

PROCEEDINGS OF THE INTERNATIONAL CONFERENCE ON ARCTIC MARGINS VI

Introduction

S.N. Kashubin, et. al. Crustal thickness in the circumpolar Arctic

Carla Susanne Tomsich, et. al. New zircon U-Pb ages for the Lower Cantwell Formation: Implications for the Late Cretaceous paleoecology and paleoenvironment of the Lower Cantwell Formation near Sable Mountain, Denali National Park and Preserve, central Alaska Range, USA

M.I. Tuchkova, et. al. Permian and Triassic deposits of Siberian and Chukotka passive margins: Sedimentation setting and provenances

Sokolov S.D., et. al. Chukchi arctic continental margins: Tectonic evolution, link to the opening of the Amerasia Basin

Galina V. Ledneva, et. al. Intra-plate gabbroic rocks of Permo-Triassic to early-middle Triassic dike-and-sill province of Chukotka (Russia)

M.V. Luchitskaya, et. al. U-Pb ages and tectonic setting of mid-Cretaceous magmatism in Chukotka (NE Russia)

V. V. Akinin, et. al. Age and composition of final stage of volcanism in Okhotsk-Chukotka volcanic belt: An example from the Ola Plateau (Okhotsk segment)

E.B. Suvorova, et. al. Lithofacies features of Carboniferous through Lower Permian strata from the Pechora Sea

Malyshev N.A., et. al. Tectonics of the sedimentary basins in the Russian sector of the Chuckchi Sea

Garrik Grikurov, et. al. Zircon geochronology of bottom rocks in the central Arctic Ocean: Analytical results and some geological implications

V. Poselov, et. al. The structural integrity of the Lomonosov Ridge with the North American and Siberian continental margins

Sergey Alekseev, et. al. The Arctic-2010 Cruise: Bathymetric survey for delineation of the extended continental shelf of the Russian Federation in the Arctic

V. A. Vernikovskiy, et. al. Early evolution stages of the Arctic margins (Neoproterozoic-Paleozoic) and plate reconstructions

L.I. Lobkovskiy, et. al. 3D geodynamics of Arctic region and model of Amerasian Basin formation



PROCEEDINGS OF THE INTERNATIONAL CONFERENCE ON ARCTIC MARGINS VI • MAY 2011

PROCEEDINGS OF THE INTERNATIONAL CONFERENCE ON ARCTIC MARGINS VI

FAIRBANKS, ALASKA
MAY 2011



EDITED BY:

DAVID B. STONE
GARRIK E. GRIKUROV
JAMES G. CLOUGH
GORDON N. OAKEY
DENNIS K. THURSTON

ICAM VI

Proceedings of the International Conference on Arctic Margins VI

Fairbanks, Alaska, May 2011

Edited by: David B. Stone, Garrik E. Grikurov,
James G. Clough, Gordon N. Oakey, Dennis K. Thurston



UDC: 005.745(100(98))

**ICAM VI: Proceedings of the International Conference on Arctic Margins VI,
Fairbanks, Alaska, May 2011.** – SPb.: Press VSEGEI, 2014. – 332 p.

ISBN 978-5-93761-217-5

Edited by: David B. Stone, Garrik E. Grikurov,
James G. Clough, Gordon N. Oakey, Dennis K. Thurston

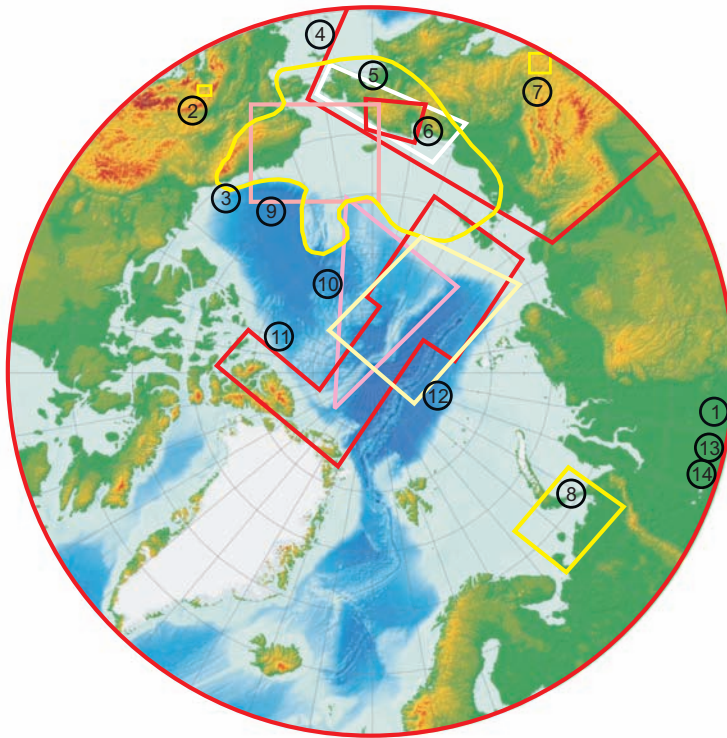
Copyright © 2014, VSEGEI

Cover photo of Kogasukruk River,
North Slope, Alaska, courtesy of Peter Flaig

Cover concept by Meghan Murphy
Layout by Vicki Daniels, Design Services,
University of Alaska Fairbanks

ISBN 978-5-93761-217-5

Table of Contents



CHAPTER 1	1
Crustal thickness in the circumpolar Arctic	
S.N. Kashubin, O.V. Petrov, E.A. Androsoy, A.F. Morozov, V.D. Kaminsky, V.A. Poselov	
CHAPTER 2	19
New zircon U-Pb ages for the Lower Cantwell Formation: Implications for the Late Cretaceous paleoecology and paleoenvironment of the Lower Cantwell Formation near Sable Mountain, Denali National Park and Preserve, central Alaska Range, USA	
Carla Susanne Tomsich, Paul J. McCarthy, Anthony R. Fiorillo, David B. Stone, Jeff A. Benowitz, and Paul B. O'Sullivan	
CHAPTER 3	61
Permian and Triassic deposits of Siberian and Chukotka passive margins: Sedimentation setting and provenances	
M.I. Tuchkova, S.D. Sokolov, A.K. Khudoley, V.E. Verzhbitsky, Y.Hayasaka, A.V. Moiseev	
CHAPTER 4	97
Chukchi arctic continental margins: Tectonic evolution, link to the opening of the Amerasia Basin	
Sokolov S.D., Ledneva G.V., Tuchkova M.I., Luchitskaya M.V., Ganelin A.V., and Verzhbitsky V.E.	
CHAPTER 5	115
Intra-plate gabbroic rocks of Permo-Triassic to early-middle Triassic dike-and-sill province of Chukotka (Russia)	
Galina V. Ledneva, Boris A. Bazylev, Paul W. Layer, Akira Ishiwatari, Sergey D. Sokolov, Natalia N. Kononkova, Petr L. Tikhomirov and Maria S. Novikova	

Table of Contents

CHAPTER 6	157
U-Pb ages and tectonic setting of mid-Cretaceous magmatism in Chukotka (NE Russia)	
M.V. Luchitskaya, P.L. Tikhomirov, and A.L. Shats	
CHAPTER 7	171
Age and composition of final stage of volcanism in Okhotsk-Chukotka volcanic belt: An example from the Ola Plateau (Okhotsk segment)	
V. V. Akinin, P. Layer, J. Benowitz, Ntaflos, Th.	
CHAPTER 8	195
Lithofacies features of Carboniferous through Lower Permian strata from the Pechora Sea	
E.B. Suvorova, T.V. Matveeva	
CHAPTER 9	203
Tectonics of the sedimentary basins in the Russian sector of the Chuckchi Sea	
Malyshev N.A., Obmetko V.V., Borodulin A.A., Barinova E.M., and Ikhsanov B.I.	
CHAPTER 10	211
Zircon geochronology of bottom rocks in the central Arctic Ocean: Analytical results and some geological implications	
Garrik Grikurov, Oleg Petrov, Sergey Shokalsky, Pavel Rekant, Alexey Krylov, Anatoly Laiba, Boris Belyatsky, Mikhail Rozinov and Sergey Sergeev	
CHAPTER 11	233
The structural integrity of the Lomonosov Ridge with the North American and Siberian continental margins	
V. Poselov, V. Butsenko, A. Chernykh, V. Glebovsky, H.R. Jackson, D. P. Potter, G. Oakey, J. Shimeld and C. Marcussen	
CHAPTER 12	259
The Arctic-2010 Cruise: Bathymetric survey for delineation of the extended continental shelf of the Russian Federation in the Arctic	
Sergey Alekseev, Ivan Glumov, Andrey Morozov, Konstantin Stavrov, Andrey Zen'kov, and Denis Zhilin	
CHAPTER 13	265
Early evolution stages of the Arctic margins (Neoproterozoic-Paleozoic) and plate reconstructions	
V. A. Vernikovskiy, D. V. Metelkin, A. E. Vernikovskaya, N. Yu. Matushkin, L. I. Lobkovskiy, E. V. Shipilov	
CHAPTER 14	287
3D geodynamics of Arctic region and model of Amerasian Basin formation	
L.I. Lobkovskiy, M.V. Kononov, I.A. Garagash, V.E. Verzhbitskiy, and V.D. Kotelkin	

ICAM VI

Proceedings of the International Conference on Arctic Margins VI Fairbanks, Alaska, May 2011

Edited by: David B. Stone, Garrik E. Grikurov, James G. Clough, Gordon N. Oakey, Dennis K. Thurston

INTRODUCTION

The Sixth International Conference on Arctic Margins was held at the University of Alaska, Fairbanks from May 30 to June 2, 2011. It was convened by Bernard Coakley together with David Stone, Garrik Grikurov, Harald Brekke, James Clough, Ruth Jackson, Paul Layer, Naja Mikkelsen, Victoria Pease, and Dennis Thurston. There were over 130 participants and 112 presentations. In addition there was ample time for discussion at the Student Union pub for lunch and poster sessions, and during the evening dinner excursions to the Pioneer Park outdoor Salmon Bake, and a Dinner cruise down the Chena River. (For photos of these activities a CD is available from the authors or can be downloaded from: <http://www2.gi.alaska.edu/ICAMVI>).

One highlight of the meeting was the wealth of new data on display, much of it collected to support Extended Continental Shelf (ECS) claims under Article 76 of the Law of the Sea. To establish the seaward limit of their ECS in accordance with the provisions of Article 76, it is necessary for each country to identify the 2500 meter isobath and the foot of slope from bathymetric data, and to collect seismic reflection and refraction data to estimate sediment thickness.

The circum-arctic countries, Denmark, Canada, Norway, Russia and the US have organized and executed Arctic Ocean cruises, airborne geophysics campaigns and ice island expeditions to collect the bathymetry, seismic reflection, seismic refraction and potential field data to support their ECS claims. The programs have also collected seafloor samples to support the geophysical interpretations.

These surveys were not planned to answer science questions, but to characterize the seafloor and sediments on a regional scale, typically with line spacing at about 100 km. Because of the regular nature of the surveys, they have visited places that would not be included under hypothesis-driven science-focused studies. As a result, we can glimpse

surprising and unexpected observations in the ECS data sets. The surprises are just starting to emerge into the wider scientific community, to be incorporated into the larger body of knowledge about the Arctic Ocean and to become the basis for planning future cruises to answer the questions these unexpected observations pose. These data are likely to be the basis for a new revolution in our understanding of the Arctic Ocean and its history.

Organization of this Volume

The papers submitted for this volume divide into three general categories, onshore geology, marine studies, large scale tectonics plus one paper that presents a framework for the whole region. This latter paper leads off followed by papers in the other three categories going more or less from east to west. The numbers for each of the areas shown on the map accompanying the Table of Contents are the Chapter numbers for each area.

In addition to this volume a CD containing power points and copies of posters from many of the presenters is available from David Stone (dstone@gi.alaska.edu) or the contents can be downloaded from <http://www2.gi.alaska.edu/ICAMVI>

ICAM Student Recognition Awards

These awards, sponsored by the Alaska Geological Society and University of Alaska Geophysical Institute, went to Anne Hegewald for the Outstanding Oral Presentation, *Sedimentary structures and horizon ages in the Amerasian Basin between the Chukchi Plateau and Mendeleev Ridge* and to Sonja Suckro for the Outstanding Poster Presentation, *Tectonic evolution of southern Baffin Bay: implications from a refraction survey*.

Field trips

Two Field Trips were offered, plus several informal ones.

Field Trip 1. *Friday and Saturday, June 3 and 4. Geology, tectonics and gold mineralization of the Fairbanks area.*

Day One focused on the broad geologic setting of the Fairbanks area, with eclogite facies rocks on top of amphibolite facies rocks on top of greenschist facies rocks. Igneous rocks include the within-plate early Tertiary basalt and the mid-Cretaceous subduction-related plutons. Day Two examined mining and mineralization in the Fairbanks area including a trip to Fort Knox, an open pit mine with 3.6 million troy ounces of proven and probable reserves. 2010 gold production at Fort Knox was 349,729 troy ounces of gold. The Fairbanks mining district is a northeast trending belt of lode and placer gold deposits that comprise one of the largest gold producing areas in the state of Alaska.

Led by Rainer Newberry, Professor, Department of Geology and Geophysics, University of Alaska Fairbanks.

Field Trip 2. *Stratigraphy, sedimentology and paleoenvironment of the Cantwell Formation, Denali National Park, Alaska.*

The Cantwell Formation of central Alaska comprises a late Cretaceous plant fossil, and dinosaur and bird track-bearing fluvial-alluvial fan sequence and an overlying Paleocene to Eocene predominantly volcanic succession. The formation is located between two fault strands forming the northern bend of the arcuate transcontinental Denali strike-slip fault. The sediments were deposited following the accretion of the Wrangellia Terrane.

The trip led into canyons and steep drainages cut into mountains composed entirely of overlying Cantwell Formation and a thick section of volcanic flows pierced by numerous mafic and felsic subvolcanic intrusions. We stopped at a particularly fossiliferous section showing facies distributions, plant fossils, invertebrate traces and vertebrate tracks.

The rocks of the sedimentary Cantwell Formation are interpreted as having been deposited in a variety of closely spaced ancient river, lake,

alluvial plain and alluvial fan floodplain sedimentary environments. The boundaries between finest-grained and coarser-grained sedimentary facies commonly preserve vertebrate and invertebrate tracks and plant fossils plus numerous large theropod and hadrosaur footprints. The finer-grained facies preserve delicate invertebrate traces and angiosperm leaf, fern frond, and conifer shoot, cone, seed and wood impressions.

Led by Paul McCarthy (Professor) and Suzanne Tomsich (PhD candidate), Department of Geology and Geophysics, University of Alaska Fairbanks.

Thanks

The local organizers headed by Bernard Coakley would like to thank the university staff and students for their part, and particularly the Pub staff who helped oil the wheels of communication.

The editors would also like to thank the external reviewers, listed below, for their sometimes thankless task of carefully reading early versions of the papers presented here: Vyacheslav Akinin, Jeff Amato, Arthur Banet, Robert Blodgett, Kelley Brumley, Douglas Christensen, Bernard Coakley, Sonya A. Dehler, George Dellagiarrino, Dieter Franke, Carmen Gaina, Chris Harrison, Larry Lane, Lotte Melchior Larsen, Keith Meekins, Elizabeth Miller, Anne Pasch, Kirk Sherwood.

Special thanks are due to Federal Agency for Mineral Resources of the Russian Federation (ROSNEDRA) and the A.P. Karpinsky All-Russia Geological Institute (VSEGEI) for active participation in the work of the conference and assistance in printing this proceedings volume.

HISTORY OF ICAM

The International Conference on Arctic Margins (ICAM) was founded by the U.S. Department of the Interior Bureau of Ocean Energy Management, Regulation and Enforcement (BOEMRE), formerly the Minerals Management Service, in 1991 with the underlying two-point theme of 1) Arctic understanding, 2) international cooperation in Arctic research. To these ends, the ICAM meetings have provided a forum for the exchange of information and presentation of research and a platform to explore collaborative programs. For more information see <http://boem.gov/ICAM/>



The core! Participants who attended all six ICAM meetings. From left to right, Back row: Larry Lawver, Tom Buntzen, Paul Layer, David Stone, Larry Lane, Warren Nokleberg, Jim Clough, Mikhail Kos'ko. Front row: Andrei Prokopiev, Dennis Thurston, Jan Inge Faleide, Tom Moore, Gordon Oakey, Garrik Grikurov.



Almost all of the participants at ICAM VI

Meeting Summaries

ICAM I—*convened in September, 2-4, 1992, Anchorage, Alaska*

- Over 400 participants from 12 countries,
- 198 presentations (90 by US; 40 Russian; 32 Canada; 25 from Scandinavia; 8 from the rest of Europe and 6 from Australia)
- 6 workshops
- 5 invited symposia
- 11 general oral sessions
- 12 poster sessions
- 5 geological field trips
- Hosted by the Alaska Geological Society
- Sponsored by BOEMRE, formerly MMS

An abstract volume containing over 250 abstracts was published in limited supply and given to all participants. The proceedings were published in 1994 as: 1992 proceedings International Conference on Arctic Margins : Anchorage, Alaska, September 1992, Thurston D.K., Fujita, K., OCS Study MMS 94-0040, 1994. <http://boem.gov/ICAM/>

ICAM II—*convened in September, 6-10, 1994, Magadan, Russia*

- 130 people participated representing 45 different organizations from 10 countries (60 non-Russian participants)
- 7 technical sessions, involving many scientific, industrial and public organizations and private companies of Magadan
- 4 symposia and a round-table session
- 103 oral and 43 poster presentations
- Hosted by the Russian Academy of Sciences, Far East Branch and the University of Alaska Geophysical Institute, Fairbanks
- Field trip “Golden Ring of Kolyma” was conducted on September 9-20, and its participants were 11 representatives of mining industry of Canada, U.S., Australia and Japan.

An abstract volume containing over 280 abstracts was published in limited supply and given to all participants.

The 1994 ICAM Proceedings was published in 1995 by the Russian Academy of Sciences Far East Branch, Northeast Science Center, Magadan: *ICAM 1994: Summary of Conference, Magadan, Russia*, and is available at <http://boem.gov/ICAM/>.

ICAM III—*convened in October 12-16, 1998, Celle, Germany*

- 200 participants from 14 countries
- 15 Technical Sessions
- 142 oral presentations and 70 posters
- Hosted by the Federal Institute for Geosciences and Natural Resources (BGR), the German Society for Polar Research, and the Alfred Wegener Institute for Polar and Marine Research
- Supported by the Russian Academy of Sciences, the University of Alaska Geophysical Institute, and MMS.
- 220 Abstracts received

The ICAM III Proceedings were published as two special volumes of the Journal *Polarforschung* (*Polarforschung 68, 1998 (printed 2000)* and *Polarforschung 69, 1998 (printed 2002)*) by the German Society for Polar Research and Alfred Wegener Institute for Polar and Marine Research.

ICAM IV—*September 30-October 3, 2003, Dartmouth, Nova Scotia*

A special event in the form of Hurricane Juan inflicted considerable damage to Halifax and Dartmouth the day before the meeting started. The organizing committee managed to find space for the meeting and food and hotels for the attendees. A remarkable achievement in the light of power and transportation outages and delays.

- 130 participants
- Featuring 9 technical sessions
- Workshops
- Hosted by Natural Resources Canada through Geological Survey of Canada (Atlantic)
- Supported by the Canadian Polar Commission and MMS
- A special meeting of the Nansen Arctic Drilling Program was held
- Field Trip: Marine Geophysical Tour of Halifax Harbour aboard the Harbour Queen

Proceedings edited by Robert Scott of Cambridge Arctic Shelf Program and Dennis Thurston, BOEMRE and published through BOEMRE-Alaska as Study MMS 2006-003. <http://boem.gov/ICAM/>

ICAM V—September 3-5, 2007, Tromsø, Norway.

- More than 300 participants
- 106 Oral presentations
- 86 Posters
- 9 Thematic Sessions
- Sponsored by the Geological Society of Norway (NGF) in cooperation with the European Association of Geoscientists and Engineers (EAGE).

ICAM V was held in conjunction with “Arctic Conference Days 2007” which included The Arctic Geology, Resources and Environment Conference (AGReE) and The Shelf Edge and Shoreline Trajectories Conference (SEST).

The Proceedings contained 11 invited papers published by the Norwegian Journal of Geology as *ICAM V Special Volume NJG 2008 Volume 88 Nr. 4*.

ICAM VI—May 31-June 2, 2010 in Fairbanks, Alaska, USA

Hosted by the Geophysical Institute and the College of Natural Sciences and Mathematics of the University of Alaska, Fairbanks.

- More than 130 participants
- 77 Oral presentations
- 45 Posters
- 5 Thematic Sessions
- Sponsored by BP Alaska, Shell, ConocoPhillips and the Alaska Division of Geological and Geophysical Survey.

The program can be obtained from www.gi.alaska.edu/icam6

Outlines of talks and posters submitted by their authors can be obtained from: <http://www2.gi.alaska.edu/ICAMVI>

We are planning to have this volume available on the internet through both the University of Alaska and VSEGEI following the printed version.

Crustal thickness in the Circum Arctic

S.N. Kashubin¹, O.V. Petrov¹, E.A. Androsov¹, A.F. Morozov², V.D. Kaminsky³, V.A. Poselov³

¹VSEGEI, St. Petersburg, Russia

²ROSNEDRA, Moscow, Russia

³VNIOkeangeologia, St. Petersburg, Russia

ABSTRACT

Crustal thickness data are used in calculating the corrections necessary for developing seismological and global geophysical models. Such data also offer some criterion for distinguishing the types of crust in zones of transition from continents to oceans. Extensive seismic investigations performed in the Arctic in recent years have considerably improved the accuracy of previous compilations and have enabled the development of a more detailed digital model of the Earth's crust. All available deep seismic geotranssects acquired north of 60°N during the period 1960-2010 were used. This dataset includes more than 200 seismic profiles totaling approximately 110 000 line km. The new map is an important contribution to geophysical and geotectonic interpretations of the Arctic region and has global implications.

INTRODUCTION

Information on the Earth's crustal thickness plays an important role in studying the deep (down to 80-100km) structure of the Earth. It is necessary for calculating the corrections in seismological and global geophysical modeling, as well as for structural and geodynamic interpretations. In zones of transition from continents to oceans, the change of crustal thickness is often a defining criterion for determining the position of the continent-ocean boundary.

Seismic methods play a leading role in studying the thickness of the crust, where the base of the crust is identified by the depth of the Mohorovičić (M or Moho) discontinuity. The most common method is deep seismic sounding (DSS) in which Moho depth is determined from refracted and post-critically reflected wave data, often called wide-angle seismic (Mooney, 2007). Sometimes the base of the crust can be recognized in seismic sections obtained from sub-critical reflections using the multi-channel

seismic (MCS) methods (Suleimanov et al., 2007), and sometimes by the receiver function methods (Zolotov et al., 1998). In the absence of seismic data, crustal thickness estimations can be made using the correlations between the Moho depth, topography and Bouguer anomalies (Demenitskaya, 1967; Kunin et al., 1987).

Under the international project "Atlas of geological maps of the Circumpolar Arctic at 1:5 000 000 scale" (BULLETIN 54 CGMW, 2006), Russia coordinates the compilation of the Tectonic map of the Arctic which includes the Earth's crustal thickness map as one of its components. Earlier compilations for individual parts of the area north of 60°N included a depth to Moho map from seismic data (Ritzmann et al., 2006; Grad et al., 2007; Erinchek et al., 2007) and crustal thickness maps derived from gravity anomalies (Verba et al., 2000; Braun et al., 2007; Alvey et al., 2008). However, due to the sparsity of seismic profiles in the Arctic and a lack of representative data on correlations between crustal thickness and gravity anomalies, these maps were not integrated and, indeed, show marked inconsistency. The only compilation of Moho depths for the entire Arctic region was the CRUST2.0 map based on the 2° x 2° global model (Laske et al., 2000) but it appeared too coarsely sampled for the purposes of tectonic interpretations (Fig. 1). Inconsistencies of Moho depths in overlapping areas of regional maps created by different authors group are within the range ±0–4 km in onshore and offshore areas supported by deep seismic investigations. Inconsistencies in offshore areas where Moho depths were derived mainly from gravity data are ±4–12 km. North American and West Greenland part is represented by the single CRUST 2.0 map, so its accuracy is not estimated. Extensive recent seismic investigations in the Arctic (Matveev et al., 2007; Poselov et al., 2007; Kaminsky, 2009; etc.) have greatly improved the accuracy of previous mapped products and have

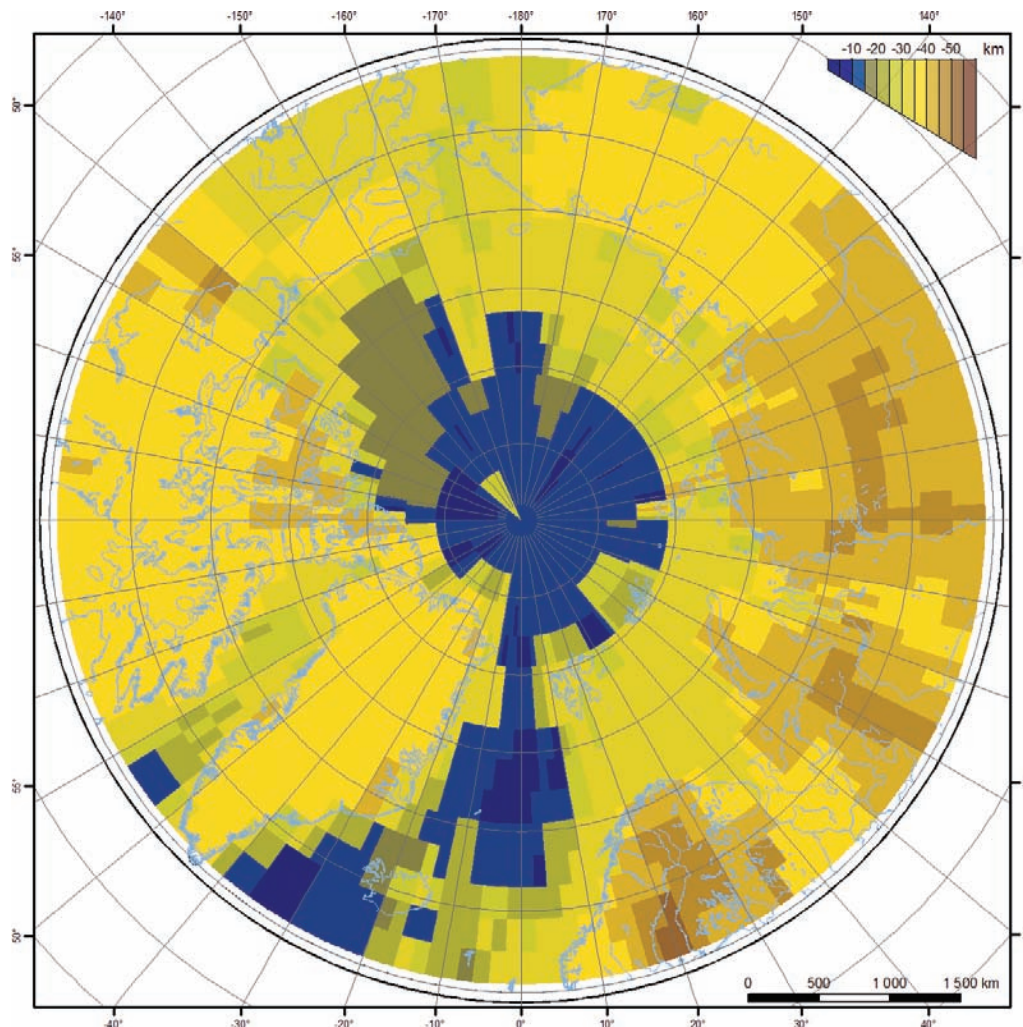


Fig. 1. Crustal thickness in the Circum Arctic based on the global crustal model CRUST 2.0 (Laske et al, 2000)

made possible a new digital model of the Earth's crustal thickness for the Circumpolar Arctic.

SEISMIC DATA

All available crustal seismic sections north of 60°N produced by earlier investigators between 1960 and 2010 were utilized in the compilation of the new map. This database includes more than 200 seismic sections totaling approximately 110 000 km in length (Fig. 2). About 75% of sections are based on wide-angle seismic data, the rest are based on MCS reflection and receiver function data.

As can be seen in Fig. 2, the coverage of the Arctic region by deep seismic methods is very irregular. The density of profiles in North Eurasia and in the Barents Sea is approximately 5 km per 1 000 km², whereas in North America and in the Canada Basin deep seismic profiles are virtually

absent. Most seismic lines (c. 73 000 km) are located on land while about 32 000 km are located offshore.

A detailed list of publications (see Bibliography), describing approximately 180 crustal sections, plus more than 20 previously unpublished seismic sections kindly provided by RosGeolFond and individual research teams have been incorporated in this compilation.

CORRELATION BETWEEN MOHO DEPTH, TOPOGRAPHY AND BOUGUER ANOMALIES

A significant part of the Circum Arctic is not characterized by DSS observations and required utilization of additional information, in particular from gravity data. Due to peculiarities of deep seismic studies, information on Moho depth is commonly much more generalized than surface

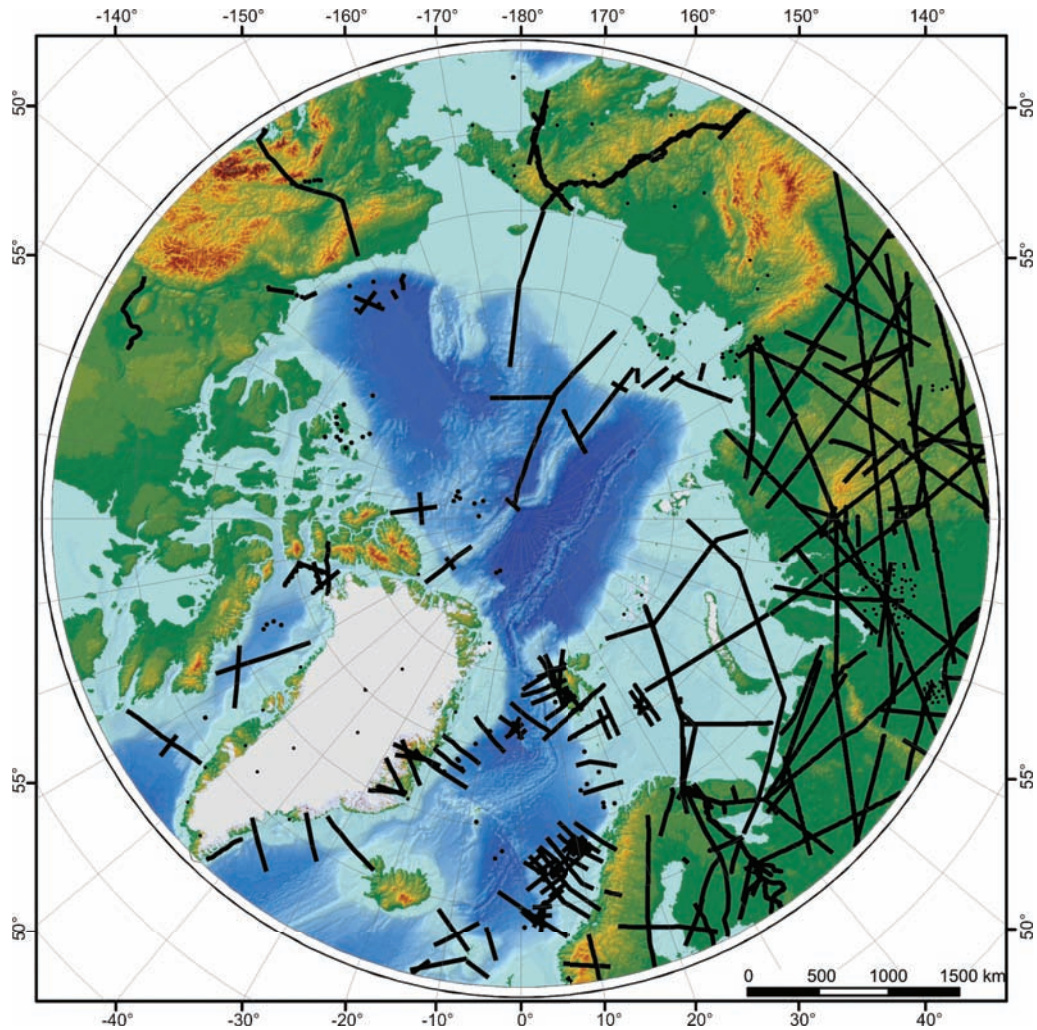


Fig. 2. Location of deep seismic profiles and points of determination of Moho depths from seismic data

topography and gravity data. Therefore, to achieve a more homogeneous view of crustal structure, we analyzed the correlation between the Moho depth, topography, and gravity anomalies smoothed by different averaging radii. To increase the representativeness of the correlation, the seismic data from the Circum Arctic (where the variations in model parameters, especially on land, are relatively small) were supplemented by seismic, topographic and gravity data from the whole of Eurasia, including highly mountainous fold belts.

The best correlation with Moho depth was found for topographic and Bouguer anomaly values calculated with an intermediate layer density of 2.67 g/cm^3 and smoothed by a 100 km window. Figure 3 shows scatter plot correlations of the model parameters: Moho depth (Z_M in km), topographic elevations averaged over a 100 km radius (h_{100} in m), and Bou-

guer anomalies, averaged over a 100 km radius (G_{100} in mGal).

It can be observed that the slopes of the regressions for land and marine data differ, notably in the Z_M-G_{100} plane (Fig. 3b), while remaining almost constant in the Z_M-h_{100} plane (Fig. 3c). This may be caused by a different relationship between the Bouguer reductions selected for onshore and offshore topography (Fig. 3d). Consequently, two bivariate regressions were selected to estimate values of Moho depth from known values of topographic elevation and Bouguer anomaly: the first one for land ($h_{100} > 0$), and the other for marine areas ($h_{100} < 0$) (Table). Both regressions have similar values of correlation coefficients equal to 0.83-0.84, that result in a root-mean-square error of Z_M estimates of 5 km.

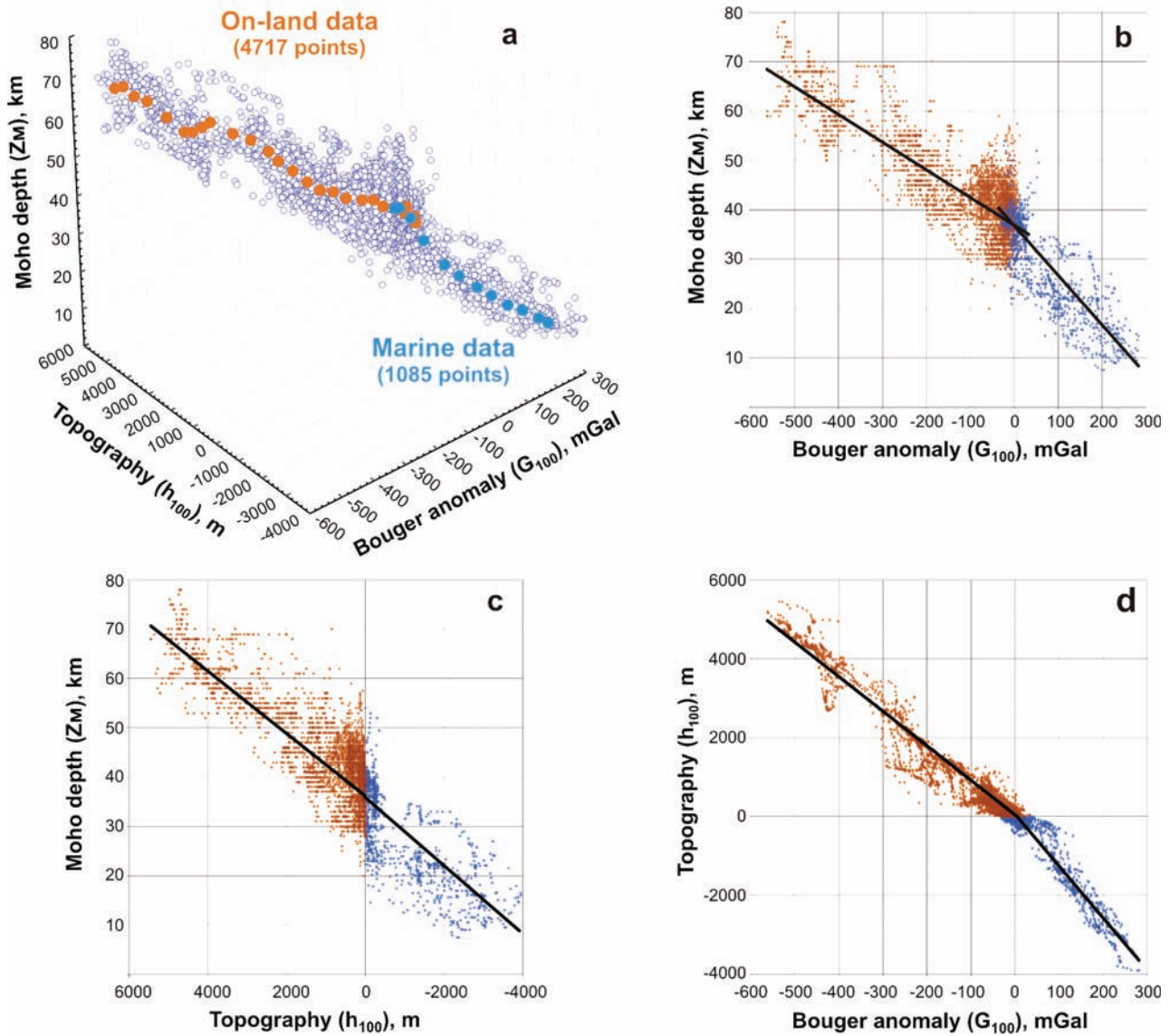


Fig. 3. Scatter plots and correlations between Moho depth, Bouguer anomalies and topography: a – regression domain for Z_M , G_{100} and h_{100} , where Z_M is depth to Moho (km), G_{100} is Bouguer anomaly (mGal) averaged over a 100 km radius, h_{100} is topographic elevation (m) averaged over a 100 km radius; b, c, d – projections of the regression domain on corresponding planes

Table. Empirical expression for estimating Moho depth from the smoothed Bouguer anomaly and topography. The first expression is for land areas while the second is for marine areas.

Equation	Range of values variation, dimensions		
	Z_M	G_{100}	h_{100}
$Z_M = 36.3 - 0.038G_{100} + 0.003h_{100}$	20.0 ÷ 80.0 km	-560 ÷ +35 mGal	0 ÷ 5400 m
$Z_M = 36.3 - 0.137G_{100} + 0.003h_{100}$	7.5 ÷ 48.0 km	-30 ÷ +280 mGal	-4200 ÷ 0 m

COMPILATION PROCEDURE AND ERROR APPRAISAL

The Moho depth values were taken from seismic sections at 25 km interval and plotted on the data location map. Altogether this map included approximately 1000 Z_M values in the Arctic Ocean and its marginal seas, and about 2600 Z_M values in the continental part of the Circum Arctic.

In spaces between profiles and in vast areas devoid of seismic data, the Moho depth values were derived from digital maps of gravity anomalies (Gaina et al., 2009) and of onshore topography and offshore bathymetry (IBCAO ver 2.23). After averaging the Bouguer anomaly values and topographic elevations over a 100 km radius in accordance with the formulas shown in Table, Z_M values were estimated separately for offshore and onshore areas using a 10 km x 10 km grid. The two grids were merged into a single model with subsequent Moho depth mis-tie correction along the coastline. Based on the adjusted data, a new digital dataset was calculated and integrated with earlier digital maps of Moho depths (Ritzmann et al., 2006; Grad et al., 2007; Erinchek et al., 2007) The resultant map is represented as a Z_M digital model with cell size of 10 km x 10 km for the entire studied region.

An appraisal of interpolation error during recalculation of the Z_M values into a uniform grid was made by comparing interpolated and initial values for 3600 locations where the depth values were also found from seismic data. The root-mean-square deviation between interpolated and initial values amounted to 1.7 km against 5 km contour interval in the final Moho depth map. Figure 4a shows the difference between gravity-derived and seismic-derived values for onshore areas, and Figure 4b – for offshore areas.

After subtracting ocean depth values and correcting for observation altitude on land, the map of Moho depth values was transformed into the map of the Earth's crustal thickness for the Circum Arctic (Fig. 5).

The main significance of the crustal thickness map in the Arctic region lies in its potential for interpretation of the tectonic structure of the Central Arctic bathymetric highs which include the Lomonosov Ridge and the Mendeleev-Alpha

system separated by the Podvodnikov-Makarov Basin and the Chukchi Borderland. The map's value in this respect rests on the fact that its compilation is, for the first time, based on extensive findings from multinational deep seismic studies conducted in this area and its juxtaposition with the adjacent Eurasian and North American continental margins (“Transarctica-1989-92”, “Arctica-2000”, “Arctica-2005”, “Arctica-2007”, “Arta-2008 on the Alpha Ridge”, “Lorita-2006 on the Lomonosov Ridge”) (Jackson et al., 2010; Lebedeva-Ivanova et al., 2006; Poselov et al., 2007).

CONCLUSION

A new digital model of the Earth's crustal thickness in the Circum Arctic significantly differs from the earlier CRUST2.0 global model (Laske et al., 2000) in capturing a much greater level of detail (compare Fig. 1 and Fig. 5). In the compilation we succeeded in incorporating a large amount of recent seismic data and interpretations, as well as in considerably less data smoothing compared to the global model and made all possible effort to avoid global data smoothing.

Crustal thickness in the Circum Arctic varies in a wide range from 5-10 km in the Norwegian-Greenland and Eurasia oceanic basins to 55-60 km in Scandinavia and the Urals. Horizontal size and configuration of the crustal thickness anomalies are comparable with those of regional geological structures. In our opinion, this new map is suitable both for introducing crustal-based corrections during seismic and global geophysical modeling, and for constructing geotectonic interpretations in the Arctic.

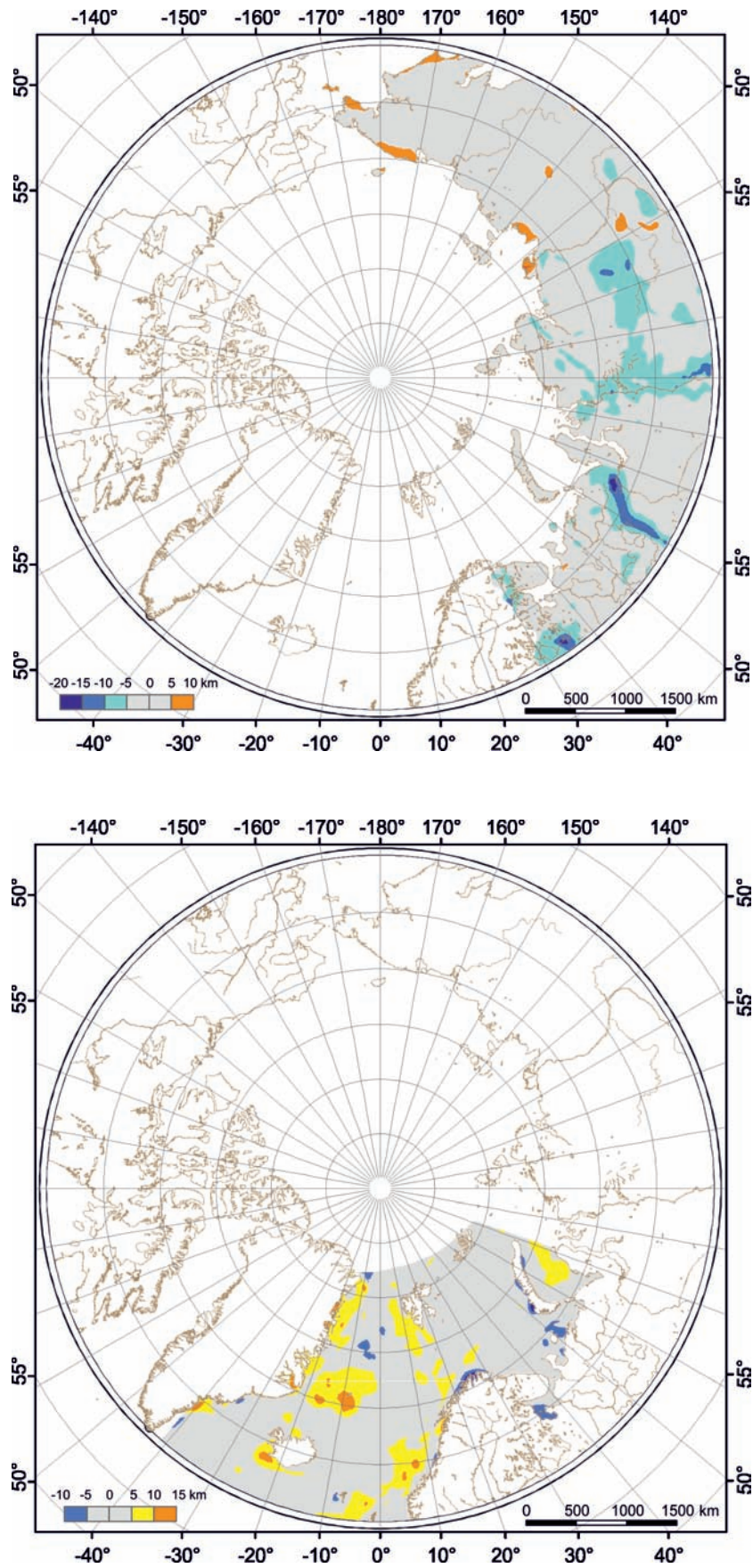


Fig. 4. Difference between the Moho depth map constructed on the basis of seismic data and the map constructed on the basis of bi-parameter correlation dependencies of Moho depth from Bouguer anomalies and topography: a – onshore areas, b – offshore areas

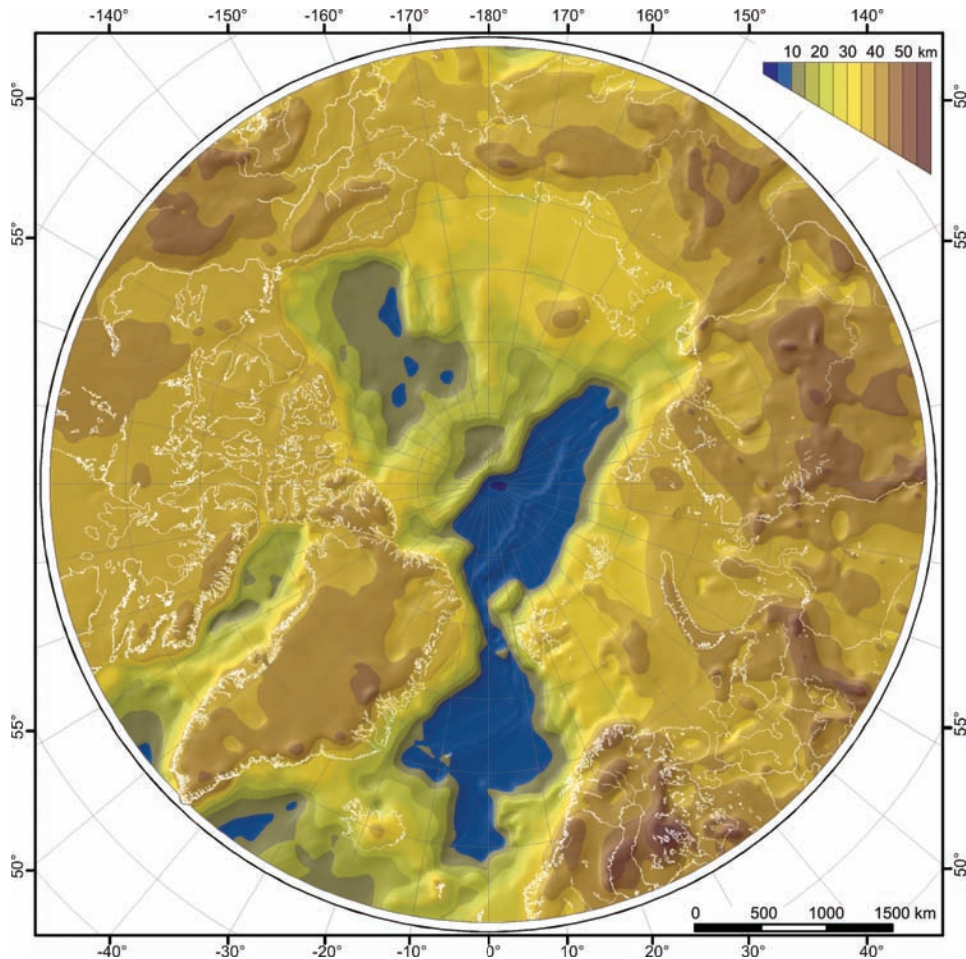


Fig. 5. Crustal thickness in the Circum Arctic

ACKNOWLEDGEMENTS

The authors would like to express their gratitude to their colleagues V. Yu. Glebovsky, V. V. Butsenko, S. M. Zholondz, E. D. Milshtein, V. N. Mukhin and Yu. M. Erinchek for a great contribution to initial data processing and fruitful ideas on the map compilation procedure. We acknowledge experts from RosGeolFond and Russian geological-geophysical enterprises and institutes: Sevmorgeo, VESGEI, SNIIGGiMS, Bazhenov Geophysical Expedition, and UIEPRAS, for seismic data selection. We would also like to thank representatives of the geological surveys of Canada, Denmark and Germany, R. Jackson, T. Funck, and S. Suckro, for the materials they provided, and N. Lebedeva-Ivanova who kindly shared her yet unpublished results for the preparation of this paper. Our special thanks go to Olga Bogdanova who translated the original manuscript into English and to Phil Christie who edited the manuscript after translation.

REFERENCES

- Alvey, A., Gaina, C., Kuszniir, N.J., Torsvik, T.H., 2008. Integrated crustal thickness mapping and plate reconstructions for the high Arctic. *Earth and Planetary Science Letters*, 274, 310–321.
- Braun, A., Kim, H.R., Csatho, B., von Frese, R.R.B., 2007. Gravity-inferred crustal thickness of Greenland. *Earth and Planetary Science Letters*, 262, 138-158.
- BULLETIN 54 (2005-2006) of Commission for the Geological Map of the World. Resolutions of the General Assembly, Paris, UNESCO – 8-10 February 2006, 1-92.
- Demenetskaya, R.M., 1967. Crust and mantle of the Earth. Moscow, Nedra (in Russian).
- Erinchek, Yu.M., Milshtein, E.D., Egorkin, A.V., Verba, V.V., 2007. Structure of Moho in the territory of Russia and adjacent water areas. - *Models of the Earth's crust and upper mantle*

- after deep seismic profiling. Proceedings of the international scientific-practical seminar. St. Petersburg, VSEGEI, 241-244 (in Russian).
- Gaina, C. and CAMP-GM working group, 2009. Gravity anomaly map of the Arctic. Geological Survey of Norway.
- Grad, M., Tiira, T. and working group, 2007. The Moho depth of the European plate. <http://www.seismo.helsinki.fi/mohomap>, <http://www.igf.fuw.edu.pl/mohomap2007>.
- Grantz A., Clark D., Phillips R. et al. 1998. Phanerozoic stratigraphy of Northwind ridge, magnetic anomalies in the Canada basin and timing of rifting in the Amerasian basin, Arctic ocean. *Geol. Soc. Amer. Bull.* V. 110, 6, 801-820.
- Jackson H.R., Dahl-Jensen T., the LORITA working group, 2010. Sedimentary and crustal structure from the Ellesmere Island and Greenland continental shelves onto the Lomonosov Ridge, Arctic Ocean. *Geophys. J. Int.*, 182, 11-35.
- Kabankov V.Ya., Andreeva I.A., Ivanov V.I., Petrova V.I., 2004. On the geotectonic nature of the Central Arctic morphostructures system and geological significance of bottom sediments in its determination. *Geotectonics*, 6, 33-48 (in Russian).
- Kaminsky, V.D., 2009. Deep structure of the Central Arctic Basin (due to substantiation of the outer continental shelf limit of the Russian Federation and hydrocarbon resource estimation). Ph.D. thesis in geology and mineralogy. VNIIOkeangeologia (in Russian).
- Kunin, N.Ya., Goncharova, N.V., Semenova, G.I. et al., 1987. Topography map for Eurasian mantle. Moscow, IFZ AN USSR, Mingeo RSFSR (in Russian).
- Laske, G., Masters, G., Reif, C., 2000. CRUST 2.0: A new global crustal model at 2x2 degrees. <http://igppweb.ucsd.edu/~gabi/rem.html>.
- Lebedeva-Ivanova N.N., Zamansky Y.Ya., Langinen A.E., Sorokin M.Yu., 2006. Seismic profiling across the Mendeleev Ridge at 82°N: evidence of continental crust. *Geophys. J. Int.*, 165, 527-544.
- Matveev, Yu.I., Verba, M.L., Lipilin, A.V., Roslov, Yu.V., 2007. Deep seismic studies in the Barents-Kara Region. - Models of the Earth's crust and upper mantle after deep seismic profiling. Proceedings of the international scientific-practical seminar. Rosnedra, VSEGEI. St.Petersburg, VSEGEI press, 90-93 (in Russian).
- Mooney, W. D., 2007. Crust and Lithospheric Structure – Global Crustal Structure. *Treatise on Geophysics*, vol. 1: Seismology and Structure of the Earth. (Eds. B. Romanowicz & A. Dziewonski). Elsevier, 361-417.
- Poselov, V.A., Kaminsky, V.D., Avetisov, G.P., Butsenko, V.V., Andreeva, I.A., Pavlenkin, A.D., 2007. Deep structure of continental margin in the Mendeleev Rise area (East Arctic) after geological-geophysical studies in “ARKTIKA-2005” transect. - Models of the Earth's crust and upper mantle after deep seismic profiling. Proceedings of the international scientific-practical seminar. Rosnedra, VSEGEI. St.Petersburg, VSEGEI Press, 163-167 (in Russian).
- Ritzmann, O., Maercklin, N., Faleide, J.I., Bungum, H., Mooney, W.D., Detweiler, S.T., 2006. A 3D geophysical model of the crust in the Barents sea region: model construction and basement characterization. In: 28th Seismic Research Review: Ground-Based Nuclear Explosion Monitoring Technologies, 229-237.
- Suleimanov, A.K., Berzin, R.G., Zamozhnyaya, N.G., Lipilin, A.V., 2007. Results of integrated geological-geophysical studies in the East European Craton (1EV geophysical transect). In: Models of the Earth's crust and upper mantle after deep seismic profiling. Proceedings of the international scientific-practical seminar. Rosnedra, VSEGEI. St.Petersburg, VSEGEI Press, 215-223 (in Russian).
- Verba, B.B., Volk, V.E., Kaminsky, V.D., Kim, B.I. 2000. Potential fields of the Arctic Ocean and their association with structural features of the Earth's crust. In: Geological structure and geomorphology of the Arctic Ocean in the context of the problem with the outer continental shelf limit of the Russian Federation in the Arctic Basin, St.Petersburg, VNIIO, 73-84 (in Russian).
- Zolotov, E.E., Kostyuchenko, S.L., Rakitov, V.A., 1998. Tomographic lithosphere sections in the

East European Platform. In: Seismological model of the North European lithosphere: Barents Region. Ed. F.P. Mitrofanov, N.V. Sharov. Apatity: KSC RAS. P. 1, 71-79 (in Russian).

BIBLIOGRAPHY

- Abramovitz, T., Thybo, H., Perchuc, E., 2002. Tomographic inversion of seismic P- and S-wave velocities from the Baltic Shield based on FENNOLOGRA data. *Tectonophysics*, 358, 151–174.
- Alekseev, A.S., Yegorkin, A.V., Pavlenkova, N.I., 1988. Shear waves in lithosphere studies on the territory of the USSR. *Tectonophysics*, v.154, No. 3/4, 227-239.
- Avetisov, G.P., Kaminsky, V.D., Lipilin, A.V., Poselov, V.A., Palamarchuk, V.K., Rekant, P.V., 2007. Preliminary results of deep geological-geophysical studies on the continental crust boundary delineation in the Lomonosov Ridge area, Arctic Ocean (“Arctica-2007” expedition). – Models of the Earth’s crust and upper mantle after deep seismic profiling. Proceedings of the international scientific-practical seminar. Rosnedra, VSEGEI. St.Petersburg, VSEGEI Press, 11-15. (in Russian).
- Avetistov, T.P., Golubkov, V.S., 1984. Deep structure of the central Norilsk Region after DSS – receiver function data. *Soviet geology*, 10, 86-94. (in Russian).
- Avetistov, T.P., Golubkov, V.S., 1996. Deep structure of the central Norilsk Region after DSS – receiver function data. In: Geological-geophysical characteristics of the Arctic Region lithosphere. SPb: VNIIOkeangeologia, issue I, part 2, 186-197 (in Russian).
- Baggeroer, A.B., Falconer, R., 1982. Array Refraction Profiles and Crustal Models of the Canada Basin. *Journal of geophysical research*, Vol. 87, N. B7, July 10, 5461-5476.
- Belyaevsky, N.A., Volvovsky, B.S., Volvovsky, I.S. et al., 1976. Earth’s crust of main tectonic structures in the West USSR (along the Black Sea – Kara Sea transect). – In: Geophysical studies of the Earth’s crust. Moscow, Nedra, 48-58. (in Russian).
- Belyaevsky, N.A., Volvovsky, B.S., Volvovsky, I.S. et al., 1976. Lithosphere structure along a profile from the Black sea to the Polar Urals. *Tectonophysics*, v. 33, No. 3/4, 359-378.
- Berzin, R.G., Zamozhnyaya, N.G., Kulakov, S.I. et al., 1998. Seismogeological model of the Earth’s crust for the northern part of I-EV transect. – In: Seismological model of the North European lithosphere. Ed. F.P. Mitrofanov, N.V. Sharov. Apatity: KSC RAS, P. 1, 93-109 (in Russian).
- Bialas, J., Flueh, E.R., Jokat, W., 1990. Seismic investigations of the Ringkoebing-Fyn High on Langeland, Denmark. *Tectonophysics*, 176, 25-41.
- Bogolepov, A.K., Zhuravlev, V.A., Shipilov, E.V., Yunov, A.Yu., 1991. Deep structure of the western sector of the Eurasian-Arctic continent – ocean transition. In: Deep structure of the USSR territory. Ed. V.V. Belousov, N.I. Pavlenkova. Moscow, Nauka, 31-41. (in Russian).
- Bohnhoff, M., Makris, J., 2004. Crustal structure of the southeastern Iceland-Faeroe Ridge (IFR) from wide aperture seismic data. *Journal of Geodynamics*, 37, 2, 233-252.
- Breivik, A.J., Faleide, J.I., Mjelde, R., Flueh, E.R., 2009. Magma productivity and early seafloor spreading rate correlation on the northern Vøring Margin, Norway – Constraints on mantle melting. *Tectonophysics*, 468, 206–223.
- Breivik, A.J., Mjelde, R., Grogan, P., Shimamura, H., Murai, Y., Nishimura, Y., Kuwano, A., 2002. A possible Caledonide arm through the Barents Sea imaged by OBS data. *Tectonophysics*, 355, 67–97.
- Breivik, A.J., Mjelde, R., Grogan, P., Shimamura, H., Murai, Y., Nishimura, Y., 2003. Crustal structure and transform margin development south of Svalbard based on ocean bottom seismometer data. *Tectonophysics*, 369, 37–70.
- Breivik, A.J., Mjelde, R., Grogan, P., Shimamura, H., Murai, Y., Nishimura Y., 2005. Caledonide development offshore–onshore Svalbard based on ocean bottom seismometer, conventional seismic, and potential field data. *Tectonophysics*, 401, 79–117.
- Bulin, N.K., 1971. New data of the Earth’s crust structure in the Baltic Shield. *FEB AS USSR*, vol. 198, 3, 657-660 (in Russian).

- Bulin, N.K., Afanasiev, K.A., Pronyaeva, E.A. et al., 1972. Deep section of the Southeast Siberian Platform and its folded framing after seismic data. *Soviet geology*, 10, 134-140 (in Russian).
- Bulin, N.K., Afanasiev, K.A., Pronyaeva, E.A., 1972. Profile seismological investigations in the South Baltic Shield. *Applied geophysics*, issue 69, 69-81 (in Russian).
- Bulin, N.K., Egorokin, A.V., 1993. Application of multi-wave CDP during small-scale predictive studies for mineralization and diamond content. *Geology and geophysics*, 9, 92-106. (in Russian).
- Bulin, N.K., Egorokin, A.V., 1994. Multi-wave deep seismic sounding during small-scale predictive studies. – *National geology*, 4, 43-50 (in Russian).
- Bulin, N.K., Itsykson, M.I., 1975. Some metallogenic features in activation areas of the Aldan Shield and Mongol-Okhotsk fold system and their reflection in deep geological structure. In: *Regularities of mineral distribution*. Moscow, Nauka, vol. 11: Problems of metallogeny in tectonic magmatic activation areas, 276-286 (in Russian).
- Bulin, N.K., Shcheglov, A.D., Egorokin, A.V. et al., 1999. New seismic lithosphere marks of areas with large hydrocarbon accumulations. *RAS papers*, vol. 364, 6, 792-795 (in Russian).
- Bulin, N.K., Yegorkin, A.V., 1995. Deep control of gold-sulfide mineralization in Russia and Kazakhstan. In: Persava et al. (eds.) *Mineral deposits*. Rotterdam, 101-104.
- Chernyshev, N.M., Egorokin, A.V., Danilova, E.G. et al., 1978. Deep structure of the north West Siberian Plate after seismic data. – *Soviet geology*, 9, 46-58 (in Russian).
- Czuba, W., Grad, M., Guterch, A., 1999. Crustal structure of north-western Spitsbergen from DSS measurements. *Polish Polar Research*, 20, 2, 131-148.
- Czuba, W., Grad, M., Guterch, A., Majdanski, M., Malinowski, M., Mjelde, R., Moskalik, M., Sroda, P., Wilde-Piorko, M., Nishimura, Y., 2008. Seismic crustal structure along the deep transect Horsted'05, Svalbard. *Polish polar research*, 29, 3, 279–290.
- Czuba, W., Ritzmann, O., Nishimura, Y., Grad, M., Mjelde, R., Guterch, A., Jokat, W., 2005. Crustal structure of northern Spitsbergen along the deep seismic transect between the Molloy Deep and Nordaustlandet. *Geophys. J. Int.*, 161, 347–364.
- Czuba, W., Ritzmann, O., Nishimura, Yu., Grad, M., Mjelde, R., Guterch, A., Jokat, W., 2004. Crustal structure of the continent–ocean transition zone along two deep seismic transects in north-western Spitsbergen. *Polish Polar Research*, v. 25, 3–4, 205–221.
- Dahl-Jensen, T., Larsen, T.B., Woelbern, I., Bach, T., Hanka, W., Kind, R., Gregersen, S., Mosegaard, K., Voss, P., Gudmundsson, O., 2003. Depth to Moho in Greenland: receiver-function analysis suggests two Proterozoic blocks in Greenland. *Earth and Planetary Science Letters*, 205, 379-393.
- Darbyshire, F.A., White, R.S., Priestley, K.F., 2000. Structure of the crust and uppermost mantle of Iceland from a combined seismic and gravity study. *Earth and Planetary Science Letters*, 181, 409-428.
- Deep structure along Kem-Kalevala transect, 2001. Petrozavodsk: KSC RAS, 1-194 (in Russian).
- Detkov, V.A., Valchak, V.I., Goryunov, N.A., Evgrafov, A.A., 2007. Structural features of the Earth's crust and upper mantle in the South Siberian Platform in section of reference routes Batholite and Altai – Severnaya Zemlya. - *Models of the Earth's crust and upper mantle after deep seismic profiling*. Proceedings of the international scientific-practical seminar. Rosnedra, VSEGEI. St.Petersburg, VSEGEI Press, 26-31 (in Russian).
- Digranes, P., Mjelde, R., Kodaira, S., Shimamura, H., Kanazawa, T., Shiobara, H., Berg, E.W., 1998. A regional shear-wave velocity model in the central Vøring Basin, N. Norway, using three-component Ocean Bottom Seismographs. *Tectonophysics*, 293, 157–174.
- Dossing, A., Funck, T., 2012. Greenland Fracture Zone–East Greenland Ridge(s) revisited: Indications of a C22-change in plate motion? *Journal of geophysical research*, 117, B01103, doi:10.1029/2011JB008393.
- Dukhovskiy, A.A., Belyaev, G.M., Bulin, N.K. et al., 1984. Deep structure of the Yakutia diamond-bearing province. Leningrad, VSEGEI funds,

- 1-256 (in Russian).
- Earth's crust structure of the Magadan sector of Russia after geological-geophysical data: Coll. sc. p. A.S. Salnikov (ed.) Novosibirsk, Nauka, 2007, 1-173 (in Russian).
- Eccles, J.D., White, R.S., Christie, P.A.F., 2009. Identification and inversion of converted shear waves: case studies from the European North Atlantic continental margins. *Geophys. J. Int.*, 179, 381–400, doi: 10.1111/j.1365-246X.2009.04290.x.
- Egorkin, A.V., 1999. Deep seismic studies with three-component registration of soil displacement. – *Earth's physics*, 7-8, 44-64 (in Russian).
- Egorkin, A.V., Anisina, L.V., Artemenko, L.S. et al., 2002. Crystalline crust structure in Siberia along Khanty-Mansiysk – Lena line. Prospect and protection of mineral resources (*Razvedka i okhrana nedr*), 2, 33-35 (in Russian).
- Egorkin, A.V., Chernyshev, N.M., Danilov, E.G. et al., 1980. Regional section across the Asian Continent north, Vorkuta – Tiksi line. In: *Lithospheric seismic models of main geostructures in the USSR territory*. Moscow, Nauka, 61-67 (in Russian).
- Egorkin, A.V., Danilova, E.G., Zyuganov, S.K. et al., 1980. Vilui Syncline. In: *Seismic lithosphere models of main geostructures in the USSR territory*. Moscow, Nauka, 96-98 (in Russian).
- Egorkin, A.V., Kostyuchenko, S.L., 1991. Heterogeneity of the upper mantle structure. In: V.V. Belousov, N.I. Pavlenkova (eds.). *Deep structure of the USSR territory*. Moscow, Nauka, 135-143 (in Russian).
- Egorkin, A.V., Pavlenkova, N.I., Romanyuk, T.V. et al., 1996. Upper mantle structure along Baikal – Yamal transect (“Rift”) obtained using nuclear explosions. *Geology and geophysics*, vol. 37, 9, 66-76. (in Russian).
- Egorkin, A.V., Zyuganov, S.K., Chernyshev, N.M., 1984. Siberian upper mantle. In: 27th International Geological Congress. *Geophysics. Section S.08. Papers*. Moscow, vol. 8, 27-42. (in Russian).
- Egorkin, A.V., Zyuganov, S.K., Pavlenkova, N.I., Chernyshev, N.M., 1988. Results of lithospheric structure investigations in transects in Siberia. *Geology and geophysics*, 5, 120-128 (in Russian).
- Egorkin, A.V., Zyuganov, S.K., Chernyshev, N.M., 1987. Some results of multiwave regional studies in Siberia. – In: *Multiwave seismic studies*. Novosibirsk, Nauka, 125-131 (in Russian).
- Egorov, A.S., 1989. Construction of 3D structural models of different-type crustal blocks for the USSR territory using geotraverse data. Leningrad, VSEGEI funds, b. 1 - 312 p., b. 2 - 45 p. (in Russian).
- Egorov, A.S., 1993. Lithospheric structure along composite geotraverse Murmansk town – Berezovo village – River Kochechum. *Regional geology and metallogeny*, 2, 25-41 (in Russian).
- Engen, Ø., Gjengedal, J.A., Faleide, J.I., Kristoffersen, Y., Eldholm, O., 2009. Seismic stratigraphy and sediment thickness of the Nansen Basin, Arctic Ocean. *Geophys. J. Int.*, 176, 805–821.
- Faleide, J.I., Tsikalas, F., Breivik, A.J., Mjelde, R., Ritzmann, O., Engen, Ø., Wilson, J., Eldholm, O., 2008. Structure and evolution of the continental margin off Norway and the Barents Sea. *Episodes*, 31, 1, 82-91.
- Fernández, M., Afonso, J.C., Ranalli, G., 2010. The deep lithospheric structure of the Namibian volcanic margin. *Tectonophysics*, 481, 68–81.
- Fliedner, M.M., Klempner, S.L., 2000. Crustal structure transition from oceanic arc to continental arc, eastern Aleutian Islands and Alaska Peninsula. *Earth and Planetary Science Letters*, 179, 567-579.
- Flovenz, O.G., Gunnarsson, K., 1991. Seismic crustal structure in Iceland and surrounding area. *Tectonophysics*, 191, 1-17.
- Forsyth, D.A., Asudeh, I., Green, A.G., Jackson, H.R., 1986. Crustal structure of the northern Alpha Ridge beneath the Arctic Ocean. *Nature*, 322, 349-352.
- Franke, D., Hinz, K., Onchen, O., 2001. The Laptev Sea Rift. *Marine and Petroleum Geology*, 18, 1083-1127.
- Funck, T., Andersen, M.S., Neish, J.K., Dahl-Jensen, T., 2008. A refraction seismic transect from the Faroe Islands to the Hatton-Rockall Basin, *Journal of geophysical research*, 113, B12405, doi:10.1029/2008JB005675.

- Funck, T., Dehler, S.A., Jackson, H.R., Salisbury, M.H., Reid, I.D., 2004. A Refraction Seismic Image of the Sediments in Kennedy Channel, Northern Nares Strait. *Polarforschung*, 74 (1-3), 41–50.
- Funck, T., Gohl, K., Damm, V., Heyde, I., 2012. Tectonic evolution of southern Baffin Bay and Davis Strait: Results from a seismic refraction transect between Canada and Greenland. *Journal of geophysical research*, Vol. 117, B04107, doi:10.1029/2011JB009110, 2012.
- Funck, T., Hopper, J.R., Larsen, H.C., Loudon, K.E., Tucholke, B.E., Holbrook, W.S., 2003. Crustal structure of the ocean-continent transition at Flemish Cap: Seismic refraction results. *Journal of geophysical research*, Vol. 108 (B11), 2531, doi: 10.1029/2003JB002434, 2003.
- Funck, T., Jackson, H.R., Dehler, S.A., Reid, I.D., 2004. A Refraction Seismic Transect from Greenland to Ellesmere Island, Canada: The Crustal Structure in Southern Nares Strait. *Polarforschung*, 74 (1-3), 97–112.
- Funck, T., Jackson, H.R., Loudon, K.E., Dehler, S.A., Wu, Y., 2004. Crustal structure of the northern Nova Scotia rifted continental margin (eastern Canada), *Journal of geophysical research*, Vol. 109, B09102, doi: 10.1029/2004JB003008.
- Funck, T., Jackson, H.R., Loudon, K.E., Klingelhofer, F., 2007. Seismic study of the transform-rifted margin in Davis Strait between Baffin Island (Canada) and Greenland: What happens when a plume meets a transform, *Journal of geophysical research*, 112, B04402, doi:10.1029/2006JB004308.
- Funck, T., Jackson, H.R., Shimeld, J., 2011. The crustal structure of the Alpha Ridge at the transition to the Canadian Polar Margin: Results from a seismic refraction experiment. *J. Geophys. Res.*, 116, B12101, doi:10.1029/2011JB008411.
- Funck, T., Loudon K.E., 1998. Wide-angle seismic imaging of pristine Archean crust in the Nain Province, Labrador. *Can. J. Earth Sci.*, 35, 672-685.
- Funck, T., Loudon, K.E., 1999. Wide-angle seismic transect across the Torngat Orogen, northern Labrador: Evidence for a Proterozoic crustal root. *Journal of geophysical research*, Vol. 104, N. B4, April 10, 7463-7480.
- Funck, T., Loudon, K.E., Reid, I.D., 2000. Wide-angle seismic imaging of a Mesoproterozoic anorthosite complex: The Nain Plutonic Suite in Labrador, Canada. *Journal of geophysical research*, Vol. 105, N. B11, , November 10, pp. 25, 693-25, 707.
- Geology and deep structure of the East Baltic Shield, 1968. A.A. Logachev (ed.) Leningrad, Nauka. 1 196 (in Russian).
- Gerlings, J., Funck, T., Jackson, H.R., Loudon, K.E., Klingelhofer, F., 2009. Seismic evidence for plume-derived volcanism during formation of the continental margin in southern Davis Strait and northern Labrador Sea. *Geophys. J. Int.*, 176, 980–994, doi: 10.1111/j.1365-246X.2008.04021.x.
- Glaznev, V.N., Zagorodny, V.G., Skopenko, G.B., Sharov, N.V., 1991. Baltic Shield: geological structure and history. In: V.V. Belousov, N.I. Pavlenkova (eds.). *Deep structure of the USSR territory*. Moscow, Nauka, 21-31. (in Russian).
- Gohl, K., Schreckenberger, B., Funck, Th., 2009. The Expedition of the Research Vessel “Maria S. Merian” to the Davis Strait and Baffin Bay in 2008 (MSM09/3). *Berichte zur Polar- und Meeresforschung N. 587*, Reports of Polar and Marine Research, Alfred Wegener Institute for Polar and Marine Research, Bremerhaven.
- GRANITE geotraverse: East European Platform – Urals – West Siberia (Earth’s crust structure after integrated geological-geophysical studies). S.N. Kashubin (editor), 2002. Yekaterinburg, 1-312 (in Russian).
- Hatzky, J., 2009. Analysis of bathymetry and acoustic backscatter from different multibeam sonar and sediment echosounder systems for the characterisation and classification of the seafloor at the Gakkel Ridge, Arctic Ocean. *Berichte zur Polar- und Meeresforschung, N. 601*, Reports of Polar and Marine Research, Alfred Wegener Institute for Polar and Marine Research, Bremerhaven.
- Holbrook, W.S., Mooney, W.D., 1987. The crustal structure of the axis of the Great Valley, California, from seismic refraction measurements. *Tectonophysics*, 140, 49-63.
- Hopper, J.R., Dahl-Jensen, T., Holbrook, W.S., Larsen, H.C., Lizarralde, D., Korenaga, J., Kent,

- G.M., Kelemen, P.B., 2003. Structure of the SE Greenland margin from seismic reflection and refraction data: Implications for nascent spreading center subsidence and asymmetric crustal accretion during North Atlantic opening. *Journal of geophysical research*, v. 108, N B5, 1-22.
- Isanina, E.V., Sharov, N.V. et al., 1995. Atlas of regional seismic lines for the European North of Russia. St.Petersburg, Rosgeofizika (in Russian).
- Ivanova, N.M., Sakoulina, T.S., Roslov, Yu.V., 2006. Deep seismic investigation across the Barents–Kara region and Novozemelskiy Fold Belt (Arctic Shelf). *Tectonophysics*, 420, 123–140.
- Jokat, W., 1998. The Sediment Distribution below the North Greenland Continental Margin and the adjacent Lena Trough. *Polarforschung*, 68, 71-82.
- Jokat, W., 2003. Seismic investigations along the western sector of Alpha Ridge, Central Arctic Ocean. *Geophys. J. Int.*, 152, 185–201.
- Jokat, W., Schmidt-Aursch, M.C., 2007. Geophysical characteristics of the ultraslow spreading Gakkel Ridge, Arctic Ocean. *Geophys. J. Int.*, 168, 983–998.
- Kaminsky, V.D., 2009. Deep structure of the Central Arctic Basin (due to substantiation of the outer continental shelf limit of the Russian Federation and hydrocarbon resource estimation). Ph.D. thesis in geology and mineralogy. VNIIOkeangeologia (in Russian).
- Konstantinov, M.M., Cherkasov, S.V., Donkovtsev, P.P., Yegorkin, A.V., 1999. Specific crustal features for large and superlarge endogenic gold deposits (Siberia and Far East regions). In: *Global tectonics and metallogeny*, v. 7, 2, 143-147.
- Kostyuchenko, S.L., 2000. Crustal structure and deep mechanisms of the cis-Arctic continental sedimentary basins formation in Siberia. *Regional geology and metallogeny*, 10, 125-135 (in Russian).
- Kostyuchenko, S.L., 1994. Structure and tectonic model of the Earth's crust in the Timan-Pechora Basin after integrated geological-geophysical study. – In: *Tectonics and magmatism of the East European Platform. Proceedings of the international conference “Intraplate tectonics and geodynamics of sedimentary basins”*. □: “Nauka Rossii” Fund, Geo-Invekr, 121-133 (in Russian).
- Kostyuchenko, S.L., Egorkin, A.V., 1994. Intracrustal elements of the North East European Platform. *Prospect and protection of mineral resources (Razvedka i okhrana nedr)*, 10, 12-15 (in Russian).
- Kostyuchenko, S.L., Egorkin, A.V., Solodilov, L.N., 2000. Features of structure and physical fields of the Earth's crust and upper mantle in some regions of Eurasia. In: *Tectonics, geodynamics, and seismicity in North Eurasia*. □oscow, 291-308. (in Russian).
- Kostyuchenko, S.L., Egorkin, A.V., Solodilov, L.N., 1998. Features of the Urals lithospheric structure after multiwave deep seismic sounding. *Geotectonics*, 4, 3-18 (in Russian).
- Kostyuchenko, S.L., Egorkin, A.V., Zolotov, E.E. et al., 2000. Structure of intracrustal stresses in the North East European Platform after deep study results. *Regional geology and metallogeny*, 10, 98-105 (in Russian).
- Kostyuchenko, S.L., Romanyuk, T.V., 1997. Nature of the Mezen gravity maximum. *Earth's physics*, 12, 3-22 (in Russian).
- Kunin, N.Ya., Goncharova, N.V., Semenova, G.I. et al., 1987. Topography map for Eurasian mantle. Moscow, IEP AR USSR, Mingeo RSFSR (in Russian).
- Kuznetsov, V.L., Titarenko, V.V., 1988. Seismic models of consolidated crust for the West Siberian Platform and its junction with the West Siberian Plate. *Geology and geophysics*, 5, 128-135 (in Russian).
- Langinen, A.E., Gee, D.G., Lebedeva-Ivanova, N.N., Zamansky, Yu.Ya., 2006. Velocity structure and correlation of the sedimentary cover on the Lomonosov ridge and in the Amerasian basin, Arctic Ocean. *Proceedings of the Fourth International conference on Arctic margins (ICAM IV)*, U.S. Department of the Interior, 179-188.
- Larsen, H.C., Dahl-Jensen, T., Hopper, J.R., 1998. Crustal structure along the Leg 152 drilling transect. *Proceedings of the Ocean Drilling Program, Scientific Results*, v. 152, 463-476.

- Lau, K.W.H., White, R.S., Christie, P.A.F., 2010. Integrating streamer and ocean-bottom seismic data for sub-basalt imaging on the Atlantic Margin. *Petroleum Geoscience*, Vol. 16, 349–366, doi: 10.1144/1354-0793/10-023.
- Lebedeva-Ivanova, N.N., 2010. Geophysical Studies Bearing on the Origin of the Arctic Basin. *Acta Universitatis Upsaliensis. Digital Comprehensive Summaries of Uppsala Dissertations from the Faculty of Science and Technology* 729, 1-80.
- Lebedeva-Ivanova, N.N., Gee, D.G., Sergeev, M.B., 2011. Crustal structure of the East Siberian continental margin, Podvodnikov and Makarov basins, based on refraction seismic data (TransArctic 1989–1991). In: A.M.Spencer, A.F.Embry, D.L.Gautier, A.Stoupakova, K.Sorensen (eds.). *Arctic Petroleum Geology*, 395-411.
- Litvinenko, I.V., Ankudinov, S.A., Gavrilov, I.A. et al., 1981. Deep crustal section in Central Karelia and its seismic model. In: *LMI proceedings*, vol. 89, 12-17 (in Russian).
- Ljones, F., Kuwano A., Mjelde R., Breivik A., Shimamura H., Murai Y., Nishimura Y., 2004. Crustal transect from the North Atlantic Knipovich Ridge to the Svalbard Margin west of Hornsund. *Tectonophysics*, 378, 17-41.
- Mair, J.A., Lyons, J.A., 1981. Crustal structure and velocity anisotropy beneath the Beaufort sea. *Can. J. Earth Sci.*, Vol. 18, 724-741.
- Malr, J.A., Forsyth, D.A., 1982. Crustal structures of the Canada basin near Alaska, the Lomonosov ridge and adjoining basins near the North Pole. *Tectonophysics*, 89, 239-253.
- Marillier, F., Hall, J., Hughes, S., Loudon, K., Reid, I., Roberts, B., Clowes, R., Cote, T., Fowler, J., Guest, S., Lu, H., Luetgert, J., Quinlan, G., Spencer, C., Wright, J., 1994. Lithoprobe East onshore-offshore seismic refraction survey – constraints on interpretation of reflection data in the Newfoundland Appalachians. *Tectonophysics*, 232, 43-58.
- Milshtein, E.D., Nikitin, A.A., Kalicheva, T.I., Naumova, E.V., Erinchek, Yu.M., 2007. Multiparameter geology-geophysical deep model of East Fennoscandia (based on seismic profiling, gravity & magnetic data). In: *Models of the Earth's crust and upper mantle after deep seismic profiling. Proceedings of the international scientific-practical seminar. Rosnedra, VSEGEI. St.Petersburg, VSEGEI Press*, 99-105 (in Russian).
- Mints, M., Suleimanov, A., Zamozhniaya, N., Stupak, V., 2009. A three-dimensional model of the Early Precambrian crust under the southeastern Fennoscandian Shield: Karelia craton and Belomorian tectonic province. *Tectonophysics* 472, 323–339.
- Mints, M.V., Suleimanov, A.K., Zamozhnyaya, N.G., Stupak, M.V., 2007. 3-d model of the deep crustal structure of the Kola-Lapland region of the Fennoscandian shield: 1-EU, EGGI and FIRE1 transects. In: *Models of the Earth's crust and upper mantle after deep seismic profiling. Proceedings of the international scientific-practical seminar. Rosnedra, VSEGEI. St.Petersburg, VSEGEI Press*, 115-119 (in Russian).
- Mjelde, R., Digranes, P., Shimamura, H., Shiobara, H., Kodaira, S., Brekke, H., Egebjerg, T., Sørensen N., Thorbjørnsen S., 1998. Crustal structure of the northern part of the Vøring Basin, mid-Norway margin, from wide-angle seismic and gravity data. *Tectonophysics*, 293, 175–205.
- Mjelde, R., Faleide, J.I., Breivik, A.J., Raum, T., 2009. Lower crustal composition and crustal lineaments on the Vøring Margin, NE Atlantic: A review. *Tectonophysics*, 472, 183–193.
- Mjelde, R., Kodaira, S., Shimamura, H., Kanazawa, T., Shiobara, H., Berg, E.W., Riise, O., 1997. Crustal structure of the central part of the Voring Basin, mid-Norway margin, from ocean bottom seismographs. *Tectonophysics*, 277, 235-257.
- Mjelde, R., Raum, T., Kandilarov, A., Murai, Y., Takanami, T., 2009. Crustal structure and evolution of the outer Møre Margin, NE Atlantic. *Tectonophysics*, 468, 224-243.
- Mjelde, R., Sellevoll, M.A., Shimamura, H., Iwasaki, T., Kanazawa, T., 1992. A crustal study off Lofoten, N. Norway, by use of 3-component Ocean Bottom Seismographs. *Tectonophysics*, 212, 269–288.
- Mjelde, R., Shimamura, H., Kanazawa, T., Kodaira, S., Raum, T., Shiobara, H., 2003. Crustal

- lineaments, distribution of lower crustal intrusives and structural evolution of the Vøring Margin, NE Atlantic; new insight from wide-angle seismic models. *Tectonophysics*, 369, 199–218.
- Mooney, W.D., Laske, G., Masters, G., 1998. CRUST 5.1: A global crustal model at 5x5 degrees. <http://igppweb.ucsd.edu/~gabi/rem.html>.
- Myhre, A.M., Eldholm, O., 1988. The Western Svalbard margin (74°-80°N). *Marine and Petroleum Geology*, 5, 134-156.
- Neprochnov, Yu.P., Semenov, G.A., Sharov, N.V., Yliniemi, J., Komminaho, K., Luosto, U., Heikkinen, P., 2000. Comparison of the crustal structures of the Barents Sea and the Baltic Shield from seismic data. *Tectonophysics*, 321, 429–447.
- Nielsen, L., Balling, N., Jacobsen, B.H. and MONA LISA Working Group, 2000. Seismic and gravity modelling of crustal structure in the Central Graben, North Sea. Observations along MONA LISA profile 3. *Tectonophysics*, 328, 229–244.
- Oakey, G.N., Stephenson, R., 2008. Crustal structure of the Inuitian region of Arctic Canada and Greenland from gravity modelling: implications for the Palaeogene Eureka orogen. *Geophys. J. Int.*, doi: 10.1111/j.1365-246X.2008.03784.x.
- Osler, J.C., Loudon, K.E., 1992. Crustal structure of an extinct rift axis in the Labrador Sea: preliminary results from a seismic refraction survey. *Earth and Planetary Science Letters*, 108, 243-258.
- Ostrovsky, A.A., Flueh, E.R., Luosto, U., 1994. Deep seismic structure of the Earth's crust along the Baltic Sea profile. *Tectonophysics*, 233, 279-292.
- Pavlenkova, G.A., 2000. New data of the Earth's crust and upper mantle structure along QUARTZ transect. Prospect and protection of mineral resources (Razvedka i okhrana nedr), 2, 11-15 (in Russian).
- Poselov, V.A., Avetisov, G.P., Kaminsky, V.D. (eds.), 2011. Russian arctic geotraverses. St.Petersburg, FGUP I.S.Gramberg VNIIOkeangeologia, 1-172.
- Poselov, V.A., Butsenko, V.V., Kaminsky, V.D., Sakulina, T.S., 2012. Mendeleev Rise (Arctic Ocean) as a geological continuation of the continental margin of the Eastern Siberia. *Geophysika*, 443, 232-235 (in Russian).
- Poselov, V.A., Verba, V.V., Zholondz, S.M., 2004. Earth's crust typification in the Central Arctic uplifts of the Arctic Ocean. *Geotectonics*, 4 (in Russian).
- Potapiev, S.V., 1983. Earth's crust structure in the East Siberian Platform. AS USSR. Editorial board of "Geology and geophysics" periodical. Novosibirsk, 1-26. (in Russian).
- Raum, T., Mjelde, R., Digranes, P., Shimamura, H., Shiobara, H., Kodaira, S., Haatvedt, G., Sørensen, N., Thorbjørnsen, T., 2002. Crustal structure of the southern part of the Vøring Basin, mid-Norway margin, from wide-angle seismic and gravity data. *Tectonophysics*, 355, 99–126.
- Raum, T., Mjelde, R., Shimamura, H., Murai, Y., Bråstein, E., Karpuz, R.M., Kravik, K., Kolstø, H.J., 2006. Crustal structure and evolution of the southern Vøring Basin and Vøring Transform Margin, NE Atlantic. *Tectonophysics*, 415, 167–202.
- Reid, I., Jackson, H.R., 1997. Crustal structure of northern Baffin Bay: Seismic refraction results and tectonic implications. *Journal of geophysical research*, Vol. 102, N. B1, January 10, 523-542.
- Ritzmann, O., Jokat, W., 2003. Crustal structure of northwestern Svalbard and the adjacent Yermak Plateau: evidence for Oligocene detachment tectonics and non-volcanic breakup. *Geophys. J. Int.*, 152, 139–159.
- Ritzmann, O., Jokat, W., Czuba, W., Guterch, A., Mjelde, R., Nishimura, Y., 2004. A deep seismic transect from Hovgard Ridge to northwestern Svalbard across the continental-ocean transition: A sheared margin study. *Geophys. J. Int.*, 157, 683–702.
- Romanyuk, T.B., Egorin, A.V., Kun, V.V. et al., 1985. Experience of $r = f(V)$ dependence reconstruction for long transects in Siberia. – In: Forward and inverse solution in gravimetry and magnetometry. Moscow, 191-225 (in Russian).
- Roslov, Yu.V., Sakoulina, T.S., Pavlenkova, N.I., 2009. Deep seismic investigations in the Barents and Kara Seas. *Tectonophysics*, 472, 301–308.

- Ryberg, T., Wenzel, F., Mechie, J. et al., 1996. Two-dimensional velocity structure beneath Northern Eurasia derived from long-range seismic profile. *Quartz. Bull. Seismol. Soc. Am.* v. 86, 3, 857-867.
- Ryberg, T., Wenzel, F., Yegorkin, A.V., Solodilov, L.N., 1997. Short-period observation of the 520 km discontinuity in northern Eurasia. *J. Geophys. Res.*, v. 102, 133, 5413-5422.
- Ryberg, T., Yegorkin, A.V., Fuchs, K., Solodilov, L.N., 1995. Observation of high-frequency teleseismic Pn on the long-range Quartz profile across northern Eurasia. *J. Geophys. Res.*, v. 100, 89, 18151-18163.
- Sakoulina, T.S., Telegin, A.N., Tikhonova, I.M., Verba, M.L., Matveev, Y.I., Vinnick, A.A., Kopylova, A.V., Dvornicov, L.G., 2000. The results of Deep Seismic Investigation on Geotraverses in the Barents Sea from Kola peninsula to Franz-Joseph Land. *Tectonophysics*, 329, 319-331.
- Sakulina, T.S., Telegin, A.N., Tikhonova, I.M., 1999. Deep seismic studies in Zapolyarny – Heiss geotranssect. *Earth's physics*. 9, 76-85. (in Russian).
- Sakulina, T.S., Verba, M.L., Ivanova, N.M., Krupnova, N.A., Belyaev I.V., 2007. Deep structure of the north Barents-Kara Region along 4AR transect (Taimyr Peninsula – Franz Joseph Land). In: *Models of the Earth's crust and upper mantle after deep seismic profiling. Proceedings of the international scientific-practical seminar. Rosnedra, VSEGEI. St.Petersburg, VSEGEI Press, 197-200* (in Russian).
- Sakulina, T.S., Verba, M.L., Kashubina, T.V., Krupnova, N.A., Ivanov, G.I., 2011. Integrated geological-geophysical studies at the 5-AR geotranssect in the East-Siberian Sea. *Prospect and protection of mineral resources (Razvedka i okhrana nedr)*, 10, 17-23 (in Russian).
- Schlindwein, V., Jokat, W., 1999. Structure and evolution of the continental crust of northern east Greenland from integrated geophysical studies. *Journal of geophysical research*, v. 104, N. B7, 15,227-15,245.
- Schmidt-Aursch, M., 2002. The crustal structure of the East Greenland Fjord Region between the Precambrian shield and the recent mid-oceanic ridges: Results from seismic and gravity modelling. *Berichte zur Polarforschung, Alfred Wegener Institute for Polar and Marine Research, Bremerhaven*, 1-145.
- Schmidt-Aursch, M.C., Jokat, W., 2005. The crustal structure of central East Greenland-I: From the Caledonian orogen to the Tertiary igneous province. *Geophys. J. Int.*, 160, 736-752.
- Schmidt-Aursch, M.C., Jokat, W., 2005. The crustal structure of central East Greenland-II: From the Precambrian shield to the recent mid-oceanic ridges. *Geophys. J. Int.*, 160, 753-760.
- Seismic lithosphere models of main geostructures in the USSR territory. S.M. Zverev, I.P. Kosminskaya (eds.), 1980. Moscow, Nauka, 1-184 (in Russian).
- Sellevoll, M.A., Duda, S.J., Guterch, A., Pajchel, J., Perchuc, E., Thyssen, F., 1991. Crustal structure in the Svalbard region from seismic measurements. *Tectonophysics*, 189, 55-71.
- Sollogub, V.B., Chekunov, A.V., Litvinenko, I.V. et al., 1987. Lithosphere of Central and East Europe: I, II, V geotraverses. Ex. Ed. V.B. Sollogub. Kiev, Naukova Dumka, 1-167 (in Russian).
- Solodilov, L.N., 1994. "GEON" Center – 25 years of deep studies. *Prospect and protection of mineral resources (Razvedka i okhrana nedr)*, 10, 2-8 (in Russian).
- Sorokin, M.Yu., Zamansky, Yu.Ya., Langinen, A.Ye., Jackson, H.R., Macnab, R., 1999. Crustal structure of the Makarov Basin, Arctic Ocean determined by seismic refraction. *Earth and Planetary Science Letters*, 168, 187–199.
- Stephenson, R.A., Coffin, □.C., Lane, L.S., Dietrich, J.R., 1994. Crustal structure and tectonics of the southeastern Beaufort Sea continental margin. *Tectonics*, Vol. 13, 2, April, 389-400.
- Suckro, S.K., Gohl, K., Funck, T., Heyde, I., Ehrhardt, A., Schreckenberger, B., Gerlings, J., Damm, V., Jokat, W., 2012. The crustal structure of southern Baffin Bay: implications from a seismic refraction experiment. *Geophys. J. Int.*, doi: 10.1111/j.1365-246X.2012.05477.x.
- Surkov, V.S., Kuznetsov, V.L., Staroseltsev, V.S., Salnikov, A.S., 2000. Seismic tomography during the Earth's crust study in Siberia. *Regional geology and metallogeny*, 10, 117-124

- (in Russian).
- Surkov, V.S., Salnikov, A.S., Kuznetsov, V.L., Seleznev, V.S., Emanov, A.F., Soloviev, V.M., 2007. Earth's crust structure along 2DV transect (Northeast Russia) after a new technology of deep seismic soundings. In: Models of the Earth's crust and upper mantle after deep seismic profiling. Proceedings of the international scientific-practical seminar. Rosnedra, VSEGEI. St.Petersburg, VSEGEI Press, 233-236 (in Russian).
- Sweeney, J.F., Weber, J.R., Blasco, S.M., 1982. Continental ridges in the Arctic Ocean: LOREX constraints. *Tectonophysics*, 89, 217-237.
- Tsikalas, F., Eldholm, O., Faleide, J.I., 2005. Crustal structure of the Lofoten–Vesterålen continental margin, off Norway. *Tectonophysics*, 404, 151–174.
- Uenzelmann-Neben, G. with contributions of the participants, 2009. The Expedition of the Research Vessel “Maria S. Merian” to the Labrador Sea in 2009 (MSM12/2). *Berichte zur Polar- und Meeresforschung*, N. 599, Reports of Polar and Marine Research, Alfred Wegener Institute for Polar and Marine Research, Bremerhaven.
- Verba, M.L., Ivanova, N.M., Katsev, V.A., Roslov, Yu.V., Sakulina, T.S., Telegin, A.N., 2001. Results of seismic studies in AR-1 and AR-2 transects in the Barents and Kara seas. Prospect and protection of mineral resources (*Razvedka i okhrana nedr*), 10, 3-7 (in Russian).
- Verba, M.L., Matveev, Yu.I., Rzhovsky, N.N., Telegin, A.N., Sakulina, T.S., 1997. Geotransects in the Arctic Shelf. Prospect and protection of mineral resources (*Razvedka i okhrana nedr*). 3, 31-33 (in Russian).
- Verba, M.L., Matveev, Yu.I., Sakulina, T.S., Telegin, A.N., Evdokimova, N.K., 1999. Oil-and-gas bearing complexes in the Baltic Shield and Barents Sea shelf plate junction zone after geophysical data. – Prospect and protection of mineral resources (*Razvedka i okhrana nedr*), 2, 19-24 (in Russian).
- Verba, M.L., Telegin, A.N., Sakulina, T.S., Atakov, A.I. et al., 1998. Earth's crust structure in the Baltic Shield and Barents Sea shelf plate junction zone (after integrated geophysical investigations in the southern part of AR-1 regional geotraverse). In: F.P. Mitrofanov, N.V. Sharov (eds.). *Seismic model of Northern Europe lithosphere: Barents Region*. Apatity, KSC RAS, P. 2, 40-81 (in Russian).
- Vinnik, L.P., Egorkin, A.V., 1981. Low-velocity layer in the ancient platforms mantle after seismic studies in long transects. *Proc. AS USSR, Earth's physics*, 12, 12-18 (in Russian).
- Volvovsky, I.S., Volvovsky, B.S., 1975. Earth's crust sections in the USSR territory after deep seismic sounding data. Moscow, Soviet radio, 1-258 (in Russian).
- Voss, M., Jokat, W., 2007. Continent–ocean transition and voluminous magmatic underplating derived from P-wave velocity modelling of the East Greenland continental margin. *Geophys. J. Int.*, 170, 580–604.
- Voss, M., Schmidt-Aursch, M.C., Jokat W., 2009. Variations in magmatic processes along the East Greenland volcanic margin. *Geophys. J. Int.*, 177, 755–782.
- Westbrook, G.K., Chand, S., Rossi, G., Long, C., Bünz, S., Camerlenghi, A., Carcione, J.M., Dean, S., Foucher, J.-P., Flueh, E., Gei, D., Haacke, R.R., Madrussani, G., Mienert, J., Minshull, T.A., Nouzé, H., Peacock, S., Reston, T.J., Vanneste, M., Zillmer, M., 2008. Estimation of gas hydrate concentration from multi-component seismic data at sites on the continental margins of NW Svalbard and the Storegga region of Norway. *Marine and Petroleum Geology*, v. 25, Is. 8, 744-758.
- Wolf, L.W., McCaleb, R.C., Stone, D.B., Brocher, T.M., Fujita, K., Klemperer, S.L., 2002. Crustal structure across the Bering Strait, Alaska: Onshore recordings of a marine seismic survey. In Miller E.L., Grantz A., and Klemperer S.L., eds., *Tectonic Evolution of the Bering Shelf –Chukchi Sea – Arctic Margin and Adjacent Landmasses: Boulder, Colorado, Geological Society of America Special Paper 360*, 25–37.
- Zehnder, C.M., Mutter, J.C., Buhl, P., 1990. Deep seismic and geochemical constraints on the nature of rift-induced magmatism during breakup of the North Atlantic. *Tectonophysics*, 173, 545-565.

New zircon U-Pb ages for the lower Cantwell Formation: implications for the Late Cretaceous paleoecology and paleoenvironment of the lower Cantwell Formation near Sable Mountain, Denali National Park and Preserve, central Alaska Range, USA

Carla Susanne Tomsich¹, Paul J. McCarthy¹, Anthony R. Fiorillo², David B. Stone³, Jeff A. Benowitz⁴, and Paul B. O'Sullivan⁵

¹Department of Geology and Geophysics, and Geophysical Institute, University of Alaska, P.O. Box 755780, Fairbanks, Alaska 99775

²Perot Museum of Nature and Science, 2201 North Field Street, Dallas, Texas 75201

³Geophysical Institute, University of Alaska, P.O. Box 757320, Fairbanks, Alaska 99775

⁴Geophysical Institute, University of Alaska, P.O. Box 755940, Fairbanks, Alaska 99775

⁵Apatite to Zircon, Inc. 1075 Matson Road Viola, Idaho 83872-9709

ABSTRACT

The up to 4000 m-thick dinosaur (including birds) track-bearing Late Cretaceous (Campanian–Maastrichtian) lower Cantwell Formation, central Alaska Range, USA, was deposited at the suture zone between the North American continent and the allochthonous Wrangellia Composite Terrane during a time of protracted plate convergence. A combined total of 2500 m of measured section at Sable Mountain in Denali National Park and Preserve yields pterosaur manus tracks, non-avian and avian dinosaur footprints, diverse invertebrate traces, and abundant plant megafossils. Paleomagnetic data place the Cantwell basin between 65 to 75° N. The ecological data serve as climate proxies for high-latitude paleoenvironments. Two mid-section ash layers, separated temporally by 24 m of section, yield zircon U–Pb ages of 71.5 ± 0.9 Ma and 71.0 ± 1.1 Ma, respectively. These first radiometric ages for the lower Cantwell Formation suggest that exposures at Sable Mountain straddle the Campanian/Maastrichtian boundary, a time for which significant cooling and subsequent global sea level fall of an estimated 40 m is predicted. In this paper, we review sedimentological, paleoecological and paleomagnetic data and paleoclimate estimates previously reported from the Cantwell basin and interpret these data in light of the new age assignments. These new numerical ages enable more direct correlations between disparate fossil sites both within the Cantwell basin as well as across the Late

Cretaceous Arctic, with implications for floral and faunal exchanges between Asia and North America and ecological responses to paleoclimate changes.

Keywords: Late Cretaceous high-latitude dinosaur and fossil bird fauna, fossil flora, and paleoenvironments, U–Pb zircon geochronology, stratigraphic correlation, Prince Creek Formation, Chignik Formation, Cantwell Formation

INTRODUCTION

The biodiversity of ancient high-latitude ecosystems is not only of interest for the study of species evolution and palinspastic restorations, but also for the ecological response signal for an amplified climate change rate (Otto-Bliesner and Upchurch, 1997; Upchurch et al., 1998). Climate modelers thus focus increasingly on proxies of Arctic regions where taxonomic and physiological adaptations can be linked more clearly to climate perturbations. For pre-anthropogenic global climate models, temperature and precipitation proxies, which invariably are based on the geologic record, should be independent, temporally well-resolved, and representative of large geographic regions (Palaeosens Project Members, 2012). Given the limitations of available data for the distant past, the scale used by climate modelers is admittedly coarse (see, for instance, Markwick and Valdes, 2004), resulting in hypothesized long-term biological responses to climate change being incidental and blurring cause and effect relationships.

Radiometric dating allows a more direct correlation of paleoclimate records from different localities and different proxies and permits comparative evaluations of the factors contributing to regional climate variability such as vegetation distribution patterns, topography and paleogeography (Upchurch et al., 1998; Markwick and Valdes, 2004; Sewall et al., 2007; Spicer and Herman, 2010). Equally important, it provides valuable insights into regional dynamics of ancient terrestrial ecosystems, such as floral and faunal evolution and migration patterns.

The Late Cretaceous period was a time of significant climate instability. Continued, but cyclic polar warmth is predicted from the fossil biota and sedimentary rocks of Arctic and subarctic regions (e.g., Spicer, 1987; Herman and Spicer, 1995; Otto-Bliesner and Upchurch, 1997; Upchurch et al., 1998; Zakharov et al., 1999; Golovneva, 2000a; Spicer, 2003; Spicer and Parrish, 1990a,b; Rich et al., 2002; Fiorillo, 2006, 2008; Herman et al., 2009; Godefroit et al., 2009; Spicer and Herman, 2010).

A rich fossil floral and faunal record indicative of a temperate high-latitude paleoclimate is presently emerging from the Late Cretaceous sedimentary rocks of the Cantwell Formation in Denali National Park (formerly Mount McKinley National Park) and Preserve, Alaska, USA. The formation crops out on the northern flanks of the central Alaska Range (Fig. 1) and comprises a Late Campanian to Early Maastrichtian non-marine to marginal marine sedimentary succession (Ridgway et al., 1997), and an overlying Late Paleocene to Early Eocene volcanic succession (Gilbert et al., 1976; Csejtey et al., 1992; Cole et al., 1999), herein referred to as the lower and upper Cantwell Formation, respectively (Figs. 1 and 2).

The up to 4000 m-thick (Hickman, 1974; Hickman et al., 1990) non-avian and avian dinosaur track-bearing lower Cantwell Formation was deposited at the northern part of a Late Cretaceous suture zone between the Wrangellia Terrane, the northernmost subterrane of the allochthonous Wrangellia Composite Terrane, and the North

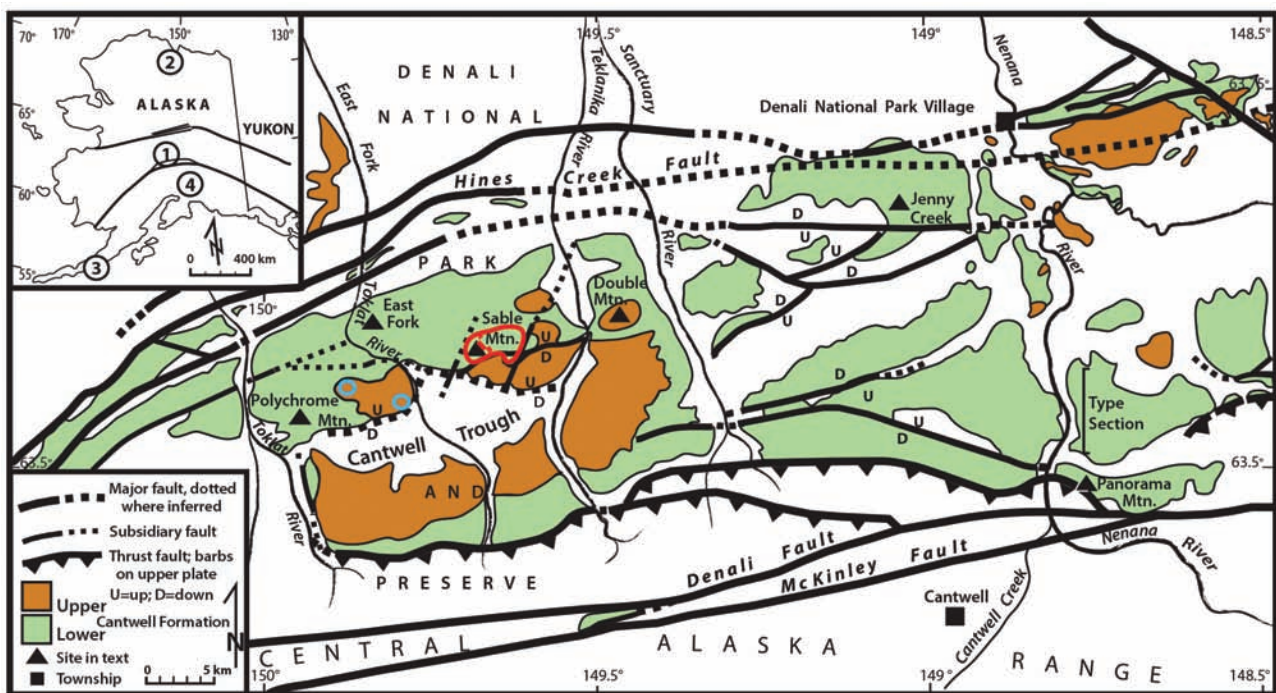


Fig. 1. Regional distribution of Cantwell Formation between longitudes -148.5 and -150.5° . Green fields: lower sedimentary unit; orange fields: upper volcanic unit; blank areas: all other lithologies and Quaternary alluvium. Red circle and lines: study area with composite measured section. Blue circles: paleomagnetic study sites of Sontag (1992). Geologic units from Csejtey et al. (1992), Gilbert and Redman (1975), and Wilson et al. (1998). Insert: Map of Alaska showing major strike-slip fault systems of central Alaska and locations of coeval Late Cretaceous fossil-bearing formations discussed in text: 1 = Cantwell, 2 = Prince Creek, 3 = Chignik, 4 = Matanuska.



Fig. 2. Cantwell Formation exposed at Sable Mountain. Reddish-weathered upper Cantwell volcanic strata in foreground are downfaulted against organic-rich sedimentary lower Cantwell Formation in the distance. A heterogeneous lithology is evident from numerous lateral and vertical facies changes. Shown exposure is ~1 km wide. View is to the northwest.

American continent during the final stages of accretion (Ridgway et al., 1997; Cole et al., 1999; Ridgway et al., 2002). Whereas previous research has focused on the tectono-sedimentary history of the Cantwell basin, current studies aim to reconstruct details of the paleoecology, paleoclimate and sedimentary subenvironments of this high-latitude basin for a fully integrated (geologic and paleoecological data) paleoenvironmental model. The discovery of a pterosaur and diverse dinosaur (including birds) ichnofauna at Sable Mountain, within Denali National Park, (Fiorillo et al., 2007, 2009a, 2011; Fiorillo and Adams, 2012; Fiorillo et al., 2014), in addition to a diverse invertebrate ichnofauna (Hasiotis et al., 2009, 2011) and plant fossils (Tomsich et al., 2010), suggests a remarkable paleo-Arctic biodiversity.

The presence of large-bodied herbivores in ancient polar regions is difficult to reconcile with extreme light and temperature seasonality. Yet,

dinosaur fossil localities are well-known from the Late Cretaceous circum-Arctic (see Parrish et al., 1987; Clemens and Nelms, 1993; Clemens, 1994; Rich et al., 1997, 2002; Fiorillo and Gangloff, 2001; Godefroit et al., 2009; Fiorillo et al., 2010). The biodiversity of the Cantwell Formation can be compared with the mid-to-late Maastrichtian Kakanaut Formation of the Okhotsk–Chukotka province in northeastern Russia (Golovneva, 1994; Golovneva, 2000a; Godefroit et al., 2009; Spicer and Herman, 2010) and with the polar dinosaur fossil-bearing section of the Late Cretaceous Prince Creek Formation on the North Slope of Alaska (Parrish et al., 1987; Parrish and Spicer, 1988; Spicer and Parrish, 1990a,b; Clemens and Nelms, 1993; Clemens, 1994; Rich et al., 2002; Fiorillo and Gangloff, 2000; Fiorillo, 2004, 2006; Gangloff and Fiorillo, 2010; Fiorillo et al., 2010; Fiorillo and Tykoski, 2012). However, identifiable bones in the Cantwell Formation have not been found to-date, and

the spatial and temporal relationships of complexly distributed fossil-bearing lithofacies at isolated, fault-bounded outcrops are still poorly understood.

In comparison, the Prince Creek Formation is well-exposed in a ~50 km long semi-continuous bluff along the Colville River. Strata include numerous bentonites and tuffs, and the ages of the fossil bone beds are fairly well-resolved (Conrad et al., 1992; Flaig, 2010; Flaig et al., 2013). Early Maastrichtian bone-bearing strata of the Prince Creek Formation are approximately the same age as sections of the lower Cantwell Formation. The Prince Creek vertebrate fauna thus hints at the kind of species that may have left footprints in the Cantwell Formation.

The age of the lower Cantwell Formation, on the other hand, is based on sparse pollen data collected from five widely spaced localities (Ridgway et al., 1997), and until now no reliable age constraint existed for the Sable Mountain area. Strata include few, mostly thin layers of highly altered bentonites that were preserved in local depressions. Recent advances in geochronological analyses of uranium and lead (U–Pb) isotope systems for residual uranium-rich minerals, such as zircon, provide new possibilities for obtaining high-resolution geochronological ages from sedimentary successions lacking datable fossils and unaltered potassium-bearing minerals required for K–Ar or $^{40}\text{Ar}/^{39}\text{Ar}$ dating. The laser ablation–inductively coupled plasma–mass spectrometry (LA–ICP–MS) technique is now widely applied, especially for large (≥ 100) zircon grain populations, as various statistical strategies have been adopted to account for isobaric interferences during analytical runs, determine detrital component, correct for common lead, and analyze zircon variability and error (Corfu, 2013). Here we report on the first radiometric ages obtained for two closely spaced lower Cantwell Formation bentonites from Sable Mountain and review regional paleoecological, paleoenvironmental and paleogeographical information to investigate the implications of improved correlations with coeval fossil-bearing sites of North America and northeastern Asia.

This research is part of an ongoing study in Denali National Park. Detailed measured sections (Fig. 3), facies analyses, channel trend mapping, and fossil and geochronological data are used to

characterize the sedimentary subenvironments, habitat conditions and paleoecological trends in order to determine influences on deposition and the paleoenvironment.

GEOLOGIC SETTING

Regional Geology

The geology of central and southern Alaska has been profoundly impacted by the juxtaposition of numerous terranes and continental slivers containing different rock types as old as the Proterozoic, and by geologic processes in effect during the past nearly 120 Ma including tectonic activity caused by the still-moving Pacific Plates. The Cantwell basin is an east–west-trending, ~135 km long and ~35 km wide structure bracketed by the Hines Creek Fault and the McKinley Fault strands at the northern apex of the arcuate Denali Fault (Fig. 1). The Denali Fault is a segmented 1200 km-long right-lateral transform fault system that bounds the large pericratonic Yukon Tanana Terrane of interior and eastern Alaska and British Columbia, Canada, and sheared-off continental margin slivers on the north side, and the Wrangellia Composite Terrane on the south side (Jones et al., 1983; Panuska and Stone, 1981; Stone, 1981; Nokleberg et al., 1985, 1994; Plafker and Berg, 1994; Ridgway et al., 2002; Nokleberg and Richter, 2007; Trop and Ridgway, 2007). The boundary represents the late Mesozoic suture zone or the Alaska Range suture zone (Ridgway et al., 2002). The Wrangellia Composite Terrane is southern Alaska's largest accreted tectono-stratigraphic terrane assemblage and consists of the Wrangellia Terrane of central and south-central Alaska, the Peninsula Terrane of west-central and southwestern Alaska, and the Alexander Terrane of southeast Alaska (Nokleberg et al., 1994). The collision and accretion is thought to have been time-transgressive (Trop and Ridgway, 2007; Hampton et al., 2007) along the > 2000 km long boundary. In the northern part of this suture zone (which includes our study area), onset of accretion is constrained to the early Late Cretaceous (Nokleberg et al., 1994; Hampton et al., 2010). Between the Hines Creek Fault strand and the northern edge of the oceanic Wrangellia Terrane lies an accretionary and post-accretionary complex that includes juxtaposed slivers of dislodged stratigraphic assemblages of continental margin and

oceanic affinity, and syncollisional melange and thick siliciclastic deposits of an ocean basin that closed during the mid to early Late Cretaceous (Hampton et al., 2007; 2010). The turbiditic sediments that filled this basin are now widely exposed within a ~400 km long arcuate belt at the Alaska Range suture zone and are collectively assigned to the Kahiltna assemblage (Csejtey et al., 1992; Ridgway et al., 2002; Trop and Ridgway, 2007; Hampton et al., 2007; Hampton et al., 2010). Csejtey et al. (1992) postulate the thick flysch sequence to have been thrust-emplaced during the collisional orogeny. These accreted units are overlain by or are in fault-contact with post-collisional non-marine sedimentary and igneous rocks (e.g., Cantwell Formation and younger fluvial successions).

Following the accretion of the Wrangellia Composite Terrane, the southern margin of Alaska continued to grow by subduction, arc magmatism and accretion. Continued convergence in the Alaska Range suture zone resulted in folding, uplift and partial exhumation of post-collisional sequences in the Cenozoic (Trop and Ridgway, 2007; Benowitz et al., 2011, 2013). High heat flow, possibly due to oblique subduction of a mid-ocean ridge and a resultant mantle window, is the inferred cause of extensive early Tertiary intracontinental extension and plutonism (Bradley et al., 2003; Cole et al., 2006, 2007; Benowitz et al., 2012) that may have contributed to the deposition of the volcanic upper Cantwell Formation. Subsequent Cenozoic strike-slip faulting on the margin-parallel Tintina and Denali Fault systems, and associated strain partitioning of the intervening crust, led to widespread high-angle normal and reverse faulting and block rotation (Hickman et al., 1990; Csejtey et al., 1992; Plafker and Berg, 1994; Ridgway et al., 2002; Till et al., 2007a,b; Trop and Ridgway, 2007). Today, the Cantwell Formation is preserved in a regional synclinorium commonly referred to as the Cantwell Trough (Fig. 2).

The Cantwell Formation

The Late Cretaceous to early Tertiary Cantwell Formation comprises a lower non-marine to marginal marine sedimentary unit (Ridgway et al., 1997), and an upper, predominantly bimodal (mafic and felsic) volcanic unit (Figs. 1 and 2; Gilbert et

al., 1976; Csejtey et al., 1992; Ridgway et al., 1997; Cole et al., 1999). The lower Cantwell Formation is abundantly fossiliferous, and consists of numerous successions of conglomerate, sandstone, mudstone and, locally, thin coal seams and altered tuffs (Fig. 3). The sedimentary rocks rest unconformably on weakly metamorphosed and locally, intensely folded Late Jurassic to Cretaceous flysch deposits that may be correlative to the Kahiltna assemblage (see Csejtey et al., 1992; Ridgway et al., 2002); Triassic marine basalts; mid-Paleozoic to Triassic shelf-margin sedimentary strata of dismembered tectonostratigraphic terranes; and Proterozoic to early Paleozoic schists of the Yukon Tanana Terrane (Csejtey et al., 1992; Ridgway et al., 1997; Trop and Ridgway, 1997; Till et al., 2007).

The top of the lower Cantwell Formation is thought to have eroded to various depths (Wolfe and Wahrhaftig, 1970). A total thickness of up to 4000 m is estimated for the alluvial deposits near the basin axis from isopach mapping in the Nenana River corridor (Fig. 1) where the stratigraphy is best resolved (Hickman, 1974; Hickman et al., 1990). The fluvial succession is commonly intruded and overlain (locally on a shallow angular unconformity) by volcanic deposits of the upper Cantwell Formation. The igneous succession, preserved in local synclines and downfaulted blocks, comprises up to 2750 m of volcanic and subvolcanic flows, pyroclastic deposits, and associated volcanoclastic deposits (Cole et al., 1999). The igneous unit is often informally referred to as the Teklanika formation (Gilbert and Redman, 1975; Gilbert et al., 1976) or Teklanika volcanics (Sontag, 1992), but it has never been officially designated as a separate formation or member.

METHODS

Stratigraphic Analyses and Data Collection

Stratigraphic sections with a combined total of 2500 vertical m were measured and described in detail from 18 sites near Sable Mountain (Denali National Park, Alaska). A composite section for a 640 m long interval is depicted in Fig. 3, and the lithofacies are described in Table 1.

Paleocurrent trends were recorded from trough cross-beds. Trace fossils were photo-documented in the field and described in terms of location, rock type, and track size, shape, depth, and quality

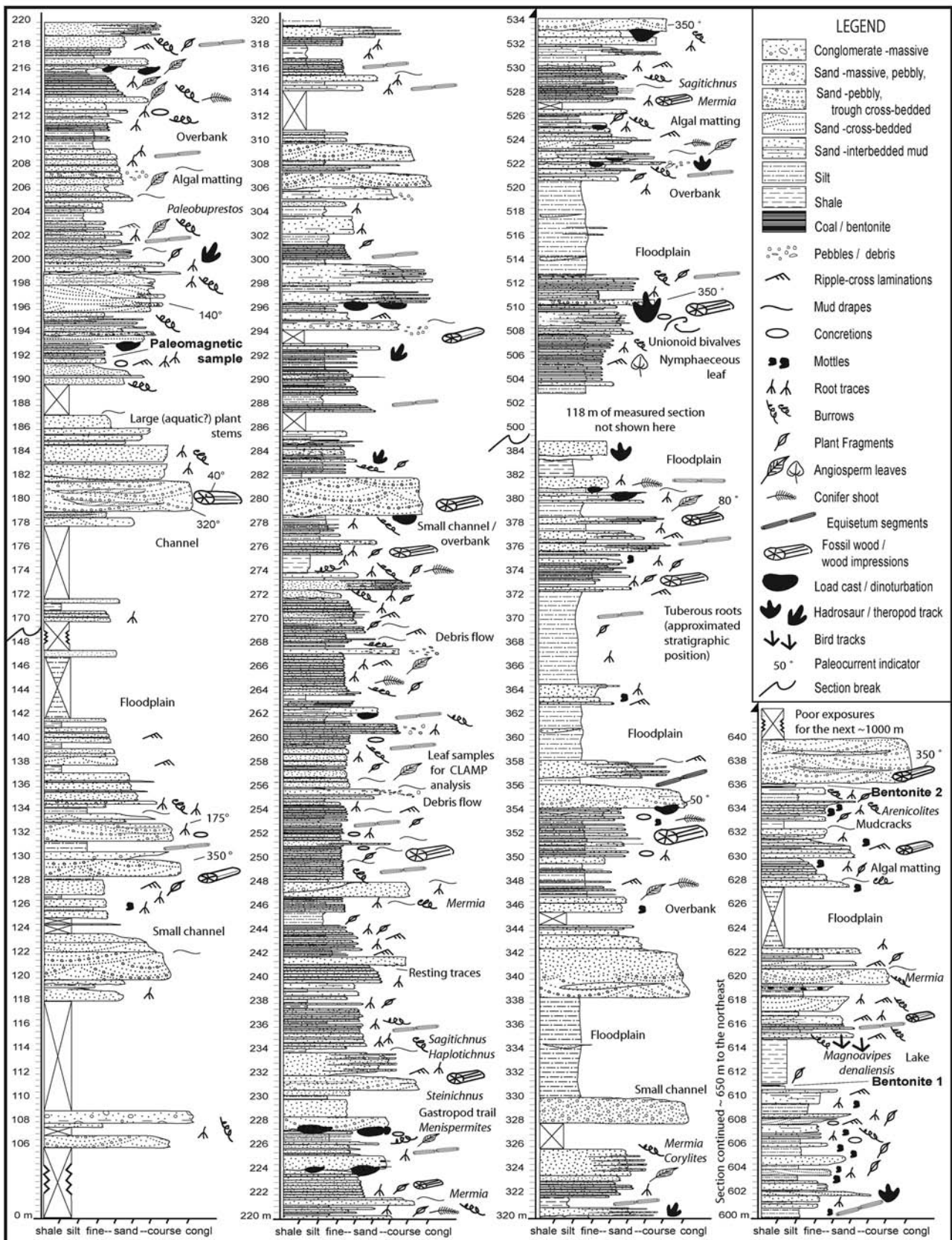


Fig. 3. Stratigraphic columns for a composite measured section at Sable Mountain, showing lithologies, sedimentary structures, fossils, and radiometrically dated bentonite horizons. See legend for explanations.

Table 1. Lithofacies and facies associations of the lower Cantwell Formation at Sable Mountain

Facies (Facies Association)	Thickness	Description	Interpretation
F 1 (FA 1) Matrix-rich, non-stratified, unsorted conglomerate	0.2 to 1.5 m average: ~ 1 m	Tabular or wedge-shaped, laterally discontinuous deposits locally encased in floodplain or channel facies. Contacts sharp or shallow irregular. Widths range from a few to 10's of meters. Texture massive with poorly sorted floating clasts up to 15 cm in diameter, woody debris and plant matter in muddy or sandy, organic-rich matrix. Capped by F 2, F 5, or F 7. Contains tree stump impressions and plant fossils.	Debris flow associated with bank or slope failure, storm events and high sediment supply (Harvey and Wells, 1987; Miall, 2006; Kumar et al., 2007)
F 2 (FA 1) Massive conglomerate	dm to 6 m average: < 2 m	Sharp-based tabular and shallow trough-shaped, laterally discontinuous deposits encased in floodplain or channel facies. Widths range from 10 m to 250 m. Texture matrix-supported and less commonly clast-supported. Poorly stratified subangular to well-rounded clasts are moderately sorted and weakly to locally well-imbricated. Average clast sizes range between 4 to 8 cm; maximum size is 15 cm. Polymictic clast lithology, including intraformational mud- and sandstones. Matrix fine to coarse-grained, predominantly subangular; well-cemented. Includes sandstone lenses and thin layers (up to 3 cm) of mudstone that divide deposits into multiple stories. F 2 commonly fines to stratified or massive medium-grained sandstone. Includes tree log or stump impressions.	Hyperconcentrated flow deposit as a result of high sediment supply and unconfined channel flow conditions on alluvial fan (Kumar et al., 2007). Textural variations suggest deposit is transitional to traction flow (Wells and Harvey, 1987; Miall, 2006).
F 3 (FA 2) Bedded conglomerate FA 2	dm to 2 m average: 1 m	Tabular and shallow lenticular-shaped clast and matrix-supported deposits co-occurring with F4, F5 and F6 to form bodies 10's of meters to up to 400 m wide. Clasts consist of moderately to well-sorted, subangular to well-rounded pebbles and cobbles that are planar bedded or trough cross-bedded. Clasts locally imbricated or aligned on low-angle foresets. Average clast diameter 3 to 5 cm, maximal 10 cm. Matrix medium to coarse-grained subangular sand that commonly fines to medium, horizontally stratified granular sand. Rare upward-coarsening. Single or multiple stories; include thin layers of mudstone and sandstone lenses. Mud drapes commonly on top. Tree log impressions common.	Traction flow deposits in gravely braided channels on alluvial fan and in interfan areas including axial alluvial plain. Clasts interpreted as bedload and channel lag. Structures represent migration of channels and bars. Mudstone indicates rapid abandonment (Wells and Harvey, 1987; Kumar et al., 2007; Miall, 2006).
F 4 (FA 2) Pebbly sandstone	cm to 2 m average: 1.2 m	Tabular and shallow lenticular geometries. Pebbles angular to well-rounded, 0.3 to 5cm in size. Matrix coarse- to medium-grained. Beds horizontally or low-angle cross-stratified with pebbles on foresets. Normal and reverse grading; commonly grades into medium sandstone at top. Occurs in association with F 3, F 5, and F 6.	Traction flow deposits in sandy braided channel (Miall, 2006)
F 5 (FA 2) Cross-bedded coarse to fine-grained sandstone	0.3 to 1.5 m average: < 1 m	Planar cross-bedded bodies with granules or mud on foresets. Grains subangular to subrounded. Rare. Associated with sandstone facies F 4, F 6, F 7, and F 8.	Traction flow across a channel bar (Miall, 2006)
F 6 (FA 2) Coarse-to medium-grained sandstone	0.5 m to 8 m average: 0.9 m	Tabular and shallow lenticular geometries. Horizontally bedded or apparently massive with faint bedding structures. Forms sand lenses and multistory deposits. Grains subangular to subrounded and moderately sorted. Moderately cemented and rooted. Contains concretions and tree log impressions. Upper contacts predominantly sharp	Rapid deposition in confined and unconfined channels Amalgamated in confined channel. Massive sandstone may be homogenized by post-depositional burrowing or soft-sediment deformation

Table 1. Continued.

Facies (Facies Association)	Thickness	Description	Interpretation
F 7 (FA 2, FA 3) Massive medium-to fine-grained sandstone	0.2 to 4 m average: < 1 m	Tabular and shallow lenticular sandstone typically embedded in finer-grained deposits. Fining upwards fine-grained sandstone, not medium sandstone. Contacts commonly sharp. Well-indurated, but poorly cemented in a few places. Contains granules and small floating pebbles. Grains predominantly subangular and moderately-well sorted. Locally burrowed and rooted. May contain iron oxide nodules, <i>Equisetites</i> rhizomes and stems, lithified and partly coalified and sideritized wood, and impressions of tree trunks, stumps and roots, conifer shoot axes, plant tubers, and partial angiosperm leaves that were folded and/or fragmented during high energy transport.	Rapid deposition under waning flow stage in flood channel and unconfined overbank stream flow (Bull, 1977; Miall, 2006). Presence of burrows and roots suggests periodic fluctuations of water table.
F 8 (FA 2, FA 3, FA 4) Tabular trough cross-bedded coarse to fine-grained sandstone	0.3 to 1.5 m average: < 1 m	Occurs in form of extensive sheets and shallow lenticular bodies. Deposits typically are sharp-based and upward fining. Grains are subrounded to rounded; include granules and minor small pebbles. Amplitude of trough cross-beds 2 to 15 cm. Burrowed and moderately rooted. May contain <i>Equisetites</i> rhizomes and stems, lithified wood, conifer shoots, and angiosperm leaf impressions. Associated with F 5, F 6, F 7, F 9, and F 10.	High-density flow or unconfined flow (including sheet-flood/ stream flow; Bull, 1977; Miall, 2006) deposits in distal alluvial fan and proximal alluvial plain settings. F 8 also occurs in inferred channel bar and crevasse splay deposits
F 9 (FA 4) Ripple-cross-laminated to massive fine- to very fine-grained sandstone	<5 cm to 1.5 m average: < 1 m	Tabular or lenticular bodies. Occurs in association with F 7, F 8, F 9, and F 11. Contacts can be gradational or sharp. Grains subangular to subrounded. Ripples include climbing ripples and herring bone patterns. Burrowed and moderately rooted. Contains conifer sprigs, leaves and cones, <i>Equisetites</i> rhizomes and stems, wood and angiosperm leaf impressions at base.	Overbank including crevasse splay channel deposits. Ripples indicate unidirectional flow. Climbing ripples suggest rapid sedimentation and herring bone structures signify reverse flow direction (Miall, 2006). Burrows and roots signal a fluctuating water table.
F 10 (FA 5) Interbedded fine to very fine-grained sand- and mudstone	<5 cm to > 10 m average: < 1 m	Numerous vertical successions of laterally continuous centimeter- to decimeter-scale interbeds form stacks 10's of meters thick. Sandstone is massive or rippled. Contains concretions, iron nodules, roots, abundant plant megafossils, and beetle and freshwater crustacean feeding traces.	Overbank deposits under waxing and waning flow stages on levee or distal crevasse splay. Well-preserved plant fossils indicate rapid deposition and short transport distance.
F 11 (FA 5) Siltstone	cm to >10 m average: 10 cm	Dark grey to black organic-rich siltstone. Commonly interlaminated with very fine sandstone and mudstone. Contains conifer needles, <i>Equisetites</i> rhizomes, carbonaceous roots and other plant fragments, iron concretions or nodules. Relief at top common.	Vegetated floodplain, lake, and pond settings. Abundant organic matter, nodules and concretions suggest high water table on alluvial fan and proximity to alluvial channels.
F 12 (FA 5) Organic-rich mudstone	mm to 1 m	Dark grey clay-rich siltstone and shale. Locally calcareous and yellow-weathering. Forms mud drapes and lenses. Mudcracks or irregular relief at top. Commonly contains plant fragments and trace fossils such as algal matting, <i>Mermia</i> and <i>Cochlichnus</i> .	Suspension settling from stagnant flood waters in floodplain lows; abandoned channel fill; bar tops (Miall, 2006).
F 13 (FA 6) Carbonaceous shale	cm to 10 m average: 20 cm	Dark grey to black; organic-rich. Locally calcareous. Mudcracks or irregular relief at top. Commonly seen in form of black or yellow-weathering rip-up clasts. Contains <i>Equisetites</i> segments, small, frequently coalified, plant fragments, rootlets, iron oxide nodules, and freshwater bivalve and gastropod shells and trails.	Backwater swamps and marshes proximal to streams (Miall, 2006)

Table 1. Continued.

Facies (Facies Association)	Thickness	Description	Interpretation
F 14 (FA 6) Coal	0.5 to 2 cm	Rare thin coal seams up to 2 cm thick. Laterally discontinuous. Commonly associated with bentonite.	Decaying plant matter in backwater swamps and marshes.
F 15 (FA 6) Bentonite	0.5 to 4 cm average: 1 cm	Volcanic ash deposit altered to white or light brown clay. Rare and discontinuous over 20 m. Commonly associated with thin coal seams. Contains minor amounts of zircon, apatite, volcanic glass, quartz, and altered feldspar.	Suspension settling in backwater ponds and lakes
F 16 (FA 1) Organic-rich gritty mudstone	0.5 to 1.5 m average: ~ 1 m	Laterally discontinuous, commonly wedge-shaped, unsorted, non-stratified deposits with variably sized free-floating small clasts, woody debris, plant fragments, mud rip-up clasts and sand and granule-sized grains in organic-rich mudstone matrix. Poorly consolidated. Sharp undulated bases and tops. Incorporates in-situ tree stump impressions and small unionid bivalves and gastropods that are commonly attached to plant stems.	Gravity mud flow deposit associated with slope or bank failure on alluvial fan, and along channel and lake margins (Bull, 1977; Miall, 2006).
Facies 17 Igneous rocks		Mafic dikes, sills and plugs consisting of aphanitic basalt to rare microcrystalline gabbro metamorphosed to greenschist facies. Host sedimentary rocks are locally hornfelsed.	Subterranean lava flows and intrusions of Latest Cretaceous and early Tertiary age.

of preservation. All trace fossils were analyzed for potential track-maker identification, animal size, social behavior, diversity and depositional environment. Fossil plant information was compiled on taxonomy, distribution, and community and lithofacies associations from on site outcrops and samples collected from float. We note here that in compliance with National Park regulations and permit application agreements, quarrying was not conducted. Palynomorphs were extracted from siltstones and shales and analyzed under the microscope for taxonomic identification and species distribution where possible. Collected plant megafossils and palynological slides will be archived at the University of Alaska Museum of the North.

Geochronological Analyses

Bentonite samples were collected from two volcanic ash layers at Sable Mountain, spaced 24 m apart in vertical section (Fig. 3). Bentonite 1 is a ~2 cm thick, brown-weathering altered tuff that consists of clay with minor zircon, apatite, altered feldspars,

and volcanic glass. Bentonite 2 is a ~10 cm thick, white-weathering tuff with a similar mineralogy. Both bentonites are bracketed by thin coal seams and are laterally discontinuous. The samples were brought to the University of Alaska Geochronology Laboratory where they were washed repeatedly to remove all clay, allowing time for the heavier minerals to settle between rinses. The mineral separates were sent to Apatite to Zircon, Inc., Viola, Idaho, USA, where zircon grains were isolated, mounted in epoxy, and polished for a LA-ICP-MS (laser ablation-inductively coupled plasma-mass spectrometry) analysis. The ablation was conducted at the Donelick Properties dba Institute on a Resonetics Resolution M-50 instrument using an ArF Excimer 193 nm laser and a spot diameter of 26 µm. Inductively coupled plasma mass spectrometry measurements were made on an Agilent 7700X Quadrupole ICP-MS. To calibrate fractionation factors for the relevant isotope ratios and determine absolute errors, two zircon U-Pb age standards with conventionally accepted ages of 1099.00 Ma (primary standard)

and 1065.40 Ma (secondary standard) were scanned prior to, during, and after each standard and sample batch spot analysis. Results were smoothed to establish collective values for each sample analysis session; these were then used to correct for cumulative radiation damage (for more detailed information on calibration procedures, see Donelick et al., 2010). Concordance was monitored separately for each ablation spot. Ages for the ratios $^{207}\text{Pb}/^{235}\text{U}$, $^{206}\text{Pb}/^{238}\text{U}$, and $^{207}\text{Pb}/^{206}\text{Pb}$ were calculated for each scan (25 to 32 individual scans performed on each spot) and checked for concordance; concordance here was defined as congruence of all three isotopic ages at the 2σ level. If the number of concordant data scans for a spot was greater than zero, the more precise age from the concordant-scan-weighted ratio $^{207}\text{Pb}/^{235}\text{U}$, $^{206}\text{Pb}/^{238}\text{U}$ or $^{207}\text{Pb}/^{206}\text{Pb}$ was chosen as the preferred age. $^{206}\text{Pb}/^{238}\text{U}$ ratios were used to calibrate ages for grains younger than 1.1 Ga, and $^{207}\text{Pb}/^{235}\text{U}$ ratios were used to calculate ages for grains older than 1.1 Ga. Asymmetrical negative and positive errors for each age were calculated by subtracting and adding, respectively, the isotopic ratio errors in the appropriate age equation (Chew and Donelick, 2012). Both samples were scanned and re-scanned in 2 separate sessions. Twenty-five single grain analyses per sample is standard practice for the constraint of

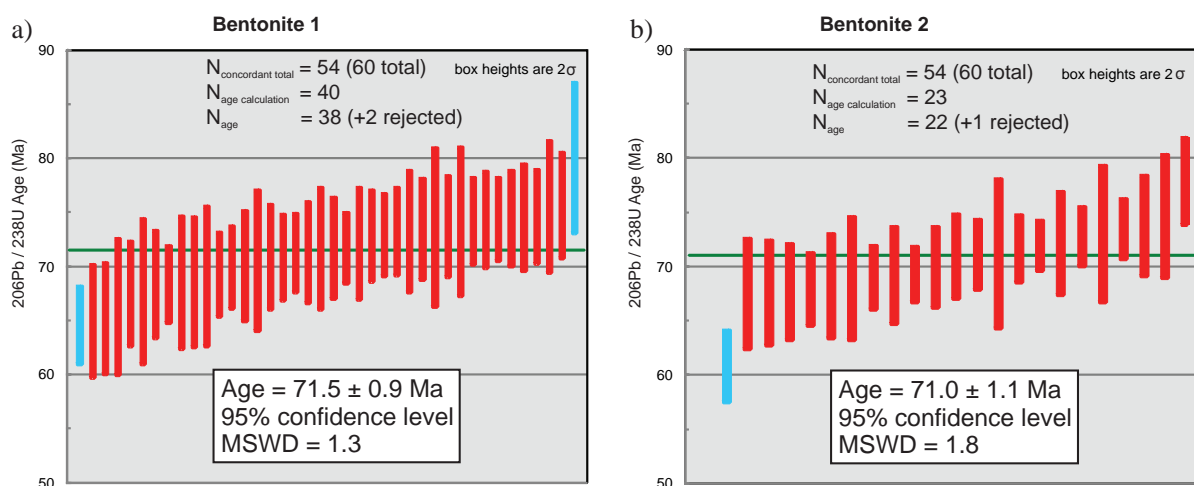
the crystallization age of a tephra. Additional single grain spot analyses were performed to identify potential detrital and xenocrystic components. The results for the measured isotope ratios and preferred ages are listed in Appendix A, Tables A-1 and A-2.

The preferred ages were filtered according to the probable age, e.g., grains older than 81 Ma were considered detrital, and grains younger than 60 Ma were also excluded on grounds of improbability. The latter may reflect localized anomalous concentration of uranium within a grain or Pb loss. In addition, error size was limited to 10% at the 2σ level. The remaining probable ages were used to calibrate the weighted mean age for each sample using Isoplot (Ludwig, 2003). The data were plotted as histograms showing concordant and overlapping results for single zircon grain analyses and the weighted mean age for each sample (Figs. 4a and 4b).

PREVIOUS WORK

Lithofacies and Depositional Models

The lower Cantwell Formation was first described by United States Geological Survey (U.S.G.S.) geologist G. H. Eldridge (1900) from the east bank of the Nenana River near Panorama Mountain ~22 km south of Denali National Park during a reconnaissance study in 1898. The site



Figs. 4 a), b). Histograms showing concordant results and overlap for LA-MS-ICP single zircon grain analyses. Weighted mean U-Pb ages are given by the green bar. 4a) Bentonite 1. The weighted mean age is 71.5 ± 0.9 Ma based on 38 single grain ages. 4b) Bentonite 2. The weighted mean age is 71.0 ± 1.1 Ma based on 22 single grain ages. Two grains from Bentonite 1 and 1 grain from Bentonite 2 (blue bars) were rejected because they do not overlap the weighted average and error margin of the accepted single zircon grain ages (at a modified 2-sigma error). Data is plotted in Isoplot (Ludwig et al., 2003).

later became the type section locality for the sedimentary succession (Capps, 1940; Wolfe and Wahrhaftig, 1970). Initial geologic investigations into the Cantwell Formation were aimed at resource estimation and resolving the geologic history of the Alaska Range. With the advance of plate tectonics and large-scale fault displacement concepts in the latter half of the nineteenth century, interest shifted to intracontinental basin evolution and the accretionary history of oceanic terranes.

The sedimentary succession has been described from a number of places and the complexity of lithofacies distribution was emphasized by all authors (Pogue, 1915, Capps, 1919, 1940; Wolfe and Wahrhaftig, 1970; Hickman, 1974; Billingsley, 1977; Stanley, 1987; Hickman et al., 1990; and Csejtey et al., 1992). Capps (1919, 1940) described lithologies and structures from a number of sites in Denali National Park and remarked on the heterogeneity of the rocks and their relationship to adjacent lithological units. Hickman (1974) isopach-mapped the distribution of the lower Cantwell Formation in the eastern parts of the Cantwell basin along the Nenana River corridor (Fig. 1) and outlined an east–west-trending southward deepening basin and several subbasins that are oriented obliquely to the basin margins.

Believing the sedimentary and volcanic members both to be of early Paleocene age, Hickman et al. (1990) characterized the Cantwell basin as a pull-apart structure that had formed in response to early Tertiary strike-slip deformation along the Denali Fault. Csejtey et al. (1992) contended that the siliciclastic sedimentary fill records regional crustal shortening associated with the amalgamation of the Wrangellia Composite Terrane. From a structural analysis, Cole et al. (1999) established multiple episodes of syn- and post-depositional deformation caused by initial northward thrusting followed by post-volcanism northwest-ward thrusting and subsequent strike-slip faulting along the Denali Fault system. The most comprehensive study of the lower Cantwell Formation thus far was conducted by Ridgway et al. (1997) and Trop and Ridgway (1997) who used paleoflow directions, grain size and facies trends from eleven sites across the basin to interpret the depositional environment as a stream-dominated alluvial fan system drained by an eastward-flowing

sandy-braided axial river. Based on their revision of the age of the sedimentary succession (Campanian / Early Maastrichtian), basin-wide facies distributions, and evidence for intraformational unconformities and growth strata, Ridgway et al. (1997) re-interpreted the Cantwell basin as a syn-orogenic thrust top basin that formed in the later stages of plate convergence between the Wrangellia Terrane and the late Mesozoic continental margin of North America. In this model, the Hines Creek Fault (Fig. 1) is an active thrust fault that underlies the leading thrust panel of a northward-propagating fold-and-thrust sheet on which the Cantwell basin formed.

From their regional facies analysis of the lower Cantwell Formation, Ridgway et al. (1997) defined five facies associations as follows:

- i) cobble conglomerate, thin mudstone and coal seams—interpreted as proximal braided stream
- ii) pebble conglomerate, sandstone and mudstone—interpreted as braided stream
- iii) interbedded sandstone and mudstone—interpreted as sheetflood
- iv) conglomerate and cross-bedded sandstone—interpreted as axial sandy river
- v) sandstone and mudstone—interpreted as lacustrine and lacustrine deltaic deposits.

According to these authors, the coarsest-grained facies are located near the northern basin margin and facies fine toward the basin axis. The lithology is polymictic, and clast composition varies greatly between outcrops reflecting a variety of different sediment source areas. On the basis of the facies distributions, Ridgway et al. (1997) interpreted the deposition as a stream-dominated alluvial fan system in a two-sided asymmetrically aligned basin drained by an axial sandy braided river.

The Age of the Lower Cantwell Formation

For nearly a century, age estimates for the non-marine to marginal marine (Ridgway et al., 1997) lower Cantwell Formation were based on diverse, but often poorly preserved fossil florules that included fragmentary angiosperm leaf impressions that reflected a broad stratigraphic range and morphological variation. The first age assessments were based on sparse material collected from single sites rather than from a combined data set, and results thus ranged from early Cretaceous

to Eocene (Pogue, 1915; Capps, 1919; Imlay and Reeside, 1954; Wolfe and Wahrhaftig, 1970). In 1937, Paleobotanist Ralph Chaney made generic and species identifications for 8 specimens from a larger collection of fragmentary plant fossils from the northern part of the basin and cautiously assigned a Cretaceous age to the formation (Capps, 1940). In a reevaluation of Chaney's taxonomic assignments, Wolfe (in Wolfe and Wahrhaftig, 1970) identified four taxa also known from the Paleocene Chickaloon Formation of southern Alaska and consequently assigned a Paleocene age to the formation. This early Tertiary age designation remained accepted even as subsequently published whole-rock and single mineral K–Ar ages for igneous intrusions indicated a much older age for the sedimentary sequence (Hickman, 1974; Hickman and Craddock, 1976; Sherwood and Craddock, 1979). Recalculated K–Ar ages for these intrusions range from 79.1 ± 6.0 to 71.9 ± 2.6 Ma (Csejtey et al., 1992).

More recently, less ambiguous age constraints brought clarity on several levels. From sparse fossil pollen data obtained for a basin-wide tectonostratigraphic study, Ridgway et al. (1997) were able to assign a Late Campanian and early Maastrichtian (~80 to ~70 Ma) age to a number of outcrop exposures of lower Cantwell Formation. Using newer $^{40}\text{Ar}/^{39}\text{Ar}$ techniques, Cole et al. (1999) subsequently re-dated the volcanic upper Cantwell Formation to 60 to 55 ± 0.2 Ma, revealing thereby a 10 to 15 Ma hiatus during which upper layers of the lower Cantwell Formation were eroded.

The Late Cretaceous age for the terrestrial sedimentary sequence then became a driving factor in the search for paleoecological data. The new age designation proved to be in good agreement with first dinosaur footprint documentations in the Cantwell Formation near Sable Mountain and Double Mountain in 2005 (Fiorillo et al., 2007). Since then, the paleoecological database has grown considerably enumerating thousands of dinosaur tracks while adding bird and pterosaur tracks to the list. From their palynological analyses, Ridgway et al. (1997) determined that some sections (Double Mountain and Jenny Creek) are entirely of Campanian age, while others (Polychrome Mountain, East Fork Toklat River and Dean Creek) include the early Maastrichtian.

Several palynological samples we processed for chronostratigraphic control proved to be inconclusive. Fossil pollen in the lower Cantwell Formation is commonly poorly preserved, and yields were inadequate to confidently assign an age to any outcrop. It appears that palynomorphs were degraded by heat, either due to Tertiary volcanism or burial, or both.

Paleolatitude of the Lower Cantwell Formation

Paleomagnetic pole positions and the composite apparent pole wander path (APW) for North America suggest that the northern geographic pole was positioned close to the coast of northwestern Alaska starting at about 130 Ma (Kent and Irving, 2010). Between ~120 and ~50 Ma, the North Pole remained at a relative standstill less than 1000 km off the northern Alaskan and northeastern Russian coastlines (present-day geography). This coincides with a time during which several floral turnovers took place. Most notably is the replacement of coniferous-dominated biota with northward migrating angiosperm communities leading to development of the mixed polar broad-leaved deciduous forest (Wolfe, 1987; Spicer et al., 1987; Spicer, 2003). Paleolatitude estimates for the Paleocene Cantwell basin range from $83^\circ \text{N} \pm 9^\circ$ (Hillhouse and Grommé, 1982), to $75^\circ \text{N} \pm 6^\circ$ (Sontag, 1992), to $71^\circ \text{N} \pm 10^\circ$ (Hillhouse and Coe, 1994). All of these calculations are based on paleomagnetic poles determined from the volcanic upper Cantwell Formation.

Previous paleomagnetic results for the lower sedimentary strata were found to be inconsistent and were not further evaluated. To test this further, we analyzed the magnetic properties of a single, spatially oriented organic-rich siltstone/very fine sandstone sample with preserved bedding structures and very few roots indicating only insignificant post-depositional sediment modification. The sample was collected from our composite section at a stratigraphic height of 191 m (Fig. 3).

Tilt-corrected magnetic inclination and declination for this sample were measured in the Paleomagnetism Laboratory of the University of Western Washington and yielded -65.4° and 149.7° , respectively. The demagnetization steps reveal that magnetic remanence is preserved. The measured magnetic inclination gave a paleolatitude of 47.5°

N. This number represents an anomalously low paleolatitude. One source for bias is an inclination error in sedimentary rocks caused by the shallowing of the magnetic inclination as a result of burial compaction and/or initial depositional factors. Such shallowing is common in clay-rich terrestrial sedimentary rocks; however, when a correction factor for the predicted mean flattening under compaction of 0.55 is applied (see for instance Kent and Irving, 2010), the paleolatitude increases to a more plausible 63.3° N. The result, which we recognize has no statistical value, is displayed in Table 2 to show that there is potential for future magnetostratigraphic and paleomagnetic studies to be successful. For comparison, we also reprint in Table 2 the results from a paleomagnetic study conducted by Sontag (1992) on upper Cantwell Formation volcanic rocks from the East Fork Toklat River and Polychrome Mountain located about 7 and 10 km, respectively, to the west of our study site.

RESULTS

Stratigraphic Analyses

The sedimentary facies documented along the incised ridges of the 1805 m tall Sable Mountain are described in Table 1 and are graphically depicted in Fig. 3. Therefore, we provide only a brief description of the lithofacies here.

The coarsest-grained deposits consist of tabular and shallow lenticular-shaped, laterally discontinuous bodies of predominantly matrix-supported and moderately sorted pebble to cobble conglomerate up to 6 m thick. Subangular to well-rounded polymictic clasts have a wide range of sizes between < 1 and 15 cm in diameter. The texture is massive to trough cross-bedded and includes sandstone lenses. Conglomerates typically fine upward to a medium-grained granular sandstone that is capped by mud drapes.

The sandy fraction consists of tabular to shallow lenticular trough cross-bedded sandstone and pebble sandstone up to 2.5 m thick; horizontally bedded (rarely cross-stratified) to massive upward-fining coarse to medium-grained sandstone up to a rare 8 m thick; and massive upward-fining coarse to medium-grained sandstone up to 1.5 m thick. Laterally continuous thinly and thickly interbedded tabular sand- and mudstones form numerous upward-

fining successions tens of meters to hundreds of meters thick. The organic-rich finer-grained fraction (very fine sandstone, mudstone and shale) makes up approximately 60 % of the section. Mudstone and carbonaceous shale range in thickness from a few cm to more than 14 m and locally contain thin seams (<10 cm) of coal and interbedded bentonite (Fig. 3). We also recorded intercalated, sharp-based non-structured deposits that incorporate clasts and woody debris in a fine-grained organic-rich matrix. Rocks are well-indurated, have a dark grey to black color, and commonly preserve primary bedding features. In a few places, beds are truncated by dikes and interleaved by sills.

Dominant sedimentary features include muddy partings in sandstone and conglomerate, trough cross-bedding, current ripples, and soft-sediment deformation. Channel scour is rare (Tomsich et al., 2010). Paleoflow measurements record bimodal directions (SE and NW) in near equal proportions.

Geochronological Analyses

The weighted mean or best fit U–Pb zircon ages for two bentonites from Sable Mountain yielded 71.5 ± 0.9 Ma and 71.0 ± 1.1 Ma ages, respectively. For the lower bentonite (Bentonite 1), a total of 60 zircon grains were analyzed of which 54 grains yielded concordant results. Eleven grains yielded ages older than the probable age of the Cantwell Formation (based on the biostratigraphy of Ridgway et al., 1997), and 3 failed to pass an applied error filter set at 10%. Of the remaining 40 grains, two more were rejected at the 95% confidence level (shown as blue bars in the histogram; Fig. 4a). The age span for the older grains ranges from 195.3 to 2556.8 Ma. These grains are considered detrital zircons that were either incorporated into the ash during magma ascent and/or were sourced from the sedimentary environment. Ages for the remaining zircon grains, for which the weighted mean age was constrained, range from 64.57 to 80.06 Ma (Fig. 4a). U/Th ratios, a discriminator for the source rock type, range from 1.06 to 3.42 with an average of 2.09 (Appendix A, Table A-1), which suggests that all zircon grains are igneous-sourced (see Hoskin and Schaltegger, 2003). For the upper bentonite (Bentonite 2), a total of 60 zircon grains were scanned. Twenty-eight grains yielded ages older than the probable stratigraphic

Table 2. Paleomagnetic results for lower (this study) and upper Cantwell Formation (Sontag, 1992). Application of a mean flattening factor (see Kent and Irving, 2010) yielded a plausible paleolatitude of 63.3° N for the sedimentary rocks. Paleomagnetic data from Sontag (1992) presented here for comparison consistently gave high inclinations yielding a mean paleolatitude of 74.3° ± 6° N and paleopole of 177° E, 75° N for ~ 60–58 Ma volcanic strata near Polychrome Mountain. Polarity is reversed in all samples.

Sample Location	Geographic Coordinates	Approx. Age (Ma)	DeMag step	Intensity (mA/m)	GeoDec	GeoInc	StratDec	StratInc	2 σ	Paleo-latitude	Notes
Sable Mountain	63.6/-149.45	~ 72	NRM	0.187601	108.9	78.6	330.9	9.6			This study
			NRM after liquid nitrogen	0.098443	119.8	42.6	5.2	25.8			
			10 mT AF	0.088212	355.4	-30.2	149.7	-65.4		47.5	
Polychrome Mountain		59.8 ± 0.2								Sontag, 1992	
North limb 1	63.6/-149.6				153	-45	149	-68	13.1		
North limb 2					167	-40	185	-71	7.2		
North limb 3					174	-41	193	-62	3.3		
North limb 4					178	-57	224	-73	26.9		
North limb 5					157	-43	142	-64	2.1		
North limb 6					154	-51	132	-71	2.1		
North limb 7					169	-47	341	-85	13.6		
North limb -- Mean					164	-47	169	-74	11.1		
South limb 1	63.5/-149.6				32	-41	73	-79	5.9		
South limb 2					22	-52	184	-87	40.7		
South limb 3					20	-45	141	-81	2.8		
South limb 4					22	-40	29	-75	28.8		
South limb 5					39	-46	84	-75	6		
South limb 6					25	-48	337	-89	9.1		
South limb 7					31	-44	126	-76	5.5		
South limb 8					25	-33	73	-77	2.5		
South limb -- Mean					27	-44	86	-82	6.1		
East Toklat Ridge	63.5/-149.55	57.8 ± 2.7	n/a	n/a	127	-39	156	-53	5.4		Sontag, 1992
East Toklat Ridge					84	-47	65	-69	19.8		
East Toklat Ridge					98	-63	158	-75	4.4		
East Toklat Ridge					110	-68	327	-88	4.5		
East Toklat Ridge					125	-51	253	-75	41		
East Toklat Ridge					137	-46	231	-71	9.2		
East Toklat Ridge					94	-50	109	-82	21.8		
East Toklat Ridge					106	-57	192	-85	3.1		
East Toklat Ridge-- Mean					111	-54	166	-82	12.3		
Polychrome Mountain-- Mean	63.5/-149.6	~ 60 – 58			98	-64	149	-82	2.3	74.3 ± 6	Sontag, 1992

age, 2 grains yielded ages <60 Ma, 5 grains failed to meet concordance tests and 2 grains failed to pass the 10% error limit. Of the remaining 23 grains, one more was rejected at the 95% confidence level (Fig. 4b). The older grains range in age from 81.8 to 2595.4 Ma and are likely detrital in nature. Ages for the remaining zircon grains ranged from 67.53 to 77.91 Ma yielding a weighted mean age of 71.0 ± 1.1 Ma at the 95% confidence level (Fig. 4b). U/Th ratios vary from 0.61 – 5.30 (Appendix A, Table A-2) with an average of 2.32, indicating that all are igneous-sourced.

Fossil Fauna of the Lower Cantwell Formation at Sable Mountain

The most important fossil vertebrate information for the lower Cantwell Formation is derived from

the ichnofossil record. Only a few poorly preserved bone fragments have been recovered to-date; thus, well-preserved vertebrate tracks play an important role in the reconstruction of faunal communities. Dinosaur tracks have been found in coarse-grained facies but are relatively common in the finer-grained, heterolithic facies of the lower Cantwell Formation. Many well-defined footprints are preserved as casts (Figs. 5 and 6) at a depositional break. Moreover, numerous small to large bulbous load casts have weathered out on the underside of more resistant beds. It is not uncommon for two or more tracks to form a short trackway along the bottom of a more resistant sandstone bed from which stride and mode of locomotion is determined and hip heights may be estimated (see Wright and Breithaupt, 2002). The majority of the dinosaur tracks in the Sable



Fig. 5. Hadrosaur footprints and manus print (above hammer) on underside of inclined bedding plane. Foot length is 32 cm. This translates into an ornithischian hip height of ~ 1.9 m (after Wright and Breithaupt, 2002). Tracks are of inferred late Campanian age. Hammer is 42 cm long.



Fig. 6. *Saurexallopus* sp., a therizinosaur footprint (Fiorillo and Adams, 2012). The 23 cm long and 20 cm wide track occurs above Bentonite 2 and is of inferred early Maastrichtian age. Form and age are comparable to *Saurexallopus lovei*, a therizinosaur footprint from the Maastrichtian of northwestern Wyoming. Similar tracks were reported from Poland implying a wide biogeographic range. Scale bar = 5 cm.

Mountain area are underprints and the variability of preserved detail is likely related to floodplain dynamics (Jackson et al., 2009). A few exquisitely preserved tracks exhibit evidence for direct contact with the sediment, such as those with distinctive impressions of foot skin tubercles.

Five Late Cretaceous dinosaur groups have been recognized from the track record. They are attributable to theropods (including birds and therizosaurs), hadrosaurs (duck-billed dinosaurs, Fig. 5), ceratopsians (horned dinosaurs) and ankylosaurs (club-tail dinosaurs). Hadrosaur tracks are the most abundant and vary in length from 10 to 60 cm, with ceratopsian tracks being the next most common. Definitive tracks attributable to ankylosaurs are rare.

Non-avian three-toed theropod tracks are

small to medium-sized; the largest footprint of this predatory dinosaur group found to-date at Sable Mountain is 25 cm long. Recent discoveries include the four-toed tracks of a therizinosaurid dinosaur (Fig. 6), an unusual herbivorous theropod (Fiorillo and Adams, 2012). Tracks and body fossils of this enigmatic group of animals are found in Asia and North America (Harris et al., 1996), and contribute to the model of faunal exchange between these two continents during the Late Cretaceous (Fiorillo, 2008; Fiorillo and Adams, 2012).

Avian dinosaur tracks include seven types of bird tracks and probable feeding traces (Fiorillo et al., 2007; 2011). Track sizes range from small wading shore bird traces to large tracks (Fig. 7) comparable to a sandhill crane (*Grus canadensis*). The morphology of the smaller traces is similar to the tracks of a willet



Fig. 7. *Magnoavipes denaliensis*, a new ichnospecies (Fiorillo et al. 2011) dated to 71.5 ± 0.9 Ma. Shown are three well-defined bird tracks and one overlapping faint bird trace (arrow). The well-defined tracks preserved toe pad detail. Imprinted medium is a bioturbated, laminated siltstone interpreted as lake margin sediment. Unidirectional track orientation indicates that the birds moved as a group. Prints are 25 cm long and compare in size and form to those of sandhill cranes. Card shown for scale is 8.5 cm long.

(*Catoptrophorus semipalmatus*) or a sand piper (*Actitis hypoleucos*). Two new ichnospecies were established on account of detailed morphological features that distinguish them from those previously described under the same ichnogenus. Alluding to their size, Fiorillo et al. (2011) named the smallest tracks *Gruipeda vegrandiunus* and, alluding to Denali, North America's highest mountain, Fiorillo et al. (2011) called the largest tracks, found at Sable Mountain just above Bentonite 1, *Magnoavipes denaliensis* (Figs. 3 and 7).

Four-toed ornithischian footprints record the presence of either ceratopsian dinosaurs (e.g., triceratops) or ankylosaurs, or both, as the hind tracks of these quadrupedal animals are indistinguishable from one another and skeletal remains of both groups have been identified from Late Cretaceous bone fossil localities of Alaska. Skeletal parts and skulls of several ceratopsids (e.g., *Pachyrhinosaurus perotorum*; Fiorillo and Tykoski, 2012) were recovered from the coeval Prince Creek

Formation on the North Slope, and the skull of a dermal armor-plated ankylosaur (*Edmontonia longiceps*) was unearthed from the Maastrichtian Matanuska Formation of southern Alaska (Gangloff, 1995; Fiorillo, 2006).

Non-dinosaurian vertebrate ichnofossils include fish fin traces (*Undichna*) and pterosaur manus prints (Fiorillo et al., 2009a). In reference to the Cretaceous paleopole, the pterosaur tracks from Sable Mountain are the northernmost documentation to-date for this unusual, extinct reptile group. Their habitat evidently extended inland suggesting rich fishing grounds for the Cantwell basin as this group would have fed primarily on fish (Fiorillo et al., 2009a).

Invertebrate trace fossils occur mainly at or just below a depositional break and, although not abundant, are quite diverse (Fiorillo et al., 2009a; Hasiotis, 2009, 2011). They include back-filled burrows made by mud-burrowing beetles (*Steinichnus*; Hasiotis et al., 2009, 2011), U-shaped

burrows of fly larvae (c.f. *Arenicolites*), crayfish burrows (*Camborygma*), and intricate ostracod (*Sagitichnus*), freshwater gastropod (*Scolicia*; cf. *Isopodichnus*), and other subsurface grazing trails (e.g., *Mermia*; Hasiotis, 2002). Sinusoidal traces (*Cochlichnus* sp.) attributable to nematodes and oligochaetes were imprinted at the sediment–water interface of standing water bodies as were microbial matting patterns. Also found were subaerial beetle trackways, channelized fossil wood (*Paleobuprestos*) from which we infer the presence of wood-burrowing beetles (S. Hasiotis, pers. comm.) and minor leaf fossil evidence for insect herbivory.

Fossil Flora of the Lower Cantwell Formation at Sable Mountain

The lower Cantwell Formation contains abundant plant impression and compression fossils and lithified wood. A total of 42 species were counted from the Sable Mountain study area. Gymnosperm fossils consist of conifer leaves, leafy shoots, cones (Fig. 8), seeds, sideritized wood, and tree bark and trunk impressions up to 2.5 m long. Leafy shoots of deciduous conifers of the family Cupressaceae

are abundant and are identified as *Taxodium* sp., *Metasequoia* sp., *Glyptostrobus* sp., possible *Parataxodium* sp., and *Sequoia*-like forms. Other conifers resemble *Tumion* (*Torreya*), a member of the Taxaceae, and the form genera *Cephalotaxopsis* and c.f. *Pityophyllum* of unknown affinities (Tomsich et al., 2010). Needles, isolated or in bundles, and cones (Fig. 8) referable to piceoid conifers (e.g., *Pinus*, *Larix*, and possibly *Picea*) were also observed, albeit less frequently. The low abundance of these taxa could signify that they retained their foliage for several years or that they grew outside the locus of deposition.

Dicot angiosperm leaf fossil impressions consist of simple entire and simple lobate leaf forms and include the following taxa: *Corylites beringianus* (Krysht.) Moiseeva, *Corylites* sp., and other betulaceous taxa; *Celastrinites* (*C. kundurensis?*); and hamamelidaceous, nymphaeaceous (cf. *Nuphar*) and platanoid taxa. The latter include *Pseudoprotophyllum* sp., *P. boreale*, *Platanites* sp., and several other platanoids of unclear generic affinities. Palmate-acrodromously veined leaf forms are assigned to *Menispermites*



Fig. 8. Longitudinal section of piceoid conifer seed cone showing hollow center axis and ovuliferous scales. Fossil is embedded in gritty siltstone interpreted as a mud flow. Scale bar = 1 cm.

sp., *M. septentrionalis*; *Trochodendroides* sp. 1,2, *T. richardsonii*, *T. taipinglinchanica*; and *Macclintockia* sp. Three additional morphotypes, including one aquatic? angiosperm leaf form resembling Trapago and another resembling *Ulmus-Zelkova*, remain unidentified due to poor preservation of higher-order venation.

The plant fossil collection also includes magnoliid seeds, several linear (*Phragmites*- and *Typha*-like) and broad-leaved (*Potamogeton*- and *Alisma*-like) monocot angiosperm taxa, the fern genera *Asplenium*, *Cladophlebis*, *Coniopteris*, and *Gleichenites*, mosses (*Lycopodium*), and abundant horsetail (*Equisetites*) stems and rhizomes of varying diameter and segment lengths (Tomsich et al., 2010). Ginkgophyte and cycadophyte leaf fossils are suspiciously absent in our study area, but have been observed elsewhere. For example, we noted Ginkgo leaves (e.g., *G. adiantoides*) from outcrops in the northwestern Cantwell basin and cycadophyte material from Double Mountain and at an outcrop above the East Fork Toklat River. *Ginkgo* leaves and *Nilssonia yukonensis* were also reported from the base of the Cantwell Formation east of the Nenana River (Alaska Paleontological Database, 2014).

Plant fossil assemblages differ in composition across the Cantwell basin because they reflect climate variability through time, various stages of floral successions, or various local depositional parameters. Distinctive plant communities appear to have been endemic to specific sedimentary subenvironments, likely for edaphic reasons. Accordingly, a *Taxodium*—*Glyptostrobus*—*Alnites* assemblage is associated with poorly-drained fine-grained floodplain sediments, and a *Metasequoia*—*Corylites*—*Trochodendroides* assemblage is associated with more heterogeneous and better-drained floodplain deposits. These mixed conifer and broad-leaved angiosperm leaf fossil assemblages commonly also include ferns and horsetails and contrast starkly with platanoid-dominant leaf assemblages found in what we interpret as channel and overbank deposits and a low-diversity community of *Equisetites* and cycadophytes observed at Double Mountain for which we infer growth in a marshland.

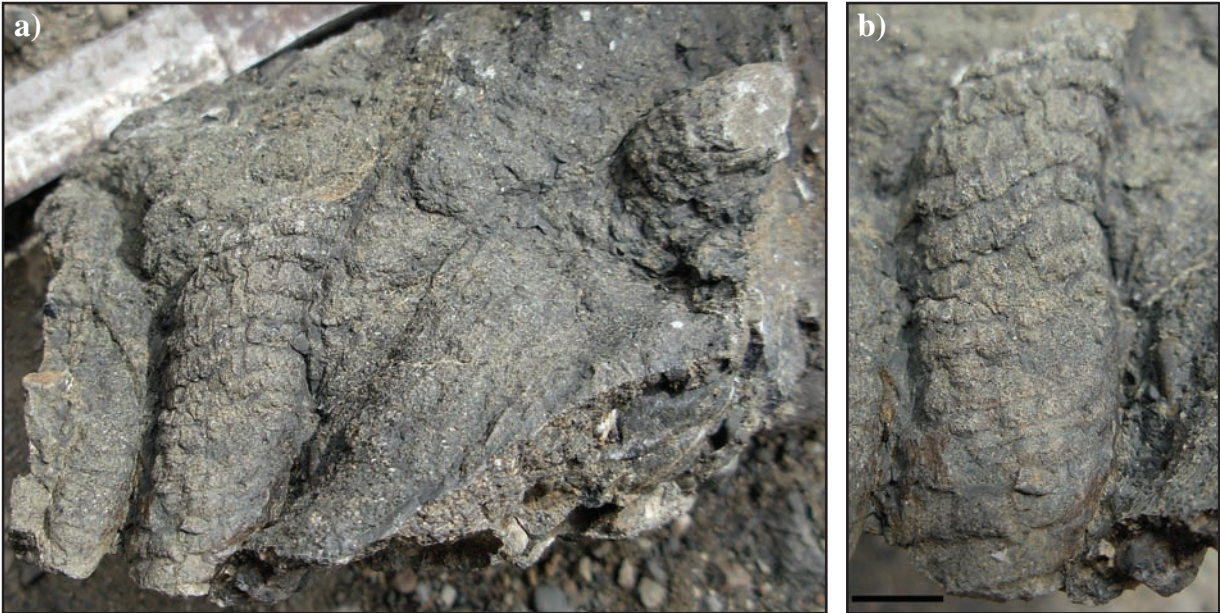
The generic taxonomy of the Sable Mountain flora shows a strong similarity to the late Maastrichtian Koryak flora of northeastern Russia

(Tomsich et al. 2010). It also partly overlaps the Campanian–Maastrichtian Hanson Point flora from Ellesmere Island in the Canadian Arctic Archipelago (Falcon-Lang et al., 2004), the Edmonton flora of the central Alberta Foothills described by Bell (1949), and older floras such as the Cenomanian (and Turonian?) Melozi and Kaltag Formation floras of the Yukon River basin (Hollick, 1930; Patton et al., 1994). Taxa are characteristic of a Pan-Beringian flora, the Late Cretaceous–early Tertiary polar broad-leaved deciduous forest. This unique fossil flora was characterized by a prevalence of deciduous conifers and angiosperms of low familial diversity (Wolfe, 1987; Spicer et al., 1987; Herman, 2007; Krassilov et al., 2009; Spicer and Herman, 2010). Woody angiosperms exhibit a high degree of polymorphism and speciation (Spicer and Herman 2010). Herbaceous angiosperms may have been present also, but are not preserved except in the pollen record and, possibly, in form of root casts (as shown in Fig. 9). Casts and impressions of tree trunks no more than 10 cm in diameter indicate that woody angiosperms had a shrub-like habit. Conifer tree trunk diameters, on the other hand, vary from 25 cm to an estimated 1 m or more at the base. Several trunk impressions may indicate buttressed bases (Fig. 10).

The taxa listed above constitute the principal floodplain vegetation in the Sable Mountain area. The relative abundance of deciduous cupressaceous conifer fossils suggests that members of this family were dominant in this part of the basin. Rare detached, pine-like conifer needles indicate they were only minor constituents of the floral community. However, a pinaceous seed cone embedded in a gritty siltstone (Fig. 8) suggests that it, too, was in situ.

Paleoclimatic Reconstruction of the Lower Cantwell Formation at Sable Mountain

The Late Cretaceous high-latitude (>65° N) terrestrial faunal and floral fossil data record species expansion in a habitat governed by a temperate climate and polar light regime (Wolfe, 1987) which may have led to unique adaptation strategies. Dinosaur egg shell fragments (Godefroit et al., 2009), juvenile dinosaur bones (Clemens, 1994; Gangloff and Fiorillo, 2010; Fiorillo et al., 2010) and small, possibly juvenile hadrosaur footprints suggest



Figs. 9 a), b). Tuberos roots cast in coarse-grained granular sandstone. 9a) Cluster of tubers. Hammer shaft for scale is 2 cm wide. 9b) Single tuber, enlarged. Scale bar = 1 cm. Although probably of little taxonomic value, we report this fossil for its evolutionary and paleoclimate implications. Selection for asexual reproduction may have been an adaptive response to short growing seasons and suggests a frost-free substrate.



Fig. 10. Conifer tree trunk impression 2.5 m long (arrows) in inferred rapidly aggraded channel deposits of Campanian age. Tree base diameter is estimated at >1 m diameter and appears buttressed. Note the shallow spread of the root system which suggests a wet floodplain. Person for scale.

that environmental conditions were sufficiently hospitable for dinosaurs to remain year-round (see also Fiorillo and Gangloff, 2001; Chinsamy et al., 2012). Being sessile, plants are genetically coded to cope with climate, low-light settings, and surface boundary interactions. For example, tuberous root casts (Fig. 9), tree trunk impressions and casts (Fig. 10), and lithified wood provide a glimpse into the boreal forest structure that has been considered one of the causes of amplified polar warming (Otto-Bliesner and Upchurch, 1997; Upchurch et al., 1998). Woody dicot leaf physiognomies are important paleoclimate proxies because leaves are highly sensitive to, and therefore responsive to, climate and insolation (Wolfe and Spicer, 1999; Spicer and Herman, 2010).

A paleoclimate analysis (Climate Leaf Analysis Multivariate Program or CLAMP for short) for 19 dicotyledonous angiosperm leaf fossil types yields a mean annual temperature (MAT) of $7.4 \pm 1.2^\circ \text{C}$, a warmest monthly mean temperature (WMMT) of $17.1 \pm 1.6^\circ \text{C}$ and a coldest monthly mean temperature (CMMT) of $-2.3 \pm 1.9^\circ \text{C}$ (Tomsich et al., 2010). Growing season precipitation is estimated at $229 \pm 336 \text{ mm}$, and the length of the growing season is estimated at 4.8 ± 0.7 months. The annual temperature range is $19.4 \pm 3.5^\circ \text{C}$ (Table 3). Results indicate a cool temperate, highly seasonal paleoclimate. Closely spaced and well-pronounced tree rings in fossil conifer wood suggest short, rather abrupt-ending growing seasons. The reduction of sunlight in late summer likely limited annual growth (Tomsich et al., 2010).

Growing season precipitation is rather low compared to other Maastrichtian sites (Table 3), but precipitation estimates have a large error margin likely because of missing data that codes for precipitation such as the leaf apex on the larger-sized leaf fossils (Spicer et al., 2005; Tomsich et al., 2010). However, if the low precipitation estimate for the growing season is valid, it could have important implications for the paleographic setting. Tree diameter size, leaf size and the occurrence of tuberous root casts (Fig. 9) also have important climate implications and are discussed below.

DISCUSSION

Depositional Environments at Sable Mountain

The Sable Mountain lithofacies (Table 1) are

characterized by a mix of fine-grained and coarse-grained facies that correspond largely to facies association (FA) 2, 3 and 4 of Ridgway et al. (1997).

On an alluvial fan, sediment grain size decreases sharply with increasing distance from the fan apex (Ridgway et al., 1997; Kumar et al., 2007). From the high proportion of fine-grained facies (60% of very fine sandstone or finer), we infer a medial to distal location for the site of deposition. We interpret the matrix-rich, non-stratified gravelly facies (F 1) as debris flow and the predominantly massive matrix-supported clast-conglomerates (F 2) as gravelly stream deposits that accumulated rapidly under hyper-concentrated flow conditions in non-channelized gravelly stream beds and flood channels (Blair and McPherson, 1994; Miall, 2006; Kumar et al., 2007). Deposition may have been triggered by a storm or flood event and was facilitated by steep alluvial slope angle and high sediment to water supply ratio (Wells and Harvey, 1987). In contrast, stratified conglomerate (F 3), cross-stratified pebbly sandstone (F 4), and thick massive, cross-bedded or horizontally stratified sandstone (F 5, F 6) are interpreted as in-channel traction flow deposits (Miall, 2006) with the lesser-organized facies being transitional to dilute flow (Wells and Harvey, 1987). Thick sandstone deposits up to 8 m high (F 6) represent amalgamated multistory sandy channel fill. Main flow direction was to the south. However, north-directed paleocurrent measurements from cross-stratified conglomerates along the southern part of the study area suggest interfingering deposition by a sinuous axial river.

Laterally continuous tabular sandstone beds up to 1 m thick are inferred to be sheetflood deposits (F 7, F 8). Numerous depositional breaks, reactivation surfaces, stringers of mudstone, lateral continuity of beds and the near-absence of scour marks imply unconfined sheet-flow under a flash-flood discharge regime and changes in sediment influx (Bull, 1977; Miall, 2006). Mud drapes indicate waning flow and flow abandonment. Lush floodplain vegetation may have significantly slowed currents thus promoting deposition on the fan (Bull, 1977).

Fine to very fine sandstone (F 9) and interbedded sandstone and mudstone (F 10) were deposited under waxing and waning flow stages during overbank flow. These facies associations

Table 3. Paleobotanical climate estimates for the lower Cantwell Formation flora at Sable Mountain and other Maastrichtian floras of North America and northeastern Russia. Results from Parrish et al. (1987); Spicer and Parrish (1990a); Golovneva (1994; 2000); Moiseeva (2005); Spicer and Herman (2010), Tomsich et al. (2010) and Flaig et al. (2013). Estimates for the Cantwell, Kakanaut, Sakhalin Island and Alberta floras were obtained from CLAMP. Uncertainties represent 2 sigma deviations of the residuals about the calibration regressions. Estimates for the Koryak flora and the Chignik flora were obtained from LMA. Temperature variables for the Prince Creek Formation were extrapolated from a latitudinal temperature curve and the floristic composition; precipitation estimates were obtained from stable isotope analyses. Paleolatitudes were approximated from paleopole positions using the Maastrichtian (70 Ma) mean pole and 2-sigma confidence level of Enkins (2006, in Kent and Irving, 2010).

Formation, Locality (Present Latitude)	Age (Ma)	Paleo-Latitude (°N)	Mean Annual Temperature (C°)	Warmest Monthly Mean Temp. (C°)	Coldest Monthly Mean Temp. (C°)	Length of Growing Season (Months)	Mean Annual Precipitation (mm)	Growing Season Precipitation (mm)	Three Driest Months Precipitation (mm)
Cantwell Sable Mtn. S.-central Alaska (63.5°N)	~ 72	~ 70 ± 5	7.4 ± 2.4	17.1 ± 3.2	-2.3 ± 3.8	4.8 ± 1.4	n/a	229 ± 672	141 ± 186
Prince Creek Northern Alaska (70°N)	~ 70	80 ± 5	2.5 – 6	10 – 12	2 – 4	n/a	500-1500	n/a	n/a
Koryak NE Russia (63°N)	Mid- to late Maastrichtian	75 ± 5	3 – 4	n/a	n/a	n/a	n/a	n/a	n/a
Kakanaut NE Russia (63°N)	Mid- to late Maastrichtian	75 ± 5	10	19	3	6.3	1414	948	181
Sakhalin (49°N)	Maastrichtian	56 ± 5	14	20	8	8	1892	1214	293
Chignik, Chignik Bay (56°N)	Late Campanian to early Maastrichtian	~ 60 ± 5	11 – 13	n/a	n/a	n/a	n/a	n/a	n/a
Edmonton Group, Alberta, Canada (53°N)	Mid- Maastrichtian	54 ± 5	12	19	5	7.1	1804	1586	335

include thick successions of thinly interbedded sand- and mudstones and small channel sandstone bodies that are indicative of distal crevasse splay complexes. Laterally extensive siltstone and thinly bedded sandstone–mudstone couplets typify levee and floodplain deposits, respectively.

Shale and laminated mudstone (F 11, F 12) are inferred to have accumulated in abandoned

channel beds, on inactive channel bars, on the floodplain, and in marginal well-drained lacustrine environments. Carbonaceous mudstone and coal (F 13, F 14) are inferred to have accumulated in poorly drained stagnant backwater swamps. These low-energy environments also preserved Late Cretaceous pyroclastic fall-out suspension deposits that altered to bentonite (F 15). Gritty siltstone accumulations

(F 16) are interpreted as mud flows. Lastly, igneous intrusive rocks (F 17) formed of near-surface basaltic lava flows in the Latest Cretaceous and Tertiary. The microcrystalline texture of a few small plugs could indicate significant burial depths.

Overall, the dark color of the rocks and minimal post-depositional sediment modification imply that the depositional environments were saturated most of the time. The lateral discontinuity of the beds, numerous depositional breaks and facies changes, an extremely low channel inter-connectedness, and predominantly matrix-supported stream-flow and gravity flow deposits are all architectural elements of wet alluvial fan systems (Bull, 1977; Wells and Harvey, 1987; Blair and McPherson, 1994; Talling et al., 1995; Miall, 2006; Kumar et al., 2007). Strongly bimodal (NW and SE) paleocurrent directions suggest frequent shifting of sinuous channels possibly as a result of periodic basin margin uplift and load-induced subsidence (Talling et al., 1995). From the large fraction of finer-grained facies, the sandstone sheets and the evidence for vertically aggraded channel sandstone deposits with a total width in excess of 150 m, we conclude that the locus of deposition was near the basin axis and entailed the following subenvironments located in close proximity: distal alluvial fan (including gravelly braided and sandy braided distributary channel, flood channel and sheet flow, alluvial slope floodplain and lacustrine settings), fan toe, and possibly interfingering axial river and alluvial floodplain deposition (Tomsich et al., in prep.).

Clast identification and petrographic analyses (Trop and Ridgway, 1997; Tomsich et al., in prep.) reveal a polymictic lithology derived from greenschist metavolcanic and plutonic rocks, greenschist-facies metasedimentary rocks, tectonite, chert, argillite, limestone, and reworked lower Cantwell Formation. Detritus was sourced from uplifted basin margins, mountainous hinterland and eroding intrabasinal highs. Trop and Ridgway (1997) showed that sandstone modal compositions vary greatly across the basin, which they attribute to the complexity of a collaged suture zone and uplifted plate margins. Source-diagnostic discrimination diagrams (Dickinson et al., 1983, Zahid and Barbeau, 2012) indicate a recycled orogen and a dissected magmatic arc (Trop and Ridgway, 1997; Tomsich et

al., in prep.).

Implications of New Numerical Ages for the Lower Cantwell Formation

Present research on the lower Cantwell Formation in Denali National Park and Preserve (Salazar Jaramillo et al., in prep. and this study) has provided the first numerical ages for the formation. Our U–Pb zircon ages of 71.5 ± 0.9 Ma and 71.0 ± 1.1 Ma for two bentonites separated by 24 m of section at Sable Mountain are within error of each other and therefore, constitute very robust data. Our results place the bird ichnospecies *Magnoavipes denaliensis* of Fiorillo et al. (2011) (Fig. 7) at and the pterosaur manus track near 71.5 ± 0.9 Ma and permit relative age determinations for all other strata. In 2012, the International Commission on Stratigraphy (ICS) placed the Campanian / Maastrichtian boundary at 72.1 Ma (Walker et al., 2013). Accordingly, the Sable Mountain deposits straddle this important boundary, which is marked by significant global cooling and sea level fall (Hay, 2008). The age of the basal section above the Sable Mountain fault is therefore Campanian, and most likely late Campanian. Correspondingly, the upper part of our section (not shown in Fig. 3) is likely of Mid-Maastrichtian age or younger. All dinosaur footprints at Sable Mountain are now interpreted to be of both upper late Campanian and early Maastrichtian age with the majority occurring in the former, provided that all beds of our composite section are in sequential order (e.g., not duplicated by blind thrust faults). Moreover, we consider the age of the plant fossil data used for a paleobotanical climate analysis (CLAMP; Tomsich et al., 2010) earliest Maastrichtian. The Sable Mountain exposures containing the bentonites correlate with upper strata at Polychrome Mountain, which were dated by Ridgway et al. (1997) to the early Maastrichtian based on the occurrence of the stratigraphically restricted pollen taxon *Kurtzipites andersonii*. This taxon ranges from 72.5 to 71.1 Ma according to biostratigraphic zonations determined for the Canadian basins (Braman and Sweet, 2012).

Outside the Cantwell basin, the lower Cantwell Formation at Sable Mountain correlates well in time with the Campanian–Maastrichtian Prince Creek Formation on the North Slope of Alaska and the Chignik Formation of southwestern Alaska. Further

away, more chronostratigraphic correlations can be made with the upper Bonnet Plume Formation in Yukon Territory, Canada, which has also yielded avian fossils (Rich et al., 2002), the upper part of the marine East Fork and the Summit Creek formations of the Brackett Basin in the Northwest Territories (Sweet et al., 1989; Braman and Sweet, 2012), the plant fossil beds of the Hanson Point Volcanics at Emma Fjord, NW Ellesmere Island in the Canadian Arctic (Falcon-Lang et al., 2004), the Horseshoe Canyon Formation in southern and central Alberta and the St. Mary River Formation of southwestern Alberta (Braman and Sweet, 2012), all of which straddle the Campanian/Maastrichtian boundary. Across the Bering Sea, the lower Cantwell Formation at Sable Mountain is partly correlative to Campanian plant megafossil-yielding strata of the Kundur Formation (Golovneva et al., 2008) and the late Campanian and early Maastrichtian dinosaur fossil-bearing strata of the Kundur and lower Udurchukan formations in the Amur River region of eastern Russia (Van Itterbeeck et al., 2005).

Assessing the Paleomagnetic Data

Our paleomagnetic sample from Sable Mountain shows sufficient remanence after demagnetization and an inclination of -65.4° indicating a reverse polarity. This reversal can be used to help define the age of the section. The new numerical age constraints reveal that the Sable Mountain section correlates to Magnetochrons 31 and 32. Lerbekmo and Braman (2005) used densely spaced paleomagnetic inclination measurements from the Canadian Pacific Oil and Gas Strathmore (CPOG) well core to identify eleven reversals in Magnetochron 32 (seven in Subchron 1 and four in Subchron 2) in the late Campanian Bearpaw and latest Campanian to early Maastrichtian Horseshoe Canyon formations. Our sample is consistent with deposition during one of the Chron 32 reversals. More paleomagnetic data are needed to determine the reversal stratigraphy and paleopole position for the lower Cantwell Formation.

In contrast to the sedimentary samples, the volcanic rocks of the Paleocene upper Cantwell Formation gave consistently high paleomagnetic inclinations (Sontag, 1992). The mean paleomagnetic pole is 177° E longitude and 75° N latitude with an

average error of 10.4° at the 95% confidence level. This result matches the position for the 120 to 60 Ma relative still-stand of the paleopole for North America (193.9° E, 76.2° N $\pm 1.6^\circ$) (see Kent and Irving, 2010) with fully overlapping circles of 95% confidence. The calculated paleolatitude for the composite volcanic sample set is $74.3^\circ \pm 6^\circ$ (Table 2; also see Sontag, 1992). Since Sontag's study, the volcanic rocks have been dated, using K–Ar, to 58.7 ± 3.5 Ma (Csejtey et al., 1992) at or near the East Fork sample site and, using $^{40}\text{Ar}/^{39}\text{Ar}$, to 59.8 ± 0.2 Ma (Cole et al., 1999) at or near the Polychrome paleomagnetic sample site. Thus, the maximal difference between the new numerical ages at Sable Mountain and Sontag's samples is approximately 13.3 ± 4.4 Ma. Northwestward displacement of 450 km along the Tintina Fault during the latest Cretaceous and earliest Tertiary (Till's et al., 2007b) would result in approximately 2 - 3° of latitude difference between the lower and upper Cantwell Formation. This translates into the lower Cantwell Formation being within a few degrees north of its present location during the Late Cretaceous.

Age of Plant Fossils and Paleoclimate Implications

Fluctuating climates leading up to the Cretaceous terminal event and the demise of many of the ecological groups that lived therein, have produced a mosaic of late Cretaceous biogeographic species distribution, ecosystems, and species radiation. While immediate effects of these oscillations are still being evaluated, data recovered to-date have been applied to model the complex interactions between land surfaces, oceans, atmosphere and biosphere of the past. These models depend heavily on accurate, high-resolution paleoecological information from different paleogeographic regions. Much insight can be gained from the comparison of co-eval sites that were subjected to similar conditions.

The new numerical ages allow us to surmise that the Sable Mountain florule used for the paleobotanical climate analysis (Table 3) (Tomsich et al. 2010) date to ~72 to 71.5 Ma or earliest Maastrichtian. This was a time marked by the onset of significant cooling as suggested by marine isotope data (Frakes, 1999; Zakharov et al., 1999; Hay, 2008; Zakharov et al., 2011). Thus, the MAT of $7.4 \pm 2.4^\circ$ C, a WMMT of $17.1 \pm 3.2^\circ$ C and a CMMT

of $-2.3 \pm 3.8^\circ\text{C}$ calculated for the Sable Mountain flora corresponds to this cooling trend (Table 3). Our temperatures are cooler than temperature estimates for the mid-to-late Maastrichtian Kakanaut flora of the Koryak Uplands located at a paleolatitude of 70 to 75°N (Godefroit et al., 2009), but warmer than estimates for the coeval Prince Creek Formation (~ 2.5 to 6°C ; Spicer and Parrish, 1990a; Herman and Spicer, 2010; Flaig, 2010; Flaig et al., 2013), which are based on a polar temperature curve for paleobotanical climate data of lower latitudes and on comparative analyses for conifer tree ring growth characteristics (Spicer and Parrish, 1990a,b; Spicer, 2003). They are also warmer than a MAT of 3 to 4°C obtained for the mid to late Maastrichtian Koryak flora from a Leaf Margin Analysis (LMA) (Golovneva, 2000a; Herman et al., 2009). They are significantly lower than a MAT of 12°C estimated for the Maastrichtian Edmonton flora (see Table 3 and Golovneva, 2000a). The Edmonton Group was deposited proximal to the Cretaceous Western Interior Seaway (CWIS) in west-central Alberta, Canada, at a paleolatitude of $\sim 54^\circ\text{N} \pm 5^\circ$ using the paleopole for North America of Enkins (2006; in Kent and Irving, 2010). However, our new numerical ages suggest that the Sable Mountain flora is somewhat older than the Edmonton flora. Winter temperatures below freezing (CMMT of $-2.3 \pm 3.8^\circ\text{C}$) have not been reported from any other Campanian–Maastrichtian CLAMP data set for the North Pacific region (Table 3), but are therefore in good agreement with an early Maastrichtian geologic age and the predicted cooling trend for this interval. They are also in good agreement with an observed absence of cycadophyte fossil material regarded by many researchers (e.g., Golovneva, 2000a; Spicer and Herman, 2010) as thermophilic and with an observed reduction for tree stump diameters and angiosperm leaf sizes in inferred Maastrichtian strata.

The $19.4 \pm 5.2^\circ\text{C}$ mean annual temperature range contrasts with 16°C estimated for the Kakanaut flora, and $\sim 10^\circ\text{C}$ for the Prince Creek Formation (Table 3). Continentality and higher elevation remain a plausible explanation for low winter temperature estimates and greater temperature ranges. Ridgway et al. (1997) identified a marine incursion from marine to brackish water dinoflagellate cysts in samples from Double Mountain that they tentatively

correlate with the Bearpaw Transgression (~ 74 to ~ 72 Ma; Braman and Sweet, 2012). The end of this transgressive cycle also coincides with a transition from deep marine to subaerial exposure along the coast of southern Alaska beginning at ~ 72 to ~ 71 Ma (Trop and Ridgway, 2007). The predicted early Maastrichtian global sea level fall of 40 m (Hay, 2008) could thus have increased continentality during that time.

Additional evidence for a mountainous terrain comes from modal lithic sandstone composition analyses (Dickinson et al., 1983; Zahid and Barbeau, 2012) for the lower Cantwell Formation (Trop and Ridgway, 1997; Tomsich et al., in prep.) and from sandstone detrital zircon age populations (Hults and Tomsich, unpubl. data). These data, which are discussed further below, indicate that the Cantwell basin was surrounded by moderate topography associated with the late Mesozoic plate convergence (Csejtey et al., 1992; Ridgway et al., 1997; Cole et al., 1999), a factor that would have had a profound bearing on the local climate and the ecosystem. The influence of topography on atmospheric boundary conditions and associated cooling effect has been shown, for example, by Markwick and Valdes (2004). If valid, the paleobotanical temperature estimates for the Sable Mountain flora are consistent with a seasonal and cool temperate, continental climate (Tomsich et al., 2010). A similar suggestion was made by Golovneva et al. (2008) for a comparison of the late Campanian floras of the Amur River region in the Russian Far East and Sakhalin Island. The flora of Sakhalin Island contains more thermophilic taxa and was influenced by a warm maritime climate.

Paleogeographic Implications

Subduction-related Late Cretaceous (~ 80 to 66 Ma) continental margin arc magmatism was widespread in southern, central, and western Alaska (Moll-Stalcup, 1994; Trop and Ridgway, 2007; Cole et al., 2007), resulting in the emplacement of Late Cretaceous to early Tertiary granitoid plutons on either side of the late Mesozoic suture zone (Csejtey et al., 1992) and significant deformation along an orogenic belt stretching from eastern Alaska to the Bering Sea (Moll-Stalcup, 1994, Foster et al., 1994; Trop and Ridgway, 2007; Till et al., 2007b).

Regionwide uplift prior to a period of Late

Table 3. Paleobotanical Climate Estimates from Upper Late Cretaceous Floras of North America and Northeastern Russia

Formation, Locality (Present Latitude)	Age (Ma)	Paleo-Latitude (°N)	Mean Annual Temperature (C°)	Warmest Monthly Mean Temp. (C°)	Coldest Monthly Mean Temp. (C°)	Length of Growing Season (Months)	Mean Annual Precipitation (mm)	Growing Season Precip. (mm)	Three Driest Months Precip. (mm)
Cantwell Sable Mtn. S.-central Alaska (63.5°N)	~ 72	~ 70 ± 5	7.4 ± 2.4	17.1 ± 3.2	-2.3 ± 3.8	4.8 ± 1.4	n/a	229 ± 672	141 ± 186
Prince Creek Northern Alaska (70°N)	~ 70	80 ± 5	2.5 – 6	10 – 12	2 – 4	n/a	500-1500	n/a	n/a
Koryak NE Russia (63°N)	Mid- to late Maastrichtian	75 ± 5	3 – 4	n/a	n/a	n/a	n/a	n/a	n/a
Kakanaut NE Russia (63°N)	Mid- to late Maastrichtian	75 ± 5	10	19	3	6.3	1414	948	181
Sakhalin (49°N)	Maastrichtian	56 ± 5	14	20	8	8	1892	1214	293
Chignik, Chignik Bay (56°N)	Late Campanian to early Maastrichtian	~ 60 ± 5	11 – 13	n/a	n/a	n/a	n/a	n/a	n/a
Edmonton Group, Alberta, Canada (53°N)	Mid-Maastrichtian	54 ± 5	12	19	5	7.1	1804	1586	335

Paleocene to Early Eocene intracontinental extension (Cole et al., 2007) is also suggested by petrographic data and detrital zircon ages for a sandstone from the basal section at Sable Mountain (Hults and Tomsich, unpubl. data). The majority of zircon grains are Precambrian in age. The oldest rocks of the Wrangellia Terrane are not older than Pennsylvanian (Nokleberg et al., 1994; Plafker and Berg, 1994). Zircons older than Pennsylvanian therefore were sourced from the Yukon Tanana Terrane exposed to the north and east. A ~69 Ma caldera in the Sixty Mile Butte area (Bacon et al., 1990) overlies the schist of the Yukon Tanana Terrane about 200 km to the east of our study site indicating that no intervening lithological unit existed at the time and the schist was at or near the surface. In the eastern part of the basin, lower Cantwell Formation overlies Proterozoic schist and a

~95 Ma pluton (Wolfe and Wahrhaftig, 1970). North of the Hines Creek Fault, upper Cantwell volcanic strata overlie Precambrian schist (Fig. 1; Csejtey et al., 1992). While the Cantwell basin remained at a low to moderate elevation as suggested by a marine excursion interpreted to coincide with the Bear Paw transgression (Ridgway et al., 1997), the landform surrounding the basin margin may have been one of uplands, if not highlands. Topographic basins like the Cantwell basin may have existed all around the orogenic belt, but little of the sedimentary fill was preserved (Foster and Igarashi, 1990; Foster et al., 1994).

Elevated regional topography is also assumed by climate modelers. To calibrate surface boundary conditions for their GCM, Sewall et al., (2007) model the early Maastrichtian topography of the

southern Alaska region in the range of 200 to 800 m with isolated areas of up to 1000 m. In their model, the lowland vegetation constitutes a mixed evergreen and deciduous forest. Upland vegetation is inferred to have been composed of closed canopy evergreen conifer forest; the paleolatitudinal position of this area is presumed to have supported evergreen habit (Sewall et al., 2007). To this end, some conifer taxa such as *Sequoia* and some members of the Pinaceae are thought to have had an evergreen habit (Golovneva and Herman, 1998). Although a small number of *Sequoia*-like leafy shoots have been observed in the Cantwell Formation, no evidence for secondary (multi-year) growth has been observed to-date on any fossil conifer shoots. Because evergreens are low-littering plants, it is not clear whether the small collection of *Sequoia*-like shoots and pinaceous needles and cones represent minor constituents of the floodplain/alluvial slope vegetation or whether these taxa preferred the drier soils outside the floodplain and fossil material was upland-derived. The piceoid seed cone shown in Fig. 8 is preserved in a thick gritty siltstone that could imply that the fossil was sourced from within the basin.

The apparent dominance of hydrophilic deciduous conifers in floodplain deposits, indications for weak pedogenic processes and ichnofossil evidence for standing water bodies could support a wet climate interpretation. However, this is not supported by the low precipitation estimate for the Sable Mountain flora (Table 3). A possible explanation for the discrepancy is that in Arctic environments, water take-up from the substrate is severely reduced from the lack of transpiration following leaf abscission in response to late summer light reduction (Spicer 2003). Coupled with an apparent absence or low distribution of evergreen plants, the floodplain would have remained saturated for many months. As high water tables and high sediment influx are adverse to deep-rooting plants, the composition of the floodplain flora was likely influenced by tolerance thresholds corresponding to autogenic factors not applicable to bordering uplands. Elevation is thus an important factor in the climate reconstructions.

The Late Cretaceous climate of central and southern Alaska may have been largely frost-free

at low elevations and supported a more diverse flora that included temperature-sensitive taxa during warm intervals while mountainous regions supported hardier, better adapted, but possibly less diverse plant groups. A diverse and superbly preserved flora from non-marine interbeds of the mostly marine Chignik Formation on the Alaska Peninsula, southwestern Alaska, was described by Hollick (1930). The Alaska Peninsula is part of the Peninsula Terrane, the western subterrane of the Wrangellia Composite Terrane. The Chignik Formation was deposited on the shelf and shoreline of a fore-arc basin and includes up to 600 m (at the type section at Chignik Bay) of coastal-plain and alluvial fan sedimentary rocks (Mancini et al., 1978; Detterman et al., 1996) which also yield dinosaur footprints (Fiorillo and Parrish, 2004). Non-marine palynomorphs and a molluscan fauna indicate a late Campanian to early Maastrichtian age (Mancini et al., 1978; Detterman et al., 1996). Thus, the Chignik flora may be correlative to the Sable Mountain flora.

A high diversity is thought to indicate a warm and humid climate (Golovneva and Herman, 1998). The Chignik florule as described by Hollick (1930) from six different collections made at the beginning of the 20th century between Chignik Bay and Pavlof Bay on the Alaska Peninsula in southwest Alaska includes the cycadophyte *Nilssonia serotina* Heer, a small leaf ginkgophyte, and a significant number of dicot angiosperm morphotypes including thermophilic taxa such as *Cupanites*, '*Cornus*,' and magnoliid and lauroid forms in addition to the cupressaceous conifer genera *Cephalotaxopsis*, *Sequoia*, *Metasequoia* and possible *Glyptostrobus*. The taxonomy is in need of revision. Many of Hollick's (1930) taxonomical designations represent morphological variations of a single genus and many of the familial and generic designations are invalid by the standards of current plant systematics. However, it is evident that the dicot angiosperm diversity is significantly greater than that of the Sable Mountain flora. For a comparison, we constrained 34 angiosperm morphotypes from the figured and described specimens of the Chignik florule. The largest collection, the T. W. Stanton collection from Chignik Bay, comprises 13 morphotypes; the proportion of entire leaf blades is 31%. This compares to about 10% for the Sable Mountain flora.

If the T. W. Stanton collection were to represent the full angiosperm diversity for the time of deposition, an LMA application using the regression equation of Wolfe (1979) would indicate a MAT estimate of 11° C for the florule at Chignik Bay. Additional entire-margined leaves are described by Hollick (1930) from the other five collections, and if any two or all of these are coeval with Chignik Bay specimens, the MAT estimate could rise to 13° C. More data are needed, however, to support this supposition.

It is not clear how the fossil localities compare with those of the lower Cantwell Formation. The alluvial fan interpretation for the coarser-grained non-marine facies of the Chignik Formation (Mancini et al., 1978) suggests a mountainous terrain bordering a narrow coastal plain consistent with an active plate margin. Thus, aspects of the depositional system may have been similar to that of the lower Cantwell Formation. The paleolatitudinal position of the Chignik Formation is poorly constrained from paleomagnetic analyses of the Chignik, and the more distally deposited Hoodoo and overlying late Paleocene Tolstoi formations, all of which yielded anomalously low and inconsistent paleolatitude results (Stone et al., 1982; Hillhouse and Coe, 1994). The Cretaceous paleoposition of the Alaska Peninsula remains controversial because of the difficulty in predicting the amount and timing of northward translation of outboard terranes along the Tintina and Denali fault systems during the late Cretaceous and earliest Tertiary and because of a possible 40 – 50° counterclockwise rotation of southern and southwestern Alaska during early Tertiary time (Hillhouse and Coe, 1994; Till et al., 2007b). However, a relatively high paleolatitude can be assumed from 2 well-constrained paleomagnetic sites located in relative proximity on either side of the late Mesozoic terrane boundary: Latest Cretaceous volcanic rocks on Hagemester Island (paleolatitude 65° ± 4° N) and near Lake Clark, located on the northern Peninsula Terrane ~350 km to the northeast (paleolatitude 63° ± 9° N). The similarity of the results indicates that the two sites have not moved significantly along meridional lines relative to each other within error since 66 Ma (Hillhouse and Coe, 1994). Thus, if the age of the Chignik florule is indeed coeval with the Sable Mountain florule, the apparent MAT differences may indicate a stronger

polar temperature gradient than previously thought.

Evidence for a warm climate at a relatively high latitude may be correlative with proximity to an ocean. Both the Prince Creek Formation and the Chignik Formation depositional environments may have been warmed by a maritime climate (Fiorillo, 2008; Fiorillo et al., 2010). Frakes (1999) and Zakharov et al. (1999, 2011) independently suggest a warm period during the latest Campanian. Frakes (1999) calculated sea surface temperatures between 15 and 20° C at paleolatitudes ranging from 35 to 65° N. Zakharov et al. (2011) obtained seawater temperatures of 19.4 – 25.5° C for the latest Campanian from oxygen isotope ratios of aragonitic ammonoid and inoceramid bivalve shells from the Matanuska Formation of southern Alaska. The many marine tongues of the Chignik Formation and a coal-bearing member suggest that it was deposited in a paralic setting. Thus, the high proportion of entire-margined woody dicot leaves in the Chignik flora was likely a result of warm sea surface temperatures.

By the earliest Maastrichtian, sea surface temperatures had declined to 10 to 15° C at high latitudes (Frakes, 1999; Zakharov et al., 2011) and continued to fall to 7° C at Sakhalin Island as determined by Zakharov et al. (1999) using brachiopods and ammonite carbon and oxygen isotope paleotemperature estimates. Therefore, the high diversity of the Chignik flora, including its thermophilic connotation, is more compatible with a latest Campanian age and climate optimum. Moreover, a magnoliid taxon ("*Magnolia*" *palaeauriculata* Hollick) described by Hollick (1930) from the Chignik Formation has also been identified from a basal and therefore possibly older section of the Cantwell Formation in addition to cycadophyte and ginkgophyte fossil material (Alaska Paleontological Database, 2014).

In contrast, the less thermophilic Sable Mountain floral composition was likely influenced by the cooler climate of the early Maastrichtian. The retreat of the CWIS could also have led to cooler inland temperatures reducing poleward heat transfer and increasing continentality. This could explain the larger proportion of toothed leaf margins and lower angiosperm diversity, which correlate with cooler temperatures (Wolfe, 1987; Wolfe and Spicer, 1999; Spicer and Herman, 2010). To solve the

puzzle posed by the richness of the Chignik florule, better chronostratigraphic control is required for the Chignik Formation. As long as refined age constraints are lacking, we must conclude that the two floras represent two very different phytogeographic provinces, one with a cool temperate continental flora and the other with a warm temperate maritime-influenced flora. The strong temperature gradient implied by the paleobotanical data for the southern half of ancient Alaska, however, is inconsistent with the predicted more shallow latitudinal temperature gradient for the Maastrichtian (see Spicer and Herman, 2010).

Implications for Paleoecology and Paleoenvironment

The new U–Pb zircon ages and paleolatitude assessments validate the comparisons and correlations of fossil and stratigraphic data, both intra- and extra-basinal. Age differences could be an explanation for observed differences in the floral compositions. To-date, the Sable Mountain flora comprises 42 species; the Chignik flora (as described by Hollick, 1930) comprises an estimated 50 species, yet the two megaflores have few genera in common. Shared taxa are the fern genera *Cladophlebis*, the conifer genera *Cephalotaxopsis*, *Metasequoia* and possibly *Glyptostrobus* and the angiosperm genera *Trochodendroides*, *McClintockia*, and *Celastrinites*. Conifer diversity appears to be greater in the Sable Mountain flora. Angiosperm diversity is higher in the Chignik flora; yet, it lacks long-ranging taxa, most notably menispermoids and platanoids and newer taxa such as *Corylites*. Platanoids are an important taxonomic group in the Cantwell flora, the more southerly deposited Kundur Formation (Van Itterbeeck et al., 2005; Golovneva et al., 2008), and the Koryak and Kakanaut formations (Golovneva et al., 2008; Moiseeva, 2008; Krassilov et al., 2009).

Perhaps as a result of the early Maastrichtian cooling and greater continentality including along the Beringian land bridge, hamamelidaceous and betulaceous dicot taxa and several different monocot taxa become more dominant, replacing platanoid groups. For example, *Corylites beringianus* and other betulaceous leaves, and linear (*Phragmites*- and *Typha*-like) and broad-leaved (*Potamogeton*- and *Alisma*-like) monocots appear in the lower Cantwell Formation by the earliest Maastrichtian and in the

Far North by the mid- to late Maastrichtian where they remain dominant throughout the Paleocene in the northeast Asian floras and the Danian–Selandian Sagwon flora of northern Alaska (Sagavanirktok river basin) (Golovneva, 2000b; Moiseeva, 2008; Moiseeva et al., 2009; Herman et al., 2009; Krassilov et al., 2009). The floristic data from the lower Cantwell Formation contradict the hypothesis that late Cretaceous plants radiated in, and spread from, northeastern Russia to North America. A major floral reorganization, similar to the one occurring at high latitudes at the early Maastrichtian boundary, is not observed at the K/T boundary in the Beringian realm (Herman et al., 2009; Krassilov et al., 2009) likely because the succeeding low diversity boreal flora was well-adapted to short seasons and temperature variability.

One intriguing attribute of the Sable Mountain florule and other floral assemblages of the lower Cantwell Formation (Wolfe and Wahrhaftig, 1970; Wright, unpublished data) is the co-occurrence of ferns, sphenophytes, conifers, and dicot and monocot angiosperms all evidently having grown in close proximity. Ten to possibly twelve conifer genera were reported. These are c.f. *Pityophyllum*, *Cephalotaxopsis*, *Tumion*, *Taxodium*, *Metasequoia*, possible *Parataxodium*, *Glyptostrobus*, *Sequoia*, *Larix*, *Pinus*, *Picea*, and specimens assignable to *Thuja* or *Mesocyparis*. Except for the latter, all of these occur at Sable Mountain. This great conifer diversity is similar to what Golovneva et al. (2008) and Herman et al. (2009) report from the Kundur and Taipinglinchang formations of the Amur region and might suggest similar geographic attributes. The mix of arboreal and non-arboreal taxa shows that edaphic conditions were frequently changing. This could be the result of infrequent and uneven deposition. For example, in his study on alluvial fan depositional processes, Bull (1977) writes that vegetation has an important role in alluvial fan deposition and suggests that lush low-growing vegetation could have slowed sheet flow currents resulting in rapid sediment accumulation on the alluvial fan slope. Consequently, floodplain forests remained immature, providing room for invaders.

Unlike the Sable Mountain flora, the Chignik flora does not appear to contain relict angiosperm genera. Possibly, the Arctic provided niches for

early late Cretaceous taxa that had gradually migrated north. For example, very large leaves of *Pseudoprotophyllum* and *Menispermites* were recovered from the base to mid-section at Sable Mountain in deposits that we interpret to be of late Campanian age. Higher in our section, in inferred Maastrichtian strata, leaf size is notably reduced for both taxa. Hollick (1930) described several specimens of *Pseudoprotophyllum* from the Cenomanian (and Turonian?) Melozi Formation of the Yukon River Valley in west-central Alaska that are now considered to be synonyms of *Pseudoprotophyllum boreale* (Dawson) Hollick, emend. Golovneva (Golovneva, 2009) and include very large leaf forms. *Pseudoprotophyllum boreale* (or synonyms) were described from Cenomanian to Coniacian fossil localities throughout northern and northeastern Asia, the North Slope of Alaska, and Northwestern Canada (Hollick, 1930; Herman, 2007; Golovneva, 2009), indicating it was widely distributed at a time when platanoid groups were highly diversified (Golovneva, 2009). *Pseudoprotophyllum* is apparently absent from the Maastrichtian Kakanaut and Koryak floras and the Chignik flora, but has been observed in a concretion from Paleocene strata on the North Slope of Alaska (Peter Flaig and Dolores van der Kolk, pers. comm.) and in early Tertiary beds of Axel Heiberg Island in the Canadian Arctic Archipelago (McIver and Basinger, 1999). The fact that such long-ranging species or relict species occur in the Cantwell Formation and in the High Arctic during the early Tertiary indicates that inland basins like the Cantwell basin could have served as temporary refugia during the warm stage of the late Campanian.

Leaves of non-woody angiosperms are rarely preserved in the megafloral record because they wilt on the plant and wither. Evidence for the presence of herbaceous plants therefore comes from pollen records. A relatively diverse angiosperm pollen flora recorded from the Prince Creek Formation (Frederiksen, 1991; Brandlen, 2008; Flaig et al., 2013) is poorly matched by the plant megafossil record (Spicer and Parrish, 1990a; Spicer and Herman, 2010). As a consequence, Spicer and Herman (2010) suggested the presence of herbaceous plants which would have left no foliar record. Additional evidence for herbaceous plant growth comes from root casts. Perennial root structures (rhizomes, bulbs, tubers;

Fig. 9), from which new shoots grow, allow plants to reproduce asexually. Their ability to store nutrients, food, and water and enter dormancy protects them against drought, lack of nutrients, a short growing season, and foraging (Shewry, 2003; Bell, 2008; Gómez-García et al., 2009). This provides for more regulated growth and a competitive advantage in places where adverse growing conditions prevail (Gómez-García et al., 2009). Botanical evidence seems to suggest that perennating plants are more successful at colonizing environmental niches marked by extremes (Geneve, 2006).

Tubers form by thickening along a portion of a root. Although apparently rare and probably of little taxonomic value, we report on two specimens resembling casts of tubers (Fig. 9) that indicate that some, possibly herbaceous plants entered dormancy at the onset of the low-level light season or a drought period. The significance of the find is appreciated, because it suggests that a) grounds were basically frost-free, b) growing conditions were periodically unfavorable for some plants, and c) the tubers could have provided food for ground-dwelling mammals and possibly for herbivorous dinosaurs. Selection for asexual reproduction may have been an adaptive response to short growing seasons and periodically adverse growing conditions.

As with the paleobotanical data, helpful taxonomic information for vertebrate track-makers can be learned from coeval fossil-bearing beds of other high-latitude localities. In southern Alaska, an ankylosaur skull was excavated from Campanian–Maastrichtian? Matanuska Formation (Gangloff, 1995; Fiorillo, 2006). In northern Alaska, the teeth, bones, and several skulls of small and large theropods, troodontids (e.g., *Troodon formosus*; Fiorillo and Gangloff, 2000; Fiorillo et al., 2009b), hypsilophodontids, dromaeosaurids, ornithomimids, ceratopsids (e.g., *Pachyrhinosaurus perotorum*) and hadrosaurids (e.g., *Edmontosaurus*) have been excavated from the world-renowned early Maastrichtian bonebeds of the Prince Creek Formation along the Colville River on the North Slope (Rich et al., 2002; Fiorillo, 2006; Fiorillo et al., 2009b; Fiorillo et al., 2010; Gangloff and Fiorillo, 2010).

From northeastern Russia, Godefroit et al. (2009) report on a highly diverse fossil bone fauna

from a late Maastrichtian section of the Kakanaut Formation. These authors list teeth and fragmentary bone remains that can be tentatively identified to basal ornithopods, theropods, troodontids (including *Troodon cf. formosus*), dromaeosaurids, ceratopsids (ankylosaurs) and hadrosaurids. The close taxonomic association with the fauna of the Prince Creek Formation suggests similar food sources and supports the hypothesized bidirectional exchange along a surmised continental bridge (Fiorillo, 2008; Godefroit et al., 2009). The argument that dinosaurs resided year-round is strengthened by abundant skeletal remains of juvenile hadrosaurs and egg shell fragments (Golovneva, 2000a; Clemens and Nelms, 1993; Godefroit et al., 2009; Gangloff and Fiorillo, 2010; Fiorillo et al., 2010) in combination with *Edmontosaurus* bone histology data (Chinsamy et al., 2012). Krassilov et al. (2009) suggest that herbivorous dinosaurs fed on non-deciduous freshwater plants. The latest Campanian and Maastrichtian megafloral record of Eurasia and North America contains diverse monocots and dicot angiosperms that are thought to have formed aquatic communities. Their adaptive radiation occurred seemingly parallel in the northern hemisphere and, in a mutual dependence, may have corresponded closely with the expansion of dinosaurs into the boreal realm (Krassilov et al., 2009).

CONCLUSIONS

New numerical ages of 71.5 ± 0.9 Ma and 71.0 ± 1.1 Ma for the non-marine lower Cantwell Formation at Sable Mountain in Denali National Park, Alaska, establish a concise temporal framework for the Sable Mountain deposits, provide stratigraphic control, and enable valid biostratigraphic and geographic correlations. The new ages place dinosaur, pterosaur and bird footprints, and the Sable Mountain florule into the late Campanian and earliest Maastrichtian and approximate the boundary between these two important epochs. Early Maastrichtian lower Cantwell strata at Sable Mountain are the same age as the dinosaur bone-bearing beds of the Prince Creek Formation on the North Slope of Alaska which may serve as an analogue for ecological reconstructions of the lower Cantwell Formation. Dating of the bird ichnotaxa provides correlation with both Northern Asian and North American faunas supporting the

concept of a Panberingian land connection during a period of global warmth. The Sable Mountain section may also be correlative to the Chignik Formation of southwestern Alaska; however, the latter bears a warm temperate flora while the Sable Mountain flora is characterized as a cool temperate flora, suggesting that the two floras represent different phytogeographic provinces located in relative proximity. The Cantwell flora is characteristic of the polar broad-leaved deciduous forest that was widely distributed across the Arctic in the Late Cretaceous and early Tertiary and was highly adapted to withstand adverse conditions. Several taxonomic groups resemble those described from the mid to late Maastrichtian Koryak flora of the Othotsk-Chukotka volcanogenic belt in northeastern Russia. The fluvial valleys that supported these two floras were similarly surrounded by dissected uplands. The late Campanian to early Maastrichtian age for the Cantwell strata negates the idea put forward by previous workers that the Koryak flora radiated and expanded from Russia to the North Slope of Alaska. The morphological similarities between the Asian and North American taxa support the supposition of floristic and faunal exchanges across the Beringian landbridge, but the timing remains poorly constrained. We argue that the diversity and structure of different phytogeographic regions is closely linked to the migration of faunal groups in a mutual dependence and to local environmental and geographic factors.

Age relationships between outcrops at Sable Mountain, Polychrome Mountain and Double Mountain in Denali National Park and Preserve reveal that complexly distributed lithofacies are correlative at least in part and are the result of point-sourcing and local controls on deposition related to an alluvial fan depositional system and adjacent environments. Debris flows, rapid basin center subsidence, and a high sediment supply from synchronously uplifted basin margins are consistent with an inferred location in an orogenic belt.

ACKNOWLEDGMENTS

This research was generously funded by BP, the Alaska Geological Society and the National Park Service. We also thank the Denali National Park Administration, especially Paul Anderson, Philip

Hooge, Lucy Tyrrell, Linda Stromquist, Denny Capps, and the late Phil Brease for supporting this research and for much appreciated logistical support. Bernie Housen of the University of Western Washington and his graduate students are thanked for analyzing and measuring magnetic vectors on our paleomagnetic sample. Furthermore, we thank Anne Pasch for her time and willingness to review this manuscript and much appreciate her comments. Sarah Fowell is acknowledged for her time in the field and her professional advice. Equally so, we are much indebted to field assistants Eric Brandlen, Ephy Wheeler, Anja Kircher, Todd Jacobus, Joshua Payne, Colby Wright and Anna Liljedahl, and to Maciej Slivinski for help in the laboratory.

REFERENCES

- Alaska Paleontological Database, 2014. [<http://www.alaskafossil.org>] Last accessed January 24, 2014.
- Bacon, C.R., Foster, H.L., and Smith, J.G., 1990. Rhyolitic Calderas of the Yukon-Tanana Terrane, East-central Alaska: Volcanic Remnants of a Mid-Cretaceous Magmatic Arc. *Journal of Geophysical Research* 95, B13, 21-451–21-461.
- Bell, A.D., 2008. *Plant Forms: An Illustrated Guide to Flowering Plant Morphology*. Timber Press Portland–London, 432 p.
- Bell, W.A., 1949. Uppermost Cretaceous and Paleocene floras of western Alberta. *Geological Survey of Canada Bulletin* 13, 231 p.
- Benowitz, J.A., Layer, P.J., Armstrong, P., Perry, S.E., Haeussler, P.J., Fitzgerald P.G., and VanLaningham, S., 2011. Spatial variations in focused exhumation along a continental-scale strike-slip fault: The Denali Fault of the eastern Alaska Range. *Geosphere* 7 (3), 455–467, DOI: 10.1130/GES00589.1.
- Benowitz, J.A., Haeussler, P.J., Layer, P.W., O’Sullivan, P.B., Wallace, W.K., and Gillis, R.J., 2012. Cenozoic tectono-thermal history of the Tordrillo Mountains, Alaska: Paleocene–Eocene ridge subduction, decreasing relief, and late Neogene faulting. *Geochemistry, Geophysics, Geosystems*, 13, Q04009, DOI: 10.1029/2011GC003951.
- Benowitz, J.A., Haeussler, P.J., Layer, P.W., O’Sullivan, P.B., Wallace, W.K., and Gillis, R.J., 2012. Cenozoic tectono-thermal history of the Tordrillo Mountains, Alaska: Paleocene–Eocene ridge subduction, decreasing relief, and late Neogene faulting. *Geochemistry, Geophysics, Geosystems*, 13, Q04009, DOI: 10.1029/2011GC003951.
- Billingsley, R.L. 1977. The Cantwell Formation (Paleocene) as a possible offset feature along the Denali Fault, central Alaska Range, Alaska. [M.S. Thesis], University of Wisconsin, Madison, Wisconsin, 86 p.
- Blair T. C. and McPherson, J.G., 1994. Alluvial fans and their natural distinction from rivers based on morphology, hydraulic processes, sedimentary

- processes, and facies assemblages. *Sedimentary Geology* A64 (3), 450–489.
- Bradley, D.C., Kusky, T.M., Haeussler, P.J., Rowley, D.C., Goldfarb, R.J., and Nelson, S.W., 2003. Geologic signature of early Tertiary ridge subduction in the accretionary wedge, forearc basin, and magmatic arc of south-central Alaska. In: Sisson, V.B., Roeske, S., and Pavlis, T.L. (eds.) *Geology of a Transpressional Orogen Developed during a Ridge–Trench Interaction along the North Pacific Margin*. Geological Society of America Special Paper 371, 19–50.
- Braman, D.R. and Sweet, A.R., 2012. Biostratigraphically useful Late Cretaceous–Paleocene Terrestrial palynomorphs from the Canadian Western Interior Sedimentary Basin. *Palynology* 36 (1), 8–35. DOI:10.1080/01916122.2011.642127.
- Brandlen, E., 2008. Paleoenvironmental reconstruction of the Late Cretaceous (Maastrichtian) Prince Creek Formation, near the Kikak Tegoseak dinosaur quarry, North Slope, Alaska. [Unpublished M.S. Thesis], University of Alaska Fairbanks, Fairbanks, Alaska, 225 p.
- Bull, W.B., 1977. The alluvial fan environment. *Progress in Physical Geography* 1, pp. 222–270.
- Capps, S.R., 1919. The Kantishna Region, Alaska. *United States Geologic Survey Bulletin* 687, 30–45.
- Capps, S.R., 1940. The Geology of the Alaska Railroad region. *United States Geologic Survey Bulletin* 907, 201 p.
- Chinsamy, A., Thomas, D.B., Tumarkin-Deratzian, A.R., and Fiorillo, A.R., 2012. Hadrosaurs were perennial polar residents. *The Anatomical Record* 295, 610–614.
- Chew, D.M. and Donelick, R.A., 2012. Combined apatite fission track and U–Pb dating by LA–ICP–MS and its application in apatite provenance analysis. In: Sylvester, P., *Quantitative Mineralogy and Microanalysis of Sediments and Sedimentary Rocks*. Mineralogical Association of Canada Short Course 42, St. John's, Newfoundland and Labrador, 219–247.
- Clemens, W.A., 1994. Continental vertebrates from the Late Cretaceous of the North Slope, Alaska. In: Thurston, D. K. and Fujita, K. (eds.) 1992 *International Conference on Arctic Margins, Proceedings*. United States Department of Interior Mineral Management Service, Outer Continental Shelf Study MMS 94-0040, pp. 395–398.
- Clemens, W.A. and Nelms, L.G., 1993. Paleocological implications of Alaskan terrestrial vertebrate fauna in latest Cretaceous time at high paleolatitudes. *Geology* 21, 503–506.
- Cole, R.B., Ridgway, K.D., Layer, P.W., and Drake, J., 1999. Kinematics of basin development during the transition from terrane accretion to strike-slip tectonics, Late Cretaceous-early Tertiary Cantwell Formation, south-central Alaska. *Tectonics* 18 (6), 1224–1244, DOI: 10.1029/1999TC900033.
- Cole, R.B., Nelson, S.W., Layer, P.W., and Oswald, P.J., 2006. Eocene volcanism above a depleted slab window in southern Alaska. *Geological Society of America Bulletin* 118 (1/2), 140–158, DOI: 10.1130/B25658.1.
- Cole, R.B., Layer, P.W., Hooks, B., Cyr, A., and Turner, J., 2007. Magmatism and deformation in a terrane suture zone south of the Denali Fault, northern Talkeetna Mountains, Alaska. In: Ridgway, K.D., Trop, J.M., Glen, J.M., and O'Neil, J.M. (eds.) *Tectonic Growth of a Collisional Continental Margin: Crustal Evolution of Southern Alaska*. Geological Society of America Special Paper 431, 447–506, DOI: 10.1130/2007.2431(19).
- Conrad, J.E., McKee, E.H., and Turrin, B.D., 1992. Age of Tephra Beds at the Ocean Point Dinosaur Locality, North Slope, Alaska, based on K–Ar and $^{40}\text{Ar}/^{39}\text{Ar}$ analyses. *United States Geological Survey Bulletin* 1990-C, C1–C12.
- Corfu, F., 2013. A century of U–Pb geochronology: The long quest towards concordance. *Geological Society of America Bulletin* 125 (1–2), 33–47, DOI: 10.1130/B30698.1.
- Csejtey, B., Mullen, M.W., Cox, D.P., and Stricker, G.D., 1992. Geology and geochronology of the Healy quadrangle, south-central Alaska. *United States Geological Survey Miscellaneous Investigation Series I-1961*, 63 p., 2 plates, scale 1:250,000.

- Detterman, R.L., Case, J.E., Miller, J.W., Wilson, F.H., Yount, M.E., 1996. Stratigraphic framework of the Alaska Peninsula. United States Geological Survey Bulletin 1969-A, 1–74.
- Dickinson, W.R., Beard, L.S., Brackenridge, G.R., Erjavec, J.L., Ferguson, R.C., Inman, K.F., Knepp, R.A., Lindberg, F.A., and Ryberg, P.T., 1983. Provenance of North American Phanerozoic sandstones in relation to tectonic setting. *Geological Society of America Bulletin* 94 (2), 222–235.
- Donelick, R.A., O’Sullivan, P.B., and Donelick, M.B., 2010. A Discordia-Based Method of Zircon U-Pb Dating from LA-ICP-MS Analysis of Single Spots. *Smart Science for Exploration and Mining*, v. 1 and 2, p. 276–278.
- Eldridge, G.H., 1900. A reconnaissance in the Sushitna Basin and adjacent territory, Alaska, in 1898. United States Geological Survey 20th Ann. Report, part 7, 1–29.
- Falcon-Lang, H.J., McRhae, R.A., and Czank, A.Z., 2004. Palaeoecology of Late Cretaceous polar vegetation preserved in the Hansen Point Volcanics, NW Ellesmere Island, Canada. *Palaeogeography. Palaeoclimatology. Palaeoecology* 212 (3), 45–64.
- Fiorillo, A.R., 2004. The dinosaurs of Arctic Alaska. *Scientific American* 291 (6), 84–91.
- Fiorillo, A.R., 2006. Review of the dinosaur record of Alaska with comments regarding Korean dinosaurs as comparable high-latitude fossil faunas. *Journal of Paleontological Society of Korea* 22 (1), 15–27.
- Fiorillo, A.R., 2008. Cretaceous dinosaurs of Alaska: Implications for the origins of Beringia. In: Blodgett, R.B., and Stanley, G. (eds.) *The Terrane Puzzle: new perspectives on paleontology and stratigraphy from the North American Cordillera*. Geological Society of America Special Paper 442, 313–326, DOI: 10.1130/2008.442(15).
- Fiorillo, A.R., and Gangloff, R.A., 2000. Theropod teeth from the Prince Creek Formation (Cretaceous of Northern Alaska, with speculations on Arctic Dinosaur paleoecology. *Journal of Vertebrate Paleontology* 20 (4), 675–682.
- Fiorillo, A.R. and Gangloff, R.A., 2001. The caribou migration model for Arctic hadrosaurs (Ornithischia: Dinosauria): a reassessment. *Historical Biology* 15, 323–334.
- Fiorillo, A.R. and Parrish, J.T., 2004. The first record of a dinosaur from southwestern Alaska. *Cretaceous Research* 25, 453–458.
- Fiorillo, A.R. and Adams, T., 2012. A therizinosaur track from the lower Cantwell Formation (Upper Cretaceous) of Denali National Park, Alaska. *Palaios* 27, 395–400, DOI: 10.2110/palo.2011.p11-083r.
- Fiorillo, A.R. and Tykoski, R.S., 2012. A new species of the centrosaurine ceratopsid *Pachyrhinosaurus* from the North Slope (Prince Creek Formation: Maastrichtian) of Alaska. *Acta Palaeontologica Polonica* 57 (3), 561–573.
- Fiorillo, A.R., McCarthy, P.J., Breithaupt, B.H., and Brease, P.F., 2007. Dinosauria and fossil aves footprints from the lower Cantwell Formation (Latest Cretaceous), Denali National Park and Preserve. *Alaska Park Science* 6, 41–43.
- Fiorillo, A.R., Hasiotis, S.T., Kobayashi, Y. and Tomsich, C.S., 2009a. A pterosaur manus track from Denali National Park, Alaska Range, Alaska, United States. *Palaios* 24, 466–472, DOI: 10.2110/palo.2008.p08-129r.
- Fiorillo, A.R., Tykoski, R.S., Currie, P.J., McCarthy, P.J., and Flaig, P., 2009b. Description of Two Partial *Troodon* Braincases from the Prince Creek Formation (Upper Cretaceous), North Slope Alaska. *Journal of Vertebrate Paleontology* 29, 178–187.
- Fiorillo, A.R., McCarthy, P.J., and Flaig, P.P., 2010. Taphonomic and sedimentologic interpretations of the dinosaur-bearing upper Cretaceous strata of the Prince Creek formation, Northern Alaska: Insights from an ancient high-latitude terrestrial ecosystem. *Palaeogeography. Palaeoclimatology. Palaeoecology* 295 (3), 376–388, DOI: 10.1016/j.palaeo.2010.02.029.
- Fiorillo, A.R., Hasiotis, S.T., Breithaupt, B.H., Kobayashi, Y., and McCarthy, P.J., 2011. Bird tracks from the Upper Cretaceous Cantwell Formation of Denali National Park, Alaska, USA: a new perspective on ancient northern polar vertebrate biodiversity. *Journal of Systematic Paleontology* 9 (1), 33–49, DOI: 10.1080/14772019.2010.509356.

- Fiorillo A.R., Contessi, M., Kobayashi, Y., and McCarthy, P.J., 2014. Theropod tracks from the lower Cantwell Formation (Upper Cretaceous) of Denali National Park, Alaska, USA with comments on theropod diversity in an ancient, high-latitude terrestrial ecosystem. In: Lockley, M. and Lucas, S.G. (eds.) *Tracking Dinosaurs and other tetrapods in North America*. New Mexico Museum of Natural History and Science, pp. 429-439.
- Flaig, P.P., 2010. Depositional environments of the Late Cretaceous (Maastrichtian) dinosaur-bearing Prince Creek Formation: Colville River region, North Slope, Alaska. [Unpublished Ph.D. Dissertation], University of Alaska Fairbanks, Fairbanks, Alaska, 311 p.
- Flaig, P.P., McCarthy, P.J., and Fiorillo, A.R., 2013. Anatomy, evolution and paleoenvironmental interpretation of an ancient Arctic coastal plain: Integrated paleopedology and palynology from the Upper Cretaceous (Maastrichtian) Prince Creek Formation, North Slope, Alaska, USA. In: Driese, S.G. and Nordt, L.C. (eds) *New Frontiers in Paleopedology and Terrestrial Paleoclimatology*. SEPM Special Publication 104, 179–230.
- Foster, H.L. and Igarashi, Y., 1990. Fossil pollen from non-marine sedimentary rocks of the eastern Yukon-Tanana region, east-central Alaska. In: Dover, J.H. and Galloway, J.P. (eds.) *Geologic Studies in Alaska by the United States Geological Survey in 1989*. United States Geological Survey Bulletin 1946, 11–20.
- Foster, H.L., Keith, T.E.C., and Menzie, W.D., 1994. The geology of the Yukon Tanana area of east-central Alaska. In: Plafker, G. and Berg, H.C. (eds.) *The Geology of Alaska*. Boulder, Colorado, Geological Society of America. *The Geology of North America*, Vol. G-1, pp. 205–214.
- Frakes, L.A., 1999. Estimating global thermal state from Cretaceous sea surface and continental temperature data. In: Barrera, E. and Johnson, C.C. (eds.) *Evolution of the Cretaceous Ocean–Climate System*. Geological Society of America Special Paper 332, 49–57.
- Frederiksen, N.O., 1991. Pollen zonation and correlation of Maastrichtian marine beds and associated strata, Ocean Point dinosaur locality, North Slope, Alaska. United States Geological Survey Bulletin 1990-E, E1–E24, 7 plates.
- Gangloff, R.A., 1995. *Edmontonia* sp., the first record of an ankylosaur from Alaska. *Vertebrate Paleontology* 15 (1), 195–200.
- Gangloff, R.A. and Fiorillo, A.R., 2010. Taphonomy and paleoecology of a bonebed from the Prince Creek Formation. *Palaios* 25, 299–317.
- Geneve, R.L., 2006. Alternative strategies for clonal plant reproduction. *Combined Proceedings International Plant Propagators' Society* 56, pp. 269-273.
- Gilbert, W.G. and Redman, E., 1975. Geologic map and structure sections of Healy C-6 Quadrangle, Alaska: Alaska Division of Geological and Geophysical Surveys Open-File Report 80, 1 sheet, scale 1:40,000.
- Gilbert, W.G., Ferrell, V.M., and Turner, D.L., 1976. The Teklanika Formation—A new Paleocene volcanic formation in the central Alaska Range. Alaska Division of Geological and Geophysical Surveys Geologic Report 47, 16 p.
- Godefroit, P., Golovneva, L., Shczepetov, S., Garcia, G., and Alekseev, P., 2009. The last polar dinosaurs: High diversity of latest Cretaceous arctic dinosaurs in Russia. *Naturwissenschaften* 96, 495–501.
- Golovneva, L.B., 1994. The flora of the Maastrichtian-Danian deposits of the Koryak Uplands, Northeast Russia. *Cretaceous Research* 15 (1), 89–100.
- Golovneva, L.B., 2000a. Maastrichtian Climate in the Northern Hemisphere. *Geological Society of London Special Publication* 181, 43–54.
- Golovneva, L.B., 2000b. Aquatic plant communities at the Cretaceous-Palaeogene boundary in northeastern Russia. *Acta Paleobotanica* 42 (2), 139–151.
- Golovneva, L.B., 2009. The Morphology, Taxonomy, and Occurrence of the Genus *Pseudoprotophyllum* Hollick (Platanaceae) in Late Cretaceous Floras of Northern Asia. *Paleontological Journal* 43 (10), 1230–1244.
- Golovneva, L.B. and Herman, A.B., 1998. Regularities in the Late Cretaceous flora evolution. *Stratigraphy and Geological*

- Correlation 6 (6), 537–549.
- Golovneva, L. B., Sun, G., and Bugdaeva, E. V., 2008. Campanian Flora of the Bureya River Basin (Late Cretaceous of the Amur River region). *Paleontological Journal* 42 (5), 554–567.
- Gómez-García, D., Azorín, J., and Aguirre, A.J., 2009. Effects of small-scale disturbances and elevation on the morphology, phenology and reproduction of a successful geophyte. *Journal of Plant Ecology* 2 (1), 13–20, DOI: 10.1093/jpe/rtp003.
- Hampton, B.A., Ridgway, K.D., O’Neill, J.M., Gehrels, G.E., Schmidt, J., and Blodgett, R.B., 2007. Pre-, syn-, and post-collisional stratigraphic framework and provenance of Upper Triassic–Upper Cretaceous strata in the northwestern Talkeetna Mountains, Alaska. In: Ridgway, K.D., Trop, J.M., Glen, J.M., and O’Neil, J.M. (eds.) *Tectonic Growth of a Collisional Continental Margin: Crustal Evolution of Southern Alaska*. Geological Society of America Special Paper 431, 401–438, DOI: 10.1130/2007.2431(16).
- Hampton, B.A., Ridgway, K.D., and Gehrels, G.E., 2010. A detrital record of Mesozoic island arc accretion and exhumation in the North American Cordillera: U–Pb geochronology of the Kahiltna basin, southern Alaska. *Tectonics* 29 TC 4015, 1–21, DOI: 10.1029/2009TC002544.
- Harris, J.D., Johnson, K.R., Hicks, J., and Tauxe, L., 1996. Four-toed theropod footprints and a paleomagnetic age from the Whetstone Falls Member of the Harebell Formation (Upper Cretaceous: Maastrichtian), northwestern Wyoming. *Cretaceous Research* 17, 381–401.
- Hasiotis, S. T., 2002. Continental Trace Fossils. *SEPM Short Course Notes* 51, 132 p.
- Hasiotis, S.T., Fiorillo, A.R., Kobayashi, Y., and Brease, P., 2009. Preliminary report on the microbial, invertebrate, and vertebrate trace fossils from Denali National Park and Preserve, Alaska: Insights into the biodiversity of a polar ecosystem. *Geological Society of America Abstracts with Programs* 41 (7), p. 162.
- Hasiotis, S.T., Fiorillo, A.R., and Kobayashi, Y., 2011. Invertebrate and vertebrate ichnofossils from the lower part of the Upper Cretaceous Cantwell Formation, Denali National Park, Alaska: Insights into the paleoenvironments, paleo-hydrology and paleoclimate of high-latitude continental paleoecosystems: AAPG Pacific Section Program with Abstracts, Anchorage Alaska, May 6–14, 2011, p. 60.
- Hay, W.W., 2008. Evolving ideas about the Cretaceous climate and ocean circulation. *Cretaceous Research* 29, 725–753, DOI: 10.1016/j.cretres.2008.05.025.
- Herman, A.B., 2007. Comparative Paleofloristics of the Albian–Early Paleocene in the Anadyr–Koryak and North Alaska Subregions. Part 3: Comparison of Floras and Floristic Changes across the Cretaceous–Paleogene Boundary. *Stratigraphy and Geological Correlation* 150 (5), 512–524.
- Herman, A.B. and Spicer, R.A., 1995. Latest Cretaceous Flora of Northeastern Russia and the Terminal Cretaceous Event. *Paleontological Journal* 29 (2), 22–35.
- Herman, A.B., Akhmetiev, M.A., Kodrul, M., Moiseeva, M.G., and Iakovleva, A.I., 2009. Flora Development in Northeastern Asia and Northern Alaska during the Cretaceous–Paleogene Transitional Epoch. *Stratigraphic and Geological Correlation* 17 (1), 79–97.
- Hickman, R.G., 1974. Structural geology and stratigraphy along a segment of the Denali Fault system, central Alaska Range, Alaska. [Ph.D. Dissertation], University of Wisconsin, Madison, 276 p., scale 1:63,360.
- Hickman, R.G. and Craddock C., 1976. Geologic map of the central Healy Quadrangle, Alaska. Alaska Division of Geological and Geophysical Survey Open–File Report AOF-95: 1 p.
- Hickman, R.G., Sherwood, K.W. and Craddock C., 1990. Structural evolution of the early Tertiary Cantwell basin, south-central Alaska. *Tectonics* 9 (6), 1433–1449.
- Hillhouse J.W. and Gromme, C.S., 1982. Limits to northward drift of the Paleocene Cantwell Formation, central Alaska. *Geology* 10, 552–556.
- Hillhouse, J.W. and Coe, R.S., 1994. Paleomagnetic data from Alaska. In: Plafker, G., and Berg, H.C., (eds.) *The Geology of Alaska*. Boulder, Colorado, Geological Society of America. *The Geology of North America Vol. G-1*, pp. 797–812.

- Hollick, A., 1930. The upper Cretaceous floras of Alaska. United States Geological Survey Professional Paper 159, 123 p., 86 plates.
- Hoskin, P.W.O. and Schaltegger, U., 2003. The composition of zircon and igneous and metamorphic petrogenesis. *Zircon* 53, 27–62.
- Imlay R.W. and Reeside, J.B., 1954. Correlations of the Cretaceous formations of Greenland and Alaska: Geological Society of America Bulletin 65, 223–246.
- Jackson, S.J., Whyte, M.A., and Romano, M., 2009. Laboratory-controlled simulations of dinosaur footprints in sand: A key to understanding vertebrate track formation and preservation. *Palaios* 24, 222–238, DOI: 10.2110/palo.2007.p07-070r.
- Jones, D.L., Silberling, N.J., and Coney, P.J., 1983. Tectonostratigraphic and interpretive bedrock geologic map of the Mount McKinley region, Alaska. United States Geological Survey Open-File Report 83–11, scale 1:250,000.
- Kent, D.V. and Irving, E., 2010. Influence of inclination error in sedimentary rocks on the Triassic and Jurassic apparent pole wander path for North America and implications for cordilleran tectonics. *Journal of Geophysical Research* 115, B10103, 1–25, DOI: 10.1029/2009JB007205.
- Krassilov, V.A., Kodrul, T.M., and Maslova, N.P., 2009. Plant systematics and differentiation of species over trans-Beringian land connections including a newly recognized cupressaceous conifer *Ditaxocladus* Guo & Sun. *Bulletin of Geosciences* 85 (1), 95–110.
- Kumar, R., Suresh, N., Sangode, S.J., and Kumaravel, V., 2007. Evolution of the Quaternary alluvial fan system in the Himalayan foreland basin: Implications for tectonic and climatic decoupling. *Quaternary International* 159, 6–20, DOI: 10.1016/j.quaint.2006.08.010.
- Lerbekmo, J.F. and Braman, D.R., 2005. Magnetostratigraphic and palynostratigraphic correlation of late Campanian to early Maastrichtian strata of the Bearpaw and Horseshoe Canyon formations between the CPOG Strathmore corehole and the Red Deer Valley section, Alberta, Canada. *Bulletin of Canadian Petroleum Geology* 53 (2), 154–164.
- Ludwig, K.R., 2003. User's manual for Isoplot 3.00—A geochronological toolkit for Microsoft Excel. Berkeley Geochronology Center Special Publication 4, 71 p.
- Mancini, E.A. Deeter, T.M., and Wingate, F.H., 1978. Upper Cretaceous arc–trench gap sedimentation on the Alaska Peninsula. *Geology* 6, 437–439.
- Markwick, P.J. and Valdes, P.J., 2004. Palaeodigital elevation models for use as boundary conditions in coupled ocean–atmosphere GCM experiments: A Maastrichtian (late Cretaceous) example. *Palaeogeography, Palaeoclimatology, Palaeoecology* 213, 37–63, DOI: 10.1016/j.palaeo.2004.06.015.
- McIver and Basinger, 1999. Early Tertiary floral evolution in the Canadian High Arctic. *Annals of the Missouri Botanical Garden* 86 (2), 523–545.
- Miall, A.D., 2006. *The Geology of Fluvial Deposits: Sedimentary Facies, Basin Analysis and Petroleum Geology*. Springer Verlag Berlin, 389 p.
- Moiseeva, M.G., 2008. New angiosperms from the Maastrichtian of the Amaam Lagoon area, Northeastern Russia. *Paleontological Journal* 42 (3), 313–327.
- Moiseeva, M.G., Herman, A.B., and Spicer, R.A., 2009. Late Paleocene Flora of the Northern Alaska Peninsula: The Role of Transberingian Plant Migrations and Climatic Change. *Paleontological Journal* 43 (10), 1298–1308.
- Moll-Stalcup, E.J., 1994. Latest Cretaceous and Cenozoic magmatism in mainland Alaska. In: Plafker, G., and Berg, H.C. (eds.) *The Geology of Alaska*. Boulder, Colorado, Geological Society of America. *The Geology of North America*, Vol. G-1, pp. 589–619.
- Nokleberg, W.J. and Richter, D.H., 2007. Origin of narrow terranes and adjacent major terranes occurring along the Denali Fault and in the eastern and central Alaska Range, Alaska. In: Ridgway, K.D., Trop, J.M., Glen, J.M.G., and O'Neill, J.M. (eds.) *Growth of a collisional continental margin: Crustal evolution of southern Alaska*. Geological Society of America Special Paper 431, 129–154, DOI: 10.1130/2007.2431(06).
- Nokleberg, W.J., Jones, D.L., and Silberling, N.J.,

1985. Origin and tectonic evolution of the Maclaren and Wrangellia terranes, eastern Alaska Range, Alaska. *Geologic Society of America Bulletin* 96, 1251–1270, DOI: 10.1130/0016-7606(1985)96<1251:OATEOT>2.0.CO;2.
- Nokleberg, W.J., Plafker, G. and Wilson, F.H., 1994. Geology of south-central Alaska. In: Plafker, G., and Berg, H.C. (eds.) *The Geology of Alaska*. Boulder, Colorado, Geological Society of America. *The Geology of North America*, Vol. G-1, pp. 311–366.
- Otto-Bliesner, B.L. and Upchurch, G.R., Jr., 1997. Vegetation-induced warming of high latitudes during the latest Cretaceous. *Nature* 385, 804–807.
- Palaeosens Project Members, 2012. Making sense of palaeoclimate sensitivity. *Nature* 491, 683–691, DOI: 10.1038/nature11574.
- Panuska, B.C. and D.B. Stone, 1981. Late Palaeozoic palaeomagnetic data for Wrangellia: Resolution of the polarity ambiguity. *Nature* 293, 561–563.
- Parrish, J.M., Parrish, J.T., Hutchison, J.H., and Spicer, R.A., 1987. Late Cretaceous vertebrate fossils from the North Slope of Alaska and implications for dinosaur ecology. *Palaios* 2, 377–389.
- Parrish, J.T. and Spicer, R.A., 1988. Late Cretaceous terrestrial vegetation: A near-polar temperature curve. *Geology* 16, 22–25.
- Patton, W.W., Jr., Box, S.E., and Moll-Stalcup, E.J., 1994. Geology of west-central Alaska. In: Plafker, G., and Berg, H.C., (eds.) *The Geology of Alaska*. Boulder, Colorado, Geological Society of America. *The Geology of North America*, Vol. G-1, pp. 241–269.
- Plafker, G., and Berg, H.C., 1994. Overview of the geology and tectonic evolution of Alaska. In: Plafker, G., and Berg, H.C., (eds.) *The Geology of Alaska*. Boulder, Colorado, Geological Society of America. *The Geology of North America*, Vol. G-1, pp. 989–1017.
- Pogue, J., 1915. The Cantwell Formation: A continental deposit of Tertiary age in the Alaska Range. *Journal of Geology* 23 (2), 118–128.
- Rich, T.H., Gangloff, R.A., and Hammer, W.R., 1997. Polar dinosaurs. In: Currie, P.J. and Padian, K. (eds.) *Encyclopedia of Dinosaurs*. Academic Press, San Diego, CA, 562–572.
- Rich, T.H., Vickers-Rich, P., and Gangloff, R.A., 2002. Polar dinosaurs. *Science* 295, 979–980.
- Ridgway, K.D., Trop, J.M. and Sweet, A.R., 1997. Thrust-top basin formation along a suture zone, Cantwell basin, Alaska Range: Implications for the development of the Denali Fault system. *Geological Society of America Bulletin* 109 (5), 505–523, DOI: 10.1130/0016-7606(1997)109<0505:TTB-FAA>2.3.CO;2.
- Ridgway, K.D., Trop, J.M., Nokleberg, W.J., Davidson, C.M., and Eastham, K.R., 2002. Mesozoic and Cenozoic tectonics of the eastern and central Alaska Range: Progressive basin development and deformation in a suture zone. *Geological Society of America Bulletin* 114 (12), 1480–1504, DOI: 10.1130/0016-7606(2002)114<1480:MACTOT>2.0.CO;2.
- Salazar-Jaramillo, S., McCarthy, P.J., Fowell, S.J., Benowitz, J.A., and Slivinski, M., in preparation. Sedimentology, terrestrial carbon isotope record, and a ~ 69.5 Ma radiometric age for the lower Cantwell Formation at the East Fork Toklat River, Denali National Park and Preserve, Alaska: Implications for mid-Maastrichtian high-latitude paleoenvironments and paleoclimate.
- Sewall, J.O., van de Wal, R.S.W., van der Zwan, K., van Oosterhout, C., Dijkstra, H.A., and Scotese, C.R., 2007. Climate model boundary conditions for four Cretaceous time slices. *Climate of the Past* 3, 647–657.
- Sherwood, K.W., and Craddock, C., 1979. General geology of the central Alaska Range between the Nenana River and Mount Deborah: Alaska Division of Geological & Geophysical Surveys Alaska Open-File Report 116, 24 p., scale 1:63,360.
- Shewry, P.R., 2003. Tuber storage proteins. *Annals of Botany* 91, 755–769, DOI: 10.1093/aob/mcg084.
- Sontag, L.J., 1992. Paleomagnetism of the Paleocene Teklanika Volcanics, Central Alaska Range, Alaska. [M.S. Thesis], Mississippi State University, Mississippi, 70 p.
- Spicer, R. A., 1987. Late Cretaceous floras and terrestrial environment of Northern Alaska. In: *Alaskan North Slope Geology—Pacific*

- Section, Society of Economic Paleontologists and Mineralogists 50, 497–512.
- Spicer, R.A., 2003. Changing climate and biota. In: Skelton, P.W., Spicer, R.A., Kelley, S.P., and Gilmour, I., (eds.) *The Cretaceous World*. Cambridge University Press, 360 p.
- Spicer, R.A. and Parrish, J.T., 1990a. Late Cretaceous—early Tertiary palaeoclimates of northern high latitudes: a quantitative view. *Journal of the Geological Society, London*, 147, 329–341.
- Spicer, R.A. and Parrish, J.T., 1990b. Latest Cretaceous woods of the central North Slope, Alaska. *United States Geological Survey Circular 998*, 225–242.
- Spicer, R.A., and Herman, A.B., 2010. The Late Cretaceous environment of the Arctic: a quantitative reassessment based on plant fossils. In: Fiorillo, A.R. and McCarthy, P.J. (eds.) *Ancient Polar Ecosystems. Palaeogeography, Palaeoclimatology, Palaeoecology* 295, 423–442, DOI: 10.1016/j.palaeo.2010.02.025.
- Spicer, R.A., Wolfe, J.A., and Nichols, D.J., 1987. Alaskan Cretaceous–Tertiary floras and Arctic origins. *Paleobiology* 13 (1), 73–83.
- Spicer, R.A., Herman, A.B., and Kennedy, E.M., 2005. The sensitivity of CLAMP to taphonomic loss of foliar physiognomic characters. *Palaios* 20, 429–438.
- Stanley, R.G., 1987. Thermal maturity and petroleum source potential of the Cantwell Formation (Paleocene), Alaska Range. In: Hamilton, T.D. and Galloway, J.P., (eds.) *Geologic studies in Alaska by the United States Geological Survey during 1986*. United States Geological Survey Circular 998, 104–107.
- Stone, D. B., 1981. Triassic paleomagnetic data and paleolatitudes for Wrangellia, Alaska. *Geological Report Alaska Division Geological and Geophysical Survey* 73, 55–62.
- Stone, D.B., Panuska, B.C., and Packer, D.R., 1982. Paleolatitude versus time for southern Alaska. *Journal of Geophysical Research* 87, B5, 3697–3707.
- Sweet, A.R., Ricketts B.D., Cameron A.R., Norris D.K., 1989. An integrated analysis of the Brackett Coal Basin, Northwest Territories. *Geological Survey of Canada Paper* 89-1G, 85–99.
- Talling, P.J., Lawton, T.F., Burbanks, D.W., and Hobbs, R.S., 1995. Evolution of latest Cretaceous–Eocene non-marine deposystems in the Axhandle piggyback basin of central Utah: *Geological Society of America Bulletin* 107 (3), 297–315.
- Till, A.B., Harris, A.G., Wardlaw, B.R., and Mullen, M., 2007a. Upper Triassic continental strata of the central Alaska Range: Implications for paleogeographic reconstruction. In: Ridgway, K.D., Trop, J.M., Glen, J.M.G., and O’Neill, J.M., (eds.) *Tectonic Growth of a Collisional Continental Margin: Crustal Evolution of Southern Alaska*. Geological Society of America Special Paper 431, 191–205, DOI: 10.1130/2007.2431(08).
- Till, A.B., Roeske, S.M., Bradley, D.C., Friedman, R., and Layer, P.W., 2007b. Early Tertiary ransension-related deformation and magmatism long the Tintina fault system. Alaska. In: Till, A.B., Roeske, S.M., Foster, D.A., and Sample, J. (eds.) *Exhumation and Continental Strike-Slip Fault Systems*. Geological Society of America Special Paper 434, 233–264, DOI: 10.1130/2007.2434(11).
- Tomsich, C.S., McCarthy, P.J., Fowell, S.J. and Sunderlin, D., 2010. Paleofloristic and paleoenvironmental information from a Late Cretaceous (Maastrichtian) flora of the lower Cantwell Formation near Sable Mountain, Denali National Park, Alaska. *Palaeogeography, Palaeoclimatology, Palaeoecology* 295 (3), 389–408, DOI: 10.1016/j.palaeo.2010.02.023.
- Tomsich, C.S., McCarthy, P.J. and Fiorillo, A.R., in preparation. The depositional system and environments of the Late Cretaceous (Campanian–Maastrichtian) lower Cantwell Formation at Sable Mountain, Denali National Park and Preserve, Alaska.
- Trop, J.M. and Ridgway, K.D., 1997. Petrofacies and provenance of a Late Cretaceous suture zone thrust-top basin, Cantwell basin, central Alaska Range: *Journal of Sedimentary Research* 67 (3), 469–485.
- Trop, J.M. and Ridgway, K.D., 2007. Mesozoic and Cenozoic tectonic growth of southern Alaska: A sedimentary basin perspective. In: Ridgway,

- K.D., Trop, J.M., Glen, J.M.G., and O'Neill, J.M., (eds.) *Tectonic Growth of a Collisional Continental Margin: Crustal Evolution of Southern Alaska*. Geological Society of America Special Paper 431, 55–94, DOI: 10.1130/2007.2431(04).
- Upchurch, G., R., Otto-Bliesner, B.L., and Scotese, C., 1998. Vegetation–atmosphere interactions and their role in global warming during latest Cretaceous. *Philosophical Transactions of the Royal Society of London B* 353, 97–112.
- Van Itterbeeck, J., Bolotsky, Y., Bultynck, P., and Godefroit, P., 2005. Stratigraphy, sedimentology and palaeoecology of the dinosaur-bearing Kundur section (Zeya-Bureya Basin, Amur Region, Far Eastern Russia). *Geological Magazine* 142 (6), 735–750.
- Walker, J.D., Geissman, J.W., Bowring, S.A., and Babcock, L.E., 2013. The Geological Society of America Geologic Time Scale. *Geological Society of America Bulletin* 125 (3/4), 259–272, DOI: 10.1130/B30712.1.
- Wells, S.G. and Harvey, A.M., 1987. Sedimentologic and geomorphic variations in storm-generated alluvial fans, Howgill Fells, northwest England. *Geological Society of America Bulletin* 98, 182–198.
- Wilson, F.H., Dover, J.H., Bradley, D.C., Weber, F.R., Bundtzen, T.K., and Haeussler, P.J., 1998. Geologic map of central (Interior) Alaska. United States Geological Survey Open File Report 98-133, 2 sheets, scale 1:250,000.
- Wolfe, J.A., 1979. Temperature parameters of humid to mesic forests of Eastern Asia and relation to forests of other regions of the Northern Hemisphere and Australia. *United States Geological Survey Professional Paper* 1106, 1–37.
- Wolfe, J.A., 1987. Late Cretaceous–Cenozoic history of deciduousness and the terminal Cretaceous event. *Paleobiology* 13 (2), 215–226.
- Wolfe, J.A. and Wahrhaftig, C., 1970. The Cantwell Formation of the central Alaska Range. In: Cohee, G.V., Bates, R.G., and Wright, W.B., (eds.) *Changes in stratigraphic nomenclature by the United States Geological Survey in 1968*. United States Geological Survey Bulletin 1294-A, 41–46.
- Wolfe, J.A. and Spicer, R.A., 1999. Fossil leaf character states: multivariate analyses. In: Jones, T.P. and Rowe, N.P., (eds.) *Fossil Plants and Spores: Modern Techniques*. Geological Society, London, 233–239.
- Wright, J.L. and Breithaupt, B.H., 2002. Walking in Their Footsteps and What They Left Us: Dinosaur Tracks and Traces. In: Scotchmoor, J.G., Breithaupt, B.H., Springer, D.A., and Fiorillo, A.R., (eds.) *Dinosaurs—The Science Behind the Stories*. Society of Vertebrate Paleontology, American Geologic Institute, pp. 117–126.
- Zahid, K.M. and Barbeau, D.L., Jr., 2012. Constructing sandstone provenance and classification ternary diagrams using an electronic spreadsheet. *Journal of Sedimentary Research* 82, 131–132, DOI: 10.2110/jsr.2012.12.
- Zakharov, Y.D., Boriskina, N.G., Ignatyev, A.V., Tanabe, K., Shigeta, Y., Popov, A.M., Afanasyeva, T.B., Maeda, H., 1999. Palaeo-temperature curve for the Late Cretaceous of the northeastern circum-Pacific. *Cretaceous Research* 20, 685–697.
- Zakharov, Y.D., Shigeta, Y., Popov, A.M., Velivetskaya, T.A., and Afanasyeva, T.B., 2011. Cretaceous climatic oscillations in the Bering area (Alaska and Koryak Upland): isotopic and paleontological evidence. *Sedimentary Geology* 235, 122–131, DOI: 10.1016/j.sedgeo.2010.03.012.

Appendix A

Table A-1. Isotopic U–Pb ratios and ages measured with LA–ICP–MS on zircon grains for Bentonite 1. Errors were calculated at the 2-sigma level.

Bentonite 1	Isotopic Ratios									Apparent Ages (Concordant Scans)						Preferred Age		
	U (ppm)	U/Th	²⁰⁷ Pb/ ²³⁵ U	2σ (%)	²⁰⁶ Pb/ ²³⁸ U	2σ (%)	²⁰⁷ Pb/ ²⁰⁶ Pb	2σ (%)	error corr.	²⁰⁷ Pb/ ²³⁵ U	2σ (Ma)	²⁰⁶ Pb/ ²³⁸ U	2σ (Ma)	²⁰⁷ Pb/ ²⁰⁶ Pb	-2σ (Ma)	+2σ (Ma)	(Ma)	2σ (Ma)
1322-01-1	240	2	0.08381	1.29	0.01163	0.08	0.05227	0.80	0.20	81.7	12.1	74.5	4.9	297.4	370.4	332.4	74.5	4.9
1322-01-2	212	3	2.10254	10.59	0.20254	0.86	0.07529	0.34	0.48	1149.6	34.7	1189.0	46.4	1076.2	90.7	88.1	1149.6	34.7
1322-01-3	216	2	0.08032	1.08	0.01180	0.08	0.04935	0.68	0.16	78.4	10.2	75.6	4.9	164.7	329.4	307.9	75.6	4.9
1322-01-4	573	2	0.08235	0.92	0.01142	0.06	0.05228	0.57	0.25	80.4	8.6	73.2	4.1	297.8	260.5	241.1	73.2	4.1
1322-01-5	66	2	0.55929	6.88	0.07294	0.45	0.05562	0.68	0.25	451.1	44.8	453.8	27.3	437.0	282.5	259.6	453.8	27.3
1322-01-6	339	1	0.07859	1.01	0.01066	0.06	0.05346	0.70	0.11	76.8	9.5	68.4	3.6	348.5	310.0	282.8	68.4	3.6
1322-01-7	109	3	0.08718	3.45	0.01068	0.10	0.05919	2.37	0.05	84.9	32.2	68.5	6.1	574.1	1015.0	768.7	68.5	6.1
1322-01-8	204	2	0.07975	6.29	0.01105	0.13	0.05235	4.16	0.03	77.9	59.2	70.8	8.2	300.8	601.5	1433.5	70.8	8.2
1322-01-9	102	3	0.10751	5.45	0.01247	0.28	0.06252	3.38	0.07	103.7	50.0	79.9	18.0	691.8	1383.6	980.3	79.9	18.0
1322-01-10	285	2	0.07828	1.62	0.01146	0.07	0.04953	1.05	0.08	76.5	15.3	73.5	4.7	173.1	346.2	458.5	73.5	4.7
1322-01-11	199	3	0.08097	2.18	0.01100	0.10	0.05339	1.48	0.08	79.1	20.5	70.5	6.5	345.4	690.8	572.5	70.5	6.5
1322-01-12	290	2	0.07821	1.17	0.01162	0.07	0.04884	0.75	0.09	76.5	11.0	74.4	4.5	140.0	280.0	343.7	74.4	4.5
1322-01-13	393	1	0.08083	1.11	0.01158	0.06	0.05064	0.70	0.15	78.9	10.5	74.2	4.0	224.6	338.1	306.3	74.2	4.0
1322-01-14	286	3	0.07694	1.33	0.01080	0.06	0.05167	0.89	0.16	75.3	12.6	69.3	3.9	270.7	421.2	372.8	69.3	3.9
1322-01-15	404	1	0.07251	1.04	0.01090	0.06	0.04823	0.69	0.16	71.1	9.9	69.9	3.8	110.5	221.0	322.8	69.9	3.8
1322-01-16	230	3	0.07438	1.35	0.01118	0.09	0.04826	0.87	0.21	72.8	12.7	71.7	5.7	111.9	223.7	401.0	71.7	5.7
1322-01-17	302	1	0.07206	1.48	0.01033	0.10	0.05059	1.05	0.21	70.7	14.1	66.3	6.3	222.3	444.7	446.0	66.3	6.3
1322-01-18	409	1	0.07982	1.57	0.01157	0.11	0.05003	0.96	0.28	78.0	14.8	74.2	6.9	196.6	393.2	418.3	74.2	6.9
1322-01-19	349	3	0.07361	0.98	0.01093	0.08	0.04886	0.67	0.21	72.1	9.3	70.1	5.1	141.0	282.0	305.0	70.1	5.1
1322-01-20	304	2	0.08054	1.56	0.01118	0.07	0.05224	1.03	0.10	78.7	14.6	71.7	4.7	296.0	483.1	420.3	71.7	4.7
1322-01-21	292	2	0.07505	1.75	0.01105	0.08	0.04926	1.16	0.08	73.5	16.5	70.8	4.9	160.3	320.5	510.5	70.8	4.9
1322-01-22	202	2	0.08924	1.58	0.01250	0.11	0.05179	0.98	0.09	86.8	14.7	80.1	7.0	276.3	463.5	405.5	80.1	7.0
1322-01-23	294	3	0.07758	1.99	0.01137	0.06	0.04947	1.27	0.08	75.9	18.8	72.9	3.8	170.2	340.5	551.6	72.9	3.8
1322-01-24	-	-	-	-	-	-	-	-	-	-	-	-	-	-	-	-	failed	-
1322-01-25	339	2	0.07587	1.71	0.01159	0.07	0.04746	1.08	0.06	74.3	16.1	74.3	4.5	72.3	144.5	502.7	74.3	4.5
1322-01-26	471	2	0.07649	0.93	0.01150	0.07	0.04824	0.58	0.28	74.8	8.8	73.7	4.7	110.8	221.7	270.2	73.7	4.7
1322-01-27	781	2	0.06655	1.08	0.01059	0.06	0.04558	0.72	0.24	65.4	10.3	67.9	4.1	0.0	0.0	314.4	0.0	0.0
1322-01-28	227	1	0.07826	12.69	0.01066	0.08	0.05327	8.64	0.01	76.5	119.7	68.3	5.0	340.2	680.4	2434.2	68.3	5.0
1322-01-29	142	2	0.07311	2.47	0.01077	0.10	0.04921	1.71	0.04	71.6	23.4	69.1	6.5	158.0	316.1	724.5	69.1	6.5
1322-01-30	315	3	0.22391	3.07	0.03076	0.21	0.05280	0.70	0.31	205.2	25.5	195.3	13.3	320.2	314.6	286.7	195.3	13.3
1322-01-31	257	2.4	0.07543	1.05	0.01137	0.07	0.04813	0.69	0.08	73.8	9.9	72.9	4.2	105.9	211.7	323.6	72.86	4.2
1322-01-32	281	2.8	0.07635	1.14	0.01164	0.07	0.04757	0.71	0.18	74.7	10.8	74.6	4.3	77.9	155.8	335.8	74.61	4.3
1322-01-33	506	2.1	0.22528	2.44	0.03224	0.21	0.05068	0.49	0.45	206.3	20.2	204.5	13.2	226.3	232.4	216.9	204.55	13.2
1322-01-34	483	1.5	0.08032	0.95	0.01118	0.05	0.05209	0.61	0.18	78.4	8.9	71.7	3.3	289.5	278.3	256.2	71.68	3.3
1322-01-35	30	3.4	0.51561	92.50	0.04091	7.32	0.09142	11.98	0.73	422.2	640.1	258.5	453.4	1455.3	2910.6	1811.6	422.22	640.3
1322-01-36	351	2.9	0.08142	1.33	0.01160	0.06	0.05092	0.82	0.19	79.5	12.5	74.3	3.9	237.1	393.8	351.3	74.33	3.9
1322-01-37	-	-	-	-	-	-	-	-	-	-	-	-	-	-	-	-	failed	-
1322-01-38	348	1.3	0.09067	1.87	0.01179	0.10	0.05577	1.15	0.20	88.1	17.4	75.6	6.1	443.4	492.5	426.9	75.56	6.1
1322-01-39	304	1.8	0.52812	3.06	0.06991	0.30	0.05479	0.29	0.44	430.6	20.3	435.6	18.2	403.5	118.9	114.6	435.64	18.2
1322-01-40	90	1.6	11.40454	65.85	0.47185	2.18	0.17530	0.86	0.54	2556.8	53.9	2491.7	96.0	2608.9	82.6	80.3	2556.80	53.9
1322-01-41	216	1.5	0.38818	3.79	0.04979	0.31	0.05655	0.54	0.33	333.0	27.7	313.2	19.2	473.9	216.9	203.2	313.22	19.2
1322-01-42	643	1.1	0.07498	0.95	0.01105	0.06	0.04922	0.62	0.21	73.4	9.0	70.8	4.0	158.1	308.3	281.7	70.84	4.0
1322-01-43	293	2.8	0.07068	1.11	0.01043	0.11	0.04917	0.88	0.09	69.3	10.5	66.9	7.2	156.1	312.1	395.2	66.86	7.2
1322-01-44	254	1.7	0.06859	1.21	0.01159	0.07	0.04292	0.77	0.07	67.4	11.5	74.3	4.4	0.0	0.0	75.7	0.00	0.0
1322-01-45	221	1.6	0.07718	1.86	0.01143	0.09	0.04899	1.22	0.04	75.5	17.5	73.2	5.7	147.1	294.2	535.9	73.25	5.7
1322-01-46	155	2.4	0.07586	1.96	0.01112	0.07	0.04947	1.29	0.07	74.2	18.5	71.3	4.7	170.4	340.8	558.5	71.29	4.7
1322-01-47	180	2.3	0.06797	2.46	0.01130	0.09	0.04361	1.58	0.08	66.8	23.4	72.5	5.7	0.0	0.0	528.8	0.00	0.0
1322-01-48	434	0.9	0.25637	2.42	0.03591	0.16	0.05178	0.46	0.35	231.7	19.5	227.4	9.8	275.7	208.9	196.3	227.43	9.8
1322-01-49	166	2.0	0.07784	2.68	0.01149	0.12	0.04914	1.73	0.05	76.1	25.2	73.6	7.3	154.4	308.8	736.3	73.64	7.3
1322-01-50	1145	3.9	0.95201	5.14	0.10778	0.44	0.06406	0.29	0.54	679.1	26.7	659.8	25.7	743.7	97.7	94.8	659.83	25.7
1322-01-51	323	1.4	0.07314	1.22	0.01052	0.08	0.05043	0.85	0.15	71.7	11.5	67.5	4.8	214.7	418.2	370.6	67.45	4.8
1322-01-52	342	2.3	0.07805	0.99	0.01111	0.06	0.05094	0.66	0.10	76.3	9.4	71.2	3.7	238.2	314.8	287.0	71.24	3.7
1322-01-53	426	3.4	0.07216	1.21	0.01125	0.08	0.04652	0.77	0.23	70.7	11.4	72.1	5.2	24.7	49.3	373.5	72.12	5.2
1322-01-54	140	1.7	0.07845	2.03	0.01069	0.09	0.05322	1.41	0.09	76.7	19.1	68.6	6.0	338.2	662.4	549.5	68.56	6.0
1322-01-55	389	1.4	0.06780	1.79	0.01016	0.08	0.04839	1.29	0.09	66.6	17.0	65.2	5.2	118.4	236.8	575.6	65.17	5.2
1322-01-56	-	-	-	-	-	-	-	-	-	-	-	-	-	-	-	-	failed	-
1322-01-57	290	2.6	0.07397	1.48	0.01055	0.11	0.05084	1.10	0.07	72.5	14.0	67.7	6.7	233.7	467.3	463.0	67.67	6.7
1322-01-58	556	5.1	0.26656	2.09	0.03740	0.14	0.05169	0.38	0.36	239.9	16.7	236.7	8.6	271.5	173.1	164.4	236.72	8.6
1322-01-59	307	1.9	0.06852	1.04	0.01007	0.06	0.04937	0.76	0.11	67.3	9.8	64.6	3.6	165.5	330.9	339.7	64.57	3.6
1322-01-60	258	2.3	0.06511	1.92	0.01012	0.08	0.04664	1.38	0.13	64.1	18.3	64.9	5.3	31.0	62.1	640.1	64.94	5.3

Table A-2. Isotopic U–Pb ratios and ages measured with LA–ICP–MS on zircon grains for Bentonite 2. Errors were calculated at the 2-sigma level.

Bentonite 2	Isotopic Ratios						Apparent Ages (Concordant Scans)						Preferred Age					
	U (ppm)	U/Th	²⁰⁷ Pb/ ²³⁵ U c	2 σ (%)	²⁰⁶ Pb/ ²³⁸ U	2 σ (%)	²⁰⁷ Pb/ ²⁰⁶ Pb	2 σ (%)	error corr.	²⁰⁷ Pb/ ²³⁵ U	2 σ (Ma)	²⁰⁶ Pb/ ²³⁸ U	2 σ (Ma)	²⁰⁷ Pb/ ²⁰⁶ Pb	-2 σ (Ma)	+2 σ (Ma)	(Ma)	2 σ (Ma)
1322-02-1	290	2.2	0.07402	1.29	0.01064	0.08	0.05044	0.89	0.14	72.5	12.2	68.3	4.8	215.1	430.2	386.7	68.3	4.8
1322-02-2	1572	1.1	0.12159	0.93	0.01771	0.09	0.04979	0.33	0.50	116.5	8.4	113.2	5.6	185.4	157.5	150.3	113.2	5.6
1322-02-3	355	1.8	0.17388	1.80	0.02579	0.13	0.04891	0.52	0.16	162.8	15.5	164.1	8.1	143.4	257.1	238.4	164.1	8.1
1322-02-4	475	1.8	0.17515	1.47	0.02507	0.10	0.05067	0.42	0.22	163.9	12.7	159.6	6.4	225.8	196.6	185.4	159.6	6.4
1322-02-5	127	1.5	0.23304	2.87	0.03117	0.16	0.05422	0.67	0.18	212.7	23.6	197.9	10.1	380.1	289.1	265.3	197.9	10.1
1322-02-6	533	3.5	0.07291	1.47	0.01118	0.05	0.04731	0.95	0.11	71.5	13.9	71.6	3.1	64.9	129.9	445.8	71.6	3.1
1322-02-7	318	2.4	0.07416	1.61	0.01111	0.11	0.04841	1.06	0.20	72.6	15.2	71.2	6.9	119.1	238.3	477.9	71.2	6.9
1322-02-8	756	3.0	0.07590	0.76	0.01146	0.04	0.04803	0.48	0.17	74.3	7.2	73.5	2.8	100.6	201.2	228.4	73.5	2.8
1322-02-9	280	2.2	0.07922	1.63	0.01140	0.10	0.05042	1.08	0.09	77.4	15.3	73.0	6.3	214.6	429.2	462.6	73.0	6.3
1322-02-10	-	-	-	-	-	-	-	-	-	-	-	-	-	-	-	-	failed	-
1322-02-11	216	3.9	0.07660	1.74	0.01165	0.09	0.04771	1.11	0.09	74.9	16.5	74.6	5.7	84.7	169.4	509.5	74.6	5.7
1322-02-12	1598	2.3	0.07916	0.68	0.01123	0.04	0.05112	0.43	0.21	77.4	6.4	72.0	2.3	246.3	198.4	187.0	72.0	2.3
1322-02-13	237	2.7	0.22422	2.16	0.03285	0.12	0.04950	0.47	0.21	205.4	17.9	208.4	7.7	171.5	227.8	212.9	208.4	7.7
1322-02-14	258	2.9	0.08917	1.40	0.01216	0.06	0.05319	0.84	0.13	86.7	13.0	77.9	4.0	336.9	378.2	338.6	77.9	4.0
1322-02-15	1086	0.9	0.07402	0.81	0.01107	0.06	0.04850	0.52	0.26	72.5	7.7	71.0	3.9	123.8	247.5	244.8	71.0	3.9
1322-02-16	3476	1.0	0.07761	0.49	0.01136	0.04	0.04955	0.29	0.38	75.9	4.6	72.8	2.7	173.8	139.7	134.0	72.8	2.7
1322-02-17	734	3.3	0.21391	1.62	0.03084	0.12	0.05031	0.38	0.22	196.8	13.6	195.8	7.7	209.2	179.4	170.1	195.8	7.7
1322-02-18	236	2.2	0.22763	2.12	0.03201	0.15	0.05158	0.48	0.23	208.2	17.5	203.1	9.3	266.8	220.0	206.1	203.1	9.3
1322-02-19	135	2.0	0.30527	3.63	0.04047	0.22	0.05471	0.62	0.33	270.5	28.3	255.7	13.5	400.4	263.4	243.5	255.7	13.5
1322-02-20	571	2.1	0.06969	0.75	0.01056	0.07	0.04785	0.52	0.29	68.4	7.1	67.7	4.4	92.1	184.2	245.8	67.7	4.4
1322-02-21	293	1.0	0.79861	4.91	0.09620	0.37	0.06021	0.34	0.42	596.0	27.7	592.1	21.7	611.1	122.9	118.4	592.1	21.7
1322-02-22	295	1.9	0.20363	2.22	0.02807	0.11	0.05261	0.58	0.14	188.2	18.7	178.5	7.1	312.1	258.8	239.6	178.5	7.1
1322-02-23	240	1.7	0.21580	1.85	0.03217	0.15	0.04866	0.42	0.23	198.4	15.4	204.1	9.1	131.3	207.4	195.1	204.1	9.1
1322-02-24	101	1.6	11.87201	58.76	0.48931	1.84	0.17597	0.71	0.58	2594.4	46.4	2567.7	79.9	2615.3	68.1	66.5	2594.4	46.4
1322-02-25	354	1.9	0.19936	2.49	0.02828	0.12	0.05112	0.63	0.18	184.6	21.1	179.8	7.7	246.3	298.2	273.2	179.8	7.7
1322-02-26	112	4.0	9.18545	78.58	0.37680	3.11	0.17680	1.11	0.71	2356.7	78.4	2061.3	145.8	2623.1	106.3	102.5	2356.7	78.4
1322-02-27	173	1.2	0.17474	2.80	0.02446	0.13	0.05181	0.84	0.12	163.5	24.2	155.8	8.3	277.0	393.0	350.5	155.8	8.3
1322-02-28	367	2.9	0.39523	5.19	0.05327	0.25	0.05381	0.70	0.21	338.2	37.8	334.5	15.6	363.3	305.6	279.1	334.5	15.6
1322-02-29	266	2.0	0.79823	5.27	0.09840	0.36	0.05883	0.37	0.30	595.8	29.8	605.0	21.2	561.0	141.5	135.5	605.0	21.2
1322-02-30	954	3.1	0.07452	0.72	0.01081	0.04	0.04999	0.48	0.17	73.0	6.8	69.3	2.6	194.4	232.6	217.1	69.3	2.6
1322-02-31	168	1.3	6.05904	31.23	0.35926	1.39	0.12232	0.52	0.58	1984.4	45.4	1978.7	66.2	1990.3	76.3	74.4	1984.4	44.9
1322-02-32	-	-	-	-	-	-	-	-	-	-	-	-	-	-	-	-	failed	-
1322-02-33	406	3.7	0.07182	0.99	0.01091	0.06	0.04773	0.66	0.12	70.4	9.4	70.0	3.7	85.7	171.5	314.5	70.0	3.7
1322-02-34	645	0.8	0.14528	1.30	0.02076	0.13	0.05076	0.44	0.38	137.7	11.6	132.4	8.3	230.0	204.5	192.4	132.4	8.3
1322-02-35	1666	3.3	0.05819	0.54	0.00851	0.05	0.04957	0.48	0.22	57.4	5.2	54.7	3.2	174.7	232.2	216.8	54.7	3.2
1322-02-36	157	2.3	0.07692	1.85	0.01075	0.09	0.05188	1.26	0.13	75.2	17.5	69.0	5.7	280.1	560.1	512.8	69.0	5.7
1322-02-37	657	1.9	0.07296	0.94	0.01060	0.05	0.04993	0.65	0.10	71.5	8.9	68.0	3.4	191.8	318.3	290.0	68.0	3.4
1322-02-38	470	2.4	0.08261	1.32	0.01126	0.08	0.05323	0.88	0.09	80.6	12.4	72.2	4.8	338.6	399.4	355.4	72.2	4.8
1322-02-39	303	2.7	0.07792	1.45	0.01054	0.08	0.05360	1.01	0.14	76.2	13.7	67.6	4.9	354.1	457.0	400.3	67.6	4.9
1322-02-40	601	3.3	0.11193	1.14	0.01557	0.07	0.05215	0.53	0.16	107.7	10.5	99.6	4.1	291.9	240.9	224.2	99.6	4.1
1322-02-41	296	1.9	0.22398	2.21	0.03091	0.13	0.05255	0.51	0.19	205.2	18.4	196.3	7.9	309.5	229.6	214.4	196.3	7.9
1322-02-42	693	3.0	0.06833	1.14	0.01076	0.05	0.04606	0.76	0.17	67.1	10.9	69.0	2.9	0.9	1.7	373.9	69.0	2.9
1322-02-43	293	2.0	0.07633	1.39	0.01080	0.07	0.05126	0.94	0.14	74.7	13.2	69.3	4.5	252.4	451.7	396.6	69.3	4.5
1322-02-44	746	2.6	0.06625	0.92	0.00949	0.05	0.05065	0.70	0.20	65.1	8.8	60.9	3.3	225.0	335.1	303.8	60.9	3.3
1322-02-45	919	1.7	0.07684	1.22	0.01053	0.08	0.05292	0.81	0.30	75.2	11.5	67.5	5.1	325.4	366.8	329.4	67.5	5.1
1322-02-46	111	2.6	0.15590	8.34	0.01048	0.29	0.10790	6.21	0.11	147.1	74.7	67.2	18.7	1764.2	1294.8	900.2	67.2	18.7
1322-02-47	288	1.5	0.11735	5.49	0.01276	0.25	0.06669	3.22	0.13	112.7	50.5	81.8	16.1	828.0	1211.8	872.3	81.8	16.1
1322-02-48	121	5.3	1.62781	12.14	0.17132	0.66	0.06891	0.49	0.30	981.0	47.5	1019.4	36.6	896.1	150.7	143.8	1019.4	36.5
1322-02-49	294	2.9	0.08024	1.43	0.01151	0.07	0.05055	0.92	0.09	78.4	13.4	73.8	4.6	220.3	440.6	395.2	73.8	4.6
1322-02-50	416	3.7	0.57981	3.64	0.07216	0.29	0.05828	0.36	0.27	464.3	23.5	449.2	17.2	540.2	137.1	131.5	449.2	17.2
1322-02-51	-	-	-	-	-	-	-	-	-	-	-	-	-	-	-	-	failed	-
1322-02-52	153	1.2	0.04873	2.20	0.00501	0.08	0.07056	3.31	0.07	48.3	21.4	32.2	5.3	944.8	1146.3	836.4	32.2	5.3
1322-02-53	654	4.3	0.25962	2.32	0.02495	0.13	0.07548	0.62	0.40	234.4	18.8	158.8	8.1	1081.3	169.7	160.9	158.8	8.1
1322-02-54	106	0.6	5.50767	28.81	0.33901	1.25	0.11783	0.56	0.43	1901.8	45.5	1881.9	60.4	1923.6	85.7	83.3	1901.8	45.0
1322-02-55	656	2.2	0.41316	2.48	0.05460	0.22	0.05488	0.31	0.37	351.1	17.9	342.7	13.4	407.2	127.7	122.8	342.7	13.4
1322-02-56	557	1.9	0.18717	1.26	0.02788	0.12	0.04870	0.31	0.34	174.2	10.8	177.2	7.5	133.2	153.6	146.8	177.2	7.5
1322-02-57	-	-	-	-	-	-	-	-	-	-	-	-	-	-	-	-	failed	-
1322-02-58	-	-	-	-	-	-	-	-	-	-	-	-	-	-	-	-	failed	-
1322-02-59	376	2.9	0.18237	1.98	0.02649	0.12	0.04993	0.53	0.23	170.1	17.1	168.6	7.8	191.6	257.1	238.3	168.6	7.8
1322-02-60	1205	1.4	0.07681	0.65	0.01110	0.05	0.05020	0.44	0.12	75.1	6.2	71.1	3.2	204.4	211.9	199.0	71.1	3.2

Permian and Triassic deposits of Siberian and Chukotka passive margins: sedimentation setting and provenances

M.I. Tuchkova¹, S.D. Sokolov¹, A.K. Khudoley², V.E. Verzhbitsky³, Y. Hayasaka⁴, A.V. Moiseev¹

¹Geological Institute of Russian Academia of Sciences, Moscow, Russia, Pyzhevsky per., 7

²Saint Petersburg State University, Saint Petersburg, Russia,

³P.P. Shirshov Institute of Oceanology RAS, Moscow, Russia

⁴Hiroshima University, Hiroshima, Japan

ABSTRACT

The numerous current hypotheses on structural evolution of the present day Arctic require validation using data from regional geological studies. We are focusing on terrigenous deposits of Triassic age, which are the key to correlate geological events from the Eastern Arctic and the Verkhoyansk-Kolyma and Anyui-Chukotka fold systems. Triassic deposits of the Verkhoyansk–Kolyma fold system formed along the eastern margin of the Siberian continent. In the Anyui-Chukotka fold system, Triassic deposits accumulated on the southern margin of the Chukotka microcontinent. In present day structure heavily deformed sedimentary complexes of the two passive margins are brought closely together as a result of collision. The Siberian continent collided with the Kolyma – Omolon superterrane to form the Verkhoyansk–Kolyma fold belt. The Anyui-Chukotka fold system was formed as the result of collision between the Siberian continent and the Chukotka microcontinent associated with opening of the Canada Basin within the Amerasia Basin. The main results of our studies are: the directions of sedimentary supply and shelf zone progradation in the present day structure of the Verkhoyansk region and Chukotka differ by almost 180°. Changes in the sandstone mineral composition during the Triassic provide evidence of different source provinces for deposits of the Verkhoyansk and Chukotka passive margins. Changes in the chemical composition imply different evolutionary patterns of the rocks. Compositions of detrital zircon assemblages show dominant spikes of different ages: Verkhoyansk region is dominated by Proterozoic assemblages, and Chukotka by Phanerozoic ones. The level and type of deformation in both cases is represented by folds-and-thrusts of different vergence.

INTRODUCTION

Many paleotectonic reconstructions published in recent years are based on the U-Pb detrital zircon geochronology. This approach has proved to be effective for localizing and estimating the age ranges of provenances and for dating the deformed sedimentary complexes of fold belts (Rohr et al., 2008; Brandon, Vance., 1992; Crowley et al., 2005; and other works). Conclusions of this kind are inferable from age correlation of detrital zircon populations, which presumably coexisted in a provenance of clastic sediments. By analyzing the distribution of averaged geochronological ages of zircon populations, paying particular attention to the most significant peaks in the distribution, plus zircon ages from single samples, the pattern of ages can be extrapolated over vast regions.

One of the reconstructions under consideration is the problem of how and when the Amerasian basin opened. Among the diverse viewpoints on how the basin developed, the most popular is the rotational model suggesting that the Arctic Alaska–Chukotka continental block was detached from the Canadian Arctic margin with subsequent counterclockwise rotation around a pole located in the McKenzie Delta region (Sweeney, J.F., 1985; Grantz et al., 1990, 2011; Embry and Dixon, 1994; Lawver, et al., 2002; 2011).

The rotational hypothesis has been criticized in several recent publications (Miller et al., 2006; Kuzmichev, 2009; Beranek et al., 2010). The comparative geochronological analysis of detrital zircon populations from Triassic sandstones of the circum-Arctic region showed that in Triassic time Chukotka was situated apart from the Canadian Arctic margin on a continuation of the West Siberian rift system eastward of the Polar Urals. This is evident from data, according to which clastic material of Triassic deposits in Chukotka dated at

235–265 Ma was derived from the Siberian traps and associated intrusive and volcanoclastic rocks (Miller et al., 2006).

Hence, the problem of provenances for Triassic deposits of the Chukotka and Verkhoyansk regions is critical for testing the paleotectonic reconstructions. Sedimentological links between the Siberian passive margin and Triassic terrigenous deposits of the Verkhoyansk region are well established (Parfenov, 1984; Zonenshain et al., 1990) and have never been doubted. Sedimentology of these deposits is known in detail (Kossovskaya, 1962; Yapaskurt, 1992). The Triassic terrigenous deposits of Chukotka also accumulated in passive margin settings (Zonenshain et al., 1990; Parfenov et al., 1993; Sokolov, 1992, 2010). On the other hand, relatively old Russian

publications (for example Til'man, 1980) showed an overall similarity of Paleozoic-Mesozoic deposits of Chukotka and the Verkhoyansk range but also drew attention to the considerable differences in their structure and stratigraphy

The main objective of this work is to discuss sedimentological differences (sedimentation settings, facies, lithology and geochemistry) and detrital zircon geochronology of Triassic sandstones from the Verkhoyansk region and Chukotka. In both regions, the best studied sections of Permian and Triassic deposits have been chosen for the comparative study. A. Prokopiev (IGABM, Yakutsk) kindly permitted us to use results of his chemical and isotopic studies in this paper. However, we are wholly responsible for our interpretation.

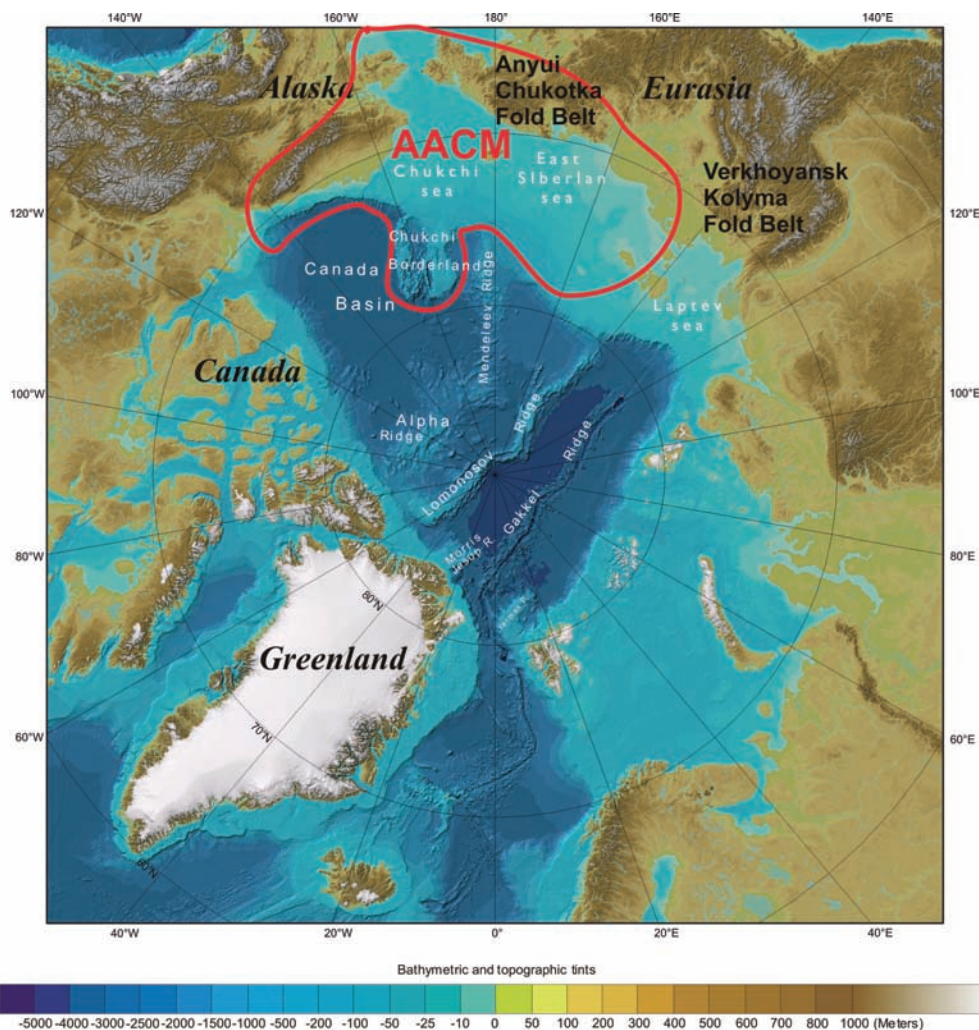


Fig. 1. The assumed outline of the Arctic Alaska –Chukotka microcontinent (AACM), IBCAO_ver2_23_Letter (Jakobsson et al., 2008).

GEOLOGICAL BACKGROUND

The Verkhoyansk-Kolyma and Anyui-Chukotka fold belts (Fig.1) are located to the east of the Siberian craton (North Asian craton in the terminology by Parfenov et al., 1993; Nokleberg et al., 1994). They were formed in the Late Mesozoic as a result of Siberia colliding with the Kolyma-Omolon and Chukotka microcontinents respectively (Zonenshain et al., 1990; Parfenov et al., 1993; Tectonics, geodynamics and metallogeny..., 2001; Geodynamic, Magmatism, and Metallogeny..., 2006; Sokolov, 2010).

The Verkhoyansk terrane between the Siberian craton and Kular-Nera terrane is bounded by thrust faults of western vergence (Parfenov et al., 1993, 1995; Tectonics, geodynamics and metallogeny...,

2001). It is divided into four tectono-stratigraphic units of the Riphean–Vendian carbonate-terrigenous deposits, the Lower–Middle Paleozoic predominantly carbonate rocks, the Upper Paleozoic–Lower Mesozoic terrigenous sediments (Verkhoyansk complex), and Upper Jurassic–Lower Cretaceous foredeep sediments. The Verkhoyansk complex corresponds to the thick (14–16 km) terrigenous sequence of the Carboniferous, Permian, Triassic, and Jurassic rocks. The basal Viséan sediments of the sequence characterize a sharp transition from carbonate to terrigenous sedimentation. The uppermost part is of the Bathonian–Callovian in age.

The Chukotka (New Siberian Islands–Chukchi) fold belt stretches from the New Siberian Islands to the Chukchi Peninsula over the continental

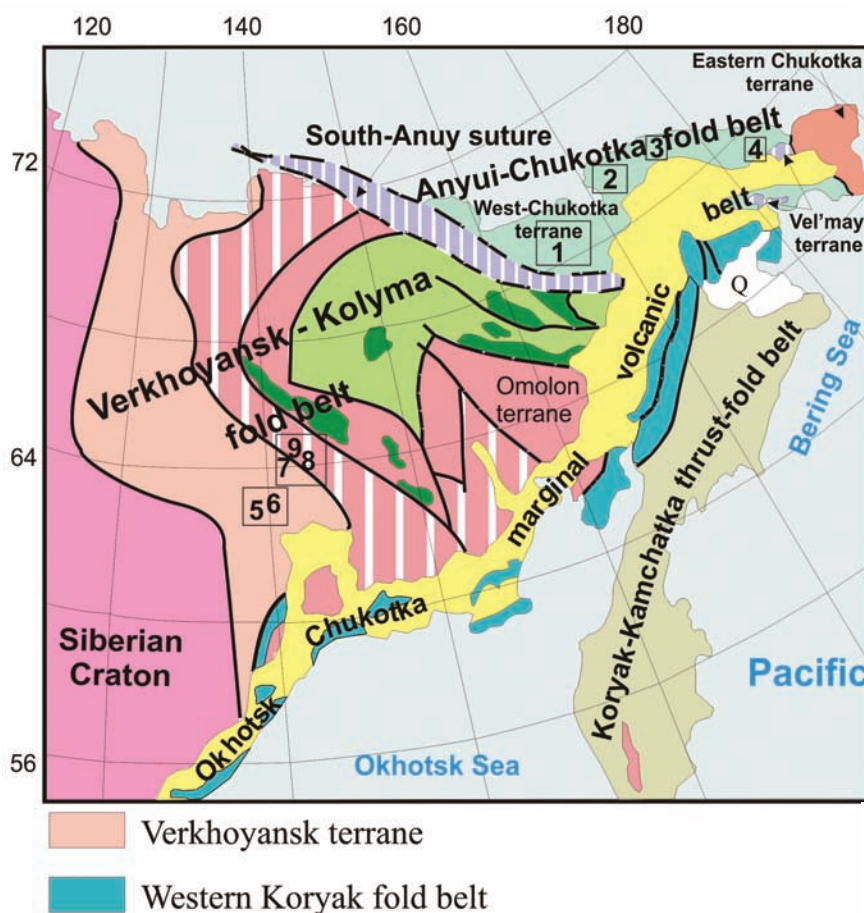


Fig. 2. Tectonic scheme of Northeastern Asia, after (Sokolov et al., 2001), Chukotka fold belt consists of the Anyui-Chukotka fold belt and South-Anuy suture. Number in squares are the main areas referred to in text: 1 – Anyui subterrane, Western Chukotka; 2 – Chaun subterrane, near Pevek, 3 – Chaun terrane, Tanyurer River; 4 – Chaun terrane, Velmay River, 5 – Northern part of the South Verkhoyansk, Kobume River; 6 – Northern part of the South Verkhoyansk, Setarym and Khandyga Rivers; 7 – Distal part of Verkhoyansk margin, Talalakh stream and Bazovsky stream, 8 – Kular-Nera terrane, Malyutka stream, 9 – Kular-Nera terrane, Northwestern flank of Ayan-Yurakh anticlinorium.

margin and vast Arctic shelf. In the Anyui-Chukchi (AChFB) and South Anyui (SAS) fold belts, crystalline basement is overlain by the Paleozoic–Mesozoic sedimentary cover intensely deformed in the terminal Early Cretaceous. In the paleotectonic aspect, this is a continental block or the Chukchi microcontinent commonly considered as a part of the Arctic Alaska–Chukotka microplate (AACM, Grantz et al., 2011; Lawver et al., 2011) or the Bennett-Borovia one (Natal'in et al., 1999). As is assumed in work by Drachev (2011), the AACM consists of three independent blocks (New Siberian–Chukchi, Arctic Alaska, and Chukchi Borderland), in which tectonic movements and deformations did not depend on the Amerasian basin formation.

The AChFB is divided (Figs. 1 and 2) into the West Chukotka, East Chukotka, and Vel'may terranes (Parfenov et al., 1993; Nokleberg et al., 1994). Crystalline basement and Ordovician–Silurian deposits are exposed in the East Chukotka terrane only. The Paleozoic–Mesozoic platform and shelf deposits of the West Chukotka and East

Chukotka terranes are similar in composition. These facies variations in the West Chukotka terrane resulted in identifying the Anyui and Chaun subterrane (Geodynamic, Magmatism, and Metallogeny..., 2006). The Devonian–Lower Carboniferous carbonate deposits with subordinate intercalations of terrigenous rocks are exposed in granite-metamorphic domes and usually show greenschist metamorphic grade, whereas amphibolite grade is less common (Gel'man, 1995). Upper Carboniferous and Permian deposits are missing. The Anyui complex, a terrigenous sequence with abundant turbidite members, is from 1 to 5 km thick in total. In the Rauchua River basin, fossils of the Lower Jurassic have been found in the upper part of the sequence (Til'man, 1980). The Triassic deposits are overlain with angular unconformity by the Upper Jurassic–Lower Cretaceous clastic sediments.

The Vel'may terrane has distinctive lithology which includes ultramafic rocks, gabbroids, plagiogranites, and volcanogenic-cherty deposits

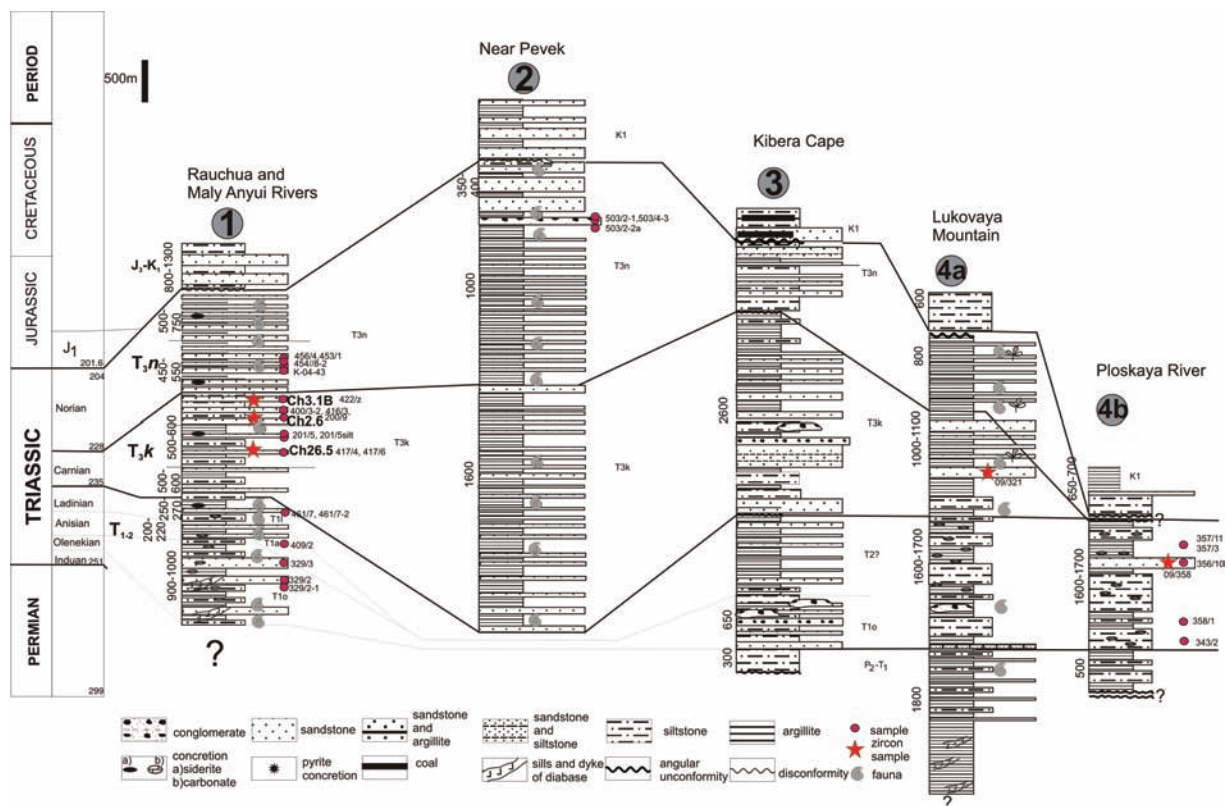


Fig. 4. Correlation chart of the main sections of the Permian and Triassic rock units of Anyui-Chukotka fold belt. Data source for compiled sections are unpublished reports. For numbers of units see figures 2 and 3 and description in text.

widespread in East Chukotka. The age of these rocks is controversial. According to some researchers the whole complex is Late Jurassic–Early Cretaceous in age (Kosygin et al., 1974), while the others argue for Late Triassic age of the rocks (Tynankergav, 1987; Bychkov, 1987). The Vel'may terrane is interpreted as a continuation of the South Anyui Suture (SAS).

The SAS is a collisional suture separating structures of Chukotka from the Verkhoyansk–Kolyma fold belt (VKFB). It represents a result of the collision between the Chukotka microcontinent and the Siberian active margin (Parfenov et al., 1993; Sokolov et al., 2002, 2009; Byalobjesky and Goryachev, 2004). At the time of collision, tectono-stratigraphic units of the SAS were thrust northward onto the passive margin of the Chukotka microcontinent. Ultimate stages of that collision were accompanied by development of dextral strike-slip faults (Sokolov et al., 2001; Bondarenko, 2004).

PERMIAN AND TRIASSIC DEPOSITS OF THE AChFB

Anyui subterrane. The Triassic terrigenous deposits unconformably overlie older Paleozoic strata and are represented by three sedimentary

complexes of Early–Middle, Carnian and Norian Late Triassic ages. The K-Ar ages of abundant sills and hypabyssal dolerite and gabbro bodies characteristic of the Early Triassic range from 233 to 218 Ma (Geodynamic, Magmatism, and Metallogeny..., 2006). The U-Pb zircon age of hypabyssal gabbro from the Kolyuchinskaya Guba area corresponds to 252 ± 4 Ma (Ledneva et al., 2011) and suggests occurrence of the Upper Permian deposits at the base of the Anyui complex.

The Triassic sequence (locality 1 in Fig. 3) is composed of rhythmically interlayered thin beds of silty mudstones, and sandstones occurring in variable proportions from section to section (Tuchkova et al., 2007, 2009). A characteristic feature of the Lower and Middle Triassic sandstones is their graded and cross bedding (Figs. 4 and 5). Typical for these rock units are slump folds and mud chips. The rocks also contain abundant siderite concretions (Fig. 6). The Carnian sandstone unit contains unconformities at the base. Sandstones are usually massive, sporadically intercalated with graded and cross-bedded sets. The Norian fine rhythmic sequence contains abundant *Monotis* shells and trace fossils (worm burrows or fucoids).

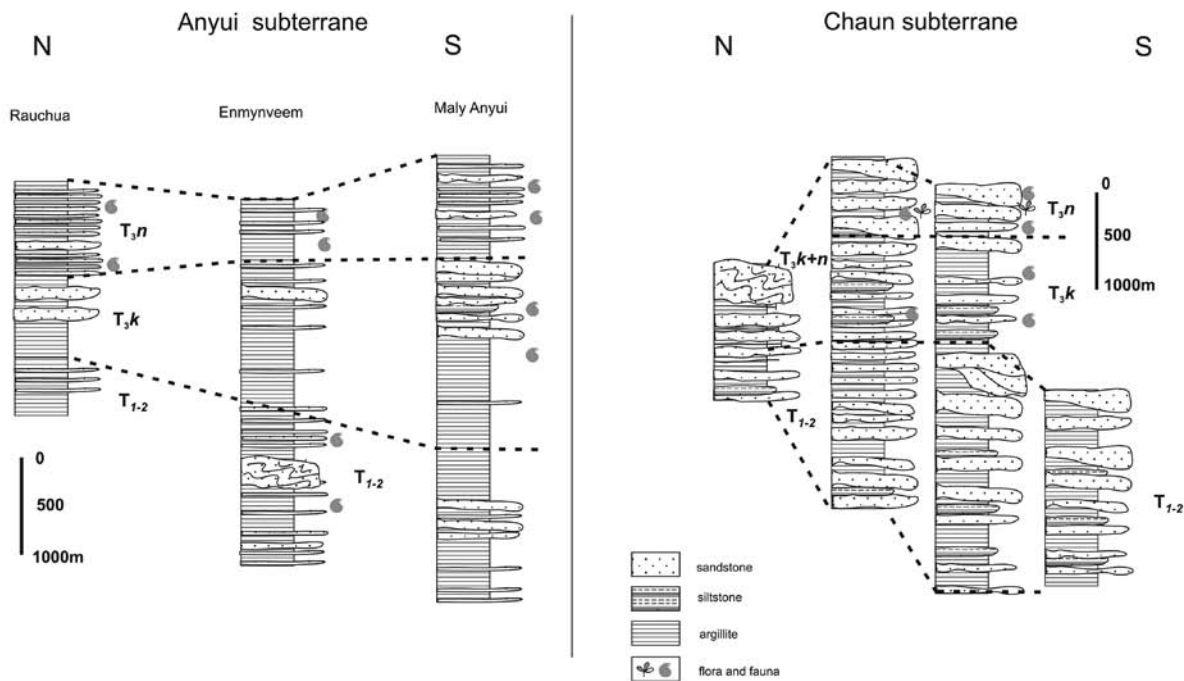


Fig. 5. Correlation of type sections in the northern and southern parts of the Anyui and Chaun subterranea (after Tuchkova et al., 2009, Morgan, 2001).

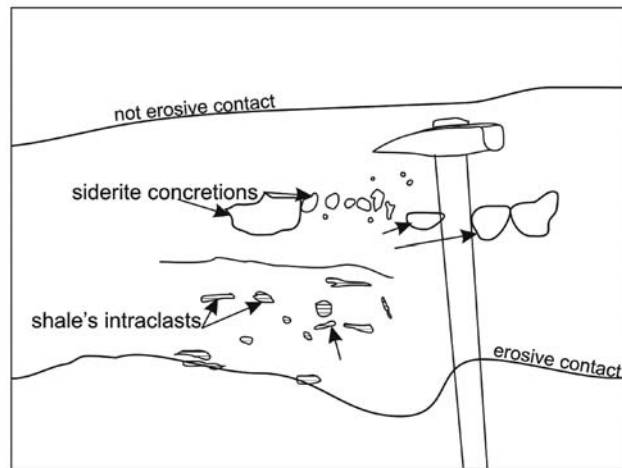


Fig. 6. Fragment of the Aalenian section at the Enmyveem River. The photo shows small clayey intraclasts oriented parallel to the turbidity flow; in the middle part, rounded siderite concretions (light) with the upper surface eroded by the flow. Photo by M.I. Tuchkova.



Fig. 7. Fragments of the Upper Triassic section of the Chaun terrane, Outcrop 44, samples 503/4-3 and 503/2-1. (a) different types of bedding (cross and lenticular, alternating with the laminar bedding) in a sandstone bed; (b) lenticular bed of gravelly coarse-grained sandstone with rounded grains of milky quartz.

Sedimentation in the basin was controlled by a large deltaic system. Distribution of sedimentary facies suggests that the basin was deepening southwestward in present-day coordinates with gradual progradation of the shelf into deeper zones of the basin (Tuchkova, 2011; Fig. 5).

Chauna subterrane.

In the Chauna Bay area and southward of Kibera Cape (locality 2 in Fig. 3), Permian and Triassic terrigenous deposits are represented by siltstones and shales with sandstone interlayers that are locally calcareous. Among the Olenekian strata there are rare lenticular intercalations of small-

pebbled conglomerate (Fig. 7).

On the east of the Chauna subterrane (locality 3 in Fig. 3), Permian and Triassic deposits are exposed along northern spurs of the Pekulney Range and in the Amguema riverhead area (Morozov, 2001). A sequence of interlayered sandstones, siltstones, and mudstones 250–300 m thick in total is tentatively attributed here to the Permian. The undivided Lower–Middle Triassic, Carnian, and Norian deposits conformably rest on this sequence. The maximum thickness of Triassic rocks is estimated as 3.5–4.5 km (Figs. 4 and 5). The Lower–Middle Triassic deposits of the Amguema riverhead area are represented by interlayered sandstone, siltstone, and silty mudstone

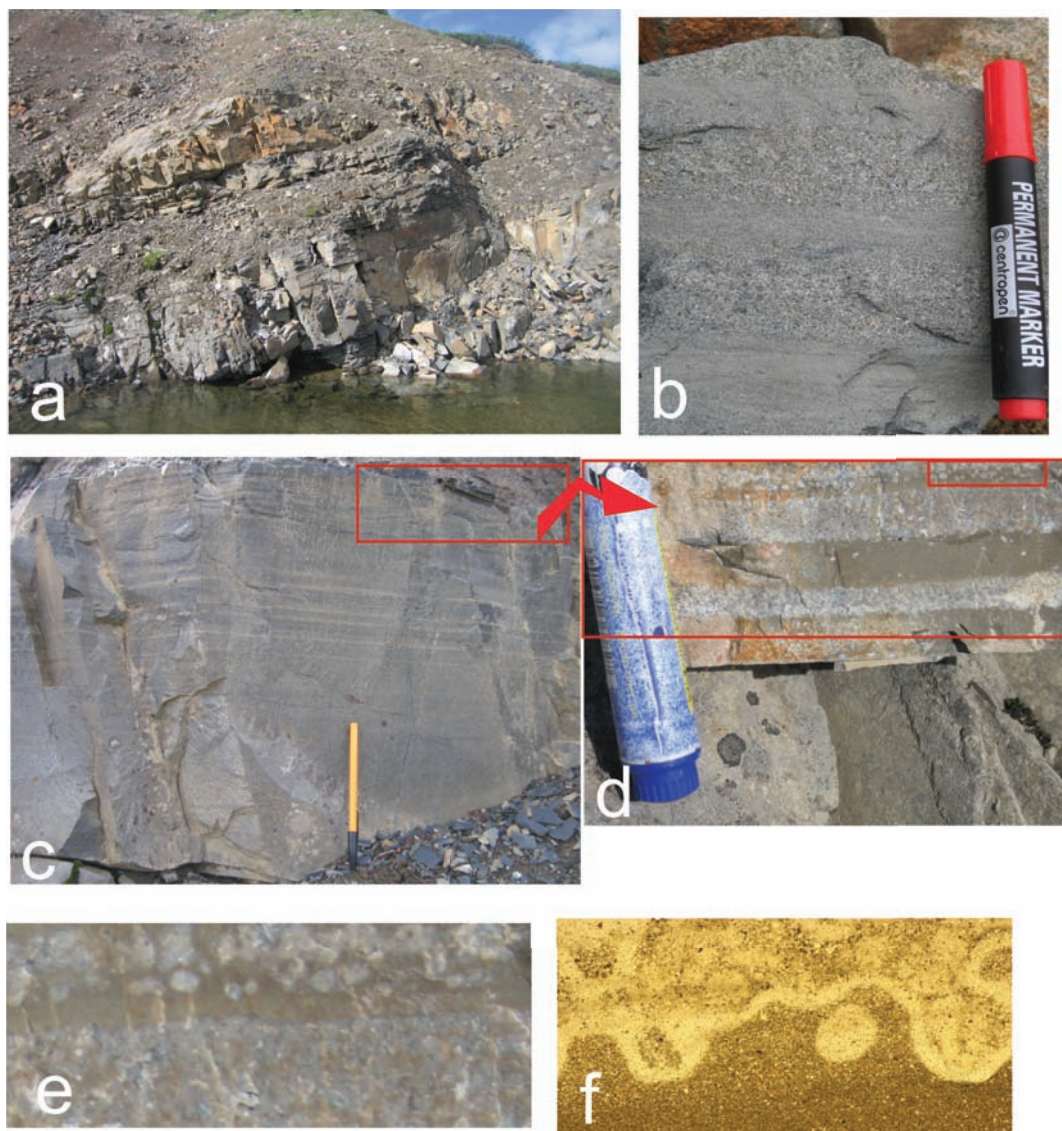


Fig. 8. The Lower–Middle Triassic section along the Ploskaya River. (a) photo by S.D. Sokolov; (b) sediments of density volcanoclastic flows alternating with host silty shales; (c) fragment of the section at the Ploskaya River, host silty shales with laminar bedding, rectangle designates a zone shown in (b); (d) fragment of a bed of brown host silty shales with isolated rounded or slightly flattened structures (hot lava drops); (e) detail of photo (d); (f) microimage of a thin section with rounded volcanoclastic structures intruded into host wet unconsolidated sediments, Sample 357/11.

beds. Gray to greenish gray frequently calcareous sandstones contain siderite concretions.

The Lower–Middle Triassic deposits have of a distinct rhythmic structure. Elements of the rhythms show massive, cross- and laminar bedding. Sole marks and slump structures are typical for the base of the sandstone beds. Upward in the sequence, rhythms become thicker, and sandstone content increases.

In southern and southeastern areas of the subterrane, the Carnian–Norian deposits have the same structure. Concurrent beds of a lesser thickness having lenticular bedding and ripple marks are

observed to the north and northeast of the Amguema riverhead area, where abundant faunal remains and fucoids have been found. Large plant fossils are known from the Norian sandstones and siltstones.

Early–Middle Triassic deposition occurred on a continental slope and rise and was controlled by gravity mass flows, and sandstone bodies increased in abundance by the end of the Middle Triassic (Morozov, 2001). Northward and upward in the sequence shelf sediments replace turbidites. This facies zonation indicates southerly shelf progradation.

In the Ploskaya River basin (locality 4 in Fig.

3), the Permian and Triassic sequence of rhythmic structures is up to 600 m thick, composed of silty sandstone and siltstones with rare sandstone interbeds (Blagodatsky and Bychkov, ed., 1978). Cross- and laminar bedding are characteristic of gray to greenish gray sandstones sometimes containing an admixture of carbonate material (Fig. 8). In the background sediments (argillaceous and silty interlayers) original bedding is often disturbed by impacts of small drop-shaped lapilli. These Permian

and Triassic deposits accumulated most likely on a shallow shelf presumably in coastal marine settings.

Paleogeographic schemes for the Early–Middle and Late Triassic times are shown in Fig. 9. Deltaic systems that controlled discharge of sedimentary material derived from provenances are established in the Anyui terrane and provisionally in the central part of the Chauna subterrane (Tuchkova et al., 2007, 2009).

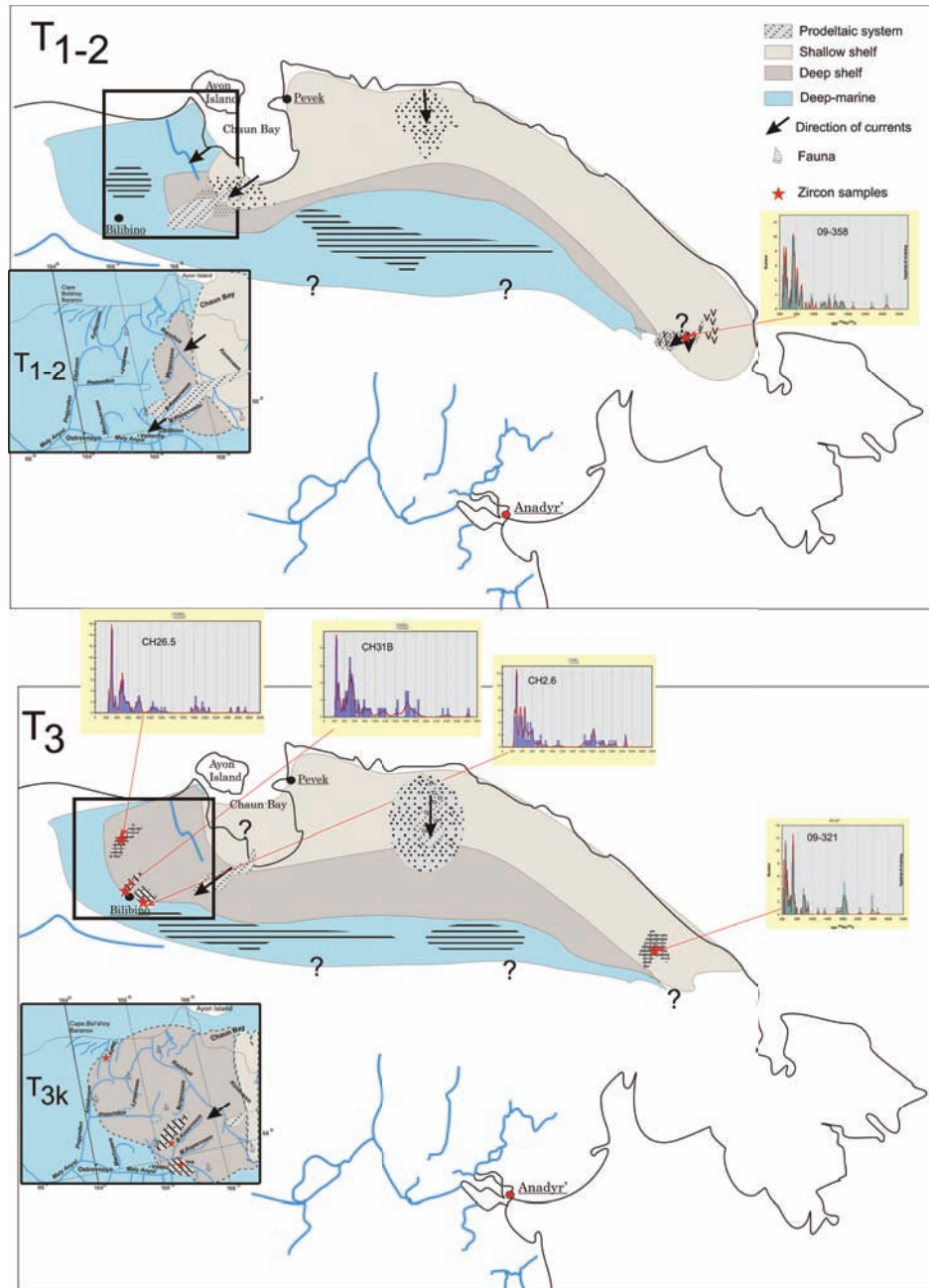


Fig. 9. Paleogeographic reconstruction of the Chukotka basin for the Early-Middle Triassic time (a) and Late Triassic time (b). Black rectangle corresponds to the area shown in the magnified lower part of the figure. Histograms correspond to detrital zircons from sandy rocks; sample positions are shown by arrows.

PERMIAN AND TRIASSIC DEPOSITS OF THE VKFB

Verkhoyansk

On the north of the southern Verkhoyansk region (Figs. 10 and 11), Permian deposits have been studied along the Setorym and Kobyume rivers. These are interlayered beds of poorly sorted sandstones, siltstones, and silty mudstones with rare conglomerate intercalations. The Permian sequence is conformably overlain by Triassic deposits, although some researchers argue for an angular

unconformity at this level (Tectonics, geodynamics and metallogeny of the Sakha Republic, 2001).

The Triassic deposits of the Verkhoyansk terrane are widespread on the north of the South Verkhoyansk (localities 5 and 6 in Figs. 4, 10, 11) and comprise all three series of the system. Near the frontal zone, they overlie Permian strata with an erosion surface at the base, whereas in the inner parts a gradual transition between Triassic and Permian deposits was documented (Parfenov, 1984; Tectonics, geodynamics and metallogeny of

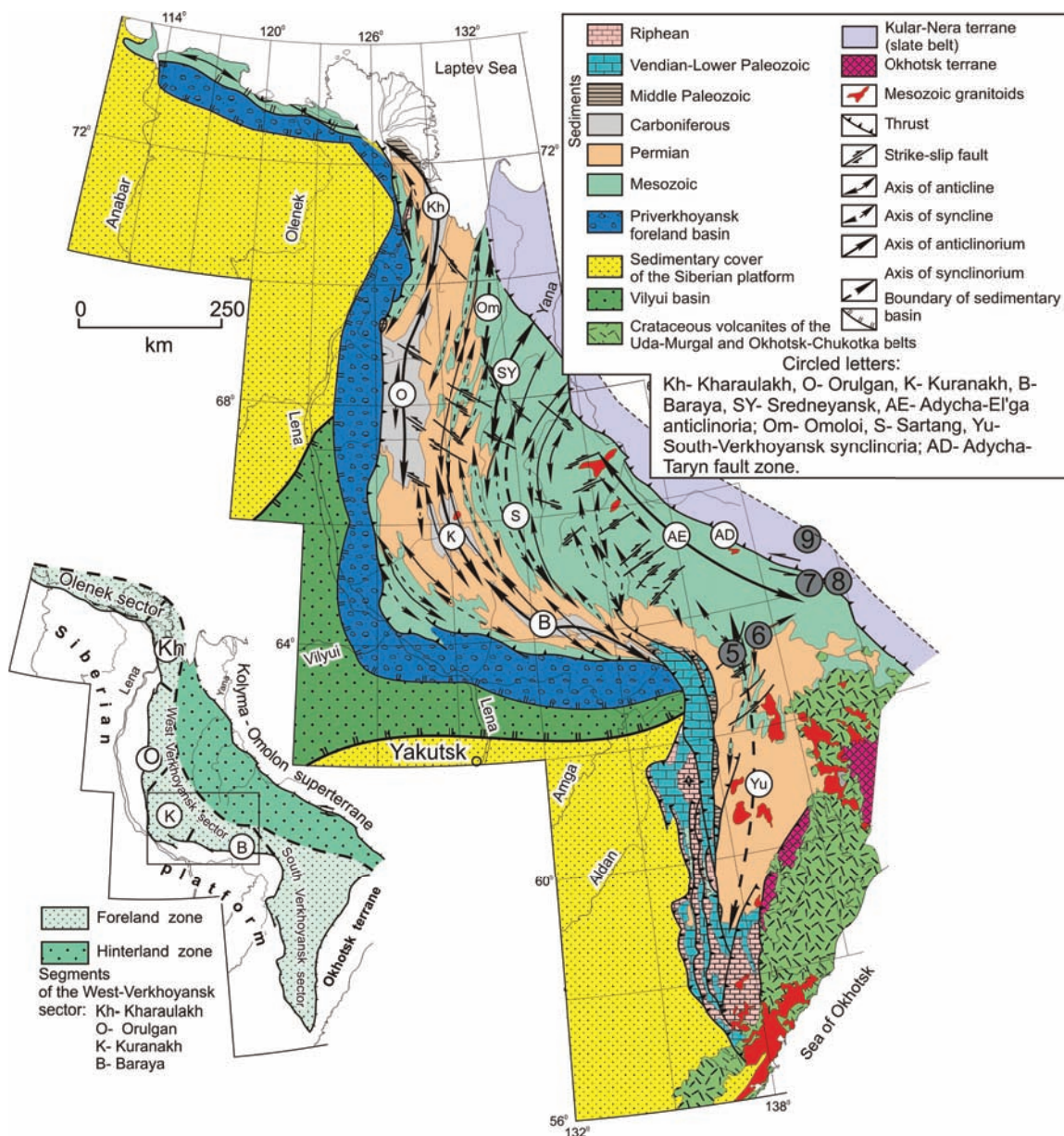


Fig. 10. The main tectonic elements of Verkhoyansk-Kolyma fold belt (Parfenov et al., 1995; Prokopiev et al., 2008). Number in gray circles are the main areas referred to in text and figure 11: 5- Northern part of South Verkhoyansk, Kobyume and Setarym Rivers; 6 – South Verkhoyansk, Allakh-Yun' zone; 7 – Distal part of Verkhoyansk margin; 8, 9 – Kular-Nera terrane (shists belt)

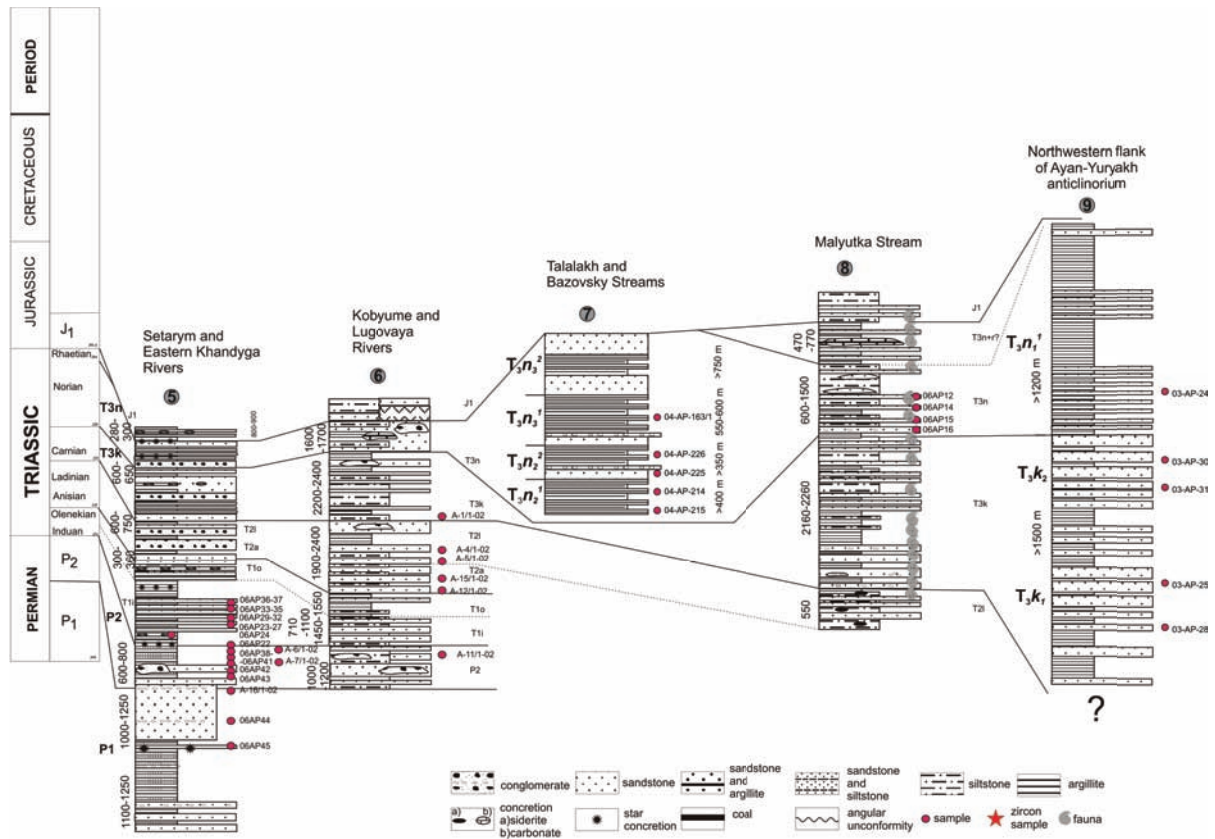


Fig. 11. Correlation chart of the main sections of the Permian and Triassic rock units of Verkhoyansk-Kolyma fold belt. Data source for compiled sections are from Prokopiev et al.,2001; Prokopiev,Ivensen, 2008. Numbers of units are the same that in figure 2 and 10. See description in text.

the Sakha Republic, 2001). This distinction led to recognition of the proximal and distal parts of the Verkhoyansk passive margin.

The Triassic sequence is composed of dark gray to gray and greenish gray sandstones and siltstones, locally intercalated shales and fine-grained calcareous sandstones (Figs 12a, 12b, 12c). Carbonate and clay-carbonate nodules are characteristic of the Lower Triassic strata. Sandstone beds and conglomerate intercalations are more typical for the Carnian–Norian rock units. Total thickness of the sequence is over 7 km.

Characteristic Permian and Triassic rocks of the Allakh-Yun zone (East Khandyga River, locality 6 in Figs. 10, 11) are tuffaceous sandstones and siltstones, as well as mafic to felsic volcanic rocks (Prokopiev and Ivensen, 2008). Submarine fans and associated deep-water deposition occurred here during the Early Permian time, and deltaic systems appeared in the Late Permian (Khudoley and

Guriev, 1994). The Induan Stage corresponds to an epoch of predominantly shallow-water terrigenous sedimentation (Korostelev, 1982; Khudoley and Guriev, 1994).

The Upper Triassic sequence of the Kular–Nera terrane (localities 8 and 9 in Figs. 10, 11) and distal part of the Verkhoyansk margin (locality 7 in Figs. 10, 11) is composed of shales, siltstones, and rare sandstone beds. Among these deposits slope apron facies are identified giving place northeastward to more distal medium- to fine-grained turbidites of a submarine fan (Prokopiev and Tronin, 2004). The Carnian–Norian rocks are over 1000 m thick. Turbidites in the distal part of the Verkhoyansk passive margin (Prokopiev and Tronin, 2004) accumulated clastic material transported into this part of the basin (Fig. 13) by the large rivers paleo-Lena and paleo-Aldan (Prokopiev et al., 2008). The largest rivers run through the area of the present-day Vilyui syncline having sources in the Baikal Mountain system



Fig. 12a. Bedded Permian rocks of the southern Verkhoyansk region. Photo by A.V. Prokopiev. **12b.** Alternating sandstones and silty shales in the Triassic section of the southern Verkhoyansk region. **12c.** Fragments of the section with lenticular bedding

(Kossovskaya et al., 1960; Prokopiev et al., 2008, Fig. 13). The other fluvial system was hypothetically situated at the southern margin of Siberian platform (Korostelev, 1982; Prokopiev et al., 2008).

Triassic sedimentation on the Verkhoyansk passive margin inherited trends of the Paleozoic sedimentation regime. Nevertheless, new facies boundaries were displaced eastward relative to those of the Paleozoic that has been interpreted as evidence

of the passive margin progradation in an easterly direction (Parfenov, 1984; Tectonics, geodynamics and metallogeny of the Sakha Republic, 2001). It has also been postulated that a gradual transition from continental to marine sedimentation and deepening of sea basin progressed from the southwest to the northeast (Korostelev, 1982).

PROVENANCE STUDY

Data on mineral composition, geochemistry, and isotopic characteristics of Triassic sediments from the Chukotka and Verkhoyansk regions (Tables 1a, b and 2a, b) are discussed below to determine paleogeography and tectonic evolution of the respective sedimentary basins.

Petrographic data

According to the classification of Pettijohn (1981), the Lower–Middle and Upper Triassic sandstones of Chukotka correspond respectively to graywackes with more than 15% of matrix and litharenites with 3–10% of matrix. The mineral composition of sandstones is as follows: quartz 10–65%, feldspars 5–45%, lithoclasts 20–75% (Tuchkova et al., 2009). The association of rock-forming components of sandstones suggests that clastic material of Triassic rocks was derived from a provenance composed of metamorphic rocks and subjected to gradual erosion (Tuchkova et al., 2009). In addition, some components of the Lower Triassic sandstones could be derived from volcanogenic rocks of basaltic andesite composition (Tuchkova et al., 2007). As lithoclasts of the Upper Triassic

sandstones are more diverse than in underlying rocks, this can be regarded as an indication of orogenesis and drainage area expansion with time.

Triassic sandstones of the Verkhoyansk region correspond in composition to sublitharenites and lithic arenites (Prokopyev et al., 2008). By the transition from the Lower to Upper Triassic sandstones, increasing quartz content of up to 80–95% of the rock volume is reported. In general, these sandstones consist of quartz (35–65%), feldspars (5–30%), lithoclasts (25–45%), and matrix (5–10%). Rock types identified among lithoclasts are granodiorite, volcanics, and cherts. The amount of lithoclasts decreases upward in the sequence.

Geochemistry

XRF and ICP-MS analyses of sandstones from both study regions are shown in tables 1a, b and 2 a, b. Classification diagrams based on the chemical composition of the analyzed rocks are shown in Figs. 14a and 14b. Data points characterizing the Lower–Middle Triassic sandstones of Chukotka plot, with considerable dispersion, predominantly in the field of graywackes, whereas data points of the Upper Triassic sandstones are displaced into the

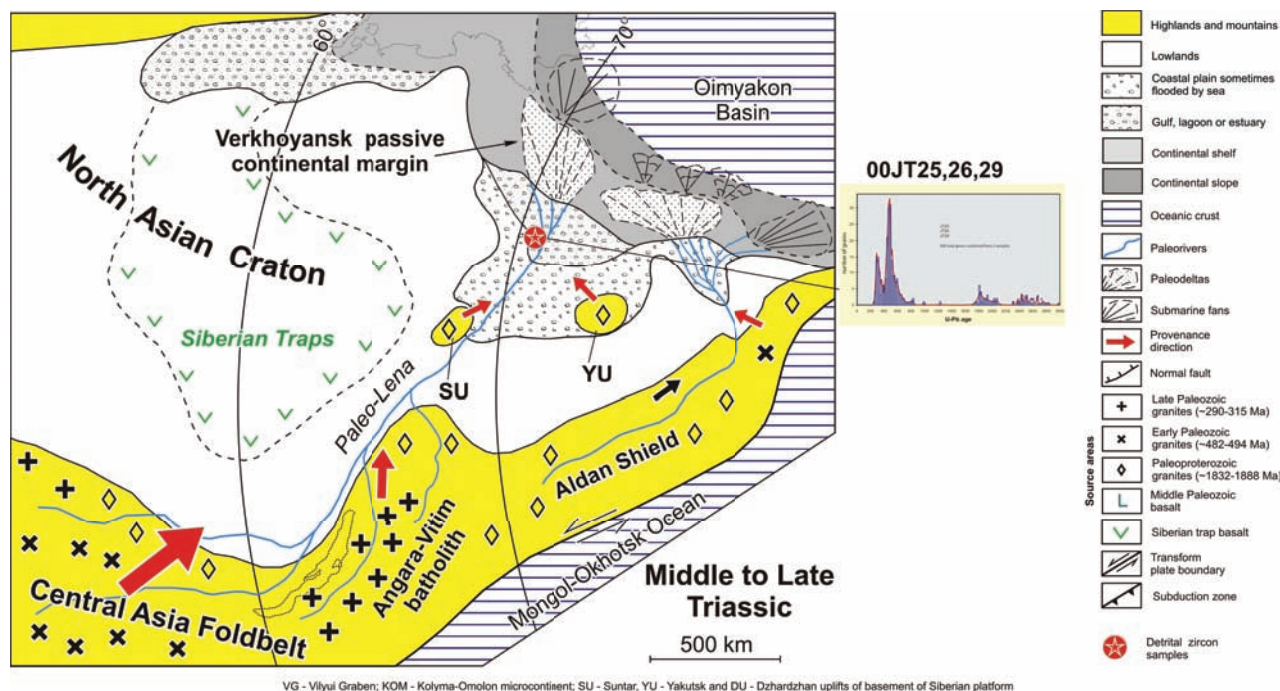


Fig. 13. The schematic paleogeographic map of the Verkhoyansk basin for the Middle–Late Triassic time (from Prokopyev et al., 2009).

Table 1a. Contents of major elements in sandstones of Chukotka region, Triassic unit. Major element were analyzed by XRF method, GIN RAS, Moscow

Map area	sample	Group	Position	SiO2	TiO2	Al2O3	Fe2O3	FeO	MnO	MgO	CaO	Na2O	K2O	H2O-	H2O+	PPP	P2O5	CO2	Sum	
1	329/2-1	T1-2	Enmyneveem River	56,83	1,2	16	2,34	7,67	0,07	3,71	2,41	0,54		2,04		6,48	0,21	1,71	101,21	
	329/2	T1-2	Enmyneveem River	55,92	1,25	15,58	3,54	6,89	0,08	3,82	1,97	2,17		2,05		6,12	0,25	1,04	100,68	
	329/3	T1-2	Enmyneveem River	49,12	1,19	12,03	2,32	5,39	0,11	2,81	11,8	2,32		0,67		11,91	0,18	9,31	109,16	
	404/3	T1-2	Yanramkyvaam River	67,55	0,98	13,46	3,19	3,62	0,05	1,76	0,96	0,49		2,51		4,67	0,2	0,24	99,68	
	405/4n	T1-2	Yanramkyvaam River	47,81	1,71	16,6	4,1	8,83	0,11	4,49	4,29	2,47		1,24		7,38	0,23	2,08	101,34	
	406/3	T1-2	Lyupeveem River	67,68	1,27	11,13	1,64	6,4	0,06	3,63	1,07	2,17		0,22		3,95	0,17	0,34	99,73	
	407/6	T1-2	Lyupeveem River	59,67	0,98	17,92	2,39	3,96	0,07	2,61	1,4	7,67		0,42		2,04	0,18	<0,2	99,31	
	409/2n	T1-2	Str. Tundryoy	71,33	0,99	12,07	1,74	4,19	0,04	1,84	0,61	3,55		0,7		2,47	0,15	0,27	99,95	
	461/7	T1-2?	Vernitakayveem River	65,81	1,34	12,51	0,71	8,32	0,06	3,30	0,25	2,57		0,28		4,17	0,15	0,20	99,67	
	461/7-2	T1-2?	Vernitakayveem River	70,90	1,02	11,78	0,20	6,43	0,04	2,46	0,62	1,28		0,83		4,23	0,14	0,20	100,13	
	460/7	T1-2	Vernitakayveem River	50,04	2	13,53	3,47	9,7	0,17	7,23	5,84	1,74		0,07	0,16	3,89	5,4	0,19	0,83	104,26
	201/5silt	T3k	Maly Anyui River	77,18	0,77	9,51	1,9	2,52	0,07	2,58	0,26	1,9		1,06		0,17	2,2	0,14	0,46	100,72
	201/5san	T3k	Maly Anyui River	75,94	0,59	8,68	1,76	2,95	0,1	2,34	1,06	1,42		0,9		0,22	3,49	0,13	1,33	100,91
	422/z	T3k	Maly Anyui River	67,72	0,73	12,68	1,04	3,88	0,07	2,18	1,98	1,05		1,93		6,16	0,13	3,05	102,60	
200/9a	T3k	Billibino	68,53	0,77	11,9	2,06	6,36	0,13	1,94	1,2	1,52		1,16		3,92	0,17	0,29	99,95		
400-3-2	T3k	Maly Keperveem River	70,85	0,55	9,29	4,12	3,97	0,13	1,69	1,25	1,52		0,77		5,13	0,15	1,76	101,18		
414/3n	T3k	Kytepguytenyveem R.	76,46	0,56	5,23	1,73	4,35	0,06	1,62	1,82	0,27		0,65		6,57	0,11	5,43	104,86		
414/7	T3k	Kytepguytenyveem R.	76,97	0,6	9,67	2,54	2,69	0,04	1,15	0,23	0,97		1,48		2,99	0,14	0,35	99,82		
416/3	T3k	Srt. Gnom	73,27	0,59	8,66	2,2	2,63	0,08	1,64	2,36	1,91		0,75		5,2	0,12	3,41	102,82		
417/4	T3k	Str.Ugol	73,9	0,58	9,43	1,93	2,47	0,03	1,1	1,31	2,1		0,99		5,54	0,15	4,14	103,67		
417/6	T3k	Str.Ugol	68,18	0,68	11,46	2,35	4,25	0,03	1,36	0,82	2,34		1,35		6,73	0,14	4,56	104,25		
454/3	T3n	Machvavaam River	71,82	0,82	10,9	2,63	2,52	0,05	1,21	0,56	1,17		1,51	0,57	2,37	6,3	0,08	2,95	105,46	
K-04-43	T3n	Machvavaam River	67,68	0,82	13,08	1,67	3,9	0,15	1,38	0,56	1,19		1,78	0,8	3,31	7,55	0,11	3,45	107,43	
454/8-2	T3n	Machvavaam River	72,8	0,59	10,44	1,37	4,86	0,17	1,72	0,74	1,54		1,05	0,52	2,58	4,15	0,1	0,92	103,55	
456/4	T3n	Pyrkanay Ridge	75,08	0,4	8,23	2,88	1,72	0,3	1,41	2,41	1,42		0,93	0,39	1,68	5,04	0,11	2,99	104,99	
453/1	T3n	Irguneyveem River	71,3	0,63	10,42	0,63	6,48	0,13	1,56	0,87	1,71		0,97	0,6	2,15	4,51	0,17	1,68	103,81	
358/1	P-T	Ploskaya River	56,84	0,9	14,24	1,48	4,56	0,13	2,71	5,1	1,3		2,05		9,83	0,24	4,81	104,19		
357/3	P-T	Ploskaya River	56,64	1,11	20	2,2	4,85	0,06	3,6	0,5	0,69		3,89		5,48	0,25	0,24	99,51		
343/5	P-T	Lukovaya Mts	64,68	0,83	12,46	1,43	4,53	0,09	2,87	3,52	1,85		1,02		5,69	0,24	2,54	101,75		

Table 1b. Contents of major elements in sandstones of the Verkhoyansk region, Permian-Triassic unit. Major element were analyzed by XRF method, VSEGEI, Spetersburg

Map area	sample	Group	Position	SiO2	TiO2	Al2O3	Fe2O3	FeO	MnO	MgO	CaO	Na2O	K2O	H2O-	H2O+	PPP	P2O5	CO2	Sum
5	06AP21	<i>P₂im₂</i>		84,28	0,24	6,78	0	1,52	0,07	0,67	0,77	2,52	0,93	0,18	0,65	0	0,38	0,53	99,47
	06AP25	<i>T₁nc₁</i>		63,88	0,61	10,17	1,94	6,64	0,45	1,96	5,41	0,99	0,99	0,28	3,36	0,14	0,92	2,33	99,93
	06AP29	<i>T₁nc₂</i>		62,21	0,87	12,72	1,34	5,85	0,18	2,77	4,03	1,74	1,7	0,32	3,73	0	0,34	2,38	100
	06AP31	<i>T₁nc₂</i>		76,64	0,4	11,03	0,44	2,39	0,09	1,19	0,98	2,76	1,54	0,22	1,25	0	0,38	0,25	99,35
	06AP32	<i>T₁nc₂</i>	South part of	67,66	0,64	15,18	1,1	3,61	0,09	1,6	0,45	2,6	3,77	0,08	2,41	0	0,38	0	99,51
	06AP34	<i>T₁nc₂</i>	Verkhoyansk	73,51	0,63	11,83	0,88	3,04	0,06	1,04	1,07	3,29	2,28	0,02	1,52	0	0,38	0	99,54
	06AP36	<i>T₁nc₂</i>		76,71	0,34	10,12	0,15	1,49	0	0,83	2,35	3,33	1,97	0,1	0,93	0	0,36	1,35	99,94
	06AP37	<i>T₁nc₂</i>		76,94	0,35	11,26	0,26	2,23	0	0,75	0,71	3,55	2,3	0,24	0,88	0,13	0,36	0	99,74
	06AP38	<i>P₂im₂</i>		63,47	0,62	13,33	1,04	1,89	0,22	1,93	5,16	3,65	2,51	0,22	1,97	0	0,36	3,44	99,86
	06AP39	<i>P₂im₂</i>		62,69	0,8	17,3	2,26	2,17	0,04	3,1	0,3	3,6	3,99	0,56	2,21	0	0,42	0	99,88
04-AP-215	<i>T3nor</i>	Str.Bazovsky	81,63	0,33	7,9	2,75	0,47	0,05	0,31	0,71	2,17	1,25			1,53	0,38	0	99,48	
04-AP-225	<i>T3nor</i>	Str.Bazovsky	89,43	0,12	3,99	0,86	0,36	0,03	0,72	1,03	1,24	0,4			0,89	0,11	1,05	100,3	
04-AP-226	<i>T3nor</i>	Str.Bazovsky	79,35	0,47	8,62	0,95	1,57	0,05	0,91	1,24	2,43	1,17			1,72	0,19	1,62	100,3	
04-AP-163/2	<i>T3nor</i>	Str.Talalakh	62,1	0,72	10,76	0,78	3,85	0,31	2,84	6,43	1,47	1,86			2,76	0,48	5,45	99,86	
04-AP-164	<i>T3nor</i>	Str.Talalakh	62,92	0,81	11,7	0,75	4,65	0,22	2,9	4,98	1,38	2			2,76	0,45	3,86	99,41	
04-AP-192	<i>T3nor</i>	Str.Bazovsky	80,67	0,28	9,39	1,15	1,71	0,03	0,7	0,56	1,8	1,51			1,53	0,19	0	99,58	
04-AP-211	<i>T3nor</i>	Str.Bazovsky	76,47	1,28	9,41	3,32	0,89	0,05	0,6	1,5	1,6	1,83			2,13	0,33	0,55	100	
04-AP-212	<i>T3nor</i>	Str.Bazovsky	57,84	0,63	11,49	1,01	3,91	0,36	2,31	6,42	2,98	1,94			2,4	0,39	8,28	99,96	
04-AP-214	<i>T3nor</i>	Str.Bazovsky	80,09	0,16	9,59	2,5	0,48	0,05	0,51	0,43	2,36	1,63			1,89	0,16	0	99,85	
04-AP-220	<i>T3nor</i>	Str.Bazovsky	65,08	0,84	13,57	3,61	2,17	0,09	1,7	0,96	2,07	2,72			3,57	0,48	2,48	99,36	
04-AP-221	<i>T3nor</i>	Str.Bazovsky	57,82	0,99	15,55	3,6	3,73	0,04	3,09	0,53	2,33	3,36			4,96	0,48	2,7	99,23	
04-AP-223	<i>T3nor</i>	Str.Bazovsky	60,41	1,03	15,11	0,83	4,95	0,05	2,64	0,96	2,17	3,09			4,05	0,58	3,7	99,59	
04-AP-219	<i>T3nor</i>	Str.Bazovsky	52,43	1,18	18,98	2,75	3,3	0,05	2,9	0,87	2,39	4,32			7,32	0,45	2,21	99,22	
04-AP-221	<i>T3nor</i>	Str.Bazovsky	58,46	1,07	17,1	2,7	2,76	0,03	2,12	0,56	2,57	3,56			5,97	0,45	2,17	99,57	
04-AP-233	<i>T3nor</i>	Str.Bazovsky	57,42	1,19	19,4	4,83	3,23	0,04	2,04	0,22	2,26	3,56			4,6	0,48	0	99,34	
8	06AP12	<i>T3</i>	Str.Pyl'	48,28	0,69	11,77	1,19	6,1	0,48	3,51	8,55	1,43	2,12	0,06	3,34	0	0,33	12,08	99,95
	06AP14	<i>T3</i>	Str.Malyutka	72,17	0,25	6,02	0,4	3,86	0,11	1,71	4,64	1,5	0,96	0,08	0,73	0	0,53	6,37	99,27
PROK-1	<i>T₁tl</i>	Western part of	71,18	0,81	11,27	2,15	3,86	0,07	1,55	1,24	2,67	1	0,26	2,67	0,26	0,39	0,27	99,39	
PROK-2	<i>T₁tl</i>	Verkhoyansk	69,95	0,78	13,28	1,5	2,89	0,06	1,05	1,09	3,62	1,92	0,24	2,14	0	0,37	0,82	99,51	
PROK-3	<i>P₂dl</i>	margin	68	0,36	11,02	0,35	1,4	0,1	0,41	5,69	3,27	1,85	0,16	1,98	0	0,32	4,89	99,65	

Table 2a. Minor and Rare earth element composition (ppm) of Permian and Triassic sandstones of Chukotka basin

Map		Co	Ni	Zn	Sc	V	Cr	Y	Ba	La	Ce	Pr	Nd	Sm	Eu	Gd	Tb	Dy	Ho	Er	Tm	Yb	Lu	Hf	Ta	Th	U	
1	B-1-1/1	T1-2	18,8	69,5	129	14,1	143	57,4	21,7	591	30,1	64,2	6,6	24,6	4,9	1,2	4,5	0,66	3,9	0,78	2,4	0,34	2,3	0,32	4,0	0,63	6,0	2,2
	329/3-3	T1-2	10,4	41,4	62,0	9,0	80,5	31,1	15,6	243	18,8	45,6	4,6	17,8	3,5	0,52	3,3	0,47	2,6	0,56	1,7	0,25	1,6	0,23	3,2	0,43	4,9	1,5
	422/z	T3k	19,3	58,5	122	11,8	99,6	62,0	17,8	214	24,6	53,2	5,2	20,1	3,9	0,80	3,8	0,56	3,2	0,64	1,9	0,27	1,9	0,26	3,1	0,59	6,6	1,8
2	503/2-1	T3	9,0	40,4	65,9	13,3	139	109	29,8	518	33,9	68,4	7,8	31,4	6,1	1,2	5,4	0,84	5,2	1,1	3,3	0,47	3,3	0,48	6,4	1,1	13,2	2,7
	357/1	P-T	10,4	35,8	72,5	9,7	59,5	55,5	6,6	164	16,0	35,4	3,7	14,6	2,7	0,55	1,9	0,23	1,6	0,23	0,7	0,10	0,9	0,13	1,5	0,33	4,9	1,3
4	343/5	P-T	9,7	77,5	84,9	19,0	234	126	14,2	744	24,1	71,6	5,9	23,5	4,9	1,2	4,3	0,60	3,4	0,71	2,2	0,34	2,5	0,40	4,5	1,0	7,2	3,4
	358/1	P-T	9,8	61,4	104	14,2	125	131	12,5	246	19,8	47,2	5,5	22,8	5,0	1,1	4,5	0,64	3,3	0,62	1,7	0,26	1,8	0,26	2,2	0,50	4,9	1,7
			12,0	65,3	297	16,1	142	99,1	21,9	354	19,5	49,0	5,9	25,8	5,9	1,6	5,9	0,89	5,0	0,97	2,8	0,40	2,7	0,41	3,3	0,70	6,1	2,6

Table 2b. Minor and Rare earth element composition (ppm) of Permian and Triassic sandstones of Verkoyansk basin

Map		Co	Ni	Zn	Sc	V	Cr	Y	Ba	La	Ce	Pr	Nd	Sm	Eu	Gd	Tb	Dy	Ho	Er	Tm	Yb	Lu	Hf	Ta	Th	U		
5	06AP21	<i>P₂im₂</i>	8,16	43,2	28,4	2,87	20,5	326	8,09	118	16,6	33,1	3,51	12,9	2,12	0,52	2,19	0,3	1,58	0,31	0,91	0,13	0,91	0,14	2,81	0,74	3,64	1,05	
	06AP25	<i>T₁nc₁</i>	28,2	37,4	71,3	14,3	129	111	39,2	159	38,6	92,8	12,1	54,5	13,9	3,75	15,5	1,98	10,1	1,63	3,77	0,46	2,92	0,43	5,02	1,27	6,08	1,39	
	06AP29	<i>T₁nc₂</i>	28,2	41,8	86,9	16,6	151	80	28,3	264	34,4	77,4	8,88	35,1	6,6	1,7	7,43	1	5,7	1,1	3,09	0,46	3,03	0,45	7,02	1,7	8,5	2,1	
	06AP31	<i>T₁nc₂</i>	9,94	23,7	41,1	6,78	55,2	145	15,9	290	33,8	68,7	7,78	28,5	4,94	1,14	4,92	0,61	3,23	0,61	1,73	0,28	1,8	0,27	7,24	1,31	7,73	1,64	
	06AP32	<i>T₁nc₂</i>	19,5	28,3	87,1	9,2	71,7	71,8	25,3	980	43,2	90,1	10,3	39,1	7,47	1,44	6,84	0,94	5,11	1,01	2,9	0,4	2,74	0,4	8,43	1,92	11,3	2,45	
	06AP34	<i>T₁nc₂</i>	16,5	20	64,4	7,23	61	107	20,5	791	44	89,4	10,2	36,6	6,32	1,7	6,2	0,81	4,19	0,74	2,2	0,31	2,07	0,35	10,8	1,72	13,8	2,18	
	06AP36	<i>T₁nc₂</i>	8,18	14,5	35,3	5,25	28,1	151	13,3	667	32,5	64,3	6,83	25,1	4,26	1,1	4,12	0,54	2,79	0,49	1,36	0,2	1,23	0,2	4,86	0,94	7,7	1,15	
	06AP37	<i>T₁nc₂</i>	10,5	17,4	36,1	4,85	34,7	129	13,4	822	29,8	64	6,91	25,5	4,3	1,12	4,42	0,53	2,86	0,52	1,5	0,22	1,39	0,22	5,56	1,19	7,85	1,34	
	06AP38	<i>P₂im₂</i>	13,8	14,7	70,5	8,75	51,1	83,4	23,5	701	30,6	64,3	7,55	28,5	5,44	1,43	5,66	0,81	4,6	0,85	2,4	0,33	2,23	0,36	7,39	1,29	8,72	2,52	
	06AP39	<i>P₂im₂</i>	16,6	16,9	50,2	8,62	67,5	61,4	22,2	791	41,5	85,1	9,6	35,4	6,12	1,36	6,25	0,82	4,5	0,9	2,57	0,39	2,76	0,42	8,76	1,69	11	2,96	
	8	06AP12	<i>T₃</i>	22,5	42,6	92,2	13	87,4	57,7	24,3	278	24,5	50,1	5,88	23,6	5,34	1,57	6,48	0,85	4,86	0,9	2,34	0,33	2,12	0,32	3,92	1,43	6,25	1,81
		06AP14	<i>T₃</i>	8,55	30,1	46,9	6,39	95,5	164	22,4	157	16,5	39,4	4,87	20,9	5,1	1,44	6,14	0,85	4,77	0,89	2,14	0,27	1,65	0,25	2,36	0,75	5,6	1,49
	9	A3/S-1	<i>T₃</i>	9,4	37,3	65,9	8,5	87,6	44,4	15,8	561	30,9	64,4	6,5	24,1	4,4	0,89	3,9	0,54	3	0,6	1,8	0,26	1,8	0,25	4,1	0,61	7,1	1,8
03AΠ25		<i>T₃</i>	8,7	66,1	120	4,5	46,5	20,2	10,7	60,0	14,4	31,3	3,5	14,4	3,3	0,64	2,9	0,4	1,9	0,36	1,1	0,15	1,1	0,16	2,8	0,32	4,4	1,1	

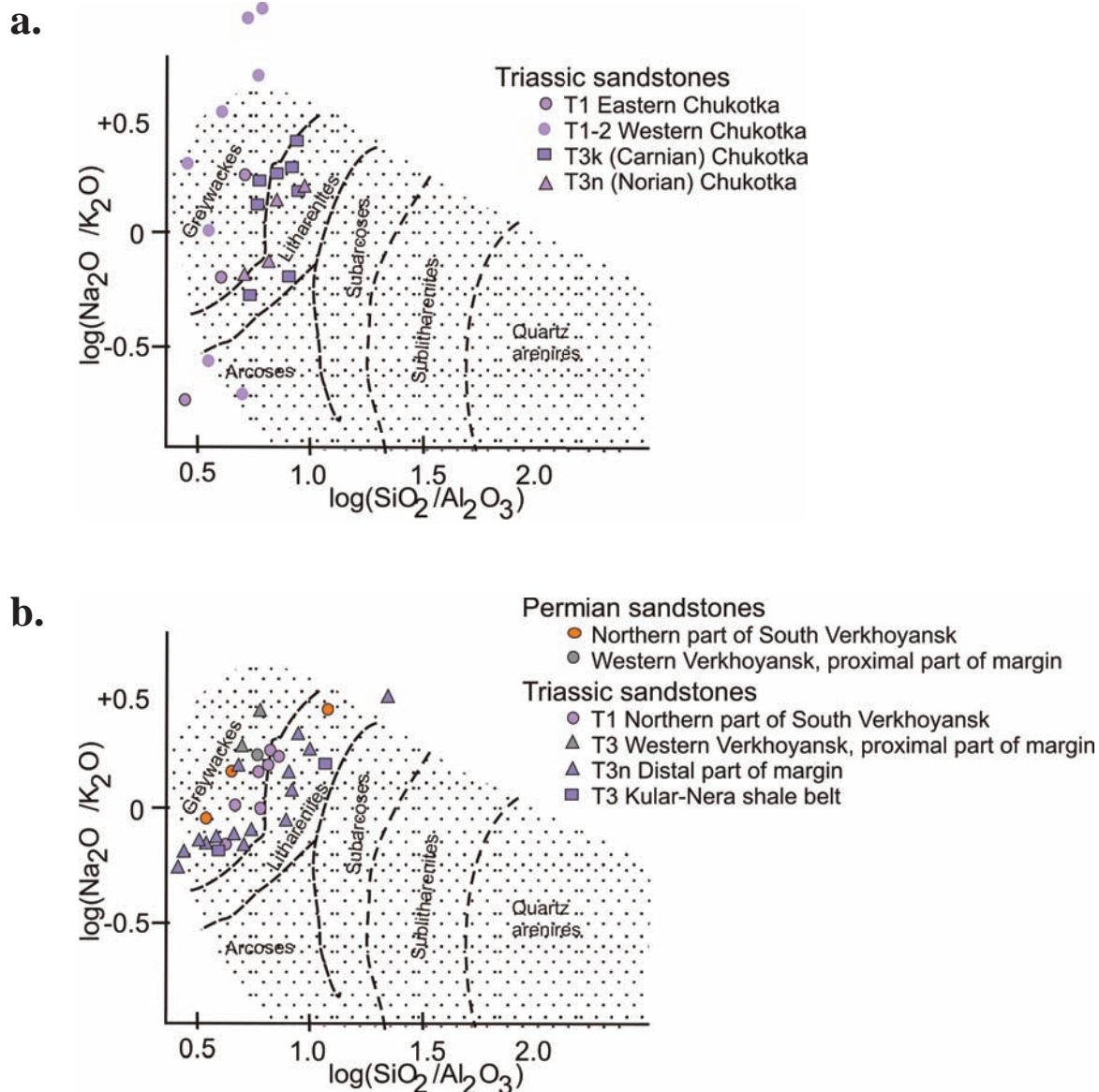


Fig. 14a. Classification diagram after Pettijohn et al. (1987) showing distribution of major components in the Triassic sandstones of the Anyui-Chukotka fold belt. Triassic sandstones: T1 Eastern Chukotka; T1-2 Western Chukotka; T3k Chukotka; T3n Chukotka. **Fig. 14b.** Classification diagram after Pettijohn et al. (1987) showing distribution of major components in the Permian and Triassic sandstones of the Verkhoyansk-Kolyma fold belt. Permian sandstones: Northern part of the South Verkhoyansk region; Western Verkhoyansk region, proximal part of the Verkhoyansk margin; Triassic sandstones: Northern part of the South Verkhoyansk region, T1; Western Verkhoyansk region, proximal part of the Verkhoyansk margin, T3; Distal part of the Verkhoyansk margin, T3n; Kular-Nera shale belt, T3.

field of litharenites. In general Fig. 14a illustrates growing compositional maturity of clastic material during the Triassic.

Triassic sandstones of the Verkhoyansk-Kolyma belt are divisible in two groups (Fig. 14b), of graywackes and litharenites with different $\log \text{Na}_2\text{O}/\text{K}_2\text{O}$ values. Graywackes with negative values of this parameter are from the distal part of the Verkhoyansk margin, whereas positive values are

characteristic of litharenites from the proximal part of that margin (Fig. 14b). This trend in distribution of data points can be regarded as indicating the previous existence of several provenances of clastic material in the Verkhoyansk region.

The chondrite-normalized rare earth elements (REE) distribution patterns for sandstones from both regions (Figs. 15a and 15b) are sufficiently uniform and typical of terrigenous sediments from

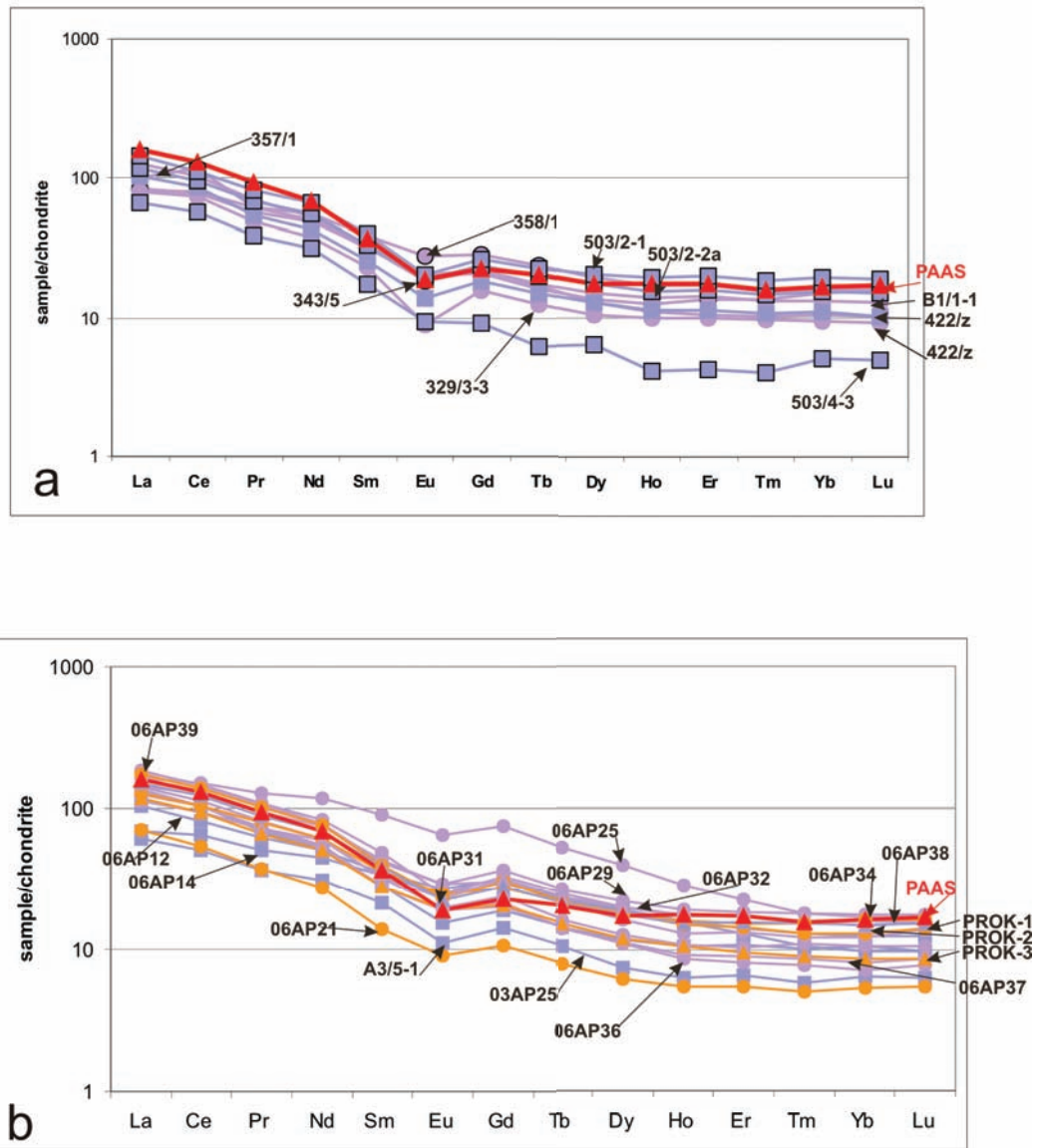


Figure 15. Plots of REE distribution in the Triassic sandy rocks of the Anyui–Chukotka (a) and Triassic sections of the Verkhoyansk–Kolyma (b) fold belts; red line shows the PAAS spectrum.

passive continental margins. As for distinctions between separate groups of rocks, it should be noted that practically all Triassic sandstones from Chukotka are depleted in REE relative to their concentrations in the Post-Arhean Australian Shale (PAAS). On the other hand, the REE concentrations in the Lower Triassic sandstones of the Verkhoyansk region are somewhat higher than in concurrent rocks of Chukotka, whereas the other sandstones of this region are relatively depleted in REE. These geochemical characteristics presumably suggest the polycyclic formation of the Lower Triassic deposits in the north of the southern Verkhoyansk region.

The high Th/U ratios (>4 , from 3.45 to 6.69, Tables 2 b) in sandstones of this region are also indicative of their polycyclic origin and suggest a considerable influence of the Old Upper Continental Crust (Taylor and McLennan, 1988) on their composition that is clearly seen in the Lower Triassic rocks. In the Lower–Middle Triassic sandstones of Chukotka, the Th/U ratio changes from 2 to 3.5 and rises up to 3.4–5 in the Upper Triassic rocks. This geochemical trend excluding the polycyclic origin of rocks suggests the influence of the Young Undifferentiated Arc source on their composition (Tables 2a and 2b).

To determine the rock types of provenances,

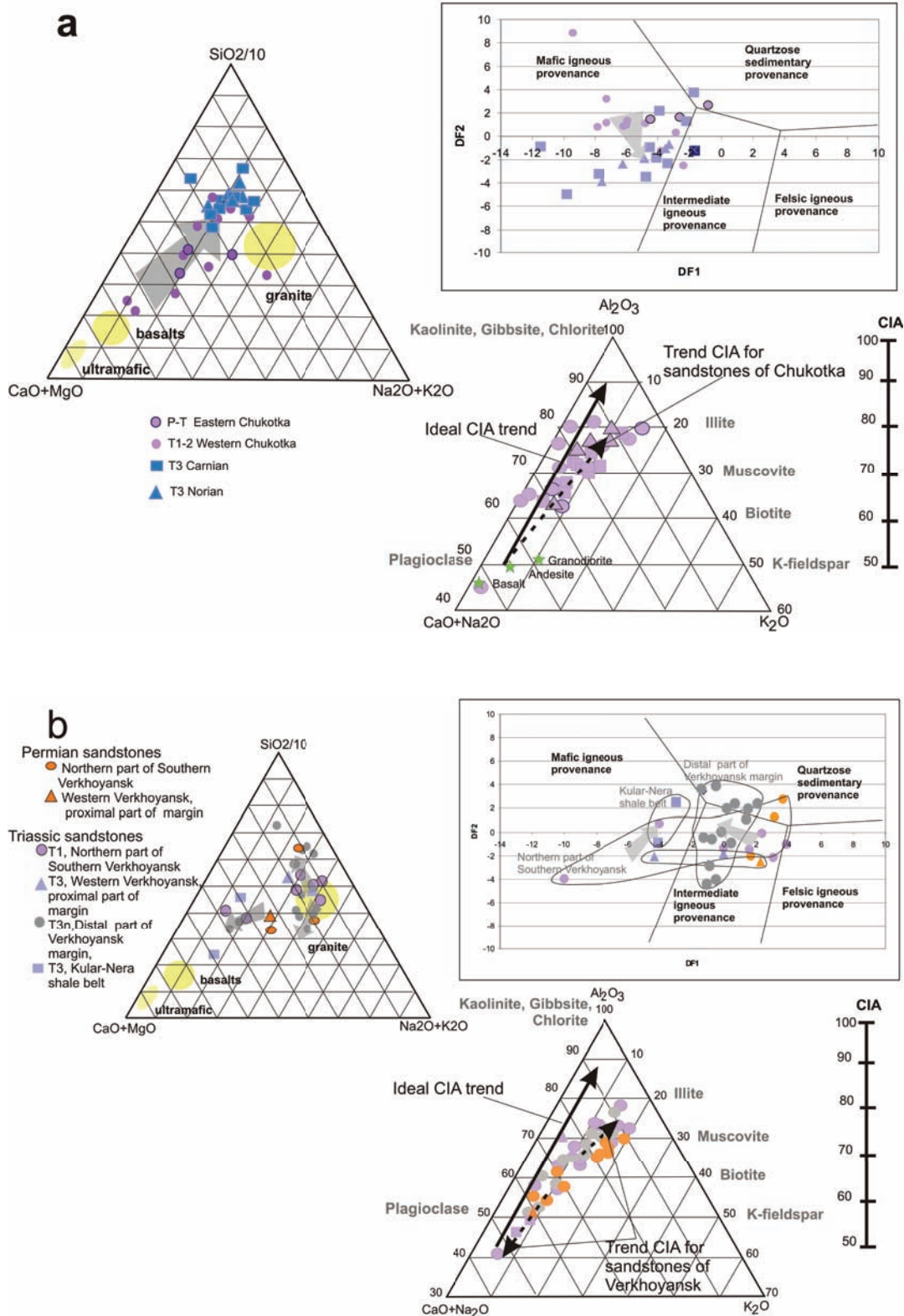


Fig. 16. Discriminant diagrams for compositions of provenances for Triassic sandy rocks of the Anyui–Chukotka (a) and Verkhoyansk–Kolyma (b) fold belts. The arrow shows the evolutionary trend of rock compositions during the Triassic. Left diagram after Taylor and McLennan (1988); Upper right discriminant diagram for major component provenance, after Roser and Korsch (1988). Discriminants and fields are $DF1=30.6038TiO_2/Al_2O_3-12.541Fe_2O_3(total)/Al_2O_3+7.329MgO/Al_2O_3+12.031 Na_2O/Al_2O_3+35.42K_2O/Al_2O_3-6.382$. $DF2=56.500TiO_2/Al_2O_3-10.879 Fe_2O_3(total)/Al_2O_3 +30.875MgO/Al_2O_3-5.404Na_2O/Al_2O_3+11.112K_2O/Al_2O_3-3.89$. Bottom right, $Al_2O_3-CaO+Na_2O-K_2O$ diagram (CIA, Nesbitt and Young, 1984) showing compositions for Permian and Triassic sandstone of the Chukotka (a) and Verkhoyansk (b) basins (molar proportions). Average values for basalt, andesite, and granodiorite are from McLennan et al. (2003).

we used diagrams by Taylor and McLennan (1995) and by Roser and Korsch (1988), in which the rocks studied are compared with typical rocks of ultramafic, mafic, and felsic compositions. In the $\text{CaO} + \text{MgO} - \text{Na}_2\text{O} + \text{K}_2\text{O} - \text{SiO}_2/10$ diagram (Taylor and McLennan, 1988, Figs. 16a and 16b), Triassic sandstones from Chukotka suggests mixing of material derived from basaltic and granitoid rocks, its gradual compositional maturation, and increase of felsic components in the rocks by the end of the Late Triassic (Fig. 16a).

In the discriminant function (DF1–DF2) diagram (after Roser and Korsch, 1988), the Triassic sandstones of Chukotka are indicative of mafic provenances (Fig. 16a). The Upper Triassic sandstones appear to be slightly displaced toward the field of the intermediate igneous provenance, which implies an elevated content of the silicate component and presumably, higher maturity of clastic material.

The behavior of rock-forming elements provides grounds for estimating the degree of clastic material weathering in the provenance (Chemical Index of Alteration, CIA, after Nesbitt and Yang, 1982, Fig. 16a). Ideally, the CIA trend reflects the degree of rock weathering in the provenance and the loss of K_2O and Al_2O_3 ; therefore, it is oriented parallel to the left side of the triangle. For the Chukotka sandstones, the CIA trend exhibits directions similar to an ideal one, though displaced toward higher K_2O concentrations. Potassium enrichment is typical for diagenetic and/or later hydrothermal processes.

In the diagram $\text{CaO} + \text{MgO} - \text{Na}_2\text{O} + \text{K}_2\text{O} - \text{SiO}_2/10$ (after Taylor and McLennan, 1988), Permian–Triassic rocks of the Verkhoyansk region form two fields (Fig. 16b). In one of them, the rocks point to a granite source. Another field corresponds to basalts. Moreover, they demonstrate differently directed compositional changes through the section from the base upward. In the first case, the content of $\text{CaO} + \text{MgO}$ content increases from proximal to distal parts of the margin, while in the second one, no regular changes are observed in the sandstone lithology. Such distributions of oxides in sandstones suggest different provenances.

In the DF1–DF2 diagram (after Roser and Korsch, 1988), Permian and Lower Triassic sandstones of the southern Verkhoyansk region and Upper Triassic rocks of the distal part of the margin

are located in the field of the intermediate and quartzose sedimentary provenance (Fig. 16b). The sandstones of the Kular–Nera terrane correspond to the field of mafic rocks.

The index CIA calculated for Permian–Triassic rocks of the Verkhoyansk basin shows that they are immature in composition, i.e., the degree of weathering in the provenance was insignificant (Fig. 16b). The CIA determined for Permian sandstones is similar to that inferred for their Triassic counterparts. Therefore, it may be concluded that sandstones of the Verkhoyansk region are characterized by the trend opposite to maturation (Fig. 16b). This may be explained only by mixing of clastic material from different sources and different duration of its transportation, which prevented maturation in the provenance.

The $\text{SiO}_2/\text{Al}_2\text{O}_3$ ratio, which is sensitive to fractionation of terrigenous material during its transportation and deposition, represents another indicator of maturity. For the Permian–Triassic rocks of the Verkhoyansk region, this ratio is highly variable ranging from 2.6 to 10.3. Moreover, synchronous rocks may be characterized by different fractionation levels. The $\text{SiO}_2/\text{Al}_2\text{O}_3$ ratio in Chukotka sandstones increases from 2.5–4.0 in the Lower Triassic to 6–8 in Upper Triassic parts of the section (Tables 2a, 2b). These data point to substantially lower fractionation of clastic material during its transportation to the Chukotka basin in the Early Triassic as compared with that in the Late Triassic.

Figures 17a and 17b present diagrams that allow the composition of rocks in provenances to be evaluated. They are based on proportions of minor elements in sedimentary rocks, which are less sensitive to post-sedimentary transformations of clastic rocks as compared with oxides. In the Ti–Zr diagram, Triassic sandstones of Chukotka form a very uniform field, which characterizes erosional products of andesites (Fig. 17a). In the other diagram based on $\text{Co}/\text{Th} - \text{La}/\text{Sc}$ ratios, the Chukotka sandstones correspond to erosional products of rocks lithologically close to average composition of the continental crust. Nevertheless, the transition from Lower to Upper Triassic sandstones is marked by a slight tendency for growth of the granodiorite constituent (Fig. 17 a). The Th/Sc versus Zr/Sc

diagram demonstrates the recycling trend from the Early to Late Triassic (Fig. 17a).

The same diagrams (Ti–Zr, Co/Th–La/Sc, Th/Sc versus Zr/Sc) available for the Verkhoyansk region exhibit gradual increase in the role of basic components in the Permian to Upper Triassic sandstone succession. It should be noted, however, that the influence of rocks compositionally close to the continental crust is sufficiently high for Co/Th and Zr/Sc ratio in both the Verkhoyansk and Chukotka basins. The distinct compositional evolution of sandstones is also evident from the Cr/V–Y/Ni diagram. The “granite” composition of clastic material in the Permian sandstones gives way to the significant role of the mafic constituent in the Lower and Middle Triassic sandstones (Fig. 17b). In the Th/Sc versus Zr/Sc diagram, sandstones of the Verkhoyansk region demonstrate a tendency opposite to maturation (Fig. 17b).

Geochronology

The age of detrital zircons in sandstones provides important information for defining their provenances. In this work, we use the U–Pb dating of detrital zircons by the ICPMS-LA and Sm–Nd isotope ratio methods for rocks with a wide grain-size spectrum. For correlating populations of detrital zircons, the published (Miller et al., 2006; Prokopiev et al., 2007) and original data (Tables 3, 4) are used.

Distribution of ages obtained for detrital zircons from Upper Triassic sandstones of the Verkhoyansk region demonstrate peaks at 331, 353, 381, 422, and 470 Ma (Sample JT25). The peaks corresponding to 292, 321, 439, and 483 Ma are recorded for Sample JT26 and to 292, 308, 459, 485, and 517 Ma for Sample Jt29. In the sample from the Lower Permian section (00JT18), the peaks for zircons are documented at 288, 494, 782, and 854 Ma (Prokopiev et al., 2008). All three Triassic samples contain populations of ancient zircons with ages of approximately 1832 Ma; in the Permian sample, the zircon population is much older: 1863 Ma (Prokopiev et al., 2008). The Paleozoic population demonstrates two notable peaks: at 288 and 482 Ma.

The association of detrital zircons from the Upper Triassic sandstones of the Anyui subterrane includes several populations 235–265, 321–399, 425–545, 545–011, 1061–1273, and 1606–2725 Ma

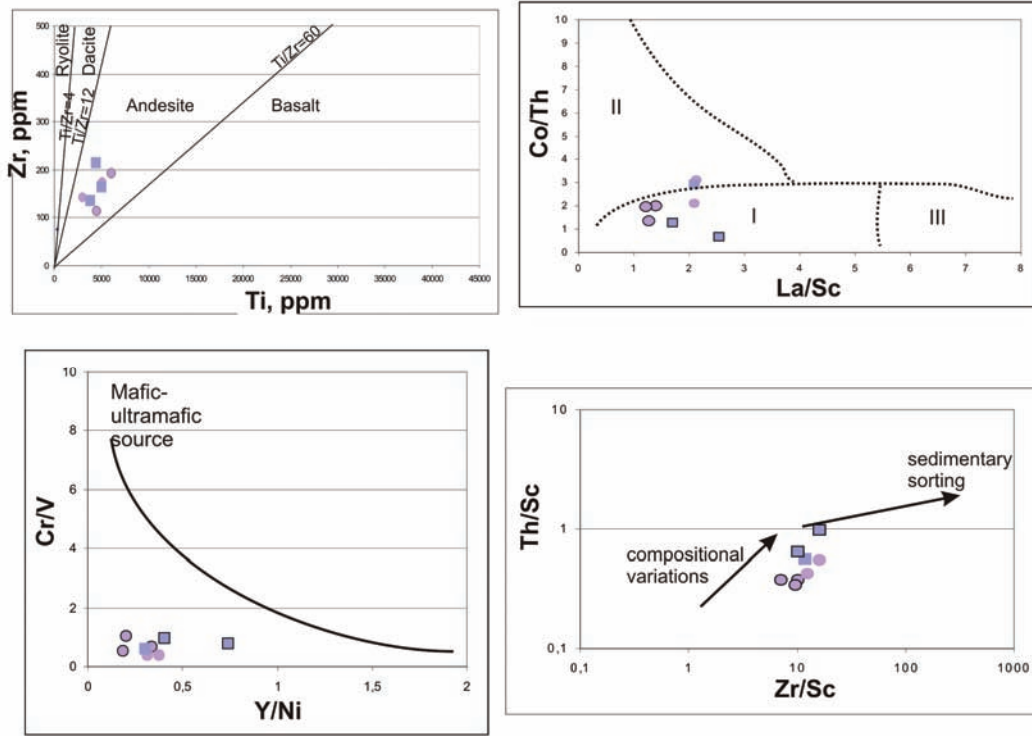
old (Miller et al., 2006). The young population is represented by zircon grains dated back to 236–265 Ma (Miller et al., 2006). No such ages were recorded for sandstones from the Verkhoyansk region. The Upper Triassic sandstones from Wrangel Island yield ages ranging from 215 to 260 Ma (Miller et al., 2009).

Y. Hayasaka (Hiroshima University) and A. Moiseev (Geological Institute Russian Academy of Science, GIN RAS) have dated two samples of the Triassic sandstones from the Chaun subterrane by the ICP-MS LA method. Sandstone sample 09/358 was taken in the Ploskaya River basin (locality 4 in Fig. 3) from the Lower Triassic sequence of alternating siltstones and sandstones with tuff intercalations. Sample 09/321 was collected from the Upper Triassic (?) member of alternating sandstones and siltstones (Mount Lukovaya, Table 2). The first sample contains zircon populations with peaks at 272–286, 435–613, 671–793, and single older grains dated back to 1000–1969, 2397, and 2672 Ma. Zircons from Sample 09/321 exhibit only two peaks at 255–295 and 424–548 Ma; a small population yielded older ages of 1669–1986 Ma (Fig. 18).

It should be noted that both samples are barren of the young population 235–265 Ma old that is characteristic of the Upper Triassic rocks from the Anyui subterrane (Miller et al., 2006) and Wrangel Island (Miller et al., 2009) despite the occurrence of tuff intercalations and gabbro–dolerite sills in the relatively shallow-water Ploskaya River section. The young zircon population is missing also from the coeval Sadlerochit Group and Blind Fiord Formation sandstones of the Sverdrup basin (Miller et al., 2006; Omma et al., 2011).

The ancient zircon populations of the Verkhoyansk and Chukotka regions demonstrate certain differences as well. The sandstones from the Verkhoyansk region are barren of zircons with ages ranging from 900 to 1700 Ma (Sample JT25); samples JT26 and JT29 each yielded the only zircon grains dated back to 988.6 ± 18.0 and 1234 ± 90 Ma (Miller et al., 2006). Three sandstone samples from Verkhoyansk contain 6, 20, and 22 zircon grains. It is noteworthy that the sample of the Lower Triassic sandstones from the Sadlerochit Mountains (Sample 96DH102) appeared to contain 17 grains with similar ages. The Lisburne Hills Sandstones yielded 4 and

a.



b.

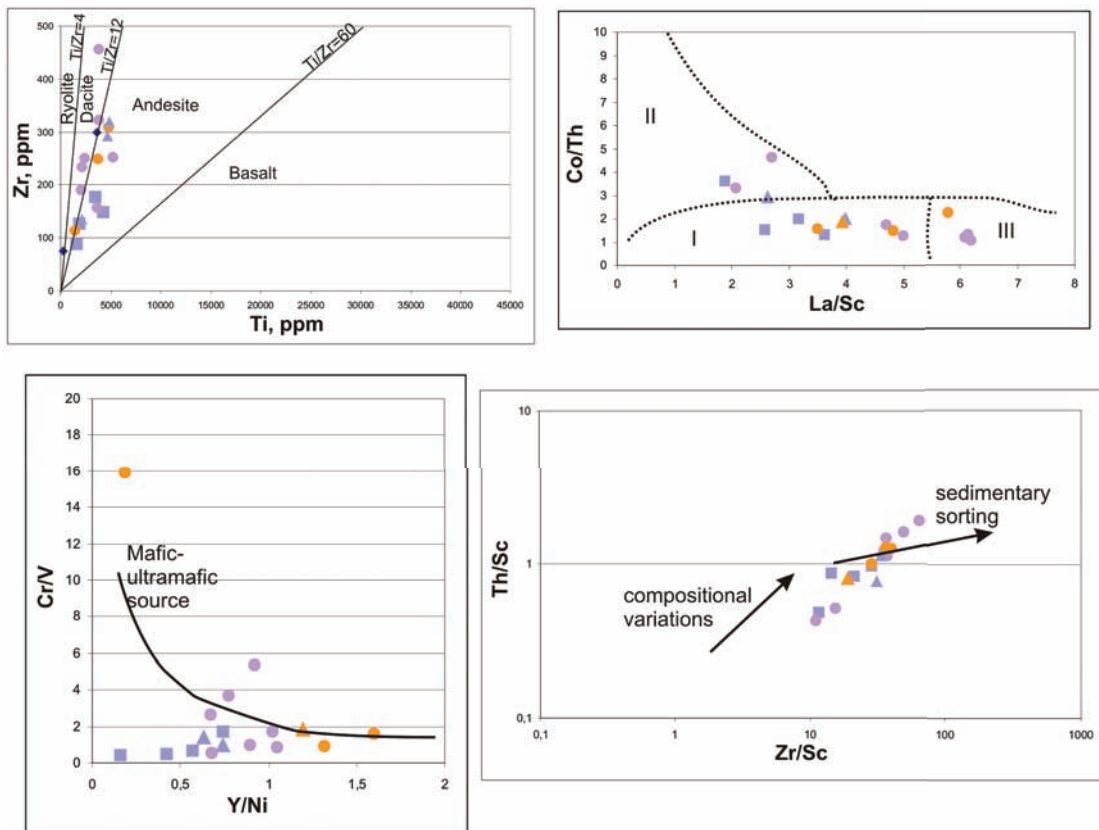


Fig. 17a. Diagrams illustrating the compositions of assumed provenances for Triassic deposits of the Anyui–Chukotka fold belt, diagrams by Roser and Korsch (1989), McLennan (1988), McLennan et al., (1993). For legend, see Figure 16. **17b.** Diagrams illustrating the compositions of assumed provenances for Triassic deposits of the Verkhoyansk–Kolyma fold belt. For legend, see Figure 16.

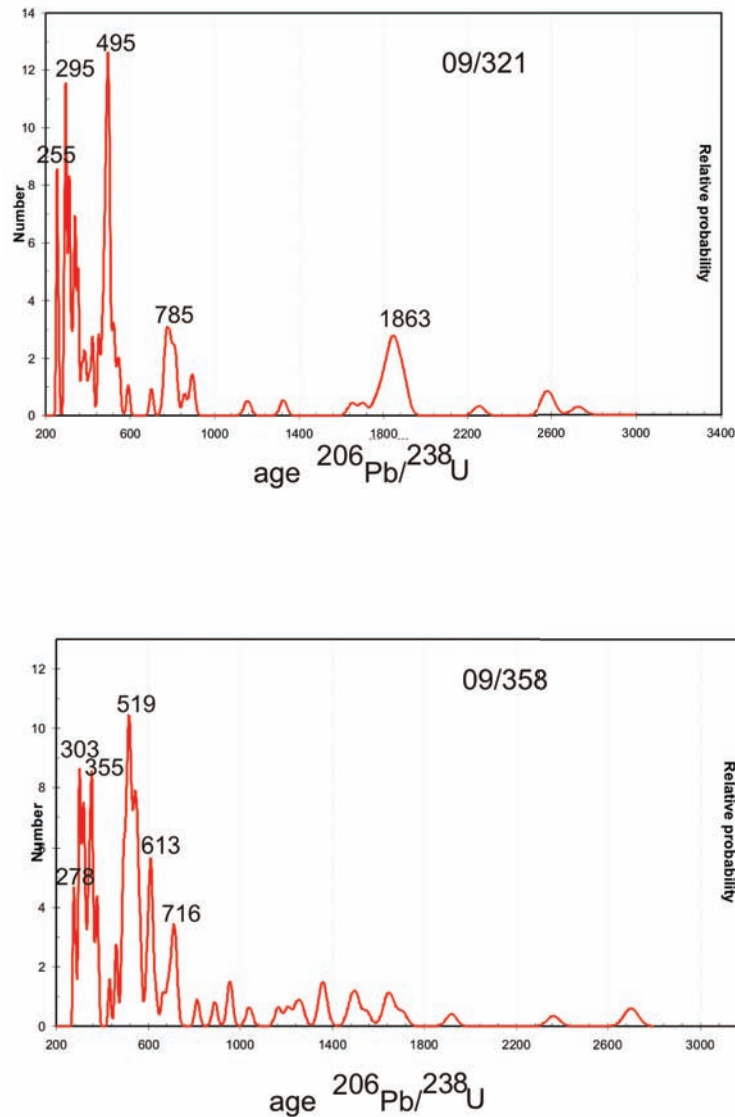


Fig. 18. Zircon populations from the Triassic sandy rocks of eastern Chukotka, samples 09/321 and 09/358. The positions of samples and zircon ages are shown in Tables 2 and 3, respectively.

11 grains with similar ages. Thus, the sandstones of Alaska and Chukotka are close to each other by this parameter.

The Sm-Nd isotopic system of sandstone samples was studied in the Institute of Geology and Geochronology of Precambrian. The Nd isotopic system is widely used in recent studies of sedimentary rocks. It is assumed that the chemical fractionation of Sm and Nd occurs mostly during differentiation of mantle material and formation of the continental crust and that these elements avoid fractionation during sedimentation and diagenesis (Taylor and McLennan, 1988). For sediments, the

Nd model age offers an opportunity to determine the crust formation age of the provenance. The samples from the Verkhoyansk region imply erosion of the old continental crust with the ϵNd varying from -5 to -20 (Fig. 19). In Chukotka rocks, the content of eroded juvenile material is slightly higher; therefore, they occupy the higher position in the diagram. Consequently, erosion in the Chukotka provenance involved an ancient orogen with relicts of the oceanic crust. The Sm-Nd ages of zircons range from 1033 to 2297 and from 1038 to 1785 Ma for sandstones from the Verkhoyansk and Chukotka regions, respectively (Table 4).

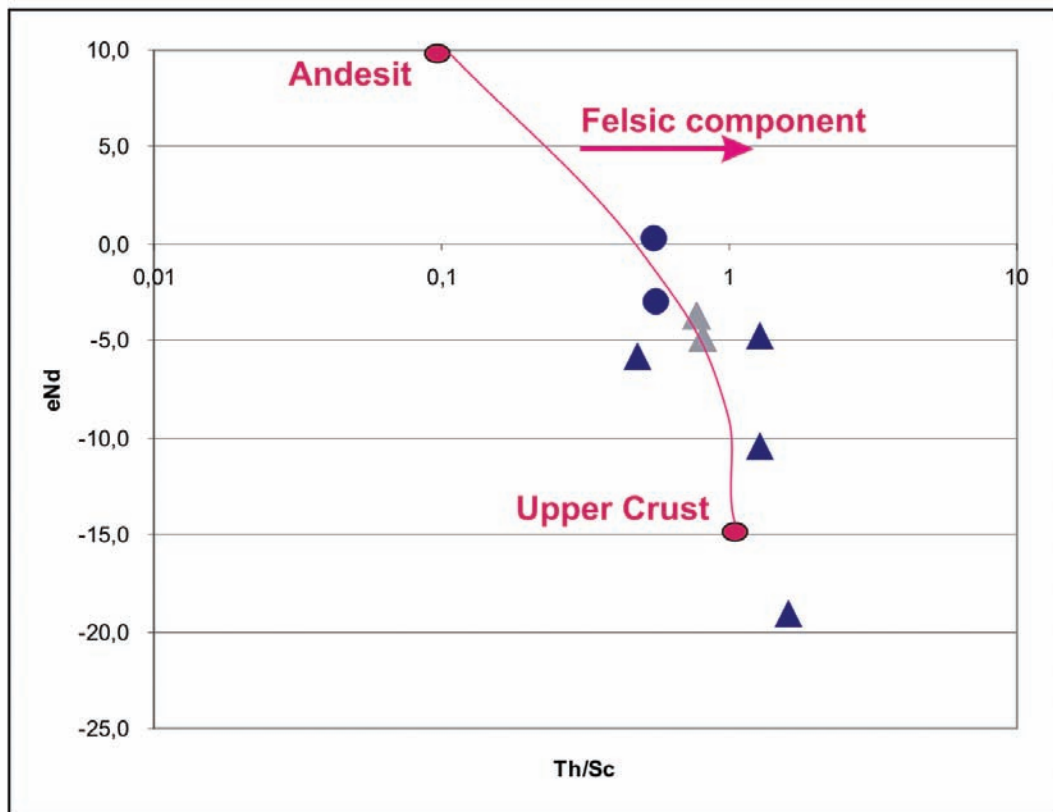


Fig. 19. eNd – Th/Sc systematic in the Permian-Triassic rocks of the southern (dark triangles) and western (gray triangles) Verkhoyansk region. Circles designate Triassic rocks of Chukotka.

STRUCTURAL STYLE

Collisional deformation in the West Verkhoyansk region began in Late Jurassic time and was most active during Early Cretaceous. In the Chukotka fold belt the main phase of collisional deformation took place at the end of Early Cretaceous (Hauterivian-Barremian). It is notable that the well-known Tithonian-Neocomian clastic sequence of Myrgovaam/Rauchua area of Chukotka is traditionally regarded as synorogenic/syncollisional (Bondarenko et al., 2003; Miller et al., 2008, and references therein). Nevertheless the unit still lacks any identified intra-formational unconformities or evidence of synsedimentary contractional deformation, although the some slump folds were described. It means that strictly speaking we do not have enough data to state that the deposition of Tithonian-Neocomian clastic sequence took place in a compressional collision-related setting. Nevertheless the earlier (pre-Neocomian) stage of contraction (?) certainly took place and caused the deformation

of Triassic strata (in Early Jurassic?) and general uplift of the entire area (Tuchkova et al., 2007). The latter in turn caused very limited occurrence of Lower Jurassic and total absence of Middle Jurassic sequences. Another principal difference between these two regions is that the main collisional stage in Verkhoyansk area lasted significantly longer (up to Late Cretaceous) than those of Chukotka (was pretty much over prior Aptian). It is also notable that collisional deformations in the South Verkhoyansk region was completed much earlier, before Tithonian-Neocomian time (Prokopiev and Deikunenko, 2001). The predominant west-vergent fold-and-thrust structural pattern of West Verkhoyansk region is cut by post-kinematic granite plutons of Main Batholith Belt of and Northern Batholith Belt with $^{40}\text{Ar}/^{39}\text{Ar}$ age of 160-134 Ma (Oxfordian-Valanginian) and 127-120 Ma (Barremian-Aptian) respectively (Layer et al., 2001; Prokopiev and Deikunenko, 2001). In general the age of deformation becomes younger westward, established by post-kinematic granite

Table 3. Sample data for sandstones analyzed for detrital zircons

Sample number	Area	Latitude	Longitude	Age
09/321	Eastern Chukotka	66° 41 53.6	W176°43 40.9	Upper Triassic
09/358	Eastern Chukotka	67°09 27.6	W178°08 29.5	Lower-Middle Triassic

Table 4. Interpreted zircon ages. Ages are in Ma.

Lukovaya mountains Sample 09/321		Ploskaya River Sample 09/358		Lukovaya mountains Sample 09/321		Ploskaya River Sample 09/358	
Used Age±2σ				Used Age±2σ			
09-321-01	252,33±6,79	09-358-01	275,22±7,26	09-321-52	503,81±13,10	09-358-53	551,78±14,79
09-321-02	253,61±7,09	09-358-02	278,17±7,39	09-321-53	518,69±13,53	09-358-54	553,38±15,01
09-321-03	254,73±7,05	09-358-03	285,48±7,62	09-321-54	521,19±13,67	09-358-55	555,00±15,76
09-321-04	257,25±7,87	09-358-04	298,64±8,24	09-321-55	527,52±13,99	09-358-56	565,95±14,42
09-321-05	262,12±7,77	09-358-05	298,92±7,74	09-321-56	542,26±14,10	09-358-57	566,46±15,17
09-321-06	286,63±7,52	09-358-06	302,03±8,00	09-321-57	550,01±14,69	09-358-58	593,33±15,72
09-321-07	292,17±7,93	09-358-07	303,97±8,18	09-321-58	591,87±15,50	09-358-59	603,10±16,29
09-321-08a	293,55±7,80	09-358-08	307,00±8,17	09-321-59	701,59±17,73	09-358-60	604,39±23,70
09-321-08b	294,26±7,86	09-358-09	312,18±8,75	09-321-60	762,61±19,82	09-358-61	609,45±15,35
09-321-09	294,91±7,80	09-358-10	314,96±8,46	09-321-61	771,31±20,67	09-358-62	612,63±17,08
09-321-10	297,51±7,97	09-358-11	318,43±8,41	09-321-62	773,25±19,73	09-358-63	614,07±15,62
09-321-11	297,99±7,72	09-358-12	320,18±8,51	09-321-63	783,22±23,47	09-358-64	615,72±16,24
09-321-12	303,47±8,16	09-358-13	324,47±8,87	09-321-64	790,44±20,16	09-358-65	632,76±16,85
09-321-13	308,65±8,29	09-358-14	327,00±8,97	09-321-65	790,68±20,63	09-358-66	663,96±16,94
09-321-14	310,89±8,26	09-358-15	335,65±8,82	09-321-66	806,76±20,68	09-358-67	684,03±18,18
09-321-15	311,49±8,26	09-358-16	342,74±9,35	09-321-67	813,98±20,86	09-358-68	697,20±17,71
09-321-16	314,57±8,24	09-358-17	343,72±9,29	09-321-68	816,93±20,68	09-358-69	707,30±17,77
09-321-17	316,89±8,52	09-358-18	348,67±9,54	09-321-69	859,08±22,08	09-358-70	712,93±17,98
09-321-18	323,86±8,58	09-358-19	353,81±9,81	09-321-70	893,28±22,10	09-358-71	715,65±18,07
09-321-19	331,5±8,708	09-358-20	354,24±9,78	09-321-71	896,84±23,15	09-358-72	725,01±18,32
09-321-20	337,16±8,86	09-358-21	355,79±9,80	09-321-72	1785,97±42,63	09-358-73	813,26±20,52
09-321-21	339,78±9,04	09-358-22	355,87±9,29	09-321-73	1827,73±43,67	09-358-74	889,69±22,18
09-321-22	339,92±9,16	09-358-23	365,33±9,99	09-321-74	1841,32±44,38	09-358-75	953,38±23,69
09-321-23	343,50±9,07	09-358-24	374,79±10,19	09-321-75	1850,11±42,76	09-358-76	957,14±23,70
09-321-24	351,94±9,13	09-358-25	377,73±10,09	09-321-76	1858,55±42,56	09-358-77	1052,68±76,06
09-321-25	354,77±9,67	09-358-26	382,99±9,99	09-321-77	1863,32±44,56	09-358-78	1196,20±44,81
09-321-26	355,66±9,60	09-358-27	432,23±11,27	09-321-78	1863,36±45,72	09-358-79	1241,42±47,65
09-321-27	371,38±9,89	09-358-28	459,25±12,00	09-321-79	1868,24±40,97	09-358-80	1296,59±52,02
09-321-28	382,44±10,00	09-358-29	463,74±12,46	09-321-80	1871,57±46,21	09-358-81	1302,27±46,09
09-321-29	391,36±10,90	09-358-30	485,65±13,11	09-321-81	1879,76±44,89	09-358-82	1319,81±45,55
09-321-30	406,56±12,00	09-358-31	491,94±12,54	09-321-82	1885,36±43,96	09-358-83	1351,16±46,19
09-321-31	420,67±11,9	09-358-32	492,05±12,79	09-321-83	1889,77±68,34	09-358-84	1453,72±47,51
09-321-32	424,18±11,28	09-358-33	497,69±13,26	09-321-84	1891,58±43,27	09-358-85	1489,24±55,47
09-321-33	450,95±11,95	09-358-34	499,38±12,85	09-321-85	1897,15±50,53	09-358-86	1524,98±46,93
09-321-34	452,24±11,92	09-358-35	504,90±13,02	09-321-86	1961,13±45,66	09-358-87	1547,96±46,59
09-321-35	466,23±12,00	09-358-36	508,34±13,00	09-321-87	1982,78±42,15	09-358-88	1653,46±42,63
09-321-36	471,55±12,47	09-358-37	509,82±12,99	09-321-88	2025,60±39,35	09-358-89	1687,73±61,75
09-321-37	479,61±12,37	09-358-38	513,65±13,71	09-321-89	2366,22±42,46	09-358-90	1696,75±42,59
09-321-38	480,44±12,43	09-358-39	514,79±13,81	09-321-90	2576,94±40,17	09-358-91	1703,02±40,96
09-321-39	482,34±12,59	09-358-40	515,80±13,29	09-321-91	2585,71±65,94	09-358-92	1852,75±44,13
09-321-40	483,49±12,58	09-358-41	518,23±13,35	09-321-92	2601,71±40,78	09-358-93	1855,34±45,34
09-321-41	487,96±12,83	09-358-42	518,35±13,39	09-321-93	2615,60±40,53	09-358-94	2584,56±42,76
09-321-42	491,67±12,50	09-358-43	521,65±13,33	09-321-94	2846,59±39,60	09-358-95	2660,44±39,28
09-321-43	493,16±13,04	09-358-44	526,01±13,72	09-321-95	3593,07±60,22	09-358-96	2698,26±36,18
09-321-44	493,34±12,94	09-358-45	526,73±13,41				
09-321-45	494,40±13,01	09-358-46	528,93±13,79				
09-321-46	495,12±13,02	09-358-47	534,99±13,65				
09-321-47	495,20±13,37	09-358-48	539,13±14,12				
09-321-48	499,78±13,19	09-358-49	540,12±13,80				
09-321-49	500,16±13,12	09-358-50	543,23±14,00				
09-321-50	501,30±13,34	09-358-51	545,05±14,73				
09-321-51	501,84±13,02	09-358-52	550,63±14,86				

plutons dating from 132 Ma (Hauterivian) on the east to 98 Ma (Cenomanian) on the west (Prokopiev and Deikunenko, 2001; Layer et al., 2001). On the western margin of the Verkhoyansk belt the youngest rocks involved in contractional deformation are Cenomanian and Turonian (100-89 Ma) (Khudoley and Prokopiev, 2007). Post-collisional (undeformed) granite plutons of Chukotka were recently dated by U-Pb (SHRIMP) as Aptian-Albian, i.e. ~ 117-108 Ma (Katkov et al., 2007; Miller et al., 2009). These ages are in a better agreement with those of the Northern Batholith Belt.

The general structural style of the Verkhoyansk region is a fold-and-thrust belt with thin-skinned tectonics. It was also noted that in the outer (west) zones thrust tectonics predominates whereas in the inner (east) the open folds are more common (e.g., Parfenov et al., 1995; Prokopiev and Deikunenko, 2001; Khudoley and Prokopiev, 2007). The recent application of the critical wedge model to the Verkhoyansk fold-and-thrust belt led to the conclusion that inner and outer zones of the belt corresponds to two different thrust wedges instead of single one (Khudoley and Prokopiev, 2007). The boundary between these two wedges was interpreted by the cited authors as the eastern limit of North Asian cratonic basement. The authors also proposed that structural and stratigraphic peculiarities of the inner fold belt (likely underlain by blocks with transitional continental crust separated by rifted basins) require a basal detachment related to salt and evaporate deposits of Middle and Upper Devonian(?).

The tectonic basement of the Chukotka fold belt is not exposed over most of the area and the number and quality of published deep seismic lines is extremely poor. So we do not have enough data to understand whether we have a regional predominance of thick-skinned or thin-skinned tectonics in Chukotka. On the other hand thick-skinned tectonics is identified on Wrangel Island where the metamorphic basement of Paleozoic-Triassic sedimentary cover (Neoproterozoic Wrangel complex) is certainly involved in the thrust and fold deformation (e.g. Kos'ko et al., 1993; 2003). Nevertheless the majority of the thrusts and folds (up to isoclinal and recumbent) of mainly northern and east-northeastern vergence were identified and mapped for the onshore Chukotka fold belt,

including Wrangel Island (Sokolov et al., 2002; 2009; Kos'ko et al., 1993; 2003). Recently some seismic lines demonstrated the occurrence of low-angle north-vergent thrust faults within the Late Mesozoic tectonic basement of the southern part of Russian Chukchi Sea (Verzhbitsky et al., 2008; 2010).

Imbricate thrust fans normally characterize the frontal ranges of the Verkhoyansk fold-and-thrust belt (e.g., Parfenov et al., 1995; Prokopiev and Deikunenko, 2001; Khudoley and Prokopiev, 2007), whereas the Chukotkan deformation front of (revealed by offshore seismic only) demonstrate transpressional (pop-ups, positive flower-like) structural pattern (Verzhbitsky et al., 2008; Drachev et al., 2001; Drachev, 2011).

DISCUSSION: CORRELATION OF SEDI-MENTOLOGIC AND TECTONIC EVENTS

Typical passive margins are characterized by rift-related volcanism and thick sedimentary successions consisting of material transported by major rivers and/or carbonates. Passive margins usually occupy wide areas with similar sedimentary histories, and significant stratigraphic unconformities and/or lithological complexes are traceable throughout the wide area related to a continental margin.

The Permian-Triassic sedimentary basins of the Verkhoyansk and Chukotka regions were formed on passive margins (Til'man, 1980; Parfenov, 1984; Zonenshain et al., 1990; Parfenov et al., 1993; Nokleberg, 1994). For convenience in comparison between geological events, the tectono-stratigraphic units of both regions are correlated with units of the North America scale: Ellesmerian, Beaufortian, and Brookian megasequences (Bird et al., 2001).

As follows from published data and that presented here, the sedimentary and tectonic evolution of the Ellesmerian and Beaufortian stages in the Chukotka and Verkhoyansk basins are different. The sections of the Chukotka passive margin are characterized by two major unconformities at the base of the Anyui Complex (Triassic) and the Upper Jurassic sequences (Figs. 20, 21). The Middle Jurassic deposits are missing from the region under consideration, while thin Lower Jurassic strata are developed only in the Rauchua River basin. The total thickness of the Triassic section is approximately 4-5 km.

On the Siberian passive margin, the Verkhoyansk complex forms a continuous Lower Carboniferous–Jurassic section 14–16 km thick in total. Its Permian–Triassic part constitutes approximately 7 km (Khudoley and Prokopiev, 2007).

The Triassic section in both fold belts is characterized by the regressive structures implying general shoaling of the sea basin up to deposition of shallow-water–shelf and terrestrial sediments in the Chukotka and Verkhoyansk basins, respectively (Figs. 9, 13).

The river systems that controlled the influx of

clastic material in both basins demonstrate different delta structures. In the Chukotka basin, the deltaic system may be attributed to fine-grained deltas (Nichols, 2009). Such deltas are characterized by a mixed feeding mode and accumulation of fine-grained sediments in their frontal parts with development of small mouth sand bars probably grading into slope sediments and turbidites. In the Verkhoyansk basin, the delta belonged to the coarse-grained type (Nichols, 2009). Coarse-grained deltas are fed by solid bottom material and characterized by a proximal mouth gravelly bar. The distal mouth

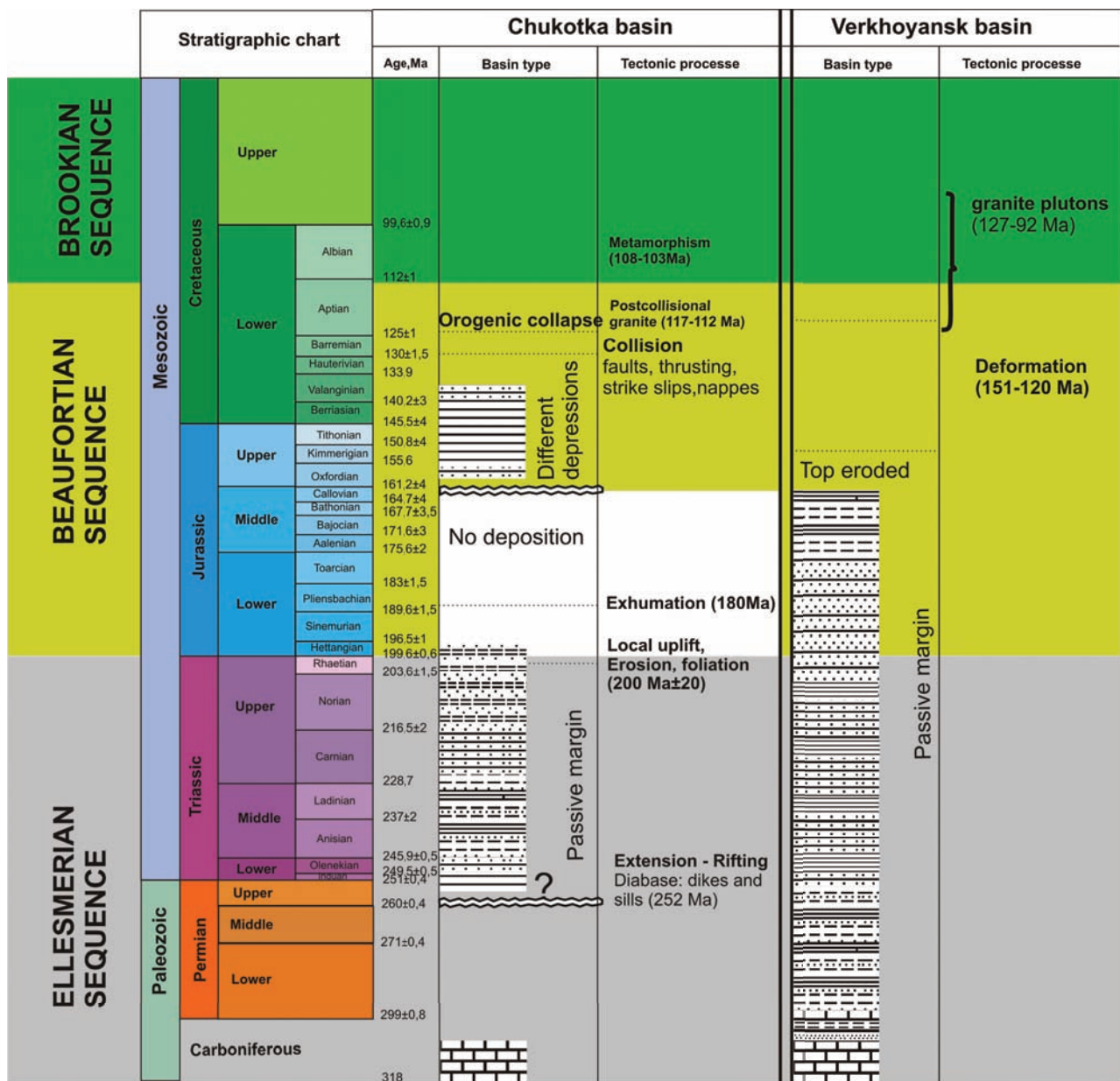


Fig. 20. Correlation between sedimentological and tectonic events in the Verkhoyansk–Kolyma and Anyui–Chukotka fold belts.

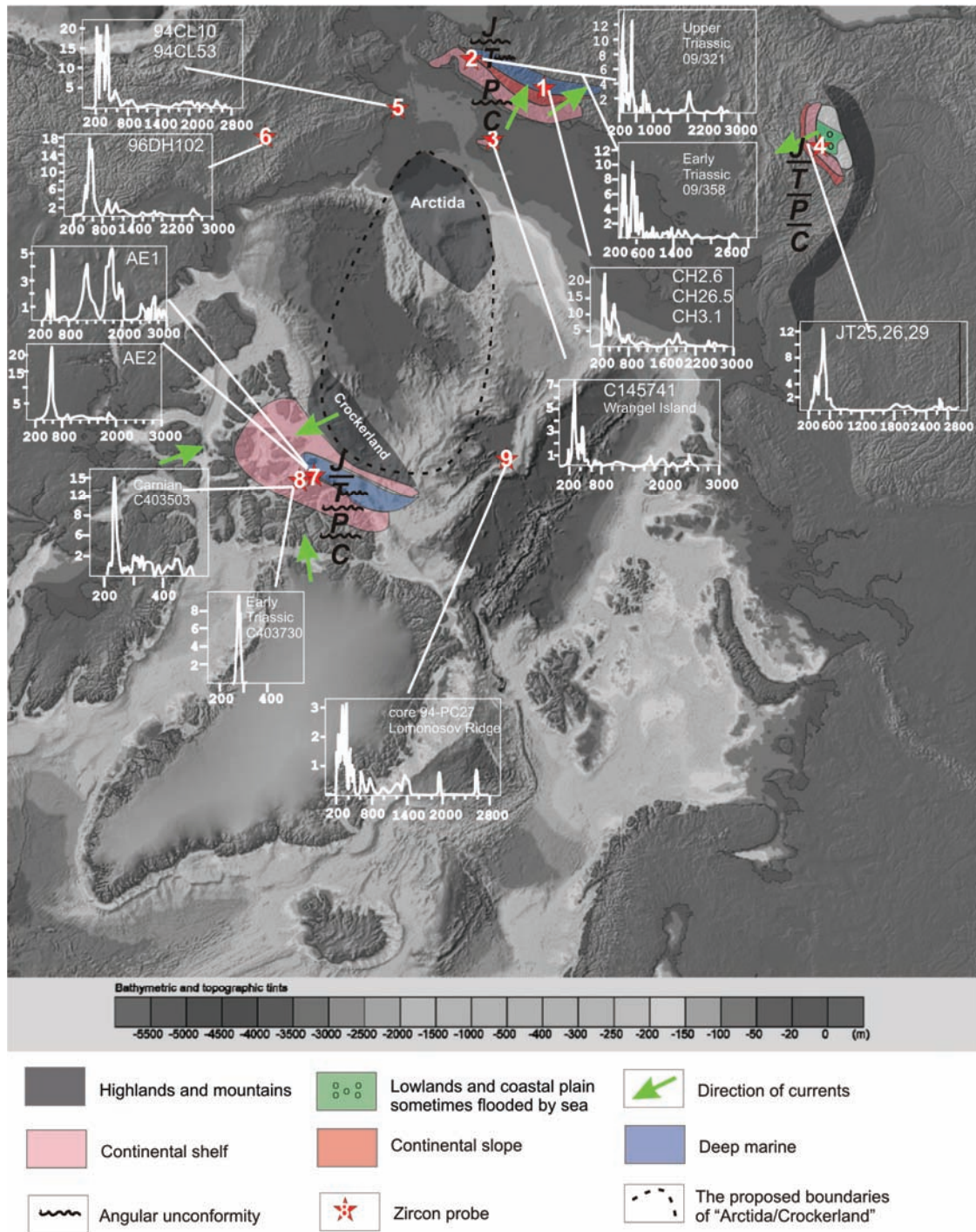


Fig. 21. The schematic position of paleogeographic zones in the present-day geography of the Arctic region. The positions of deltaic and prodeltaic systems are consistent with the directions of the clastic material transport. It is seen that the material transport for the Permian-Triassic deposits of the Verkhoyansk and Chukotka regions was characterized by almost opposite directions. The dashed line shows the contour of the hypothetical microcontinent (Arctida?, Crockerland?). Asterisks with numbers designate positions of samples with detrital zircons discussed in the text. (1) Western Chukotka terrane, Upper Triassic sandstones, cited from Miller et al., 2006; (2) Chaun terrane, Lower and Upper Triassic sandstones discussed in this work; (3) Wrangel Island, Upper Triassic sandstones, cited from Miller et al., 2006. (4) Verkhoyansk terrane, Permian and Triassic sandstones, cited from Miller et al., 2006, Prokopiev et al., 2008. (5) Cape Lisburne, Two samples, data combined, cited from Miller et al., 2006. (6) Sadlerochit Mts, Eastern Alaska: Ivashak sandstones, cited from Miller et al., 2006. (7) Arctic Alaska, Canada, Sverdrup basin, cited from Miller et al., 2006. (8) Arctic Alaska, Canada, Sverdrup basin, cited from Omma et al., 2010. (9) Lomonosov Ridge, Grantz et al., 2001, cited from Miller et al., 2006.

bar and delta front are composed of sand material, and the muddy prodeltaic zone is narrow.

The facies analysis reveals that the Chukotka and Verkhoyansk Triassic basins deepened in opposite directions. In the Chukotka basin, sediments transformed from shallow- to deepwater varieties and the shelf zone gradually prograded from the north (northeast) southward (southwestward). The section thicknesses increase in the same direction (Fig. 5). The distal facies of Upper Triassic turbidites are known from the South Anyui suture (Sokolov et al., 2002). The eastern Lower Triassic sections (locality 4 in Figure 3) exhibit the significantly reduced thickness and imply coastal –marine depositional environments accompanied by volcanism (Ledneva et al., 2011).

In the Verkhoyansk basin, shallow-water facies are replaced by deepwater sediments in the SW–NE direction (Figs. 13, 21) and distal turbidite facies are documented in the Kular–Nera terrane (Kossovskaya et al., 1960; Parfenov, 1984; Yapaskurt, 1992; Prokopiev, Khudoley, 2007).

The analysis of paleogeographic and geochemical data provides grounds for the assumption that the provenance of the Chukotka basin was characterized by a low hilly topography without high mountains. The Triassic was marked by enhanced weathering, which is evident from the CIA trend close to the ideal one (Tuchkova et al., 2009). Hence, clastic material was subjected to weathering immediately in the provenance, not only during its mixing and transport. This resulted in the supply to the sedimentation basin of sediments with the average weighted composition. The compositional similarity between Triassic sandstones and the averaged crust as well as almost complete lack of conglomerates confirms this assumption.

Quite different Permian and Triassic paleogeographic settings are reconstructed for the Verkhoyansk basin. In the south and west the basin was surrounded by relatively high mountains which graded northward into a spacious plain with coal-bearing deposits. Numerous rivers and creeks eroded complexes with variable lithology, while no weathering occurred in the provenance, which is supported by CIA trends (Fig. 17a).

The geochemical evolution of clastic material constituting Triassic rocks of the Verkhoyansk and

Anyui complexes demonstrate different trends. The sandstones of the Chukotka basin reflect the reduced influence of basic rocks, mature composition of sedimentary material, and increased role of the quartz constituent. In the Verkhoyansk basin, the influence of basic rocks becomes notable in the Upper Triassic sandstones, while their Lower Triassic and Permian counterparts are mostly characterized by quartzose composition of clastic material. The distal sandstones demonstrate the significant contribution of granites.

The assumption of the “trap provenance” requires close relations between Chukotka and Siberia. At the same time, geochemical data and composition of rock clasts indicate no influence of basic and intermediate rocks on the Carnian and Norian deposits of Chukotka. The absence of these relations in the Late Triassic is difficult to explain taking into consideration development of large river systems and continuous sedimentary succession. There are no indications of Chukotka moving or of tectonic reorganizations in the assumed provenance during the Triassic. At the same time, the typical Verkhoyansk passive margin demonstrates the opposite geochemical trend with the increased role of mafic clastic material in the Late Triassic and substantial influence of acid material in Permian and Lower Triassic deposits (Fig. 17b). Diagrams of the REE distribution constructed for both regions point to depositional environments typical of passive margins. Nevertheless, different trends of changes in the composition of sandstones in the Permian–Upper Triassic succession are notable; i.e., they point to different passive margins, and correspondingly, different provenances.

The age of detrital zircons provides important information on provenances. Despite intense Permian–Triassic trap volcanism on the Siberian Platform, no indications of their erosion are revealed in detrital zircons of the Verkhoyansk complex (Miller et al., 2006; Prokopiev et al., 2008), although the Upper Permian and Lower Triassic sections of the southern Verkhoyansk region include volcanogenic–sedimentary rocks and abundant basic pyroclastic material (Prokopiev and Ivensen, 2008). The population of detrital zircons with the peak at 288 Ma corresponds to erosion of the Angara–Vitim batholith. The main peak at 488 Ma points to the increased role of clastic material from the Altai–

Sayany region. It is also conceivable that clastic material was transported from the Suntar and Yakutsk uplifts, Aldan Shield (?) (2300–2800 Ma), northern Transbaikal and eastern Sayany regions (1863 Ma) (Kossovskaya, 1960; Prokopiev et al., 2007).

Unfortunately, it is impossible to correlate zircon age peaks and assumed provenances for the Chukotka continental margin. This is primarily explained by the underwater position of its “northern province.” Among Upper Triassic detrital zircons of Chukotka and Wrangel Island, is the remarkable Permian–Triassic population (235–265 Ma), which provides grounds for considering them as originating from the Siberian traps and assuming a westerly position for Chukotka near the Urals, Taimyr, and Siberia (Miller et al., 2006). Indeed, some displacement of Chukotka in an easterly direction in response to the opening of the Eurasia Basin and rifting on the Laptev Sea shelf cannot be ruled out (Drachev et al., 2003). In addition, some displacement could be determined by dextral syncollisional shifts along strike-slip faults established in the South Anyui fold system, a result of from the oblique subduction of the Chukotka microcontinent (Sokolov et al., 2002, 2009). At the same time, the amplitude of such shifts cannot explain significant near-latitudinal AACM displacements.

Coeval zircon population dated at 220–265 Ma is known from the Upper Triassic Lisburne Hills Sandstones (Miller et al., 2006). Nevertheless, taking into consideration the shelf affinity of these sandstones, it is impossible to assume an origin for the zircon population in question from the Urals, Taimyr, or Siberia provenances.

The zircon populations with ages of 750–1000 and 1000–1300 Ma from the Triassic sandstones of Chukotka imply erosion of an ancient metamorphic complex. The lack of these populations, except several grains in sandstones (samples JT 26, JT 29) of the Verkhoyansk region (Miller et al., 2006) points to another, not “Siberian” source for the sandstones of Chukotka.

According to (Miller et al., 2006), the Triassic sandstones of the Sverdrup basin yielded 20 and 37 zircon grains aged in the interval of 959–1700 Ma. The Lower Triassic sandstones provided the population dated back to 265–290 Ma (19 grains), Mesoproterozoic zircons with ages of 959–1206 Ma

(eight grains) and 1356–1497 Ma (12 grains), and single Archean grain (3100 Ma). The Paleozoic rock yielded a zircon population dated at 268–493 Ma, 34 grains with peaks at 302, 327, 348, and 447 Ma, and 21 Precambrian grains exhibiting no distinct peaks. The Proterozoic zircon population (900–1700 Ma) in sandstones of Chukotka, the Sverdrup basin, and Alaska point presumably to a single source in common. It is clear that neither Siberia nor Laurentia could serve as such a source.

The new data on Chukotka show that populations of detrital zircons from Chukotka, the Sverdrup basin, and Alaska, the Sadlerochit Mountains included, demonstrate greater similarity than it was previously thought. Consequently, it may be assumed that they originate from a single source.

The data on zircon ages of gabbro–dolerite magmatism in eastern Chukotka (252 Ma. Ledneva et al., 2011) and K–Ar ages obtained for sills and small intrusive bodies (Geodynamic, Magmatism, and Metallogeny..., 2006) in Lower Triassic deposits allow the local (Chukotka), not Siberian provenance to be assumed. The presence of products of synchronous magmatism and shallow-water facies in the Lower Triassic sequences (Fig. 8 and 9) confirm this assumption. At the same time, coeval zircons appear only in the Upper Triassic strata. It is conceivable that the young zircon population originates from intrusive, not volcanic rocks, which were subjected to erosion only in the Late Triassic.

In our opinion, the assumption of the local source with synchronous magmatism is consistent with the evolution of the petrological–mineralogical and geochemical compositions in the Anyui Complex of Chukotka. The Devonian zircon population (340–390 Ma) of Chukotka and Lisburne Hills may also originate from a local magmatic source, indications of which are established in metamorphic complexes of eastern Chukotka and Alaska (Natal'in, 1999; Amato, 2009).

For solving the problem of a northern “local” source of clastic material for Triassic deposits of the Chukotka basin, the available reconstructions should be taken into consideration. The existence of a large continental block in the central Arctic region was assumed in previous works: the Hyperborean Platform (Shatsky, 1935, 1963), the Ancient Arctida (Eardly, 1948). Zonenshain et al. (1990) substantiated the

existence of the Arctida continent that resulted from Rodinia break-up (Vernikovskiy and Vernikovskaya, 2001). In the present-day structure, fragments of Arctida basement are preserved along the periphery of the Arctic Ocean: Kara massif, northern Taimyr, Chukotka, Brooks Range, Wrangel Island, and others. According to subsequent studies (Kuznetsov et al., 2007; Vernikovskiy and Vernikovskaya, 2001), the Arctida continent included also the Barentsia and Timanides. When investigating the provenances for sediments of the Sverdrup basin, Embry (1993, 2011) assumed existence of a northerly located, hypothetical, Crockerland continent. The Sverdrup basin was formed in response to rifting in the Carboniferous, which is consistent with the Lower Ellesmere Sequence and onset of the formation of the Verkhoyansk and Anyui complexes (Fig. 21).

Figure 21 illustrates the present-day positions of the Chukotka, Verkhoyansk, and Sverdrup basins and their provenances. The sediments of the Chukotka basin and its paleogeographic zones extend now in approximately east-west direction (Fig. 8). In contrast, the paleogeographic zones of the Verkhoyansk basin are oriented in almost north-south directions (Fig. 13). The last basins are separated by major tectonic elements: SAS and cratonic and island-arc terranes of the Kolyma loop.

Two important inferences follow from this geodynamic situation. First, the facies distribution and clastic material transport for the Sverdrup and Chukotka basins point to the existence of the continental provenance north of them: Arctida (Zonenshain et al., 1990) or Crockerland (Embry, 1990, 1992; Anfinson et al., 2012). This provenance is characterized by the Mesoproterozoic and Permian–Triassic zircon populations with ages of 900–1700 and 236–263 Ma, respectively. The Arctida–Crockerland continent was subjected to most intense erosion in the post-Jurassic period after structural reorganization, which is evident from the appearance of significant peaks (at 1900–1950 Ma and single grains dated back to 2200, 2400, 2600, and 2800 Ma) in zircons from the Lower Cretaceous rocks of Chukotka (Miller et al., 2006). The ancient zircon populations (978–1978 Ma, Omma et al., 2010) appear also in Jurassic deposits of the Sverdrup basin.

Second, the displacement of Chukotka only

along strike-slip faults toward Taimyr and the Urals provides no grounds for considering traps as a potential source for the Permian–Triassic zircon population (236–263 Ma). This requires also rotation of the Chukotka block by approximately 100–180°. In addition, the westward AACM displacement requires the opening of the oceanic basin in its rear part. No suture of the basin closed in the Late Cretaceous is recognizable in the present-day structure of eastern Alaska. If it is assumed that the Lisburne thrust represents such a structure then the Chukotka terrane along with the Seward Peninsula and Arctic Alaska terrane can be considered autonomous microcontinents (Grantz et al., 1990; Nockleberg et al., 1993). Such a scenario may be considered possible, when fragments of the oceanic crust are found along the Lisburne thrust.

Differences in sedimentary evolution of the Verkhoyansk and Chukotka basins are determined by their different tectonic histories. The formation of the Verkhoyansk passive margin was initiated in the Devonian (Til'man, 1980; Parfenov, 1984; Khudoley and Prokopiev, 2007). In the Chukotka basin, extension of the continental crust occurred at the Permian–Triassic transition determined by the replacement of carbonate sedimentation with a terrigenous one.

The structural patterns of the Verkhoyansk complex conform to thrust–wedge models with the western vergence of thrusts and folds. The age of deformation and intruded syncollisional granites becomes younger westward. In the east, granite plutons of the Main Batholith Belt are dated back to 135–160 Ma ($^{40}\text{Ar}/^{39}\text{Ar}$), although most plutons range in age from 136 to 144 Ma (Layer et al., 2001). The granite pluton closest to the frontal thrust yielded a $^{40}\text{Ar}/^{39}\text{Ar}$ age of 98 Ma. The folded and thrust structures of Chukotka exhibit the northern vergence (Sokolov et al., 2009; Sokolov, 2010). The Anyui complex is deformed into complex isoclinal and recumbent folds. The postcollisional granites are 115–117 in age (Katkov et al., 2007).

CONCLUSIONS

1. The comparison of sedimentary and tectonic events documented in the two regions under consideration reveals significant differences. The thick continuous section of the Verkhoyansk

complex differs from its thinner Anyui counterpart in Chukotka, which was formed during a shorter period.

2. In contrast to the Verkhoyansk region, the continental margin of Chukotka is devoid of Upper Carboniferous, Lower Permian, and Middle Jurassic deposits and its section encloses unconformities at the bases of the Anyui Complex and Upper Jurassic–Lower Cretaceous sequence.
3. The geochemical composition of sandstones from the Chukotka basin is characterized by the distinct maturation trend reflected in the lower influence of basic rocks and increased role of the quartzose constituent. For Permian–Triassic sediments of the Verkhoyansk basin an opposite geochemical trend is reported.
4. The analysis of detrital zircons reveals several similar coeval populations, though these belong to different provenances, in addition to differences in ancient populations. The compositions of provenances are shown to be different. For the Chukotka basin, the provenance was dominated by low- to medium-metamorphosed rock complexes; in the Early Triassic, the notable role belonged to basic–intermediate rocks. For the Verkhoyansk basin, dominant rocks in the provenance were represented by granitoids; beginning in the Late Triassic, they were added to by basic rocks.
5. New dates obtained for detrital zircons from the Chukotka basin are similar to those available for Alaska and the Sverdrup basin, which provides grounds for assuming a single provenance for them (Crockerland–Arctida microcontinent).

ACKNOWLEDGMENTS

This study was supported by the Russian Foundation for Basic Research (project nos. 11-05-00074, 11-05-00787, 13-05-00943, 14-05-00031), 12-05-31432, project NSh-5177.2012.5, Department of Earth Sciences of RAS (program no. 10), and State contract № 01/14/20/11 and grant from St. Petersburg State University.

REFERENCES

Amato, J. M., Toro, J., Miller, E. L., Gehrels, G. E., Farmer, G. L., Gottlieb, E. S., and A.

B., Till, 2009, Late Proterozoic–Paleozoic evolution of the Arctic Alaska–Chukotka terrane based on U–Pb igneous and detrital zircon ages: implications for Neoproterozoic paleogeographic reconstructions. *Geological Society of America Bulletin*, 121, 1219–1235.

Anfinson O. A., Leier A.L., Embry A. F., and Dewing K. 2012, Detrital zircon geochronology and provenance of the Neoproterozoic to Late Devonian Franklinian Basin, Canadian Arctic Islands // *GSA Bulletin*; March/April; v. 124; no. 3/4; p. 415–430; doi: 10.1130/B30503.

Beranek, L.P., Mortensen, J.K., Lane, L.S., Allen, T.L., Fraser, T.A., Hadlari, T., and Zantvoort, W.G., 2010. Detrital zircon geochronology of the western Ellesmerian clastic wedge, northwestern Canada: Insights on Arctic tectonics and the evolution of the northern Cordilleran miogeocline: *Geological Society of America Bulletin*, v. 122, no. 11/12, p. XX

Bird, K. J., 2001. Alaska: a twenty-first-century petroleum province. In: Downey, M. W., Threet, J. C. & Morgan, W. A. (eds) *Petroleum Provinces of the Twenty-First Century*. American Association of Petroleum Geologists, Tulsa, OK, *Memoirs*, 74, 137–165.

Bondarenko, G.E.: 2004. *Tectonics and Geodynamic Evolution of the Mesozoic Fold Belts Along the Northern Circum-Pacific*, abstract of thesis, Moscow State University, Moscow, (in Russian).

Bondarenko, G. E., A. V. Soloviev, M. I. Tuchkova, J. I. Garver, and I. I. Podgorny, 2003, Age of detrital zircons from sandstones of the Mesozoic flysch formation in the South Anyui suture zone (western Chukotka): *Lithology and Mineral Resources*, 38, no. 2, 162–176.

Brandon M. T., Vance J.A., 1992, Tectonic evolution of the Cenozoic Olympic subduction complex, western Washington State, as deduced from fission track ages for detrital zircon // *American Journal of Science*, 292, 565–636.

Byalobzhesky S. G. and Goryachev N. A. 2004, “On the Origin of the Kolyma Structural Loop,” in *Proceedings of All_Russia Conference on Evolution of Tectonic Processes*, Novosibirsk, February 10–13, (Novosibirsk, 2004), 1 (in Russian).

- Bychkov, Yu. M. 1959: Stratigraphic scheme of the Triassic deposits of the central part of the Chaun region, in *Trudy Mezhdovedomstvennogo SoveshchaniyapoRazrabotkeUnifitsirovannykh Stratigraficheskikh Skhem Severo-Vostoka SSSR*, Magadan, 239–242, (in Russian).
- Crowley J.I., Myers J.S., Sylvester P.J., Cox R.A., 2005, Detrital Zircon from the Jack Hills and Mount Narryer, Western Australia: Evidence for Diverse > 4.0 Ga Source Rock // *Journal of Geology*, 113, 239-263.
- Drachev, S. S., 2011, Tectonic setting, structure and petroleum geology of the Siberian Arctic offshore sedimentary basins, From: Spencer, A. M., Embry, A. F., Gautier, D. L., Stoupakova, A. V. & Sørensen, K. (eds) *Arctic Petroleum Geology*. Geological Society, London, *Memoirs*, 35, 369–394. 0435-4052/11/\$15.00 # The Geological Society of London. DOI: 10.1144/M35,25.
- Drachev, S. S., Elistratov A. V., and Savostin L. A., 2001, Structure and Seismostratigraphy of the East Siberian Sea Shelf along the Indigirka Bay–Jannetta Island Seismic Profile: *Transactions (Doklady) of the Russian Academy of Sciences/Earth Science Section*. v. 377A, no. 3, P. 293-297.
- Drachev, S. S., Kaul, N. & Beliaev, V. N. 2003. Eurasia spreading basin to Laptev Shelf transition: structural pattern and heat flow. *Geophysical Journal International*, 152, p. 688–698.
- Eardly, A.J., 1948. Ancient Arctic. *Journal of Geology*, 56, 409-436.
- Embry, A. F. 2011, Petroleum prospectivity of the Triassic-Jurassic succession of Svedrup Basin, Canadian Arctic Archipelago. From: Spencer, A. M., Embry, A. F., Gautier, D. L., Stoupakova, A. V. & Sørensen, K. (eds) *Arctic Petroleum Geology*. Geological Society, London, *Memoirs*, 35, p. 545–558. 0435-4052/11/\$15.00 # The Geological Society of London. DOI: 10.1144/M35, 36.
- Embry, A. F. & Dixon, J. 1994. The age of the Amerasia Basin. In: Thurston, D. K. & Fujita, K. (eds) *Proceedings of the 1992 International Conference on Arctic Margins*. US Department of the Interior, Minerals Management Service, Anchorage, AK, p. 289–294.
- Embry A., 1993, Crockerland – the northern source area for the Sverdrup Basin, Canadian Arctic Archipelago. In: Vorren, E. Bergsager, O. Dahl-Stammes, E. Holter, B. Johansen, E. Lie and T. Lund (eds). *Arctic Geology and Petroleum Potential*. T. Norwegian Petroleum Society, Special Publication, 2, 205–216.
- Embry, A. F. 1992. Crocker Land: the northwest source area for the Sverdrup Basin, Canadian Arctic Archipelago. In: Vorren, T. O. (ed.) *Arctic Geology and Petroleum Potential*. Elsevier, Amsterdam. Norwegian Petroleum Society Special Publications, 2, p. 204–216.
- Embry, A. F. 1990. Geological and geophysical evidence in support of the hypothesis of anticlockwise rotation of Northern Alaska. *Marine Geology*, 93, p. 317–329.
- Gelman, M. L., 1995, Phanerozoic Granite–Metamorphic Domes in Northeastern Siberia. Article 1. Geological History of the Paleozoic and Mesozoic Domes. *Tikhookeanskaya Geologiya*, 14, 5, 102–115 (in Russian).
- Geodynamic, Magmatism, and Metallogeny of the Eastern Russia. 2006. Khanchuk (ed). Vladivostok, Dal'nauka, 1, 572. (in Russian).
- Grantz, A., Johnson, L. & Sweeney, J. F. (eds) 1990. *The Arctic Ocean Region. The Geology of North America*, L. Geological Society of America, Boulder, CO.
- Grantz A., Scott R. Drachev S., Moore T., & Zenon C. 2011, Sedimentary successions of the Arctic Region (58–648 to 908N) that may be prospective for hydrocarbons From: Spencer, A. M., Embry, A. F., Gautier, D. L., Stoupakova, A. V. & Sørensen, K. (eds) *Arctic Petroleum Geology*. Geological Society, London, *Memoirs*, 35, 17–37. 0435-4052/11/\$15.00 # The Geological Society of London. DOI: 10.1144/M35,2.
- Katkov, S. M., A. Strickland, E. L. Miller, and J. Toro, 2007, Ages of granite batholiths from Anyui-Chukotka Foldbelt: *Doklady Earth Sciences*, 414, no. 4, 515-518.
- Khudoley A.K. and Guriev G.A. 1994. The formation and development of late Paleozoic basin on the passive margin of the Siberian paleocontinent. In: *Pangea: Global Environments and*

- Resources, B. Beauchamp, A.F. Embry and D. Glass eds., Canadian Society of Petroleum Geologists Memoir 17, 131–143.
- Khudoley, A.K. and Prokopiev, A.V., 2007, Defining the eastern boundary of the North Asian craton from structural and subsidence history studies of the Verkhoyansk fold-and-thrust belt, in Sears, J.W., Harms, T.A., and Evenchick, C.A., eds., *Whence the Mountains? Inquiries into the evolution of orogenic systems: A volume in honor of Raymond A. Price*: Geological Society of America Special Paper 433, p. 391–410, doi: 10.1130/2007.2433(19)
- Korostylev V.I., 1982, Geology and Tectonic of South Verkhoyansk zone. Novosibirsk. Nauka. 282. (in Russian)
- Kos'ko, M. K., M. P. Cecile, J. C. Harrison, V. G. Ganelin, N. V. Khandoshko, and B. G. Lopatin, 1993, Geology of Wrangel Island, between Chukchi and East Siberian seas, northeastern Russia: Geological Survey Canada Bulletin, 461, 101.
- Kos'ko, M. K., Avdyunichiev V. V., Ganelin V. G., Opeskunov A. Yu., Opeslunova M. G., Cecile M. P., Smirnov A. N., Ushakov V. I., Khandozhko N. V., Harrison J. C., and Shul'ga D. Yu., 2003, The Wrangel Island: geological structure, mineragenesis, environmental geology (in Russian): Saint Petersburg, VNIIOkeangeologia, 137.
- Kossovskaya A. G., 1962, Mineralogy of the Mesozoic Terrigenous Complex in the Vilyui Basin and the West Verkhoyan'e, Academy of Sciences of the USSR, Moscow, 63, 234 (in Russian).
- Kossovskaya, A.G., Shutov, V.D., and Muraviev, V.I., 1960, Mesozoic and Upper Paleozoic Rocks of West Verkhoyanye and the Vilyui Basin, Academy of Sciences of the USSR, Moscow, 34, 276. (in Russian).
- Kosygin, Yu. A., Voevodin, V. N., Zhitkov, N. G., and V. A., Solov'yov, 1974, Eastern Chukotka volcanic zone and tectonic nature of volcanic belts, Dokl. Akad. Nauk SSSR, 216, 4, 885–888 (in Russian).
- Kuzmichev, A.B., 2009, Where does the South Anyui suture go in the New Siberian islands and Laptev Sea? *Tectonophysics*, 463, 86–108.
- Kuznetsov N.B., Soboleva A.A., Udoratina O.V., Hertseva M.V., Andreichev V.L. Pre-Ordovician tectonic evolution and volcano-plutonic associations of the Timanides and northern Pre-Uralides, northeast part of the East European Craton // *Gondwana Research*. 2007. 12. 305-323.
- Lawver, L. A., Grantz, A. & Gahagan, L. M. 2002. Plate kinematic evolution of the present Arctic region since the Ordovician. In: Miller, E. L., Grantz, A. & Klemperer, S. L. (eds) *Tectonic Evolution of the Bering Shelf-Chukchi Sea-Arctic Margin and Adjacent Landmasses*. Geological Society of America, Boulder, CO, Special Papers, 360, p. 333–358 and pl. 6.
- Lawver L.A., Ganagan L.M., and I., Norton, 2011, Palaeogeographic and tectonic evolution of the Arctic region during the Palaeozoic. In: Spencer, A. M., Embry, A. F., Gautier, D. L., Stoupakova, A. V. and K., Sørensen (eds.) *Arctic Petroleum Geology*. Geological Society, London, Memoirs, 35, 61–77.
- Layer, P.W., Newberry, R., Fujita, K., Parfenov, L.M., Trunilina, V.A., and Bakharev, A.G., 2001, Tectonic setting of the plutonic belts of Yakutia, northeast Russia, based on $^{40}\text{Ar}/^{39}\text{Ar}$ geochronology and trace element geochemistry: *Geology*, v. 29, p. 167–170, doi: 10.1130/0091-7613(2001)029<0167:TSOTPB>2.0.CO;2.
- Ledneva G.V., Pease V.L., and Sokolov S.D., 2011, Permo-Triassic hypabyssal mafic intrusions and associated tholeiitic basalts of the Kolyuchinskaya Bay, Chukotka (NE Russia): Links to the Siberian LIP. *Journal of Asian Earth Sciences*, 40, 737–745.
- McLennan S.M., Hemming S., McDaniel D.K., Hanson G.N., 1993, Geochemical approaches to sedimentation, provenance and tectonics // In Jonsson M.J. and Basu A. (eds) *Processes Controlling the composition of Clastic sediments*: Boulder, Colorado, Geological Society of America, Spec. Paper, 284, 21–40
- McLennan S.M., Bock B., Hemming S.R., Hurowitz J.A., Lev S.M., McDaniel D.K. The role of provenance and sedimentary processes in geochemistry of sedimentary rocks. 2003. In: Lentz D., editor. *Geochemistry of Sediments and Sedimentary Rocks: Evolutionary*

- Considerations to Mineral Deposit-Forming Environments. St. John's, Geol. Assoc. of Canada, 7-38
- Miller E., Toro J., Gehrels G., Amato J., Prokopiev A., Tuckkova M., Akinin V., Dumitru T., Moore T., Embry A. and Cecile M. 2006, New Insights into Arctic Paleogeography and Tectonics from U-Pb Detrital Zircon Geochronology // *Tectonics*. 25. TC3013. doi:10.1029/2005TC001830.
- Miller, E. L., Soloviev, A., Kuzmichev, A., Gehrels, G., Toro, J., and Tuckkova, M., 2008, Jura-Cretaceous foreland basin deposits of the Russian Arctic: Separated by birth of Makarov Basin?: *Norwegian Journal of Geology*, 88, 227–250.
- Miller, E.L., S. M. Katkov, A. Strickland, J. Toro, V. V. Akinin, and T. A. Dumitru, 2009, Geochronology and thermochronology of Cretaceous plutons and metamorphic country rocks, Anyui-Chukotka fold belt, northeastern Arctic Russia, in D. B. Stone, K. Fujita, P. W. Layer, E. L. Miller, A. V. Prokopiev, and J. Toro, eds., *Geology, geophysics and tectonics of Northeastern Russia: a tribute to Leonid Parfenov*: European Geosciences Union, Stephan Mueller Publication Series, 4, 157–175.
- Morozov O.L., 2001, Geological structure and tectonic evolution of Central Chukotka. Moscow, GEOS, Trudy GIN RAS, 523, 201 (in Russian).
- Natal'in, B., Amato, J.M., Toro, J., and Wright J.E., 1999, Paleozoic rocks of the northern Chukotka Peninsula, Russian Far East: implications for the tectonics of the Arctic region // *Tectonics*, 18, 6, 977-1004.
- Nesbitt, H.W., Young, G.M., 1982. Early Proterozoic climates and plate motions inferred from major element chemistry of lutites. *Nature* 299, p. 715-717.
- Nichols G. 2009, *Sedimentology and Stratigraphy*, Second Edition, Wiley-Blackwell, 419.
- Nokleberg W.J., Parfenov L.M., Monger J.W.H., Baranov B.V., Byalobzhesky S.G., Bundtzen T.K., Feeney T.D., Fujita K., Gordey S.P., Grantz A., Khanchuk A.I., Natal'in B.A., Natapov L.M., Norton I.O., Patton W.W., Jr., Plafker G., Scholl D.W., Sokolov S.D., Sosunov G.M., Stone D.B., Tabor R.W., Tsukanov N.V., Vallier T.L., and K., Wakita, 1994. Circum-North Pacific tectonostratigraphic terrane map: U.S. Geological Survey Open-File Report 94-714 (2 sheets, scale 1:5 000 000, 1 sheets, scale 1:10 000 000), 433
- Omma J. E., Pease V. & Scott R. A., 2011, U–Pb SIMS zircon geochronology of Triassic and Jurassic sandstones on northwestern Axel Heiberg Island, northern Sverdrup Basin, Arctic Canada // From: Spencer, A. M., Embry, A. F., Gautier, D. L., Stoupakova, A. V. & Sørensen, K. (eds) *Arctic Petroleum Geology*. Geological Society, London, *Memoirs*, 35, 559-556. 0435-4052/11/\$15.00 # The Geological Society of London 2011. DOI: 10.1144/M35.25
- Parfenov, L.M. 1984. *Continental Margins and Island Arcs of the Mesozoics of Northeast Asia*. Nauka, Novosibirsk, 192 (in Russian).
- Parfenov, L.M., 1995, Terranes and history of formation of Mesozoic orogenic belts of the eastern Yakutia: *Pacific Geology*, 14, no. 6, 3–10.
- Parfenov, L. M., Natapov, L. M., Sokolov, S. D., and N.V., Tsukanov, 1993, Terranes analysis and accretion in northeast Asia, *The Islands Arc*, 2, 35–54.
- Parfenov, L.M., Prokopiev, A.V., and Gaiduk, V.V., 1995, Cretaceous frontal thrusts of the Verkhoyansk fold belt, eastern Siberia: *Tectonics*, v. 14, p. 342–358, doi: 10.1029/94TC03088.
- Pettijohn F. J., 1981, *Sedimentary Rocks*, 3rd Ed. (Harper and Row, New York, Moscow, Nedra, 475. (in Russian).
- Prokopiev A.V., Toro J., Miller E.L., Gehrels G.T., 2008, The paleo-Lena River – 200 m.y. of transcontinental zircon transport in Siberia // *Geology*. 36, no. 9, 699–702.
- Prokopiev, A.V., and Deikunenko, A.V., 2001, Deformational structures of fold-and-thrust belts, in: Parfenov, L.M., and Kuzmin, M.I., eds., *Tectonics, geodynamics and metallogeny of the Sakha Republic (Yakutia)*: Moscow, International Academic Publishing Company “Nauka/Interperiodica,” 156–198 (in Russian).
- Prokopiev A.V. and Ivensen G.V., 2008, Reconstruction of source of pyroclastic materials if Permian and Triassic South-

- Verkhoyansk basin (North-Eastern part of Asia) by lithochemical data // *Russian Geology*, 5, 119-127 (in Russian).
- Prokopiev, A. V., Toro, J., Miller, E. L., Wooden, J., Trunilina, V. A., and Bakharev, A. G.: Granitoids of the Main batholith belt (northeast Asia): new U-Pb SHRIMP geochronological and geochemical data, Tectonics and metallogeny of the Circum North Pacific and East Asia, Khabarovsk, Institute of Tectonics and Geophysics, 2007, p. 286–288 (in Russian).
- Prokopiev A.V. and Tronin A.V., 2004, Structure and sedimentological data for Kular-Nera schist's belt and In'aly-Debin synclinorium // *Russian Geology*, 4, 49–56. (in Russian).
- Report on 1:200 000 Geological Mapping and General Exploration, Quadrangle Q-1-1X,X, Chukotka, 1978, Blagodatsky S.V., Bychkov Yu.M. (ed.). North-Eastern Geological Survey, 62 (in Russian).
- Rohr T. S., Andersen T. & Dyrvik H., 2008, Provenance of Lower Cretaceous sediments in the Wandel Sea Basin, North Greenland // *Journal of the Geological Society*. London. 165, 755–767.
- Roser B.P. & Korsch R.J., 1988, Provenance signatures of sandstone-mudstone suites determined using discriminant function analysis of major-element data. *Chemical Geology*. 67, 119-139.
- Shatsky, N. S. 1935. On Tectonics of the Arctic. *Geology and Mineral Resources of the USSR's North*. Glavsevmorput', Leningrad, 149–165 (in Russian).
- Shatsky N.S., 1963, Revisit Arctic tectonics // *Selected issues Russian Academy of Sciences*, Moscow, 1, 426-444. (in Russian).
- Sokolov S.D., 1992, Accretionary tectonics of the Koryak - Chukotka segment of the Pacific belt, *Trans. of Geological Institute Russian Academy of Sciences*, 479, Moscow, Nauka, 182 (in Russian).
- Sokolov, S. D., Bondarenko, G. E., Morozov, O. L., and Luchitskaya, M. V., 2001, The tectonics of the junction zone between the Verkhoyansk-Chukotka and Koryak-Kamchatka fold belts, *Byull. Mosk. O-va Ispyt. Prirody. Otd. Geol*, 76, 24–37, (in Russian).
- Sokolov, S. D., G. Ye. Bondarenko, O. L. Morozov, V. A. Shekhovtsov, S. P. Glotov, A. V. Ganelin, and I. R. Kravchenko-Berezhnoy, 2002, Souyh Anyui suture, northeast Arctic Russia: Facts and problems, in E. L. Miller, A. Grantz, and S. L. Klemperer, eds., *Tectonic Evolution of the Bering Shelf-Chukchi Sea-Arctic Margin and Adjacent Landmasses: Geological Society of America Special Paper 360*, 209-224.
- Sokolov, S. D., G. Ye. Bondarenko, P. W. Layer, and I. R. Kravchenko-Berezhnoy, 2009, South Anyui suture: tectono-stratigraphy, deformations, and principal tectonic events, in D. B. Stone, K. Fujita, P. W. Layer, and E. L. Miller, A. V. Prokopiev, and J. Toro, eds., *Geology, geophysics and tectonics of Northeastern Russia: a tribute to Leonid Parfenov*, European Geosciences Union, Stephan Mueller Publication Series, v. 4, p. 201-221.
- Sokolov S. D., 2010, Tectonics of Northeast Asia: An Overview. *Geotectonics*, 44, 6, 493-509.
- Sweeney, J.F., 1985, Comments about the age of the Canada Basin: *Tectonics*, v. 114, p. 1–10
- Taylor S.R., McLennan S.M., 1985, *The Continental Crust: its Composition and Evolution*. Moscow, Mir, 1988, 384 (in Russian).
- Taylor S.R., McLennan S.M., 1995, The geochemical evolution of continental crust // *Reviews of Geophysics*, 33, 241-265.
- Tectonics, geodynamics and metallogeny of the Sakha Republic (Yakutia), 2001, Moscow, MAIL Nauka/Interperiodika, 571 (in Russian).
- Til'man, S.M., 1980, Regions with the continental crust formed to the beginning of the Riphean: miogeosyncline systems. In: Markov, M.S., Pustcharovsky, Yu.M., Til'man, S.M., Fedorovsky, V.S. and N.A., Shilo, (eds.) *Tectonics of the continental margins of the northwestern Pacific Ocean*. Moscow, Nauka, 26-48 (In Russian).
- Tuchkova M.I., Bondarenko G.Ye., Buyakaite M.I., Golovin D.I., Galuskina I.O., and E.V., Pokrovskaya, 2007, Results from sedimentological and radiometric studies of the Upper Triassic deposits of the Chukotka microcontinent, *Geotektonika*, 5, 76-96 (in Russian).
- Tuchkova M.I., Katkov S.M., Galuskina E.O., and

- I.M.Simanovich, 2011, Postsedimentation Transformation of Triassic Terrigenous Rocks in West Chukotka as an Indicator of Folding Conditions // *Geotectonics*, 45, 3, 225–239.
- Tuchkova M.I., Sokolov S.D., and Kravchenko-Berezhnoy I.R., 2009, Provenance analysis and tectonic setting of the Triassic clastic deposits in Western Chukotka, Northeast Russia // *Stephan Mueller Spec. Publ. Ser.*, 4, 177–200, www.stephan-mueller-spec-publ-ser.net/4/177/2009/.
- Tynankergav, G. A. and Bychkov J. M., 1987, Upper Triassic Chert-Volcanic-Terrigenous Assemblages of Western Chukotka, *Doklady of Russian Academy of Sciences*, 296, 698–700 (in Russian)
- Vernikovskiy V.A., Vernikovskaya A.E., 2001, Central Taymyr accretionary belt (Arctic Asia): Meso-Neoproterozoic tectonic evolution and Rodinia breakup // *Precambrian Research*, 110, 127-141
- Verzhbitsky V., Frantzen E.M., Trommestad K., Savostina T., Little A., Sokolov S.D., Tuchkova M.I., Travis T., Martyntsiva O., Ullnaess M., 2008, New seismic data on the South and North Chukchi sedimentary basins and the Wrangel Arch and their significance for the geology of Chukchi Sea shelf (Russian Arctic) // “Geosciences – From New Ideas to New Discoveries”. 3rd Saint Petersburg International Conference and Exhibition of European Association of Geoscientists and Engineers (EAGE). 7-10 April 2008. Lenexpo, Saint Petersburg, Russia. Extended Abstracts and Exhibitors' Catalogue. Abstract B030.
- Verzhbitsky V.E., Sokolov S.D., Frantzen E.M., Tuchkova M.I., Bannikov G.A., 2010, Tectonics, sedimentary basins, and hydrocarbon prospects in the Chukchi Sea // “Gas Industry of Russia”, special issue “Gas and oil of the East Russia”, 654, p. 32-37 (in Russian).
- Yapaskurt, O.V., 1992, Lithogenesis and Mineral Deposits of Miogeosynclines: Moscow, Nedra, 224 (in Russian).
- Zonenshain, L. P., Kuzmin, M. I., and Natapov L. M., 1990, Plate Tectonics of the USSR Territory, Moscow, Nedra, 2 (in Russian).

Chukchi arctic continental margins: tectonic evolution, link to the opening of the Amerasia Basin

Sokolov S.D., Ledneva G.V., Tuckova M.I., Luchitskaya M.V., Ganelin A.V., and Verzhbitsky V.E.

ABSTRACT

The Arctic margin of Chukotka (Chukotka fold belt) comprises two tectonic units, namely the Anyui-Chukotka fold system (the ACh) and the South Anyui suture (the SAS). In terms of the paleotectonic reconstructions, the ACh represents the Chukotka microcontinent whereas the SAS is the suture, which is the result of collision of the Chukotka microcontinent with the Siberian active margin (the Verkhoyansk-Kolyma fold system). Tectono-stratigraphic units of the South Anyui suture were thrust northward over the passive margin of the microcontinent during the collision.

The tectonic evolution of the continental margin of Chukotka can be divided into four main tectonic stages corresponding to the Late Precambrian-Early Paleozoic, the Late Paleozoic- Early Mesozoic, the Middle Jurassic- Early Cretaceous and the Aptian-Albian. The metamorphic basement has the Neoproterozoic age and is assumed to represent a relict of the ancient Arctida continent. In the Early Paleozoic, Arctida was separated from Siberia and Laurentia by oceanic basins. The Chukotka microcontinent was situated next to Siberia until the Devonian and was accreted to Laurentia during the Ellesmerian orogeny. The wide ProtoArctic Ocean connected with the PaleoUral Ocean can be reconstructed for Late Paleozoic time. The Siberian margin was active whereas the North American margin was passive. After the closure of the PaleoUral Ocean, the ProtoArctic Ocean became a gulf of the PaleoPacific Ocean. However, it separated structures of the North American and Siberian continents. In the latest Permian-earliest Triassic, the continental crust of the Chukotka microcontinent was destroyed as Pangea broke up. The Lower Triassic turbidites contains dikes and sills of diabases.

Starting in Early Jurassic time, tectonic events taking place at the continental margin of Chukotka are well correlated with the main phases of the Amerasia Basin opening. The Late Jurassic was

characterized by termination of spreading in the ProtoArctic Ocean and transformation of the latter into the closing South Anyui turbidite basin. The Chukotka microcontinent was subducted beneath the Siberian active margin (the Oloy volcanic belt) until the Valanginian. In the Hauterivian-Barremian, an oblique collision was initiated simultaneously with spreading in the Canada Basin. This collision resulted in formation of the South Anyui suture. As both subduction and collision was terminated, formation of an oceanic crust within the Amerasia Basin ceased.

INTRODUCTION

The origin of the Amerasia Basin is broadly debated in discussions of Arctic region tectonics. Different viewpoints exist on its origin but the rotational hypothesis (Carey, 1955) and its various modifications (Embry and Dixon, 1994; Lawver, et al., 2002; 2011; Grantz, et al., 1990, 2011, and others) are the most popular positions. However, it has been recently sharply criticized (see Lane, 1997; Miller, et al., 2006; Kuz'michev, 2009; and Beranek, et al, 2010).

A composition of the crust in structures of the Amerasia Basin is widely discussed as well. A continental nature of the Lomonosov Ridge crust and an oceanic nature of the Canada Basin crust are more or less proven. However, seismic data available for the crust of the Alpha Ridge and the Mendeleev Uplift cannot currently be unambiguously interpreted based on available evidence.

In this context, the continental margin of Chukotka is an important source of information for testing the rotational hypothesis. The geological peculiarities of Chukotka must be taken into account in tectonic reconstructions. At present, our knowledge of the geology of Chukotka is insufficient to resolve the reconstructions. Therefore, new data, which have been recently obtained by different researchers including authors of this paper, allow for elucidation

of different aspects of the tectonic evolution and to construct regional correlations. This paper pays special attention to correlations of tectonic stages of the Arctic margins of Chukotka and the Canada Basin.

GEOLOGICAL SETTING

The Amerasia basin is asymmetric, which is expressed in the narrow North American shelf and the large Eurasian shelf (Fig. 1). Its western part is made of the system of the Lomonosov, Alpha and Mendeleev Uplift and separating them deep-water Makarov and Podvodnikov basins. The eastern part of the basin comprises the Canada Basin and the Chukchi plateau adjacent to the Mendeleev Uplift.

The Arctic margin of Chukotka includes the continental areas from the Kolyma river basin to Chukotka Peninsula and the large shelf of the East Siberian and Chukchi seas. One of the main structures of this region is the Chukotka (Novosibirsk-Chukotka) fold belt (Fig. 2), which is also referred to as the Chukotka Mesozoides in the Russian literature (Til'man, 1980; Zonenshain et al, 1990). The Mesozoides includes the Anyui-Chukotka fold system (the AChS) and the South Anyui Suture (the SAS). The latter is the southern boundary of the Chukotka Mesozoides and separates them for structures of the Verkhoyansk-Kolyma province.

The SAS extends from Bol'shoy Lyakhovsky

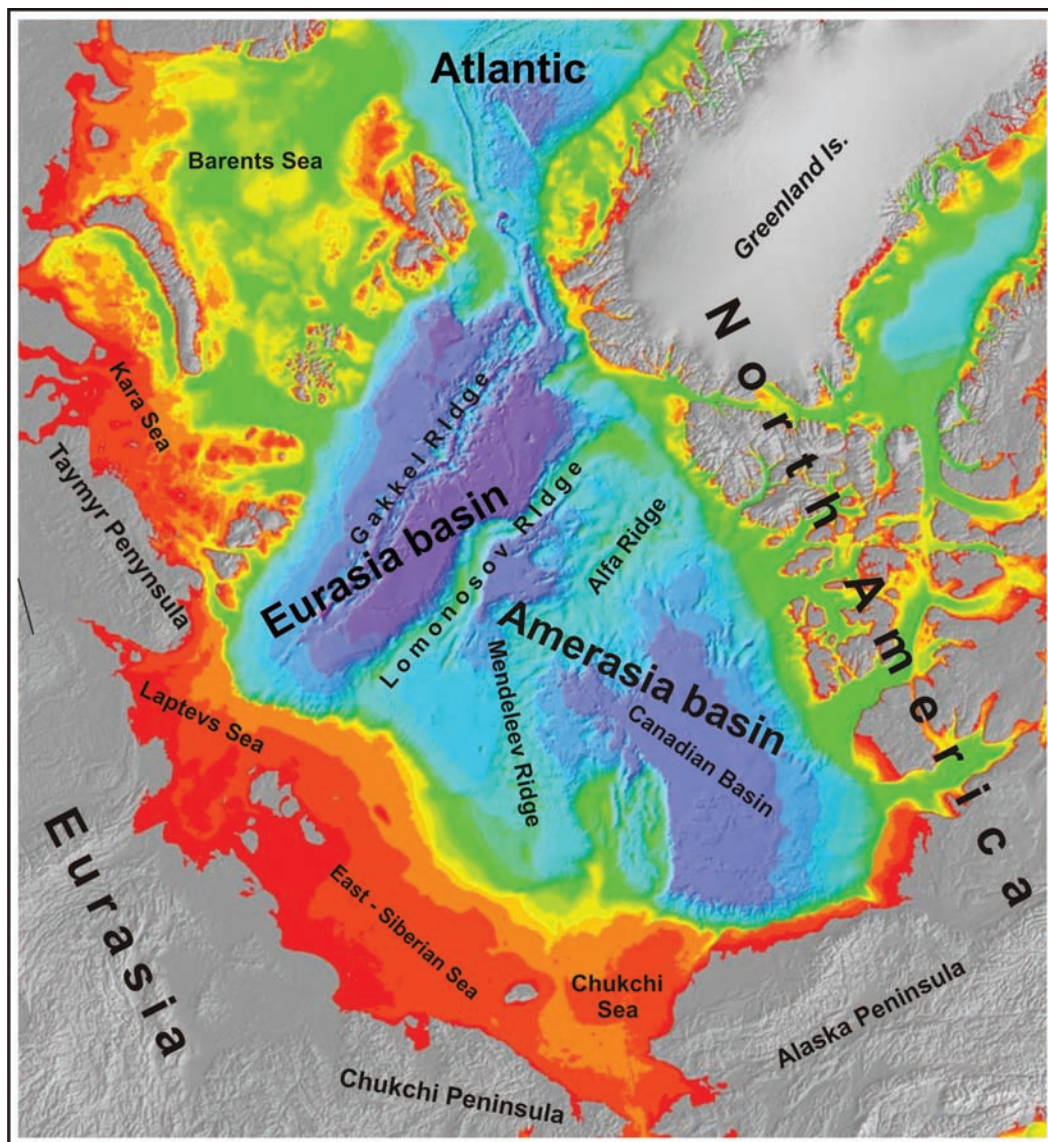
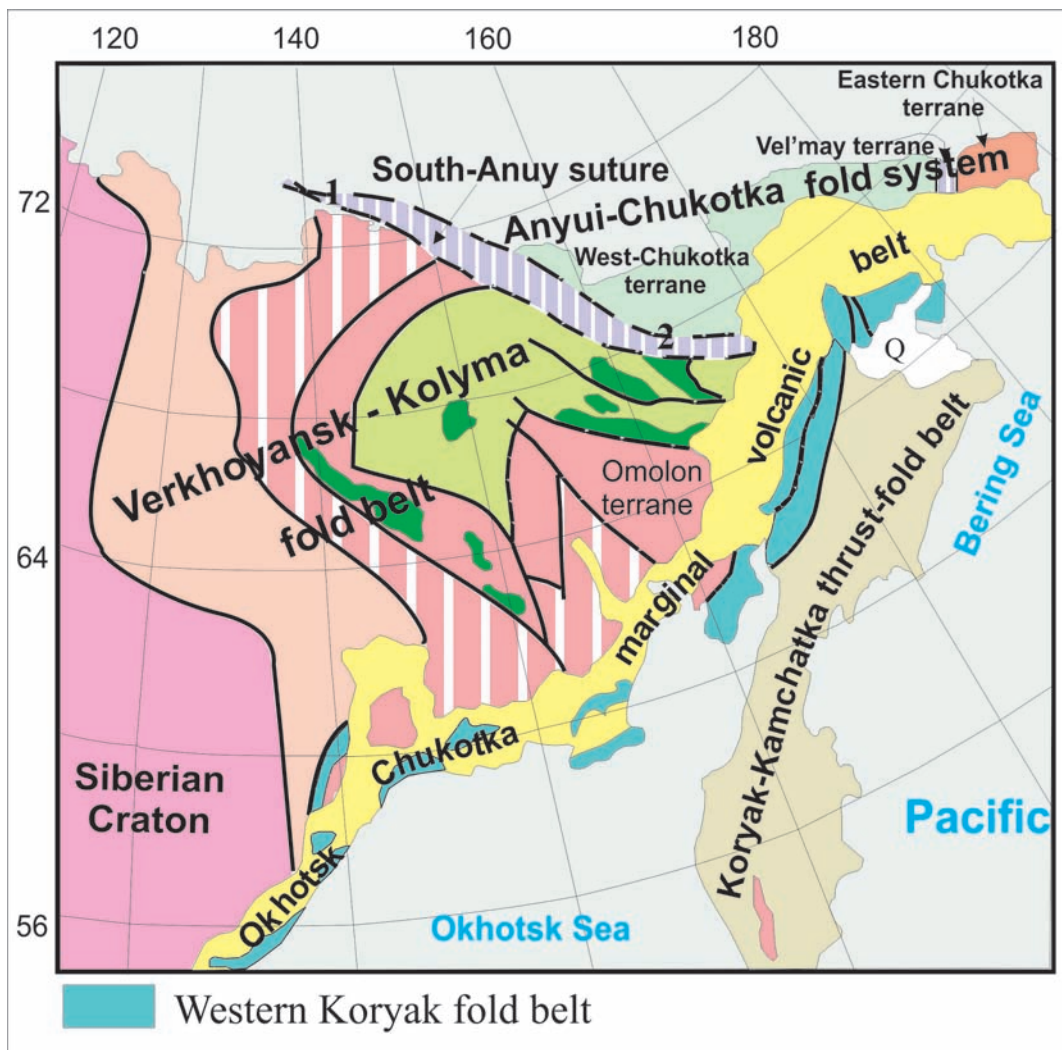


Fig. 1. Main structures of Arctic region

Island (the New Siberian Islands) up to the upper reach of the Bol'shoy and Maly Anyui rivers, where it is unconformably overlain by deposits of the Okhotsk-Chukotka volcanic belt (the OChVB). As suggested, an eastern continuity of the SAS is represented by ophiolites of the Vel'may terrane of eastern Chukotka (Parfenov, et al., 1993; Nokleberg, et al., 1994). A western continuity of this terrane is disputed. Some researchers (Zonenshain, et al., 1990; Parfenov, et al., 1993) extend it to the Polar Urals through the Taymyr. However, Kos'ko et al., (1994) stressed that data on magnetic and gravity fields for areas to the west of Bol'shoy Layakhovsky Island do not provide an unequivocal resolution of this problem. The latter allows the suggestion that a

western continuity of the SAS can be represented by ophiolites of the collisional belt of the Chersky Range (Oxman, et al., 2003). In this case, the configuration of the suture would be similar to boundaries of the Angayucham terrane in Alaska. This hypothesis has been recently discussed in detail by Kuz'michev (2009). Direct correlations between ophiolites of the Chersky Range and the SAS are hardly possible as they differ in ages.

The AChS is characterized by an ancient crystalline basement, fold-and-thrust structures of the Paleozoic and Mesozoic deposits and deformation of Kimmeridgian age. The northern boundary is assumed to be marked by the Wrangel-Herald front of deformations. Deposits of the Northern Chukchi



Chukotka fold belt consists of Anyui-Chukotka fold system and South Anyui suture (1- Shalaurova terrane, 2 - South-Anyui terrane)

Fig. 2. Tectonic scheme of the Northeastern Russia

depression located to the north of it are undeformed (Verzhbitsky, et al., 2008; Drachev, 2011).

There are differing viewpoints concerning distinguishing the New Siberian Islands as a part of the Chukotka fold area. Based on similar lithology, most researchers recognize a single structure referred to as the New Siberian-Chukotka block (Zonenshain, et al., 1990; Parfenov, et al., 1993 and others) or Bennett-Barrovia (Natal'in, et al., 1998) block. However, some recent studies suggest that the New Siberian Islands belong to the Siberian continent (Kuz'michev, 2009; Vernikovskiy, 2011, personal comm.). Geology of the New Siberian Islands is not considered in this paper.

The Anyui-Chukotka fold system (ACh)

The ACh includes several terranes and subterrane (the Wrangel, West-Chukotka and East-Chukotka) that somewhat differ in composition and stratigraphic successions of these deposits (Fig. 3). From the paleotectonic viewpoint, they are interpreted as Chukotka microcontinent (Parfenov, et al., 1993; Kos'ko, et al., 1993, 1994; Khanchuk (ed), 2006) with the ancient crystalline basement and Paleozoic-Mesozoic cover. This continent was considered either as a part of the Arctida continent (Zonenshain, et al., 1990) or as a fragment of the Arctic Alaska-Chukotka microplate (the AACM).

The basement of the ACh is exposed in Wrangel Island and in the East-Chukotka terrane. On Wrangel Island, it is composed of amphibole schists, epidote-amphibole schists and greenschists derived from sedimentary and volcanic rocks. These deposits are intruded by granites (609-677 Ma) and are unconformably overlain by Devonian-Lower Carboniferous deposits (Kos'ko, et al., 1993). In eastern Chukotka, exposures of the Precambrian basement are represented by deposits that are strongly metamorphosed to greenschist, amphibolite and locally granulite facies and there are sedimentary strata with horizons of marbles, granitic gneisses and ultrabasites (Til'man..., 1980; Zhulanova, 1990). Most of the researchers points out the similarity of metamorphic complexes of eastern Chukotka and the Seward Peninsula of Alaska and combine them into a single terrane (Parfenov, et al., 1993; Nokleberg, et al., 1994; Natal'in, et al., 1999).

The oldest dates were obtained by Rb/Sr (2565

and 1990 Ma) and K/Ar (1570 and 1680 Ma) methods (Zhulanova, 1990; Kotlyar, et al., 2001; Khanchuk (ed), 2006). Zircons from presumably Pre-Cambrian metamorphic rocks, which were chronologically dated in the last few years, yield younger Paleozoic and Cretaceous ages. They chiefly relate to granite-metamorphic domes that formed at the end of the Early Cretaceous (Gel'man, 1995; Bering Strait..., 1987). Most of orthogneisses are deformed granites of Cretaceous age (108-104 Ma, U-Pb SHRIMP zircon ages). Zircons of only two samples yielded ages of 369 ± 2 and 274.5 ± 0.5 Ma (Natal'in, et al., 1999). Zircons from metamorphic rocks of the Chegitun complex have ages that vary between 650-540 Ma (Natal'in, et al., 1999).

Paleozoic strata are represented by carbonate, carbonate-terrigenous and terrigenous deposits of the Middle Ordovician to Middle Carboniferous ages (Fig. 3). In the granite-metamorphic domes, they are metamorphosed to greenschist and amphibolite facies. Upper Carboniferous and Permian marine deposits do not occur in the Chukotka Peninsula. On Wrangel Island, they are represented by carbonate and terrigenous rocks that accumulated in shallow water conditions to the north and deeper water conditions to the south (Kos'ko, et al., 1993).

Triassic deposits rest unconformably on Paleozoic strata and are mainly represented by shelf, continental slope and rise turbidites (Tuchkova, et al., 2007b). Sediment provinces were located to the north or northeast. In the lower part, this sequence is cut by numerous sills and small intrusions of gabbro, gabbro-diabases and gabbro-dolerites. They are dated at 218-233 Ma (Khanchuk (ed), 2006). The first U-Pb zircon age of 252 ± 4 Ma of gabbroic rocks from the area of the Kolyuchinskaya Bay (Ledneva et al., 2011) proves the existence of the Permian deposits in the cover. Unique findings of flora, spore and pollen indicative of the continental genesis were previously known.

Upper Jurassic – Lower Cretaceous deposits are represented by clastic rocks with horizons of conglomerate and slates with plant detritus. Some units contain tuff and volcanic material.

The South Anyui Suture (SAS)

The SAS is the result of collision of the Chukotka microcontinent with structures of the active margin

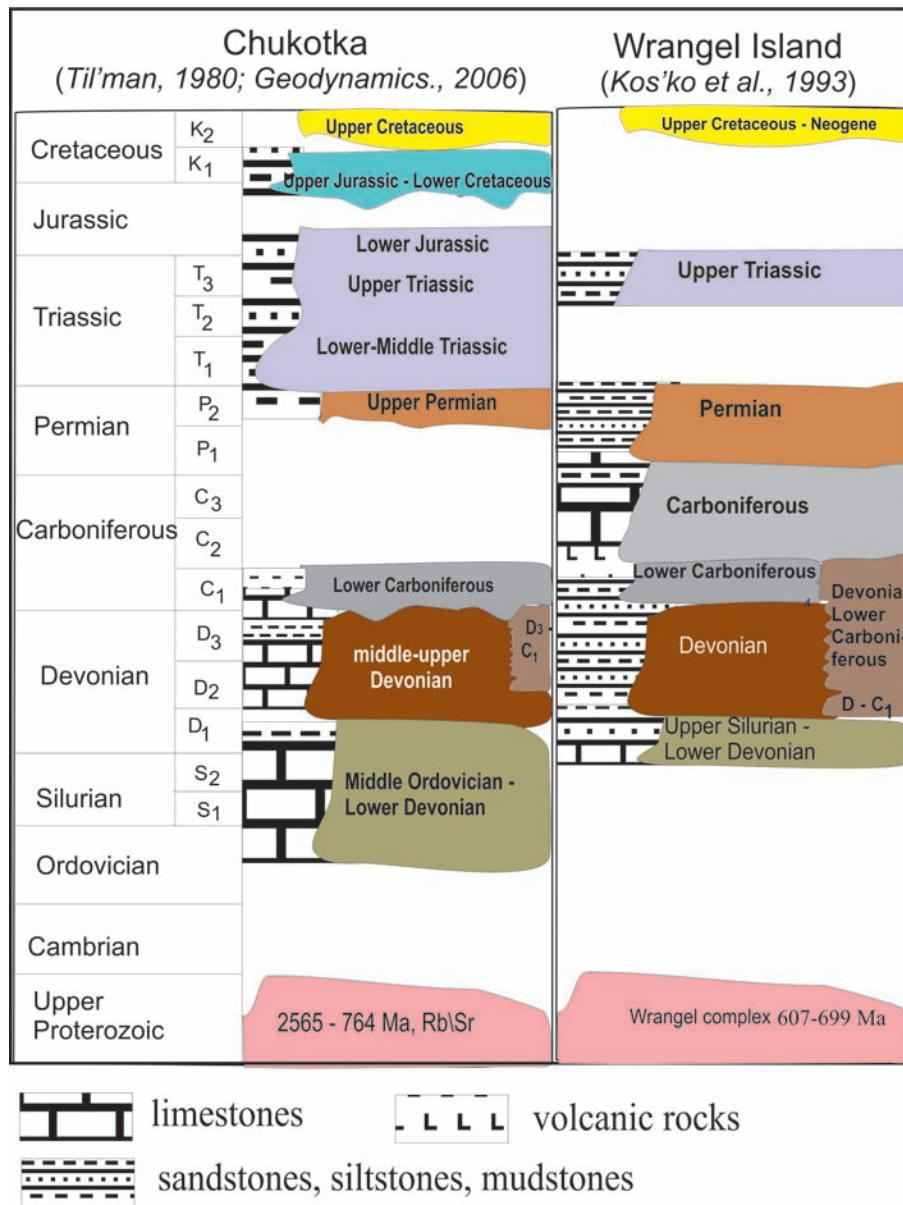


Fig. 3. Stratigraphic schemes of Chukotka and Wrangel Island

of the Siberian continent (Seslavinsky, 1979; Natal'in, 1984; Zonenshain, et al, 1990; Parfenov, et al, 1993). The SAS includes three terranes, which are separated by overlying Cretaceous, Tertiary and Quaternary deposits. The Shalaurova terrane is located in the northwestern part of the suture; the South Anyui terrane is situated in its central part; and the Vel'may terrane occurs in its eastern part. Main features of the geological structure and model of tectonic evolution of the SAS are discussed in detail in several publications (Natal'in, 1984; Sokolov, et al., 2001, 2002, 2009; Khanchuk (ed), 2006) and are only briefly considered in this paper.

The Shalaurova terrane is situated in the southeastern part of Bol'shoy Lyakhovsky Island (Parfenov, et al, 1993; Tectonics..., 2001; Kuz'michev, 2009). It comprises serpentinized peridotites, gabbro-diabases, pillow MORB lavas, amphibolites and glaucophane schists. Metamorphic rocks and ophiolites are thrust over Upper Jurassic – Lower Cretaceous flysch deposits. It is assumed that the flysch was deposited in a foredeep formed via the collision of the Svyatoy Nos arc and the Novosibirsk continental block. Postcollisional granites show ⁴⁰Ar/³⁹Ar biotite plateau age of 114.4±0.5 Ma (Layer, et al., 2001)).

Geochronological data on metamorphic rocks and ophiolites are not reliable. For example, bulk-rock pillow basalts are dated at 291 ± 62 Ma; K-Ar bulk-rock amphibolites age is 473 Ma (Drachev and Savostin, 1993). Metamorphic minerals from basalts exhibit K-Ar age of 133.5 ± 4.5 and 139 ± 8 Ma (Kuz'michev, 2009) that can be treated as an age of young alteration.

The South Anyui terrane is situated in the interflaves of the Bol'shoy and Maly Anyui rivers. It is made of a system of intensively deformed tectonic nappes. Four stages of deformation are distinguished (Sokolov et al., 2002, 2009). The first and second stages of deformation is characterized by thrusts and folds of northern and southern vergence, respectively. The collision between Chukotka microcontinent and North-Asian craton that occurred in the Early Cretaceous was oblique and resulted in the formation of dextral strike-slip faults. Deformation of the final stage was related to nearly latitudinal sinistral brittle strike-slip faults that exerted an influence on

the Albian-Cenomanian deposits of the Okhotsk-Chukotka volcanic belt.

Tectonic nappes are made of the following tectono-stratigraphic units (Fig.4) that originated in different provinces of an oceanic basin and its margins:

1. The Ustieva Unit, turbidites, Upper Triassic, deposits of the continental slope. The lower structural unit is interpreted as distal turbidites of a passive margin of the Chukotka microcontinent;
2. The Polyarnyui unit, volcanic-chert-carbonate assemblage, Lower Carboniferous. The unit is interpreted as a fragment of the oceanic crust composing the base of the Kulpolney island arc;
3. The Kulpolney unit, volcanic and clastic rocks, Oxfordian-Kimmeridgian, a fragment of an ensimatic island arc;
4. The Tenvel unit, clastic rocks with volcanic layers, a Kimmeridgian-Lower Tithonian, forearc basin;

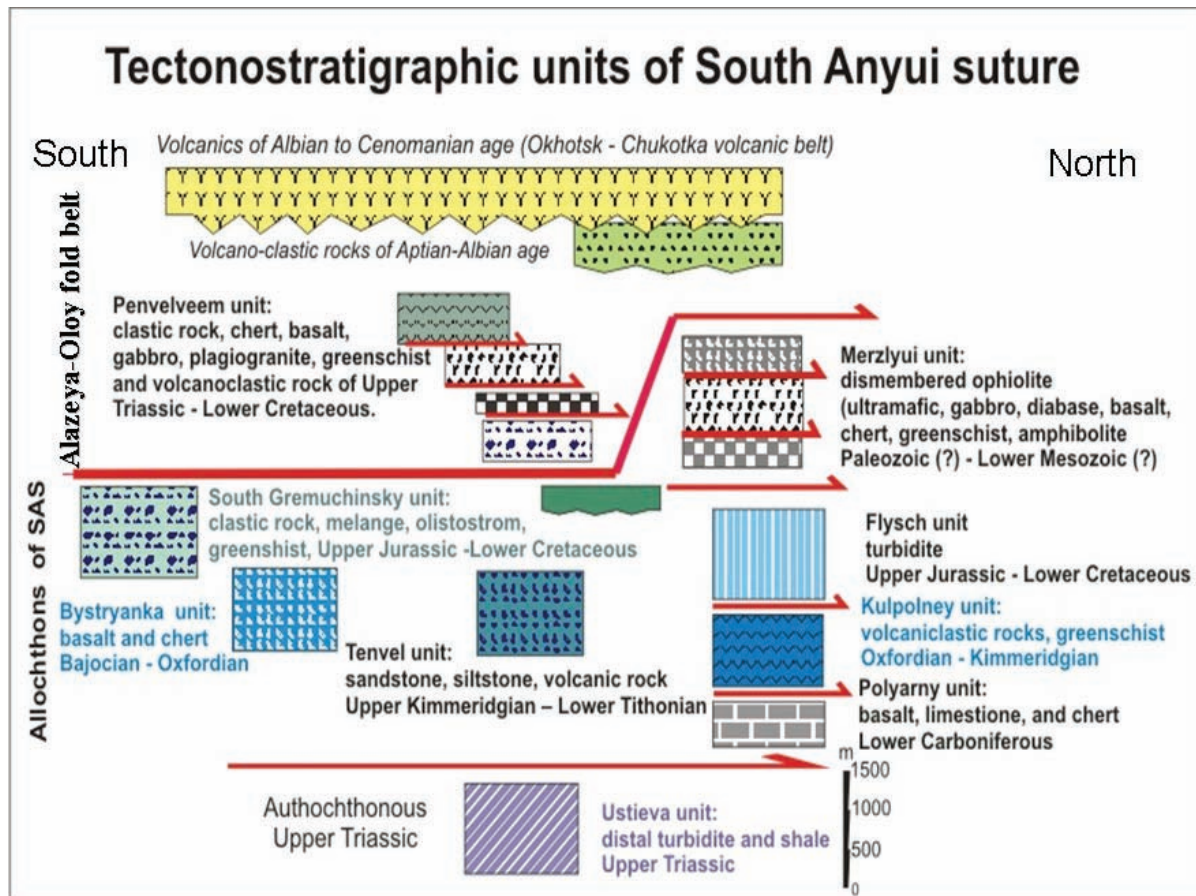


Fig. 4. Tectono-stratigraphic units of South Anyui suture.

5. The Flysch unit, turbidite, Upper Jurassic-Lower Cretaceous, the syncollisional South-Anyui basin;
6. The South Gremyachinsky unit, clastic rocks, tuffs, terrigenous mélangé, greenschists, Upper Jurassic-Lower Cretaceous, an accretionary prism;
7. The Merzlyui Unit, dismembered ophiolite, greenschists, amphibolites, Paleozoic-Early Mesozoic (?);
8. The Penvel'veem unit, volcanic-tuff-terrigenous deposits, Upper Triassic-Valanginian. A fragment of an island arc assumed to be a klippe of the Yarakvaam terrane.

The Aluchin and Vurguveem ophiolites are located along the boundary of the South Anyui and Yarakvaam terranes. They were originally included into the SAS as fragments of the Late Jurassic-Early Cretaceous oceanic crust (Seslavinsky, 1979; Natal'in, 1984). New data indicates their Paleozoic and Triassic ages and suggests their suprasubduction origin (Lychagin, et al, 1991; Ganelin et al., 2003; Ganelin and Silantyev, 2008). As a result, the age of the South-Anyui oceanic basin was revised. In relation to these new age data, we propose to refer to the oceanic basin as the ProtoArctic Ocean and to keep the South Anyui name for the Late Jurassic – Early Cretaceous basin characterized by turbidite sedimentation.

The Vel'may terrane is composed of ultrabasic rocks, gabbroids, plagiogranites and volcanic-chert-terrigenous deposits that occur in the areas to the north of Cross Bay and to the south of Kolyuchinskaya Bay. Tectonic mélanges that are typical of disintegrated ophiolite assemblages are pointed out. The age of these terrane deposits is disputed and are suggested to be either Late Jurassic-Early Cretaceous (Kosygin, et al., 1974) or Late Triassic in age (Tynankergav and Bychkov, 1987).

THE TECTONIC HISTORY: A DISCUSSION

The tectonic history of the Arctic margin of Chukotka can be divided into four periods: the Late Precambrian – Early Paleozoic, Paleozoic – Early Mesozoic, and Late Mesozoic. Marine sedimentation is terminated by the late Early Cretaceous, during Aptian-Albian time; and post-collisional, continental deposition commenced.

The Late Precambrian – Early Paleozoic time

Metamorphic complexes of the Chukotka fold belt have not been objects of sophisticated investigations thus far; therefore regional correlations and general reconstructions are invoked for reconstructing its early stages of tectonic evolution. Most of the researchers considered Chukotka as a fragment of an ancient continental block that had occupied the central part the Arctic Ocean. It was referred to as the Hyperborean platform (Shatsky, 1935), the Ancient Arctida (Eardly, 1948), Arctida (Zonenshain, et al., 1990), Crockerland (Embry, 1993), and Bennett-Barrovia block (Natal'in, et al., 1999).

Relicts of the Arctida basement are preserved as ancient Arctic continental massifs such as the Kara massif (including the northern Taymyr and the southern part of the North Zemlya Archipelago) and the Chukchi massif of Wrangel Island and Alaska (the Seward Peninsula and the Brooks Range). The basement of the Arctic Alaska and Chukotka terranes is composed of Neoproterozoic metamorphic rocks that are intruded by granites with an age of 609-677 Ma in Wrangel Island (Kos'ko, et al, 1993). Augen gneisses of eastern Chukotka contain zircons dated at 650-540 Ma (Natal'in et al., 1999). The Nome complex of the Seward Peninsula contains lenses of orthogneiss dated at 670-680 Ma (Amato, et al., 2009).

In the Early Paleozoic, Arctida represented a carbonate platform that had been separated from Siberia, Laurentia and Baltica by oceanic basins (Zonenshain, et al., 1990). The most ancient Ordovician, Silurian and Early Devonian deposits of the Chukotka block (Wrangel Island and the Eastern Chukotka terrane) are represented by shallow-water carbonate and clastic rocks.

A precise position of Arctida and the Chukotka block is not determined as no paleomagnetic data are available. Paleontological data neither help in resolving of this problem as the platform rocks of the Arctic Alaska-Chukotka microplate, especially those of Ordovician age, contain conodont faunas characterized by mixed Laurentian, Siberian, and Baltic affinities (Dumoulin, et al., 2002, 2012). Blodgett et al (2002) reviewed the evidence for Paleozoic (especially Cambrian-Devonian) megafossils from Arctic Alaska and they note that

the component terranes of Arctic Alaska show their closest affinities with Siberia and Northeast Russia. Until the Devonian, Arctic Alaska and Chukotka had been placed close to Siberia as shown in the reconstructions (Drachev, 2011; Lawver, et al., 2011). During the Ellesmerian orogeny (the Devonian), which resulted in the complete closure of the Neoproterozoic-Early Paleozoic Iapetus Ocean, they were displaced from Siberia toward Laurentia. An emplacement of deformed granites dated at 369.6 ± 1.2 and 374.8 ± 0.5 Ma from a metamorphic complex of the Chukotka terrane (Natal'in, et al., 1999) and Early Carboniferous granites of the Kiber Cape (unpublished data) probably resulted from the Ellesmerian orogeny. The findings of andesitic tuff horizons suggest that an island arc existed along the southern flank of the Bennett-Barrovia block. The Devonian volcanic arc extended to the Pacific Ocean (Plafker, 1990) and is also known in Alaska (Moore, et al., 1994).

The Late Paleozoic – Early Mesozoic time

Dates available on ophiolites of the Yarakvaam terrane (Ganelin et al., 2003; Oxman, et al., 2003; Ganelin and Silantyev, 2008; Ganelin, 2011) and fragments of an oceanic crust in the SAS (the Polyarnyui Unit) suggest the existence of the ProtoArctic oceanic basin (Sokolov, et al, 2009). In Devonian-Carboniferous time, prior the collision of Siberia and Baltica, this ocean had been connected to the Pacific and the Paleo-Urals Oceans (Zonenshain et al., 1990; Sokolov et al., 2002; Vernikovskiy, et al., 2003). Following the closure of the Pale-Urals Ocean and the collision of Kara block with Siberia and termination of the Ellesmerian orogeny, this ocean became a large gulf of the Pacific Ocean.

The southern margin of the Proto-Arctic Ocean adjacent to the Siberian continent was active and extended toward the Pacific structures (Khanchuk (ed), 2006; Sokolov, 2010). A building of this convergent margin commenced simultaneously with a termination of the Ellesmerian orogeny in Laurentia, framing the formation of a passive margin. In Paleozoic – Early Mesozoic time, this convergent margin was surrounded by enigmatic arcs: the Alazeya, Oloy, Yarakvaam and other terranes (Parfenov, et al, 1993; Nokleberg, et al., 1998). In the Yarakvaam terrane (Fig. 5), the

Aluchin and Vurguveem suprasubduction ophiolites are associated with glaucophane schists and island-arc complexes of the Carboniferous, Permian and Triassic ages (Shekhovtsov and Glotov, 2001; Sokolov, et al., 2002, Sokolov, 2010).

The Triassic dike complex of the Yarakvaam terrane originated in an island arc-marginal sea system (Ganelin, et al., 2003). It should be stressed that Triassic volcanic-sedimentary deposits of the Yarakvaam terrane contain Tethyan fauna. The occurrence of boreal fauna of the northern passive margin of the ProtoArctic Ocean mixed with the Tethyan fauna of its southern border suggests that the oceanic basin was very large in the Triassic.

Small oceanic basins (the Oymyakon) of the Verkhoyansk-Kolyma Mesozoides existed in back-arc areas adjacent to the Siberian continent (Kuzmin.&Parfenov, 2001; Oxman, et al., 2003). These basins were originated via the rifting and splitting off the large continental blocks (the Omolon, Okhotsk and other terranes) from the Siberian continent. Fragments of the oceanic crust and suprasubduction ophiolites occur in the collisional belt of the Chersky Range.

The Northern, Chukotka (or Arctic) continental margin was a passive one. Terrigenous and carbonate strata were deposited in the Devonian-Middle Carboniferous time. In Chukotka, these deposits are commonly metamorphosed and their facies changes are well documented. On Wrangel Island, shallow-water shelf sediments of the Carboniferous and Permian sequences grade southward and upward into deeper water strata (Kos'ko, et al., 1993). In the northern area of the island, Early Carboniferous (?) deposits contain rift-related volcanic rocks (Moiseev and Sokolov, 2009). Note, Upper Carboniferous and Permian deposits (Fig. 3) bearing age-dated faunas are not known in Chukotka. It was presumably an area of erosion at the time.

Late Devonian and younger faunas of the AACM have strong northern Laurentian affinities (Dumoulin, et al., 2002). The AACM was, therefore, a part of the Laurentia continent or was placed close to it. A translation of a number of blocks from the Siberian continent close to the Laurentia is substantiated in the reconstructions of Lawver, et al. (2002, 2011) and others (for example Zonenshain et al., 1990). Additionally, fusulinids occur in

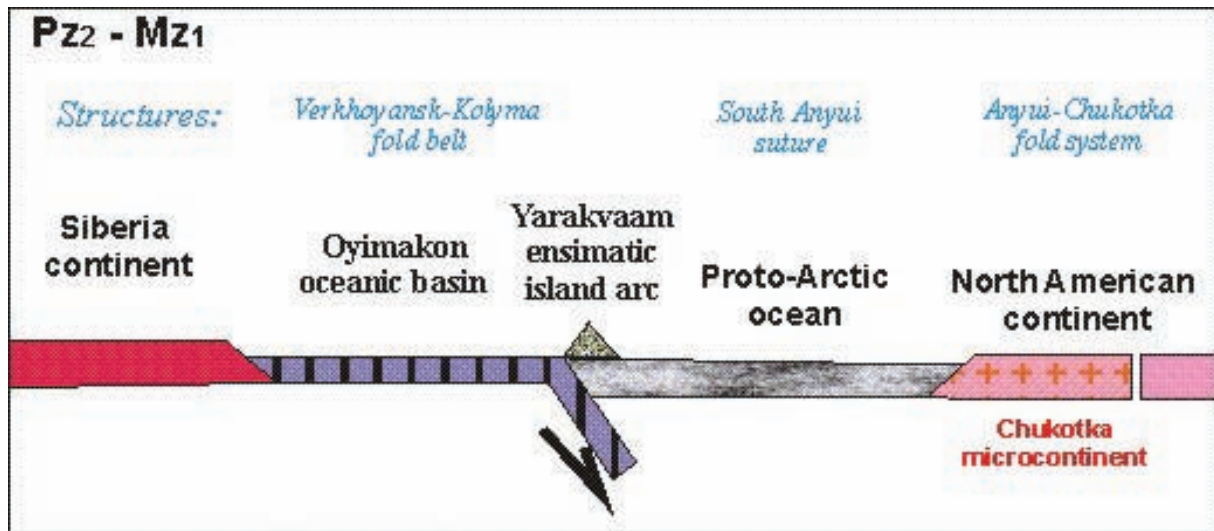


Fig. 5. Paleogeodynamic profiles for Late Paleozoic –Early Mesozoic time.

Middle Carboniferous limestones on Wrangel Island and Kotel’nyi Island, which is consistent with a sediment deposition in the relatively lower latitudes (Solovieva, 1975). Similar faunas have not been described in deposits of the Siberian passive continental margin so far. These faunas occur in allochthonous terranes of the Pacific rim (Sokolov, 1990, 1992).

In the latest Permian and earliest Triassic time, continental crust of the eastern Arctic region was destroyed (Til’man, et al., 1980; Sokolov, 2010; Ledneva, et al., 2011). Permian-Lower Triassic deposits of Chukotka are intruded by numerous sills and small hypabyssal bodies of diabases, gabbro and dolerites. Locally, tuffs and basalts geochemically similar to the Siberian traps occur (Ledneva, et al., 2011). The destruction of the continental crust was related to plume tectonics and break off from the Pangean continent. A genetic affinity of this magmatism, whether to an incipient Meso-Cenozoic Arctic plume or to one of the Siberian plume branches has yet to be investigated.

Triassic strata-bearing turbidites were deposited on the continental shelf, slope and rise. These deposits contain faunas typical of boreal provinces. The Norian carbonate-clay deposits of Kotel’nyi Island are an exception as they contain mixed boreal and Tethyan faunas (Konstantinov, et al., 2003). An occurrence of North American faunas (Yegorov, et al., 1987) and its similarity with faunas from the upper reach of the Bol’shoy Anyui

River (the Yarakvaam terrane) has been pointed out. Occurrences of faunas common to British Columbia and Yukon indicate a faunal exchange with eastern Pacific Ocean.

Upper Triassic distal turbidites of the Chukotka microcontinent are described in the tectono-stratigraphic units of the South-Anyui terrane (the Ustieva Unit). Facies distribution and orientations of turbidity currents indicate that a sedimentary province was located to the north or northeast (Morozov, 2001; Tuchkova, et al., 2007b). The source of sediments was probably situated in Arctida or Crokerland.

Early Jurassic deformation recently recognized in the Chukotka microcontinent (Tuchkova, et al., 2007a) probably resulted in a general uplift of the area, leaving only a local occurrence of Lower Jurassic deposits and a lack of Middle Jurassic strata.

The Late Mesozoic (the Middle Jurassic-Early Cretaceous)

The Middle Jurassic is an important period in the tectonic history of the Arctic and Pacific continental margins of Northeastern Russia that was characterized by structural transformation and deformation (Sokolov, 1992; Parfenov, et al., 1993; Tectonics., 2001). Its formation was coeval to the generation of an incipient system of Pacific plates that defines modern appearance of the Pacific Ocean (Larson and Hide, 1975).

Convergent margins of the Asian continent

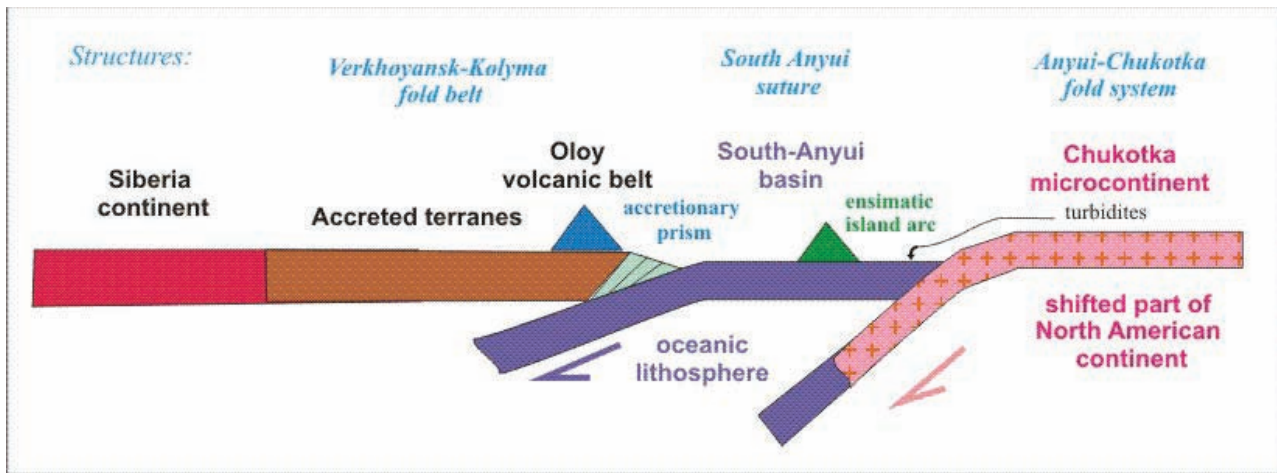


Fig. 6. Paleogeodynamic profiles for Late Jurassic –Early Cretaceous time.

were reorganized. Development of the Uda-Murgal volcanic belt commenced along its Pacific margin (Sokolov, 1992; Parfenov et al., 1993). The Verkhoyansk-Kolyma terranes were amalgamated by this time and formed the single Kolyma-Omolon superterrane (Parfenov et al., 1993; Tectonics., 2001). The collision of this superterrane with the Siberian continent commenced.

The new extended volcanic belt, referred to as the Oloy belt (Tii'man, et al., 1980) or the Oloy-Svyatoy Nos belt (Parfenov, et al., 1993), was created along the northern margin of the Kolyma-Omolon superterrane at the boundary with the ProtoArctic Ocean. Volcanic-sedimentary deposits of the Late Jurassic – Early Cretaceous unconformably overlie the older arc complexes of the Paleozoic and Early Mesozoic. Volcanic rocks of the Svyatoy Nos area can be included into the belt only partially as they show the narrow Oxfordian-Kimmeridgian age interval. They are coeval volcanic rocks of the Kupolney arc situated in the ProtoArctic Ocean (Sokolov, et al., 2002, 2009). These volcanic rocks might represent fragments of the same arc. A termination of volcanic activity in the arc coincides with termination of spreading in the ProtoArctic Ocean.

A new stage in the tectonic evolution of the ProtoArctic Ocean (Fig. 6) started in the Volgian (Tithonian) time. The spreading was terminated and the volcanism in ensimatic arcs (the Kupolney and the Svyatoy Nos) became extinct. Closure of the ProtoArctic Ocean commenced and this resulted in the formation of the syncollisional South-Anyui oceanic basin that was filled with terrigenous sediments.

Concurrently, turbidites were deposited along the northern Chukotka margin. As the ensimatic arcs became extinct, a localized subduction developed along the southern margin. An accretionary prism incorporating offscraped blocks of basalts and cherts (the South-Gremuchinsky unit) developed along its boundary with the Yarakvaam terrane. The accretion of the Kupolney arc was followed by the subduction of the Chukotka continental lithosphere.

The last stage of the collision occurred in the Hauterivian-Barremian time. A system of pull-apart basins filled with the shallow-water coarse-grained deposits developed along dextral strike-slips in the area affected by the collision.

The Middle Cretaceous (the Aptian-Albian)

The principal structural reorganizations took place during Aptian-Albian time. At approximately the same time, collision of the Chukotka microcontinent with an active margin of Siberia was completed. The accretion and collision was accompanied by the intrusion of granites indicating the formation of a new granite-metamorphic layer, which covered the Siberian, Omolon, AACM and other continental blocks. The Okhotsk-Chukotka volcanic belt then developed along the newly formed continental edge and the convergent margin was of the Andean type.

This stage was characterized by extensional structures that originated immediately after the collision of the active continental margin with the Chukotka microcontinent. The collapse of the collisional orogen and exhumation of subducted

deposits of the Chukotka microcontinent resulted in the formation of granite-metamorphic domes and superimposed depressions filled with continental volcanic-sedimentary deposits.

Correlations with the Canada basin

According to the rotation hypothesis, the formation of the Amerasian basin and the generation of the oceanic crust of the Canada basin resulted from the break-up of the Arctic Alaska-Chukotka microplate from the Laurentia, followed by the counter-clockwise rotation of this block. The Chukotka microcontinent, whose rotation had caused the closure of the Proto-Arctic Ocean and which collided with the Siberian active margin, is a part of the AACM. This collision resulted in formation of the SAS. The testing of the rotation hypothesis reveals the detailed correlation of tectonic events of the Amerasian basin and structures of the Arctic continental margin of Chukotka.

According to Grantz, et al. (2011), the Amerasia basin was formed by two phases of counterclockwise rotational opening about a pole in the Mackenzie Valley of NW Canada: (phase 1) an initial phase of extension in the Early Jurassic to Neocomian, and (phase 2) spreading (131-127 Ma) and intrusion of mid-ocean ridge basalt crust in the central part of the Amerasia Basin in the Hauterivian and Barremian.

The initiation of the Amerasia basin is attributed to the Early Jurassic, a generation of the ocean-continent transitional crust, and rifts. The coeval uplift in Chukotka appears to have resulted from deformation at the shoulders of an incipient rift. Synrift strata are 2 km thick or more and they are interbedded with volcanic rocks of the Alpha-Mendeleev Ridge. Moore, et al. (2011) suggest an Early Jurassic-Valanginian age for the synrift volcanism. This is proven by new geochronologic dates for basaltic rocks of the Frantz Josef Land (FJL) of 190.1 ± 4.4 , 156.8 ± 3.8 , and 132.5 ± 1.2 Ma (Karyakin, et al., 2009). The closure of the Eurasian basin allows the reconstruction of the large igneous province comprising the FJL, the Alpha and Mendeleev ridges, and the DeLong Massif. Compositional variations of the intraplate volcanic rocks of the FJL are consistent with the continental nature of the crust of this province.

Termination of spreading in the ProtoArctic

Ocean at the Tithonian-Kimmeridgian boundary (150 Ma) was followed by terrigenous sedimentation (the South Anyui turbidite basin). A subducted oceanic crust was intensively pulled beneath the Siberian margin. Relicts of this oceanic crust are preserved in the South Gremuchinsky accretionary prism. These processes were approximately simultaneous with the opening of the Amerasian basin. Grantz, et al. (2011) assumed that the North Chukotka depression was established at about 145.5 Ma ago. The depression could be have resulted from an extension of the AACM that caused its rapid subduction.

Later, in the Early Cretaceous, when the Chukotka microcontinent continental lithosphere had started to be consumed, the subduction process slowed and volcanism in the Oloy belt became less voluminous. The South Anyui basin continued to shorten and fill with sediments of a significant thickness.

The spreading of the second phase in the Canada Basin was simultaneous with the closure of the South Anyui basin. Turbidite sedimentation was followed by deposition of shallow-water strata during the Hauterivian-Barremian. Conglomerates in this basin contain various clastic fragments that were transported from the northern and southern provenances. Any traces of coeval volcanism are absent. It should be emphasized that Hauterivian-Barremian strata were deformed during the latest stages of the collision.

Termination of spreading in the Canada Basin coincides with a termination of collision in the Chukotka fold belt. Post-collisional granites are dated at 117-108 Ma in Chukotka (Katkov, et al., 2010) and at 114 Ma in the Shalaurova terrane (Layer, et al., 2001). Post-rift strata of the Canada Basin are Aptian-Albian in age. In Aptian-Albian time, extension taking place in Chukotka resulted creation of the Aynakhkurgun, Nutesyn and other postorogen depressions. These depressions are filled with shallow-water, lagoonal and continental volcanic-sedimentary deposits. Extensional structures partially formed during this time period in the Arctic shelf of the East Siberian and Chukchi seas (Miller and Verzhbitsky, 2007). Main stages of the tectonic evolution of the Chukotka continental margin are well correlated with stages of the Canada Basin formation.

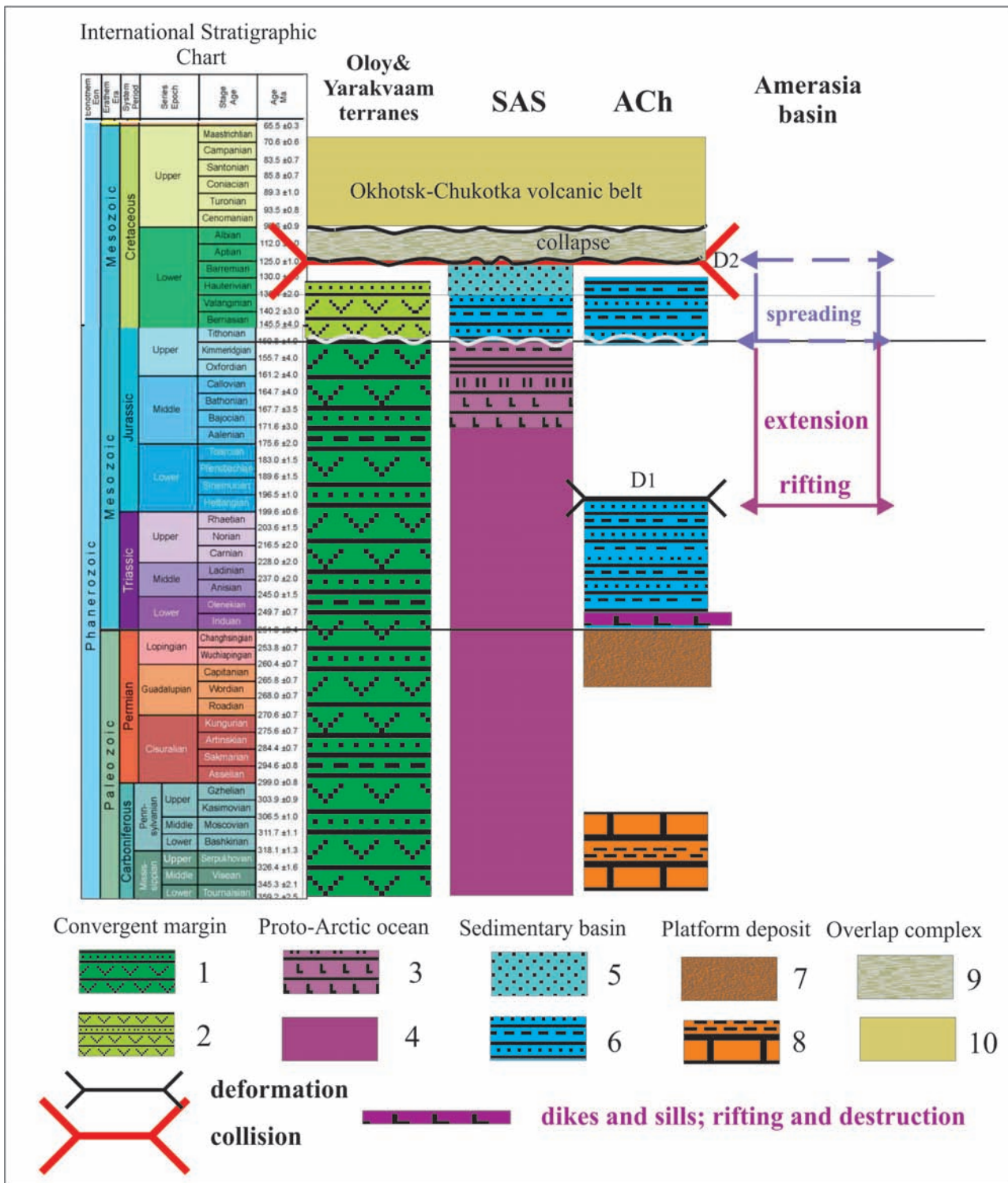


Fig. 7. Time-space diagram. 1 – island arc complexes of the Yarkvaam terrane; 2 – Oloy volcanic belt; 3 – basalt-chert assemblage (Bystryanka unit); 4 – oceanic complexes; 5 – clastic rocks; 6 – turbidites; 7 – terrestrial and shallow-water beds; 8 – limestone and clastic rocks; 9 – Aptian –Albian volcanic and sedimentary terrestrial rocks; 10 – Okhotsk-Chukotka volcanic marginal belt.

CONCLUSION

The Chukotka fold belt comprises two structural elements: the Anyui-Chukotka fold system (AChS) and the South Anyui suture. They formed during collision of the Chukotka microcontinent with the Siberian active margin. The tectono-stratigraphic units of the South Anyui suture were thrust northwards over the passive margin deposits of the microcontinent, whose sedimentary cover is strongly deformed.

Complexes of the Chukotka microcontinent were geographically placed close to Siberia in the Early Paleozoic. They became a part of Laurentia during the Ellesmerian orogeny. In the Late Paleozoic – Early Mesozoic, Laurentia and Siberia were separated from each other by the ProtoArctic Ocean. The American margin was a passive one, whereas the Siberian margin was an active one. In the latest Permian – earliest Triassic, destruction of Pangea resulted in destruction of the continental crust. However, this crustal thinning did not cause the formation of oceanic crust. In the Early Jurassic, formation of the Amerasia Basin commenced. The rifting followed by spreading in the Canada Basin caused the splitting of the Chukotka microcontinent from Laurentia. The Tithonian was characterized by the termination of spreading in the ProtoArctic Ocean that had been transformed into the South Anyui syncollisional turbidite basin. The opening of the Amerasia Basin coincided with shortening of the South-Anyui turbidite basin that was deposited on oceanic lithosphere and concurrently subducted beneath the Verkhoyansk-Kolyma foldbelt (see Fig. 6).

As a result of this collision, a large block of the continental crust which includes the Mendeleeva uplift and the Chukchi plateau was amalgamated onto Siberia. After the collision, extensional structures (the Aynakhkurgan and Nutesyn depressions) were developed along with commencement of continental and marine sedimentation. The extensional events were accompanied by volcanism and crustal thinning; however, this did not result in the destruction of the continental crust.

The good correlation and relationships between the tectonic events evident in the Amerasia Basin and the Chukotka fold belt prove the rotation hypothesis. Tectonic models based on this hypothesis will be improved when new data are obtained.

ACKNOWLEDGEMENTS

We use this opportunity to express our gratitude to D. Stone and J. Clough and R. Blodgett for helpful and valuable remarks and suggestions that were very useful during the revision of the manuscript. This study was supported by the Russian Foundation of Basic Research (project no. 11-05-00074, 14-05-0031), projects of FCNTP (NSh-2981.2014.5), Department of Earth Sciences of RAS (program no. 10), and State contract № 01/14/20/11.

REFERENCES

- Amato, J. M., Toro, J., Miller, E. L., Gehrels, G. E., Farmer, G. L., Gottlieb, E. S., and A. B., Till, 2009. Late Proterozoic–Paleozoic evolution of the Arctic Alaska–Chukotka terrane based on U–Pb igneous and detrital zircon ages: implications for Neoproterozoic paleogeographic reconstructions. *Geological Society of America Bulletin*, 121, 1219–1235.
- Beranek, L. P., Mortensen, J. K., Lane, L. S., Allen, T. L., Fraser, T.A., Hadlari, T., and W. G. Zantvoort, 2010. Detrital zircon geochronology of the western Ellesmerian clastic wedge, northwestern Canada: Insights on Arctic tectonics and the evolution of the northern Cordilleran miogeocline. *Geological Society of America Bulletin*, 122, 899-1911.
- Blodgett, R. B., Rohr, D. M., and Boucot, A. J., 2002, Paleozoic links among some Alaskan accreted terranes and Siberia based on megafossils, in Miller, E.L., Grantz, Art, and Klemperer, S.L., eds., *Tectonic Evolution of the Bering Shelf-Chukchi Sea-Arctic Margin and Adjacent Landmasses: Geological Society of America Special Paper 360*, p. 273-290.
- Bering Strait Geologic Field Party, 1997. Koolen metamorphic complex, northeastern Russia: Implications for the tectonic evolution of the Bering Strait region. *Tectonics*, 16, 713–729.
- Carey, S. W., 1958. The tectonic approach to continental drift. In: *Proceedings, Continental drift; A Symposium*. University of Tasmania, Hobart, 177–355.
- Drachev, S. S. and L. A., Savostin, 1993. Ophiolite of Bolshoi Lyakhovsky Island (Novosibirsk Archipelago). *Geotektonika*, 3, 98-107 (in

- Russian).
- Drachev, S. S., 2011. Tectonic setting, structure and petroleum geology of the Siberian Arctic offshore sedimentary basins. In: Spencer, A. M., Embry, A. F., Gautier, D. L., Stoupakova, A. V. and K., Sørensen (eds). *Arctic Petroleum Geology*. Geological Society, London, *Memoirs*, 35, 369–394.
- Dumoulin, J. A., Harris, A. G., Gagiev, M., Bradley, D. C., Repetski, J. E., 2002. Lithostratigraphic, conodont, and other faunal links between lower Paleozoic strata in northern and central Alaska and northeastern Russia. *Geological Society of America Special Paper* 360.
- Dumoulin, J. A., Till, A. B., and Bradley, D. C., 2012. Neoproterozoic-Paleozoic Paleogeographic Reconstruction of The Arctic Alaska-Chukotka Terrane. Geophysical Institute Report UAG-R-335, Compilers: D.B.Stone, J.G.Clough, D.K.Thurston, University of Alaska, Fairbanks, Alaska.
- Eardly, A.J., 1948. Ancient Arctic. *Journal of Geology*, 56, 409-436.
- Embry A., 1993. Crockerland – the northern source area for the Sverdrup Basin, Canadian Arctic Archipelago. In: Vorren, E. Bergsager, O. Dahl-Stammes, E. Holter, B. Johansen, E. Lie and T. Lund (eds). *Arctic Geology and Petroleum Potential*. T. Norwegian Petroleum Society, Special Publication, 2, 205–216.
- Embry, A. F. and J. Dixon, 1994. The age of the Amerasia Basin. In: Thurston D. and Fujita K. (eds). 1992 Proceedings International Conference on Arctic Margin. US Minerals Management Service, Anchorage, AK, Reports, MMS94-0040, 289–294.
- Ganelin, A., V., 2011. Geochemistry and Geodynamic Significance of the Dike Series of the Aluchin Ophiolite Complex, Verkhoyansk–Chukotka Fold Zone, Northeast Russia. *Geochemistry International*, 7, 654-675 (in Russian).
- Ganelin, A. V. and S. A., Silantyev, 2008. Composition and Geodynamic Conditions of Formation of the Intrusive Rocks of the Gromadnen-Vurguveem Peridotite-Gabbro Massif, Western Chukotka. *Petrology*, v. 16, 6, 565-583 (in Russian).
- Ganelin, A. V., Sokolov, S. D., Morozov, O. L., Layer, P., and J. Hourigan, 2003. Dike Complexes in Ophiolites of the South Anyui Suture: Geodynamic Implications. *Doklady Earth Sciences*, 388, 1, 26-29.
- Gelman, M. L., 1995. Phanerozoic Granite–Metamorphic Domes in Northeastern Siberia. Article 1. Geological History of the Paleozoic and Mesozoic Domes. *Tikhookeanskaya Geologiya*, v. 14, 5, 102–115 (in Russian).
- Grantz, A., May, S. D., Taylor, P. T., and L.A., Lawver, 1990. Canada Basin. In: Grantz, A., Johnson, G. L. & Sweeney, W. J. (eds.) *The Arctic Region. The Geology of North America*, L. Geological Society of America, Boulder, CO, 379–402.
- Grantz, A., Hart, P. E., and V. A., Childers, 2011. Geology and tectonic development of the Amerasia and Canada basins, Arctic Ocean. In: Spencer, A. M., Embry, A. F., Gautier, D. L., Stoupakova, A. V. and K., Sørensen (eds). *Arctic Petroleum Geology*. Geological Society, London, *Memoirs*, 35, 771–800.
- Karyakin, Yu. V., Lyapunov, S.M., Simonov V.A., Sklyarov, E.V., Travin A.V., and E.V., Shipilov, 2009. In: Karyakin (ed.) *Geology of Polar regions*. Proceeding XLII Tectonic conference. Moscow, GEOS, book 1, 257-263 (in Russian).
- Katkov, S. M., Miller, E. L., and J., Toro, 2010. Structural paragenesis and age of deformation of the Anyui-Chukotka fold system (Northeastern Russia). *Geotectonics*, 44, 5, 61-80.
- Khanchuk, A.I. (ed). *Geodynamic, Magmatism, and Metallogeny of the Eastern Russia*. 2006. Vladivostok, Dal'nauka, v.1, 572 p. (in Russian).
- Kuzmin, M.I., Parfenov, L.M. (eds.). *Tectonics, Geodynamics, and Metallogeny of the Sakha Republic (Yakutia)*, 2001. MAIK “Nauka\ Interperiodika”, 571 p.
- Konstantinov A.Yu., Sobolev E.□., and T.V., Kletc, 2003. New biostratigraphic data of Norian deposits of the Kotel'nyui Island. *Tikhookeanskaya geologia*, 3, 27-39 (in Russian).
- Kosygin, Yu. A., Voevodin, V. N., Zhitkov, N. G., and V. A., Solov'yov, 1974. Eastern Chukotka volcanic zone and tectonic nature of volcanic belts, *Dokl. Akad. Nauk SSSR*, 216, 4, 885–888, (in Russian).
- Kos'ko, M. K. 1994. Major Tectonic Interpretations

- and Constraints for the New Siberian Islands Region, Russian Arctic. In: Thurston D. Fujita K. (eds.) 1992. Proceedings International Conference on Arctic Margins, US Department of the Interior, Minerals Management, Anchorage, AK, Reports, MMS94-0040, 195–200.
- Kos'ko, M. K., Cecile, M. P., Harrison, J. C., Ganelin, V. G., Khandoshko, N. V., and B. G. Lopatin, 1993. Geology of Wrangel Island, Between Chukchi and East Siberian Seas, Northeastern Russia. Geological Survey of Canada, Ottawa, Bulletins, 461.
- Kotlyar, I.N., Zhulanova, I.L., Rusakova, T.V., and M.N., Gagieva, 2001. Isotope system in magmatic and metamorphic rock assemblages of North-eastern Russia. Magadan, NEISRI, 319 p. (in Russian).
- Kuzmichev, A.B., 2009. Where does the South Anyui suture go in the New Siberian islands and Laptev Sea? *Tectonophysics*, 463, 86-108.
- Kuzmin, M.I., Parfenov, L.M. (eds.). *Tectonics, Geodynamics, and Metallogeny of the Sakha Republic (Yakutia)*, 2001. MAIK "Nauka\ Interperiodika", 571 p.
- Lane, L.S., 1997. Canada Basin, Arctic Ocean: evidence against a rotational origin. *Tectonics*, 16, 363–387.
- Larson R.L., Hilde T.W.C., 1975. A revised time scale of magnetic reversals for the Early Cretaceous and Late Jurassic. *Journal of Geophysical Research*, 80, 2586-2594.
- Lawver L.A., Ganagan L.M., and I. Norton, 2011. Palaeogeographic and tectonic evolution of the Arctic region during the Palaeozoic. In: Spencer, A. M., Embry, A. F., Gautier, D. L., Stoupakova, A. V. and K., Sørensen (eds.) *Arctic Petroleum Geology*. Geological Society, London, *Memoirs*, 35, 61–77
- Lawver, L. A., Grantz, A., and L. M., Gahagan, 2002. Plate kinematic evolution of the present Arctic region since the Ordovician. In: Miller, E. L., Grantz, A., and S. L., Klempner (eds.) *Tectonic Evolution of the Bering Shelf—Chukchi Sea—Arctic Margin and Adjacent Landmasses*. Geological Society of America, Boulder, CO, *Special Papers*, 360, 333–358.
- Layer, P., Newberry, R., Fujita, K., Parfenov, L., Trunilina V., and A. Bakharev, 2001. Tectonic setting of the plutonic belts of Yakutia, northeast Russia, based on $^{40}\text{Ar}/^{39}\text{Ar}$ geochronology and trace element geochemistry: *Geology*, 29, p. 167–170.
- Ledneva G.V., Pease V.L., and S.D., Sokolov, 2011. Permo-Triassic hypabyssal mafic intrusions and associated tholeiitic basalts of the Kolyuchinskaya Bay, Chukotka (NE Russia): Links to the Siberian LIP. *Journal of Asian Earth Sciences*, 40, 737–745.
- Lychagin, P. P., Byalobzhessky, S. G., Kolyasnikov, Yu. A., Korago, Ye. A., and V. B., Likman, 1991. The Magmatic History of the South Anyui Folded Zone. In: *Geology of Continent-Ocean Transition Zone in Northeast Asia, Severo-Vostochnyi Kompleksnyi Nauchno-Issledovatel'skiy Institut Rossiyskoi Akademii Nauk*, Magadan, 140–157 (in Russian).
- Miller, E. L., Toro, J., Gehrels, G., Amato, J. M., Prokopiev, A., Tuchkova, M. I., Akinin, V. V., Dumitru, T. A., Moore, T. E., and M.P. Cecile, 2006. New insights into Arctic paleogeography and tectonics from U-Pb detrital zircon geochronology, *Tectonics*, 25, TC3013, doi:10.1029/2005TC001830.
- Miller E.L., Verzhbitsky V.E., 2009. Structural studies near Pevek, Russia: Implications for formation of the East Siberian Shelf and Makarov Basin of the Arctic Ocean. In: Stone, D. B., Fujita, K., Layer, P. W., Miller, E. L., Prokopiev A. V., and J. Toro (eds.) *Geology, geophysics and tectonics of Northeastern Russia: a tribute to Leonid Parfenov*. EGU Stephan Mueller Publication Series, 4, 223-241.
- Moiseev A.V. and S.D., Sokolov, 2009. Geochemistry of Paleozoic volcanics of Wrangel Island. In: Karyakin (ed.) *Geology of Polar regions Proceeding XLII Tectonic conference*. Moscow, GEOS, v. 2. 62-69 (in Russian).
- Moore, T. E., Wallace, W. K., Bird, K. J., Mul, C. G. and J. T., Dillon, 1994. Geology of northern Alaska. In: Plafker, G. and H. C., Berg (eds.) *The Geology of Alaska*. DNAG. *The Geology of North America*, G-1. Geological Society of America, Boulder, CO, 49–140.
- Morozov, O.L. 2001. Geological structure and tectonic evolution of Central Chukotka.

- Moscow, GEOS, Transactions of GIN RAS, 523, 201 p.
- Natal'in, B.A., 1984. Early Mesozoic Eugeosynclinal Systems in the Northern Part of the Circum-Pacific Belt, Moscow, Nauka, 186 p. (in Russian).
- Natal'in, B., Amato, J.M., Toro, J., and J.E., Wright, 1999. Paleozoic rocks of the northern Chukotka Peninsula, Russian Far East: implications for the tectonics of the Arctic region // *Tectonics*, v.18, 6, 977-1004.
- Nokleberg W.J., Parfenov L.M., Monger J.W.H., Baranov B.V., Byalobzhesky S.G., Bundtzen T.K., Feeney T.D., Fujita K., Gordey S.P., Grantz A., Khanchuk A.I., Natal'in B.A., Natapov L.M., Norton I.O., Patton W.W., Jr., Plafker G., Scholl D.W., Sokolov S.D., Sosunov G.M., Stone D.B., Tabor R.W., Tsukanov N.V., Vallier T.L., and K., Wakita, 1994. Circum-North Pacific tectonostratigraphic terrane map: U.S. Geological Survey Open-File Report 94-714 (2 sheets, scale 1:5 000 000, 1 sheets, scale 1:10 000 000), 433 p.
- Nokleberg, W. J., Parfenov, L. M., Monger, J. W. H., Norton, I.O., Khanchuk, A. I., Stone, D. B., Scholl, D. W., and K., Fujita, 1998. Phanerozoic Tectonic Evolution the Circum-North Pacific, U.S. Geological Survey, Open-File Report 98-754.
- Oxman, V. S., Ganelin, A. V., Sokolov, S. D., Morozov, O. L., Tretyakov, F. F., and S. A., Silant'ev, 2003. Ophiolitic belts of the Arctic regions of the Verkhoyansk-Chukotka orogenic area: A geodynamic model of formation, *Tikhookeanskaya Geologia*, 22, 62-75 (in Russian).
- Parfenov, L. M., Natapov, L. M., Sokolov, S. D., and N.V., Tsukanov, 1993. Terranes analysis and accretion in northeast Asia, *The Islands Arc*, 2, 35-54.
- Plafker G., 1990. Regional geology and tectonic evolution of Alaska and adjacent parts of the northeast Pacific ocean margin. Proceeding of the Pacific Rim Congress 90. Australasian Institute of Mining and Metallurgy, Queensland, Australia, p. 841-853.
- Seslavinskiy, K. B., 1979. The South Anyui Suture (Western Chukotka). *Doklady Akademii Nauk SSSR*, 249, 1181-1185 (in Russian).
- Shatsky N.S., 1935. O tektonike Arktiki (On tectonics of Arctic). In: *Geologiya i Poleznye iskoparmue SSSR. Trudy pervoi geologo-razvedochnoi konferencii Glavsermorputi. Geologiya, Leningrad*, 1, 3-28 (in Russian).
- Shekhovtsov, V. A. and Glotov, S. P., 2001. State Geological map of the Russian Federation, scale 1:200 000, Oloy Series, Quadrangle Q-58-XI, XII, Explanatory note, Sokolov, S.
- D., (ed.) *Anyuiskoe Gosudarstvennoe Gorno-Geologicheskoe Predpriyatie, Ministerstvo Prirodnykh Resursov, Moscow*, (in Russian).
- Sokolov, S.D., 1990. Exotic complexes (terrane) in the Koryak Highlands. *International Geology Review*, 32, 117-27.
- Sokolov S.D., 1992. Accretionary tectonics of the Koryak - Chukotka segment of the Pacific belt, *Trans. of Geological Institute Russian Academy of Sciences*, 479, Moscow, Nauka, 182 p., (in Russian).
- Sokolov S. D., 2010. Tectonics of Northeast Asia: An Overview. *Geotectonics*, 44, 6, 493-509.
- Sokolov, S. D., Bondarenko, G. Ye., Morozov, O. L., Ganelin, A. V., and I. I., Podgorny, 2001. Nappes tectonics of the South Anyui suture zone (western Chukotka), *Dokladi Akademii Nauk Rossii*, 376, 1, 80-84 (in Russian).
- Sokolov, S.D., Bondarenko, G.Ye., Morozov, O.L., Shekhovtsov, V.A., Glotov, S.P., Ganelin, A.V., and I.R., Kravchenko-Berezhnoy, 2002. The South Anyui Suture, NE Arctic Russia: facts and problems to solve. *Geol. Soc. Amer. Spec. Paper*, 360, 209-224.
- Sokolov S. D, Bondarenko G. Ye., Layer P. W., and I. R., Kravchenko-Berezhnoy, 2009. South Anyui suture: tectono-stratigraphy, deformations, and principal tectonic events. *Stephan Mueller Spec. Publ. Ser.*, 4, 201-221.
- Solovieva M.F., 1975. Biostratigraphic based on foraminiferas Lower and Middle Carboniferous deposits of Kotel'nyui, Wrangel islands and Chukotka. In: *Upper Paleozoic of USSR. Leningrad, Nauka*, 42-53 (In Russian).
- Til'man, S.M. 1980, Regions with the continental crust formed to the beginning of the Riphean: miogeosyncline systems. In: *Markov, M.S., Pustcharovsky, Yu.M., Til'man, S.M.,*

- Fedorovsky, V.S. and N.A., Shilo, (eds.)
Tectonics of the continental margins of the
northwestern Pacific Ocean. Moscow, Nauka,
26-48 (In Russian).
- Tectonics, Geodynamics, and Metallogeny of the
Sakha Republic (Yakutia), 2001. M.I.Kuzmin,
L.M.Parfenov (eds.), MAIK “Nauka\
- Interperiodika”, 571 p.
- Zhulanova I.L., 1990. Earth crust of the Northeastern
Asia in Precambrian and Phanerozoic. Moscow,
Nauka, 302 (in Russian).
- Tuchkova M.I., Bondarenko G.Ye., Buyakaite
M.I., Golovin D.I., Galuskina I.O., and
E.V., Pokrovskaya, 2007a. Results from
sedimentological and radiometric studies of
the Upper Triassic deposits of the Chukotka
microcontinent, *Geotektonika*, 5, 76-96 (in
Russian).
- Tuchkova, M.I., Morozov, O.L., and S.M., Katkov,
2007b. Lower–Middle Triassic Rocks in
the Enmynveem River (Western Chukotka).
Lithology and Mineral Resources 42, 437-452.
- Tynankergav, G. A. and J. M., Bychkov, 1987.
Upper Triassic Chert-Volcanic-Terrigenous
Assemblages of Western Chukotka, *Doklady
Akademii Nauk SSSR*, 296, 698–700 (in
Russian).
- Vernikovskiy, V., Pease, V., Vernikovskaya, A.,
Romanov, A., Gee, D. and A., Travin, 2003.
Early Triassic A-granites from Taimyr: a result
of the northern Asia superplume. *Lithos*, 66,
23–36.
- Verzhbitsky, V., Frantzen E., Savostina T., Little
A., Sokolov S.D., and M.I., Tuchkova, 2008,
The Russian Chukchi Sea shelf: GEO ExPro,
5, 3, 36-41 (full article available at [http://www.
geo365.no/TGS-Chukchi/](http://www.geo365.no/TGS-Chukchi/)).
- Yegorov A.Yu., Bogomolov Yu. A., Konstantinov
A. G., and Kurushin N. I. 1987. Stratigraphy
of Triassic deposits of the Kotel’nyui Island
(Novosibirskie Islands). *Boreal Triassic*.
Moscow, Nauka, 66-80 (in Russian).
- Zonenshain, L. P., Kuzmin, M. I., and L. M., Natapov,
1990. Plate Tectonics of the USSR Territory,
Moscow, Nedra, 2 (in Russian).

Intra-plate gabbroic rocks of Permo-Triassic to Early-Middle Triassic dike-and-sill province of Chukotka (Russia)

Galina V. Ledneva¹, Boris A. Bazylev², Paul W. Layer³, Akira Ishiwatari⁴, Sergey D. Sokolov¹, Natalia N. Kononkova², Petr L. Tikhomirov⁵ and Maria S. Novikova^{1,5}

¹Geological Institute, RAS, 7, Pyzhevsky per., Moscow 119017, Russia; ledneva@ilran.ru

²V.I. Vernadsky Institute of Geochemistry and Analytical Chemistry, RAS, 19, Kosygin st., Moscow 119991, Russia; bazylev@geokhi.ru

³College of Natural Science and Mathematics, University of Alaska Fairbanks, Fairbanks, AK, 99775, USA; pwlayer@alaska.edu

⁴Center of NE Asian Studies, Tohoku University, Kawauchi 41 Aoba-ku, Sendai 980-8576 Japan; geoishw@cneas.tohoku.ac.jp

⁵Geologic Faculty of Moscow State University, Vorob'yovy Gory, Moscow 119991, Russia; petr_tikhomirov@mail.ru

ABSTRACT

In order to provide basic materials for geodynamic and tectonic reconstruction of the Arctic region, we investigated Permo-Triassic to Early-Middle Triassic gabbroic rocks of tabular bodies in shelf and continental slope sediments of eastern Chukotka. These rocks, which are here referred to as the Anyui dike-and-sill province, are represented by gabbro, Fe-Ti gabbro, and gabbroic diorite assumed to be cogenetic to each other. The rocks from different tabular bodies can be originated from variably differentiated portions of melts at similar pressure and temperature conditions. The rocks show geochemical features of crustally contaminated intra-plate basaltic lavas and are geochemically similar to Permo-Triassic continental plateau basalts of the platformal (or the trap) stage of the Siberian large igneous province.

INTRODUCTION

Permo-Triassic to Early-Middle Triassic gabbroic rocks of the Chukotka Peninsula are an object of high interest for the tectonic evolution of the Arctic region prior to the Amerasia basin opening. The locations and extent of these volcanic rocks provide constraints on the original position of the Arctic Alaska-Chukotka continental margin (the AACM) relative to the Siberian and Canadian Arctic continental margins. According to the counterclockwise rotation model based on correlation of the Mesozoic-Paleozoic stratigraphy along with magnetic and gravity anomalies in the Amerasia basin, the AACM was pivoted from the Canadian Arctic margin during the Amerasia basin opening by

ripping commenced in the Early Cretaceous (Grantz, et al., 1990; Lawver and Scotese, 1990; Lawver, et al., 2002). Other studies taken into account geological data along with distributions of detrital zircon SHRIMP ages from sandstones of Chukotka, Wrangel Island and Alaska, petrochemical and geochemical similarity of gabbroic rocks of Chukotka and the New Siberian Islands coeval to traps of the Siberian large igneous province (LIP) (Fig. 1a), argue a close proximity of the Chukotka part of the AACM to the Siberian margin (the Taimyr and Verkhoyansk areas) in the Permo-Triassic to Early-Middle Triassic time (Miller, et al., 2006; Kuz'michov and Pease, 2007).

The similarity of Permo-Triassic magmatism of the New Siberian Islands to the Siberian LIP is well substantiated by geological observations, age (252 ± 2 Ma, U-Pb TIMS ages of igneous zircons) and bulk major- and trace-element compositions (Kuz'michov and Pease, 2007); however, correlation of the New Siberian Islands to the AACM is doubted by some researchers.

In the Chukotka Peninsula, small intrusions, dikes and sills of gabbroic rocks are widespread in the Permian - lower Triassic and lower-middle Triassic shelf and continental slope sediments. In the western Chukotka they extend for ~350 km (the Keperveem and Raucha Uplifts); in central and eastern Chukotka they are traced to a distance of ~900 km (the vicinity of Cape Schmidt and the interflaves of the Amguema and Vel'may rivers and the Kolyuchinskaya Bay area) (Fig. 1b). These gabbroic rocks were recognized as parts of a large regional complex (Til'man and Sosunov, 1960; Gel'man, 1963) named as the Amguema-Anyui Igneous Province

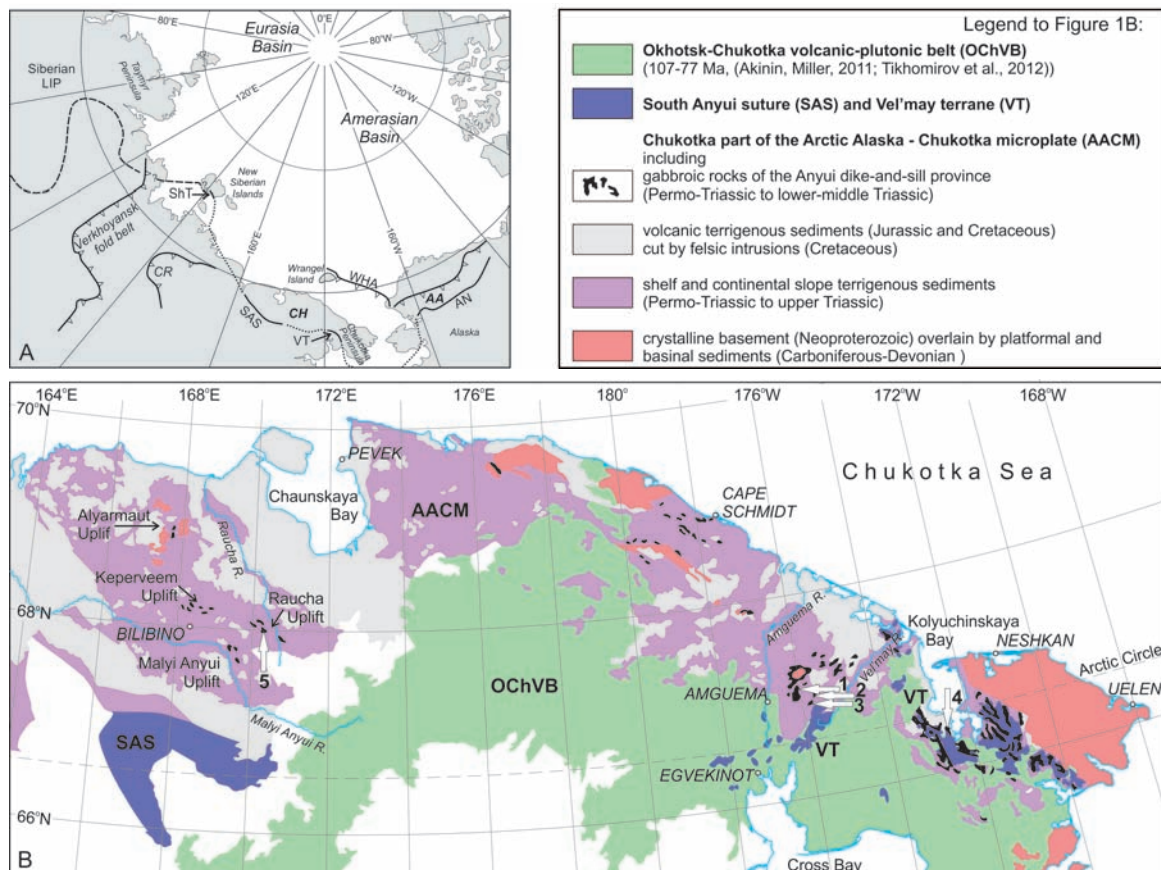


Fig. 1. Regional geological structures and locations of the studied gabbroic rocks of the Anyui dike-and-sill province.

(A) A position of the AACM among major geological structures of the Arctic region and adjacent areas (modified after Miller, et al., 2006). The AACM occupies Wrangel Island, the Chukotka (CH) and Arctic Alaska (AA) regions north of the Shalaurova terrane (ShT) in the New Siberian Islands, the South Anyui suture (SAS) in western Chukotka, the Vel'may terrane (VT) in eastern Chukotka, the Angayucham terrane (AN) in Alaska. The southern AACM boundary is shown in solid line and its inferred continuities are in the dotted line. The northern boundary of the AACM is supposedly marked by the Wrangel Herald Arch (WHA). The boundary of the Siberian LIP (dash line) is after Reichow, et al. (2009). CR is abbreviation for the Chersky Range.

(B) Sketch of the principle geological structures of Chukotka with localities of the domains investigated. The sketch is compiled using 1:2500000 geological map (Nalivkin, 1983); the Vel'may terrane is shown based on the geological scheme by Tynankergav and Bychkov (1987).

Locations of the rocks sampled and used for the comparison are shown by arrows. Numbers correspond to the domains as follows: the Gytgyl'ven pass (1), the Ploskaya River (2), Keeneyveem River (3), the Kolyuchinskaya Bay (4) and Bilibino (5).

by Degtyaryov (1975). In regional geological maps (scales 1:200000 and 1:1000000) these rocks were mapped as parts of a large regional complex referred to as the Anyui sill-and-dike series of gabbro-diorite or gabbro-dolerite. In this paper we will refer these gabbroic rocks to as the Anyui dike-and-sill province. Their Permo-Triassic to Early-Middle Triassic age is proven by their stratigraphic position within Permian - lower Triassic and lower-middle Triassic terrigenous sediments, joint deformation

of gabbroic bodies and their country rocks (Til'man and Sosunov, 1960; Gel'man, 1963), bulk-rock K-Ar determinations of 250, 231 and 223 Ma (Ivanov and Milov, 1975; Degtyaryov, 1975) and the U-Pb TIMS igneous zircon age of 252 ± 4 Ma obtained for the Kolyuchinskaya Bay gabbro (Sokolov, et al., 2009). Gel'man (1963) and Degtyaryov (1975) pointed out a similarity of bulk major-element composition of gabbroic rocks from western Chukotka (areas of the Keperveem, Malyi Anyui and Raucha Uplifts)

to continental tholeiitic basalts and Siberian trap basalts. The gabbro from the Kolyuchinskaya Bay area exhibit bulk-rock trace-element abundances, Rb-Sr and Sm-Nd isotope compositions indicative of their crystallization from variably differentiated portions of crustally contaminated basaltic magma. They are similar to intra-plate basalts in general and some tholeiitic basalts of the Siberian LIP in particular (Ledneva, et al., 2011).

Data on the Anyui dike-and-sill province of the Chukotka Peninsula are sparse and any regional correlations are speculative. In this paper we focus on characteristic of gabbroic rocks of the Anyui dike-and-sill province from several localities of eastern Chukotka. Rare samples from western Chukotka were investigated as well. We present new $^{40}\text{Ar}/^{39}\text{Ar}$ ages, major-element compositions of minerals and whole rocks, bulk-rock trace-element chemistry and Sm-Nd isotopes as well as their possible petrologic and geodynamic interpretations. This provides grounds for addressing the following issues:

- Were gabbroic rocks, which were distinguished as parts of the Anyui dike-and-sill province, generated in one magmatic event?
- Is there any connection between studied gabbroic rocks of the Chukotka Peninsula and coeval rocks of the New Siberian Islands?
- Can the Anyui dike-and-sill province be considered as a possible continuity of the Siberian LIP?

GEOLOGICAL SETTING

General geological and tectonic settings

The major tectonic units of the AACM (Fig.1b) are the Neoproterozoic crystalline basement (Bering Strait Geol. Field Party, 1997; Natal'in, et al., 1999; Cecile, et al., 1999; Amato, et al., 2009) and upper Paleozoic - Mesozoic sedimentary cover (Natal'in, et al., 1999; Tuchkova, et al., 2009). The basement is exposed in domes of high-grade metamorphic rocks that are intruded by Early Cretaceous granitoids and Late Cretaceous mafic to intermediate rocks (e.g. Bering Strait Geol. Field Party, 1997; Amato, et al., 1997, 2003; Dorofeev, et al., 1999; Layer, et al., 2001; Miller, et al., 2009; Tikhomirov, et al., 2009). The sedimentary cover comprises Carboniferous and Permian carbonate platform strata (Natal'in, et al., 1999), Permo-Triassic to upper Triassic terrigenous

continental slope and shelf sediments (Tuchkova, et al., 2009) and Jurassic volcanic-terrigenous foreland sediments (Vatrushkina and Tuchkova, 2014).

The southern boundary of the AACM is widely hidden under the Cretaceous (Albian-Cenomanian and Santonian-Campanian) Okhotsk-Chukotka volcanic belt (Akinin and Miller, 2011; Tikhomirov, et al., 2012). In western Chukotka it is marked by the South Anyui Suture, which originated via closure of an oceanic basin and collision of the ACCM with the Asian continental margin during the early Cretaceous (Seslavinsky, 1979; Fujita and Newberry, 1982; Parfenov, 1984; Parfenov, et al., 1993; Nokleberg, et al., 1998). In eastern Chukotka its position is less certain and ascribed to the Vel'may terrane (Parfenov, et al., 1993; Nokleberg, et al., 1998; Sokolov, et al., 2009).

Geological setting of rocks of the Anyui dike-and-sill province

Sampling locations are shown in Figure 1b and are listed in Table 1.

Gabbroic rocks of the Anyui dike-and-sill province form numerous tabular bodies from a few meters to a few hundred meters thick that are mainly confined to the upper Permian - lower Triassic and lower-middle Triassic strata of the AACM cover (see notes for Table 1). Upper Triassic sediments gradually overlying these older sequences are free of tabular bodies of gabbroic rocks (Til'man and Sosunov, 1960; Gel'man, 1963; Degtyaryov, 1975; authors' observations). In Paleozoic limestones underlying Permo-Triassic and Triassic sediments elongated diabase lenses of a few hundred meters long and a few meters thick were described by Gel'man (1963).

In the study areas, gabbroic rocks are commonly exposed as eluvium and diluvium deposits due to frost weathering. In talus, fresh or relatively fresh gabbroic rocks are often mixed up with mudstones, siltstones, sandstones and bedded tuffs while metagabbros are intermixed with slates, schists and amphibolites. Bedrock exposures were investigated in domains of the Ploskaya River and Gyt'gylven pass. In the steep southern bank of the Ploskaya River gabbroic rocks constitute a sill of about 30 m thick and a body of unknown thickness (one of the contacts is covered with vegetation). Gabbros intrude

Table 1. List of samples and localities.

No	Sample	Rock group*	Rock name (based on petrographic description)	Domain **	Country rocks, Formation***	Longitude	Latitude	Type of exposure
1	GY9-74	Fe-Ti gabbro	metagabbro rich in Fe-Ti oxides	Gytgyl'ven pass (1)	Iul'tin, P-T ₁	178°11,404'W	67°09,543'N	bedrock
2	GY9-76	Fe-Ti gabbro	Qtz-bearing Hbl gabbro/diorite rich in Fe-Ti oxides	Gytgyl'ven pass (1)	Iul'tin, P-T ₁	178°11,514'W	67°09,741'N	eluvium
3	GY9-78	gabbroic diorite	Qtz diorite	Gytgyl'ven pass (1)	Iul'tin, P-T ₁	178°11,845'W	67°09,951'N	eluvium
4	GY9-79	Fe-Ti gabbro	metagabbro rich in Fe-Ti oxides	Gytgyl'ven pass (1)	Iul'tin, P-T ₁	178°11,845'W	67°09,951'N	eluvium
5	GY9-81	Fe-Ti gabbro	metagabbro rich in Fe-Ti oxides	Gytgyl'ven pass (1)	Iul'tin, P-T ₁	178°08,924'W	67°08,955'N	deluvium
6	GY9-82a	gabbroic diorite	diorite	Gytgyl'ven pass (1)	Iul'tin, P-T ₁	178°08,924'W	67°08,955'N	deluvium
7	GY9-82b	gabbroic diorite	Qtz diorite	Gytgyl'ven pass (1)	Iul'tin, P-T ₁	178°08,924'W	67°08,955'N	deluvium
8	GY9-84	gabbroic diorite	Qtz-metagabbro/Qtz-metadiorite	Gytgyl'ven pass (1)	Iul'tin, P-T ₁	178°09,677'W	67°08,952'N	deluvium
9	GY9-85	gabbroic diorite	Qtz diorite	Gytgyl'ven pass (1)	Iul'tin, P-T ₁	178°09,677'W	67°08,952'N	deluvium
10	GY9-87	gabbroic diorite	Qtz diorite	Gytgyl'ven pass (1)	Iul'tin, P-T ₁	178°10,161'W	67°08,932'N	deluvium
11	GY9-98	Fe-Ti gabbro	metagabbro rich in Fe-Ti oxides	Gytgyl'ven pass (1)	Iul'tin, P-T ₁	178°08,543'W	67°09,564'N	deluvium
12	GY9-99	Fe-Ti gabbro	Qtz-bearing Bi-Hbl gabbro rich in Fe-Ti oxides	Gytgyl'ven pass (1)	Iul'tin, P-T ₁	178°08,537'W	67°09,584'N	deluvium
13	GY9-101	gabbro	Qtz-bearing Hbl gabbro	Gytgyl'ven pass (1)	Iul'tin, P-T ₁	178°08,430'W	67°09,694'N	bedrock
14	GY9-102	Fe-Ti gabbro	metagabbro rich in Fe-Ti oxides	Gytgyl'ven pass (1)	Iul'tin, P-T ₁	178°08,329'W	67°09,726'N	bedrock
15	PS9-89	Fe-Ti gabbro	Qtz-bearing Bi-Hbl gabbro/diorite rich in Fe-Ti oxides	Ploskaya River (2)	Amguema, T ₁₋₂	177°52,958'W	67°07,954'N	bedrock
16	PS9-90	Fe-Ti gabbro	metagabbro/metadiorite rich in Fe-Ti oxides	Ploskaya River (2)	Amguema, T ₁₋₂	177°52,872'W	67°07,987'N	bedrock
17	PS9-92	gabbro	Qtz-bearing Bi-Hbl gabbro	Ploskaya River (2)	Amguema, T ₁₋₂	177°52,843'W	67°08,001'N	bedrock
18	KE9-71	Fe-Ti gabbro	Qtz diorite rich in Fe-Ti oxides	Keeneyveem River (3)	Amguema, T ₁₋₂	177°40,520'W	66°56,668'N	bedrock
19	KE9-72	Fe-Ti gabbro	Qtz-bearing Hbl gabbro rich in Fe-Ti oxides	Keeneyveem River (3)	Amguema, T ₁₋₂	177°40,520'W	66°56,668'N	bedrock
20	KE9-73	Fe-Ti gabbro	Qtz-bearing Bi-Hbl gabbro rich in Fe-Ti oxides	Keeneyveem River (3)	Amguema, T ₁₋₂	177°40,690'W	66°56,599'N	bedrock
21	P-11-7	gabbro	Qtz-bearing Hbl gabbro	Bilibino area (5)	Keperveem, T ₁₋₂	169°00,768'E	67°51,082'N	bedrock
22	P-11-7a	gabbro	Qtz-bearing Hbl gabbro (brecciated)	Bilibino area (5)	Keperveem, T ₁₋₂	169°00,768'E	67°51,082'N	bedrock
23	T-05-5	gabbro	Qtz-bearing Bi gabbro	Bilibino area (5)	Keperveem, T ₁₋₂	167°55,060'E	68°04,087'N	bedrock

* Rock group distinguished based on the bulk major-element composition of rocks.

** Numbers in the brackets correspond to the localities in Figure 1b.

*** The Iul'tin Formation is made of the upper Permian-lower Triassic strongly deformed slates, carbonaceous schists, siltstones and rare sandstones. The Amguema Formation (distinguished in eastern Chukotka) is represented by lower Triassic and lower-middle Triassic sequences of rhythmically bedded sandstones, calcareous siltstone and mudstones with calcareous concretions and rare intraformational conglomerates. The Keperveem Formation (recognized in western Chukotka) is facial analogues of the Amguema Formation (Explanatory notes to the regional geologic maps).

the folded sequence of bedded mudstones, siltstones and sandstones with rare thin layers of tuffs. Inner parts of the gabbroic bodies are composed of massive medium- and coarse-grained rocks without any features of magmatic banding. The sill has chilled contacts, which are marked by pinkish hornfels in the exocontact and very fine-grained gabbros in the endocontact. In the Gyt'gylven pass sills of a few meters to a few tens meters thick are embedded in strongly folded metamorphic rocks and are made of metagabbros. The sills are folded along with host slates and schists; and primary chilled contacts are often tectonically disrupted.

Similar geological relationships between gabbroic rocks of the Anyui dike-and-sill province were described in the Kolyuchinskaya Bay area in eastern Chukotka (Ledneva, et al., 2011) and in western Chukotka (Til'man and Sosunov, 1960; Gel'man, 1963; Degtyaryov, 1975). Gel'man (1963) also pointed out that in areas of the most intensive

deformations (for example the eastern flank of the Alyarmaut Uplift) tabular bodies are boudinaged. The boudins are traced for a distance of ~1-2.5 km and they are composed of amphibolites presumably originated after gabbroic rocks.

AGE

For ⁴⁰Ar/³⁹Ar analysis, samples were submitted to the Geochronology laboratory at the University of Alaska Fairbanks where they were crushed, sieved, washed and hand-picked for mineral phases. The monitor mineral MMhb-1 (Samson and Alexander, 1987) with an age of 513.9 Ma (Lanphere and Dalrymple, 2000) was used to monitor neutron flux (and calculate the irradiation parameter, J). The samples and standards were wrapped in aluminum foil and loaded into aluminum cans of 2.5 cm diameter and 6 cm height. The samples were irradiated in position 5c of the uranium enriched research reactor of McMaster University in Hamilton, Ontario, Canada

for 20 megawatt-hours. Upon their return from the reactor, the samples and monitors were loaded into 2 mm diameter holes in a copper tray that was then loaded in an ultra-high vacuum extraction line. The monitors were fused, and samples heated, using a 6-watt argon-ion laser following the technique described in York, et al. (1981), Layer, et al. (1987) and Layer (2000). Argon purification was achieved using a liquid nitrogen cold trap and a SAES Zr-Al getter at 40°C. The samples were analyzed in a VG-3600 mass spectrometer at the Geophysical Institute, University of Alaska Fairbanks. The argon isotopes measured were corrected for system blank and mass discrimination, as well as calcium, potassium and chlorine interference reactions following procedures outlined in McDougall and Harrison (1999). System blanks generally were 2×10^{-16} mol⁴⁰Ar and 2×10^{-18} mol³⁶Ar which are 10 to 50 times smaller than fraction volumes. Mass discrimination was monitored by running both calibrated air shots and a zero-age glass sample. These measurements were made on a weekly to monthly basis to check for changes in mass discrimination.

Results of ⁴⁰Ar/³⁹Ar dating

Results of the ⁴⁰Ar/³⁹Ar dating are shown in Table 2 and Figure 2. ⁴⁰Ar/³⁹Ar plateau ages obtained are 218.3 ± 5.2 Ma for hornblende of gabbroic diorite (sample GY9-87, the Gytgyl'ven pass) and 167.8 ± 11.2 Ma for actinolite with minor relicts of primary hornblende of Fe-Ti gabbro (sample PS9-89, the Ploskaya River).

PETROGRAPHY

Studied rocks of the Anyui province can be divided into three broad groups comprising the gabbro, Fe-Ti gabbro and gabbroic diorite. Each group includes rocks that are metamorphosed to a different extent, so some samples investigated are actually metagabbro and metadiorite. Rock names and groups to which they were attributed are given in Table 1. Relicts of primary silicates occupy usually only central parts of some grains with rims being pseudomorphed by metamorphic minerals. The petrographic description is based mainly on relatively fresh samples. In general, the original modal contents of mafic minerals in the rocks are

Table 2. Results of the argon measurements.

GY9-87 hornblende																
Weighted average of J from standards = $3.624 \times 10^{-3} \pm 1.367 \times 10^{-5}$																
Laser (mW)	Cum. ³⁹ Ar	⁴⁰ Ar/ ³⁹ Ar meas.	±	³⁷ Ar/ ³⁹ Ar meas.	±	³⁶ Ar/ ³⁹ Ar meas.	±	% Atm ⁴⁰ Ar	Ca/K	±	Cl/K	±	⁴⁰ Ar*/ ³⁹ Ar _K	±	Age (Ma)	± (Ma)
400	0,0114	855,459	20,608	4,1314	0,0816	2,7331	0,0598	94,4	7,60	0,15	0,0787	0,0041	48,268	22,689	290,9	126,3
800	0,0412	330,984	9,418	4,8920	0,1374	1,0068	0,0258	89,8	9,01	0,25	0,0711	0,0028	33,978	8,363	209,5	48,7
1200	0,0745	260,902	6,582	6,0898	0,1285	0,7745	0,0160	87,5	11,22	0,24	0,0900	0,0024	32,638	6,311	201,7	36,9
1500	0,1013	195,822	5,409	5,0209	0,1213	0,5534	0,0146	83,3	9,25	0,22	0,1817	0,0053	32,793	5,112	202,6	29,9
1750	0,1268	157,683	4,153	6,3412	0,1725	0,4268	0,0122	79,7	11,69	0,32	0,2259	0,0059	32,211	4,198	199,2	24,6
2000	0,1606	112,396	3,274	6,1122	0,2006	0,2748	0,0100	71,8	11,26	0,37	0,3395	0,0103	31,815	3,449	196,9	20,2
3000	0,2845	83,216	1,975	7,9697	0,1475	0,1640	0,0036	57,5	14,71	0,27	0,5429	0,0089	35,591	1,971	218,9	11,4
5000	0,6215	73,123	1,669	7,6599	0,1241	0,1294	0,0024	51,4	14,13	0,23	0,5915	0,0087	35,683	1,650	219,4	9,6
9000	1,0000	59,303	1,382	9,2375	0,1418	0,0808	0,0015	39,0	17,06	0,26	0,6228	0,0103	36,385	1,332	223,5	7,7
Integrated		98,714	0,987	7,9648	0,0692	0,2163	0,0018	64,1	14,70	0,13	0,5304	0,0048	35,632	0,916	219,1	5,4
PS9-89 actinolite																
Weighted average of J from standards = $3.624 \times 10^{-3} \pm 1.367 \times 10^{-5}$																
Laser (mW)	Cum. ³⁹ Ar	⁴⁰ Ar/ ³⁹ Ar meas.	±	³⁷ Ar/ ³⁹ Ar meas.	±	³⁶ Ar/ ³⁹ Ar meas.	±	% Atm ⁴⁰ Ar	Ca/K	±	Cl/K	±	⁴⁰ Ar*/ ³⁹ Ar _K	±	Age (Ma)	± (Ma)
500	0,0905	506,866	14,995	8,5942	0,2966	1,6044	0,0514	93,4	15,87	0,55	0,0643	0,0036	33,660	13,623	207,7	79,4
750	0,1800	309,578	10,015	5,9250	0,2207	0,9391	0,0335	89,5	10,92	0,41	0,0507	0,0030	32,672	8,571	201,9	50,1
1000	0,2852	135,433	7,947	4,0961	0,2189	0,3698	0,0210	80,5	7,54	0,40	0,0462	0,0032	26,535	7,340	165,7	43,8
1500	0,4383	100,217	5,657	5,9873	0,3128	0,2463	0,0130	72,1	11,03	0,58	0,0626	0,0039	28,029	4,989	174,6	29,6
1750	0,5362	74,323	5,342	7,7837	0,5235	0,1713	0,0132	67,3	14,36	0,97	0,0575	0,0046	24,450	4,925	153,2	29,6
2250	0,6783	54,138	3,369	8,2545	0,5254	0,0998	0,0072	53,2	15,23	0,98	0,1243	0,0084	25,455	3,049	159,2	18,3
2750	0,7714	58,484	2,993	12,4592	0,6529	0,1154	0,0074	56,6	23,06	1,22	0,0755	0,0045	25,602	3,054	160,1	18,3
4000	0,9011	64,572	2,910	23,8160	1,1043	0,1245	0,0064	54,0	44,45	2,10	0,1200	0,0056	30,218	2,809	187,5	16,6
5000	0,9647	70,458	3,485	29,6883	1,3706	0,1384	0,0079	54,6	55,64	2,62	0,1934	0,0094	32,672	3,513	201,9	20,5
9000	1,0000	151,887	7,049	96,9457	4,3119	0,3650	0,0172	65,8	190,96	9,12	0,2022	0,0097	55,812	7,032	332,4	38,2
Integrated		141,615	2,308	14,3797	0,2633	0,3846	0,0067	79,4	26,66	0,49	0,0901	0,0018	29,415	2,012	182,8	11,9

impossible to evaluate from petrography.

Gabbro and Fe-Ti gabbro are massive fine- to medium-grained rocks of hypidiomorphic-granular texture (Fig. 3a). The rocks are mainly composed of hornblende, augite, plagioclase, ilmenite, and Ti-magnetite, and contain variable amounts of biotite, accessory apatite and sodium-potassium

feldspars, trace micrographic intergrowths of quartz with orthoclase and albite (or discrete grains of these minerals) and sulfides. Minor pigeonite and orthopyroxene are present only in a few samples studied. Mafic silicates are dominated by hornblende. The exception is sample T05-5, which seems to be hornblende-free. The plagioclase content in the

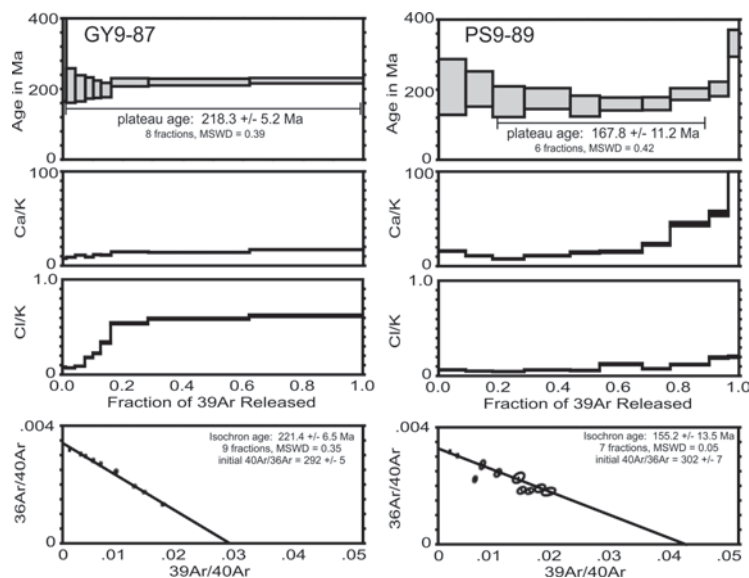


Fig 2. Age, Ca/K and Cl/K spectra and correlation diagrams for hornblende and actinolite. Plateau and isochron ages are indicated. MSWD: Mean square weighted deviations, a measure of plateau or isochron scatter.

Fig. 3. Photomicrographs and back-scattered electron (BSE) images demonstrating typical textures and other features of rocks of the Anyui province. Acronyms are as follows: Ab – albite, Afs – alkali feldspars, Amph – amphibole, Ano – anorthoclase, Ap – apatite, Aug – augite, Chl – chlorite, Ep – epidote, Hbl – hornblende, Ilm – ilmenite, Pl – plagioclase, rTi-Mag – Ti-magnetite pseudomorphly replaced by titanite, Stil – stilpnomelane, Ti-Mag – Ti-magnetite, Ttn – titanite, Qtz – quartz.

(a) Massive hypidiomorphic-granular Fe-Ti gabbro (sample KE9-73) dominated by euhedral crystals of zoned feldspars and subhedral grains of hornblende and augite; quartz and micrographic intergrowths of quartz with alkali feldspar fills interstices and constitute less than 2-3 %. Primary hornblende is partially replaced by actinolite. Cross-polarized light.

(b) BSE image showing zonation of euhedral feldspar grains and details of granophyric groundmass of Fe-Ti gabbro (sample PS9-89). The core of feldspar grain is composed of labradorite (An53); the inner and outer rims are made of oligoclase (An36) and anorthoclase, respectively. Groundmass is dominated by micrographic intergrowths of anorthoclase, albite and quartz and individual grains of orthoclase and quartz.

(c) Massive hypidiomorphic-granular Fe-Ti gabbro with micrographic groundmass (sample PS9-89). The rock is made of euhedral crystals of zoned feldspars, subhedral grains of hornblende merged in the groundmass of intergrown quartz, albite and orthoclase. Cross-polarized light.

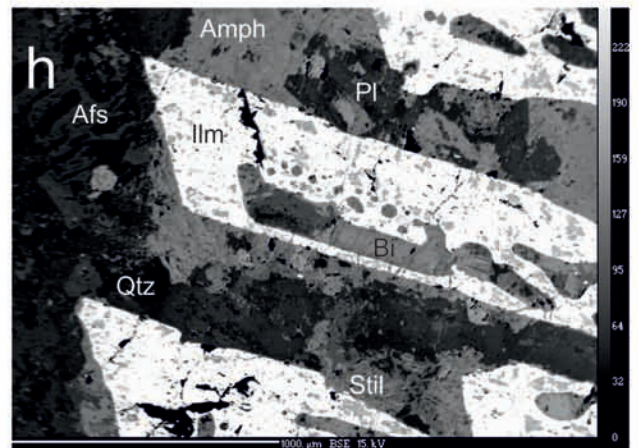
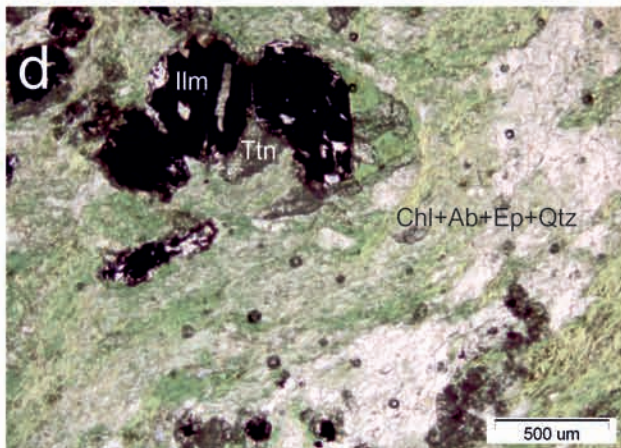
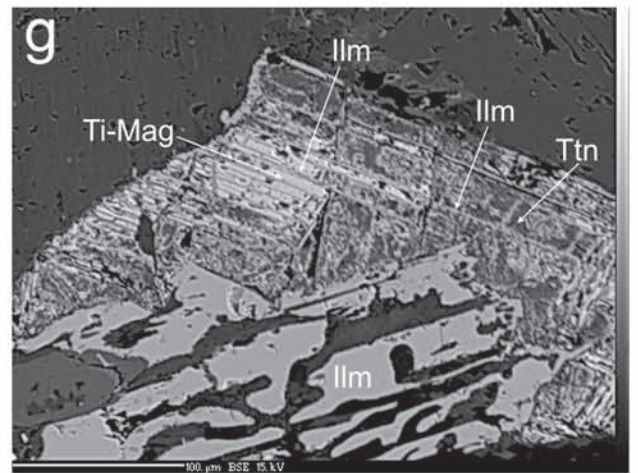
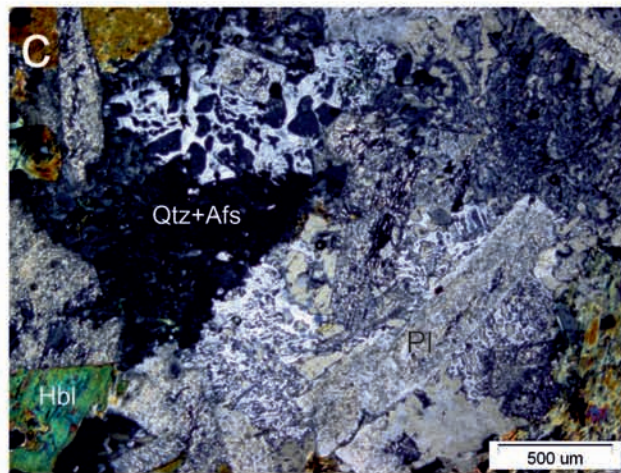
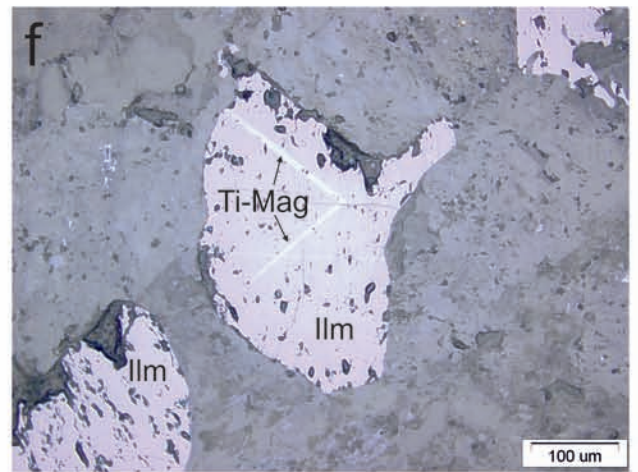
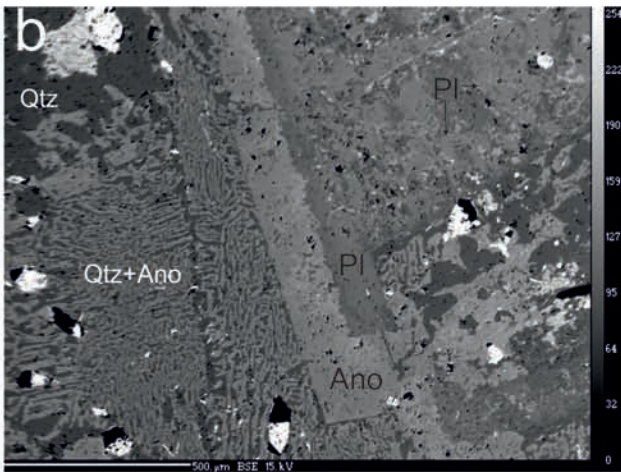
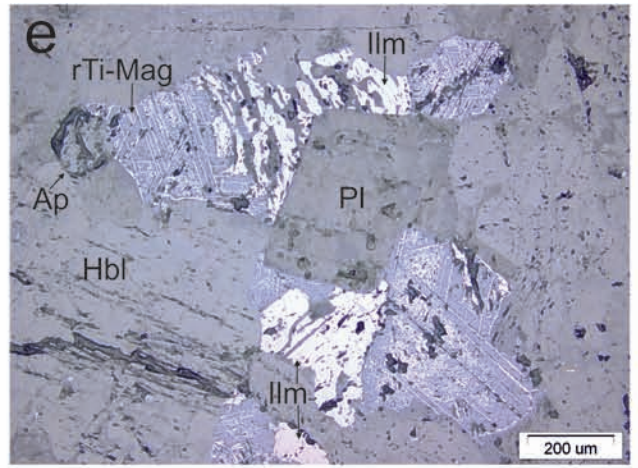
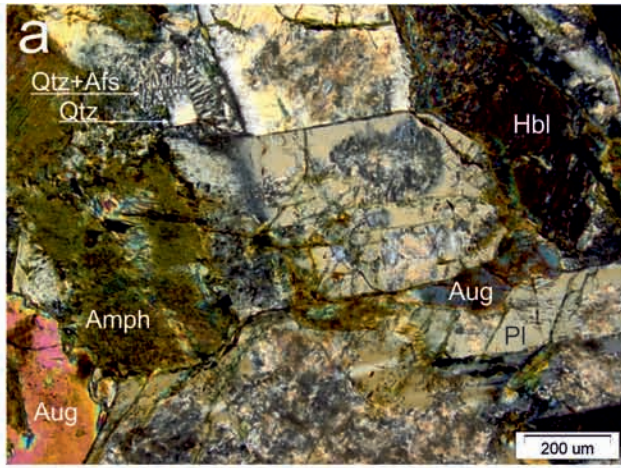
(d) Metagabbro presumably resulted from nearly complete metamorphic alteration of a gabbro (sample GY9-102). A primary texture is not preserved; metamorphic minerals are chlorite, albite, quartz, epidote, and titanite. Titanite and high-Mn ilmenites form pseudomorphs after primary Ti-magnetite and ilmenite. This rock contains only very rare relicts (a few to a few tens microns) of hornblende similar in composition to a primary one (Table 3). Plane-polarized light.

(e) Ilmenite grains and pseudomorphs of titanite after Ti-magnetite with preserved ilmenite lamellae in Fe-Ti gabbro (sample KE9-71). Reflected light.

(f) Ti-magnetite lamellae in ilmenite, Fe-Ti gabbro (sample KE9-71). Reflected light.

(g) Ilmenite intergrown with Ti-magnetite with ilmenite lamellae, Ti-magnetite is partially replaced by titanite, Fe-Ti gabbro (sample KE9-71). BSE image.

(h) Euhedral grains of ilmenites with numerous inclusions of silicate minerals (biotite, amphibole and etc.), Fe-Ti gabbro (sample PS9-89). BSE image.



rocks amounts to 30-40%. The contents of Fe-Ti oxides is evaluated at 5-10% (the highest value is typical for the Fe-Ti gabbros); ilmenite dominates over Ti-magnetite with a factor of about 2.

Hornblende forms anhedral, subhedral, or euhedral elongated, or isometric grains and displays pleochroism from greenish to brown colors. Euhedral and subhedral grains, often occurring as aggregates, show only weak pleochroism, and anhedral grains in contact with quartz have stronger pleochroism. Augite forms isometric subhedral grains without a visible pleochroism. Pigeonite was found in trace amount only in two samples (GY9-73 and T-05-5), where it forms small (a few tens of microns) subhedral crystals completely or partially embedded in augite and biotite. Orthopyroxene was found only in one sample (T-05-5), in which it forms small subhedral grains embedded in augite. Augites in this sample contain exsolution lamellae of pigeonite and vice versa; other samples studied have no pyroxenes with exsolution lamellae. Biotite is pleochroic from dark to light reddish brown. It forms small euhedral laths included in Fe-Ti oxides and anhedral grains that fill interstices along with hornblende, quartz and Fe-Ti oxides. Plagioclase forms euhedral and subhedral tabular crystals displaying sometimes clear optical compositional zoning. Polysynthetic twinning in the plagioclase grains is abundant. In some samples, tabular plagioclase grains are rimmed by anorthoclase (Fig. 3b). Micrographic intergrowths of quartz±orthoclase±albite and discrete grains of these minerals fill interstices (Fig. 3a, 3b, 3c). Fe-Ti oxides (Fig. 3e) are represented by elongated grains of ilmenite, with or without rare Ti-magnetite lamellae (Fig. 3f), and isometric grains of Ti-magnetite with numerous ilmenite lamellae (forming three systems) (Fig. 3g). Ti-magnetite is preserved as unique relicts and generally is completely replaced by titanite; the ilmenite lamellae therein seem to be much more resistant to the metamorphic replacement. Fe-Ti oxides contain inclusions of silicate minerals as, for example, shown in Fig. 3h.

Gabbroic diorites exhibit mineral assemblages and textures typical of gabbro and Fe-Ti gabbro and differ from the latter only in modal mineral abundances (chiefly elevated quartz, biotite and potassium feldspar abundances). As the gabbro and Fe-Ti gabbro, gabbroic diorites are massive fine-

to medium-grained mesocratic hypidiomorphic-granular and granophyric rocks. Their peculiar feature is the wide occurrence of micrographic intergrowths of quartz, orthoclase and albite.

Metamorphic replacement of minerals is recorded by partial to complete replacement of primary pyroxenes and hornblende by greenish actinolite and chlorite. Core plagioclases are commonly substituted by calcium-potassium-sodium zeolites. In some samples, plagioclases are totally replaced by albite or albite-oligoclase, prehnite, epidote and pumpellyite; no primary zonation was preserved in these samples. Biotite is substituted mainly by chlorite, Ti-magnetite and ilmenite by titanite. In some well-metamorphosed samples, a secondary biotite forming sharp euhedral plates and associated with chlorite and albite has formed. Traces of metamorphic calcite, stilpnomelane and muscovite also occur. A few rocks, which are completely metamorphosed, exhibit no primary magmatic textures (Fig. 3d), and relict primary minerals therein are represented by quartz, apatite and ilmenite only.

Composition of minerals

Major elements in minerals were analyzed in polished thin sections using a Cameca-SX100 electron microprobe at the V.I. Vernadsky Institute of Geochemistry and Analytical Chemistry (GEOKHI RAS) at 15kV accelerating voltage and 30 nA beam current. The diameter of the beam was 5 µm for plagioclase to predict Na loss and 1-2µm for all other minerals analyzed. Counting time was 20/10 s (peak/background). Natural standards from the Smithsonian Institution were used. The analytical accuracy for silicate minerals was monitored by regular measurements of the Cr-augite. The single point analytical errors were ±2% rel. for major components (10-100 wt %), ±5% rel. for minor components (2-10 wt %), ±10% rel. for components accounting for 1-2 wt %, and ±20 % rel. for components accounting for less than 1 wt %.

Major-element variations in minerals of the Anyui province rocks

Compositions of primary minerals are shown in Table 3. In most of the samples studied, augites have relatively high to moderate magnesium-numbers

Table 3. Primary mineral compositions.

N	1	2	3	4	5	6	7	8	9	10
Sample	KE9-71	KE9-71	KE9-71	KE9-71	KE9-71	KE9-71	KE9-71	KE9-72	KE9-72	KE9-72
Mineral	Cpx-C	Cpx-R	Bi	P11	P12/Qtz	Ilm	Ti-Mag	Cpx	Hbl	Ilm-Lam
Points	2	2	2	2	1	4	1	3	2	1
SiO ₂	50.65	50.89	35.38	55.07	65.94	0.05	0.23	50.99	47.01	0.14
TiO ₂	0.91	0.72	3.42	0.06	0.00	47.45	6.15	0.64	0.99	50.62
Al ₂ O ₃	1.70	1.56	12.37	27.90	21.64	0.06	0.87	1.38	5.33	0.03
FeO	14.05	13.31	27.66	0.48	0.22	49.37	84.49	13.62	20.64	45.45
MnO	0.42	0.41	0.08	0.00	0.00	0.96	0.00	0.46	0.36	1.45
MgO	13.68	12.36	7.06	0.06	0.01	0.08	0.02	11.77	10.42	0.06
CaO	17.29	19.52	0.04	10.41	2.92	0.03	0.36	20.21	10.25	0.59
Na ₂ O	0.26	0.26	0.09	5.28	9.48	0.00	0.05	0.24	1.74	0.03
K ₂ O	0.01	0.00	8.46	0.42	0.30	0.01	0.01	0.00	0.71	0.00
Cr ₂ O ₃	0.00	0.01	0.03	0.02	0.00	0.03	0.05	0.04	0.00	0.04
NiO						0.01				
V ₂ O ₃						0.66	1.77			
Sum	98.96	99.04	94.59	99.69	100.51	98.72	94.01	99.36	97.46	98.40
Cl										
Mg#	63.4	62.4	31.3					60.6	47.4	
xAn				50.9	14.3					

Table 3. (continued).

N	11	12	13	14	15	16	17	18	19	20
Sample	KE9-72L	KE9-73	KE9-73	KE9-73	KE9-73	KE9-73	KE9-73	KE9-73	KE9-73	KE9-73
Mineral	Ilm	Cpx	Pig	Hbl	Bi	P11	P12/Qtz	Ort/Sim Qtz	Ilm	Ti-Mag1
Points	1	3	3	2	2	2	2	2	2	2
SiO ₂	0.31	50.37	51.58	47.02	35.88	54.60	59.97	64.28	0.04	0.13
TiO ₂	50.72	0.94	0.27	1.38	3.90	0.09	0.04	0.00	47.19	12.70
Al ₂ O ₃	0.08	2.02	0.40	5.64	12.87	29.15	25.64	19.38	0.05	1.80
FeO	45.06	13.96	28.84	18.21	26.06	0.59	0.56	0.06	47.94	78.17
MnO	1.44	0.39	0.69	0.22	0.08	0.01	0.03	0.02	0.96	0.30
MgO	0.12	12.60	14.80	11.60	9.33	0.06	0.03	0.02	0.09	0.04
CaO	0.22	18.55	3.42	10.66	0.16	11.52	7.09	0.05	0.01	0.05
Na ₂ O	0.01	0.26	0.07	1.66	0.05	4.69	6.87	0.29	0.03	0.04
K ₂ O	0.01	0.01	0.01	0.73	6.66	0.32	0.72	16.28	0.01	0.00
Cr ₂ O ₃	0.03	0.02	0.02	0.02	0.00	0.00	0.01	0.00	0.03	0.07
NiO									0.00	
V ₂ O ₃									0.66	2.21
Sum	97.99	99.11	100.10	97.13	95.00	101.03	100.96	100.38	97.01	95.51
Cl										
Mg#		61.7	47.8	53.2	39.0					
xAn						56.5	34.8			

Table 3. (continued).

N	21	22	23	24	25	26	27	28	29	30
Sample	KE9-73	GY9-76	GY9-76	GY9-78	GY9-78	GY9-78	GY9-82a	GY9-82a	GY9-82a	GY9-82a
Mineral	Ti-Mag2	Hbl	Ilm	Hbl	Ap	Ilm	Hbl	Pl-C	Pl-R	Ort
Points	1	2	2	2	1	1	2	2	3	1
SiO ₂	0.12	45.14	0.04	43.63	0.19	0.04	45.93	57.61	63.51	64.79
TiO ₂	5.80	1.47	53.11	1.61	0.03	51.36	1.30	0.06	0.00	0.02
Al ₂ O ₃	2.15	5.81	0.03	6.63	0.00	0.03	5.81	27.21	24.06	18.86
FeO	85.75	22.40	43.27	26.56	0.77	45.88	20.93	0.44	0.40	0.48
MnO	0.16	0.29	2.40	0.37	0.07	1.58	0.30	0.03	0.01	0.03
MgO	0.07	8.14	0.07	5.81	0.01	0.05	9.96	0.01	0.03	0.04
CaO	0.02	10.41	0.04	10.13	53.80	0.06	10.07	8.87	4.51	0.01
Na ₂ O	0.00	1.47	0.02	1.46	0.00	0.00	1.65	5.67	8.07	0.25
K ₂ O	0.01	0.70	0.00	0.99	0.00	0.00	0.82	0.57	0.67	16.19
Cr ₂ O ₃	0.06	0.04	0.00	0.02	0.06	0.04	0.04	0.04	0.02	0.00
NiO										
V ₂ O ₃	1.89									
Sum	96.03	95.88	98.97	97.21	54.93	99.04	96.81	100.51	101.30	100.66
Cl										
Mg#		39.3		28.1			45.9			
xAn								44.8	22.7	

Table 3. (continued).

N	31	32	33	34	35	36	37	38	39	40
Sample	GY9-82b	GY9-82b	GY9-82b	GY9-82b	GY9-82b	GY9-85	GY9-85	GY9-85	GY9-85	GY9-87
Mineral	Hbl	Bi	Pl-C	Pl-R	Ort	Hbl	Bi	Ort	Ilm	Cpx
Points	3	2	2	1	1	4	3	2	1	2
SiO ₂	44.58	33.30	58.62	64.65	66.47	43.71	31.99	63.86	0.04	49.60
TiO ₂	1.33	3.57	0.02	0.00	0.01	1.38	2.58	0.03	53.11	0.60
Al ₂ O ₃	6.47	12.73	25.63	22.02	19.65	6.11	12.51	19.63	0.02	1.14
FeO	24.59	30.91	0.39	0.04	0.07	26.70	35.58	0.27	46.15	19.19
MnO	0.24	0.18	0.01	0.00	0.00	0.38	0.20	0.00	1.82	0.70
MgO	7.17	5.84	0.02	0.01	0.00	5.62	3.52	0.02	0.03	7.44
CaO	10.42	0.21	7.49	2.92	0.00	10.05	0.36	0.08	0.01	20.33
Na ₂ O	1.45	0.10	5.93	8.93	0.26	1.97	0.04	0.27	0.01	0.24
K ₂ O	0.87	6.51	0.64	0.69	14.94	0.88	5.25	14.44	0.00	0.00
Cr ₂ O ₃	0.02	0.03	0.00	0.00	0.00	0.01	0.02	0.00	0.00	0.00
NiO										
V ₂ O ₃										
Sum	97.14	93.38	98.76	99.27	101.40	96.82	92.04	98.61	101.18	99.24
Cl										
Mg#	34.2	25.2				27.3	15.0			40.9
xAn			39.4	14.7						

Table 3. (continued).

N	41	42	43	44	45	46	47	48	49	50
Sample	GY9-87	GY9-87	GY9-87	PS9-89						
Mineral	Hbl	Ort	Ilm	Cpx1	Cpx2	Hbl	Bi	Pl-C	Pl-R	Ano
Points	4	2	2	2	2	2	2	2	1	2
SiO ₂	44.64	66.19	0.06	48.03	50.52	42.68	34.95	54.76	59.13	64.49
TiO ₂	1.50	0.02	49.48	0.98	1.04	1.78	4.01	0.06	0.03	0.02
Al ₂ O ₃	6.20	19.43	0.04	3.63	1.96	7.20	12.07	28.00	25.33	19.06
FeO	25.59	0.10	47.64	13.12	12.02	25.96	28.68	0.58	0.36	0.11
MnO	0.33	0.00	2.35	0.27	0.34	0.23	0.13	0.02	0.01	0.00
MgO	7.00	0.00	0.03	12.92	12.84	5.69	5.77	0.10	0.02	0.02
CaO	10.15	0.02	0.08	18.02	19.82	10.37	0.16	10.68	7.17	0.33
Na ₂ O	2.01	0.25	0.00	0.28	0.28	1.66	0.15	5.04	6.58	3.31
K ₂ O	0.91	14.89	0.03	0.02	0.01	0.97	7.92	0.39	0.84	11.13
Cr ₂ O ₃	0.00	0.00	0.03	0.00	0.04	0.01	0.03	0.00	0.02	0.01
NiO										
V ₂ O ₃			0.89							
Sum	98.35	100.89	100.63	97.27	98.86	96.57	93.87	99.63	99.49	98.48
Cl										
Mg#	32.8			63.7	65.6	28.1	26.4			
xAn								52.7	35.7	

Table 3. (continued).

N	51	52	53	54	55	56	57	58	59	60
Sample	PS9-89	PS9-89	PS9-89	PS9-92	PS9-92	PS9-92	PS9-92	PS9-92	PS9-92	GY9-98
Mineral	Ort/Sim Qtz	Ort	Ilm	Cpx	Hbl-C	Hbl- R/Qtz	Bi	Pl/Ilm	Ort	Ilm
Points	1	1	2	2	2	2	3	1	1	1
SiO ₂	65.90	63.08	0.03	50.32	45.53	45.50	35.39	54.29	64.16	0.06
TiO ₂	0.02	0.02	48.47	1.20	1.07	1.39	4.55	0.14	0.00	55.03
Al ₂ O ₃	19.12	18.66	0.07	3.02	5.68	5.91	12.70	28.14	18.64	0.00
FeO	0.14	0.66	46.76	11.09	22.34	25.09	27.96	0.88	0.07	44.47
MnO	0.00	0.00	1.85	0.21	0.27	0.24	0.11	0.01	0.00	2.22
MgO	0.03	0.01	0.07	13.43	9.15	7.11	6.26	0.02	0.01	0.07
CaO	0.19	0.00	0.02	19.78	10.08	10.19	0.01	10.71	0.01	0.00
Na ₂ O	2.98	0.20	0.00	0.30	1.77	1.52	0.22	4.79	0.22	0.04
K ₂ O	12.14	15.50	0.00	0.01	0.83	0.64	7.97	0.40	15.84	0.00
Cr ₂ O ₃	0.00	0.02	0.00	0.05	0.03	0.04	0.06	0.04	0.01	0.05
NiO			0.02							
V ₂ O ₃			0.58							
Sum	100.53	98.15	97.88	99.41	96.73	97.64	95.23	99.42	98.96	101.93
Cl										
Mg#				68.3	42.2	33.6	28.5			
xAn								53.9		

Table 3. (continued).

N	61	62	63	64	65	66	67	68	69	70
Sample	GY9-99	GY9-99	GY9-99	GY9-99	GY9-101	GY9-101	P-11-7	P-11-7	P-11-7	P-11-7
Mineral	Hbl1	Hbl2	Bi	Ilm	Hbl	Ilm	Cpx-C	Cpx-R	Hbl1	Hbl2
Points	2	2	2	3	2	2	2	4	1	3
SiO ₂	48.05	46.85	37.52	0.05	45.73	0.08	52.14	51.57	46.81	44.13
TiO ₂	1.07	1.16	1.93	51.87	1.53	50.69	0.65	0.85	1.46	1.40
Al ₂ O ₃	4.97	5.74	12.66	0.03	6.95	0.02	2.15	2.09	6.15	5.62
FeO	19.09	20.19	25.55	45.08	21.02	43.23	10.19	12.75	16.42	25.38
MnO	0.25	0.21	0.15	2.41	0.26	2.99	0.28	0.34	0.24	0.36
MgO	10.87	9.60	8.41	0.10	8.74	0.10	14.35	14.26	12.71	7.15
CaO	10.50	10.74	0.03	0.05	10.70	0.05	19.73	17.81	10.25	9.45
Na ₂ O	1.10	1.18	0.03	0.00	1.18	0.02	0.30	0.27	2.19	1.94
K ₂ O	0.52	0.67	9.02	0.01	0.85	0.01	0.01	0.01	0.67	0.77
Cr ₂ O ₃	0.01	0.01	0.05	0.01	0.02	0.47	0.02	0.00	0.01	0.00
NiO		0.07		0.01		0.01				
V ₂ O ₃		0.08		0.53		0.63				
Sum	96.42	96.50	95.36	100.14	96.96	98.27	99.81	99.94	96.90	96.21
Cl									0.10	0.40
Mg#	50.4	45.9	37.0		42.6		71.5	66.6	58.0	33.4
xAn										

Table 3. (continued).

N	71	72	73	74	75	76	77	78	79	80
Sample	P-11-7	P-11-7	P-11-7	P-11-7a	P-11-7a	P-11-7a	P-11-7a	P-11-7a	P-11-7a	P-11-7a
Mineral	Pl	Ilm	Ap	Cpx-C	Cpx-R	Hbl-C	Hbl-R/Qtz	Pl1/Cpx	Pl2	Pl3
Points	2	2	1	2	2	2	2	2	2	2
SiO ₂	58.82	0.53	0.75	50.57	51.57	46.98	44.89	51.11	53.61	58.41
TiO ₂	0.02	52.11	0.02	0.92	0.64	1.14	1.30	0.04	0.08	0.05
Al ₂ O ₃	25.49	0.13	0.24	3.50	2.22	4.54	5.36	30.06	28.52	26.38
FeO	0.43	44.85	1.22	8.89	8.41	22.52	25.73	0.79	1.02	0.79
MnO	0.00	2.19	0.06	0.27	0.27	0.40	0.32	0.01	0.01	0.02
MgO	0.06	0.08	0.14	15.51	15.84	8.98	6.69	0.15	0.22	0.16
CaO	6.88	0.52	52.74	19.08	19.31	10.26	9.44	13.87	10.50	6.83
Na ₂ O	6.98	0.02	0.04	0.31	0.25	1.71	1.73	3.67	4.59	6.43
K ₂ O	0.69	0.01	0.01	0.00	0.00	0.67	0.62	0.17	0.72	0.89
Cr ₂ O ₃	0.00	0.01	0.03	0.14	0.08	0.00	0.02	0.00	0.02	0.03
NiO										
V ₂ O ₃										
Sum	99.38	100.46	55.25	99.18	98.58	97.20	96.10	99.86	99.28	99.99
Cl			0.06			0.22	0.39			
Mg#				75.7	77.1	41.6	31.7			
xAn	33.8							67.0	53.4	35.0

Table 3. (continued).

N	81	82	83	84	85	86	87	88	89	90
Sample	P-11-7a	P-11-7a	T-05-5							
Mineral	PI4- R/Qtz	Ilm	Cpx1	Cpx2	Pig	Opx	Bi-C	Bi-R	Pl1/Cp	Pl2/Qtz
Points	2	2	3	2	3	2	3	2	3	2
SiO ₂	65.15	0.11	49.86	50.85	50.57	49.62	35.94	34.28	54.69	59.49
TiO ₂	0.03	50.60	0.91	0.67	0.42	0.34	4.49	3.24	0.08	0.02
Al ₂ O ₃	22.08	0.07	1.90	1.31	0.69	0.32	12.60	12.85	28.48	25.51
FeO	0.41	45.87	15.64	15.61	26.61	33.00	22.89	28.29	0.67	0.34
MnO	0.02	2.06	0.39	0.48	0.74	0.91	0.09	0.14	0.00	0.03
MgO	0.03	0.10	12.46	12.22	15.24	12.65	9.30	6.67	0.07	0.03
CaO	2.22	0.17	16.96	17.99	4.74	2.64	0.05	0.11	10.92	7.18
Na ₂ O	9.02	0.03	0.26	0.26	0.10	0.06	0.23	0.05	5.22	7.14
K ₂ O	0.57	0.00	0.01	0.02	0.00	0.01	8.62	7.96	0.26	0.65
Cr ₂ O ₃	0.01	0.00	0.02	0.02	0.00	0.01	0.01	0.07	0.00	0.01
NiO										
V ₂ O ₃										
Sum	99.53	99.01	98.41	99.44	99.13	99.54	94.22	93.66	100.40	100.40
Cl							0.34	0.33		
Mg#			58.7	58.2	50.5	40.6	42.0	29.6		
xAn	11.6								52.8	34.4

Table 3. (continued).

N	91	92	93
Sample	T-05-5	T-05-5	T-05-5
Mineral	Ort	Ilm	Ti-Mag
Points	2	2	2
SiO ₂	64.24	0.07	0.10
TiO ₂	0.00	48.69	16.22
Al ₂ O ₃	18.47	0.03	1.49
FeO	1.17	46.98	74.78
MnO	0.05	1.72	0.62
MgO	0.18	0.03	0.02
CaO	0.10	0.04	0.02
Na ₂ O	0.59	0.02	0.00
K ₂ O	14.44	0.00	0.00
Cr ₂ O ₃	0.08	0.16	0.03
NiO			
V ₂ O ₃			
Sum	99.30	97.75	93.29
Cl			
Mg#			
xAn			

Notes: C – core, R – rim, numbers correspond to different mineral generations. min/min – phases at a contact. Sim – micrographic intergrowths. For other acronyms see caption to Figure 3.

(note: $mg\# = 100 * Mg / (Mg + Fe_{tot})$) was similarly calculated for all minerals and whole rocks) of 58-77 that drop as low as 41 in the gabbroic diorite (Fig. 4) with the lowest magnesium number of rock (sample GY9-87). The $mg\#$ variations of augite within a single sample commonly are negligible but in most samples outer parts of augite grains are fully replaced. Only two samples (KE9-71, P11-7) contain augite that exhibits core-to-rim zoning. All augites are relatively low in titanium (0.6-1.04 wt. %, TiO_2) and sodium (0.24-0.30 wt. %, Na_2O); concentrations of these elements remain nearly constant in the whole range of augite magnesium number variations.

Primary **hornblendes**, edenites and ferroedenites (Leake, et al., 1997), have moderate to low magnesium-numbers of 27.3-58.0 (Fig. 5) that do not cover the range of magnesium number variations in clinopyroxenes. Hornblendes generally show moderately low aluminum (4.54-7.20 wt. %, Al_2O_3), elevated titanium (0.99-1.78 wt. %, TiO_2) contents

and are rich in potassium (0.52-0.97 wt. %, K_2O). Some samples studied (GY9-92, GY9-99, P-11-7, P-11-7a) contain hornblendes of widely variable magnesium-numbers.

Biotite exhibits wide variations in FeO^{tot}/MgO ratio chiefly ranging in the interval of 2.5-5.3 and reaching 10.1 in the gabbroic diorite (sample GY9-85), i.e. biotites become richer in siderophyllite and annite components. Al_2O_3 abundances of 12.07-12.87 wt. % remain nearly constant. TiO_2 content decreases slightly as the $mg\#$ of biotite decreases. They are relatively high (2.6-4.6 wt. %, TiO_2) excluding sample GY9-99 in which somewhat lowered titanium content can be related to partial recrystallization of the biotite. In some samples biotites reveal lowered K_2O contents that can be a result of partial metamorphic recrystallization or replacement of this mineral.

Plagioclases are represented by both igneous and metamorphic (albite) generations. Primary

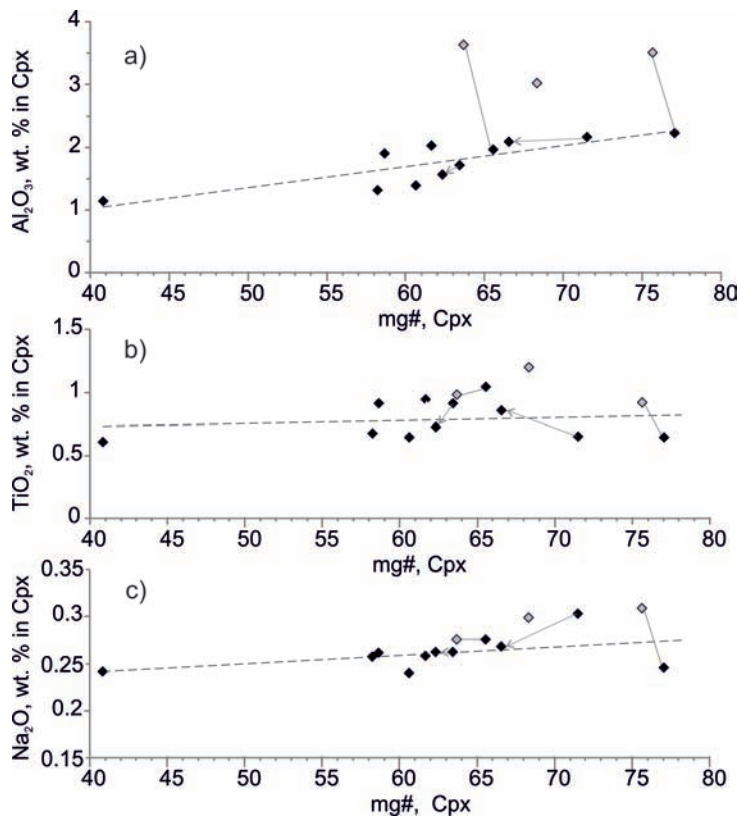


Fig. 4. Oxide, wt. % vs. $mg\#$, Cpx plot. Black and grey diamonds are for low-Al and medium-Al clinopyroxenes in the Anyui province sills, correspondingly. Grey arrows show core-to-rim zoning in the sample; grey lines connect coexisting augite generations (measured in different grains) in the sample. Individual data points characterize individual samples (in this and other diagrams for minerals).

plagioclases have appreciable admixtures of iron (0.2-0.8 wt. %, FeO) and K_2O (0.2-0.9 wt. %) and display a clear regularity in decreasing iron contents and increasing potassium contents with decreasing xAn (note: $xAn = 100 * Ca / (Ca + Na + K)$) in plagioclase. As mentioned above, primary plagioclases are zoned. In gabbro, their cores are composed of labradorite (xAn67-51) that gradually ranges into andesine (xAn36-34) rims. At the contact with quartz, rim plagioclases become sodic oligoclase (xAn14-12). In one of the samples studied (P-11-7a), they cover the whole range of compositions from labradorite xAn72 to oligoclase xAn12. Most calcium plagioclases are confined to core grains embedded in clinopyroxenes. In the gabbroic diorite, tabular feldspar grains are made of andesine (xAn45-39) cores and oligoclase (xAn23-14) rims. Therefore, in all samples studied plagioclases reveal wide compositional variations.

Alkali feldspars are represented by anorthoclase and orthoclase. Anorthoclase was measured only in one sample (PS9-89) in which it constitutes the outermost rim of the zoned tabular feldspar (Fig. 3c). In this sample, orthoclase intergrown with quartz in interstices is sodium-bearing variety (3 wt. % Na_2O) that seems to have primary magmatic composition.

In this and other (more intensively metamorphosed) samples studied, pure orthoclase; however, occurs along with sodium orthoclase in micrographyc structures. In all samples albitic plagioclase seems to have a metamorphic origin. We suppose that pure orthoclase and albite in micrographyc structures are products of metamorphic recrystallization of primary magmatic sodium orthoclase (and probably also anorthoclase) and primary magmatic plagioclase (probably sodium oligoclase or albite), respectively.

Ti-magnetites were measured only in three samples and are characterized by variable TiO_2 content of 6.15-16.22 even within a single sample. This is probably related to different degrees of the magnetite to ilmenite exsolution in different points of analyses. All Ti-magnetites demonstrate high V_2O_3 contents (1.8-2.2 wt. %), elevated Al_2O_3 contents (0.9-2.2 wt. %) and relatively low MnO contents (up to 0.6 wt. %).

Ilmenites show slight $TiO_2 - FeO_{total}$ variations with ilmenite composing grains and lamellae in Ti-magnetite in a single sample having similar compositions. The only significant admixture in ilmenites is MnO (0.96-2.40 wt. %).

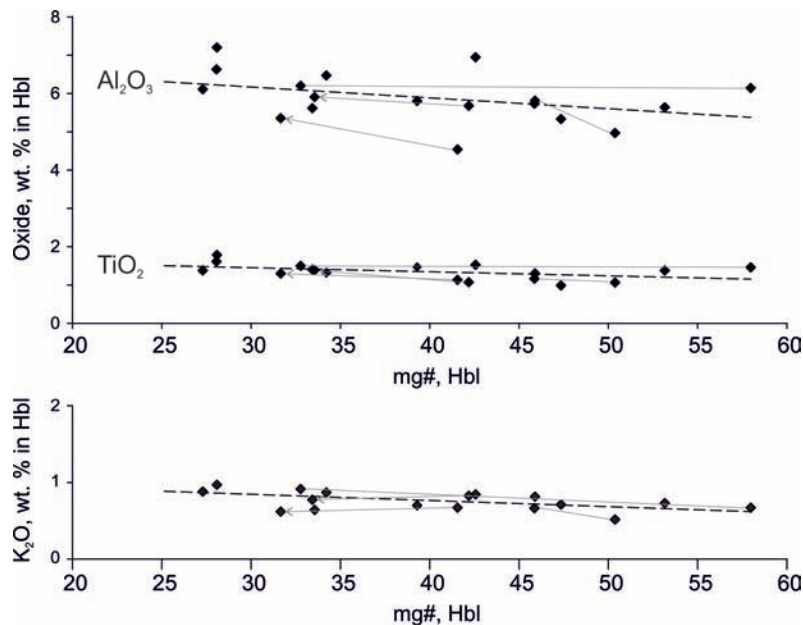


Fig. 5. Oxide, wt. % vs. mg#, Hbl plots. Grey arrows show a core-to-rim zoning; grey lines connect compositions of minerals coexisting in one sample.

BULK ROCK MAJOR AND TRACE-ELEMENT COMPOSITIONS

Major and trace elements in bulk rocks were measured at the GEOKHI RAS, Moscow, Russia. Samples were carefully cleaned before crushing but not leached. Rocks (~300-400 g) were crushed and powdered (~30-40 g) using a jaw crushing and vibrating cup mill. The major elements were determined by the XRF method with a Phillips PW-1600 equipment. The calibration was performed using international (Govindaraju, 1994) and domestic rock standards as well as internal standards. The trace-element abundances were determined by Inductively Coupled Plasma Mass Spectrometry with a Finnigan Element XR instrument. Sample

preparation was done in a microwave oven using the method of bulk rock acid digestion. The precision and accuracy of analyses were controlled by regular measurements of international (BCR-2) and internal rock standards. Detection limits were 0.01 ng/g for heavy and medium elements and 0.1 ng/g for light elements. Analytical error was 1-3% rel. (one standard deviation). Element contents were calculated using standard solutions ICP-MS-68A, HPS (A and B) with known element concentrations.

Principle features of bulk rock compositions

Bulk rock compositions are given in Table 4. In the TAS diagram (Fig. 6a) the plutonic rock samples investigated fall into the field of gabbro and gabbroic

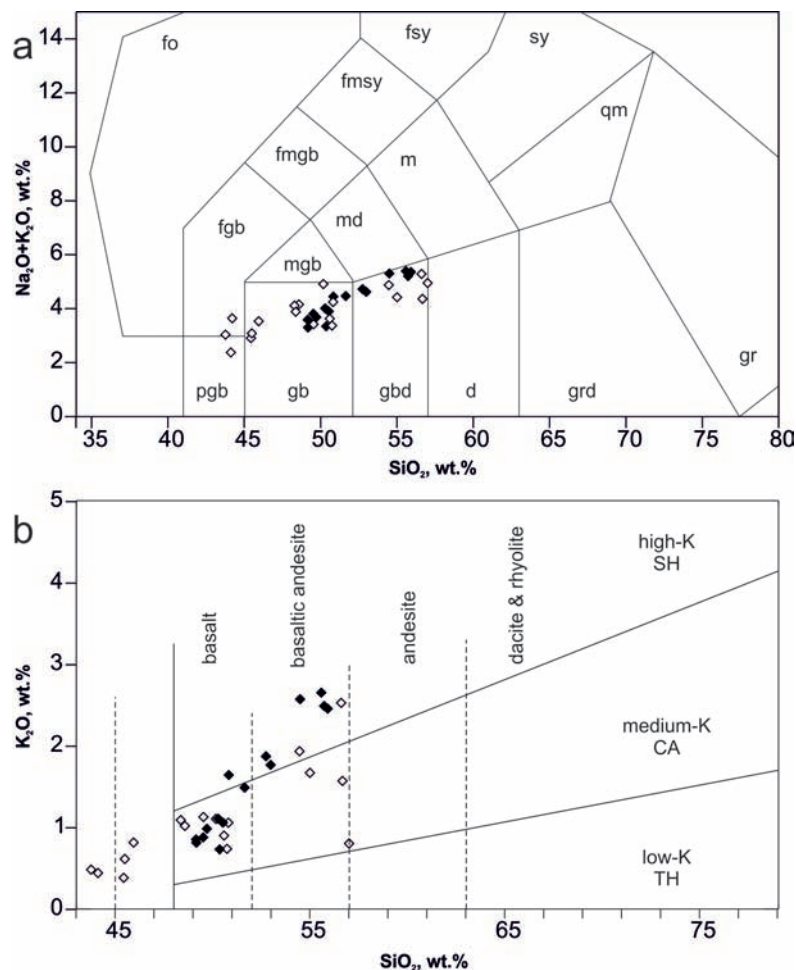


Fig. 6. Nomenclature of the rocks studied (open diamonds) and calculated melts (filled diamonds).

(a) TAS (total alkali, wt. % vs. SiO_2 , wt. %) diagram adopted for plutonic rocks (Middlemost, 1994). Acronyms are as follows: pgb – peridotgabbro; gb – gabbro; gbd – gabbroic diorite; d – diorite; grd – granodiorite; gr – granite; mgb – monzogabbro; md – monzodiorites; m – monzonite; qm – quartz monzonite; sy – syenite; fgb – foid gabbro; fmgb – foid monzogabbro; fmsy – foid monzosyenite; fsy – foid syenite; fo – foidotite.

(b) SiO_2 , wt. % vs. K_2O , wt. % diagram for volcanic rocks (LeMaitre et al., 1989) demonstrating series affinity of the melts calculated; actual rock compositions are shown for comparison.

Table 4. Bulk rock major and trace element compositions

	1	2	3	4	5	6	7	8	9
Sample	GY9-101	PS9-92	GY9-74	GY9-79	KE9-71	PS9-89	KE9-73	GY9-99	GY9-81
SiO ₂	49.25	48.59	42.55	43.94	45.03	47.21	44.61	42.08	46.83
TiO ₂	2.35	2.58	6.17	5.28	5.72	3.82	5.98	3.59	4.62
Al ₂ O ₃	13.38	13.77	11.34	11.53	12.87	12.69	12.49	10.43	11.87
FeO	12.79	13.31	18.33	16.82	16.43	15.77	17.11	21.53	17.55
MnO	0.171	0.168	0.214	0.208	0.222	0.203	0.229	0.221	0.215
MgO	6.00	4.66	6.14	6.13	5.12	4.90	5.13	8.36	3.75
CaO	9.50	8.64	9.26	9.70	8.82	8.18	9.13	6.52	7.74
Na ₂ O	2.55	3.68	2.48	2.44	2.66	3.05	2.42	1.84	2.70
K ₂ O	0.72	1.07	0.47	0.38	0.80	0.99	0.61	0.43	1.06
Cr ₂ O ₃	0.018	0.011	0.000	0.000	0.000	0.001	0.000	0.014	0.000
P ₂ O ₅	0.312	0.345	0.250	0.274	0.317	0.362	0.347	0.356	0.468
LOI	1.92	2.16	1.41	2.04	0.85	1.49	0.62	2.94	1.78
Sum	98.96	99.00	98.61	98.74	98.85	98.67	98.68	98.30	98.58
Rb	16	33	10	9	26	35	20	18	40
Ba	290	259	164	116	239	392	201	121	344
Th	2.14	2.83	1.71	1.92	2.01	2.74	2.03	2.90	3.14
U	0.68	0.78	0.56	0.62	0.67	0.88	0.70	0.79	0.97
Nb	14.7	16.2	17.8	17.2	20.4	18.9	20.9	22.5	27.6
Ta	0.66	0.77	1.19	1.00	1.12	1.09	1.07	1.21	1.44
La	18.5	22.0	15.4	16.5	18.3	21.2	18.1	26.7	28.9
Ce	43	51	37	39	44	50	43	64	68
Pb	5.84	2.11	4.09	4.31	3.84	2.80	2.98	1.31	8.33
Pr	5.8	6.7	4.9	5.3	5.9	6.6	5.8	8.3	8.9
Sr	306	172	245	291	249	316	224	72	338
Nd	27	30	23	25	28	31	27	38	41
Sm	6.5	7.4	5.9	6.3	7.0	7.5	6.8	9.3	9.8
Zr	116	91	139	117	207	179	209	126	248
Hf	3.2	2.8	3.8	3.7	5.5	5.0	5.4	3.6	6.5
Eu	2.09	2.22	1.94	1.92	2.20	2.30	2.20	2.19	3.08
Gd	7.3	8.1	6.6	7.0	7.8	8.3	7.6	10.1	11.0
Tb	1.25	1.39	1.16	1.22	1.37	1.45	1.33	1.71	1.87
Dy	7.3	8.1	7.0	7.3	8.1	8.5	7.9	10.1	11.1
Y	42	47	41	42	48	50	46	58	65
Ho	1.47	1.62	1.41	1.45	1.67	1.73	1.61	2.00	2.22
Er	4.3	4.8	4.1	4.2	4.9	5.0	4.7	5.8	6.5
Tm	0.58	0.65	0.56	0.58	0.68	0.69	0.66	0.77	0.89
Yb	3.7	4.2	3.8	3.5	4.5	4.6	4.3	4.8	5.9
Lu	0.50	0.60	0.49	0.46	0.67	0.66	0.63	0.65	0.84
V	396	391	833	754	658	618	727	495	416
Cr	235	209	11	14	13	61	16	233	14
Co	34	38	54	48	50	44	60	76	43
Ni	80	98	25	47	30	68	11	223	29
Cu	57	65	305	302	343	278	44	271	61
Zn	110	105	135	128	143	147	145	195	178

Table 4. (continued).

	10	11	12	13	14	15	16	17
Sample	GY9-102	PS9-90	GY9-76	GY9-82a	GY9-78	GY9-82b	GY9-87	GY9-84
SiO ₂	47.53	49.03	49.29	52.76	55.56	54.89	54.81	54.18
TiO ₂	3.38	3.24	4.31	2.91	2.56	2.63	2.26	2.55
Al ₂ O ₃	12.28	12.41	10.63	12.62	12.20	11.64	10.98	11.52
FeO	16.33	15.69	17.27	15.47	13.47	14.62	15.77	16.20
MnO	0.204	0.185	0.266	0.171	0.137	0.142	0.202	0.190
MgO	5.87	4.20	3.74	3.18	2.52	2.23	2.20	2.42
CaO	6.58	7.06	7.79	4.42	5.43	4.91	5.41	6.22
Na ₂ O	2.20	3.07	2.65	2.85	4.04	2.67	2.70	2.71
K ₂ O	1.09	1.03	0.88	1.88	0.79	2.46	1.52	1.65
Cr ₂ O ₃	0.006	0.005	0.000	0.002	0.000	0.000	0.000	0.001
P ₂ O ₅	0.481	0.551	0.584	0.601	0.744	0.773	0.857	0.856
LOI	2.72	2.17	1.20	1.73	1.43	1.64	1.80	0.00
Sum	98.66	98.64	98.61	98.60	98.88	98.61	98.51	98.50
Rb	50	34	38	63	28	61	45	40
Ba	377	624	250	799	196	853	438	572
Th	3.28	3.66	3.71	4.78	5.72	7.20	5.91	5.67
U	0.95	1.08	1.07	1.09	1.31	2.95	1.45	1.58
Nb	23.5	23.5	32.2	32.8	38.1	35.3	40.2	38.5
Ta	1.12	1.12	1.70	1.67	1.97	1.58	2.14	1.86
La	30.1	33.7	33.9	39.3	54.2	54.8	55.2	53.2
Ce	71	79	82	94	126	130	131	128
Pb	6.50	3.69	5.61	3.07	1.50	2.83	5.40	2.60
Pr	9.1	10.1	10.8	11.8	16.2	16.1	16.7	16.1
Sr	257	300	244	273	97	192	129	124
Nd	42	45	50	53	72	72	75	73
Sm	9.9	10.6	11.9	12.4	16.9	16.6	17.6	17.1
Zr	111	69	175	93	180	303	163	283
Hf	3.2	2.3	4.6	3.5	4.9	8.2	4.8	7.3
Eu	2.92	2.75	3.36	3.47	4.02	3.76	4.08	4.17
Gd	11.2	11.6	13.2	13.5	18.3	17.9	19.3	18.7
Tb	1.86	1.94	2.24	2.24	3.07	3.00	3.23	3.12
Dy	10.8	11.2	13.2	13.1	17.7	17.3	18.7	18.0
Y	64	66	78	78	104	104	110	108
Ho	2.14	2.24	2.62	2.61	3.53	3.45	3.71	3.58
Er	6.2	6.6	7.6	7.6	10.1	10.3	10.9	10.5
Tm	0.82	0.89	1.02	1.04	1.35	1.39	1.44	1.40
Yb	5.2	5.9	6.5	6.8	8.5	9.1	9.4	9.1
Lu	0.69	0.85	0.91	0.97	1.15	1.31	1.35	1.30
V	491	417	197	227	136	126	46	96
Cr	94	83	16	56	38	43	23	33
Co	44	40	35	31	26	31	23	27
Ni	60	51	7	40	23	38	34	35
Cu	169	112	19	56	6	7	16	26
Zn	239	128	200	111	66	107	217	171

diorite. All rock varieties follow a trend of simultaneous increase of silica and total alkali elements and belong to a moderate alkaline series. In binary diagrams (Fig. 7) gabbro and gabbroic diorite of the Anyui province of eastern Chukotka form linear and gently curved trends. The mg# of rock samples range from 19.4 to 38.1 and decreases from gabbro to gabbroic diorite. As mg# of gabbro and gabbroic diorite decreases, contents of Al_2O_3 and CaO decrease, concentrations of P_2O_5 increase and abundances of TiO_2 remain nearly constant. In contrast, Fe-Ti gabbro exhibit irregular variations and lie out of the trends in the plots for Al_2O_3 and TiO_2 .

In multi-element diagrams (Fig. 8), the gabbro, Fe-Ti gabbro and gabbroic diorite show spectra, which are principally similar in shape. The spectra reveal a relative enrichment of all investigated rocks

in more incompatible lithophile elements (such as Th, U, light REE) relative to less incompatible ones (such as Y and heavy REE). Contents of lithophile elements gradually increase from gabbro to gabbroic diorite; the Fe-Ti gabbro has trace-element contents similar to that of the gabbro or intermediate between the gabbro and gabbroic diorite. The rocks exhibit negative anomalies of Nb-Ta, Zr-Hf, Sr and P. The anomalies of Zr-Hf are very small or almost negligible in some samples of Fe-Ti gabbro and gabbroic diorite. A titanium anomaly is negligible in gabbro; it becomes positive in some Fe-Ti gabbro and negative in gabbroic diorite.

BULK ROCK SM-ND ISOTOPE COMPOSITIONS

Neodymium and strontium isotopic measure-

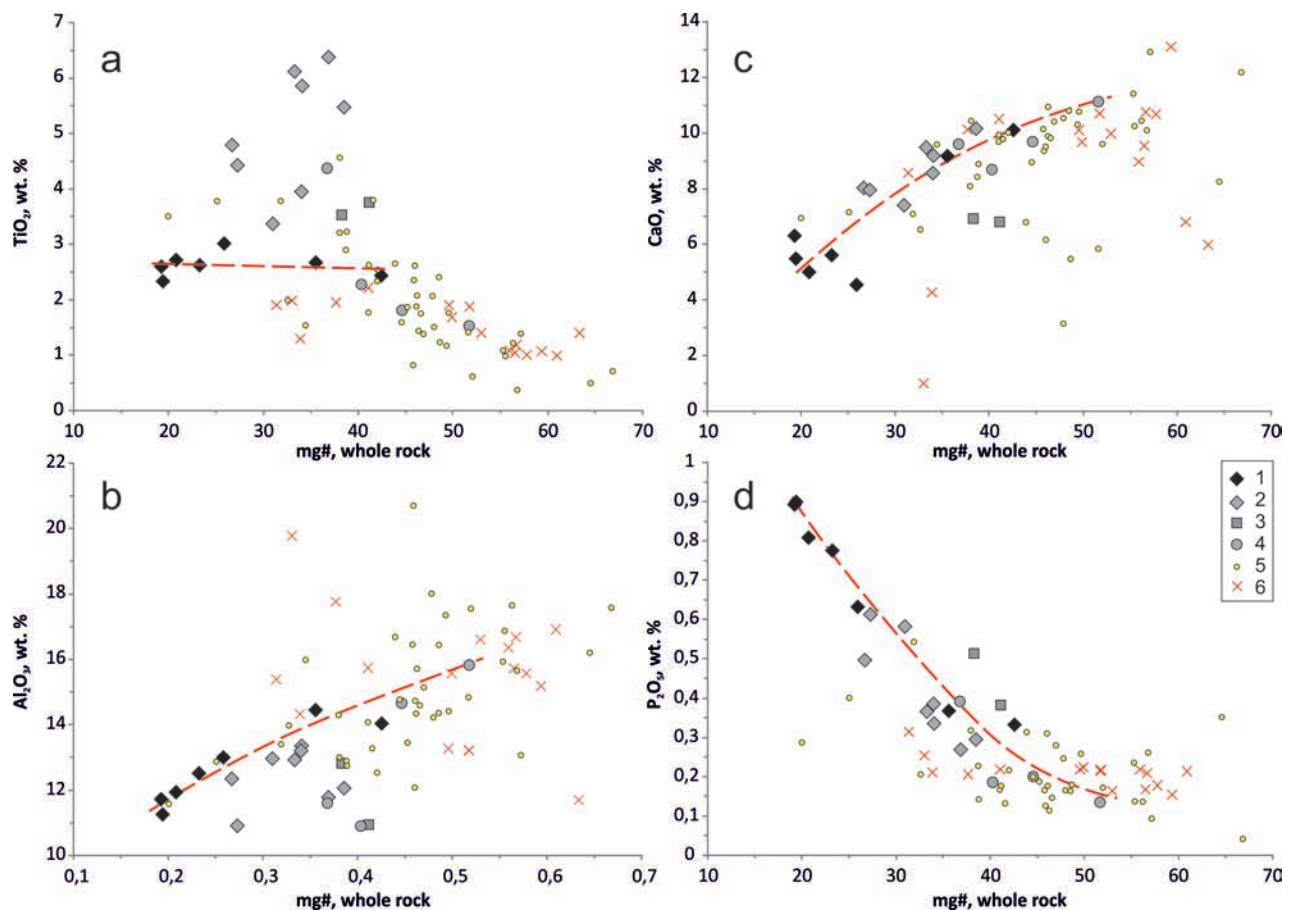


Fig. 7. Mg#, whole rock vs. oxide, wt. % diagrams. The original data are compared with those published on the Bilibino and Cape Schmidt areas (Gel'man, 1963; Degtyaryov, 1975) and the New Siberian Islands (Kuz'michov and Pease, 2007). Symbols 1 to 5 are for the Anyui province of Chukotka: gabbro and gabbroic diorite studied (1); Fe-Ti gabbro studied (2); investigated Fe-Ti gabbro with significant admixture of silicate phases or strongly allochemically metamorphosed (3); gabbroic rocks of the Kolyuchinskaya Bay (4); diabase and gabbro from the vicinities of Bilibino and Cape Schmidt (5). Dolerite of the New Siberian Islands (6).

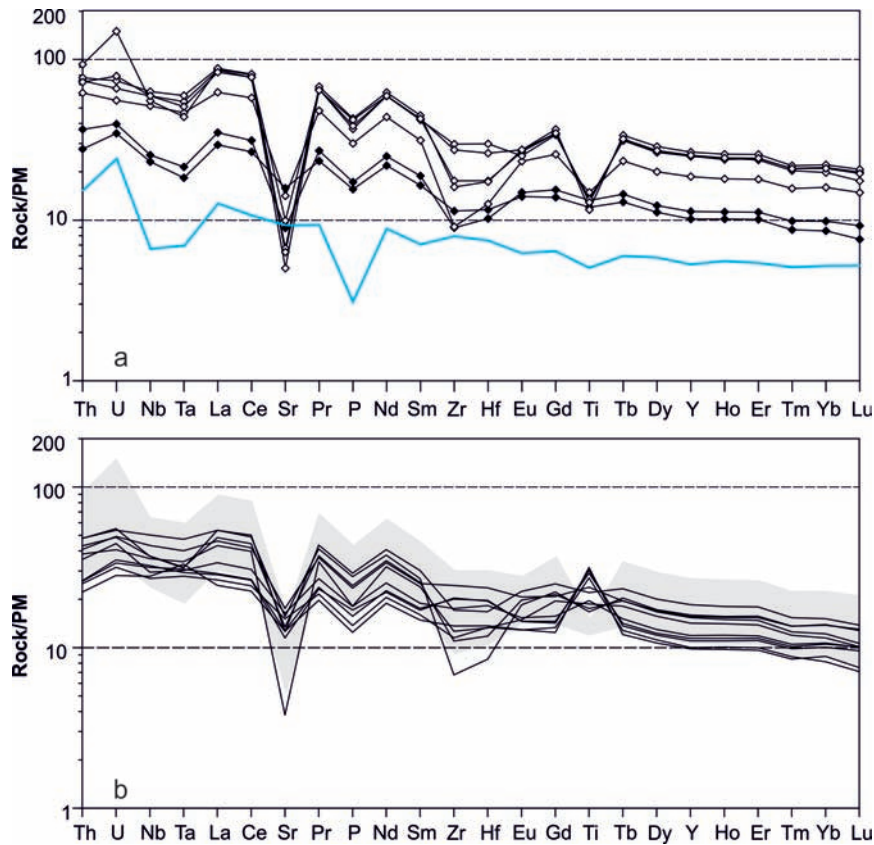


Fig. 8. Multi-element diagrams of primitive mantle (PM) normalized (Sun and McDonough, 1989) trace elements of the Anyui province gabbroic rocks. For comparison the averaged spectrum of the most basalts of the trap stage of the Siberian LIP (data from Krivolutsкая, 2013) is shown. **(a)** gabbro (filled diamonds) and gabbroic diorites (open diamonds) probably free of the admixed cumulative Fe-Ti oxides; **(b)** Fe-Ti gabbro in the comparison with gabbro and gabbroic diorite (the grey field).

ments were performed at the Geological Institute of the Kola Research Center of the Russian Academy of Sciences, Apatity, Russia with a Finnigan MAT-262 (RPQ) seven channel mass spectrometer employing the method described in detail by Bayanova (2004). During the course of measurements, the laboratory blank was lower than 0.3 ng Nd and 0.06 ng Sm. The international standard (La Jolla) gave ratios of $^{143}\text{Nd}/^{144}\text{Nd} = 0.511851 \pm 17$ ($N=20$). The uncertainty of the $^{147}\text{Sm}/^{144}\text{Nd}$ ratio was calculated from twenty measurements of Sm and Nd concentrations in the BCR-1 standard as 0.2% (2σ). The measured Nd isotopic ratios were normalized to $^{148}\text{Nd}/^{144}\text{Nd} = 0.241570$ and then adjusted to the value $^{143}\text{Nd}/^{144}\text{Nd} = 0.511860$ in the La Jolla standard. The decay constants were taken from Steiger and Jaeger (1977).

Results of the Sm-Nd isotope investigations

Results of Sm-Nd isotope measurements are

presented in Table 5. The gabbro, Fe-Ti gabbro and gabbroic diorite of the Anyui province of eastern Chukotka display positive $\epsilon\text{Nd}(t=252 \text{ Ma})$ ranging from +2.8 to +1.2. ϵNd values are well correlated with MgO contents for rocks from the areas of the Gytgyl'ven pass and Ploskaya River in western Chukotka and are lowered as MgO decreases (Fig. 9).

INTERPRETATION OF $^{40}\text{Ar}/^{39}\text{Ar}$ AGES

Sample GY9-87, gabbroic diorite of the Anyui dike-and-sill province, contains hornblende whose composition (Table 3, column 41) is close to a magmatic composition of this mineral. Despite this, the late Triassic $^{40}\text{Ar}/^{39}\text{Ar}$ plateau age of this hornblende can be hardly regarded as the time of rock crystallization. The gabbroic rocks of the Anyui province (including the sample studied) are not younger than the Early-Middle Triassic as they are folded and metamorphosed together with Permo-

Table 5. Sm-Nd isotopic composition of plutonic rocks of the Anyui province

Sample	Sm, ppm	Nd, ppm	$^{147}\text{Sm}/^{144}\text{Nd}$	$^{143}\text{Nd}/^{144}\text{Nd}$	Err	$\epsilon\text{Nd}(t=252\text{ Ma})$
GY9-101	6.479	26.236	0.149257	0.512662	0.000007	2.2
GY9-74	6.179	24.204	0.154296	0.512702	0.000004	2.8
GY9-76	12.810	51.699	0.149769	0.512638	0.000012	1.7
GY9-82a	12.899	54.411	0.143289	0.512662	0.000021	2.4
GY9-87	18.685	76.994	0.146686	0.512604	0.000008	1.2
KE9-73	6.726	26.280	0.154700	0.512642	0.000016	1.6
KE9-71	7.172	28.155	0.153968	0.512621	0.000008	1.2
PS9-89	7.928	31.920	0.150115	0.512664	0.000007	2.2
PS9-90	10.998	46.800	0.142047	0.512635	0.000007	2.0
PS9-92	7.561	30.884	0.147980	0.512663	0.000005	2.3

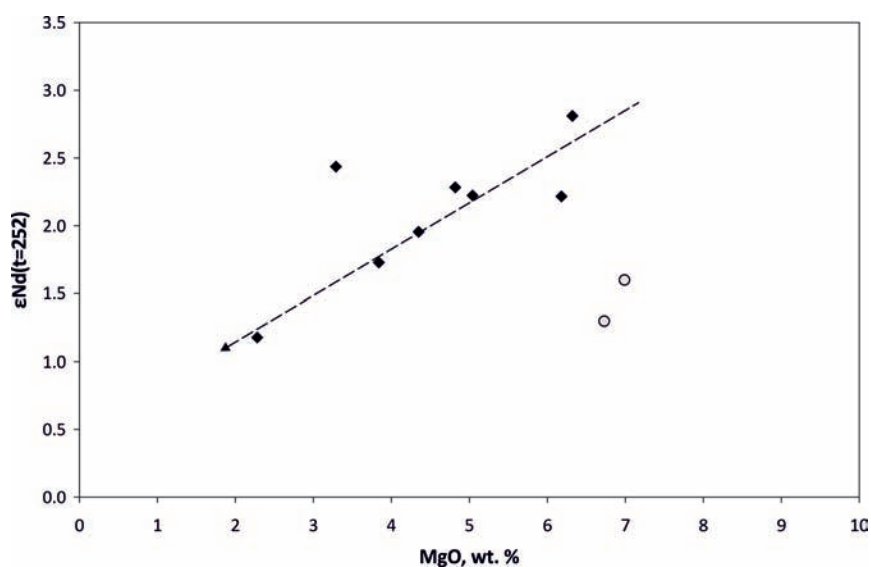


Fig. 9. MgO, wt. % vs. $\epsilon\text{Nd}(t=252\text{ Ma})$ plot for rocks of the Anyui province of eastern Chukotka. Symbols correspond to gabbroic rocks of the Gytgyl'ven pass and Ploskaya River domains (black diamond) and the Kolyuchinskaya Bay domain (grey circle). Sm-Nd data for the Kolyuchinskaya Bay area are from Ledneva, et al. (2011).

Triassic and Early-Middle Triassic strata hosting them, and they do not intrude Late Triassic and younger deposits. In general, $^{40}\text{Ar}/^{39}\text{Ar}$ plateau age of $218.3 \pm 5.2\text{ Ma}$ (Norian) might be considered as the cooling age of the gabbro to a temperature of $\sim 500 \pm 50^\circ\text{C}$, e.g. an argon closure temperature in hornblende (McDougall and Harrison, 1999). An alternative interpretation is the resetting of the argon isotope system in the hornblende without influencing its major-element composition.

In sample PS9-89 of gabbro, the primary

hornblende is preserved only as a relict mineral (Table 3, column 46), and it is largely replaced by actinolite. The $^{40}\text{Ar}/^{39}\text{Ar}$ plateau age of $167.8 \pm 11.2\text{ Ma}$ (Middle Jurassic) might therefore reflect an argon system reset during a metamorphic event. Igneous zircons from this sample yielded U-Pb LA-ICPMS age corresponding to the Middle Triassic (V.L. Pease, personal comm.).

The confines of the Anyui province rocks to Permo-Triassic and lower-middle Triassic shelf sediments of Chukotka, joint deformations of

dikes and sills with hosting them strata and U-Pb TIMS age of igneous zircons from gabbro of the Kolyuchinskaya Bay indicate that gabbroic rocks of the Anyui dike-and-sill province are Permo-Triassic to Early-Middle Triassic in age. The upper Triassic $^{40}\text{Ar}/^{39}\text{Ar}$ plateau age (218.3 ± 5.2 Ma) of hornblende is correlated with Norian magmatism which is recorded in basaltic lavas and gabbroic diorite sills (Tynankergav and Bychkov, 1987; V.L. Pease, personal comm.) of the Vel'may terrane. The tabular body dated is too thin (about 30 meters thick) to cool slowly. So we suggest that the Norian age of hornblende probably reflects a thermal event that resulted in the resetting of the argon isotope system in hornblende without influencing its major-element composition. We are unable to distinguish whether rocks of the Anyui province originated in a single or several magmatic episodes, and we assume that the studied rocks of eastern Chukotka to be coeval to each other.

PETROLOGICAL AND GEOCHEMICAL INTERPRETATIONS

An interpretation of the mineralogical data

In mg# vs. major-element oxide, wt. % plots for clinopyroxene and hornblende (Fig. 4 and 5) compositions of the minerals display linear trends. This might be indicative of a cogenetic nature of gabbro, Fe-Ti gabbro and gabbroic diorite from different bodies of the Anyui province because of the following. Abundances of both clinopyroxene and hornblende in alumina are generally sensitive to a pressure of magma crystallization. In binary diagrams, the hornblende studied follows a linear trend. This suggests crystallization of gabbro, Fe-Ti gabbro and gabbroic diorite from different tabular bodies at similar pressure or depth, which is consistent with pressure estimates as discussed below. Augite is characterized by two levels of alumina abundances (1.14-2.09 and 3.02-3.63 wt. %, Al_2O_3). Low-Al augite occurs in all samples (the only exclusion is the sample PS9-92) and forms a continuous trend of Al_2O_3 decrease with mg# decrease. This suggests a primary magmatic nature of low-Al augite and its crystallization along with plagioclase at a similar pressure in different bodies. Augite showing moderate alumina contents (samples PS9-89 and PS9-92 from the same tabular body, P-11-7a) occurs

in the body whose rocks contain low-Al augite as well. Augites with higher Al_2O_3 contents probably crystallized at a deeper level while augites with lower Al_2O_3 contents probably originated in situ in tabular bodies.

Abundances of clinopyroxene in titanium and sodium and of hornblende in titanium and potassium depend on the composition of (parent magma) equilibrium melt (e.g. Zlobin and Zakariadze, 1993) and P-T parameters of crystallization. In low-Al augite, TiO_2 contents decrease as mg# decreases. In hornblende, TiO_2 and K_2O contents slightly increase as its mg# decrease. These binary diagrams show that low-Al augite of rocks from different bodies form one trend. This is also true for hornblende. Using the mg# of the minerals as a measure of a magma differentiation degree, we conclude that different bodies were probably originated from portions of variably differentiated magmas derived from some initial melts similar in titanium, sodium and potassium contents, and crystallization of these magmas in situ took place at similar pressure and temperature conditions.

Conditions of crystallization

Pressures of rock crystallization are estimated by aluminum-in-hornblende geobarometer of Schmidt (1992) and range from 1.2 to 3.4 kbar. Pressures calculated by aluminum-in-hornblende geobarometer of Ridolfi, et al. (2009) are 0.9 ± 0.2 kbar. Although the geobarometer of Schmidt is calibrated for clinopyroxene-free assemblages and the geobarometer of Ridolfi, et al. (2009) is calibrated for volcanic hornblendes, close similarity of calculated pressures suggests that the studied rocks crystallized at very low pressures.

Equilibrium temperature for augite-pigeonite pairs (in samples KE9-73 and T-05-5) was calculated using the QUILF program (Anderson, et al., 1993) and corresponds to about $900-910(\pm 20)^\circ\text{C}$ and $840-860(\pm 50)^\circ\text{C}$ for core and rim pyroxene compositions at a pressure of 2 kbar. Temperatures of primary hornblende crystallization are estimated based on the equation of Ridolfi, et al. (2009) and vary from 710 to 780°C . In one of the samples (GY9-82a) we also estimated equilibrium temperature of coexisting hornblende with mg# of 34.2 and oligoclase with $\text{xAn}_{22.6}$ composing outer rims of grains in

contact using the geothermometer of Holland and Blundy (1984). The estimated temperature is about 720°C (for 2 kbar). A large interval of equilibrium temperatures in a single sample reflects a relatively fast rock cooling and is consistent with their crystallization at the low pressure.

An oxygen fugacity estimated by the method of Ridolfi, et al. (2009) varies from -13.2 to -15.1 which correspond to $\Delta\text{NNO}+0.4$ to $\Delta\text{NNO}+1.1$. H_2O contents in melts coexisting with hornblendes are estimated at 3.3-5.7 wt. % (Ridolfi, et al., 2009). These results are not very reliable as this calibration is proposed only for hornblendes from subduction-related lavas.

All these estimations are related to the stage of in situ rock crystallization. Crystallization at a deeper level can be inferred from the fact that rocks composing different bodies are variably differentiated and there are no signs of in situ fractionation. A pressure for the previous crystallization stage can be roughly evaluated from composition of clinopyroxenes with elevated Al_2O_3 contents (Fig. 4); estimations by the method of (Putirka, 2008) give a pressure of 4 ± 2 kbar.

Imprints of admixed cumulative minerals

The rocks studied show a strong correlation of immobile incompatible trace elements (REE, P, Nb) both with each other and with some major elements (Si, Al, Mg) as well. This suggests that rock compositions are generally similar to the compositions of the melts, and an admixture of cumulate minerals is moderate. However, it was not negligible for most of rocks. This is demonstrated by evidently elevated contents of Ti, Fe, V, which are correlated with each other but are not correlated with contents of other elements. These covariations suggest a variable amount of cumulate Fe-Ti oxide grains suspended in the melts.

Admixed cumulate Fe-Ti oxides in bulk rocks can be predicted based on comparison of titanium and REE contents. Among REE titanium has bulk distribution coefficient (a restite or cumulate to a melt) similar to Dy and Gd which is obvious from Ti/Gd and Ti/Dy ratios. These ratios are similar in different primitive mantle-derived melts (N-MORB, E-MORB and subduction melts), primitive ultramafic and mafic cumulates and in mantle sources (Sun and

McDonough, 1989; Hofmann, 1988; Kelemen, et al., 2003). These elements behave similarly during both mantle melting and melt fractionation (in the absence of Fe-Ti oxides) and normalized to primitive mantle ratio of $(\text{Ti}/\text{Gd})_N$ and $(\text{Ti}/\text{Dy})_N$ is ~ 1 in both melts and cumulates. Fe-Ti oxides will fractionate this ratio and an addition of cumulate Fe-Ti oxides will raise this ratio ($(\text{Ti}/\text{Gd})_N > 1$, $(\text{Ti}/\text{Dy})_N > 1$), while an extraction of Fe-Ti oxides will lower the ratio ($(\text{Ti}/\text{Gd})_N < 1$, $(\text{Ti}/\text{Dy})_N < 1$) (Kelemen, et al., 2003). Thus, Gd vs. TiO_2 plot can be useful to separate effects of Fe-Ti oxides addition and extraction to melts. However, Gd contents in rocks are affected with an addition of Fe-Ti oxides while the Gd/SiO_2 ratio remains constant. In Gd/SiO_2 vs. $\text{TiO}_2/\text{SiO}_2$ diagram (Fig. 10) bulk compositions of rocks with the lowest TiO_2 concentrations form trend that probably reflects evolution of melt saturated in Fe-Ti oxides. At initial stages of crystallization (before melt saturation in Fe-Ti oxides) melt compositions probably evolve along the line corresponding to $(\text{Ti}/\text{Gd})_N = 1$. Rock samples plotting above these trends are interpreted to be a mixture of melt and cumulative Fe-Ti oxides.

The amount of these phases can be evaluated from the quantity of excess Ti and Fe over the level

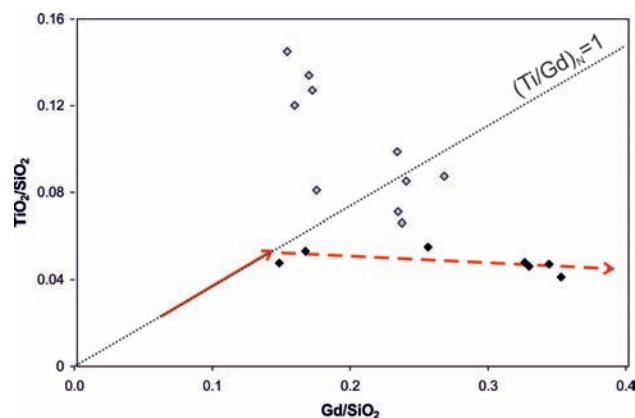


Fig. 10. Covariations of Gd and TiO_2 in bulk rocks. Contents of Gd (ppm) and TiO_2 (wt. %) are normalized to SiO_2 (wt. %). Black diamond is the symbol for the gabbro and gabbroic diorite with the lowest TiO_2 contents; grey diamond is the symbol the Fe-Ti gabbro. The solid arrow corresponds to a probable melt evolution before melt saturation in Fe-Ti oxides; the dashed arrow shows probable melt evolution after melt saturation in Fe-Ti oxides. The excess of titanium in the Fe-Ti gabbro relative to the level of melt saturation in Fe-Ti oxides is attributed to various amounts of admixed cumulative Fe-Ti oxides in the rocks.

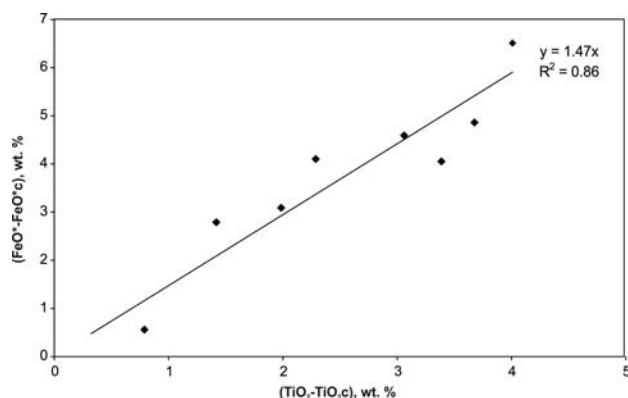


Fig. 11. Correlation of excess amounts of TiO_2 and FeO^* in the Fe-Ti gabbro demonstrating nearly constant ratio of Ti-magnetite/ilmenite in cumulate Fe-Ti oxides.

of melt saturation in respect to these elements (see Appendix for details of calculations). In the Fe-Ti gabbros studied, the excess quantities of Ti and Fe display a good correlation (Fig. 11), which indicates FeO/TiO_2 value of 1.47. This value corresponds to Ti-magnetite/ilmenite ratio of 0.3/0.7 in the rocks (if the average compositions of these minerals are used), which is supported by petrographic observations.

Some rocks studied show chemical imprints of a possible addition not only of Fe-Ti oxides but also of cumulative silicate phases. Samples GY9-99 and GY9-102 display anomalously high MgO contents that can be attributed to significant amounts of cumulative magnesium clinopyroxenes or orthopyroxenes. Samples GY9-99, PS9-92 and GY9-101 have slightly elevated bulk-rock Cr contents, which can be indicative of admixture of pyroxenes with detectable Cr contents (Table 3). However, we cannot numerically estimate the quantity of cumulative silicates in these rocks as we don't know the composition of admixed cumulative minerals.

Mobility of elements due to metamorphism

Bulk rock compositions were modified due to metamorphism. This is evident from comparison of contents of alkali elements, Ba and Ca with both contents of immobile incompatible elements and contents of major elements (Si, Al, P) (Fig. 12). Metamorphic replacements of biotite suggest the potassium loss. Relicts of primary biotite are preserved only in the freshest samples and its metamorphism does not usually result in potassium-

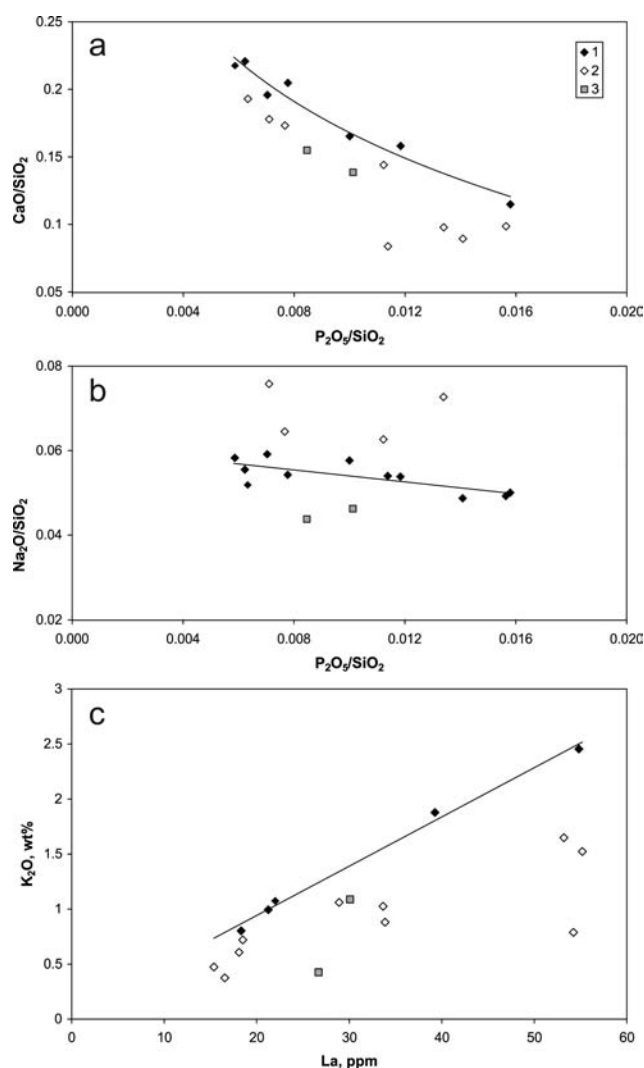


Fig. 12. The diagrams demonstrating the loss of calcium (a), gain of sodium (b) and loss of potassium (c) during metamorphic alteration of rocks. Black diamond (1) corresponds to the rocks probably characterized by primary element abundances; open diamonds (2) are allochemically (in respect to a considered element) metamorphosed rocks; grey squares (3) are rocks with significant admixture of silicate phases or strongly allochemically metamorphosed.

rich minerals. Stilpnomelane after biotite, which contains a much lower potassium contents, is rather rare and was found only in a few samples. Clinopyroxene replacement by secondary amphibole and plagioclase replacement by albite, which are common in the rocks studied, suggest the likelihood of calcium loss. Thus, potassium contents close to original (e.g. existed prior to metamorphism) concentrations of this element in rocks are expected to remain only in samples with the highest ratios of potassium to high incompatible elements such

as K/La. Calcium contents close to its original concentrations in rocks are expected in samples with the highest ratios of calcium to moderate incompatible or moderate compatible immobile elements such as CaO/SiO_2 and $\text{CaO}/\text{Al}_2\text{O}_3$. Sodium behavior is not clear from petrography. As various binary correlations indicate, sodium contents in most of the rocks are close to its original concentrations. Only a few samples have elevated sodium concentrations; which can be attributed to plagioclase albitization. In several rocks studied, Ca, K, Rb, Ba (and probably Sr) were removed and Na was added during metamorphism. In general, this tendency is typical for sea-floor spilitization. Hence, the contents of alkali elements and Ca in the rocks should be corrected to reconstruct original rock compositions prior to metamorphism that should be used for evaluation of the modal mineral modes of the rocks and a correct rock chemical and mineralogical classification.

Primary bulk rock chemical and modal mineral compositions

The original contents of calcium, sodium and potassium in the rocks were evaluated using a set of binary element correlations of the same type as demonstrated in the Appendix. For mineral mode calculations, the real mineral compositions (averaged or generalized) (Table 3) were used. The calculations were performed by the least square sum minimization procedure for optimization using a difference between real and calculated oxide contents normalized to the probable value of the integrated analytical uncertainty (both XRF for bulk rock and electron microprobe for minerals). In the calculations, wt. % contents of SiO_2 , TiO_2 , Al_2O_3 , $\text{FeO}_{\text{total}}$, MgO , CaO , Na_2O , K_2O and P_2O_5 were used. In order to make the calculations some assumptions were required. Fe-Ti oxides were treated as a single phase with a composition reflecting the Ti-magnetite/ilmenite ratio of 0.3/0.7. Pigeonite and orthopyroxene were excluded from the calculations (based on their scarcity in the rocks studied). Instead of using both the compositions of anorthoclase and probable igneous orthoclase, an average composition of pure orthoclase was used. To choose compositions of clinopyroxene and biotite for each sample, we used correlations between measured compositions

of these minerals and wt. % MgO in the bulk rock. Integral composition of plagioclase in the rocks was estimated from relative quantities of xAn-rich and xAn-poor plagioclase that were used in calculations as distinct phases. Optimization was reached by varying the integral hornblende composition (along the trend demonstrated by real compositions). The results of calculations are presented in Table 6.

These data are consistent both with real assemblages of primary minerals in the rocks and with measured compositions of hornblende and plagioclase (where they were analyzed). As demonstrated in Table 6, the content of clinopyroxene is below 10% in gabbro and mainly below 5% in gabbroic diorites. The amount of Fe-Ti oxides is 3.5-5.2 % in gabbro and gabbroic diorite, and 6.0-14.2 % in Fe-Ti gabbro. Contents of orthoclase are below 4 % in gabbro and 5-9 % in gabbroic diorite. Contents of biotite are below 10 % in gabbro and 5-13% in gabbroic diorites.

Calculation of melt compositions

The procedure of reconstruction of original calcium, sodium and potassium contents in the rocks prior to metamorphism is a first step to approach probable melt composition for the rocks studied. The second step is eliminating the influence of cumulative Fe-Ti oxides on the bulk composition of Fe-Ti gabbro. To do this, we used a set of binary correlations of iron, titanium, manganese, vanadium and niobium (i.e. components showing elevated contents in the Fe-Ti gabbro relative to the gabbro and gabbroic diorite low in titanium) with both major oxides (SiO_2 , Al_2O_3 , MgO) and immobile trace elements in rocks which were probably free of cumulative Fe-Ti oxides (i.e. gabbro and gabbroic diorite). The results of these calculations are shown in Table 7 (see Appendix for details of the calculations) demonstrate a similarity of probable melt compositions calculated for gabbro, gabbroic diorite and Fe-Ti gabbro (Fig. 6 and 13). The resulting calculations for samples GY9-99 and GY9-102 do not correspond to melt compositions, probably because these rocks contain abundant cumulative silicate minerals or underwent loss/gain not only CaO , Na_2O and K_2O but other major elements as well.

Despite this, the calculations for the Fe-Ti

Table 6. Calculated modal mineral composition of the rocks (wt. %) and integral average compositions of hornblende and plagioclase

#	Sample	Rock group	Rock (QAPF)	Cpx	Hbl	Bi	Pl	Ksp	FTO	Qtz	Ap	Mg# Hbl	xAn Pl
1	GY9-74	FTG	D	5.6	47.7	1.8	29.7	0.4	14.2	0.0	0.6	50	48
2	GY9-79	FTG	D	9.5	43.8	1.8	30.6	1.0	12.0	0.7	0.7	49	49
3	GY9-101	G	Qtz G	6.1	45.7	2.6	35.6	1.1	4.2	4.0	0.8	50	54
4	KE9-71	FTG	Qtz D	2.5	41.5	2.1	35.8	1.0	13.2	3.0	0.8	51	49
5	PS9-92	G	Qtz D	4.3	42.0	3.5	38.4	1.8	4.9	4.2	0.9	44	48
6	PS9-89	FTG	Qtz D	2.2	47.5	2.4	33.3	1.6	8.0	4.0	0.9	44	48
7	KE9-73	FTG	Qtz G	5.2	39.4	2.7	33.4	1.4	13.7	3.3	0.9	49	52
8	GY9-102*	FTG	Qtz G	2.0	48.6	8.3	27.6	1.2	6.1	4.8	1.2	47	55
9	GY9-81	FTG	Qtz D	2.0	41.9	5.7	31.1	2.0	9.9	6.2	1.3	37	39
10	PS9-90	FTG	Qtz D	4.8	37.7	9.5	32.2	1.6	6.0	6.8	1.5	38	40
11	GY9-82a	D	Qtz MD	1.7	39.0	6.4	31.5	4.7	5.2	9.9	1.6	32	36
12	GY9-76	FTG	Qtz MD	8.4	36.4	5.7	26.8	4.0	9.0	8.1	1.6	33	29
13	GY9-78	D	Qtz MD	3.7	31.1	5.5	30.4	9.3	4.7	13.2	2.1	30	28
14	GY9-82b	D	Qtz MD	1.8	32.3	8.0	27.7	7.9	4.7	15.2	2.2	26	28
15	GY9-84	D	GD	1.5	32.4	13.5	26.6	5.2	4.0	14.3	2.4	26	24
16	GY9-87	D	GD	3.5	31.7	12.0	25.2	6.6	3.4	15.1	2.5	23	19

Notes: FTG – Fe-Ti gabbro, G – gabbro, D – diorite, B – basalt, Rock (QAPF) corresponds to the rock named in accordance with the QAPF nomenclature of plutonic rocks (Streckeisen, 1974, 1976). Qtz G – quartz gabbro, Qtz D – quartz diorite, Qtz MD – quartz monzodiorite, GD – granodiorite. For mineral abbreviations see the caption to Figure 3. * is rocks containing cumulative silicate minerals.

Table 7. Calculated melt compositions

#	1	2	3	4	5	6	7
Sample	GY9-101	PS9-92	GY9-74	GY9-79	KE9-71	PS9-89	KE9-73
Rock	G	G	FTG	FTG	FTG	FTG	FTG
Melt	Bas	Bas	Bas	Bas	Bas	Bas	Bas
SiO ₂	50.37	50.30	48.99	49.16	49.75	50.54	49.72
TiO ₂	2.40	2.67	2.49	2.48	2.58	2.58	2.56
Al ₂ O ₃	13.68	14.25	13.06	12.89	14.22	13.59	13.92
FeO	13.08	13.78	13.61	13.68	13.68	13.89	13.65
MnO	0.175	0.174	0.166	0.178	0.178	0.176	0.182
MgO	6.13	4.83	7.07	6.86	5.66	5.25	5.71
CaO	10.47	9.61	10.66	10.85	9.74	9.69	10.18
Na ₂ O	2.61	2.90	2.86	2.73	2.94	2.84	2.70
K ₂ O	0.74	1.11	0.82	0.86	0.89	1.06	0.99
Cr ₂ O ₃	0.019	0.012	0.000	0.000	0.000	0.002	0.000
P ₂ O ₅	0.319	0.357	0.287	0.306	0.350	0.387	0.387
Sum	100.00	100.00	100.00	100.00	100.00	100.00	100.00
Mg#	45.5	38.4	48.1	47.2	42.5	40.2	42.7

Table 7. (continued).

#	8	9	10	11	12	13	14
Sample	GY9-99*	GY9-81	GY9-102*	PS9-90	GY9-76	GY9-82a	GY9-78
Rock	FTG	FTG	FTG	FTG	FTG	D	D
Melt		Bas		Bas	AB	AB	AB
SiO ₂	44.21	51.66	48.31	50.85	53.00	52.75	55.96
TiO ₂	<u>2.18</u>	<u>2.58</u>	<u>2.42</u>	<u>2.54</u>	<u>2.50</u>	2.90	2.58
Al ₂ O ₃	10.96	13.10	12.48	12.88	11.44	12.62	12.29
FeO	<u>18.91</u>	<u>14.84</u>	<u>16.61</u>	<u>15.70</u>	<u>15.25</u>	15.47	13.57
MnO	<u>0.141</u>	<u>0.174</u>	<u>0.164</u>	<u>0.173</u>	<u>0.171</u>	0.171	0.138
MgO	8.78	4.13	5.97	4.35	4.02	3.18	2.53
CaO	<u>10.78</u>	8.53	<u>9.45</u>	<u>8.49</u>	8.38	<u>7.58</u>	<u>6.82</u>
Na ₂ O	2.40	2.98	2.68	<u>2.80</u>	2.85	2.85	<u>2.90</u>
K ₂ O	<u>1.24</u>	<u>1.49</u>	<u>1.43</u>	<u>1.65</u>	<u>1.77</u>	1.88	<u>2.46</u>
Cr ₂ O ₃	0.015	0.000	0.006	0.005	0.000	0.002	0.000
P ₂ O ₅	0.374	0.517	0.489	0.571	0.628	0.600	0.749
Sum	100.00	100.00	100.00	100.00	100.00	100.00	100.00
Mg#	45.3	33.2	39.0	33.1	32.0	26.8	25.0

Table 7. (continued).

#	15	16	17
Sample	GY9-82b	GY9-87	GY9-84
Rock	D	D	D
Melt	AB	AB	AB
SiO ₂	55.76	55.58	54.50
TiO ₂	2.67	2.29	2.57
Al ₂ O ₃	11.83	11.13	11.58
FeO	14.85	16.00	16.29
MnO	0.144	0.205	0.192
MgO	2.27	2.23	2.44
CaO	<u>6.47</u>	<u>6.29</u>	6.26
Na ₂ O	2.72	2.74	2.73
K ₂ O	2.49	<u>2.66</u>	<u>2.58</u>
Cr ₂ O ₃	0.000	0.000	0.001
P ₂ O ₅	0.785	0.870	0.861
Sum	100.00	100.00	100.00
Mg#	21.4	19.9	21.0

Notes: Corrected values are underlined. * is samples probably containing cumulative silicates along with Fe-Ti oxides, contents of FeO* and CaO in melts are poorly constrained. Bas – melts of the basaltic composition, AB – melts of basaltic andesitic composition. See Appendix for the details of calculations.

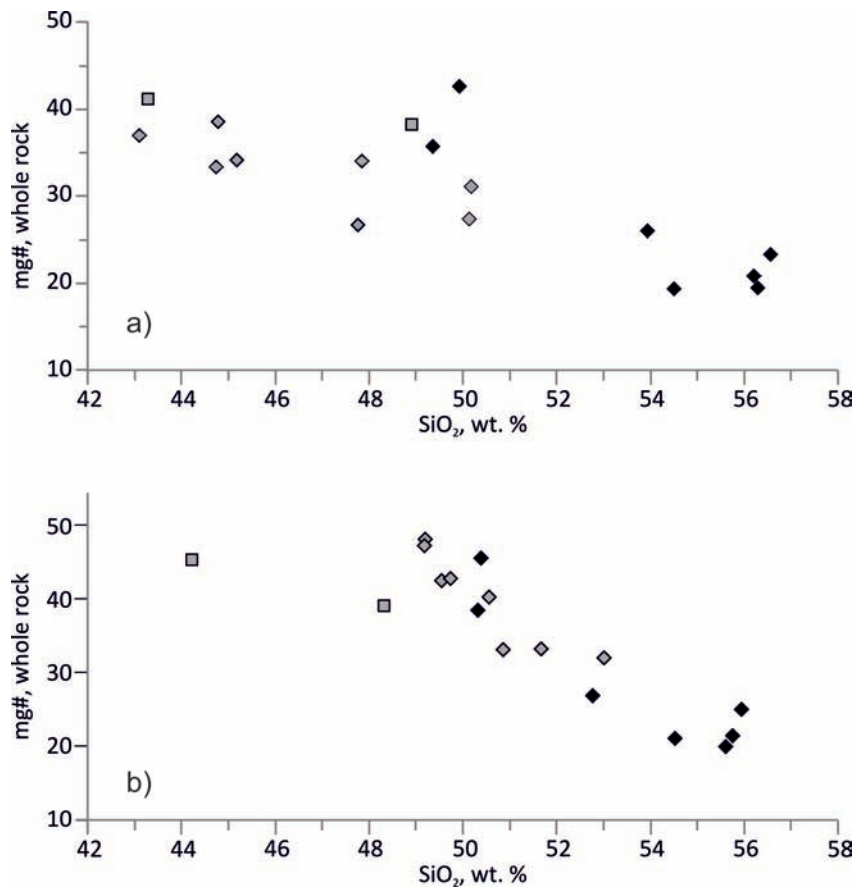


Fig. 13. SiO₂ vs. mg# of whole rocks (a) and SiO₂ vs. mg# of calculated melts (b) for rocks of the Anyui province of eastern Chukotka. Black diamond (1) corresponds to the gabbro and gabbroic diorite; grey diamond (2) is the Fe-Ti gabbro; grey square (3) is rocks with significant admixture of silicate phases or strongly allochemically metamorphosed.

gabbro excess contents of manganese, vanadium and niobium demonstrate good correlation with excess content of titanium. This is in accordance with assumption that contents of these elements in bulk rocks are influenced by admixed cumulative Fe-Ti oxides. It can be inferred from these correlations that the content of MnO in the bulk Fe-Ti oxide consists of 0.85 wt. %, that of V₂O₃ is 0.65% and that of Nb is about 60 ppm.

Figure 13 demonstrates covariations of SiO₂ and mg# of measured whole rock compositions and calculated melts. In comparison with calculated melts, actual rocks show a wider range of SiO₂ and Fe-Ti gabbros are generally lower in SiO₂ contents. This reflects their abundances in Fe-Ti oxides as discussed above. Parent melts for gabbro, Fe-Ti gabbro and gabbroic diorites form trend

of increasing SiO₂ with decreasing mg# which suggests that all rocks investigated originated from melt portions via crystal fractionation of magmas of similar compositions. Compositions of parent melts for gabbros fall into the range of parent melts for Fe-Ti gabbros. The least differentiated melts formed the Fe-Ti gabbro (samples GY9-74 and GY9-79) of the Anyui province in eastern Chukotka which were basaltic with SiO₂ ~49 wt. % and mg# ~47-48. These basaltic compositions are far from primitive (i.e. equilibrated with residual mantle peridotites) and suggests primary melt differentiation in a deeper magma-chamber. The degree of crystal fractionation of the most differentiated gabbroic diorites was probably up to 60-65%, inferred from enrichment in highly incompatible elements (La, Ce) relative to parental melt (sample GY9-74) (see the Appendix).

In the TAS diagram (Fig. 6a) for plutonic rocks and SiO_2 vs. K_2O plot for volcanic rocks (Fig. 6b) alkali elements exhibit irregular variations in measured rock samples because of mobility of sodium and potassium in the metamorphic process as discussed above. This prevents the correct definition of rock series affinity from bulk rock compositions. In contrast, calculated melts form systematic trends showing the affinity of calculated melts to moderately alkaline series. Basaltic compositions (calculated from most of the gabbro and Fe-Ti gabbro) belong to medium-potassium (calc-alkaline) series and basaltic andesite compositions (calculated from gabbroic diorites) belong to high-potassium (shoshonitic) series.

Interpretation of Sm-Nd isotope

Sm-Nd isotopes indicate that the gabbro, Fe-Ti gabbro and gabbroic diorite studied are crustally contaminated rocks. The most evolved samples show the lowest ϵNd value, which could be interpreted to reflect a greater crustal input. It is hard to distinguish whether a source or a melt at some stage of its evolution was contaminated. However assuming the rocks from the Gytgyl'ven pass and Ploskaya River domains (for which Sm-Nd data are presented here) to be coeval and cogenetic we argue that contamination of melts by crustal material could be important for these rocks. Nonetheless, it does not exclude a source contamination by a crustal material. The gabbro from the Kolyuchinskaya Bay area lies out of the trend formed by the rocks investigated, and this suggests either source heterogeneity beneath the eastern Chukotka area and/or different compositions of the source of contamination. In the Nb/Yb vs. Th/Yb and $(\text{La}/\text{Nb})_{\text{PM}}$ vs. $(\text{Th}/\text{Ta})_{\text{PM}}$ plots (Fig. 14) the gabbro, Fe-Ti gabbro and gabbroic diorite exhibit variations that are consistent with contamination of mantle-derived enriched melts either by upper crustal material or by sediments.

GEODYNAMIC INTERPRETATIONS

Geodynamic setting of the Anyui province rocks

The data on mineral and whole rock compositions presented above suggest that the investigated gabbro, Fe-Ti gabbro and gabbroic diorite from eastern Chukotka can probably be treated as cogenetic rocks derived from several portions of variably

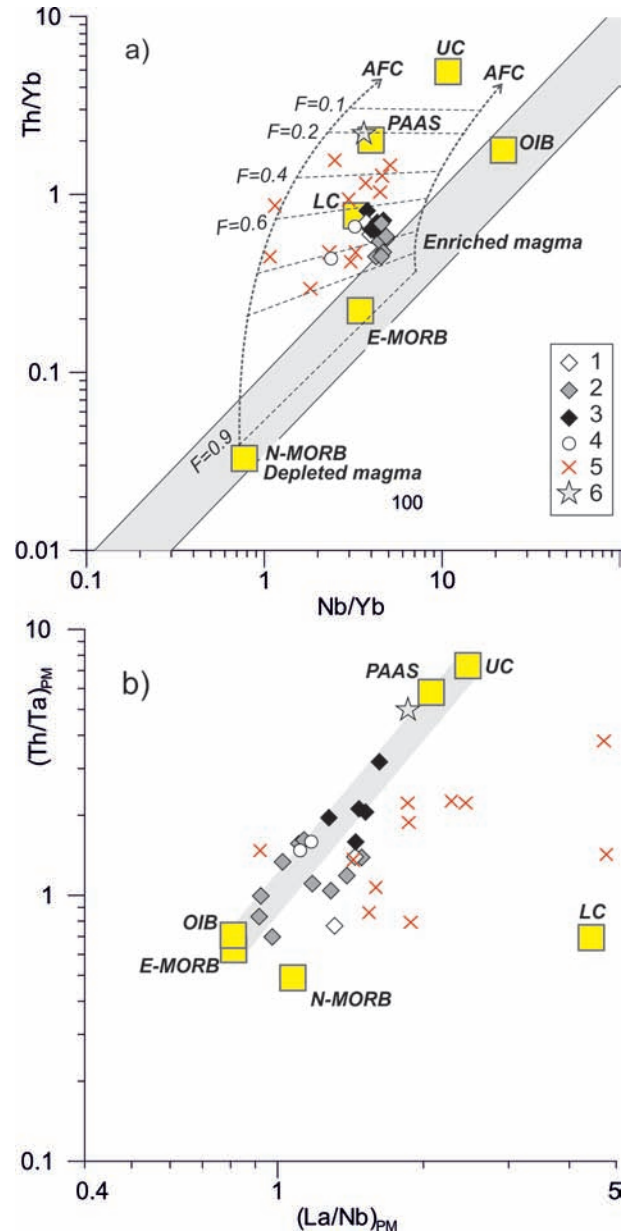


Fig. 14. Nb/Yb vs. Th/Yb (a) (Pearce, 2008) and $(\text{La}/\text{Nb})_{\text{PM}}$ versus $(\text{Th}/\text{Ta})_{\text{PM}}$ (b) (Neal, et al., 2002) diagrams, showing probable contamination of rocks of the Anyui province of eastern Chukotka by crustal material. N-MORB, E-MORB and OIB are from (Sun and McDonough, 1989); average lower crust (LC) and upper crust (UC) are from (Rudnick and Fountain, 1995); the post-Archean Australian shale (PAAS) is from (Taylor and McLennan, 1985). In plot (a), modeling curves of combined fractional crystallization and contamination (AFC) are from (Pearce, 2008). Wide grey line in plot (b) indicates probable contamination of mantle-derived enriched melts by crustal material.

Symbols 1 to 3 correspond to gabbro (1), Fe-Ti gabbro (2), gabbroic diorite (3). Other symbols are for gabbroic rocks of the Kolyuchinskaya Bay (4) and the New Siberian Islands (5), and terrigenous sediments (unpublished authors' data) hosting the investigated sills in eastern Chukotka (6).

differentiated melts of a similar initial composition. The studied rocks have compositions similar to that of the calculated melts with little or no admixture of cumulate Fe-Ti oxides (and silicates). Thus, discrimination diagrams proposed for the volcanic rocks can be generally applied for geodynamic interpretation of geochemical data. Samples GY9-99 and GY9-102 probably contain a significant amount of cumulative silicate minerals and are ignored in this summary.

The multi-element spectra (Fig. 8) and some ratios of incompatible elements (Fig. 14) are characteristic of rocks produced from enriched mantle-derived basic melts. The negative anomalies of Nb-Ta and Zr-Hf observed in the rocks can be attributed to crustal contamination, as discussed. The spectra of the rocks studied are similar in shape to that of trap basalts of the Siberian LIP (Fig. 16a) which also exhibit negative anomalies of Nb-Ta attributed to a crustal input (Lightfoot, et al., 1993; Wooden, et al., 1993; Al'Mukhamedov, et al., 1999; Medvedev, 2004; Krivolutskaya, 2013). The difference in trace-element abundance between the rocks investigated and the Siberian traps is probably due to a different degree of magma crystallization (Siberian basalts have higher mg# than the rocks investigated). In the La-Y-Nb plot (Fig. 15a) the gabbro and Fe-Ti gabbro compactly fall in the field of continental basalts; the Fe-Ti gabbro (despite admixed cumulative Fe-Ti oxides concentrating Nb) are only slightly displaced relative to the gabbro toward a more Nb-rich compositions. In the Th-Hf-Ta plot (Fig. 15b) the Fe-Ti gabbro partially lies in the field of intraplate basalts (which is indistinguishable from the field of E-MORB). Data points of the gabbro and some gabbroic diorites are displaced toward the field of subduction-related calc-alkaline lavas. This can be attributed to crustal contamination, as discussed above. Siberian trap basalts also lie in the field of arc lavas. We conclude that the gabbro, Fe-Ti gabbro and gabbroic diorite show geochemical features of continental intra-plate crustally contaminated lavas. A non-subduction origin of the Anuyi province rocks is also consistent with compositional variations of biotites that are typical of anorogenic granites but not of subduction-derived felsic rocks (Abdel-Rahman, 1994).

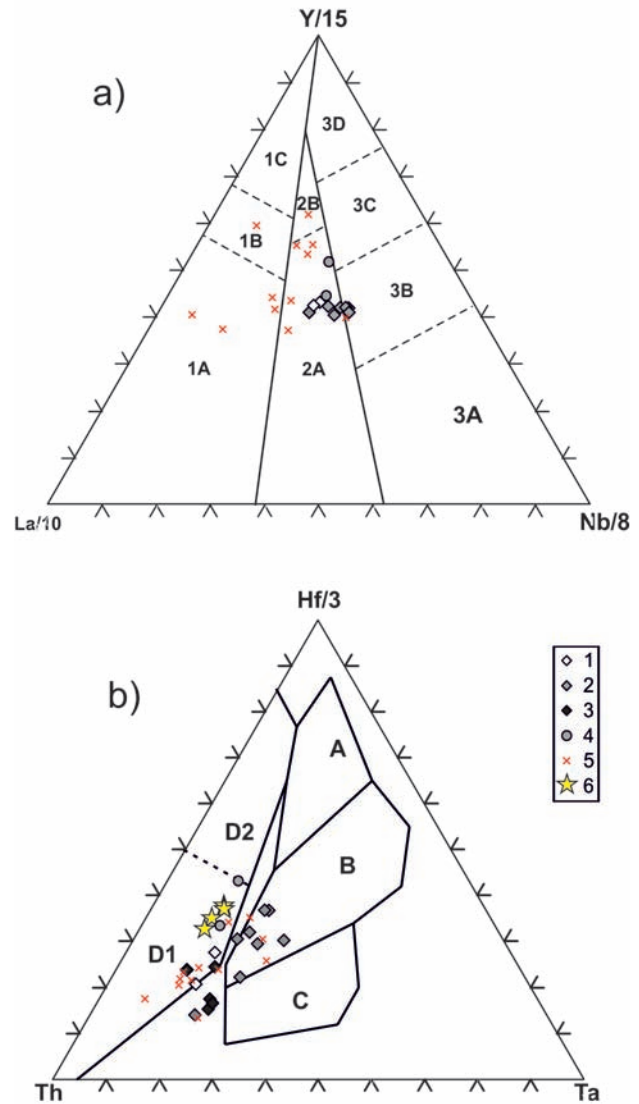


Fig. 15. Tectonomagmatic diagrams (a) La-Y-Nb (Cabanis and Lecolle, 1989) and (b) Th-Hf-Ta (Wood, 1980) for the studied rocks of eastern Chukotka.

Symbols are as follows: studied gabbro (open diamond, 1) Fe-Ti gabbro (grey diamond, 2), gabbroic diorite (black diamond, 3), gabbro of the Kolyuchinskaya Bay (grey circle, 4), rocks of the New Siberian Islands (crosses, 5) (Kuz'michov and Pease, 2007), basalts of the platformal or trap stage of the Siberian LIP (star, 6) (Al'Mukhamedov, et al., 2004; Krivolutskaya, 2013).

In plot (a) fields are as follows: 1 – basalts of the volcanic arcs (1a – calc-alkaline basalts, 1C arc tholeiites, 1B – both calc-alkaline basalts and arc tholeiites), 2 – continental basalts (2a – continental basalts, 2b – back-arc basalts), 3 – oceanic basalts (3A – alkaline basalts of continental rifts, 2b – enriched E-MORB, 3C – slightly enriched E-MORB, 3D – N-MORB).

In plot (b) fields in Fig. 14b are as follows: A – N-MORB, B – E-MORB and intraplate tholeiites, C – intraplate alkaline basalts, D1 – calc-alkaline lavas, (D2) – arc tholeiites.

REGIONAL CORRELATIONS

The material presented suggests that the shelf of the Chukotka microcontinent was an arena of intra-plate basic magmatism in the Permo-Triassic to Early-Middle Triassic time. This epoch is known for a global plate-tectonic reorganization and superplume impingements. In particular, one of such superplumes resulted in voluminous eruptions of basaltic lavas and formation of numerous mafic intrusions in the Siberian platform and West Siberian Basin referred to as the Siberian large igneous province (LIP) (e.g. Reichow, et al., 2009). In the Arctic region, manifestations of the Siberian LIP were reported in the Taimyr Peninsula, in the

islands of the Kara Sea (Vernikovskiy, et al., 2003; Dobretsov, et al., 2008) and in the New Siberian Islands (Kuz'michov and Pease, 2007).

The Anyui province rocks of eastern Chukotka are coeval to the Siberian traps in general and to the dolerite and gabbro-dolerite of the New Siberian Islands. However, rocks of eastern Chukotka and the New Siberian Islands differ in major- and trace-element chemistry (Fig. 16b). The gabbro, Fe-Ti gabbro and gabbroic diorite of eastern Chukotka from the regions investigated and from the Kolyuchinskaya Bay are much more evolved. Nonetheless the difference in geochemistry between the rocks of these two regions hardly can be

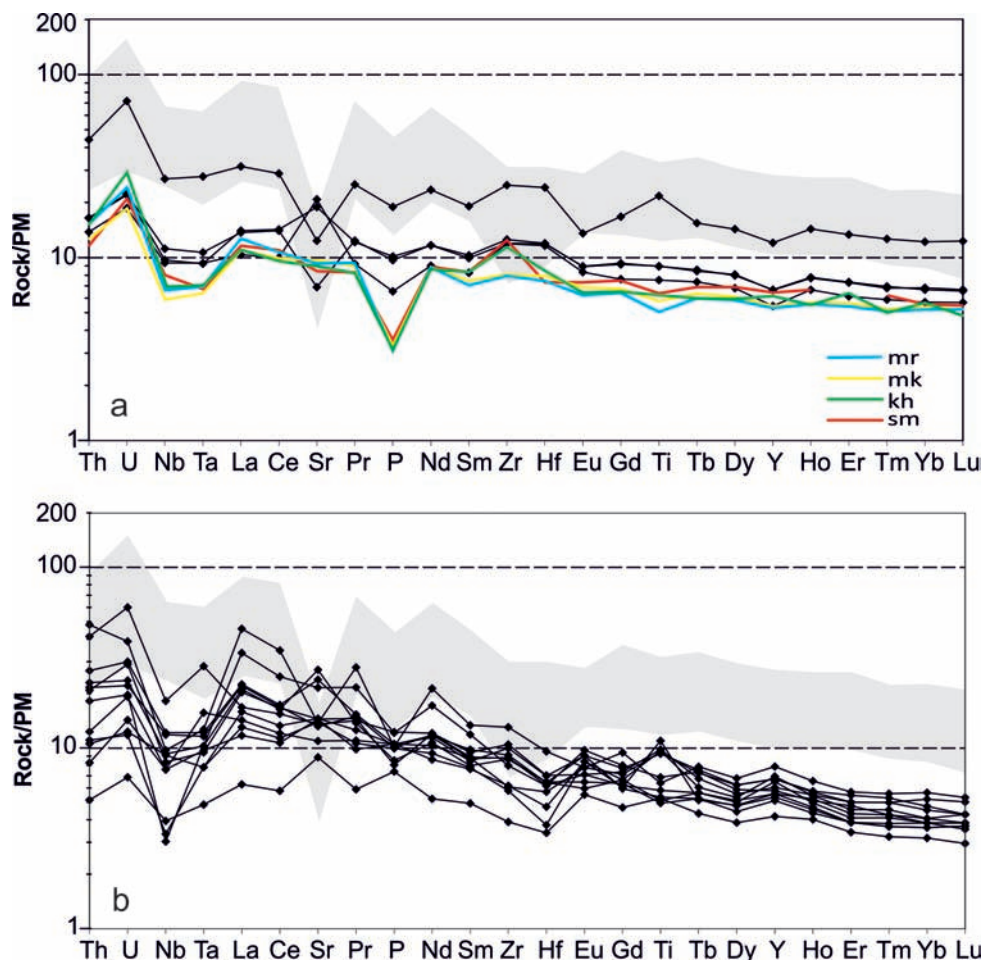


Fig. 16. Multi-element spectra shown in plot (a) demonstrate the geochemical similarity between gabbroic rocks of eastern Chukotka from the study areas and the Kolyuchinskaya Bay region (Ledneva, et al., 2011). The latter closely resembles Siberian LIP basalts of the platform or trap stage (Al'Mukhamedov, et al., 2004; Krivolutsкая, 2013), which are the most typical and widespread in the Noril'sk region (the Formations are as follows: Morongo, mr; Mokulaev, mk; Kharaelakh, kh; Samoed, sm). Plot (b) shows the difference between gabbroic rocks of eastern Chukotka and the New Siberian Islands (Kuz'michov and Pease, 2007). Normalizing values for primitive mantle (PM) are from Sun and McDonough (1989).

attributed to melt differentiation and contamination and it rather reflects a difference in sources, conditions of melting or both. To date, there are not enough data to compare rock compositions of the Anyui province from the eastern, central and western regions of Chukotka. The data on mineral composition suggest that gabbro from the vicinity of Bilibino (western Chukotka) originated from a basic melts under conditions similar to that of rocks from eastern Chukotka. As to the major elements (Fig. 7), sills and dikes from the Bilibino and Cape Schmidt areas are more similar to subvolcanic bodies of the New Siberian Islands.

In the Taimyr Peninsula and in Kara Sea, magmatism attributed to the Siberian LIP is expressed as A-type granites (Vernikovskiy, et al., 2003; Dobretsov, et al., 2008), gabbroic rocks have not been describe so far and we are unable to make comparisons.

In eastern Chukotka, the Anyui province rocks are very uniform in bulk rock geochemistry. Variations of the gabbro, Fe-Ti gabbro and gabbroic diorite studied and those from the Kolyuchinskaya Bay lie in the range of geochemical variations typical of intra-plate basalts of the platformal (Al'Mukhamedov, et al., 1999) or trap (Krivolutskaya, 2013) stage of the Siberian LIP magmatism (Fig. 16a). Analogues of the early rift picritic and basaltic lavas and the latest alkaline intrusions of the Siberian LIP are not known in Chukotka up to date. The data presented in this paper on the Anyui province rocks cannot be considered as direct evidence that the Permo-Triassic to Early-Middle Triassic intra-plate magmatism of the Chukotka microcontinent was caused by the Siberian superplume. With the same probability, the Triassic intra-plate magmatism in Chukotka could reflect an extension, which may have resulted from regional transform displacements.

ACKNOWLEDGEMENTS

This study was supported by the Russian Foundation of Basic Research (project no. 09-05-00529, 14-05-00413 and 11-05-00074), projects of FCNTP (NSh-5177.2012.5 and №14.740.11.0190), Department of Earth Sciences of RAS (program no. 10), and State contract № 01/14/20/11. We use the opportunity to thank V.V. Lebedev and A.D. Kievskiy (Georegion, Anadyr, Russia) for their help in the organization

of 2009 field studies in Chukotka. We also express our gratitude to professor Y. Hayasaka (Hiroshima University, Japan), S. Machi (Kanazawa University, Japan) and A.V. Moiseev (GIN RAS, Moscow) participated in the 2009 field studies. We cordially thank I.A. Roshchina and T.V. Romashova (GEOKHI RAS, Moscow) for analyzing whole rocks by XRF, Dr. Ya.V. Bychkova (GEOKHI RAS, Moscow) for ICP-MS determinations, and staff of the analytical center of Geological Institute of the Kola Research Center of the Russian Academy of Sciences, Apatity, Russia and especially its leader Dr. T.B. Bayanova for Sm-Nd isotope measurements.

REFERENCES

- Abdel-Rahman, A., 1994. Nature of biotites from alkaline, calc-alkaline, and peraluminous magmas. *Journal of Petrology*, 35(2), 525-541.
- Akinin, V.V. and Miller, E.L., 2011. Evolution of calc-alkaline magmas of the Okhotsk–Chukotka volcanic belt. *Petrology*, 19(3), 237–277.
- Al'Mukhamedov, A.I., Medvedev, A.Y. and Kirda, N.P., 1999. Comparative analysis of geodynamic settings of the Permo-Triassic magmatism in East Siberia and West Siberia. *Russian Geology and Geophysics*, 40(11), 1550-1561.
- Al'Mukhamedov, A.I., Medvedev, A.Y. and Zolotukhin, V.V., 2004. Chemical evolution of the Permian-Triassic basalts of the Siberian platform in space and time. *Petrology*, 12(4), 297-311.
- Amato, J.M. and Wright, J.E., 1997. Potassic mafic magmatism in the Kigluaik gneiss dome, northern Alaska: a geochemical study of arc magmatism in an extensional tectonic setting. *Journal of Geophysical Research*, 102, 8065-8084.
- Amato, J.M., Miller, E.L., Wright, J.E. and McIntosh W.C., 2003. Dike swarms on Seward Peninsula, Alaska, and their implication for kinematics of the Cretaceous extension in the Bering Strait region. *Canadian Journal of Earth Science*, 40, 865-886.
- Amato, J.M., Toro, J., Miller, E.L., Gehrels, G.E., Farmer, G.L. Gottlieb, E.S. and Till, A.B., 2009. Late Proterozoic-Paleozoic evolution of the Arctic Alaska-Chukotka terrane based

- on U-Pb igneous and detrital zircon ages: Implications for Neoproterozoic paleogeographic reconstructions. *GSA Bulletin*, 121(9/10), 1219–1235.
- Anderson, D.J., Lindsley, D.H. and Davidson, P.M., 1993. QUILF: a PASCAL program to access equilibrium among Fe-Mg-Mn-Ti oxides, pyroxenes, olivine and quartz. *Computers and geosciences*, 19, 1333-1350.
- Bayanova, T.B., 2004. Age of reference geological complexes of the Kola region and duration of magmatic processes. Nauka, St. Petersburg (in Russian).
- Bering Strait Geologic Field Party, 1997. Koolen metamorphic complex, NE Russia: implications for tectonic evolution of the Bering Strait region. *Tectonics*, 16, 713–729.
- Cabanis, B. and Lecolle, M., 1989. Le diagramme La/10-Y/15-Nb/8: un outil pour la discrimination des series volcaniques et la mise en evidence des processus de mélange et/ou de contamination crustale. *Comptes Rendus de l'Académie des Sciences. Series II*, 309, 2032-2029.
- Cecile, M.P., Lane, L.S., Khudoley, A.K. and Kos'ko M.K., 1999. Lower Paleozoic rocks around today's Arctic Ocean: two ancestral continents and associated plates; Alaskan rotation unnecessary and unlikely. *Polarforschung*, 69, 235- 241.
- Degtyaryov, V.S., 1975. Petrochemical peculiarities of the Amguema-Anyui diabase formation of the Chukotka fold region. In Shatalov, E.T. (ed.). *Magmatism of North East Asia*, part 2. Magadan book publisher, Magadan, 160-175 (in Russian).
- Dobretsov, N.L., Kirdyashkin, A.A., Kirdyashkin, A.G., Vernikovskiy, V.A. and Gladkov, I.N., 2008. Modeling of thermochemical plumes and implications for the origin of the Siberian traps. *Lithos*, 100, 66-92.
- Dorofeev, V. K., Blagoveschensky, M. G., Smirnov, A. N. and Ushakov, V. I., 1999. New Siberian Islands, geology and minerageny. *VNIIOkeangeologia*, Saint-Petersburg, 1-130 (in Russian).
- Fujita, K. and Newberry, J. T., 1982. Tectonic evolution of Northeastern Siberia and adjacent regions. *Tectonophysics*, 89, 337–357.
- Gel'man, M. L., 1963. Triassic diabase association in the Anyui fold zone (Chukotka). *Geologiya i Geofizika*, 2, 127-134 (in Russian).
- Govindaraju, K., 1994. 1994 compilation of working values and sample description for 383 geostandards. *Geostandards Newsletter*, 18 (Special Issue), 1–158.
- Grantz, A., May, S.D., Taylor, P.T. and Lawver, L.A., 1990. Canada Basin. In Grantz, A., Johnson, L. and Sweeney, J. F. *The Geology of North America*, vol. L: The Arctic Ocean Region. The Geological Society of America, Boulder, Colo, 379-402.
- Hofmann, A.W., 1988. Chemical differentiation of the Earth: the relationship between mantle, continental crust, and oceanic crust. *Earth and Planetary Science Letters*, 90, 297-314.
- Holland, T. and Blundy, J., 1994. Non-ideal interactions in calcic amphiboles and their bearing on amphibole-plagioclase thermometry. *Contributions to Mineralogy and Petrology*, 116, 433-47.
- Ivanov, O.N. and Milov, A.P., 1975. The diabase association in the Chukchi fold system and its relation to the basic magmatism in the northern portion of the Pacific Mobile Belt. In Shatalov, E.T. (ed.). *Magmatism of North East Asia*, part 2. Magadan book publisher, Magadan, 155-159 (in Russian).
- Kelemen, P.B., Hanghøj, K. and Greene, A.R., 2003. One view of the geochemistry of subduction-related magmatic arcs, with an emphasis on primitive andesite and lower crust. In Rudnick, R.L. (ed.). *The Crust*. Holland, H.D. and Turekian, K.K. (eds.) *Treatise on Geochemistry*, Volume 3. Elsevier-Pergamon, Oxford, 593–659.
- Krivolutskaya, N.A., 2013. Evolution of trap magmatism and origin of Pt-Cu-Ni ores of the Noril'sk province. Association of scientific publishers of KMK. 301 pp.
- Kuz'michov, A.B. and Pease, V.L., 2007. Siberian trap magmatism on the New Siberian Islands: constraints for Arctic Mesozoic plate tectonic reconstructions. *Journal of Geological Society*, 164, 959–968.
- Lanphere, M.A. and Dalrymple, G.B., 2000. First-principles calibration of ³⁸Ar tracers:

- Implications for the ages of $^{40}\text{Ar}/^{39}\text{Ar}$ fluence monitors. U.S. Geological Survey Professional Paper 1621, 10 p.
- Lawver, L.A. and Scotese, C.R., 1990. A review of tectonic models for the evolution of the Canada Basin. In: Grantz, A., Johnson, L. and J.F. Sweeney (eds.). *The geology of North America*, Geological Society of America, Boulder, Colorado, L (The Arctic Ocean Region), 593–618.
- Lawver, L.A., Grantz, A. and Gahagan, L.M., 2002. Plate kinematic evolution of the present Arctic region since the Ordovician. In: Miller, E.L., Grantz, A. and S.L. Klempere (eds.). *Tectonic evolution of the Bering shelf – Chukotka sea – Arctic margin and adjacent landmasses*. Geological Society of America, Special Paper 360, 333–358.
- Layer, P.W., 2000. Argon-40/argon-39 age of the El'gygytgyn impact event, Chukotka, Russia. *Meteoritics & Planetary Science*, 35, 591–599.
- Layer, P.W., Hall, C.M. and York, D., 1987. The derivation of $^{40}\text{Ar}/^{39}\text{Ar}$ age spectra of single grains of hornblende and biotite by laser step heating. *Geophysical Research Letters*, 14, 757–760.
- Layer, P.W., Newberry, R., Fujita, K., Parfenov, L., Trunilina, V. and Bakharev, A., 2001. Tectonic setting of the plutonic belts of Yakutia, northeast Russia, based on $^{39}\text{Ar}/^{40}\text{Ar}$ geochronology and trace element geochemistry. *Geology*, 29(2), 167–170.
- Leake, B.E., Woolley, A.R., Arps, C.S., Birch, W.D., Gilbert, M.C., Grice, J.D., Hawthorne, F.C., Kato, A., Kisch, H.J., Krivovichev, V. G., Linthout, K., Laird, J., Mandarino, J. A., Maresch, W.V., Nickel, E. H., Rock, N.M.S., Schumacher, J.C., Smith, D.C., Stephenson, N.C.N., Ungaretti, L., Whittaker, E.J.W. and Youzhi, G., 1997. Nomenclature of amphiboles: Report of the subcommittee on amphiboles of the international mineralogical association, commission on new minerals and mineral names. *The Canadian Mineralogist*, 35, 219–246.
- Ledneva, G.V., Sokolov, S.D. and Pease, V.L., 2011. Permo-Triassic hypabyssal mafic intrusions and associated tholeiitic basalts of the Kolyuchinskaya Bay, Chukotka (NE Russia): Links to the Siberian LIP. *Journal of Asian Earth Sciences*, 40, 737–745.
- LeMaitre, R.W., Bateman, P., Dudek, A., Keller, J., Lameyre, J., Le Bas, M.J., Sabine, P.A., Schmidt, R., Sorensen, H., Streckeisen, A., Woolley, A.R. and Zanettin, B., 1989. *A Classification of igneous rocks and glossary of terms: recommendations of the International Union of Geological Sciences Subcommittee on the systematics of igneous rocks*. Blackwell Scientific Publications, Oxford, U.K. 193 p.
- Lightfoot, P.C., Hawkesworth, C.J., Hergt, J., Naldrett, A.J., Gorbachev, N.S., Fedorenko, A.V. and Doherty, W., 1993. Remobilization of continental lithosphere by a mantle plume: major-trace-element, and Sr-, Nd- and Pb-isotopic evidence from picritic and tholeiitic lavas of the Noril'sk District, Siberian Trap, Russia. *Contributions to Mineralogy and Petrology*, 114, 171–188.
- McDougall, I. and Harrison, T.M., 1999. *Geochronology and thermochronology by the $^{40}\text{Ar}/^{39}\text{Ar}$ method-2nd ed*, Oxford University Press, New York, 269 pp.
- Medvedev, A.Ya., 2004. Permo-Triassic volcanism of the North Siberian craton (West Siberian Basin and Tunguska syncline): geochemistry, petrology and geodynamics. Doctor's thesis. Irkutsk, A.P. Vinogradov Institute of geochemistry, 306 pp (in Russian).
- Middlemost, A. K., 1994. Naming materials in the magma/igneous rock system. *Earth Science Review*, 37, 215–224.
- Miller, E. L., Katkov, S.M., Strickland, A., Toro, J., Akinin, V.V. and Dumitru, T.A., 2009. Geochronology and thermochronology of Cretaceous plutons and metamorphic country rocks, Anyui-Chukotka fold belt, North East Arctic Russia Stephan Mueller Special Publication Series, 4, 157–175.
- Miller, E.L., Toro, J., Gehrels, G., Amato, J.M., Prokopiev, A., Tuchkova, M.I., Akinin, V.V., Dumitru, T.A., Moore, T.E. and Cecile, M.P., 2006. New insights into Arctic paleogeography and tectonics from U–Pb detrital zircon geochronology. *Tectonics*, 25, 1–19.
- Nalivkin, D.V. (Ed.), 1983. *Geologic map of USSR*

- and adjacent aquatories. Scale 1:2500000. VSEGEI, St. Petersburg.
- Natal'in, B.A., Amato, J.M., Toro, J. and Wright, J.E., 1999. Paleozoic rocks of northern Chukotka Peninsula, Russian Far East: implication for the tectonics of the Arctic region. *Tectonics*, 18, 977–1003.
- Neal, C.R., Mahoney, J.J. and Chazey III, W.J., 2002. Mantle sources and the highly variable role of continental lithosphere in basalt petrogenesis of the Kerguelen plateau and Broken Ridge LIP: results from ODP Leg 183. *Journal of Petrology* 43, 1177–1205.
- Nokleberg, W.J., West, T.D., Dawson, K.M., Shpikerman, V.I., Bundtzen, T.K., Parfenov, L.M., Monger, J.W.H., Ratkin, V.V., Baranov, B.V., Byalobzhesky, S.G., Diggles, M.F., Eremin, R.A., Fujita, K., Gordey, S.P., Gorodinskiy, M.E., Goryachev, N.A., Feeney, T.D., Frolov, Y.F., Grantz, A., Khanchuck, A.I., Koch, R.D., Natal'in, B.A., Natapov, L.M., Norton, I.O., Patton Jr., W.W., Plafker, G., Pozdeev, A.I., Rozenblum, I.S., Scholl, D.W., Sokolov, S.D., Sosunov, G.M., Stone, D.B., Tabor, R.W., Tsukanov, N.V. and Vallier, T.L., 1998. Summary terrane, mineral deposit, and metallogenic belt maps of the Russian Far East, Alaska, and the Canadian Cordillera. US Geological Survey Open-File Report, 98–136.
- Parfenov, L.M., 1984. Continental margins and island arcs in the Mesozooids of Northeastern Asia. Nauka Publisher, Novosibirsk, 192 pp. (in Russian).
- Parfenov, L.M., Natapov, L.M., Sokolov, S.D. and Tsukanov, N.V. 1993. Terrane analysis and accretion in northeast Asia. *The Island Arc*, 2, 35–54.
- Pearce, J.A., 2008. Geochemical fingerprinting of oceanic basalts with applications to ophiolite classification and the search for Archean oceanic crust. *Lithos*, 100, 14–48.
- Putirka, K. D., 2008. Thermometers and barometers for volcanic systems. In: Putirka, K. D. and Tepley, F. (eds.). *Review in Mineralogy and Geochemistry*, 69, 61-120.
- Reichow, M.K., Pringle, M.S., Al'Mukhamedov, A.I., Allen, M.B., Andreichev, V.L., Buslov, M.M., Davies, C.E., Fedoseev, G.S., Fitton, J.G., Inger, S., Medvedev, A.Ya., Mitchell, C., Puchkov, V.N., Safonova, I.Yu., Scott, R.A. and Sauders, A.D. 2009. The timing and extent of the eruption of the Siberian traps large igneous province: Implication for the end-Permian environmental crisis. *Earth and Planetary Science Letters*, 277(1–2), 9–20.
- Ridolfi, F., Runzelli, A. and Puerini, M., 2009. Stability and chemical equilibrium of amphibole in calc-alkaline magmas: an overview, new thermobarometric formulations and application to subduction-related volcanoes. *Contribution to Mineralogy and Petrology*, 160(1), 45-66.
- Rudnick, R.L., and Fountain, D.M., 1995. Nature and composition of the continental crust: a lower crustal perspective. *Reviews of Geophysics*, 33, 267–309.
- Samson, S. D. and Alexander E. C., 1987. Calibration of the interlaboratory $^{40}\text{Ar}/^{39}\text{Ar}$ dating standard. *MMhb1: Chemical Geology*, 66, 27-34.
- Schmidt, M. W., 1992. Amphibole composition in tonalite as a function of pressure: an experimental calibration of the Al-in-hornblende barometer. *Contributions to Mineralogy and Petrology*, 110, 304-10.
- Seslavinsky, K.B., 1979. The South Anyui Suture (Western Chukotka). *Doklady Akademii Nauk SSSR*, 249, 1181–1185 (in Russian).
- Sokolov, S.D., Ledneva, G.V. and Pease, V.L., 2009. New data on the age and genesis of igneous rocks in the Kolyuchinskaya Guba (Eastern Chukotka). *Transactions (Doklady) of the Russian Academy of Sciences/Earth Science Section*, 425A(3), 384-388.
- Steiger, R. H. and Jaeger, E., 1977. Subcommittee on geochronology: convention on the use of decay constants in geo- and cosmochemistry. *Earth and Planetary Science Letters*, 36, 359–362.
- Streckeisen, A.L., 1974. Classification and nomenclature of plutonic rocks. Recommendations of the IUGS subcommission on the systematics of igneous rocks. *Geologische Rundschau. Internationale Zeitschrift für Geologie*. Stuttgart, 63, 773-785.
- Streckeisen, A.L., 1976. To each plutonic rock its proper name. *Earth Science Reviews*, 12, 1–33.
- Sun, S.S., and McDonough, W.F., 1989. Chemical

- and isotopic systematics of oceanic basalts: implication for mantle composition and processes. In: Saunders, A.D. and Norry, M.J. (Eds.), *Magmatism in the Oceanic Basins*. Geological Society Special Publication, 42, 313–345.
- Taylor, S.R. and McLennan, S.M., 1985. *The continental crust: Its composition and evolution*. Blackwell, Oxford, 312 pp.
- Tikhomirov, P.L., Kalinina, E.A., Moriguti, T., Makishima, A., Kobayashi, K., Cherepanova, I.Yu. and Nakamura, E., 2012. The Cretaceous Okhotsk–Chukotka Volcanic Belt (NE Russia): Geology, geochronology, magma output rates, and implications on the genesis of silicic LIPs. *Journal of Volcanology and Geothermal Research*, 221, 14–32.
- Tikhomirov, P.L., Luchitskaya, M.V. and Kravchenko-Berezhnoy, I.R., 2009. Comparison of Cretaceous granitoids of the Chaun tectonic zone to those of the Taigonos Peninsula, NE Asia: rock chemistry, composition of rock forming minerals, and conditions of formation. *Stephan Mueller Special Publication Series*, 4, 289–311.
- Til'man, S.M. and Sosunov, G.M. 1960. Some peculiarities of evolution of the Chukotka geosynclines in the Early Triassic. *Doklady Akademii Nauk SSSR*, 130(4), 834–837 (in Russian).
- Tuchkova, M.I., Sokolov, S. and Kravchenko-Berezhnoy, I.R., 2009. Provenance analysis and tectonic setting of the Triassic clastic deposits in Western Chukotka, Northeast Russia. *Stephan Mueller Special Publication Series*, 4, 177–200.
- Tynankergav, G.A. and Bychkov, J.M., 1987. Upper Triassic chert-volcanic-terrigenous assemblages of western Chukotka. *Doklady Akademii Nauk USSR* 296, 698–700 (In Russian)
- Vatrushkina, E.V. and Tuchkova M.I., 2014. Peculiarities of lithology and geochemistry of the Raucha Formation (upper Jurassic, western Chukotka). *Bulletin MOIP. Geology Branch* 89(1), 59–74 (in Russian).
- Vernikovskiy, V.A., Pease V.L., Vernikovskaya A.E., Romanov A.P., Gee D. and Travin, A.V., 2003. First report of early Triassic A-type granite and syenite intrusions from Taimyr: product of the northern Eurasian superplume? *Lithos*, 66(1–2), 23–36.
- Wood, D.A., 1980. The application of a Th-Ta-Hf diagram to problems of tectonomagmatic classification and to establishing the nature of crustal contamination of basaltic lavas of the British Tertiary volcanic province. *Earth and Planetary Science Letters*, 50, 11–30.
- Wooden, J.L., Czamanske, G.K., Fedorenko, V.A., Arndt, N.T., Chauvel, C., Bouse, R.M., King, B.W., Knight, R.J. and Siems, D.F., 1993. Isotopic and trace element constrains on mantle and crustal contributions to Siberian continental flood basalts, Noril'sk area, Siberia. *Geochemica et Cosmochemica Acta*, 57, 3677–3704.
- York, D., Hall, C.M., Yanase, Y., Hanes, J.A. and Kenyon, W.J., 1981. $^{40}\text{Ar}/^{39}\text{Ar}$ dating of terrestrial minerals with a continuous laser, *Geophysical Research Letters*, 8, 1136–1138.
- Zlobin, S. K. and Zakariadze, G. S., 1993. Composition and geodynamic setting of the plutonic series of ophiolites in the Sevan–Akerin zone (Lesser Caucasus). *Petrologiya*, 1, 413–430.

APPENDIX

Trace element contents in fractionated melt can in general be evaluated based on the Rayleigh fractionation model. Contents of major elements in melts can be evaluated using either the Rayleigh fractionation model or empirical correlations. However, both approaches have some limitations. Relationships between contents and activities of major elements deviate from Henry's law. Empirical correlations are not definite because any correlation can be described by different equations (especially when data are limited). Both these approaches are valid only for a restricted interval of fractionation, which is characterized by crystallization of a certain mineral assemblage and only limited variations of bulk element distribution coefficients.

According to the Rayleigh fractionation model, content of a trace element at a given degree of fractionation can be calculated using the equation

$$C=C_0*(1-xF)^{(KD-1)} \quad (1)$$

where KD is a bulk distribution coefficient (cumulate/melt) of an element, xF is a degree of fractionation (xF=0 for an initial melt), C₀ is a content of an element in an initial melt, C is a content of an element in fractionated melt. Correspondingly, values of xF can be estimated using an equation

$$xF=1-(C/C_0)^{(1/(KD-1))} \quad (2)$$

if values of C, C₀ and KD of a trace element are known. However, in our case compositions of actual rocks (Table 4) differ from compositions of melts due to a probable admixture of cumulative Fe-Ti oxides and a loss/gain of some major components during the rock metamorphism. Hence a content of an element in melt is related to its actual content in a rock as

$$C=C_{meas}*k, \quad (3)$$

where

$$k=100*(SiO_2+TiO_2+Al_2O_3+FeO^*+MnO+MgO+CaO+Na_2O+K_2O+Cr_2O_3+P_2O_5) \quad (4),$$

where contents of all oxides (wt. %) should correspond to their probable contents in a melt. This means that bulk rock contents of TiO₂, FeO*, MnO should be corrected to exclude the effect of an admixture of Fe-Ti oxides, and bulk rock contents of CaO, Na₂O and K₂O should be corrected to eliminate effects of element mobility (loss/gain) during metamorphism.

Additionally, values of KD for trace and major elements are not exactly known. However, one can infer from equation (1) that contents of two elements x and y in melts should correlate as

$$Cx/Cy=(Cx_0/Cy_0)*(1-xF)^{(KDx-KDy)} \quad (5),$$

so that the content of an element is related with a the content of another element as

$$Cx=Cy*k1*(1-xF)^{k2} \quad (6).$$

The values k1 and k2 can be estimated for any two elements by a least square minimization procedure of actual-calculated Cx/Cy values for a number of cogenetic melts for which Cx, Cy and xF are known.

When two elements have a similar degree of compatibility, the equation (6) can be reduced to the form

$$Cx=Cy*k1 \quad (7)$$

With a simple linear correlation between Cx and Cy.

Assuming a rock studied is a mixture of an initial melt fractionated to a certain degree and cumulative Fe-Ti oxides, the contents of FeO*, TiO₂, MnO, V and Nb in melts should correlate with contents of other elements. The correlations can be evaluated from compositions of 7 samples of the gabbro and diorite with the lowest TiO₂ contents which are assumed to be free of or contain only a little admixed Fe-Ti oxides. We prefer to use an average estimation based on values calculated using different element pairs (Table A1) in order to minimize both errors related to the deviation of iron behavior from Henry's law and analytical errors.

For evaluation of TiO₂ contents in melts at

different stages of fractionation we use correlation $TiO_2/SiO_2 - Gd/SiO_2$ (Fig. 10), correlation $TiO_2 - SiO_2$ and correlation $TiO_2 - Al_2O_3$:

$$TiO_2 = (0.0537 - 0.0302 * Gd/SiO_2) * SiO_2 \quad (8),$$

$$TiO_2 = SiO_2 * 0.0519 * (1 - xF)^{0.0901} \quad (9),$$

$$TiO_2 = Al_2O_3 * 0.182 * (1 - xF)^{-0.169} \quad (10),$$

where oxides are in wt.%, Gd (and other elements in equations below) in ppm, and xF is relative degree of crystallization. The form of equation (8) is empirical, and the form of equations (9) and (10) corresponds to the Rayleigh fractionation model.

Similarly, FeO* contents in melts can be calculated from compositions of the same reference rocks:

$$FeO^* = SiO_2 * 0.268 * (1 - xF)^{-0.0299} \quad (11),$$

$$FeO^* = Al_2O_3 * 0.931 * (1 - xF)^{-0.304} \quad (12),$$

$$FeO^* = MgO * 2.21 * (1 - xF)^{-0.962} \quad (13),$$

$$FeO^* = CaO * 1.26 * (1 - xF)^{-0.555} \quad (14).$$

In equation (14) CaO contents calculated by equations (33-35) were used in order to increase the accuracy of calculations.

Contents of MnO in melts were calculated using equations

$$MnO = SiO_2 * 0.00353 * (1 - xF)^{0.123} \quad (15),$$

$$MnO = Al_2O_3 * 0.0122 * (1 - xF)^{-0.158} \quad (16),$$

$$MnO = P_2O_5 * 0.582 * (1 - xF)^{0.918} \quad (17).$$

For calculation of V content in melts, we used equations

$$V = SiO_2 * 9.335 * (1 - xF)^{1.288} \quad (18),$$

$$V = Al_2O_3 * 33.2 * (1 - xF)^{1.090} \quad (19),$$

$$V = P_2O_5 * 1484 * (1 - xF)^{1.900} \quad (20).$$

Contents of Nb in melts were constrained using equations

$$Nb = SiO_2 * 0.305 * (1 - xF)^{-0.744} \quad (21),$$

$$Nb = Al_2O_3 * 1.058 * (1 - xF)^{-1.022} \quad (22),$$

$$Nb = Y * 0.355 * (1 - xF)^{-0.027} \quad (23),$$

$$Nb = P_2O_5 * 48.3 * (1 - xF)^{0.001} \quad (24),$$

$$Nb = La * 0.794 * (1 - xF)^{0.094} \quad (25),$$

$$Nb = Ce * 0.341 * (1 - xF)^{0.113} \quad (26).$$

Initial contents of K_2O , Na_2O and CaO in some investigated rocks seem to have changed during metamorphism (Fig. 12). However, contents of these components remain probably unchanged in a number of rocks, and this allows calculations of their initial contents in allochemically metamorphosed rock using an approach outlined above.

For potassium, using 5 rocks as reference ones (Fig. 12c),

$$K_2O = La * 0.0466 * (1 - xF)^{0.0203} \quad (27),$$

$$K_2O = Ce * 0.0199 * (1 - xF)^{0.0268} \quad (28),$$

$$K_2O = P_2O_5 * 2.72 * (1 - xF)^{-0.153} \quad (29).$$

For sodium, using 11 rocks as reference ones (Fig. 12b),

$$Na_2O = SiO_2 * 0.0567 * (1 - xF)^{0.101} \quad (30),$$

$$Na_2O = Al_2O_3 * 0.205 * (1 - xF)^{-0.144} \quad (31),$$

$$Na_2O = CaO * 0.260 * (1 - xF)^{-0.446} \quad (32).$$

In equation (32) CaO contents calculated by equations (33-35) were used in order to increase the accuracy of calculations for rocks probably experienced calcium gain/loss during metamorphism.

For calcium, using 7 rocks as reference rocks (Fig. 12a),

$$\text{CaO}=\text{SiO}_2*0.218*(1-\text{xF})^{0.519} \quad (33),$$

$$\text{CaO}=\text{Al}_2\text{O}_3*0.791*(1-\text{xF})^{0.279} \quad (34),$$

$$\text{CaO}=\text{MgO}*1.592*(1-\text{xF})^{-0.423} \quad (35).$$

At the first stage of the calculation, we estimated approximate xF (equation 2) for each rock assuming KD=0 for the most incompatible elements in cogenetic differentiated melts; in our case such elements are La and Ce. Then we calculated contents of the major elements in melts (using equations similar to 8-35). As major element contents in melts influence values of xF (equations 2-4) the calculation requires several iteration steps. Shown in equations 8-35 the values of coefficients reflecting the last step of the iteration procedure as well as the values of xF are listed in Table A1. Final contents of oxides and elements calculated using equations (8-35) along with average estimations are also presented in Table A1.

Table A1. Evaluation of relative degree of differentiation and elimination of effects of metamorphic loss/gain of some elements and cumulative Fe-Ti oxide admixture to melts.

#	1	2	3	4	5	6	7	8	9	10	11	12
Oxide/element	x _F	x _F [*]	x _F [*]	x _F [*]	TiO ₂	FeO [*]	FeO [*]					
Sample	calc	calc	calc	calc	actual	calc.	calc.	calc.	calc.	calc.	actual	calc.
	avg	us. La	us.Ce	avg		eqn.(8)	eqn.(9)	eqn.(10)	avg	excess		eqn.(11)
GY9-101	0.042	0.050	0.034	0.042	2.35	2.57	2.54	2.45	2.52	-0.17	12.79	13.22
PS9-92	0.197	0.209	0.186	0.197	2.58	2.51	2.47	2.60	2.53	0.06	13.31	13.12
GY9-74	0.000	0.000	0.000	0.000	6.17	2.21	2.21	2.06	2.16	4.01	18.33	11.41
GY9-79	0.040	0.041	0.039	0.040	5.28	2.28	2.27	2.11	2.22	3.06	16.82	11.80
KE9-71	0.107	0.106	0.105	0.105	5.72	2.32	2.31	2.38	2.34	3.39	16.43	12.12
PS9-89	0.207	0.211	0.201	0.206	3.82	2.43	2.40	2.40	2.41	1.42	15.77	12.75
KE9-73	0.113	0.112	0.115	0.114	5.98	2.30	2.29	2.32	2.30	3.68	17.11	12.01
GY9-99	0.425	0.427	0.427	0.427	3.59	2.08	2.08	2.08	2.08	1.51	21.53	11.47
GY9-81	0.439	0.442	0.434	0.438	4.62	2.32	2.31	2.38	2.34	2.29	17.55	12.78
GY9-102	0.440	0.441	0.438	0.440	3.38	2.36	2.34	2.46	2.39	0.99	16.33	12.97
PS9-90	0.494	0.497	0.491	0.494	3.24	2.43	2.39	2.53	2.45	0.79	15.69	13.42
GY9-76	0.520	0.516	0.524	0.520	4.31	2.40	2.39	2.19	2.33	1.98	17.27	13.51
GY9-82a	0.543	0.543	0.545	0.544	2.91	2.58	2.55	2.62	2.58	0.32	15.47	14.49
GY9-78	0.667	0.672	0.665	0.668	2.56	2.60	2.61	2.67	2.63	-0.06	13.47	15.40
GY9-82b	0.677	0.678	0.678	0.678	2.63	2.57	2.57	2.56	2.57	0.07	14.62	15.23
GY9-87	0.681	0.680	0.680	0.680	2.26	2.52	2.56	2.42	2.50	-0.24	15.77	15.21
GY9-84	0.669	0.666	0.670	0.668	2.55	2.51	2.54	2.52	2.53	0.03	16.20	15.02

Table A1. (continued)

#	13	14	15	16	17	18	19	20	21	22	23	24
Oxide/element	FeO [*]	MnO	MnO	MnO	MnO	MnO	MnO	V				
Sample	calc.	Calc.	Calc.	Calc.	Calc.	Actual	calc.	Calc.	Calc.	Calc.	Calc.	Actual
	eqn.(12)	eqn.(13)	eqn.(14)	avg	excess		eqn.(15)	eqn.(16)	eqn.(17)	avg	excess	
GY9-101	12.62	13.79	13.21	13.21	-0.42	0.171	0.173	0.164	0.174	0.171	0.001	396
PS9-92	13.70	12.70	13.22	13.18	0.12	0.168	0.167	0.174	0.164	0.168	0.000	391
GY9-74	10.55	13.54	11.78	11.82	6.51	0.214	0.150	0.138	0.145	0.145	0.070	833
GY9-79	10.86	14.07	12.18	12.23	4.59	0.208	0.154	0.142	0.153	0.150	0.058	754
KE9-71	12.40	12.61	12.39	12.38	4.05	0.222	0.157	0.160	0.166	0.161	0.062	658
PS9-89	12.67	13.51	12.97	12.98	2.79	0.203	0.162	0.161	0.170	0.164	0.039	618
KE9-73	12.05	12.69	12.25	12.25	4.86	0.229	0.155	0.155	0.181	0.164	0.065	727
GY9-99	11.49	31.43	17.59	17.99		0.221	0.139	0.139	0.125	0.134	0.087	495
GY9-81	13.17	14.42	13.42	13.45	4.10	0.215	0.154	0.159	0.160	0.158	0.058	416
GY9-102	13.62	22.61	16.16	16.34		0.204	0.156	0.164	0.164	0.162	0.043	491
PS9-90	14.22	17.84	15.06	15.13	0.56	0.185	0.159	0.169	0.171	0.166	0.018	417
GY9-76	12.38	16.73	14.10	14.18	3.09	0.266	0.159	0.146	0.173	0.159	0.107	197
GY9-82a	14.91	14.93	14.77	14.77	0.70	0.171	0.169	0.174	0.170	0.171	0.000	227
GY9-78	15.87	15.99	15.72	15.75	-2.27	0.137	0.171	0.177	0.158	0.169	-0.032	136
GY9-82b	15.28	14.61	15.03	15.04	-0.42	0.142	0.169	0.170	0.159	0.166	-0.024	126
GY9-87	14.46	14.56	14.73	14.74	1.03	0.202	0.168	0.160	0.175	0.168	0.034	46
GY9-84	15.00	15.47	15.13	15.15	1.04	0.190	0.167	0.167	0.180	0.172	0.019	96

Table A1. (continued)

#	25	26	27	28	29	30	31	32	33	34	35	36
Oxide/element	V	V	V	V	V	Nb	Nb	Nb	Nb	Nb	Nb	Nb
Sample	calc.	calc.	calc.	calc.	calc.	actual	calc.	calc.	calc.	calc.	calc.	calc.
	eqn.(18)	eqn.(19)	eqn.(20)	avg	excess		eqn.(21)	eqn.(22)	eqn.(23)	eqn.(24)	eqn.(25)	eqn.(26)
GY9-101	435	424	426	428	-32	14.7	15.5	14.8	15.1	15.1	14.6	14.7
PS9-92	342	360	338	347	45	16.2	17.5	18.2	16.8	16.6	17.1	16.9
GY9-74	397	377	370	381	452	17.8	13.0	12.0	14.6	12.1	12.2	12.5
GY9-79	389	366	376	377	377	17.2	13.8	12.7	14.8	13.2	13.1	13.4
KE9-71	363	378	379	373	285	20.4	15.0	15.3	17.1	15.3	14.4	14.7
PS9-89	327	327	346	333	284	18.9	17.1	17.0	17.7	17.5	16.5	16.6
KE9-73	357	364	410	377	350	20.9	14.9	14.9	16.5	16.7	14.2	14.5
GY9-99	192	189	185	189	306	22.5	19.4	19.4	21.0	17.2	20.1	20.4
GY9-81	208	210	232	216	200	27.6	22.0	22.7	23.5	22.6	21.7	21.7
GY9-102	210	217	238	222	269	23.5	22.3	23.5	22.9	23.2	22.6	22.8
PS9-90	190	196	224	203	214	23.5	24.9	26.4	24.0	26.6	25.1	25.0
GY9-76	179	159	214	184	13	32.2	26.0	23.8	28.1	28.2	25.1	25.7
GY9-82a	179	179	201	186	41	32.8	28.9	29.7	28.2	29.0	29.0	29.3
GY9-78	126	122	137	128	8	38.1	38.5	39.7	38.2	35.9	38.9	38.1
GY9-82b	120	113	134	122	3	35.3	38.9	39.1	38.2	37.3	39.2	39.2
GY9-87	118	105	146	123	-77	40.2	39.1	37.3	40.4	41.3	39.4	39.4
GY9-84	122	115	156	131	-35	38.5	37.7	37.7	39.3	41.3	38.1	38.6

Table A1. (continued)

#	37	38	39	40	41	42	43	44	45	46	47	48
Oxide/element	Nb	Nb	K ₂ O	Na ₂ O	Na ₂ O	Na ₂ O	Na ₂ O					
Sample	calc.	calc.	actual	calc.	calc.	calc.	calc.	calc.	actual	calc.	calc.	calc.
	avg	excess		eqn.(27)	eqn.(28)	eqn.(29)	avg	loss		eqn.(30)	eqn.(31)	eqn.(32)
GY9-101	15.0	-0.2	0.72	0.86	0.86	0.85	0.86	0.14	2.55	2.78	2.76	2.84
PS9-92	17.2	-1.0	1.07	1.02	1.01	0.97	1.00	-0.07	3.68	2.70	2.91	2.87
GY9-74	12.7	5.0	0.47	0.72	0.73	0.68	0.71	0.23	2.48	2.41	2.32	2.41
GY9-79	13.5	3.7	0.38	0.77	0.78	0.75	0.77	0.39	2.44	2.48	2.37	2.57
KE9-71	15.3	5.1	0.80	0.85	0.87	0.88	0.87	0.06	2.66	2.53	2.68	2.67
PS9-89	17.1	1.8	0.99	0.99	0.99	1.02	1.00	0.00	3.05	2.62	2.69	2.72
KE9-73	15.3	5.6	0.61	0.84	0.86	0.96	0.89	0.28	2.42	2.50	2.60	2.50
GY9-99	19.6	2.9	0.43	1.24	1.25	1.05	1.18	0.75	1.84	2.26	2.31	2.35
GY9-81	22.4	5.2	1.06	1.34	1.33	1.39	1.35	0.29	2.70	2.51	2.64	2.60
GY9-102	22.9	0.6	1.09	1.39	1.40	1.43	1.41	0.32	2.20	2.54	2.73	2.71
PS9-90	25.3	-1.8	1.03	1.56	1.55	1.66	1.59	0.56	3.07	2.60	2.80	2.77
GY9-76	26.2	6.0	0.88	1.57	1.60	1.78	1.65	0.77	2.65	2.60	2.42	2.81
GY9-82a	29.0	3.8	1.88	1.82	1.83	1.84	1.83	-0.05	2.85	2.77	2.89	2.91
GY9-78	38.2	-0.1	0.79	2.50	2.44	2.39	2.45	1.66	4.04	2.82	2.93	2.95
GY9-82b	38.6	-3.3	2.46	2.53	2.52	2.50	2.52	0.06	2.67	2.78	2.81	2.87
GY9-87	39.5	0.7	1.52	2.54	2.54	2.78	2.62	1.10	2.70	2.77	2.65	2.79
GY9-84	38.8	-0.3	1.65	2.45	2.48	2.76	2.56	0.91	2.71	2.75	2.76	2.65

Table A1. (continued)

#	49	50	51	52	53	54	55	56
Oxide/element	Na ₂ O	Na ₂ O	CaO	CaO	CaO	CaO	CaO	CaO
Sample	calc.	calc.	actual	calc.	calc.	calc.	calc.	calc.
	avg	gain		eqn.(33)	eqn.(34)	eqn.(35)	avg	loss
GY9-101	2.77	-0.22	9.50	10.52	10.45	9.73	10.23	0.73
PS9-92	2.80	0.88	8.64	9.47	10.24	8.15	9.29	0.64
GY9-74	2.36	0.12	9.26	9.29	8.96	9.78	9.35	0.09
GY9-79	2.45	-0.01	9.70	9.40	9.01	9.94	9.45	-0.25
KE9-71	2.60	0.06	8.82	9.27	9.86	8.56	9.23	0.41
PS9-89	2.65	0.39	8.18	9.14	9.40	8.61	9.05	0.87
KE9-73	2.51	-0.09	9.13	9.16	9.55	8.59	9.10	-0.03
GY9-99	2.29	-0.44	6.52	6.89	7.06	16.83	10.26	
GY9-81	2.56	0.14	7.74	7.58	7.99	7.62	7.73	-0.01
GY9-102	2.64	-0.44	6.58	7.68	8.25	11.95	9.30	
PS9-90	2.70	0.37	7.06	7.52	8.11	8.92	8.18	1.12
GY9-76	2.59	0.07	7.79	7.35	6.85	8.13	7.44	-0.35
GY9-82a	2.83	0.02	4.42	7.67	8.02	7.07	7.58	3.16
GY9-78	2.88	1.16	5.43	6.85	7.09	6.38	6.78	1.34
GY9-82b	2.79	-0.12	4.91	6.67	6.71	5.74	6.37	1.46
GY9-87	2.71	-0.01	5.41	6.62	6.31	5.68	6.20	0.80
GY9-84	2.70	0.01	6.22	6.67	6.69	6.15	6.50	0.28

Notes to Table A1. Contents of major elements and trace elements are in wt. % and in ppm, respectively; data are not recalculated to a water-free base as it is in Table 4. x_F is an average value of a relative degree of differentiation of an initial melt (corresponds to sample GY9-74) calculated using La and Ce concentrations in rocks and used to evaluate contents of oxides and elements, which are shown in this Table. x_{F^*} is a value of a relative degree of differentiation of an initial melt (calculations using La, Ce and average) obtained at the next step of the iteration and demonstrating the that sufficiency sufficient of the iterations were done. A difference between $x_F(\text{La})$ and $x_F(\text{Ce})$ reflects an error of x_F calculation. “Excess” is a difference between an actual concentration of an oxide or an element in a rock and its average calculated content in a melt; “excess” probably reflects an amount of an oxide or an element in a rock related to an admixed cumulative Fe-Ti oxides. “Loss/Gain” is a difference between an actual content of an oxide or an element in a rock and its average calculated content in a melt. “Loss/Gain” reflects an amount of a component removed or added during allochemical metamorphism of a rock. The reference contents of oxides and elements are shown in bold. Contents of oxides and elements calculated using different equations are similar; it and indicates that our approaches are correct. In samples Gy9-99 and GY9-102 contents of CaO and FeO estimated using different equations significantly differ. It This can be attributed either to a significant amount of cumulative silicate phases (that were not taken into account in the calculations) or to allochemical behavior of some major elements (MgO?) in metamorphism (in rest of the samples MgO is probably inert in metamorphism).

U-Pb ages and tectonic setting of mid-Cretaceous magmatism in Chukotka (NE Russia)

M.V. Luchitskaya¹, P.L. Tikhomirov², and A.L. Shats³

¹Geological Institute Russian Academy of Sciences, Moscow, Russia

²Lomonosov Moscow State University, Moscow, Russia

³Public agency "Fire and Rescue Center", Moscow, Russia

ABSTRACT

We present a brief review of recent research on the age of granitoid plutons of the Anyui-Chukotka fold system, including Chaun fold zone, together with results of SHRIMP U-Pb zircon dating of two batholiths, Velitkenay and Moltykan. Despite structural differences, granitoids of both batholiths have similar isotopic ages, 105.3 ± 1.2 and 107.0 ± 1.0 . Granitoids of Chaun fold zone including Velitkenay and Moltykan batholiths have characteristics that are similar to those of post-orogenic plutons formed in extensional tectonic settings. We suggest a transtensional stress regime for their formation. There are geochemical similarities between the lowermost Etchikun unit of the Okhotsk-Chukotka belt and the Velitkenay and Moltykan batholiths and other granitoids of the Chaun zone. These results indicate the existence of a significant Mid-Cretaceous (Albian) magmatic event in the region, preceding initiation of the northern segment of Okhotsk-Chukotka volcanic belt.

INTRODUCTION

The Alazei-Oloy fold belt, South-Anyui Suture Zone and Anyui-Chukotka fold belt are the main tectonic elements of Chukotka (Fig. 1). They formed as a result of collision between an active North-Asian (Siberian) continent and the passive margin of the Chukotka-Alaska microcontinent (Parfenov, 1984; Zonenshain et al., 1990; Sokolov, 2007). Deformation on the Siberian continent was localized in the Alazei-Oloy fold system, and deformation of the passive margin of the Arctic Alaska-Chukotka microcontinent resulted in the Anyui-Chukotka fold belt. The South-Anyui suture zone formed as a result of an oceanic basin closure between these continental blocks (Seslavinsky, 1979; Natal'in, 1984; Sokolov et al., 2002). The South-Anyui suture

zone is a large orogen with south- and north-vergent structures, complicated by strike-slip faults (Sokolov et al., 2001; Bondarenko, 2004).

Cretaceous granitic plutons are widespread across the Anyui-Chukotka fold system (nearly 10% of the area). They comprise several batholiths (up to 2000 km²) and a number of smaller intrusions of granodiorites, quartz monzonites, granites, and leucogranites (Sadovsky, and Gelman, 1970; Samorukov and Matveenkov, 1984; Varlamova et al., 2004; Tibilov and Cherepanova, 2001). Granitoids intrude folded Devonian-Carboniferous clastic and limestone sequences, Late Permian-Triassic clastic rocks, and weakly deformed Late Jurassic-Early

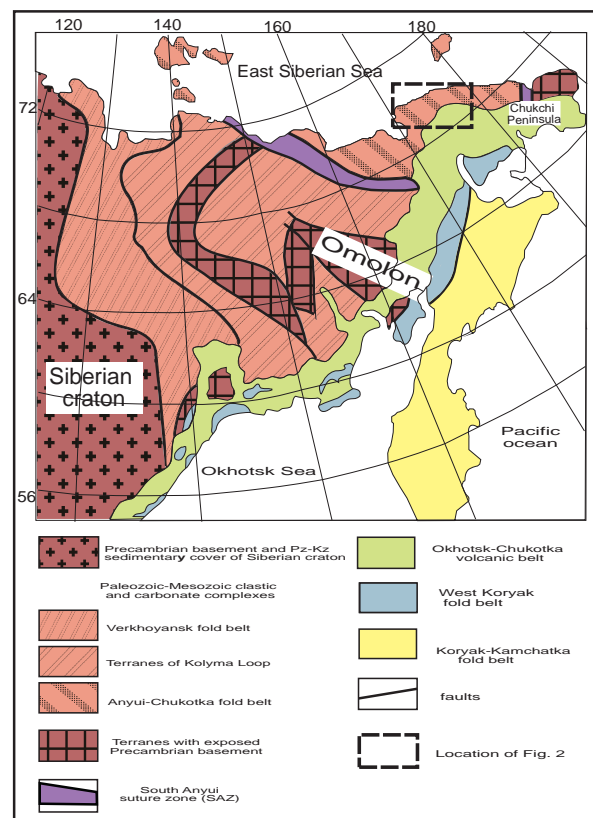


Fig. 1. Tectonic map of NE Russia (after Sokolov et al., 1999)

Cretaceous rocks, that formed in syn-collisional basins (Sadovsky and Gelman, 1970; Varlamova et al., 2004; Tibilov and Cherepanova, 2001). They are overlain by volcanic rocks of the Albian-Late Cretaceous Okhotsk-Chukotka belt (Fig. 2).

Here we present the results of SHRIMP U-Pb dating of zircons from two granitic plutons of the Chaun fold zone (CFZ), Velitkenay and Moltykan (V and M on Fig. 2). The shape and the spatial distribution of Chaun zone granitic bodies suggest their emplacement was controlled by faults of NW and NE strike (Fig. 2). The Velitkenay batholith includes gneissic granites, and some migmatites are present at its contact with Paleozoic metamorphic rocks. The Moltykan batholith consists of massive rocks and has sharp intrusive contacts with host rocks. The former may have formed in a granite-migmatite dome structure. The latter is similar to post-orogenic plutons formed in extensional tectonic settings. The observed structural diversity of the Chaun zone granitoids could result from their relation with at least two different tectonic events,

though this suggestion needs to be verified by independent methods, including isotopic dating.

GEOLOGIC SETTING OF CHAUN FOLD ZONE

The Chaun fold zone (Fig. 2) is composed of Paleozoic-Mesozoic sedimentary deposits. Lower Mesozoic (Triassic) rock assemblages accumulated on the passive margin of the Chukotka microcontinent (Parfenov, 1984; Parfenov et al., 1993; Akimenko, 2000; Tibilov and Cherepanova, 2001; Tuchkova, 2011). The northern part of this zone exposes several uplifts with outcrops of Devonian to Carboniferous metasedimentary rocks, overlain by terrigenous clastic sequences of Permian–Triassic age. The structure of these uplifts is now considered as that of granite-metamorphic core complexes, and its formation took place in Early Cretaceous (Gelman, 1995, 1996; Bondarenko and Luchitskaya, 2003; Miller et al., 2009, Luchitskaya et al., 2010). Paleozoic and Early Mesozoic strata are folded, with NW-trending fold axes. The western part of the

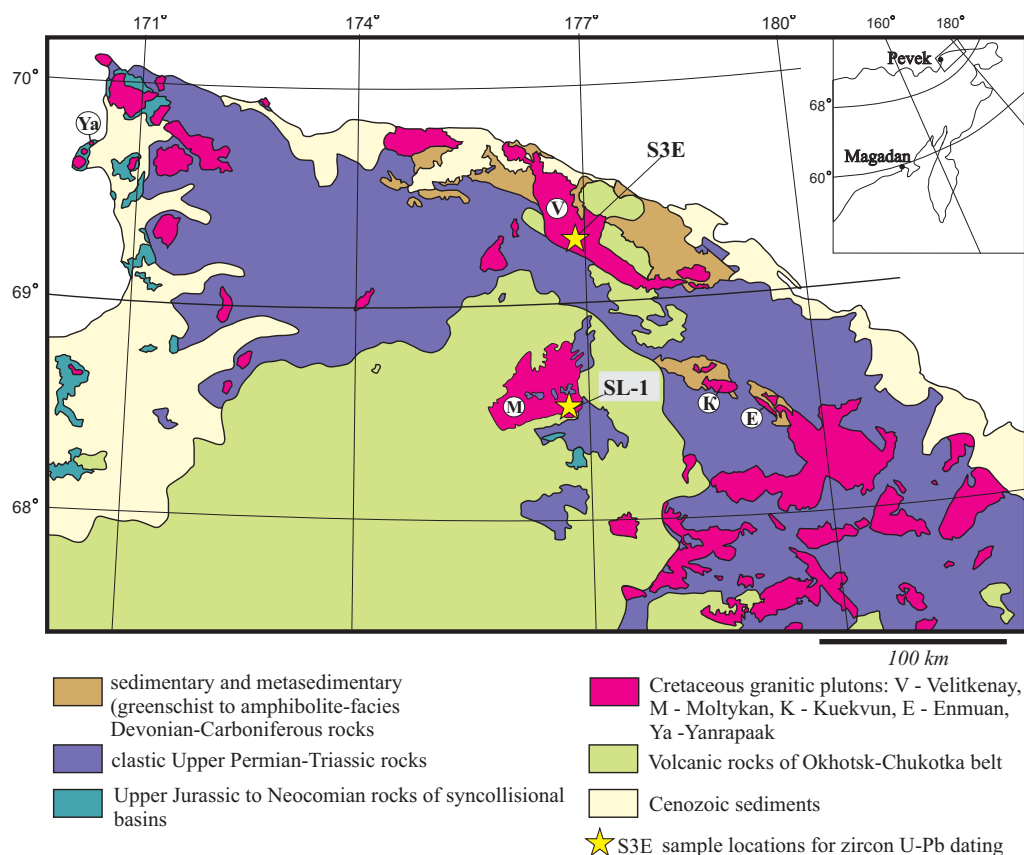


Fig. 2. Geological map of the Chaun tectonic zone (central part of Anyui-Chukotka fold system). Modified after Varlamova et al. (2004)

Chaun zone is overlain by slightly deformed Upper Jurassic to Lower Cretaceous clastic sediments of the Rauchua basin, probably of syn-collisional nature (Sokolov et al., 2002, Bondarenko, 2004, Miller et al. 2004, 2008, 2009).

To the south, structures of the Chaun zone are covered by thick (up to 3–4 km) undeformed sequences of the Okhotsk-Chukotka volcanic belt (OCVB). The OCVB was active from ~106–77 Ma (Belyui, 1977, Akinin and Miller, 2011), but the volcanic rocks which directly overlay the plutons are relatively young (89–80 Ma) (Tikhomirov et al., 2006). Granitic plutons of the Chaun zone form several linear belts with NW and NE strikes. They intrude both folded Triassic and weakly deformed Jurassic–Early Cretaceous sedimentary rocks, indicative of their emplacement during the post-orogenic stage (Miller et al., 2009).

K-Ar and Rb-Sr dating of granitoids of the Anyui-Chukotka fold system, including granitoids of Chaun fold zone, are predominantly Cretaceous, rarely Late Jurassic; single datings are Devonian (Sadovsky and Gel'man, 1970; Late Mesozoic granitoids of Chukotka, 1965; Petrology of magmatic formations of Chukotka, 1969; Milov, 1975; Zagruzina, 1977; Tibilov et al., 1986; Efremov et al., 2000; Tikhomirov, 1998; Zhulanova et al., 2007). On geological maps (Varlamova et al., 2004) all granitoid plutons are referred to as a single Early Cretaceous complex, which is called the Chukotka complex in western Chukotka and the Taurean complex in eastern Chukotka; in the central part of Chukotka the magmatic rocks are named the Telekay granitoid complex. Statistical peaks of the older K-Ar data reported from these rocks are 97 and 85 Ma (Gorbov et al., 1968; Akinin and Kotlyar, 1997; Zhulanova et al., 2007). Efremov et al., (2000) and Zhulanova et al., (2007) generalized existing K-Ar and Rb-Sr datings. The former distinguished three stages of granitoid magmatism based on a study of the granitoids of the Chaun fold zone (western part of Anyui-Chukotka fold system): 1) 144 ± 14.4 , 2) 126.8 ± 9.6 and 3) 85 ± 1.9 Ma (Efremov et al., 2000). The third stage is synchronous with Okhotsk-Chukotka volcanic belt activity. Efremov et al., (2010) noted that Rb-Sr dating of these rocks is not likely to be reliable because mixing of magmas with different initial $(^{87}\text{Sr}/^{86}\text{Sr})_0$ values may have occurred.

According to Zhulanova et al., (2007) granitoid magmatism in the Chukotka, Taurean and Telekay complexes began in the Middle to Late Jurassic (164–152 Ma). However, the main volume of granodiorite magmas corresponds to Valanginian-Hauterivian, as the most precise date is 139 ± 1.4 Ma (Zhulanova et al., 2007). Granites and leucogranites were intruded at 127 Ma (Zhulanova et al., 2007). These authors suggested that as a result of 109–106, 98–95, and 83–80 Ma thermal events, the isotopic systems of rocks of all three complexes were disturbed. More recently, U-Pb SHRIMP (Sensitive High-Resolution Ion Microprobe) dating on granitoids of the Anyui-Chukotka fold system (Natal'in et al., 1999; Miller et al., 2009; Miller and Verzhbitsky, 2009; Akinin, 2011, Akinin et al., 2012; Katkov et al., 2013), indicate both Cretaceous (Aptian-Albian, 117–100 Ma) and Devonian-Early Carboniferous (370–375 Ma, 363 ± 44 Ma, 380 Ma, 353 ± 5 Ma, 352 ± 6 Ma) ages.

The Molykan batholith is one of the largest intrusive complexes of the Chaun zone; its outcrop area is 1,630 km². In map view, the intrusive body is slightly elongated in a northeasterly direction, across the strike of the principal fold structures of the region (Fig. 2). It intrudes Late Triassic clastic sequences and produced a hornfelsic aureole up to 200 m wide. The aureole is composed of quartz-biotite, quartz-biotite-diopside, quartz-biotite-cordierite and quartz-biotite-hornblende hornfels (Milov, 1975, Varlamova et al., 2004). To the NW and SW, the batholith is unconformably overlain by volcanic strata of the OCVB. Remnants of both Triassic sediments and Late Cretaceous volcanic rocks are present within the Molykan granite, indicative of a relatively shallow depth of the erosional incision. Compositionally, the batholith is dominated by granodiorites and monzogranites. Between major rock types both sharp contacts and gradual transitions have been documented (Tikhomirov, 1998) so the batholith was likely produced by several major near-simultaneous intrusive pulses (Tikhomirov, 1998).

The Velitkenay batholith is elongated in a NE direction being 150 km in length and from 3–5 to 35 km in width and has S-shaped outlines; its outcrop area is nearly 2000 km² (Fig 2). The batholith intrudes Upper Devonian-Lower Carboniferous terrigenous and carbonate rocks, Triassic shales, siltstones and

sandstones and is overlain by Upper Cretaceous volcanic rocks (Varlamova et al., 2004; Tibilov and Cherepanova, 2001). There is a migmatite zone along the contact with host rocks, varying in width from several to 250–300 meters and granitoids contain xenoliths of Paleozoic metasedimentary rocks (Milov, 1975, Akinin and Polzunenkov, 2013). Two intrusive phases are distinguished in the batholith (Milov and Ivanov, 1965): 1) coarse- and medium-grained porphyric biotite, biotite-amphibole and amphibole quartz diorite, monzonites, granodiorites and granites of the early phase; 2) fine- and medium-grained leucocratic granites of a later phase. Granites of the late phase form dikes and stocks.

RESULTS OF U-PB STUDIES

Analytical techniques

Zircons have been extracted from two samples: a gneissic quartz monzodiorite from the Velitkenay pluton and a massive granodiorite from the Molytkan pluton. U-Pb zircon dating was carried out by E.N. Lepekhina using the high-resolution

multi-collector secondary ion mass spectrometer SHRIMP-II in the Center of Isotopic Studies of A.P. Karpinsky Russian Geological Research Institute (St. Petersburg).

Hand-picked zircons were mounted in epoxy together with standard zircons TEMORA and 91500. The zircons were ground to approximately half their original thickness and polished. To select the analysis locations optical (in transmitted and indirect light) and cathodoluminescence (CL) images were used to determine the inner structure and zoning of zircons.

Measurements of U-Pb ratios on SHRIMP-II were carried out by techniques described in Williams, (1998). The intensity of the primary beam of molecular negatively charged oxygen ions was 2 nA, and the beam diameter was 5 μm . The SQUID program (Ludwig, 2000) was used for data processing. U-Pb ratios were normalized to a 0.0668 value, attributed to standard TEMORA zircon, which corresponds to an age of 416.75 Ma age of this zircon (Black et al., 2003). Errors of single analyses (ratios

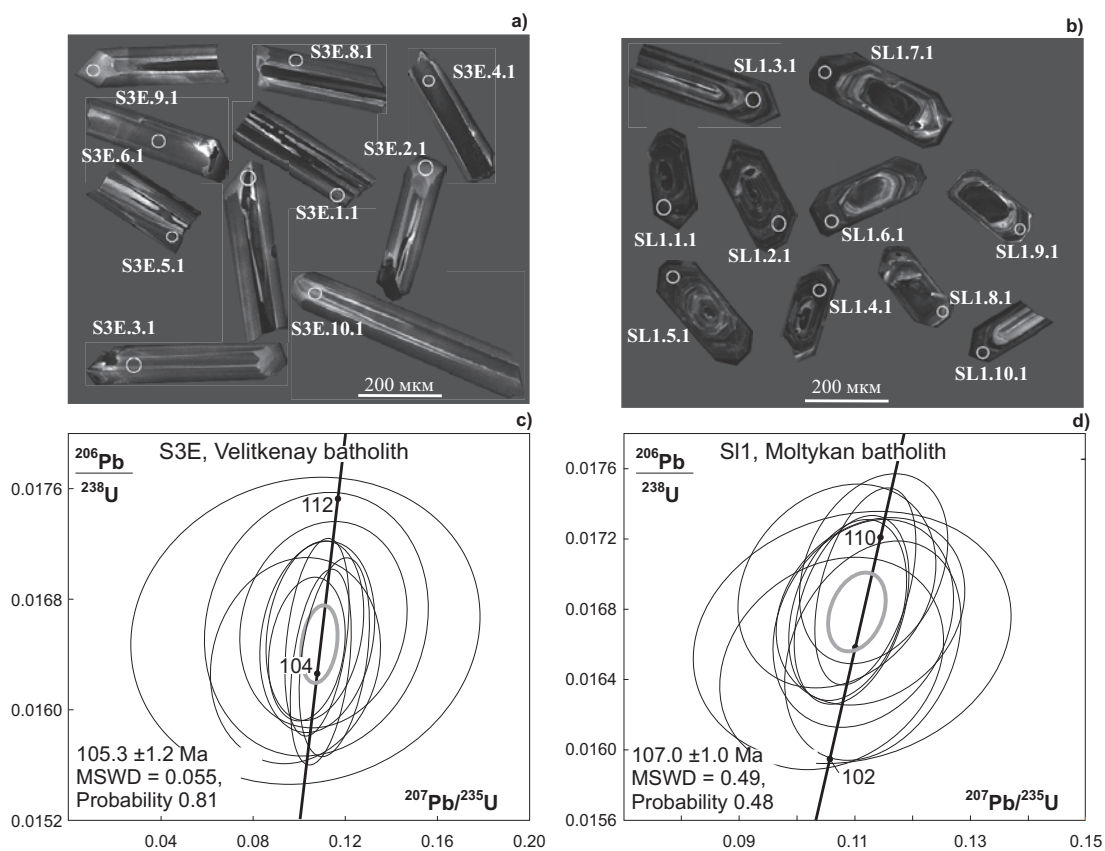


Fig. 3. CL images of zircons and concordia diagrams for granitoids of Velitkenay (a, c) and Molytkan (b, d) batholiths

Table 1.

spot	206 Pbc, %	U ppm	Th ppm	232Th /238U	206 Pb*, ppm	(1) 206Pb/ 238U age, Ma	1σ, ±%	238U/ 206Pb	1σ, ±%	207Pb/ 206Pb	1σ, ±%	207Pb* /235U	1σ, ±%	206Pb* /238U	1σ, ±%	Err corr
sample S3E (gneissic quartz monzodiorite, Velitkenay batholith, N 69°17'2.75", E 176°50'58.61")																
S3E.1.1	0.44	932	44	0.05	13.2	105.1	0.79	60.56	1.2	0.0491	2.8	0.1033	6.5	0.01644	1.3	.198
S3E.2.1	0.00	383	129	0.35	5.43	105.7	1.09	60.50	1.8	0.0472	5.0	0.1076	5.3	0.01652	1.8	.334
S3E.3.1	0.00	378	231	0.63	5.32	104.7	1.10	61.00	1.8	0.051	5.1	0.1151	5.4	0.01638	1.8	.332
S3E.4.1	0.67	618	403	0.67	8.86	105.9	0.97	59.94	1.6	0.052	3.9	0.1068	8.1	0.01657	1.6	.199
S3E.5.1	0.81	508	314	0.64	7.27	105.7	1.03	60.01	1.6	0.0538	4.2	0.1080	9.5	0.01653	1.7	.180
S3E.6.1	1.21	465	292	0.65	6.61	104.6	1.16	60.40	1.7	0.0533	4.4	0.0980	15	0.01636	1.9	.121
S3E.7.1	1.58	365	198	0.56	5.29	106.3	1.38	59.20	2.1	0.0594	4.8	0.1070	18	0.01662	2.3	.127
S3E.8.1	1.16	506	301	0.61	7.31	106.2	1.08	59.48	1.7	0.0574	4.2	0.1100	13	0.01661	1.8	.137
S3E.9.1	0.00	416	201	0.50	5.83	104.3	1.10	61.30	1.8	0.0486	4.6	0.1093	5	0.01631	1.8	.358
S3E.10.1	2.54	225	102	0.47	3.29	106.0	1.63	58.80	2.2	0.0652	5.7	0.1030	30	0.01657	2.7	.091
sample SL1 (massive porphyric granodiorite, Mol'tykan batholith, N 68°30'35.70", E 176°47'17.80")																
SL1.2.1	0.21	1966	476	0,25	28.4	107.4	1.4	59.53	1.3	0,0472	2.7	0.1094	3.7	0.01680	1.3	.354
SL1.1.1	0.37	2153	514	0,25	31.6	108.9	1.4	58.72	1.3	0,0482	2.5	0.1132	4.6	0.01703	1.3	.282
SL1.3.1	0.70	2469	482	0,20	35.9	107.3	1.4	59.57	1.3	0,0487	2.3	0.1127	5.9	0.01679	1.3	.221
SL1.4.1	0.28	2889	1303	0,47	41.8	107.4	1.3	59.54	1.2	0,0470	2.2	0.1088	3.8	0.01679	1.3	.327
SL1.5.1	0.45	1593	523	0,34	23.3	108.2	1.5	59.05	1.4	0,0458	3.0	0.1070	6.5	0.01693	1.4	.214
SL1.6.1	0.00	937	286	0,32	13.3	105.9	1.6	60.37	1.5	0,0495	5.3	0.1130	5.5	0.01656	1.5	.280
SL1.7.1	0.00	1758	338	0,20	25.6	108.2	1.4	59.06	1.4	0,0479	2.9	0.1118	3.2	0.01693	1.4	.425
SL1.8.1	0.83	682	282	0,43	9.83	106.4	1.9	60.1	1.7	0,0478	4.3	0.1100	10	0.01664	1.8	.172
SL1.9.1	0.64	1416	524	0,38	20.5	106.9	1.5	59.81	1.4	0,0483	3.1	0.1114	5.7	0.01672	1.4	.253
SL1.10.1	0.48	1252	400	0,33	17.8	105.4	1.6	60.63	1.5	0,0466	4.6	0.1060	7.4	0.01649	1.5	.202

Notes. Errors are 1-sigma; Pbc and Pb* indicate the common and radiogenic portions, respectively. Error in Standard calibration was 0.68% (not included in above errors but required when comparing data from different mounts).

(1) Common Pb corrected using measured 204Pb. Analyst E.N.Lepekhina.

and ages) are at one sigma level, errors of calculated concordant ages and intersections with concordia are at two sigma levels. Concordia plotting (Wetherill, 1956) was carried out using ISOPLOT/EX program (Ludwig, 1999).

U–Pb SHRIMP data

Zircons from gneissic quartz monzodiorite (S3E, Velitkenay batholith) are represented by colorless or yellowish idiomorphic elongate-prismatic (1:4–1:10) crystals, with lengths ranging from 300–800 μm (Fig. 3a). CL zonation of the imaged crystals is predominantly oscillatory without apparent cores,

suggesting a magmatic origin. All 10 analyses yield a weighted mean 206Pb*/238U concordant age of 105.3±1.2 Ma (MSWD=0.06, P=0.81) (Fig. 3c, Table 1). Nearly the same age (105–100 Ma) for the Velitkenay batholith was confirmed by V.V.Akinin et al., (2012).

Zircons from massive porphyric granodiorite (SL1, Moltykan batholith) are represented by colorless or yellowish idiomorphic short- and elongate-prismatic (1:2–1:5) crystals, with lengths ranging from 200–500 μm (Fig. 3b). CL zonation of the imaged crystals is predominantly oscillatory, suggesting their magmatic origin, and apparent

cores are absent. All 10 analyses yield a weighted mean $^{206}\text{Pb}^*/^{238}\text{U}$ concordant age of 107.0 ± 1.0 Ma (MSWD=0.49, P=0.48) (Fig. 3d, Table 1).

Thus the age of both batholiths corresponds to Albian Stage of Cretaceous they are the same within the analytical error despite their structural difference.

GEOCHEMISTRY

The element analysis of rock's samples was made at the laboratory of the nuclear-physical and mass-spectrum method analysis involved in the Analytic Certification Testing Center of the Institute of Microelectronics Technology and High Purity Materials of Russian Academy of Science. The content of Li, Be, Na, Mg, Al, K, Ca, Sc, Ti, V, Cr, Mn, Fe, Co, Ni, Cu, Zn, Ga, Rb, Sr, Y, Zr, Nb, Cs, Ba, La, Ce, Pr, Nd, Sm, Eu, Gd, Tb, Dy, Ho, Er, Tm, Yb, Lu, Hf, Ta, Pb, Th, and U in rocks was determined using inductively coupled plasma mass spectrometry (X-7, *Thermo Elemental*, USA) and inductively coupled plasma atomic emission

spectrometry (ICAP-61, *Thermo Jarrell Ash*, USA).

Granitoids of Chaun fold zone including Velitkenay and Molytkan batholiths have characteristics that are similar to those of post-orogenic plutons formed in extensional tectonic settings. They fall in the field of post-collisional granites on Pearce (1996) discriminant diagram (Fig. 4) and in the same fields with Chaun zone granites of QAP diagram (Le Maitre, 1989) (Fig. 5). For comparison we included mid-Cretaceous granitoids of Kigluaik pluton of the Kigluaik gneiss dome, Seward Peninsula, Alaska (Amato and Wright, 1997). These granitoids are subalkaline, typical for all granitic complexes of the Chaun fold zone (Tikhomirov, 1998; Tikhomirov and Luchitskaya, 2006; Dudkinsky et al., 1993; 1997).

Granitoids of Velitkenay and Molytkan batholiths have identical fractionated chondrite-normalized patterns with negative Eu-anomalies ($\text{La}_N/\text{Yb}_N=8.85; 10.71; \text{Eu}/\text{Eu}^*=0.43; 0.55$) (Fig. 6, Table 2). They are similar to those of granitoids of

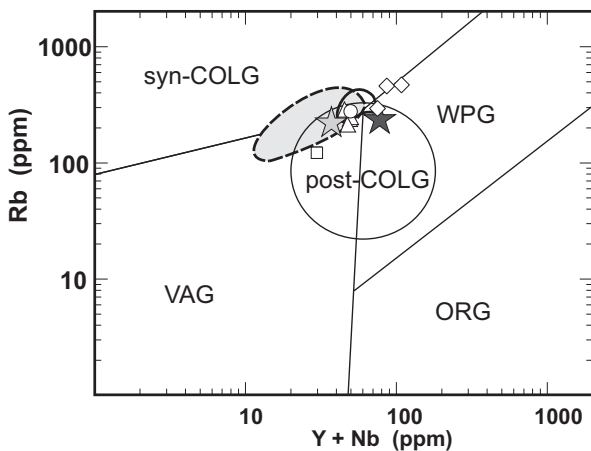


Fig. 4. Rb vs Y+Nb diagram (Pearce et al., 1984) for dated granitoids of Velitkenay and Molytkan batholiths, granites from other plutons of Chaun fold zone, Alarmaut Uplift granitoids (Chukotka) and granitoids of Kigluaik pluton, Seward Peninsula (Alaska)

- ★ Chaun fold zone
- ★ Velitkenay quartz monzodiorite (106 Ma)
- ★ Molytkan granodiorite (108 Ma)
- Molytkan granodiorite
- Telekay, southern part, adamellite ($K_{1,2}$, Tikhomirov, 1998)
- ◇ Telekay, northern part, granite, leucogranite ($K_{1,2}$, Tikhomirov, 1998)
- △ Peekiney quartz syenites ($K_{1,2}$, Tikhomirov, 1998)
- Kigluaik pluton granitoids (90 Ma, Amato, Wright, 1997)
- Alarmaut Uplift granitoids (112-117 Ma, Katkov et al., 2007; Miller et al., 2009)

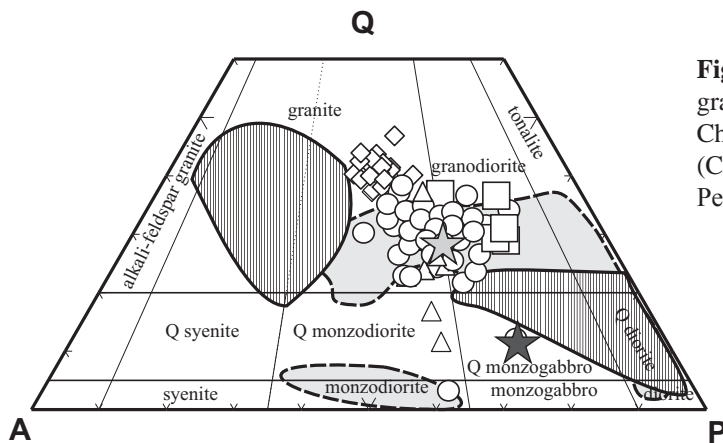


Fig. 5. QAP diagram (Le Maitre, 1989) for granitoids of Velitkenay and Molytkan batholiths, Chaun fold zone granites, Alarmaut Uplift granites (Chukotka) and granites of Kigluaik pluton, Seward Peninsula (Alaska). See fig. 4 for unit names

the other plutons of Chaun zone and Alarmaut Uplift. More differentiated leucogranites and granites of Telekay pluton (Chaun zone) and Kigluaik pluton have more pronounced negative Eu-anomaly (Fig. 6B).

Spidergrams of Velitkenay and Molytkan batholiths are characterized by enrichment of lithophile elements, light rare earths and negative Ta, Nb, Sr, Ti anomalies (Fig. 7). They are also similar to granitoids of other plutons of Chaun zone, Alarmaut Uplift and Kigluaik pluton.

DISCUSSION AND CONCLUSIONS

Comparison with other available U-Pb SHRIMP zircon data indicates that our ages are similar to those of Yanrapaak pluton near Pevek City (108.1±1.1 Ma, Miller and Verzhbitsky, 2009). Our ages are slightly younger than those of Aptian-Albian granitoids of the Alarmaut Uplift in more western part of Anyui-Chukotka fold system (116–112 Ma, Katkov et al., 2007, Miller et al., 2009). The latter are

Table 2. Major (wt.%) and trace elements (ppm) of granitoids of Velitkenay and Molytkan batholiths

	Velitkenay	Molytkan
Nosam.	S3E	SL-1
SiO ₂	58.9	69.2
TiO ₂	1.0	0.46
Al ₂ O ₃	16.1	14.8
Fe ₂ O ₃ *	7.7	3.7
MnO	0.13	0.063
MgO	3.5	1.7
CaO	6.3	2.5
Na ₂ O	3.2	3.0
K ₂ O	2.8	4.4
P ₂ O ₅	0.33	0.14
S	0.05	0.02
Total	99.97	99.99
Li	35.1	52.5
Be	5.2	4.7
Sc	16.9	11.7
V	85.6	60.3
Cr	36.3	47.7
Co	18.0	8.3
Ni	30.5	23.1
Cu	10.1	17.7
Zn	124	60.7
Ga	19.9	16.1
Rb	243	227
Sr	402	362
Y	40.4	23.0
Zr	109	173
Nb	25.2	13.1
Cs	12.7	11.8
Ba	505	900
La	48.6	39.5
Ce	105	83.7
Pr	12.3	9.6
Nd	49.0	37.6
Sm	10.0	7.4
Eu	1.3	1.2
Gd	8.8	5.9
Tb	1.3	0.84
Dy	7.2	4.6
Ho	1.4	0.88
Er	3.9	2.5
Tm	0.54	0.37
Yb	3.7	2.5
Lu	0.53	0.34
Hf	3.3	5.2
Ta	1.4	0.8
Pb	24.5	38.5
Th	16.9	23.7
U	3.0	4.3
Lan/Ybn	8.85	10.71
Eu/Eu*	0.43	0.55

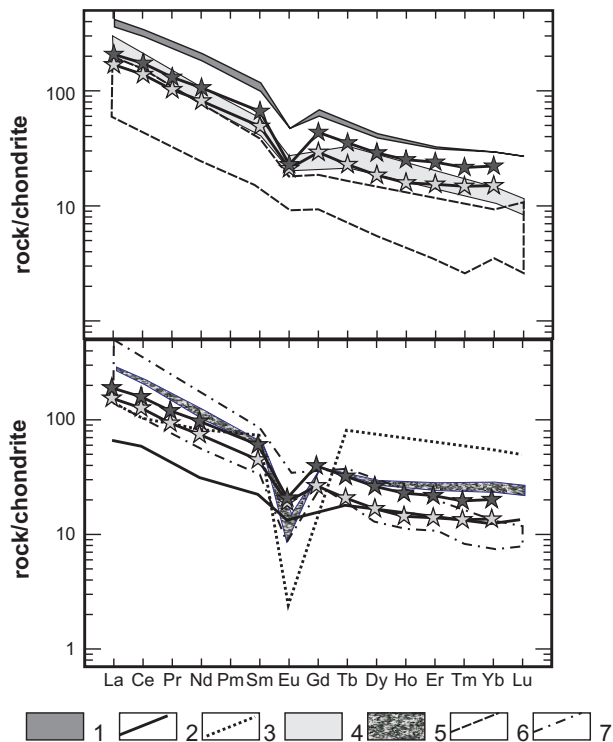


Fig. 6. Chondrite-normalized REE patterns for granitoids of Velitkenay, Molytkan batholiths and plutons of Chaun zone, Alarmaut Uplift and the Kigluaik pluton. Normalization to chondrite (Sun and Donough, 1989). For symbols see Fig. 4

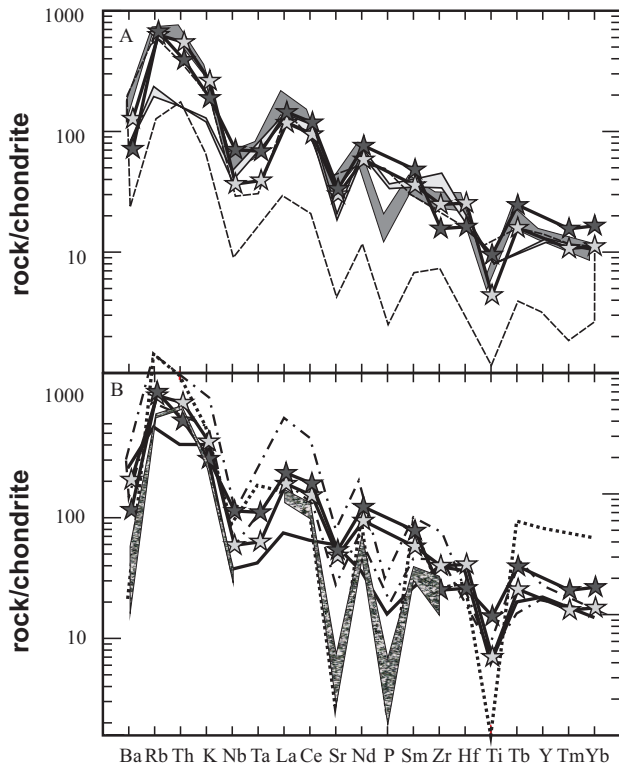


Fig. 7. Spidergrams for granitoids of Velitkenay, Molytkan batholiths and plutons of Chaun zone, Alarmaut Uplift and Kigluaik pluton. For symbols see Fig. 4 and 6.

undeformed granitoids associated with the central part of the granite-metamorphic core complex and are considered as extension-related post-collisional plutons, intruded the final stages of collision between active margin structures of North-Asian (Siberian) continent and Chukotka-Alaska microcontinent (Bondarenko and Luchitskaya, 2003, Miller et al. 2009, Miller and Verzhbitsky, 2009; Luchitskaya et al., 2010). Extension might be associated with strike-slip movements (Bondarenko, 2004). The age of Molytkan and Velitkenay batholiths is similar to the age of metamorphism in the framework of Alarmaut Uplift granitoids (109–103 Ma), that is extensional in nature and post-dates collision (Miller et al., 2009) and the age of undeformed post-tectonic granitoid plutons of the South-Anuyi zone (109 Ma) (Miller et al., 2009; Luchitskaya et al., 2010). U-Pb zircon and monazite data of Koolen' granite-metamorphic core complex of eastern part of Anyui-Chukotka fold system show that the age of metamorphism synchronous with extension (orthogneiss) (108 Ma) and deformation (deformed pegmatite) (104 Ma) coincides with the ages of Velitkenay and Molytkan

batholiths (Bering Strait Geologic Field Party, 1997; Akinin, 2011). The age of non-deformed granites of Koolen' complex is younger (94 Ma) (Bering Strait Geologic Field Party, 1997).

Many authors noted the interrelation between extension processes and the formation of plutonic belts and individual intrusions in northeastern Russia territory (e.g., Bering Strait Geologic Field Party, 1997; Layer et al., 2001, Toro et al., 2003; Miller and Verzhbitsky, 2009; Miller et al. 2009). Layer et al. (2001) used $^{40}\text{Ar}/^{39}\text{Ar}$ dating of magmatic complexes to distinguish two extensional events: an older one from 135–120 Ma and a younger one from 110–93 Ma. In their opinion the older event was probably related to post-accretionary northwest translation of the now-accreted Kolyma-Omolon terrane relative to North Asia. Subsequently the entire region was subjected to east-west extension resulting in the intrusion of plutonic belts that have within-plate characteristics. This extension could be the consequence of north-south closure of the South-Anuyi suture. The age of the second younger extensional event coincides with our ages from the Velitkenay and Molytkan batholiths.

The shape and the spatial distribution of granitic bodies of the Chaun zone suggest their emplacement was controlled by faults of north-west and north-east strike. NS and NE average dike orientations and east-west, and north-west extension directions inferred from structural data in the region were proposed by Miller and Verzhbitsky, 2009. Our data support a model of northeast-southwest extension direction (Fig. 8). To explain the synchronous formation of both NE and NW-trending plutons, we use the tectonic model which implies the combination of NW-SE extension and right-lateral strike-slip deformations within the area north of the South Anyui zone (Miller et al., 2009). The gneissic structure of some granites and the observed manifestations of regional metamorphism may be associated with the formation of gneiss domes (Gel'man, 1996; Amato and Miller, 2004; Miller et al., 2009, Akinin et al., 2009; and references therein). Such complexes could have formed in a transtensional stress regime – a suggestion consistent with the S-shaped outlines of Velitkenay pluton (Fig. 2).

The SHRIMP U-Pb zircon dates obtained for the Velitkenay and Molytkan batholiths are similar to the

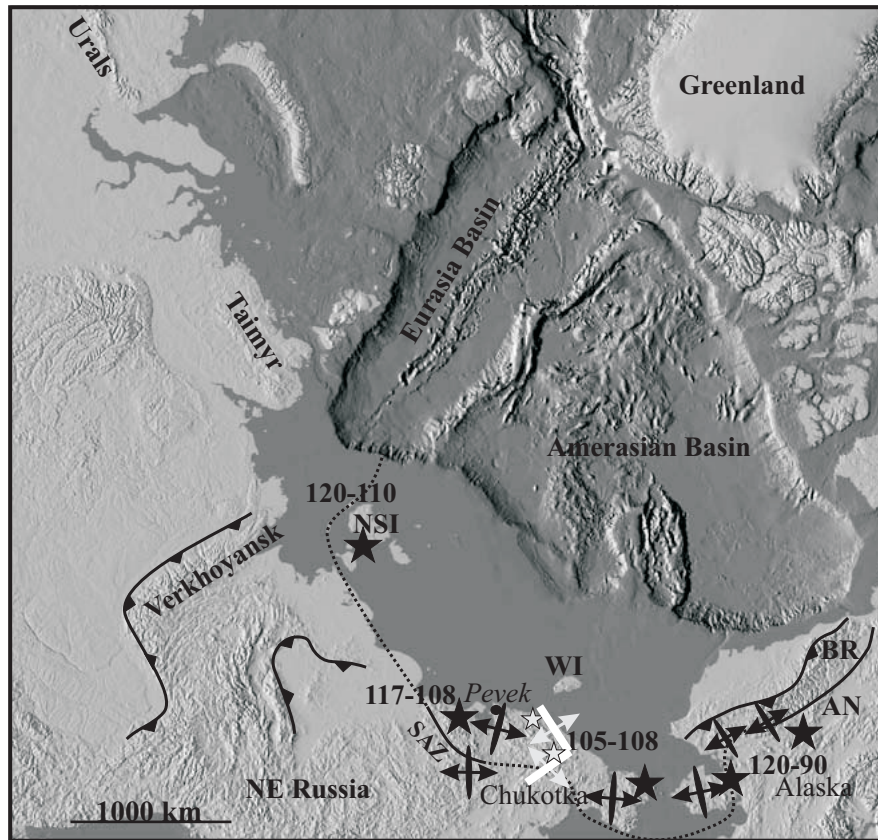


Fig. 8. Circum-Arctic map, modified after (Miller and Verzhbitsky, 2009). Black stars are Cretaceous magmatic activity and elongate ellipses are average dike orientations and inferred extension directions (thin lines) based on land geology (Miller and Verzhbitsky, 2009). White stars are Velitkenay and Moltykan batholiths and white sections are their orientations and inferred extension directions. Cretaceous extension directions in northern Alaska (south flank of Brooks Range and Seward Peninsula), the Bering Strait region and adjacent Chukotka are N-S oriented and are from Miller et al. (2002). AN – Angayucham belt, BR – Brooks Range, NSI – New Siberian Islands, WI – Wrangel Island

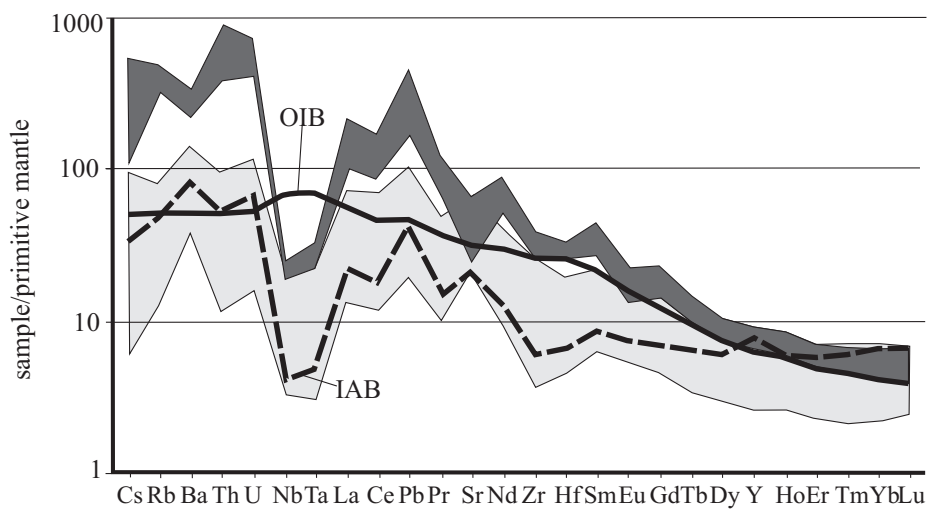


Fig. 9. Spidergrams for rocks of Etchikun Suite (dark grey), Okhotsk-Chukotka volcanic rocks, northern part (light grey). IAB, island arc basalt, OIB, oceanic island basalt (P.L.Tikhomirov, unpublished data). OIB, IAB normalization values are from Sun and Donough (1989)

age of the Etchikun suite (106 Ma – unpublished data of P.L.Tikhomirov). Within the study area this suite is considered as the lowermost unit of the Okhotsk-Chukotka volcanic belt. This suite is composed of trachybasalts, trachyandesites, latites and is shoshonitic series rocks, compositionally similar to subalkaline granitoids of Chaun zone. Spidergrams of Etchikun suite rocks are characterized by large-ion lithophile elements enrichment, depletion of high-field strength elements and pronounced Ta-Nb negative anomaly (Fig. 9). These facts, as well as a significant hiatus of about 15 m.y. at the top of the Etchikun suite, infer that the latter may be not linked to the Okhotsk-Chukotka belt. Instead, it could be related to the same mid-Cretaceous extensional event which that produced most of granitic bodies of the Chaun zone.

ACKNOWLEDGMENTS

Work is supported by RFBR (N13-05-00249), FTs-NTP leading scientific schools (NSh-2981.2014.5), kontrakts № 01.14.20.11, № 14.740.11.0190. We are indebted to E.Miller and J.Amato for in-depth reviews of an earlier version of manuscript.

REFERENCES

Akimenko, G.I. 2000. Geologic map 1:200000 scale. R-58-XXXV, XXXVI (Bilibino)

Akinin, V.V., Miller, E.L., 2011. Evolution of calc-alkaline magmas of the Okhotsk-Chukotka volcanic belt. *Petrology*, 19, 3, 237–279.

Akinin, V.V. and Kotlyar, I.N. 1997. GEOKHRON – computer data base of isotopic dating of minerals, rocks and ores of North-East. In: Ed. S.G.Byalobzhesky. *Magmatism and ore formation of Russian North-East*. Magadan: SVKNII DVO RAN, 313-318.

Akinin, V.V., Miller, E.L., Wooden, J. 2009. Petrology and Geochronology of Crustal Xenoliths from the Bering Strait Region: Linking Deep and Shallow Processes in Extending Continental Crust. In: R.B. Miller and A. W. Snoke, eds., *Crustal cross-sections from the western North America Cordillera and elsewhere: Implications for tectonic and petrologic processes*, Geological Society of America Special Paper 456, 39-68

Akinin, V.V., Miller, E.L., Gotlieb E., and

Polzunenkov G., 2012. Geochronology and geochemistry of Cretaceous magmatic rocks of Arctic Chukotka: an update of GEOCHRON2.0. *Geophysical Research Abstracts*, 14. EGU2012-3876.

Akinin, V.V. and Polzunenkov G., 2013. Composition and age of Velitkenay granite-migmatite massif (Arctic Alaska-Chukotka terrane): synchronization with tectonic-magmatic events in Amerasian basin of Arctic. Abstracts of All-Russian conference “Tectonics, deep structure and minerageny of East Asia”. 17-20 September 2013. Khabarovsk, 6-9.

Amato, J.M. and Miller, E.L., 2004. Geologic map and summary of the evolution of the Kigluaik Mountains gneiss dome, Seward Peninsula, Alaska. In: Whitney, D. L, Teyssier, C., and Siddoway, C. S. (eds) *Gneiss Domes in Orogeny*. *Geol. Soc. Am. Spec. Paper*, 380, 295–306.

Amato J.M. and Wright, J.E., 1997. Potassic mafic magmatism in the Kigluaik gneiss dome, northern Alaska: a geochemical study of arc magmatism in an extensional tectonic setting. *J. Geophys. Res.*, 102, B4, 8065–8084.

Belyui, V.F., 1977. *Stratigraphy and structures of Okhotsk-Chukotka volcanic belt*. M.: Nauka, 171 (in Russian).

Bering Strait Geologic Field Party, 1997. Koolen metamorphic complex, NE Russia: implications for the tectonic evolution of the Bering Strait region. *Tectonics*, 16, 5, 713-729.

Black, L.P., Kamo, S.L., Allen, C.M., Aleinikoff, J.N., Davis, D.W., Korsch, R.J. and Foudoulis, C., 2003. TEMORA 1: a new zircon standard for Phanerozoic U–Pb geochronology. *Chemical Geology*, 200, 155-170.

Bondarenko, G.E. 2004. Tectonics and geodynamic evolution of Mesozooids of northern framework of Pacific Ocean. Moscow: Lomonosov Moscow State University, 46 (in Russian).

Bondarenko, G.E. and Luchitskaya, M.V., 2003. Mesozoic tectonic evolution of Alarmaut Uplift. *Byulleten’ MOIP. Otdeleniye geol.*, 78, 3, 25–38 (in Russian).

Dudkinsky, D.V., Efremov, S.V., and Kozlov, V.D., 1993. Geochemical features of Mesozoic granitoides of increased basicity of Chaun Bay (Chukotka). *Pacific geology*, 6, 74–85.

- Dudkinsky, D.V., Kozlov, V.D. and Efremov, S.V. 1997. Petrological-geochemical peculiarities and geodynamic setting of Chukotka ore-bearing granitoids formation. *Geology and geophysics*, 38, 7, 1202-1216 (in Russian).
- Efremov, S.V., Kozlov, V.D. and Sandimirova, G.P., 2000. Rb/Sr age of granitoids of Central Chukotka, new sight on the history of geological evolution of the region. *Doklady Earth Sciences*, 375A, 9, 1463–1466.
- Efremov, S.V., Dril', S.I., Sandimirova, G.P. and Sandimirov, I.V., 2010. Using of Rb/Sr isotopic data for chronometry of granitoid intrusions (on the example of Severny massif, C.Chukotka). *Geology and Geophysics*, 51, 12, 1618–1624 (in Russian).
- Gel'man, M.L., 1995. Phanerozoic granite-metamorphic domes on the northeast of Russia. Paper 1. Geological evolution of Paleozoic and Mesozoic domes. *Pacific Geology*, 4, 102-115. (in Russian).
- Gel'man, M.L., 1996. Phanerozoic granite-metamorphic domes on the northeast of Russia. Paper 2. Magmatism, metamorphism and migmatization in Late Mesozoic domes. *Pacific Geology*, 1, 84-93 (in Russian).
- Gorbov, V.V., Zagruzina, I.A. and Safronov, D.N., 1968. Geochronological typification of some Mesozoic intrusive complexes of North-East Asia. In: *Magmatism of North-East Asia*. Magadan, 31–33 (in Russian)
- Katkov, S.M., Strickland, A. and Miller, E.L., 2007. On the age of granite intrusions of Anyui-Chukotka fold system. *Doklady Earth Sciences*, 414, 2, 219–222.
- Katkov, S.M., Luchitskaya, M.V., Kotov, A.B., Sal'nikova, E.B., Yakovleva, S.Z. 2013. Late Paleozoic granitoids of Central Chukotka; structural position and age foundation. *Doklady Earth Sciences*, 450, 2, 193–198 (in Russian).
- Late Mesozoic granitoids of Chukotka. *Proceedings SVKNII*, 12. 1965. Magadan, SVKNII, 242 (in Russian).
- Layer, P.W., Newberry, R., Fujita, K., Parfenov, L., Trunilina, V. and Bakharev, A., 2001. Tectonic settings of the plutonic belts of Yakutia, northeast Russia, based on $^{40}\text{Ar}/^{39}\text{Ar}$ geochronology and trace element geochemistry. *Geology*, 29, 2, 167–170.
- Le Maitre, R. W., Bateman, P., Dudek, A., Keller J., Lameyre J., Le Bas M., Sabine, P.A., Schmid, R., Sorensen, H., Streckeisen, A., Wooley, A.R. and Zanettin, B., 1989. A classification of igneous rocks and glossary of terms: recommendations of the International Union of Geological Sciences Subcommission on the systematics of igneous rocks. Oxford, Blackwell Scientific, 193.
- Luchitskaya, M. V., Sokolov, S. D., Bondarenko, G. E. and Katkov, S. M., 2010. Composition and Geodynamic Setting of Granitoid Magmatism in the Alyarmaut Uplift, Western Chukchi Peninsula. *Geochemistry International*, 48, 10, 946–971.
- Ludwig, K.R., 1999. User's manual for Isoplot/Ex, Version 2.10, a geochronological toolkit for Microsoft Excel. Berkeley Geochronology Center Special Publication, 1a.
- Ludwig, K.R., 2000. SQUID 1.00. A User's Manual. Berkeley Geochronology Center Special Publication, 2.
- Miller, E. L., Gelman, M., Parfenov, L., and Hourigan, J., 2002. Tectonic setting of Mesozoic magmatism: A comparison between northeastern Russia and the North American Cordillera. In: Miller, E. L., Grantz, A., and Klemperer, S. L. (eds.) *Tectonic Evolution of the Bering Shelf-Chukchi Sea-Arctic Margin and Adjacent Landmasses*. *Geol. Soc. Am. Spec. Paper*, 360, 333–358.
- Miller, E. L., Toro, J., Gehrels, G., Tuchkova, M. I., and Katkov, S. M., 2004. Detrital Zircon ages from Late Jurassic–Early Cretaceous Myrgovaam Basin sandstones (Rauchua Trough), Western Chukotka, NE Russia. *Eos Trans. AGU.*, 85, 47. Fall Meeting Supplement, Abstract, GP44A-04.
- Miller, E.L. and Verzhbitsky, V.E., 2009. Structural studies near Pevek, Russia: implications for formation of the East Siberian Shelf and Makarov Basin of the Arctic Ocean. *Stephan Mueller Spec. Publ. Ser.* 4, 223–241.
- Miller, E.L., Soloviev, A.V., Kuzmichev, A.B., Gehrels, G., Toro, J. and Tuchkova M.I. 2008. Jura-Cretaceous foreland basin deposits of the Russian Arctic: separated by birth of Makarov

- Basin? *Norw. J. Geol.*, 88, 227-250.
- Miller, E.L., Katkov, S.M., Strickland, A., Toro, J., Akinin, V.V. and Dumitru, T.A., 2009. Geochronology and thermochronology of Cretaceous plutons and metamorphic country rocks, Anyui-Chukotka fold belt, North East Arctic Russia. *Stephan Mueller Spec. Publ. Ser.* 4, 157–175.
- Milov, A.P., 1975. Late Mesozoic granitoid formations of Central Chukotka. *Proceedings SVKNII*; 53. Novosibirsk, SO RAS, 134.
- Milov, A.P. and Ivanov, V.S., 1965. Late Mesozoic granitoid formations of Central Chukotka. *Proceedings SVKNII DVNTs AN SSSR*, 12. Magadan, 141-187.
- Natal'in, B.A. Early Mesozoic eugeosynclinal systems in the northern part of Circum-Pacific. Moscow, Nauka, 1984. 136 (in Russian).
- Natal'in, B.A., Amato, J.M., Toro, J., and Wright, J.E., 1999. Paleozoic Rocks of Northern Chukotka Peninsula, Russian Far East. *Tectonics*, 18, 6, 977–1003.
- Parfenov, L.M., 1984. Continental margins and island arcs of North-East Asia Mesozooids. Novosibirsk, Nauka, 192 (in Russian).
- Parfenov, L.M., Natapov, L.M., Sokolov, S.D., Tsukanov, N.V., 1993. Terranes and accretionary tectonics of North-East Asia. *Geotectonics*, 1, 68–78 (in Russian).
- Pearce, J.A., Harris, N.B.W. and Tindle, A.G., 1984. Trace element discrimination diagrams for the tectonic interpretation of granitic rocks. *J. Petrology*, 25, 4, 956-983.
- Pearce J.A., 1996. Sources and settings of granitic rocks. *Episodes*, 19, 4, 120–125.
- Petrology of magmatic formations of Chukotka. *Proceedings SVKNII*, 18. 1969. Magadan, SVKNII, 205 (in Russian).
- Sadovsky, A.I. and Gel'man, M.L. 1970. Geological map of the USSR, scale 1:200000. Anyui-Chaun series. Sheet R-58-XXVII, XXVIII. Explanatory note. Leningrad: VSEGEI, 84 (in Russian).
- Samorukov, N.M. and Matveenko, S.T. 1984. Geologic map 1:200000 scale. R-59-XXIII, XXIV
- Seslavinsky, K.B., 1979. South-Anuyi suture zone (West Chukotka). *Doklady Earth Sciences*, 249, 1181-1185 (in Russian).
- Sokolov, S.D. 2007. Classification and hierarchy of fold systems. Moscow, GEOS, 71–100 (in Russian).
- Sokolov, S.D., Bondarenko, G.Ye., Morozov, O.L. and Grigoriyev, V.N., 1999. Transition zone Asian continent – northwestern Pacific in Late Jurassic-Early Cretaceous time. In: *Theoretical and regional problems of geodynamics. Proceedings GIN RAS*, 515. Moscow, Nauka, 30-83 (in Russian).
- Sokolov, S.D., Bondarenko, G.Ye., Morozov, O.L., and Luchitskaya, M.V., 2001. Tectonics of joint zone of Verkhoyan-Chukotka and Koryak-Kamchatka fold areas // *Byulleten' MOIP. Otdeleniye geol.*, 76, 6, 24–37 (in Russian).
- Sokolov, S.D., Bondarenko, G.Ye., Morozov, O.L., Shekhovtsov, V.A., Glotov, S.P., Ganelin, A.V. and Kravchenko-Berezhnoy, I.R., 2002. The South Anyui Suture, NE Arctic Russia: facts and problems to solve. In: *Tectonic Evolution of the Bering Shelf-Chukchi Sea-Arctic Margin and Adjacent Landmasses. Geol. Soc. Amer. Spec. Paper*, 360, 209-224.
- Sun, S.S. and McDonough, W.F., 1989. Chemical and isotopic systematics of oceanic basalts: implications for mantle composition and processes. *Geol. Soc. London. Spec. Publ.*, 42, 313–345.
- Toro, J., Amato, J.M., Natal'in, B.A., 2003. Cretaceous deformation, Chegitun River area, Chukotka Peninsula, Russia: implications for the tectonic evolution of the Bering Strait region. *Tectonics*, 22, 3, 1021–1040.
- Tibilov, I.V., Milov, A.P. and Davydov, I.A., 1986. On the occurrence of pre-Mesozoic granitoid magmatism on Chukotka. *Pacific Geology*, 4, 95–99 (in Russian).
- Tibilov, I.V. and Cherepanova, I.Yu., 2001. Geology of the northern part of Chukotka – modern condition and problems. Moscow, GEOS, 94 (in Russian).
- Tikhomirov, P.L., 1998. Petrology of Telekay ore region granitoids (Central Chukotka). PhD. Saint-Petersburg, 24 (in Russian).
- Tikhomirov, P.L., Akinin, V.V., Ispolatov, V.O., Alexander, P., Cherepanova, I. Yu. and Zagoskin, V.V., 2006. The Okhotsk–Chukotka Volcanic

- Belt: Age of Its Northern Part According to New Ar–Ar and U–Pb Geochronological Data. *Stratigraphy and Geological Correlation*, 14, 5, 524–537 (in Russian).
- Toro, J., Amato, J.M., Natal'in, B.A., 2003. Cretaceous deformation, Chegitun River area, Chukotka Peninsula, Russia: implications for the tectonic evolution of the Bering Strait region. *Tectonics*, 22, 3, 1021–1040.
- Tikhomirov, P.L and Luchitskaya M.V., 2006. Cretaceous granitoids of North-East Asia. Paper 1. Geology, petrography and geochemistry. *Vestnik MGU*, 5, 13–20 (in Russian).
- Tuchkova, M.I., 2011. Lithology of terrigenous rocks of fold areas of Mesozoic continental margins (Great Caucasus, North-East Asia). *GIN RAS Transactions*, 600, 334 (in Russian).
- Varlamova, V.A., Malysheva, G.M., Vyatkin, B.V., Zvizda, T.V., Zhukov, V.A., Kovalenko, A.V. and Kazinsky, V.A., 2004. Information report on unaccomplished works “The creation of digital geologic maps of 1:500000 scale for the Chukotka Autonomous Okrug area” (The monitoring of regional geologic research works, scale 1:500000). FGUGP “Georegion”, Anadyr (in Russian).
- Wetherill, G.W., 1956. Discordant uranium-lead ages, I. *Trans. Amer. Geophys. Union*, 37, 320–326.
- Williams, I.S., 1998. U-Th-Pb geochronology by ion microprobe: applications of microanalytical techniques to understanding mineralizing processes. *Reviews in Economic Geology*, 7, 1–35.
- Zagruzina, I.A., 1977. Geochronology of Mesozoic granitoids of USSR North-East. Moscow, Nauka, 278 (in Russian).
- Zhulanova, I.L., Rusakova, T.B. and Kotlyar, I.N., 2007. Geochronology and geochronometry of endogenic events in Mesozoic history of North-East Asia. Moscow, Nauka, 358 (in Russian).
- Zonenshain, L.P., Kuz'min, M.I. and Natapov, L.M., 1990. Plate tectonics on the USSR territory. Moscow, Nauka, 2, 327 (in Russian).

Age and composition of final stage of volcanism in Okhotsk-Chukotka volcanic belt: An example from the Ola Plateau (Okhotsk Segment)

V. V. Akinin¹, P. Layer², J. Benowitz², Ntaflos, Th.³

¹North-East Interdisciplinary Scientific Research Institute, FEB Russian Academy of Science, Magadan, 685000, Russian Federation

²University of Alaska, Fairbanks, AK 99775, USA

³Department of Lithospheric Research, University of Vienna, Austria

ABSTRACT

The final stage of volcanism in the subduction-related Okhotsk-Chukotka volcanic belt (OCVB) is represented by transitional basalts and andesitic basalt lava flows of the Mygdykit unit forming several separated high-altitude plateaus. One of the largest is the Ola plateau (~222 km³), which is located north of the Okhotsk Sea and yields Early Campanian (~78–80 Ma) ⁴⁰Ar/³⁹Ar and U-Pb ages. The Ola plateau basalts formed less than 2 Ma after the eruption of underlying rhyolite sequences of the main phase of the OCVB and therefore are regarded as part of OCVB. The new ages date the cessation of volcanism and time of the change in the locus of arc volcanism to more eastern locations along the margin of the paleo-Pacific ocean in the Maastrichtian and Paleocene (i.e., the Bristol-Anadyr and Koryak-Kamchatka arcs). This end of magmatism in the OCVB coincides with the timing of the final plume-related intraplate volcanism of the High Arctic Large Igneous Province (HALIP). Although the Ola plateau basalts have some subduction-related geochemical features (e.g. Nb-Ta negative anomaly) they also display geochemical discrepancies compared to basalt units in the older part of the OCVB, such as the higher contents of Ti, Zr, P, and other high field strength elements as well as more evolved Sr, Nd isotopic ratios. The origin of the late-stage basaltic magmas of the OCVB are attributed to weak assimilation and fractional crystallization processes in deep magma chambers during an interval of local extension due to the change in geodynamic setting from frontal subduction to a slab-window transform regime along the paleomargin of eastern Asia.

INTRODUCTION

One of the key problems in continental margin geology is the mechanism responsible for cessation of subduction and coeval magmatism in a continental margin arc. The cause of the demise of the arc might be reflected in changes in the chemistry of the final volcanism events which emphasizes the importance of compositional studies on such late-stage arc magmas. Another topic related to the importance of precise characterization of early and late-stage volcanism particularly in the case of two attached and/or overlaid arcs is to be able to distinguish them. Such issues have been debated for a long time for the continental margin of northeastern Russia where Okhotsk-Chukotka volcanic belt (OCVB) sits on older arcs and is, in turn, overlain by the slightly younger Bristol-Anadyr and Koryack-Kamchatka volcanic belts (e.g. Bely, 1977; Filatova, 1988; Kotlyar and Rusakova, 2004; Akinin and Miller, 2011). Hourigan and Akinin (2004) dated the final stage of volcanism in the Arman plateau using the ⁴⁰Ar/³⁹Ar method but there are other regional plateau basalts of unknown age that need to be investigated. Do they have the same age or do they show some spatial-temporal progression? For instance, Stone et al. (2009) reported about 10 Ma younger ⁴⁰Ar/³⁹Ar ages for upper basalts in Enmyvaam volcanic field of OCVB compared to Hourigan and Akinin (2004) results from the area. Additionally, compositions of these late-stage basalts are poorly studied, particularly in terms of modern trace element and isotopic geochemistry which is critical to understanding the tectonic setting and evolution of the final stages of the OCVB.

There are some fundamental topics that could also potentially be addressed if the mechanism of arc demise can be identified. Change in direction of

oceanic plate motion is one of the possible tectonic scenarios leading to subduction cessation (e.g. Matthews et al., 2012). Why do some subduction zones roll back along the trench and how fast does this process occur are still open questions. Driving mechanisms of plate reorganizations responsible for major episodes of plate motion change remain unclear (e.g. Bercovici, 2003), including the importance of top-down (plate-derived) (Anderson, 2001) versus bottom-up (mantle flow-derived) (e.g. King et al., 2002) processes. There are asymmetries on both sides of Tethys (paleo Pacific) Ocean margins in terms of occurrences of modern island arcs and back arc basins which can be related to different

angles of oceanic and continental plates interaction (frontal subduction in western Pacific vs. transform slip in north-eastern Pacific) (Seton et al., 2012). Are there any correlations in age and composition of arc magmatism on both sides of Pacific? The OCVB (Fig. 1) stretching about 3250 km along the margin of North Asian continent, from the mouth of the Uda River in the Khabarovsk District to Provideniya on the eastern Chukchi Peninsula is the perfect location to investigate both these regional and general process questions.

The OCVB comprises about 1 million km³ of Cretaceous calc-alkaline volcanic rock suites consisting of andesitic basalts, andesites, dacites,

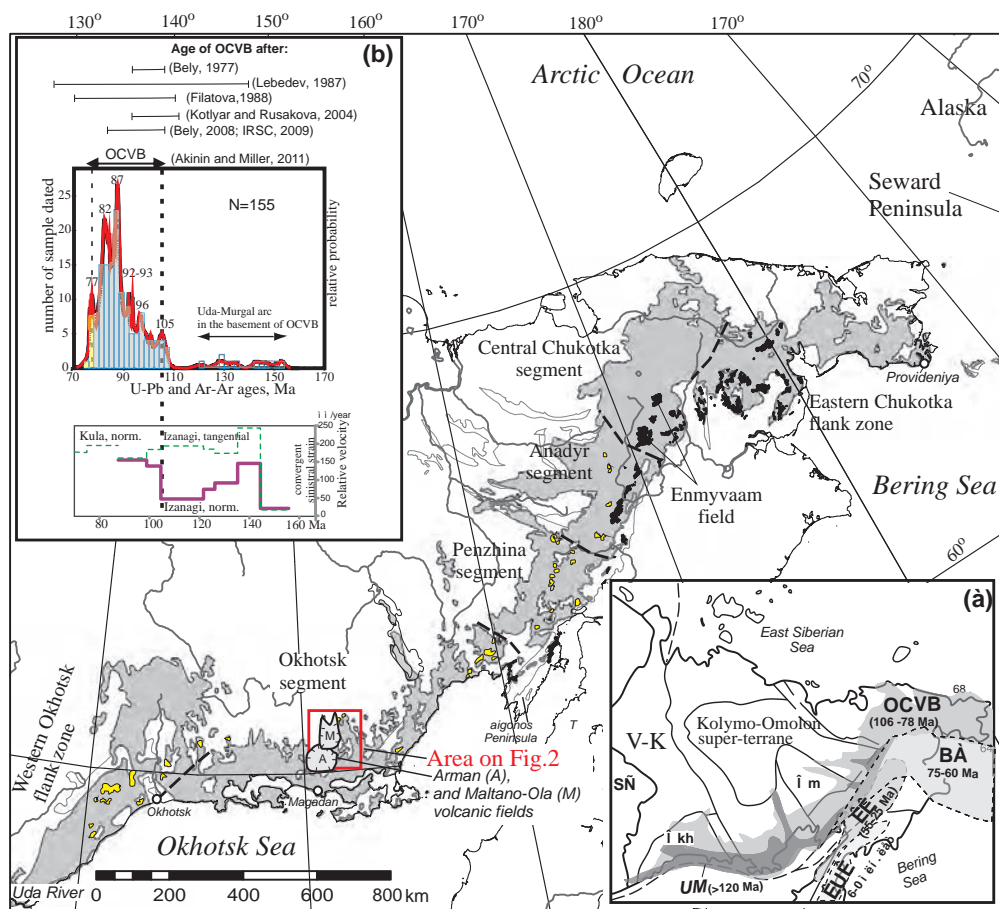


Fig. 1. Sketch map showing the Okhotsk –Chukotka volcanic belt in the continental framework of northeastern Asia (after Akinin and Miller, 2011; with minor changes). The names of the main segments and flank zones of the belt are after Belyi (1977). Gray shading shows the main volume of the Albian – Campanian calc-alkaline magmas of the OCVB, yellow areas are exposures of the Campanian late OCVB plateau basalts, and oblique hatching shows pre-OCVB island-arc volcanosedimentary complexes. Black areas are Maastrichtian-Paleocene basalts of Bristol-Anadyr and Koryak-Kamchatka belts which are located east of the OCVB. Inserts: (a) distribution of volcanogenic belts in northeastern Asia showing a decrease in age toward the paleo-Pacific (UM, Uda–Murgal; OCVB, Okhotsk–Chukotka; BA, Bristol–Anadyr; KK, Koryak–Kamchatka; and KUK, Kuril–Kamchatka). Lines show the boundaries of main terranes, and cross-hatching pattern shows Precambrian cratons and microcontinents that underlie the volcanic belts. Abbreviations: SC, Siberian craton; Okh, Okhotsk massif; and Om, Omolon massif. (b) Histogram of the U-Pb and ⁴⁰Ar/³⁹Ar ages of igneous rocks in OCVB and Uda-Murgal arc showing the correspondance of the volcanism with the changing direction and rate of movement of Pacific oceanic plates during the Cretaceous (Akinin and Miller, 2011).

rhyolites, their tuffs and tuffaceous sediments as well as coeval magnetite-bearing granitoid intrusions. The OCVB is a classical Andean-style arc but differs in some details because it was built on thinner (around ~30 to ~35 km) and variable age crust (Archean to Paleoproterozoic basement is seen in the Okhotsk and Omolon microcontinents, while Paleozoic to Early Cretaceous forms the remainder of the regional basement). All volcanic deposits of the main-stage of the OCVB are typical calc-alkaline rocks showing considerable variations in alkalinity and relatively high SiO₂ contents at low Fe/Mg. The OCVB arc is interpreted as having formed from subduction of part of the ancestral Pacific oceanic plate during the Albian to Campanian. Forearc basins are preserved in the West Kamchatka, Ekonay, and Yanranay accretionary-wedge terranes (Parfenov, 1984). One of the key aspects of the OCVB is that the belt overlaps terranes of both the Pacific and Arctic continental margins, constraining and linking their tectonic evolution.

The age span of the OCVB is still a topic of debate. It was first estimated as Neocomian–Paleogene (Ustiev, 1959; Umitbaev, 1986), then Albian–Cenomanian (Belyi, 1977; Kotlyar and Rusakova, 2004; Zhulanova et al., 2007), then Albian–Paleogene (Filatova, 1988), and then middle Albian–Santonian (Belyi, 2008; Koren' and Kotlyar, 2009). The lack of consensus is related to the original geochronological methods used (paleophytological methods and bulk rock K–Ar and Rb–Sr isotope analysis) which produced variable and non reproducible ages.

The first ⁴⁰Ar/³⁹Ar and U–Pb mineral ages from the volcanic rocks of the OCVB provided new insight into the inception, total duration, and variations in style and age of volcanism in the different segments of the belt (Kelley et al., 1999; Newberry et al., 2000; Hourigan and Akinin, 2004; Ispolatov et al., 2004; Akinin and Miller, 2011; Tikhomirov et al., 2012). The geochronologic results are fundamentally different from previously accepted ages of the OCVB and require a revision of the existing chronostratigraphic and tectonic models of the OCVB development which will continue to benefit from additional investigations using modern isotopic methods.

The volcanic rocks of the OCVB are flat-

lying, undeformed, and overlap the previously accreted Kolyma-Omolon superterrane and adjacent collisional belts in the Russian Northeast. Knowledge of the temporal evolution of the OCVB is critical for understanding the final timing of accretion of those terranes as well as the upper age limit of accretion tectonics in the region. The economic implications of any OCVB investigation are great because the belt hosts many epithermal gold-silver deposits of low sulfidation types (more than 50 epithermal deposits have been explored in northeastern Asia, from which more than 150 metric tons of gold and more than 1000 metric tons of silver have been recovered during the past 70 years; Struzhkov and Konstantinov, 2005). Of particular importance to economic development is having knowledge of the precise age of the final stage of basaltic volcanism in OCVB. Basaltic dikes mapped in many epithermal ore deposits post-date all of the units including gold-bearing quartz-adularia veins thus constraining the upper limit age of the mineralization.

The final stage of volcanism in the OCVB is represented by local basaltic plateaus (Fig. 1, yellow). One of the most renowned OCVB researchers, V.F. Belyi (Belyi, 1977; Belyi, 2008), argued that these late stage basaltic lavas should be included as part of the OCVB, although others have disagreed, pointing out discrepancies in their geochemical signatures, ages and geodynamic settings ((Filatova, 1988; Polin and Moll-Stalcup, 1998; Kotlyar and Rusakova, 2004). In our opinion, the discrepancies apply mainly to basalts in the northeastern part of the OCVB (Enmyvaam volcanic field, and Amguema–Kanchalan volcanic field (Stone et al., 2009; Sakhno et al., 2010) where ~60 to ~67 Ma-old (Maastrichtian to Paleocene) basalts overlap the OCVB and display a ~10 Ma hiatus after eruption of upper OCVB rhyolites. By this reasoning, we argue that Maastrichtian and younger volcanic rocks belong to the younger Bristol-Anadyr and Koryak-Kamchatka volcanic belts which are located east of the OCVB (Akinin et al., 2009; Akinin and Miller, 2011). If, on the other hand, hiatuses are short (within the uncertainty of age determination, ~1–~2 Ma) between arc volcano-sedimentary sequences that directly adjoin or occur in nearby areas, then it is likely that they constitute part of the same arc volcanic sequence.

In this paper we present geochronologic evidence that the Ola basaltic plateau formed between ~78 to ~80 Ma using $^{40}\text{Ar}/^{39}\text{Ar}$ and U-Pb SHRIMP dating. These ages are close to those from the underlying rhyolite sequences with the gap between the two volcanic units being no longer than 1–2 Ma. The short span of time separating the two volcanic units gives us reason to consider the plateau basalts to be part of the OCVB. Systematic weak upward compositional changes in the basaltic unit are interpreted as being related to limited fractional crystallization combined with assimilation and following alteration. The final stage of basaltic volcanism in the OCVB (ca. 78-79 Ma) reflected changes in geodynamic setting from subduction to

transform slip and closely corresponds in age to the final stage of High Arctic Large Igneous Province (HALIP) volcanism of the Arctic region (Gottlieb and Miller, 2012).

GEOLOGIC SETTING AND PREVIOUS WORK

Located along the northern shore of the Okhotsk Sea (from the town of Okhotsk to the Taigonos Peninsula), the OCVB is subdivided into segments or “sectors” on the basis of differences in the basement rock types and lithologic similarities of volcanic rocks within specific geographic regions (Bely, 1977). A typical cross-section of the OCVB in the Okhotsk segment can be seen in the Arman and

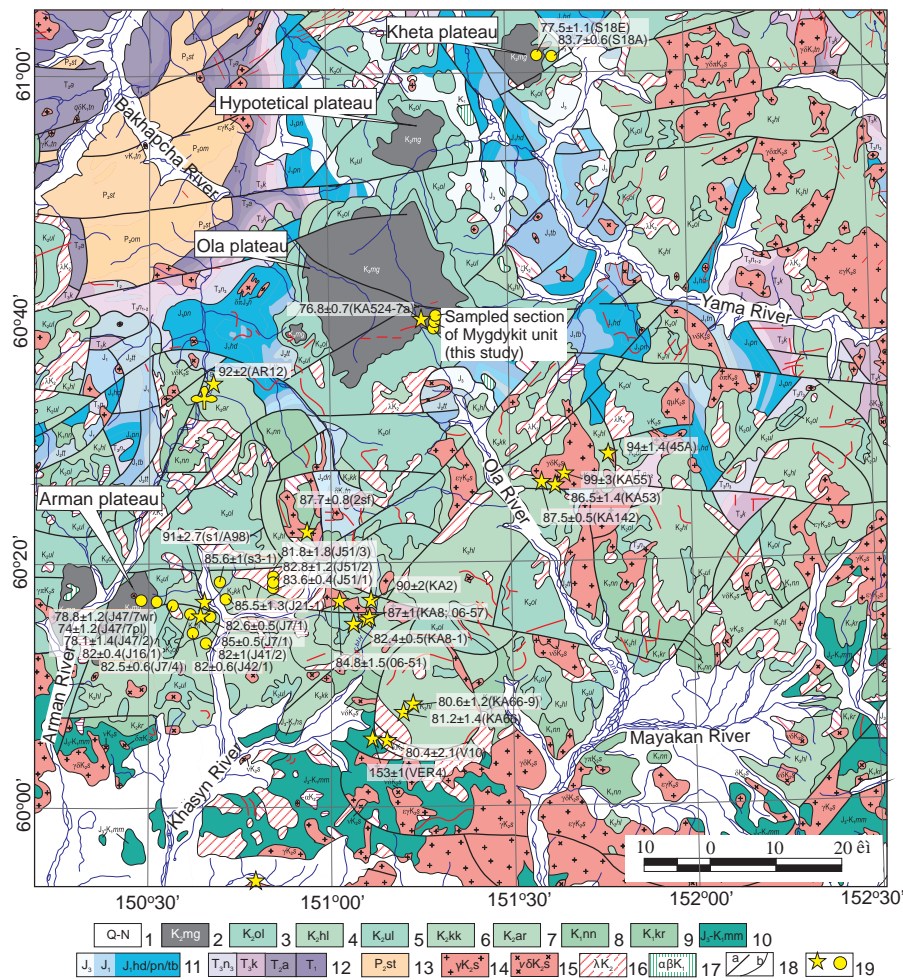


Fig. 2. Geological map of southern part of the Okhotsk segment of the Okhotsk-Chukotka volcanic belt (compiled using Gorodinsky, 1980). 1–Quaternary alluvium and lake deposits, 2–9–volcanic units of OCVB (2–Mygdykit, 3–Ola, 4–Kholchan, 5–Ulyn, 6–Kukushka or Narauli, 7–Arman, 8–Nankala, 9–Kirik, 10–Momoltykich unit of Uda-Murgal arc in the base of OCVB, 11–Jurassic sediments, 12–Triassic sediments; 13–Permian sediments, diamictites and phillites; 14–15–Upper Cretaceous granite (14), and gabbro-diorite (15) intrusions. 16–17–Upper Cretaceous subvolcanic intrusions of rhyolites (16), and basaltic andesites (17). 18–faults (a) and contacts (b). 19– samples dated by U-Pb SHRIMP (stars - Akinin and Miller, 2011) and $^{40}\text{Ar}/^{39}\text{Ar}$ (circle - Hourigan and Akinin, 2004) methods, dates and uncertainty shown in Ma, sample number in brackets.

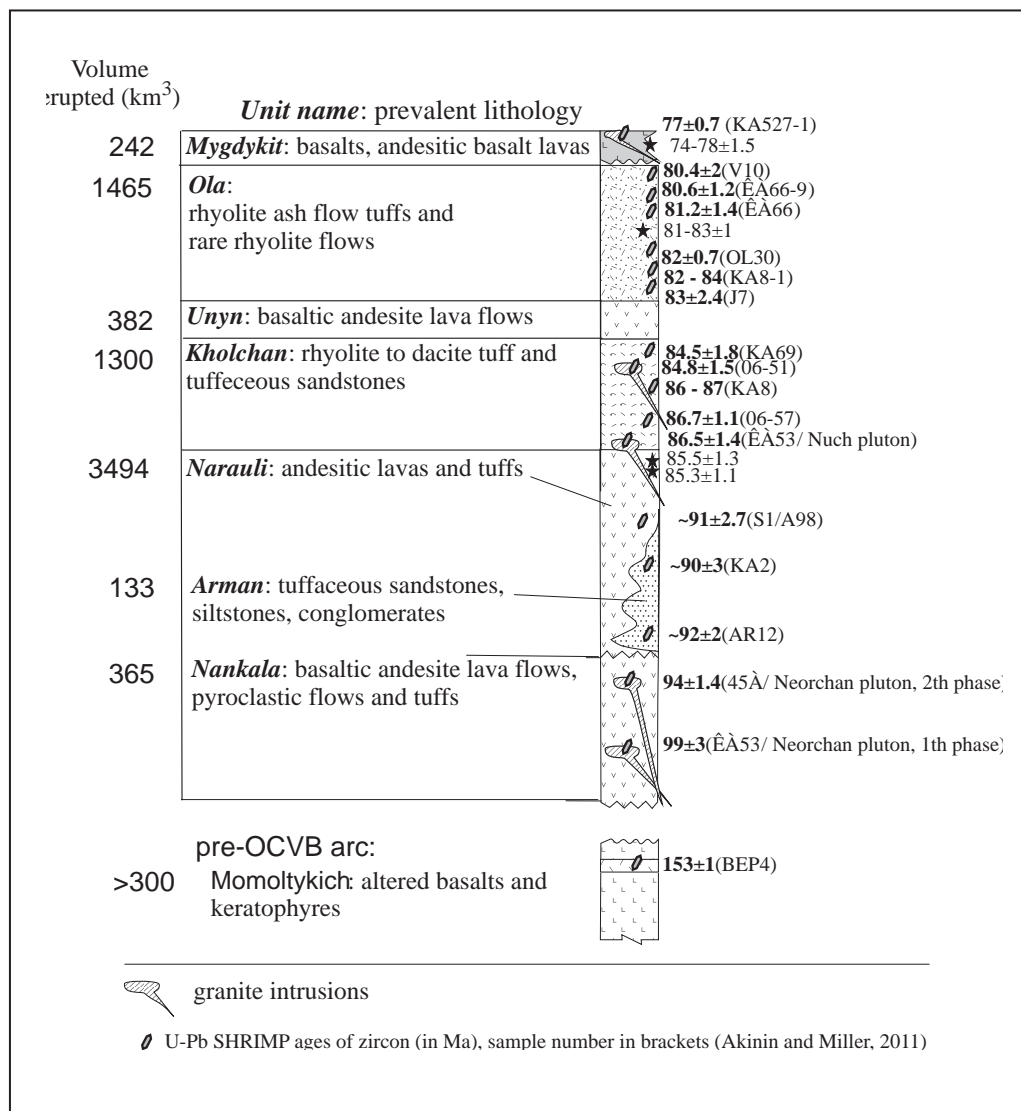


Fig. 3. Generalized stratigraphic column of volcanic units in Arman and Maltano-Ola volcanic fields (Okhotsk segment of OCVB). Volcanic units are according to (Anorov et al., 1999), volcanic volume erupted and isotopic ages are after Akinin and Miller (2011).

Maltano-Ola volcanic fields (fields called structures in Russian literature) (Figs. 1 and 2). Those two volcanic fields delineate a ~1500 km² area, where the total thickness of the volcanic sequences is 1–2 km and the thickness of each volcanic unit is highly variable. A simplified succession in the area is presented in Fig. 3.

All of the main stage volcanic products (Nankala to Ola units on Fig. 3) are typical calc alkaline rocks showing considerable variation in alkalinity and relatively high SiO₂ contents at low Fe/Mg. Late-stage basaltic volcanism of the Mygdykit unit forms several distinctive plateaus including the Yana, Arman, Kheta, Hypotetical and Ola (grey fields on Fig. 2). One can integrate Ola and Mygdykit units

into bimodal formation, but Hourigan and Akinin (2004) reported a ~3 Ma hiatus between those two units precluding bimodal origin from the single same source. They follow the conclusions of previous studies (Filatova, 1988; Polin and Moll-Stalcup, 1999) which point toward a within-plate, possibly extension-related origin of late-stage basalts of the Arman plateau, but this conclusion needs to be proved or disproved using detail geochemical and geochronological study of the different plateaus.

The Ola plateau is one of the largest, and is composed of Mygdykit unit basalts. It is also well known because of gem deposits of agates and chalcedonites associated with the basalts. The Ola plateau is located in the headwaters of Ola River,

Magadan district (north of the Okhotsk Sea) and is recognized by a planar primary surface that dips gently to the northwest at an elevation of ~1500 m (Figs. 3 and 4). Basalts of the Mygdykit unit on the Ola plateau occupy ~443 km² and have an estimated total eruptive volume of ~222 km³ (assuming an average ~500 m thickness; Akinin et al., 2007). The age of the Mygdykit basalt unit was thought to be Cenomanian (Belyi, 1977) or Maastrichtian to Paleogene (Filatova, 1988) based on early work using paleo-flora assemblages. The age of the basalts was later changed to Santonian and probably Early Campanian based on palynocomplexes and a few whole rock K-Ar and ⁴⁰Ar/³⁹Ar ages (Belyi and Belaya, 1998). Filatova (1988) first suggested that Maastrichtian-Paleocene plateau basalts located within the OCVB region and in the inner zones of Koryak-Kamchatka region are not related to subduction-related OCVB volcanism, but rather are extensional basalts deposited in local grabens formed in response to Late Cretaceous and Paleogene collision of oceanic island arcs against the Russian Far East. Alshevsky (1997) reported the first K-Ar whole-rock ages for the Ola, Kheta, and

Arman plateau basalts ranging from 81 ± 1 Ma to 63 ± 3 Ma, and concluded a Paleocene age for the upper age limit of the OCVB. Kotlyar and Rusakova (2004) suggested a Santonian – Early Campanian age (84 – 82 Ma) for the upper plateau basalts by picking a “true relict age” using only the oldest published K-Ar whole rock data. They ignored the few existing ⁴⁰Ar/³⁹Ar ages at the time and included the upper basalts of the “Khakarino-Enmyvaam intercontinental volcanic chain” which post-dates the OCVB (Kotlyar and Rusakova, 2004; Zhulanova et al., 2007) basically following the conclusions of Filatova (1988). The rhyolites of Ola units which concordantly underlie the lower basaltic flows of the Mygdykit unit, yielded ~83 to ~81 Ma ⁴⁰Ar/³⁹Ar ages (Hourigan and Akinin, 2004; Akinin and Miller, 2011). Thus the age of the Mygdykit unit has been debated for decades and needs to be resolved using modern geochemical and isotopic geochronology methods such as ⁴⁰Ar/³⁹Ar and U-Pb on other regional basalt plateaus.

This study focuses on the Ola basaltic plateau on the right bank of Grozovoi Creek where 97 individual lava flows with a total thickness of ~630 m

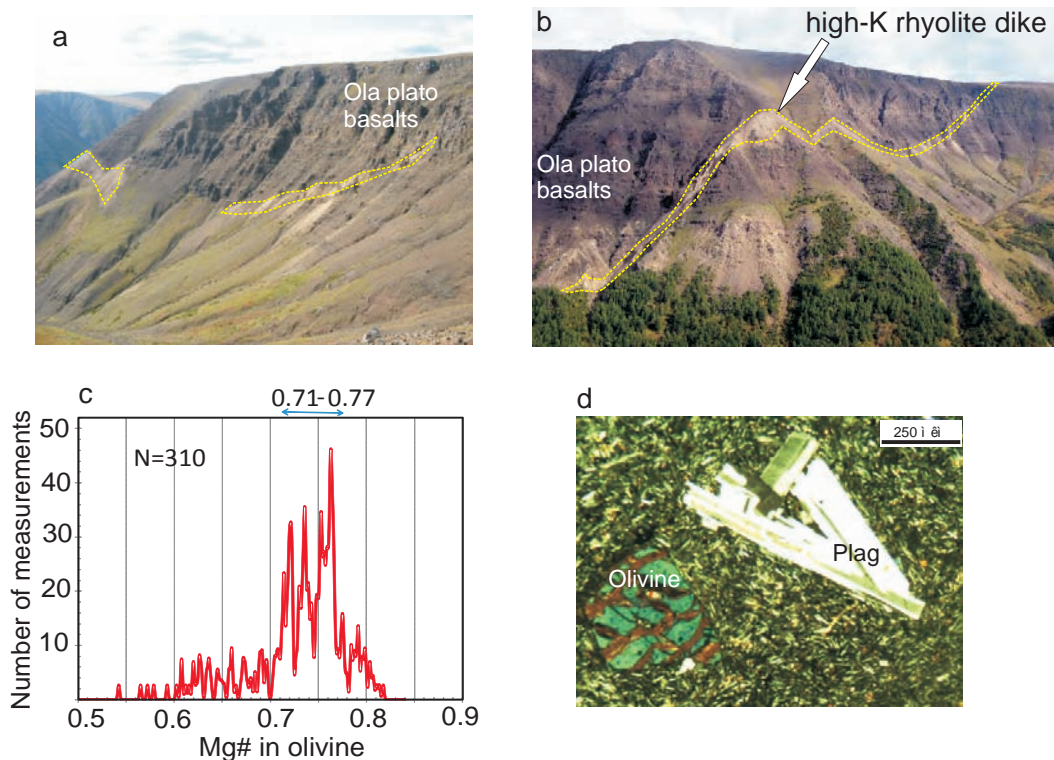


Fig. 4. Mygdykit unit basalts in Ola plateau . Yellow line in the 4a and 4b photo shows the high-potassium rhyolite dike cutting the basaltic section. 4c – Distribution of olivine phenocrysts composition (Mg# = Mg / (Mg+Fe), molar fraction). 4d – typical thin-section of Mygdykit unit basalts.

are recognized (Fig. 4). Each lava flow is 3 to 6 m thick and is composed of brecciated reddish basaltic clastic lava at the base, massive lava in the middle, and vesicular lavas at the top of each flow. Massive lava from the middle part of each flow was sampled and numbered sequentially from B1 to B97, and then samples were submitted for major and trace element geochemistry. In addition, several key samples were dated using the $^{40}\text{Ar}/^{39}\text{Ar}$ method and the composition phenocryst phases determined by microprobe analysis. The basalt flows are cut by a high-potassium rhyolite dike which provides a good constraint on upper age limit for the Mygdykit basalts on the Ola plateau.

ANALYTICAL METHODS

The samples were studied in thin-sections using classical microscopy for petrographic analysis. Mineral compositions were measured on a Camebax microprobe (NEISRI, Far East Branch, Russian Academy of Science, Magadan) and a JEOL microprobe (Vienna University, Austria), using common measurements conditions (15kV, 20nA), and a set of synthetic and natural standards. ZAF corrections were applied for matrix effects. Uncertainties of measurements were less than 5% (excluding Na). X-ray fluorescence analysis of whole rocks for major and trace elements were performed at NEISRI (Far East Branch, Russian Academy of Science, Magadan) using SRM-25 and VRA-30 spectrometers and following standard procedures. Uncertainties for major element abundances were less than 0.4% for SiO_2 and about 0.2% for other oxides; errors for trace element measurements (Rb, Sr, Zr) did not exceed 5–6%. ICP-MS analyses for trace elements were performed at the Institute of Tectonics and Geophysics (Far East Branch, Russian Academy of Science, Khabarovsk) and IEC SB RAS (Irkutsk) where repeated measurement of BHVO-1, AGV-1 and BIR-1 standards yielded a 5 to 10% standard deviation. The distribution of major and trace elements allow us to estimate the role of crystal fractionation and magma mixing in the petrogenesis of the OCVB volcanic rocks and to perform geochemical modeling using available computer software programs. Melt crystallization was simulated using COMAGMAT software (Ariskin and Barmina, 2000), and mineral thermobarometry

was carried out using olivine-melt and plagioclase-melt thermobarometers (Putirka, 2008). The mass spectrometric measurements of Sr, Nd, and Pb isotopic ratios in the bulk rocks of the OCVB were carried out using a MI-1201 mass spectrometer at NEISRI (Magadan) and a VG-Sector mass spectrometer (Stanford University, United States).

For $^{40}\text{Ar}/^{39}\text{Ar}$ analysis, samples were submitted to the Geochronology Laboratory at University of Alaska Fairbanks where they were crushed, sieved, washed and hand-picked for small phenocryst-free whole-rock chips. The mineral standard MMhb-1 (Samson and Alexander, 1987) with an age of 513.9 Ma (Lanphere and Dalrymple, 2000) was used to monitor neutron flux (and calculate the irradiation parameter, J). The samples and standards were wrapped in aluminum foil and loaded into aluminum capsules of 2.5 cm diameter and 6 cm height. The samples were irradiated in position 5c of the uranium enriched research reactor of McMaster University in Hamilton, Ontario, Canada for 20 megawatt-hours.

Upon return from the reactor, the samples and monitors were loaded into 2 mm diameter holes in a copper tray that was then loaded into an ultra-high vacuum extraction line. The monitors were fused and samples heated using a 6-watt argon-ion laser following the technique described by York et al. (1981), Layer et al. (1987) and Layer (2000). Argon purification was achieved using a liquid nitrogen cold trap and a SAES Zr-Al getter at 400C. The samples were analyzed in a VG-3600 mass spectrometer. The measurements of argon isotopes were corrected for system blank and mass discrimination, as well as calcium, potassium and chlorine interference reactions following procedures outlined in McDougall and Harrison (1999). System blanks generally were 2×10^{-16} mol ^{40}Ar and 2×10^{-18} mol ^{36}Ar which are 10 to 50 times smaller than the values for the fraction volumes. Mass discrimination was monitored by running both calibrated air shots and a zero-age glass sample. These measurements were made on a weekly to monthly basis to check for changes in mass discrimination.

A summary of all the $^{40}\text{Ar}/^{39}\text{Ar}$ results is given in Table 1, with all ages quoted to the ± 1 sigma level and calculated using the constants of Steiger and Jaeger (1977). The integrated age is the age given by the total gas measured. The spectrum provides a

plateau age if three or more consecutive gas fractions represent at least 50% of the total gas release and are within two standard deviations of each other (Mean Square Weighted Deviation less than 2.5). Each sample was run twice to both confirm age determinations and to optimize analytical precision.

RESULTS

⁴⁰Ar/³⁹Ar age of Mygdykit unit of Ola plateau

Six whole rock samples were dated using the ⁴⁰Ar/³⁹Ar method. Five samples (B2 to B7) are from the bottom of the “B” cross-section, and one sample (B91) was collected from the top of section. The ⁴⁰Ar/³⁹Ar data suggest that the emplacement of the entire section of Mygdykit unit in Ola plateau occurred between 80.6 ± 1.2 to 76.6 ± 0.7 Ma (weighted mean = 78.6 ± 1.9 [2.5%] 95% conf., MSWD = 4.3, probability = 0.001). The results

of five of the samples (B2, B3, B5, B7, and B91) are consistent and are in agreement with their stratigraphic positions in the succession (Table 1). There is a very high probability that entire section of basalts erupted almost synchronously bearing in mind the overlap of uncertainty obtained between about 78 and 79 Ma. The only exception to this interpretation is sample B4 which yielded an older plateau and inverse isochron ages of 82.0 ± 1.1 Ma (Table 1), but this age is still within two sigma error of the weighted mean age of the other four samples. The upper limit of Mygdykit unit formation can be constrained by the age of a rhyolite dike which cuts the basalt section (Fig. 5). Zircon from a dike of peralkaline rhyolites cutting the Mygdykit basalts in Ola Plateau were dated previously using SHRIMP-RG (Akinin and Miller, 2011) and yielded a mean weighted age of 76.8 ± 0.7 Ma

Table 1. Summary of ⁴⁰Ar/³⁹Ar geochronological data.

Sample	Min.	Integrated Age (Ma)	Plateau Age (Ma)	Plateau Information	Isochron Age (Ma)	Isochron Information
B2	WR	89.0± 3.3	80.6± 1.2	8 of 11 fractions 62.9% ³⁹ Ar release MSWD =0.6	79.0 ± 1.2	8 of 12 fractions ⁴⁰ Ar/ ³⁶ Ari = 304.5 ± 3.1 MSWD = 0.6
B3	WR	80.6± 1.1	78.6± 0.8	9 of 11 fractions 82.7 % ³⁹ Ar release MSWD =1.1	77.9 ± 0.9	12 of 12 fractions ⁴⁰ Ar/ ³⁶ Ari = 300.0 ± 2.0 MSWD = 1.0
B4	WR	84.5± 1.5	82.1± 1.1	7 of 12 fractions 81.1 % ³⁹ Ar release MSWD =0.6	82.0 ± 1.1	12 of 12 fractions ⁴⁰ Ar/ ³⁶ Ari = 302.8 ± 3.1 MSWD = 0.6
B5	WR	79.2± 2.2	79.3± 1.4	5 of 8 fractions 72.2 % ³⁹ Ar release MSWD =0.2	79.3.0 ± 1.4	8 of 8 fractions ⁴⁰ Ar/ ³⁶ Ari = 294.8 ± 4.2 MSWD = 0.2
B7	WR	81.2± 1.2	78.2± 0.7	4 of 9 fractions 77.2 % ³⁹ Ar release MSWD =0.1	78.0± 0.9	7 of 9 fractions ⁴⁰ Ar/ ³⁶ Ari = 298.8 ± 4.7 MSWD = 0.3
B91	WR	77.5 ± 0.5	76.6 ± 0.7	3 of 7 fractions 56% ³⁹ Ar release MSWD = 2.0	-	-

Samples analyzed with standard MMhb-1 an age of 513.9 Ma. A homogenous whole rock ground mass separate from each sample was analyzed. We prefer the plateau age (in bold) because of the higher precision, convention and because of the high atmospheric content of the first two to three steps and low K content of the final steps release. For geochemical data, see Table 2.

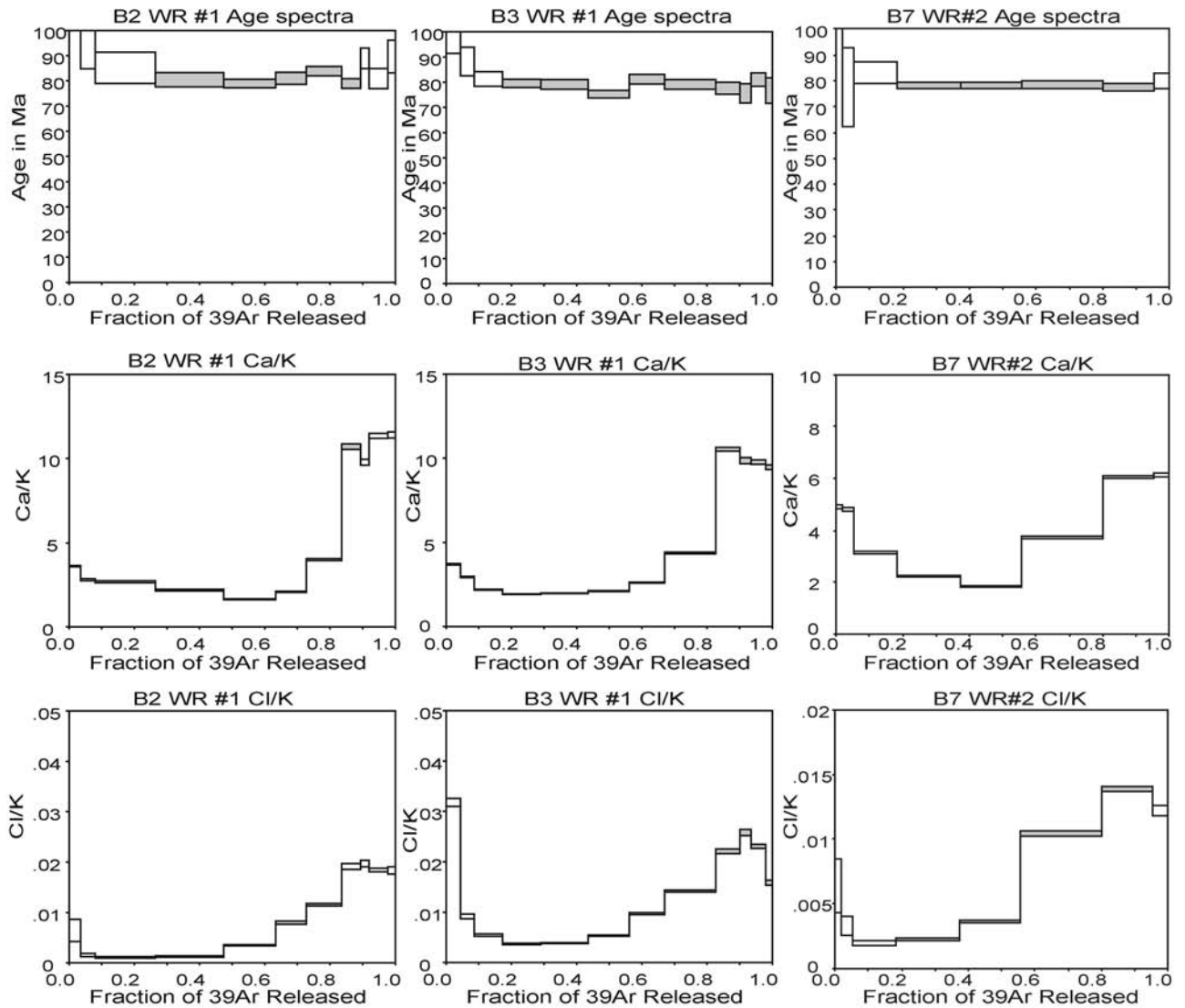


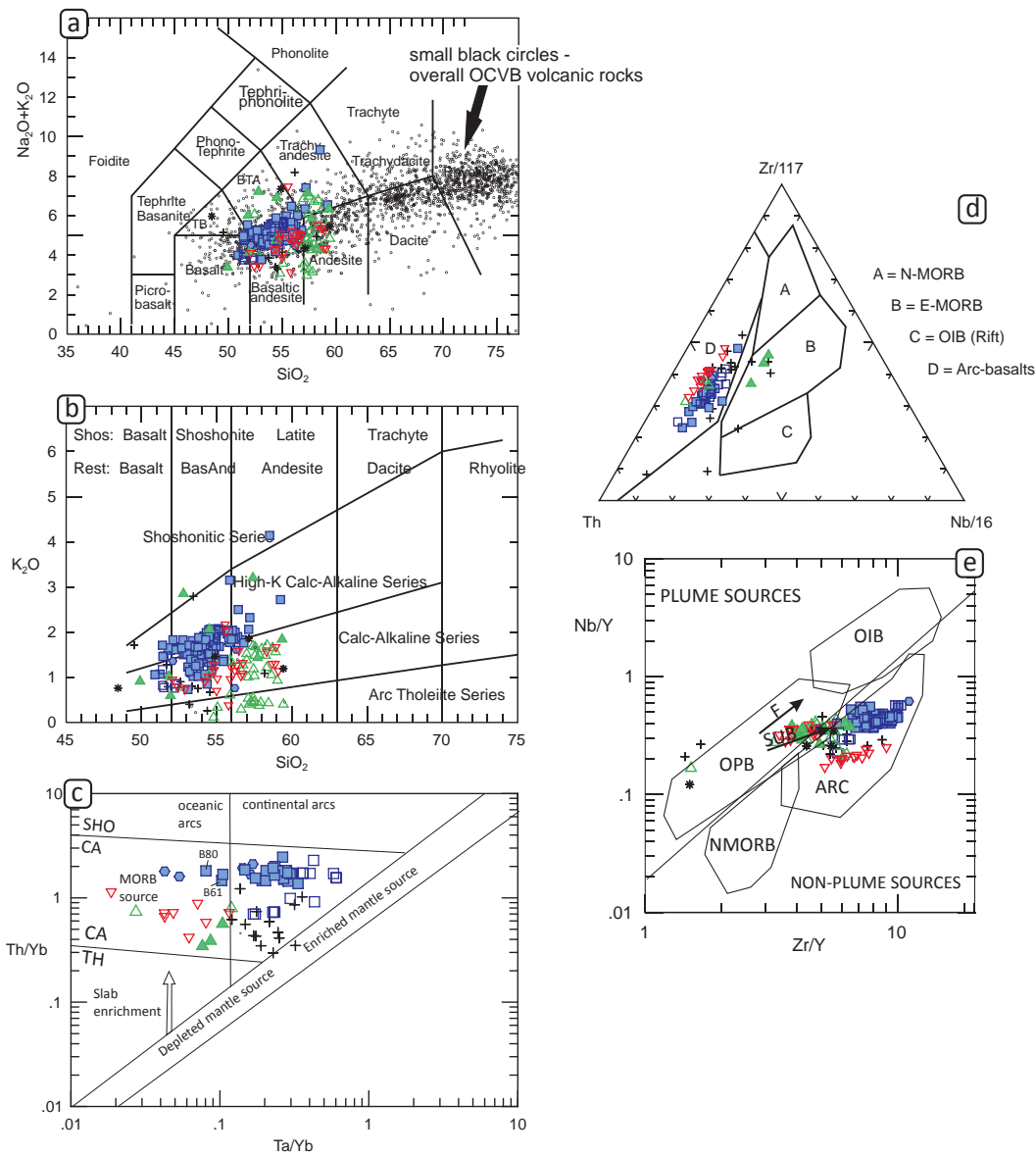
Fig. 5. Age spectrum, Ca/K, and Cl/K plots for three new $^{40}\text{Ar}/^{39}\text{Ar}$ analyses of Mygdykit unit basalts from Ola plateau. Sample localities are shown in Fig. 2.

(MSWD = 1.2, $N = 8/10$). The age of the rhyolite dike is consistent with our $^{40}\text{Ar}/^{39}\text{Ar}$ age on sample B91 and suggests a possible bimodal generation of basalts and rhyolite dikes. Previously published $^{40}\text{Ar}/^{39}\text{Ar}$ ages from the Mygdykit basalts from the Arman plateau located to the south-west from the Ola plateau yield ~ 74 to $\sim 77.5 \pm 1$ Ma ages demonstrating a quite prolonged eruption history (Hourigan and Akinin, 2004). Our new isotopic geochronologic data sets viewed as an entirety, provides an opposing view suggesting that the whole basalt section of Mygdykit unit may have been catastrophic and basalt generation occurred almost synchronously as essentially one eruptive phase, probably over a period of less than 1 Ma. The apparent difference in the two data sets loses significance if we exclude

just one sample from Hourigan and Akinin's (2004) data. The accepted 74 ± 1.2 Ma $^{40}\text{Ar}/^{39}\text{Ar}$ age for this "anomalous" sample (J47/7 plagioclase in Table 7, Hourigan and Akinin, 2004) is an isochron age which was not reproduced by an Ar-plateau age. In addition, a whole rock argon age for this sample yields an age of 78.8 ± 1.2 Ma which is 4.8 Ma older compared to its plagioclase age (J47/7 WRB in Table 7 of Hourigan and Akinin, 2004).

Variation of lava composition

Most of the studied lavas are unaltered and consist of olivine- and olivine-plagioclase porphyritic basalts and basaltic andesites (both referred to as basalts). Geochemical analyses shows that these rocks belong to normal to transitional



Basaltic to andesitic volcanic rocks of OCVB (Okhotsk segment), SiO₂ < 60 wt% in dry mode:

- top of OCVB section
 - Mygdykit unit Ola plateau ~ 78-79 Ma.
 - Mygdykit unit Hypotetical plateau ~ 76-78 Ma.
 - Mygdykit unit Arman plateau ~ 74-78 Ma (Horigan and Akinin, 2004).
- bottom of OCVB section
 - ▼ Ulyn unit ~ 85-83 Ma
 - ▲ Narauli unit ~ 85-90 Ma
 - ▲ Nankala unit ~ 100 Ma
- pre-OCVB volcanic rocks
 - + Momoltyk unit ~140-150 Ma
 - * Arman unit (pebble in conglomerate)

Fig. 6. Classification and discrimination geochemical diagrams for volcanic rocks of Okhotsk segment of OCVB located in the area outlined on Fig. 2. Mygdykit unit basaltic andesites have Arc-type signatures although they are enriched in potassium, Zr, and Ti compared to the rocks of basaltic and basaltic andesite composition from lower units of OCVB. (a, b) TAS classification diagram of LeBas et al. (1986) showing predominant basaltic andesite composition of Mygdykit unit volcanic rocks; (b) Arc rock types diagram of Peccerillo and Taylor (1976) showing trend to high-K calc-alkaline series for Mygdykit unit volcanic rocks compared to those from lower units of OCVB. (c) Ta/Yb vs. Th/Yb diagram after Pearce (1983), showing continental arc origin of Mygdykit unit basalts with enriched source of magma. SHO - shoshonitic series, CA - calc-alkaline series, TH - tholeiitic series. (d) Th-Zr-Nb diagram of Wood (1980) showing arc origin of Mygdykit unit basalts. (e) Zr/Y vs. Nd/Y diagram from (Condie, 2003) where arrows indicate effects of batch melting (F) and subduction (SUB). Abbreviations: ARC, arc-related basalts; NMORB, normal ocean ridge basalt; OIB, oceanic island basalt; OPB – oceanic plateau basalts (Pearce and Cann, 1973).

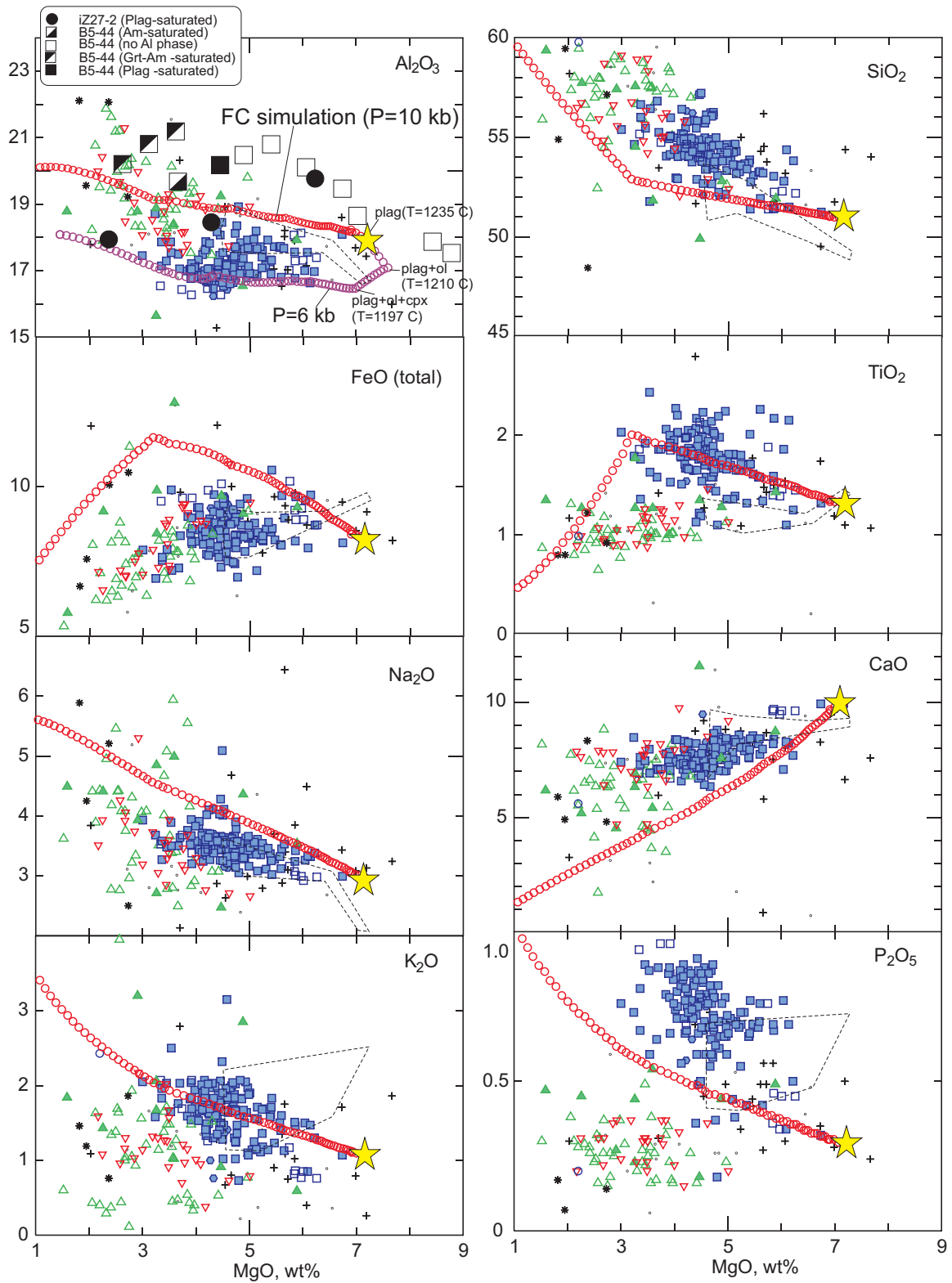


Fig. 7. Harker-type diagram for volcanic rocks of Okhotsk segment of OCVB. Red circle shows modeled fractional crystallization liquid line of descent (FC) simulated using COMAGMAT software (Ariskin and Barmina, 2000). Color symbols are OCVB samples as in Figure 6. Dashed line delineated field of basalts from Enmyvaam unit, Chukotka (Belyi and Belaya, 1998; Stone et al., 2009) which represent Maastrichtian volcanism of Bristol-Anadyr belt located east from OCVB. Black squares on SiO vs. Al_2O_3 diagram denote experimentally produced residual melts from crystallization of hydrous basalts in the lower crust. Primitive Mount Shasta basaltic andesite, sample 85-44 (mg-number 0.71), from Grove et al. (2003), at 0.8–1.2 GPa, 1045–1230° C and with >2.5 wt % added H_2O ; filled black circles denote experimental melts from Kawamoto (1996) on a Higushi-Izu high alumina basalt, sample IZ27-2 (mg-number 0.60), at 1.0 GPa, 1000–1150° C with 1 wt % added H_2O .

calc-alkaline series, and moderate to high alumina type (Figs. 6 and 7). Basalts of the Mygdykit unit are distinguished from basalts of lower units (such as Ulyn, Narauli, Nankala, and Momolykich units) because of higher contents of Ti, Zr, and rare earth elements (REE) and display some enriched intraplate-like geochemical signatures (Filatova, 1988; Polin and Moll-Stalcup, 1999; Akinin and Miller, 2011; Fig. 7). Nevertheless, Mygdykit unit basalts have a pronounced Nb-Ta negative trough on the spider diagram; a similar pattern to that as seen in the older subduction related volcanics of OCVB (Fig. 8). Depletion of tantalum and niobium relative to other incompatible elements in arc lavas has been ascribed to many processes (review in Kelemen *et al.* (2003, p.627)) including: (1) crystal fractionation of Fe-Ti oxides in the crust, (2) fractionation of titanium-rich, hydrous silicates such as phlogopite or hornblende in the mantle or crust, (3) extensive, chromatographic interaction between migrating melt and depleted peridotite, (4) the presence of phases such a rutile or sphene in the mantle wedge, (5) relative immobility of tantalum and niobium relative to REE and other elements in aqueous fluids derived from subducting material, (6) inherited, low Ta/Th and Nb/Th from subducted sediment, and (7) the presence of residual rutile during partial melting of subducted material. Following Kelemen *et al.* (2003) we prefer the hypothesis that fractionation of Nb and Ta from other highly incompatible elements via partial melting of subducting, eclogite facies basalts or sediments with residual rutile to explain the results.

Mygdykit unit basalt compositions vary slightly from plateau to plateau, and Ola Plateau basalts have higher Ni, and lower Sr content compared to rocks from the Arman and Hypotetical plateaus (Figs. 2 and 8). The major elements in the Mygdykit unit of Ola plateau vary slightly, but inconsistently (Fig. 7). The most pronounced co-variation can be seen in graphs of MgO vs SiO₂, CaO, and Na₂O which reflect concurrent fractional crystallization and assimilation processes. Fractional and equilibrium crystallization were simulated using COMAGMAT software (Ariskin and Barmina, 2000) which contains a set of empirically calibrated equations that are used to calculate equilibrium temperatures and phase relations. These equations describe mineral-melt

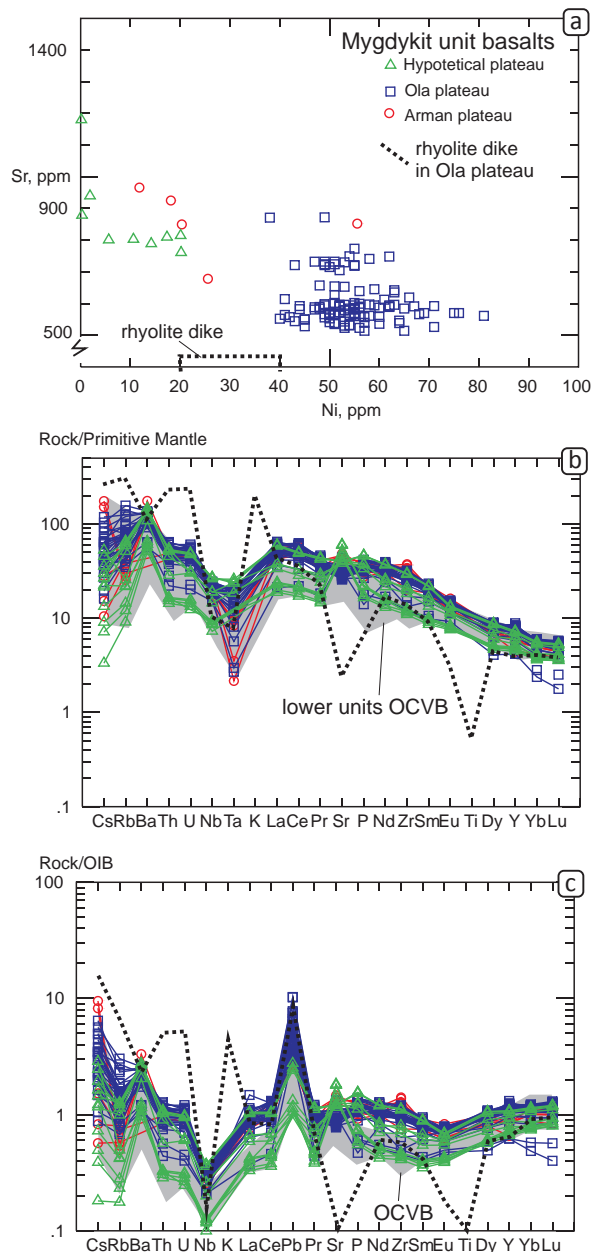


Fig. 8. Trace element diagrams for basalts and basaltic andesites of Mygdykit unit. Figure 8a graph shows compositional variation of basalts from different plateaus. Figure 6b and 6c are spider-diagrams (normalized to primitive mantle and Ocean Island Basalts – OIB, after McDonough and Sun, 1995). Gray field are composition of basalts and andesites from lower units of OCVB. The Mygdykit unit basalts in the lower units of OCVB display notable similar trace element patterns, especially for incompatible trace elements.

equilibria for major- and trace-elements in terms of pressure, temperature, oxygen fugacity and liquid composition. Based on the geothermometers, an algorithm for the simulation of the differentiation of multiply saturated magmas from primitive basalts to dacites has been developed for olivine, plagioclase,

augite, pigeonite (or opx), ilmenite, and magnetite bearing assemblages including the equilibrium mineral proportions and compositions. Simulated liquid lines of descent shows paths that are displaced from the observed major and trace element variation in the Mygdykit unit and therefore indicate that mixing and assimilation processes were involved in the fractionation process (Fig. 7).

In order to estimate the mantle sources for OCVB magmas, radiogenic isotope ratios of Sr, Nd, and Pb were measured in ten samples from the Arman volcanic field (basalts and basaltic andesites of the pre-OCVB Momoltykich Formation, belt andesite of the Narauli and Ulyn formations, rhyolitic ignimbrites of the Ola Formation, and basalts of the Mygdykit Formation). The observed variations in the initial isotopic ratios, $(^{87}\text{Sr}/^{86}\text{Sr})_0 = 0.70444\text{--}0.70332$, $(^{143}\text{Nd}/^{144}\text{Nd})_0 = 0.51286\text{--}0.51257$, ϵNd from +6.5

to +0.8, and $^{208}\text{Pb}/^{204}\text{Pb} = 38.5\text{--}38.04$, suggest that the mantle sources of magmas were rather depleted (similar to MORB) and not significantly different from one another. For instance, the basalts of the Nankala Formation of the OCVB show $(^{87}\text{Sr}/^{86}\text{Sr})_0 = 0.70378\text{--}0.70336$, $(^{143}\text{Nd}/^{144}\text{Nd})_0 = 0.51291\text{--}0.51287$, and ϵNd from +5.3 to +6.1, and the basalts of the pre-belt Momoltykich Formation have almost identical characteristics: $(^{87}\text{Sr}/^{86}\text{Sr})_0 = 0.70378\text{--}0.70336$, $(^{143}\text{Nd}/^{144}\text{Nd})_0 = 0.51291\text{--}0.51287$, and ϵNd from +5.5 to +6.0 (Table 2). The variation of isotopic composition in Mygdykit basalts is reflective of a mixed source from the end-member compositions defined by Zindler and Hart (1986) of PREMA (Prevalent Mantle), BSE (Bulk Silicate Earth), and EM I (Enriched Mantle 1) (Fig. 9). The presence of a relatively depleted MORB-like isotopic component suggests a link between the volcanism

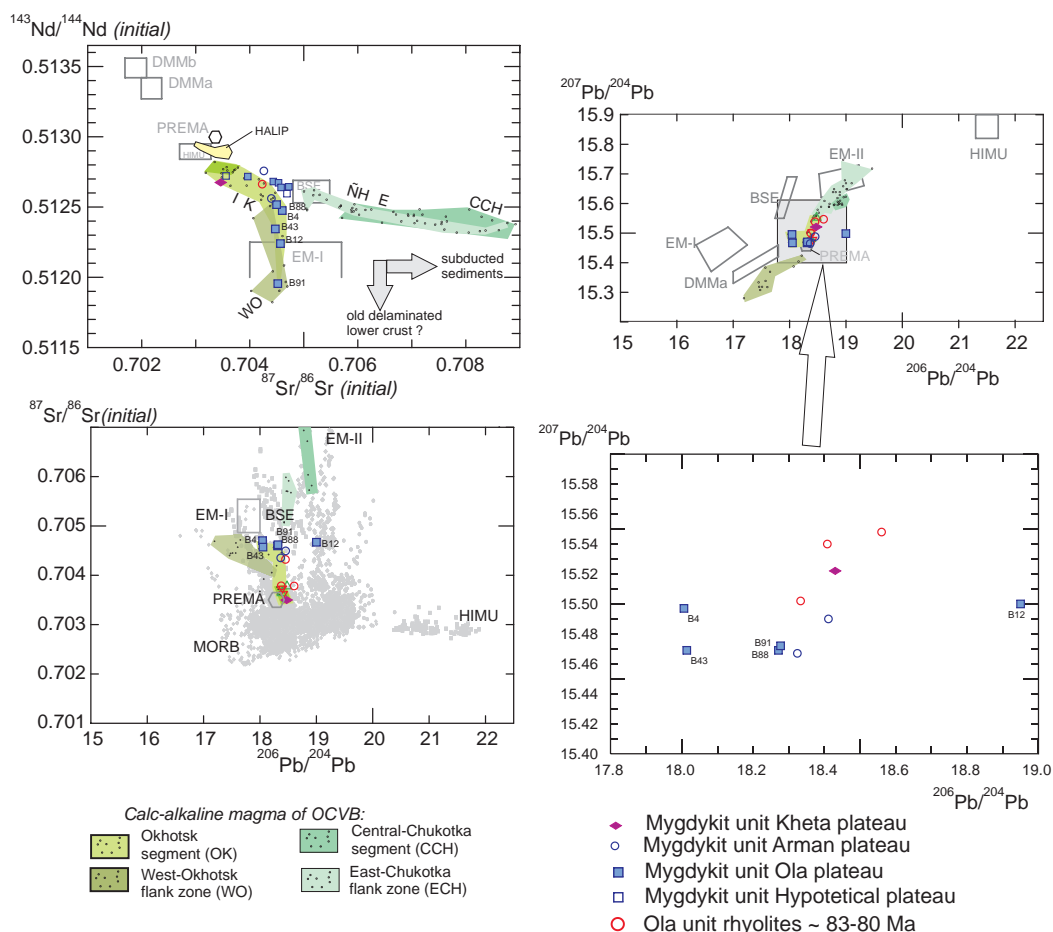


Fig. 9. Isotopic compositions (initial ratios) of the volcanic rocks of the OCVB indicating lateral heterogeneity of the mantle sources of calc-alkaline magmas in various segments and zones of the belt (Akinin and Miller, 2011; Tikhomirov et al., 2008). Symbols with different colors shows basalts of the plateaus of the final stage of OCVB volcanism discussed in this paper (data on basalts from Hypotetical and five samples of Ola plateau are from Leitner, 2010). The mantle end members (DMM, PREMA, BSE, MORB, HIMU, EM-I, EM-II) are after Zindler and Hart (1986).

of the OCVB and subducted oceanic slab. Enriched Sr-Nd isotopic ratios (admixture of EM1 on Fig. 9) may reflect contribution from an old delaminated lower crustal component in the source of magma (Tatsumi and Kogiso, 2003).

Major element compositions in the Ola section vary slightly from the bottom to the top (Fig. 10). SiO₂ increases up section from 49 to 54.5 wt. %, Al₂O₃ from 16 to 17 wt. %, magnesium number (Mg/(Mg+Fe)) from 0.4 to 0.5, K₂O from 1.5 to 2 wt. %. In contrast, TiO₂ decreases up section from 2.2 to 1.4 wt.%, CaO from 8 to 6.5 wt.%, P₂O₅ from 0.8 to 0.6 wt.% decreased up-section (Fig. 10). Trace element variations were not as clear as we found decreasing Ba, but increasing Rb and other incompatible elements with higher positions in the Ola section. In the middle part of the section (flow numbers from B45 to B64) significant shifts in whole rock geochemistry were observed. The most pronounced shifts are strong increases in CaO, Sr, ⁸⁷Sr/⁸⁶Sr isotopic ratio (from 0.7035 to 0.7077 ± 0.0001), and a coincident decrease in SiO₂, Ba, and LOI (Fig.10). The sharp changes in composition between flows 45 to 64 are interpreted to have been caused by an introduction of a CO₂-bearing, Si-rich fluid flux into the magma chamber which led to post-magmatic carbonate alteration and formation of agate and chalcedonies (Akinin et al., 2007).

Microprobe studies of rock-forming minerals (olivine, and plagioclase phenocrysts, as well as clinopyroxene, orthopyroxene, and Fe-Ti oxides in groundmass) were conducted in seventeen representative samples. A total of 310 olivine phenocrysts were studied which revealed a composition variation from Fo 81.8 to Fo 54.2 with most of the olivines having Fo 77-71. We did not find any clear gradational change in composition of olivine across the section. Plagioclase numbers vary from An 88 to An 43 with most of the grains having An 73-60. We found plagioclase with lower An number in older eruptions, whereas plagioclase with higher in anorthite content is located in the middle and upper parts of the section. Clinopyroxene in the groundmass of the lavas displays variation in magnesium number (Mg#=Mg/(Mg+Fe), mol.) within the same samples or the same mineral grains from 0.75 to 0.5, and shows little or no systematic variation with stratigraphic position in the section.

Orthopyroxene microphenocryst compositions measured in four samples have Mg# ranging from 0.73 to 0.51, generally consistent with the variation in Mg# in clinopyroxene. We suggest that the mostly weak variations in whole rock and mineral composition with locations in the section, reflect that fractional crystallization processes were limited. Weak plagioclase fractionation is suggested in magma evolution and is corroborated by the limited changes in whole rock Ca, Sr, and Ba.

DISCUSSION AND CONCLUDING REMARKS

The final stage of basaltic volcanism in Okhotsk segment of Okhotsk-Chukotka volcanic belt occurred during Early Campanian (78-80 Ma) as suggested from ⁴⁰Ar/³⁹Ar and U-Pb SHRIMP dating of the Mygdykit suite of the Ola plateau (northern coast of Okhotsk Sea). Our new ages are close to those obtained from the underlying rhyolite sequences, showing that the hiatus between rhyolite and the overlying Mygdykit basalt unit was less than 1–2 Ma. The small disparity in time between these two units suggests that these plateau basalts are part of the OCVB.

The emplacement of the Mygdykit basalts heralds the final stage of volcanism in the OCVB related to oblique subduction. Simultaneously, the transition coincided with the completion of plume-related tholeiitic volcanism in the HALIP which occurred between ~130 to ~80 Ma (Gottlieb and Miller, 2012), and is possibly linked to the opening of the Canada Basin. The HALIP is a tholeiitic suite that occurs as flood basalt lavas, sills and dykes exposed on the Canadian Arctic Islands, the Chukchi margin, Svalbard and King Charles Land, and Franz Josef Land (e.g. Tegner et al., 2011; Thorarinnsson et al., 2011). Although both final OCVB basalts and HALIP basalts represent disparate geochemical signatures and sources, they might have been caused by a global change in the geodynamics of both Pacific and Arctic regions. This suggests that during the Early Campanian, the direction of Pacific plate motion may have changed dramatically (e.g. Engebretson et al., 1985) from orthogonal subduction along the Russian Pacific margin to a regime of an overall transform margin with local extension zones or slab-windows. Simultaneously,

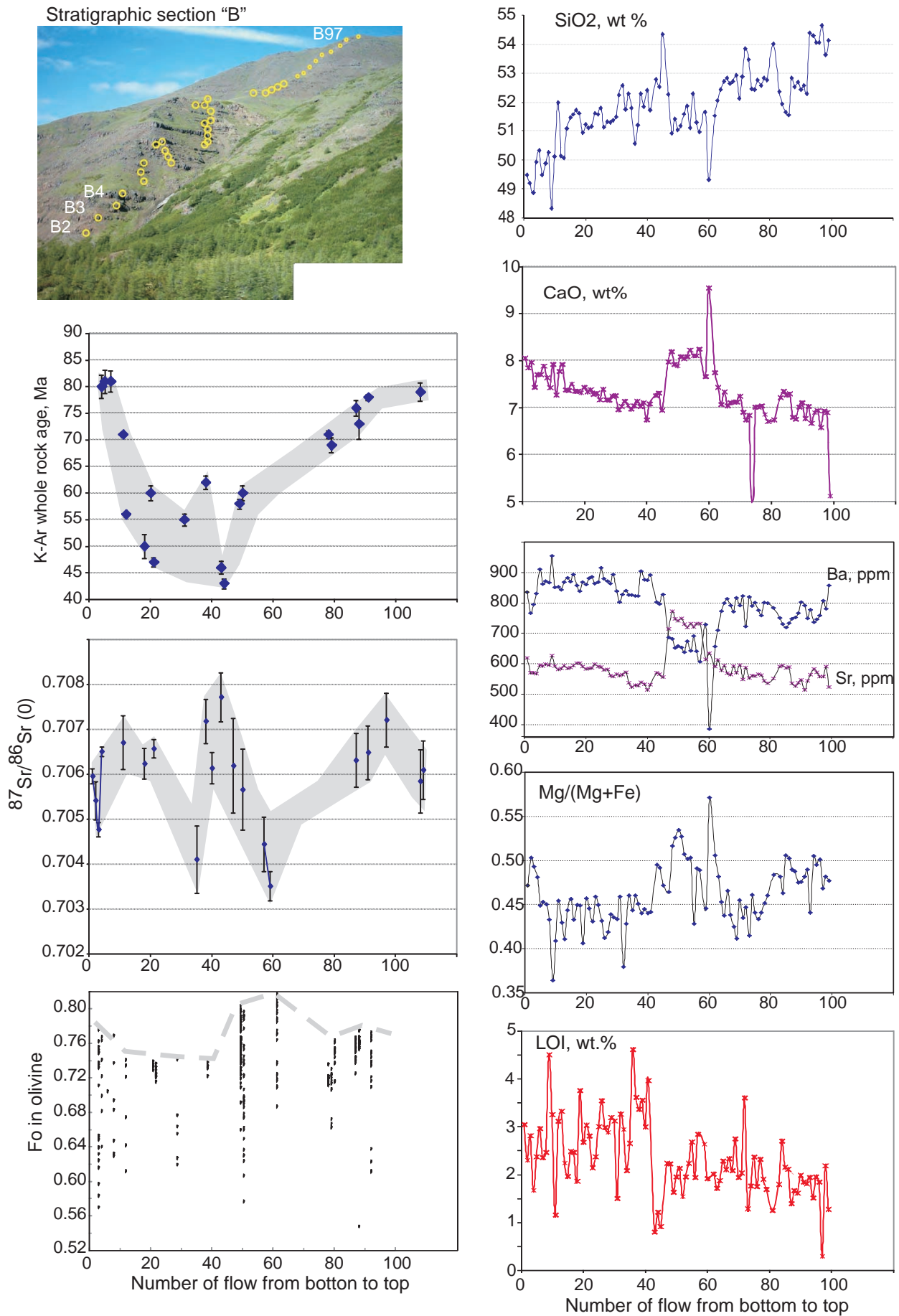


Fig. 10. Variation of composition of basalts and basaltic andesites of Mygdykit unit from Ola plateau from bottom to top of stratigraphic section "B" (Grozovoi Creek).

in the Arctic it was the beginning of extensive initial (pre-breakup) rifting in the Eurasia – Laptev Sea region of Arctic as well as compression events in the Chukchi-Bering region (e.g. Drachev, 2011).

The spiked incompatible trace element patterns of the Mygdykit unit lavas including pronounced Nb-Ta negative anomaly (Fig. 8) are indicative of a component derived from partial melting of eclogite facies subducted material with residual rutile (Kelemen et al., 2003). Volcanic rocks with MgO-rich compositions that are in equilibrium with the mantle wedge are rare in continental arcs and form only a minor component of island arcs, due to density filtering and intracrustal ‘processing’ of ascending magmas (Annen et al., 2006). The maximum values of Mg with a number of about 0.58 (sample B61: whole rock Mg# =0.581, plagioclase An80, olivine Fo81.7) in the Mygdykit unit basalts indicates that they represent a primary mantle-derived melt. On the other hand, all of the samples contain evidence of magma evolution generated during

AFC (assimilation and fractional crystallization) processes from evolved mafic magma. The parent melt probably did not reach the surface, and instead probably stalled in a middle crustal magma chamber or in MASH zones (zone of mixing, assimilation, storage and hybridization; Hildreth and Moorbath, 1988). The most magnesium-rich basalts (e.g. sample B61, B80) can be segregated at pressures of about 7 to 8 kilobars as calculated using appropriate whole rock and plagioclase-melt barometers (Albarede, 1992; Putirka, 2008), and a temperature of 1200 to 1250° C using the plagioclase-melt and olivine-melt thermometers (Putirka, 2008; Beattie, 1993). Basalts with lower contents of MgO (e.g. sample B10, whole rock Mg# =0.41, plagioclase An66, olivine Fo72), according to our calculations using Putirka’s plag-melt equation 25a (2008) were generated at T= 1150-1180° C, and P= 5-6 kb, which corresponds to a depth of about 15 to 18 km where the fractionation took place. Calculated pressures are little lower than those experimentally produced for residual melts

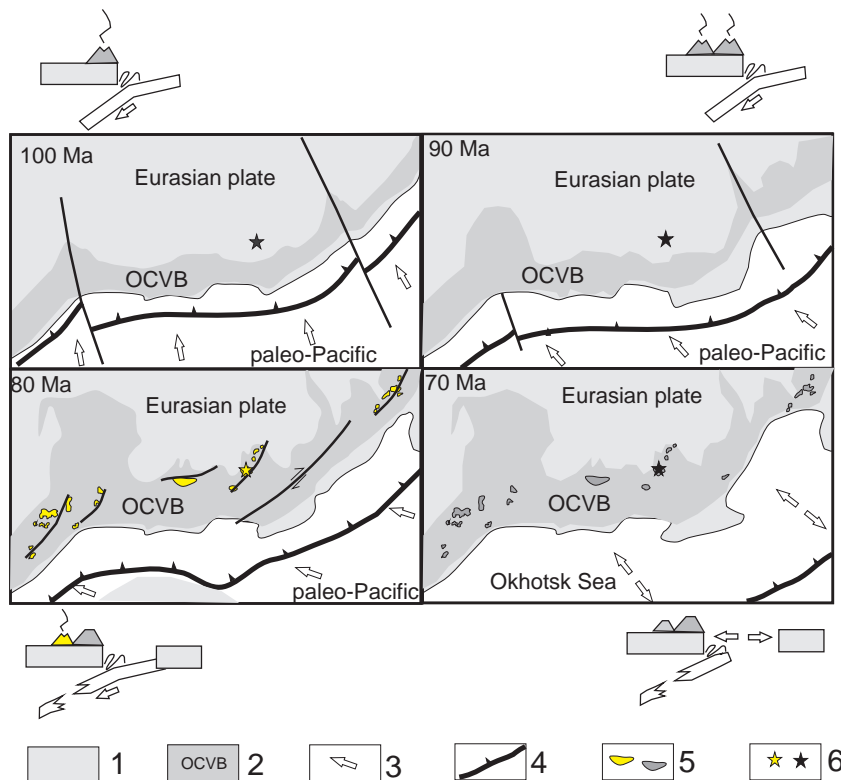


Fig. 11. Paleo-reconstruction schematic showing inferred links between development of late-stage OCVB volcanism (basaltic volcanism of the Mygdykit unit) due to change in geodynamic setting from frontal subduction to a slab-window transform regime along the paleomargin of eastern North eastern Russia. 1 - Eurasian plate, Northeastern Russia; 2 - subduction related Okhotsk-Chukotka continental margin volcanic belt; 3 - plate motion direction; 4 - subduction zone; 5 - active (yellow) and not active (grey) area of Mygdykit unit basaltic volcanism; 6 - position of Ola plateau.

from crystallization of Mount Shasta hydrous basalts in the lower crust (Fig. 7).

Although the Mygdykit unit basalts have subduction-like geochemical features (e.g. Nb-Ta negative anomaly) they display geochemical discrepancies compared to basalt units in the underlying parts of the OCVB. The plateau basalts have higher Ti, Zr, P, and other HFSE as well as more evolved Sr and Nd isotopic ratios compared to the stratigraphically lower basalts which we attribute to a slab-window volcanism or local extension-related volcanism along strike-slip faults. Principal sketch of paleodynamic reconstruction of such environment on four time-slices shown on Fig. 11. We speculate that contrasting tectonic processes in the system “rifted Arctica vs. subducted western Pacifica” at ~80 Ma affected the geodynamic setting in Northern Asia. At this time the subduction setting changed from orthogonal subduction to extension due transform-like continental margin.

Acknowledgments. We greatly appreciated a helpful review by Thomas Moore improving the draft of the manuscript. This study was financially supported by the Russian Foundation for Basic Research, project no 12-05-00874 (PI. Akinin), and CRDF-Far East Branch RAS grant no. RUG1-2994-MA-11 (PIs Akinin and Miller).

Table 2. Geochemistry of Ola plateau volcanic rocks.

Sample No	B1	B2	B3	B4	B7	B11	B18	B21	B28	B31	B35	B38
Longitude	151.313	151.307	151.307	151.307	151.307	151.306	151.306	151.306	151.304	151.304	151.303	151.303
Latitude	60.647	60.648	60.649	60.649	60.649	60.650	60.649	60.650	60.651	60.651	60.650	60.651
SiO ₂	49.49	49.19	48.87	49.92	49.89	51.99	51.62	51.10	51.29	52.25	51.80	52.29
TiO ₂	1.88	2.05	2.06	2.17	2.09	1.97	1.97	1.89	1.86	1.87	1.77	1.69
Al ₂ O ₃	16.95	15.88	15.94	16.15	16.17	16.10	16.31	15.90	15.85	16.30	16.11	15.87
FeOT	9.19	10.31	10.20	10.35	10.00	9.73	9.67	9.48	9.61	9.39	9.31	8.83
MnO	0.15	0.17	0.16	0.16	0.16	0.14	0.13	0.15	0.15	0.12	0.15	0.14
MgO	4.60	5.86	5.57	5.38	4.60	4.55	4.42	4.27	4.22	4.47	4.16	3.90
CaO	8.06	7.85	7.97	7.44	7.89	7.27	7.35	7.34	7.16	6.96	6.97	7.03
Na ₂ O	3.27	3.17	3.25	3.32	3.39	3.54	3.25	3.81	3.83	3.51	3.34	3.52
K ₂ O	1.74	1.40	1.39	1.54	1.54	1.71	1.58	1.22	1.34	1.84	1.90	1.59
P ₂ O ₅	0.58	0.66	0.64	0.73	0.78	0.74	0.74	0.74	0.71	0.73	0.79	0.78
LOI	3.04	2.30	2.81	1.67	2.35	1.15	1.86	3.03	2.88	1.50	2.65	3.36
TOTAL	98.95	98.84	98.86	98.83	98.86	98.89	98.90	98.93	98.90	98.94	98.95	99.00
Mg #	0.471	0.503	0.493	0.481	0.450	0.455	0.449	0.445	0.439	0.459	0.443	0.440
Sc	20	21		22	19	19	21	21	18	20	20	18
Cr	99	137		102	86	84	88	81	77	77	89	89
Ni	28	44		28	27	28	16	15	20	12	12	19
Rb	39	21		30	22	30	22	69	66	39	41	86
Sr	702	638		663	735	728	699	698	725	658	624	677
Y	20	25		27	26	26	27	27	26	27	27	27
Zr	176	225		290	343	370	285	276	385	280	324	441
Nb	8.1	10.8		13.2	12.7	13.4	14.3	13.2	13.7	13.8	16.5	16.2
Cs	1.15	0.81		0.77	0.74	0.91	1.14	2.49	1.90	1.46	1.28	2.18
Ba	723	566	795	708	899	524	730	848	996	764	748	1208
La	27	28		32	30	33	34	35	32	36	40	38
Ce	69	85		80	72	100	88	90	75	99	105	99
Pr	7.3	7.9		9.0	8.6	9.2	9.8	9.9	9.2	9.7	11.1	10.6
Nd	32.2	34.7		39.8	37.1	39.8	42.7	42.7	38.7	41.7	47.3	44.2
Sm	6.6	7.3		8.1	7.6	7.9	8.4	8.4	7.6	8.3	9.1	8.6
Eu	2.1	2.2		2.4	2.2	2.1	2.3	2.3	2.0	2.2	2.2	2.1
Gd	6.8	7.7		8.5	8.1	8.5	8.6	8.8	8.1	8.8	9.8	8.6
Tb	0.81	0.95		1.06	0.98	1.00	1.06	1.07	0.97	1.06	1.10	1.01
Dy	4.3	5.2		5.8	5.2	5.3	5.8	5.8	5.3	5.7	5.9	5.4
Ho	0.8	1.0		1.1	0.9	1.0	1.1	1.1	0.9	1.1	1.1	1.0
Er	2.1	2.7		2.9	2.6	2.7	2.9	2.9	2.6	2.9	3.0	2.7
Tm	0.3	0.3		0.4	0.3	0.3	0.4	0.4	0.3	0.4	0.4	0.3
Yb	1.8	2.3		2.5	2.3	2.3	2.5	2.6	2.3	2.6	2.6	2.3
Lu	0.25	0.34		0.37	0.32	0.31	0.37	0.37	0.31	0.38	0.38	0.32
Hf	3.7	4.6		5.3	4.7	5.2	5.8	5.5	5.3	5.7	6.5	6.0
Ta	0.47	0.61		0.73	0.77	0.65	0.78	0.73	0.65	0.77	0.73	0.71
Pb	16.0	17.2		20.3	15.1	32.7	32.9	20.3	24.8	24.2	18.2	18.8
Th	4.4	3.4		3.7	3.2	3.8	4.4	4.4	3.5	4.1	4.4	4.0
U	1.1	0.9		0.9	0.8	1.0	1.1	1.0	0.9	1.0	1.1	1.0
K-Ar age, Ma				80	81	71	50	47	0	55	0	62
1σ				2.2	2.0	0.5	2.2	0.9		1.1		1.3
⁸⁷ Sr/ ⁸⁶ Sr	0.70619	0.70556	0.70497	0.70484		0.70479	0.70639	0.70699			0.7044	0.70775
2σ	0.00017	0.00042	0.00016	0.000010		0.000001	0.000345	0.0002			0.00075	0.00049
(⁸⁷ Sr/ ⁸⁶ Sr) _i	0.70597	0.70542	0.70478	0.704648		0.704614	0.70624	0.70658			0.70411	0.70719
¹⁴³ Nd/ ¹⁴⁴ Nd				0.512539		0.512293						
2σ				0.00001		0.00001						
(¹⁴³ Nd/ ¹⁴⁴ Nd) _i				0.512476		0.512232						
ε _{Nd}				-1.2		-6.0						
T _{Nd} (DM)				884		1228						
²⁰⁶ Pb/ ²⁰⁴ Pb				18.01		18.95						
²⁰⁷ Pb/ ²⁰⁴ Pb				15.50		15.50						
²⁰⁸ Pb/ ²⁰⁴ Pb				37.85		37.93						

Sample numbers with * indicate late dikes, (⁸⁷Sr/⁸⁶Sr)_i and (¹⁴³Nd/¹⁴⁴Nd)_i are calculated initial ratios.

Sample No	B40	B43	B47	B50	B57	B59	B78	B87	B91	B97	BD61*	KA524-7*
Longitude	151.303	151.303	151.301	151.301	151.301	151.301	151.300	151.299	151.299	151.324	151.301	151.261
Latitude	60.651	60.651	60.652	60.652	60.653	60.653	60.655	60.656	60.656	60.661	60.653	60.661
SiO ₂	52.42	52.80	52.28	51.03	50.96	51.66	52.83	52.83	52.57	54.64	49.42	75.34
TiO ₂	1.73	1.75	1.64	1.53	1.63	1.77	1.77	1.70	1.73	1.64	1.27	0.11
Al ₂ O ₃	15.91	16.36	17.15	16.89	17.28	16.83	16.15	16.38	16.28	16.70	17.42	13.93
FeOT	8.98	9.12	8.26	8.74	8.42	8.85	8.97	8.94	8.93	8.38	8.95	0.86
MNO	0.13	0.15	0.13	0.14	0.15	0.15	0.14	0.13	0.15	0.14	0.15	0.01
MGO	3.96	5.01	4.02	5.63	4.52	3.99	4.15	4.81	4.65	4.14	6.96	0.08
CAO	6.74	7.26	7.98	7.89	8.25	7.67	6.86	6.80	6.77	6.93	9.66	0.14
NA ₂ O	3.34	3.51	3.40	3.12	3.38	3.44	3.43	3.47	3.41	3.56	2.85	1.62
K ₂ O	1.97	1.51	1.28	1.45	0.97	1.35	1.95	1.91	1.99	1.98	1.03	6.03
P ₂ O ₅	0.80	0.68	0.68	0.66	0.64	0.68	0.83	0.63	0.67	0.66	0.28	0.00
LOI	2.99	0.80	2.23	1.95	2.84	2.63	1.90	1.39	1.84	0.29	1.00	1.79
TOTAL	98.97	98.95	99.05	99.03	99.04	99.02	98.98	98.99	98.99	99.06	98.99	100.00
Mg #	0.440	0.495	0.464	0.534	0.489	0.446	0.452	0.490	0.481	0.468	0.581	0.142
Sc	21	21	23	19	20	21	18	21	15	16	26	1
Cr	91	111	96	100	79	75	91	102	90	80	142	1
Ni	12	30	9	21	16	19	21	33	28	12	38	36
Rb	50	75	40	23	35	56	44	42	37	43	21	190
Sr	625	677	875	862	886	752	641	640	524	655	809	51
Y	28	28	26	23	24	27	27	26	24	27	22	21
Zr	336	293	276	244	250	290	333	287	266	410	127	163
Nb	16.9	13.7	12.4	11.5	11.8	14.0	17.4	14.2	13.6	14.8	3.7	10.0
Cs	1.71	1.32	1.34	0.63	0.85	1.48	1.35	1.19	1.03	0.90	0.57	
Ba	712	751	572	268	227	1636	561	1549	244	329	282	707
La	42	37	36	33	32	35	41	33	31	38	24	29
Ce	97	83	84	83	79	91	100	86	76	89	56	62
Pr	11.8	10.2	10.4	9.6	9.2	10.1	11.4	9.5	8.6	10.7	6.9	6.0
Nd	49.3	43.7	44.7	41.7	39.8	43.5	48.2	40.2	37.0	45.3	30.2	21.9
Sm	9.5	8.5	8.6	8.1	7.7	8.5	9.2	7.9	7.1	8.7	6.1	3.9
Eu	2.3	2.2	2.4	2.2	2.2	2.2	2.2	2.0	1.8	2.1	1.8	0.5
Gd	9.4	8.7	8.7	7.9	7.8	8.6	9.2	8.1	7.3	8.7	6.4	4.0
Tb	1.14	1.09	1.04	0.94	0.94	1.06	1.12	1.01	0.91	1.07	0.77	0.52
Dy	6.0	5.9	5.5	5.2	5.2	5.9	6.1	5.7	5.2	5.9	4.3	3.1
Ho	1.1	1.1	1.0	0.9	0.9	1.1	1.1	1.0	1.0	1.1	0.8	0.6
Er	3.0	3.0	2.8	2.6	2.6	3.0	3.0	2.9	2.7	3.0	2.3	1.8
Tm	0.4	0.4	0.4	0.3	0.3	0.4	0.4	0.4	0.3	0.4	0.3	0.3
Yb	2.6	2.6	2.5	2.3	2.3	2.6	2.6	2.5	2.3	2.6	2.0	1.9
Lu	0.39	0.38	0.36	0.32	0.33	0.38	0.37	0.37	0.33	0.36	0.28	0.27
Hf	6.8	6.0	5.6	5.1	5.1	6.0	6.7	5.9	5.3	6.4	2.6	4.3
Ta	0.74	0.72	0.67	0.44	0.46	0.60	0.73	0.61	0.54	0.59	0.21	0.30
Pb	16.4	17.2	12.2	13.6	13.5	17.9	15.0	11.7	11.4	23.9	11.1	25.6
Th	4.8	4.8	3.8	3.4	3.3	5.1	4.5	4.5	3.8	5.0	3.0	19.0
U	1.2	1.1	0.9	0.9	0.8	1.1	1.1	1.1	1.0	1.2	0.7	5.0
K-Ar age, Ma	0	46	0	60	0	0	71	76	78	0	61	
1σ		1.2		1.4			0.7	1.4	0.5		1.2	
⁸⁷ Sr/ ⁸⁶ Sr	0.7065	0.70499	0.7064	0.7058	0.7046	0.70382		0.70484	0.70487	0.7075	0.7056	
2σ	0.00035	0.00001	0.00105	0.0009	0.0006	0.00033		0.000010	0.00002	0.0006	0.00065	
(⁸⁷ Sr/ ⁸⁶ Sr) _i	0.70614	0.704518	0.70620	0.70567	0.70445	0.70352		0.704541	0.70456	0.70722	0.70549	
¹⁴³ Nd/ ¹⁴⁴ Nd		0.51240						0.512519	0.51201			
2σ		0.00001						0.00001	0.00001			
(¹⁴³ Nd/ ¹⁴⁴ Nd) _i		0.512344						0.512519	0.51195			
ε _{Nd}		-3.8						-0.4	-11.4			
T _{Nd} (DM)		1034						409	1575			
²⁰⁶ Pb/ ²⁰⁴ Pb		18.01						18.27	18.28			
²⁰⁷ Pb/ ²⁰⁴ Pb		15.47						15.47	15.47			
²⁰⁸ Pb/ ²⁰⁴ Pb		37.93						38.06	38.07			

REFERENCES

- Akinin V.V., Miller E.L., Wooden J., 2009. Petrology and Geochronology of Crustal Xenoliths from the Bering Strait Region: Linking Deep and Shallow Processes in Extending Continental Crust. Geological Society of America Special Paper 456, 39–68.
- Akinin, V.V. and E. L. Miller, 2011. The evolution of the calc-alkalic magmas of the Okhotsk – Chukotka volcanic belt. *Petrology*. 19, № 3, 237-277.
- Akinin V.V., Alshevsky A.V., Parfenov M.I., Leonova V.V., 2007. Age and evolution of Ola plateau basaltic magma, northern Priokhotie. In: All Russian conference dedicated to academician K.V.Simakov. Abstract volume. Magadan, NEISRI FEB RAS. 5 (in Russian)
- Alshevsky A.V., 1997. About upper age limit of continental margin OCVB. In: Geological formation, magmatism, and ore deposits of North-Eastern Asia, Abstracts of Mineralogical conference, Magadan, NEISRI FEB RAS. 43-45 (in Russian)
- Albarède, F., 1992. How deep do common basaltic magmas form and differentiate? *Journal of Geophysical Research*, 97, 10997-11009.
- Anderson, D.L., 2001. Top-down tectonics? *Science*, 293, 2016–2018.
- Annen, C., J. D. Blundy, R. S. J. Sparcs, 2006. The Genesis of Intermediate and Silicic Magmas in Deep Crustal Hot Zones, *Journal of Petrology*, 47(3), 505-539.
- Anorov P.N., Bychkov Yu.M., Karavaeva N.I., Mikhailov V.P., Yudina G.M., 1999. Geological map 1:200 000 scale legend for Magadan series, Russian Federation (2th edition), Magadan, Ministry of natural resources of Russian Federation, 110 p. (in Russian)
- Ariskin A.A., Barmina G.S., 2000. Modelling phase equilibria at crystallization of basalt magmas, Moscow, Nauka, MAIK «Nauka/ Interperiodica», 363p. (in Russian)
- Beattie P., 1993. Olivine-melt and orthopyroxene-melt equilibria: Contributions to Mineralogy and Petrology, 115, 103-11.
- Belyi, V.F., 1977. Stratigraphy and Structure of the Okhotsk–Chukotka Volcanogenic Belt. Moscow: Nauka, 190p. (in Russian)
- Bely V.F., Belaya, B.V., 1998. Late stage of evolution of Okhotsk-Chukotka volcanogenic belt (upper part of Enmyvaam River). Magadan, NESRI FEB RAS, 108p. (in Russian).
- Belyi, V.F., 2008. Problems of Geological and Isotopic Age of the Okhotsk–Chukotsk Volcanogenic Belt (OCVB). *Stratigr. Geol. Correlation*, 16 (6), 639–649.
- Bercovici, D., 2003. The generation of plate tectonics from mantle convection. *Earth Planet. Sci. Lett.* 205, 107–121.
- Condie K.C., 2003. Incompatible element ratios in oceanic basalts and komatiites: Tracking deep mantle sources and continental growth rates with time: *Geochemistry, Geophysics, Geosystems*. 4(1), doi:10.1029/2002GC000333.
- Drachev S.S., 2011. Tectonic setting, structure and petroleum geology of the Siberian Arctic offshore sedimentary basins. In: Spencer A.M., Embry, A. F., Gautier, D. L., Stoupakova, A. V. & Sorensen, K. (Eds.) *Arctic Petroleum Geology, Memoirs*, 35. London: The Geological Society of London, 369–394 (DOI: 10.1144/M35.25).
- Engebretson, D.C., Cox, A., Gordon, R.G., 1985. Relative motions between oceanic and continental plates in the Pacific Basin. *Geological Society of America Special Paper*. Boulder, Colorado, 59 p.
- Filatova, N.I., 1988. Peri-oceanic Volcanogenic Belts. Moscow, Nedra, 264 p. (in Russian)
- Gottlieb, E., and Miller, E., 2012. Cretaceous Magmatism in the Arctic: Slab versus Plume? Or Slab and Plume Together?, ICAM-VI. Conference abstracts. Geophysical Institute Report UAG-R-335, Compilers: D.B.Stone, J.G.Clough, D.K.Thurston, University of Alaska, Fairbanks, Alaska, 63-64.
- Gorodinsky, M.E. (Ed.), 1980. Geological map of North East USSR, 9 sheets, 1:1,500,000 scale. *Minist. Geol. SSSR, Leningrad*, (in Russian).
- Grove, T. L., Elkins-Tanton, L. T., Parman, S. W., Chatterjee, N., Muntener, O., Gaetani, G. A., 2003. Fractional crystallisation and mantle-melting controls on calc-alkaline differentiation trends. *Contributions to Mineralogy and Petrology*, 145, 515–533.
- Hildreth, W., and Moorbath, S., 1988. Crustal

- contribution to arc magmatism in the Andes of Central Chile. *Contributions to Mineralogy and Petrology* 98, 455–489.
- Hourigan J.K. and Akinin V.V., 2004. Tectonic and chronostratigraphic implications of new $^{40}\text{Ar}/^{39}\text{Ar}$ geochronology and geochemistry of the Arman and Maltan-Ola volcanic fields, Okhotsk-Chukotka volcanic belt, northeastern Russia, *Geol. Soc. Am. Bull.*, 116 (5-6). 637-654.
- Ispolatov, V.O., Tikhomirov, P.L., Heizler, M., Cherepanova, I.Yu., 2004. New $^{40}\text{Ar}/^{39}\text{Ar}$ Ages of Cretaceous Continental Volcanics from Central Chukotka: Implications for Initiation and Duration of Volcanism within the Northern Part of the Okhotsk Chukotka Volcanic Belt (Northeastern Eurasia). *J. Geol.*, 112, 369-377.
- Kawamoto, T., 1996. Experimental constraints on differentiation and H₂O abundance of calc-alkaline magmas. *Earth and Planetary Science Letters* 144, 577–589.
- Kelemen, P.B., Hanghoj, K., and Greene, A.R., 2003. One view of the geochemistry of subduction-related magmatic arcs, with an emphasis on primitive andesite and lower crust. in *The Crust*, Rudnick R.L., Ed., *Treatise on Geochemistry*, Amsterdam: Elsevier. 3, 593–569.
- Kelley S.R., Spicer R.A., Herman A.B., 1999. New $^{40}\text{Ar}/^{39}\text{Ar}$ dates for Cretaceous Chauna Group tephra, north-eastern Russia, and their implications for the geologic history and floral evolution of the North Pacific region, *Cretaceous Research*, 20, 97-106.
- King, S.D., Lowman, J.P., Gable, C.W., 2002. Episodic tectonic plate reorganizations driven by mantle convection. *Earth Planet. Sci. Lett.*, 203, 83–91.
- Kotlyar, I.N., and Rusakova, T.B., 2004. Cretaceous Magmatism and Ore Potential of the Okhotsk–Chukotka Area: Geological–Geochronological Correlation. Magadan: SVKNII DVO RAN, 152 p. (in Russian).
- Koren', T.N. and Kotlyar, G.V., (Eds.), 2009. Resolution of the 3rd Interdisciplinary Regional Stratigraphic Conference on the Precambrian, Paleozoic, and Mesozoic of Northeastern Russia. St. Petersburg: VSEGEI, 268 p. (in Russian)
- Lanphere, M.A., and Dalrymple, G.B., 2000. First-principles calibration of ^{38}Ar tracers: Implications for the ages of $^{40}\text{Ar}/^{39}\text{Ar}$ fluence monitors, U.S. Geological Survey Professional Paper 1621, 10 p.
- Layer, P.W., 2000. Argon-40/argon-39 age of the El'gygytgyn impact event, Chukotka, Russia, *Meteoritics and Planetary Science*, 35, 591-599.
- Layer, P.W., Hall, C.M. and York, D., 1987. The derivation of $^{40}\text{Ar}/^{39}\text{Ar}$ age spectra of single grains of hornblende and biotite by laser step heating. *Geophys. Res. Lett.*, 14, 757-760.
- LeBas, M.J., LeMaitre, R.W., Streckeisen, A., and Zanettin, B., 1986. A chemical classification of volcanic rocks based on the total alkali silica diagram. *J. Pet.* 27, 745-750.
- Leitner J., 2010. Geochemical and petrological studies of the Ola- and Hypotetica-Plateau basalts in the Okhotsk-Chukotka Volcanic Belt, NE Russia. Unpublished Master Thesis, University of Vienna. 84p.
- Matthews, K. J., M. Seton, and R. D. Müller, 2012. A global-scale plate reorganization event at 105–100Ma, *Earth and Planetary Science Letters*, 355-356, 283-298.
- McDonough W.F., Sun S., 1995. The composition of the Earth, *Chemical Geology*, 120, 223-253.
- McDougall, I. and Harrison, T.M., 1999. *Geochronology and ThermoChronology by the $^{40}\text{Ar}/^{39}\text{Ar}$ method*, 2nd ed. Oxford University Press, New York, 269p.
- Newberry R., Layer, P., Gans, P., Goncharov V.I., Goryachev N.A., Voroshin S.V., 2000. Preliminary geochronology analysis of Mesozoic magmatism, tectonics, and mineralization in North-East Russia according to $^{40}\text{Ar}/^{39}\text{Ar}$ dating and trace element data on igneous and ore-bearing rocks, Gold mineralization and granitoid magmatism of North Pacific. Vol 1. Proceedings of the All-Russian Meeting. Magadan: NEISRI. FEB RAS, 158-205 (in Russian).
- Parfenov, L.M., 1984. Continental Margins and Island Arcs of Northeastern Asian Mesozoics. Novosibirsk: Nauka, 192 p. (in Russian)

- Pearce, J.A., Cann, J.R., 1973. Tectonic setting of basic volcanic rocks determined using trace element analysis. *Earth Planet. Sci. Letters*, 19, 290-300.
- Peccerillo, A. and Taylor, S.R., 1976. Geochemistry of Eocene calc-alkaline volcanic rocks from the Kastamonu area, Northern Turkey. *Contrib. Mineral. Petrol.* 58, 63-81.
- Polin, V.F. and Moll-Stalcup, E.J., 1999. Petrological–Geochemical Criteria of Tectonic Conditions of the Formation of the Chukotka Chain of the Okhotsk–Chukotka Volcanogenic Belt. *Pacific Geology*, 18 (4), 29–47.
- Putirka K.D., 2008. Thermometers and barometers for volcanic systems. *Reviews in mineralogy and geochemistry*, 69, 61-120.
- Sakhno, V.G., Polin, V.F., Akinin, V.V., Sergeev, S.A., Alenicheva, A.A., Tikhomirov, P.L., Moll-Stalcup, E.J., 2010. The diachronous formation of the Enmyvaam and Amguema–Kanchalan volcanic fields in the Okhotsk–Chukotka Volcanic Belt (NE Russia): evidence from isotopic data. *Doklady Earth Sciences* 434 (1), 1172–1178.
- Samson S. D., and Alexander E. C., 1987., Calibration of the interlaboratory $^{40}\text{Ar}/^{39}\text{Ar}$ dating standard, MMhb1. *Chemical Geology*, 66, 27-34.
- Seton, M., Müller, R. D., Zahirovic, S., Gaina, C., Torsvik, T., Shephard, G., Talsma, A., Gurnis, M., Turner, M., Maus, S., Chandler, M., 2012. Global continental and ocean basin reconstructions since 200 Ma. *Earth-Science Reviews*, 113(3-4), 212-270.
- Steiger, R.H. and Jaeger, E., 1977. Subcommittee on geochronology: Convention on the use of decay constants in geo and cosmochronology. *Earth and Planet Science Letters*, 36, 359-362.
- Stone, D.B., Layer, P.W., and Raikevich, M.I., 2009. Age and Paleomagnetism of the Okhotsk–Chukotka Volcanic Belt (OCVB) near Lake El'gygytgyn, Chukotka, Russia, *Stephan Mueller Spec. Publ. Ser.*, 4, 243–260.
- Struzhkov, S.F. and Konstantinov, M.M., 2005. *Metallogeniya zolota i serebrya Okhotsko-Chukotskogo vulkanogenogo poyasa (Gold and Silver Metallogeny of the Okhotsk–Chukotka Volcanogenic Belt)*. Moscow: Nauchnyi Mir, 320 p. (in Russian).
- Tatsumi, Y. and Kogiso, T., 2003. The subduction factory: Its role in the evolution of the Earth's crust and mantle. In: Larter, R.D., and Leat, P.T., eds., *Intra-oceanic subduction systems: tectonic and magmatic processes*. London, Geological Society Special Publication 219, 55–80.
- Tegner, C., Storey, M., Holm, P.M., Thorarinsson, S.B., Zhao, X., Lo, C.-H., and Knudsen, M.F., 2011. Magmatism and Eureka deformation in the High-Arctic Large Igneous Province: $^{40}\text{Ar}/^{39}\text{Ar}$ age of Kap Washington Group volcanics, North Greenland. *Earth Planet. Sci. Lett.* 303, 203-214.
- Tikhomirov P.L., Kalinina E.A., Kobayashi K., Nakamura E., 2008. Late Mesozoic silicic magmatism of the North Chukotka area (NE Russia): Age, magma sources, and geodynamic implications. *Lithos*, 105. 329-346.
- Tikhomirov, P. L., E. A. Kalinina, T. Moriguti, A. Makishima, K. Kobayashi, I. Y. Cherepanova, and E. Nakamura, 2012. The Cretaceous Okhotsk–Chukotka Volcanic Belt (NE Russia): Geology, geochronology, magma output rates, and implications on the genesis of silicic LIPs. *Journal of Volcanology and Geothermal Research*, 221-222, 14-32.
- Thorarinsson, S.B., Holm, P.M., Duprat, H., and Tegner, C., 2011. Silicic magmatism associated with Late Cretaceous rifting in the Arctic Basin – petrogenesis of the Kap Kane sequence, the Kap Washington Group volcanics, North Greenland. *Lithos*, 125 (1-2), 65-85.
- Umitbaev, R.B., 1986. *Okhotsko-Chaunskaya metallogenicheskaya provintsiya (Okhotsk–Chauna Metallogenic Province)*. Moscow: Nauka, (in Russian)
- Ustiev, E.K., 1959. *Okhotsk Tectonomagmatic Belt and Some Related Problems*. *Otechestvennaya geologiya*, 3, 3–26.(in Russian)
- York, D., Hall, C.M., Yanase, Y., Hanes, J.A., and Kenyon, W.J., 1981. $^{40}\text{Ar}/^{39}\text{Ar}$ dating of terrestrial minerals with a continuous laser. *Geophys. Res. Lett.*, 8, 1136-1138.
- Wood, D. A., 1980. The application of a Th-Hf-Ta diagram to problems of tectonomagmatic classification and to establishing the nature of crustal contamination of basaltic lavas of the British Tertiary volcanic province. *Earth and*

Planetary Science Letters, 50 (1), 11-30.

Zhulanova, I.L., Rusakova, T.B., and Kotlyar, I.N.,
2007. Geochronology and Geochronometry of
Endogenous Events in the Mesozoic History
of Northeast Asia. Moscow: Nauka, 358 p. (in
Russian)

Zindler A. and Hart S., 1986. Chemical Geodynamics,
Annual Review of Earth and Planetary Sciences.
14. 493-571.

Lithofacies features of Carboniferous – Lower Permian strata from the Pechora Sea

E.B. Suvorova, T.V. Matveeva

«I.S. Gramberg VNIIOkeangeologia», Saint-Petersburg, Russia

ABSTRACT

This paper shows interpreted lithofacies features of Carboniferous to Lower Permian carbonate strata from the Pechora Sea. Log and core data are used to develop lithofacies schemes and construct a lithostratigraphic section across the area. Two main sedimentation phases are revealed: 1) Late Viséan-Serpukhovian and 2) Middle Carboniferous – Early Permian. There is a gap between those phases which is confined to the Early Bashkirian time. Both phases are characterized by reef sedimentation. Available well data show that during Late Viséan–Earlier Permian time, the area of reefs distribution gradually shifted from northeast to northwest and west. In Carboniferous to Early Permian time shallow sea environments changed into much deeper environments.

INTRODUCTION

Carboniferous–Lower Permian carbonate strata comprise one of the main oil and gas-bearing reservoir objectives among all discovered fields in the Pechora Sea. The emphasis of this study is on the offshore Pechora Sea portion of the Timan-Pechora Basin province of northwest Russia. Exploration and development shows the most prospective reservoirs are Asselian to Sakmarian reef buildups (Bro, 1993; Viskunova, Suprunenko, and Preobragenskaia, 2002). Additional hydrocarbon deposits also occur in the Upper Viséan to Middle-Upper Carboniferous section. The core and log data shows the variations of lithological composition, depositional environments, and facies distribution of these rocks. Results obtained during this study may highlight areas where prospective reservoirs are most likely to occur.

Core descriptions, rock samples and thin sections, and well logging data from eleven wells

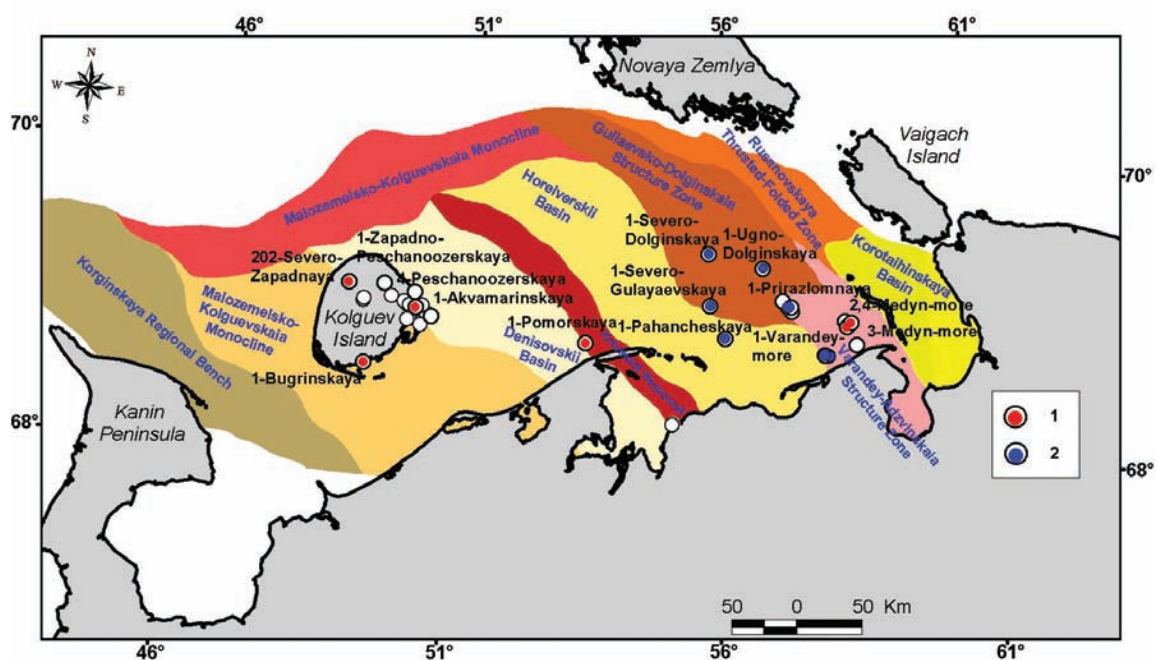


Fig. 1. Map of structural elements and well location at the Pechora sea. Deep wells: 1 – core samples, thin sections, well logging data were investigated, 2 – core description, well logging data were considered.

comprise the data for this study. Depositional environments are reconstructed from facies analyses. These wells represent the stratigraphic variations across major structural elements of the Pechora Syncline (from West to East): Malozemelsko-Kolguevskaya Monocline, Denisovsky Basin, Kolvinskii Megaswell, Horeiverskii Basin, Guliaevsko-Dolginskaya and Varandey-Adzvinikaia Structure Zones (Fig.1).

The Carboniferous–Lower Permian carbonate strata vary in thickness from 326 m in the

1-Bugrinskaya well to 620 m in the 1-Prirazlomnaya well. The age of this complex is Late Visean to Early Permian (Sakmarian, partially Artinskian). At the western part of the region, Carboniferous to Lower Permian carbonate rocks unconformably overlie Tournaisian and Upper Devonian strata (Preobragenskaia, Ustricki, and Bro, 1995). Visean rocks wedge out in a westerly direction based on seismic data (Suvorova, Viskunova, and Preobragenskaia, 2010). In contrast, in the eastern part of the basin these rocks are deposited

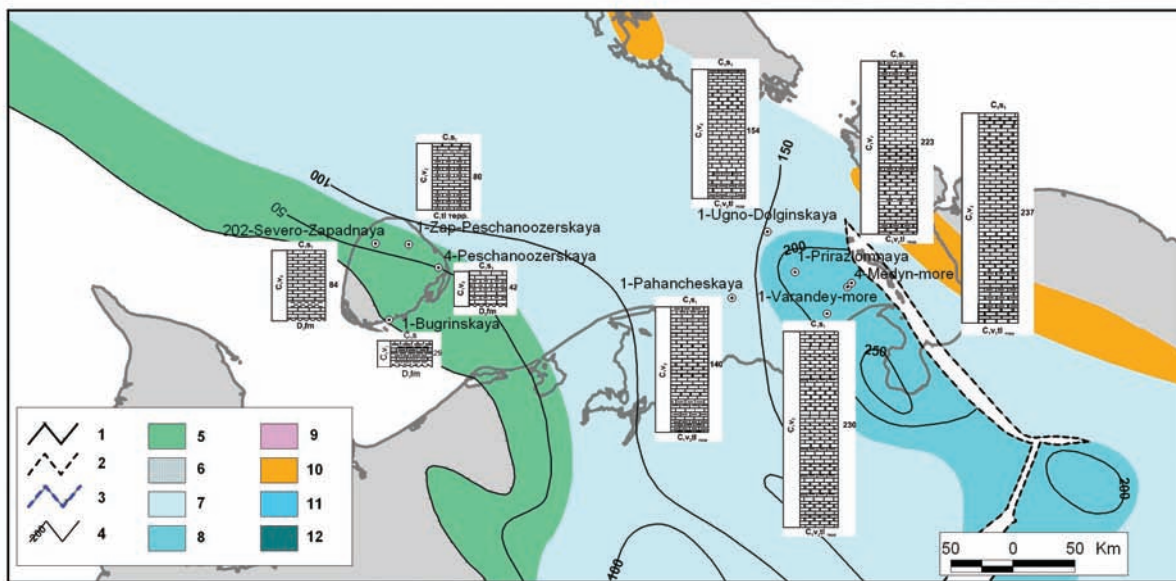


Fig. 2. Lithofacies map of Upper Visean strata. Boundaries: 1 – of modern strata distribution, 2 – strata absence, 3 - of Bashkirian strata distribution, 4 – isopachs. Environments: 5 – coastal, 6 – insular high zone, 7 - shallow shelf, 8 – depression on shallow shelf, 9 – lagoon, 10 - buildups, 11 - deep shelf, 12 – continental slope.

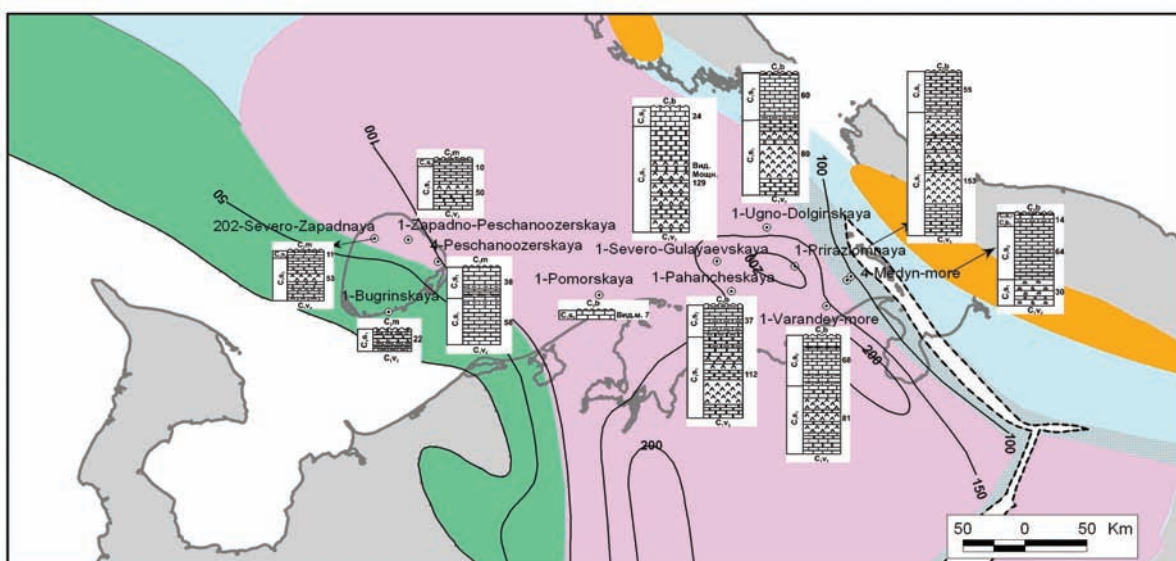


Fig. 3. Lithofacies map of Serpukhovian strata. Legend shown on fig.2.

conformably on the Devonian section in the Varandey-Adzvinskaia Structure Zone. Asselian to Sakmarian strata are overlain by Artinskian to Kungurian terrigenous rocks, and in the Medyn-Saremboj zone by Triassic argillites.

LITHOFACIES FEATURES AND ENVIRONMENTAL EVOLUTION

Early Visean of the northern Pechora basin consisted of continental and coastal environments. A marine transgression starting in the Late Visean changed the depositional condition into a shallow shelf setting, however coastal environments were preserved in the western part of the study region (Fig.2). A comparatively thick and predominantly mud-rich section on the eastern part of the shallow shelf suggests sedimentation in a deep depression in the Varandey-Adzvinskaia Structure Zone. At the end of the Late Visean sea level was lowered in the basin, and in the Medyn-Varandey zone littoral conditions with stromatolitic limestones were deposited.

In Early Serpukhovian time the sea basin became shallower. Coastal conditions were preserved in the western part of the basin. Lagoonal environments occurred over the greater part of the region (Fig.3), and sulphate-dolomite evaporites formed. At the eastern part of the basin a lagoon was bounded by an insular high zone (in modern coordinates this zone corresponds to Varandey-Adzvinskaia Structure Zone), where secondary dolomites formed by eogenetic alteration.

Upper Serpukhovian rocks across most of the area show an environment which is comparatively rich in fauna and flora such as corals, brachiopods and algae, indicating normal shallow marine environments were restored at this time.

During Visean-Serpukhovian time organogenic buildups formed in the Pechora Sea. Visean-Serpukhovian reefs can be traced in the western slope of the Urals, in southwest of Pai-Khoi (Antoshkina, 1994), and along the western coast of Novaya Zemlya (Matveev, 2008, Novaya Zemlya, 2004) (Fig.4). The distribution of these organic buildups is related to the boundary between the shallow-water Eleckaya and deep-water sediments of the Lemvinskaya formation zones. The position of this boundary has existed since the Ordovician (Sobolev,

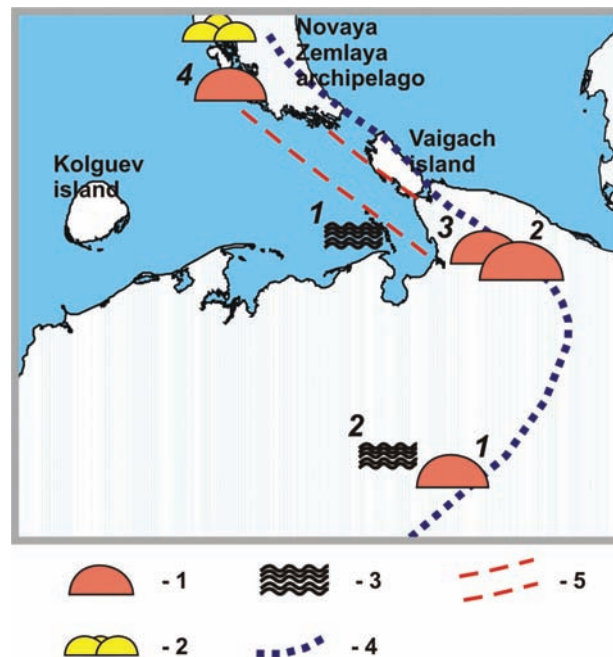


Fig. 4. Location of Visean-Serpukhovian buildups.

1- reefs: 1 - on The Bolshaya Nadota river (Eliseev, 1978), 2 - on The Sibirchata river (Antoshkina, 1994), 3 - on The Hey-Iyga river (Antoshkina, 1994), 4 - on The Chernyi cape (Novaya Zemlya, 2004); 2 - mud mounds on the Vypuklyi and Sokolova peninsulas (Novaya Zemlya, 2004); 3- stromatolites: 1 - in the Medyn-more field (Suvorova, 2010), 2 - in the Chernyshova mound (Antoshkina, 1994); 4 - paleoboundary between shallow and deep-water sediments (Sobolev, Ustrickii, Cherniak, 1985); 5 - the region, where reefs are expected.

Ustrickii, and Cherniak, 1985). We propose that the Visean-Serpukhovian buildups can be detected also in the Korotaihinskaya basin of the Pechora Sea.

The marine regression was followed by transgression in Late Serpukhovian-Early Bashkirian time, and as a result Upper Serpukhovian strata were in part eroded or simply not deposited.

In Late Bashkirian time carbonate sediments were deposited gradually from east to west across the region. In the western part of the Pechora Sea sedimentation occurred only since Late Moskovian time.

Comparatively shallow shelf environments predominated in Bashkirian and Moskovian time (Fig.5). Facies of bioclastic limestone sand and small bioherms occur in the Guliaevsko-Dolginskaya and Varandey-Adzvinskaya Structure Zones.

During Kasimovian-Gzhelian time the basin deepened (Fig.6) and shallow shelf environments

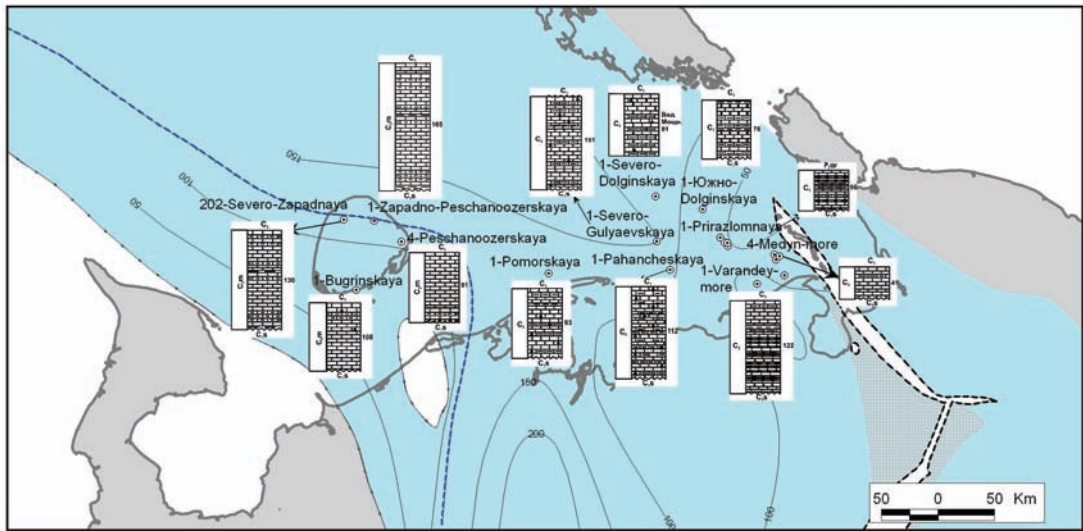


Fig. 5. Lithofacies map of Bashkirian-Moskavian strata. Legend shown on fig.2.

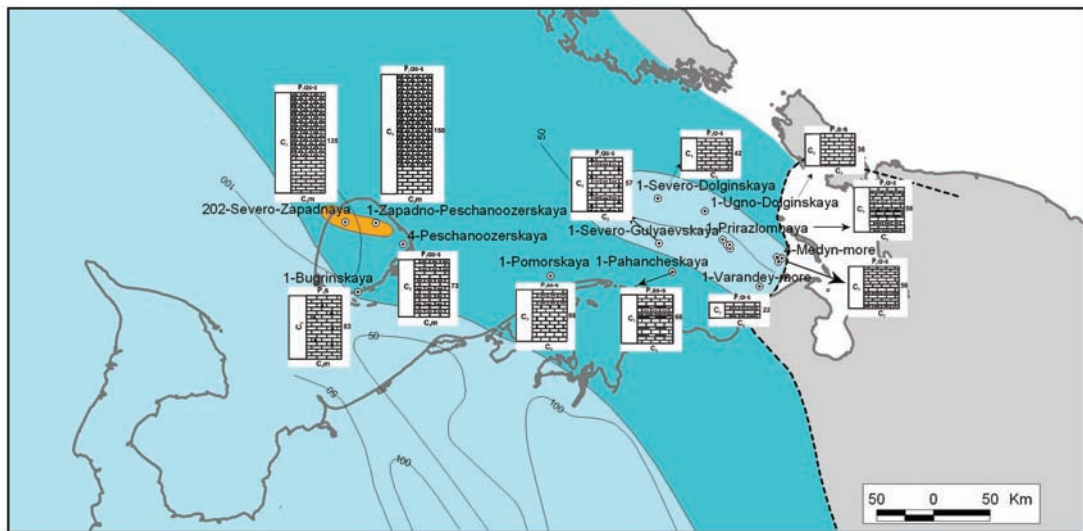


Fig. 6. Lithofacies map of Casimovian-Gzhelian strata. Legend shown on fig.2.



Fig. 7. Lithofacies map of Asselian-Sakmarian strata (By Viskunova, Suprunenko, Preobragenskaia, 2002 with changes). Legend shown on fig.2.

existed in the eastern part of the study area, where bioclastic limestones were deposited. According to published data (Preobragenskaia, Ustriski, and Bro, 1995), organogenic buildups at the western part of the region started to form in Late Pennsylvanian time.

In Early Permian time buildups were distributed to the west on Kolguev Island and to the east within the Guliaevsko-Dolginskaia and Varandey-Adzvinskaia Structure Zones (Fig.7). In the Pechora-Kolvinski, Megaswell, and Horeiverskii basins, reef buildups are observed in seismic data (Viskunova, Suprunenko, and Preobragenskaia, 2002). Seismic data also show that all lithofacies of the lower Permian are absent along the western boundary of Korotaihinskaya basin. The absence of strata is due

to post-Permian erosion.

Lithofacies schemes described in our paper can be used as a basis for predicting reservoir potential. Producing oil pools in Lower Carboniferous rocks could be associated with Upper Visean secondary dolomites, for example, such pools are present in the Medynskoe-More deposit. The porosity coefficient of these rock is 10-15%.

Oil fields with sufficient resources for commercial production from Middle to Upper Carboniferous rocks occur in the Dolginsky and Medynskoe-More fields. Oil production here is from both algal genesis rocks and calcareous sand facies that were deposited on the shelf edge. The porosity coefficient of these rocks is from 7% to 10-15%. We extrapolate that potential oil accumulations may

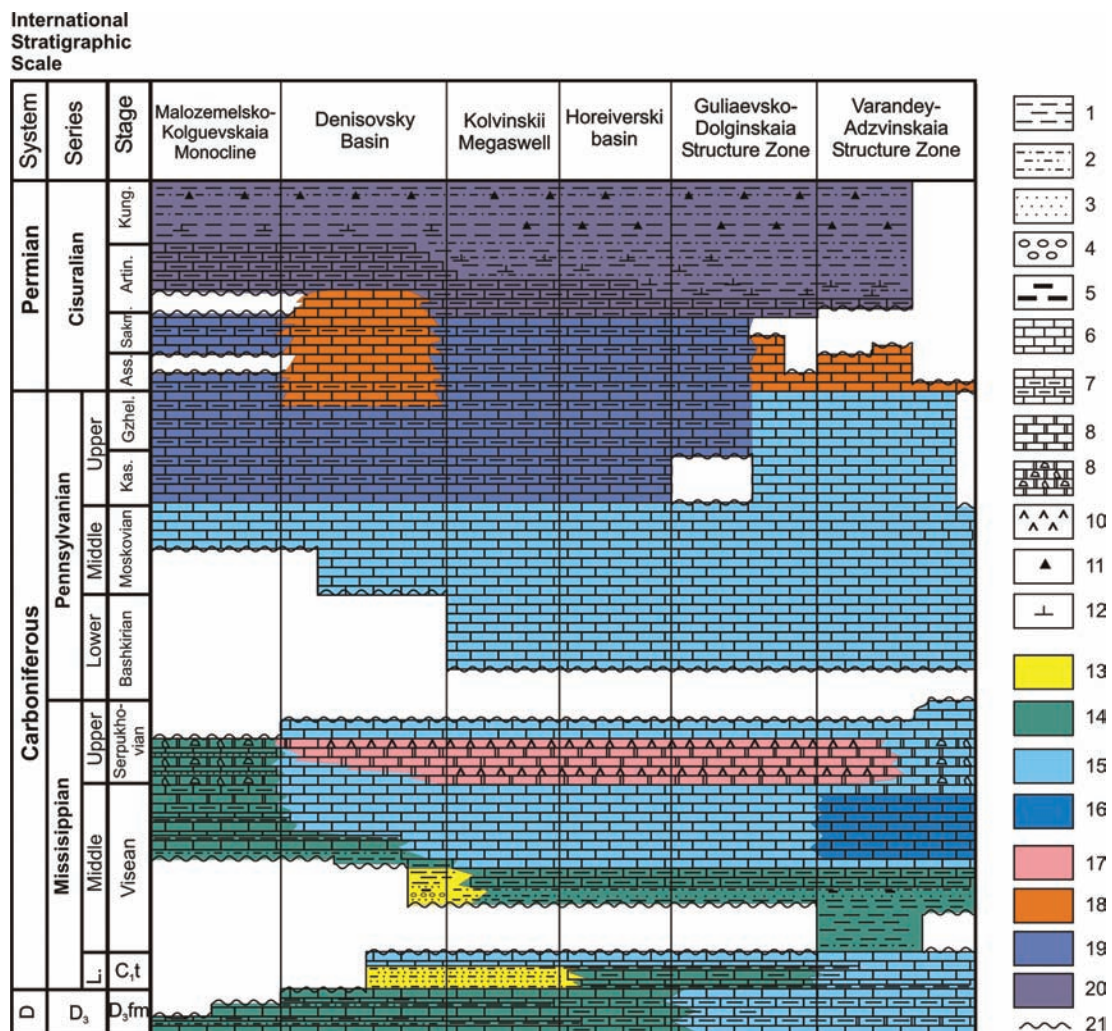


Fig. 8. Lithostratigraphic section of Upper Visean – Lower Permian strata. Lithology: 1 – claystones, 2 – siltstones, 3 – sandstones, 4 – pebbles, 5 – coal lenses, 6 – limestones, 7 – clayey limestones, 8 – dolomites, 9 – carbonate breccia, 10 – anhydrite, 11 – cherts, 12 – calcareous. Environments: 13 – continental, 14 – coastal, 15 – shallow shelf, 16 – depression on the shallow shelf, 17 – lagoon, 18 – buildups, 19 – deep shelf, 20 – shelf slope. 21 – unconformity.

occur in correlative Middle to Upper Carboniferous rocks in the north-west continuation of the Dolginsky swell.

Regional data show that the Lower Permian organogenic carbonate mound structures appear to be prospective targets for oil and gas exploration. Porosities of up to 20% are reported from similar sedimentary facies in the already discovered Prirazlomnoe, Dolginskoe, and Varandey-More oil fields. Similar prospective oil exploration targets are expected in the Kolvinsky megaswell and along the margins of the Horeiversky Basin, provided the lithologic composition, and hydrocarbon charges are similar.

CONCLUSION

Figure 8 summarizes the lithostratigraphic analysis of the evolution of Late Visean-Early Permian carbonate rocks across the northern Pechora Basin. There are two main sedimentation phases: Late Visean-Serpukhovian and Bashkirian-Sakmarian. The hiatus between these phases is confined to Early Bashkirian time in the east and Upper Serpukhovian through Middle Moskovian in the west. Carbonate facies are varied both in lateral and vertical directions. In Late Visean-Serpukhovian time coastal, shallow sea and lagoon environments predominated. The basin deepens during Bashkirian-Sakmarian time resulting in the deposition of relatively deep-water shelf sediments.

Both sedimentation phases are characterized by reef building. The distribution of reefs is related to the shelf edge boundary between shallow and deep-water environments. In particular, Visean-Serpukhovian reefs can be traced on the western slope of the Urals, south-west of Pai-Khoi (Antoshkina, 1994), and along the western coast of Novaya Zemlya (Matveev, 2008; Novaya Zemlya, 2004). Lower Permian reefs are found at the south-west border of the Denisovskii Basin (at Kolguev Island) and in the eastern part of the offshore Pechora Basin. During Late Visean-Early Permian time, the distribution of reefs gradually shifted in direction from northeast to northwest and west.

ACKNOWLEDGMENTS

Lithological and paleogeographic study of Palaeozoic strata was provided by E.G. Bro, E.N.

Preobragenskaia, V.M. Komarnicki, V.I. Ustrickii, L.G. Povysheva, E.S. Mirolubova, M.S.Zonn and others. We appreciate the thoughtful and thorough review of our paper by A. Banet, R. Blodgett and J. Clough.

REFERENCES

- Antoshkina A.I. Palaeozoic reefs at Pechora Urals // S-Pb., Nauka, 1994. 154 p.
- Bro E.G. Oil&gas bearing complexes in Palaeozoic and Mezozoic strata at the Barents offshore // Oil&gas bearing of Barents-Kara offshore. – SPb.: VNIIOkeangeologia, 1993. P.17-37.
- Eliseev A.I. Zone formations of the north-east bordering European platform (Late Devonian and Carboniferous). L.: Nauka, 1978. 192 p.
- Matveev V.P. Carbonate frame buildings in carboniferous strata at Severnyi island, Novaya Zemlya archipelago // Sedimentogenesis and lithogenesis types and their evolution in Earth history. Materials 5-th All-Russia lithological meeting. 2008. P.57-60.
- Novaya Zemlya and Vaigach Island. Geological structure and minerageny // S-Pb., VNIIOkeangeologia, 2004. 174 p.
- Preobragenskaia E.N., Ustricki V.I., and Bro E.G. Paleozoic strata of Kolguev island (the Barents Sea) // Stratigraphy. Geological correlation. 1995, № 5. Vol.3. P. 75-85.
- Sobolev N.N., Ustrickii V.I., and Cherniak G.E. Structure of Palaeozoic passive margin on the Novaya Zemlya // Geological structure of Barents-Kara offshore – L.: Sevmorgeologia, 1985. P. 34-43.
- Suvorova E.B., Viskunova K.G., and Preobragenskaia E.N. Geological structure and petroleum potential of Visean-Serpukhovian strata at the Pechora sea // Geology, geophysics and exploration of oil and gas fields, 2010. N 6. P. 7-14.
- Suvorova E.B. Litofacial characteristic of organogenic buildups and carbonate breccia of Medynskoe-more field // Reefs and carbonate psefitolits: Proceedings of All-Russia lithological meeting. Syktyvkar: Geoprint, 2010. P.171-173.
- Viskunova K.G., Suprunenko O.I., and

Preobragenskaia E.N. Lithological and facial prediction of asselian-sakmarian strata of the Pechora Sea, in petroleum case // Geological and geophysical characteristic Arctic region lithosphere. S-Pb., VNIIOkeangeologia, 2002. Vol.4. P. 147-156.

Tectonics of the sedimentary basins in the Russian sector of the Chuckchi Sea

Malyshev N.A., Obmetko V.V., Borodulin A.A., Barinova E.M., and Ikhsanov B.I.

Rosneft Oil Company, Moscow, Russia

ABSTRACT

The integrated analysis of geological and geophysical, primarily seismic data, resulted in new interpretations of the stratigraphy of the Chukchi Sea shelf in its southern and northern parts (Russian sector) and tectonics of the South and the North Chukchi basins. It is demonstrated that the sedimentary cover in the northern part of the Russian Chukchi Sea sector shares similarities with the U.S. sector but important differences are also identified. In the Russian sector, the westward extension of the Colville foredeep is reduced in thickness due to subdued scale of subsidence and deeper erosion. The sub-latitudinal marginal uplift near the hinge line along the south margin of the North Chukchi trough (analog to the Barrow Arch) is less significant. In the South Chukchi basin rift-fault structures are prominent in the earliest strata that floor the basin. Transtension structures (extension accompanied by strike-slip displacements) are widely developed. Transtensional displacements occurred in the Oligocene-Early Miocene time and are well correlated with similar features in other Eastern Arctic sedimentary basins.

INTRODUCTION

After recent (1990-2009) seismic data acquisitions, exploration interest has sharply increased in the sedimentary basins in Russian offshore sector of the Eastern Arctic, including South and North Chukchi basins. This region, in our opinion, has a number of challenges and principal problems to be addressed. Some of them are listed below:

- Absence of wells in the north and south parts of the Russian sector in the Chukchi Sea that causes an ambiguous interpretation of the sedimentary cover in the North and South Chukchi basins.
- Seismic sequence comparison with the Alaska part of the Chukchi Sea and tracking of seismic

reflector horizons are challenging, since the Hanna Trough, expressed in the sedimentary cover in the U.S. sector and described by drilling data, is separated from the North Chukchi Basin in the Russian sector by a big horst-and-graben zone with a reduced stratigraphic interval.

- The South Chukchi and North Chukchi sedimentary basins are separated by the Wrangel-Herald fold-thrust zone, which frustrates correlations of seismic reflections along submeridional lines crossing the two basins.
- Insufficient characterization of similarities and differences in the basin structure in front of the Brooks-Herald-Wrangel fold-thrust belt in Russian and American offshore sectors.
- Insufficient studies of hydrocarbon systems, regarding distribution and characterization of oil source rocks, main reservoir rocks and seals.

METHODS

The Rosneft Arctic Research team has conducted seismic mapping in the Russian sector of the Chukchi Sea in support of a hydrocarbon potential assessment. The assessment incorporates evaluations of the presence and distribution of oil source and reservoir rocks, and the impact of tectonic events and major unconformities to hydrocarbon reservoir integrity. The study results are based on traditional basin analysis using only the latest data set, which includes:

- Seismic data, acquired by Dalmorneftegeofizika (DMNG), TGS Nopec and WesternGeco in 1990-2006 in the amount of 13,400 linear km;
- Drilling data both onshore and offshore Alaska (VSP, well logs, stratigraphic tops, etc.);
- Geological information on adjacent land and islands, including the Alaska State Geological Survey reports for 2008-2009.
- Reports of DMNG, VNIIOkeangeologia and other organizations and institutes;

- Numerous publications on the U.S. and Russian sectors of the Chukchi Sea and adjacent land (i.e. Filatova and Khain, 2007; Kim et al., 2009; Kosko and Ushakov, 2003; Malyshev, et al., 2010; Orudzheva, et al., 1999; Vierzhbitsky, et al., 2009; Brown, 2009; Sherwood, et al., 1998; and Tolson, 1987).

RESULTS OF SEISMIC INTERPRETATIONS

Our stratigraphic organization of the reflecting horizons in the Russian waters was based on character matches to reflecting horizons in seismic time sections in the U.S. sector of the Chukchi Sea. The U.S. sector seismic interpretations are controlled by well and outcrop data and document major unconformities as shown in Figure 1. As a reference horizon for the seismic-stratigraphic correlation, we selected the reflecting horizon at the Cenozoic base (mBU) controlling the top of the complex, which is clearly expressed and well-defined from the seismic signature. In the Paleozoic-Early Cenozoic section of various parts in the Novosibirsk-Chukchi-

Brooks fold zone and on the Chukchi Sea shelf, five regional unconformities are clearly identified: Late Devonian?-Early Carboniferous (Ellesmerian, EU), pre-Late Permian (PU), pre-Late Jurassic (JU), pre-Aptian (BU) and Early Paleocene (mBU).

NORTH CHUKCHI BASIN

Based on seismic ties to the Crackerjack and Klondike wells in the U.S. Chukchi Sea, five tectonostratigraphic complexes were identified and mapped in the Russian sector of the North Chukchi basin: 1) Upper Devonian-Lower Carboniferous syn-rift; 2) Middle Carboniferous-Middle Jurassic post-rift; 3) Upper Jurassic-Neocomian syn-rift; 4) Aptian-Upper Cretaceous post-rift (syn-collision); and 5) Cenozoic complex of passive continental margins. As used here, the term “North Chukchi basin” refers to a composite basin that includes the “Wrangel-Herald ledge” on the south and the “North Chukchi trough” on the north.

The sedimentary cover in the northern part of the Russian sector shares some similarities with the

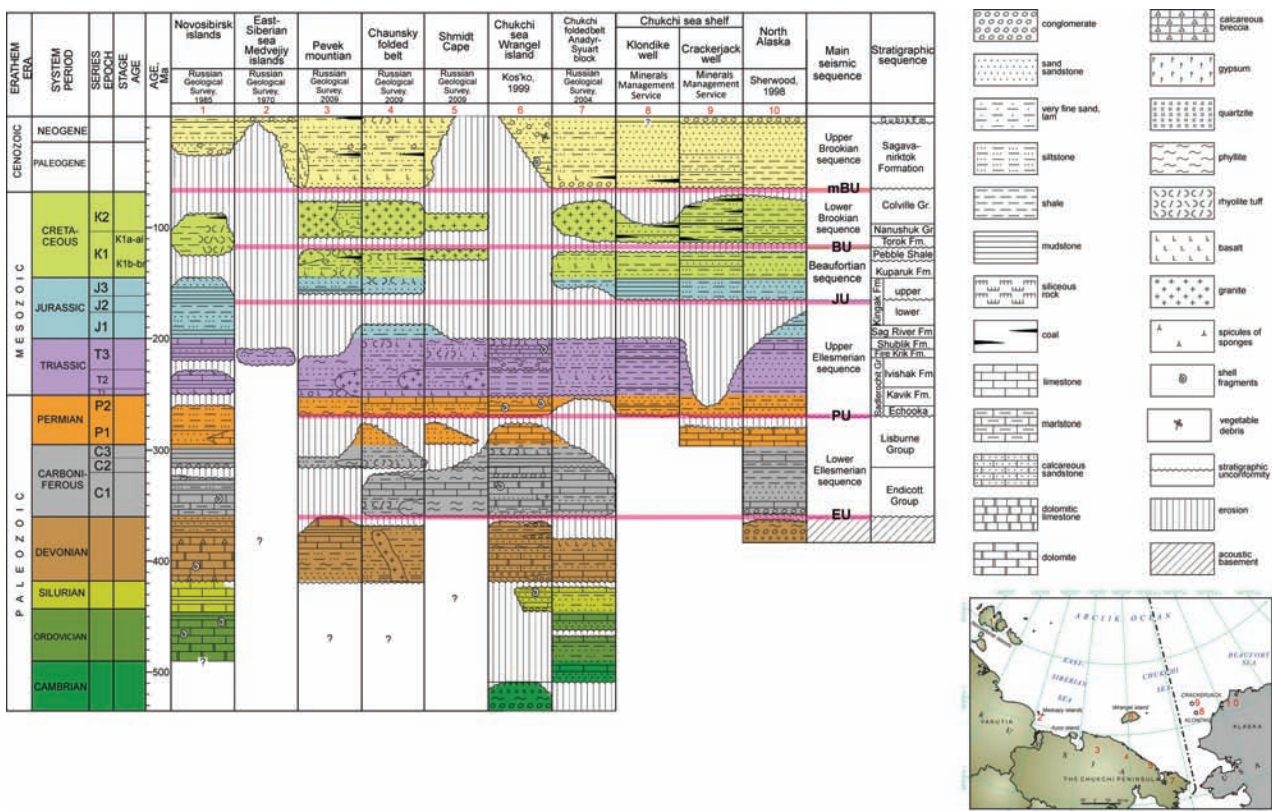


Fig. 1. Correlation through the Novosibirsk and Wrangel-Chukchi-Brooks fold zones, the Russian and U.S. sectors of the Chukchi Sea shelf, and the western North Slope of Alaska.

U.S. Chukchi Sea sector but also differs in some important aspects.

As shown in Figures 2 and 3, the North Chukchi basin is located north of the Wrangel-Herald fold-thrust zone. Its northern boundary is associated with the Andrianov uplift. The Wrangel-Herald Ledge underlies the southern part of the North Chukchi basin between the Wrangel-Herald fold-thrust zone and the North Chukchi trough. The Hinge zone separates the Wrangel-Herald ledge from the North Chukchi trough.

In the southeastern and southwestern parts of the North Chukchi basin along the Wrangel-Herald fold-thrust zone, the Russian-sector extension of the Colville foredeep of Alaska is fragmented into isolated outliers that preserve relatively thin foredeep fill sequences. The Colville foredeep outliers are isolated by large uplifts along the Wrangel-Herald ledge in the Russian sector as mapped in Figure 2. These uplifts were elevated during foredeep subsidence and blocked the establishment of a continuous basin linked to the Colville foredeep. The

Wrangel-Herald ledge was also broadly elevated in Early Paleocene time, which resulted in the foredeep sediments exposure to the surface with their full denudation in the central part.

Formed contemporary to foredeep subsidence, the sub-latitudinal marginal uplift, similar to the Barrow Arch (Alaska) in the Russian sector of the Chukchi shelf, is observed only north of the foredeep outliers. Elsewhere, the sub-latitudinal marginal uplift merges with the hinge zone along the south margin of the North Chukchi trough and does not form a distinct mappable feature.

At the base of the Ellesmerian complex of the North Chukchi basin, a rift-like trough is identified between the paleo-uplifts just north of the Wrangel-Herald-Brooks fold zone (located in Figure 2). The rift-like trough is characterized by submeridional extension and is interpreted as filled by the Early Carboniferous formations, similar to the Endicott Group. The trough has a structure similar to the Hanna Trough and the sedimentary cover of the U.S. western sector of the Chukchi Sea (Fig. 2).

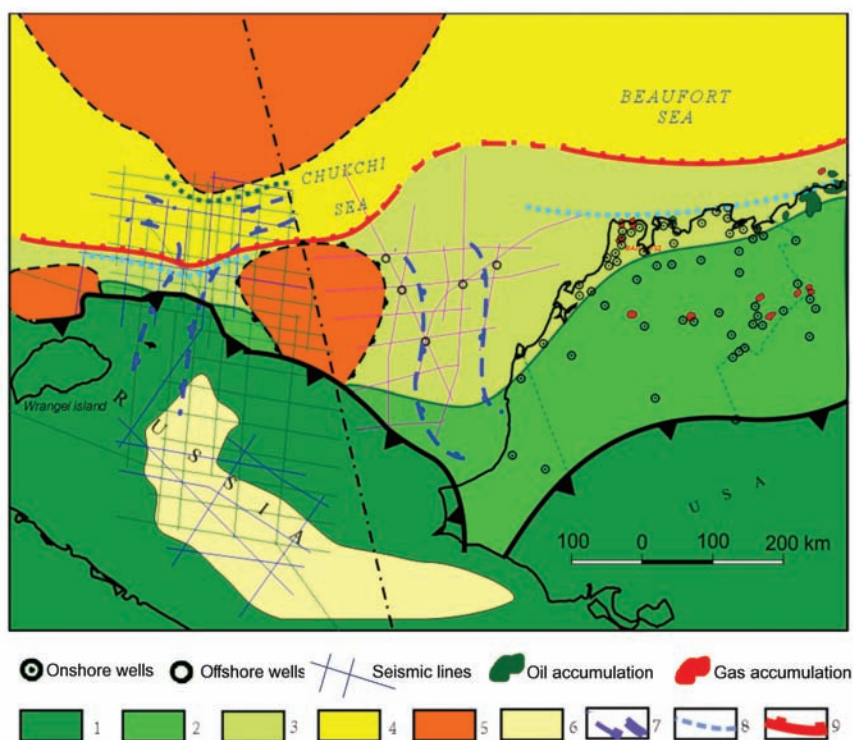


Fig. 2. Tectonic scheme of Russian and U.S. sectors of the Chukchi Sea: 1 - Wrangel-Herald Brooks fold zone, 2 - foredeep, 3 - platform, 4 - Jurassic-Cenozoic troughs, 5 - paleo-uplifts (a - Mamontov uplift, b - North Chukchi graben-and-horst zone, c - Andrianov uplift), 6 - South Chukchi-Hope basin, 7 - Early Ellesmerian rift-like troughs, 8 - Barrow Arch (Alaska), Andrianov uplift (Russia) and similar marginal uplifts, 9 - Hinge zone, 10 - wells, 11 - oil and gas fields.

SOUTH CHUKCHI BASIN

The South Chukchi sedimentary basin is located south of the north-vergent Wrangel-Herald fold-thrust zone. The South Chukchi basin is the northwest extension of the Kotzebue and Hope basins of the U.S. sector of the Chukchi Sea. Its geological history has three main phases. At the initial phase (Albian-Late Cretaceous), subsidence was driven by rift faulting, possibly during a collapse of the Wrangel-Herald-Brooks fold zone. In the Late Oligocene-Early Miocene phase, extension continued with a significant strike-slip component. Similar transtension processes took place at that time over the whole Eastern Arctic, which is expressed in widespread development of extensional incipient strike-slip structures on the shelves of the Laptev, East Siberian, and Chukchi Seas and on adjacent lands. Obviously, these events were associated with the Eurasian Basin opening and, apparently, with the plate-tectonic rearrangements during general geodynamic evolution in the Arctic region. At the final or third phase during Pliocene-Quaternary time, the South Chukchi basin experienced a regional subsidence not accompanied by faulting.

The above-described events are reflected in the sedimentary cover as major stratigraphic unconformities that can be observed on regional seismic lines. These unconformities divide the sedimentary section into three structural complexes:

- Lower - syn-rift complex (Albian-Late Cretaceous), developed in grabens and semi-grabens and absent on the separating uplifts,
- Middle - post-rift complex (Late Oligocene-Early Miocene) with development of northwest-trending transtensional structures, and
- Upper - synclise complex (Pliocene-Quaternary) of sub-horizontal strata draped upon the lower complexes and basement rocks.

In the central part of the South Chukchi basin along the main fault zone that divides the basin into two large troughs - Schmidt on the southeast and Sredinny on the northwest, there is the Ushakov anticline zone with pop-up structures. Moving away from this fault zone, the amplitudes and sizes of positive structures diminish. Fault tectonics become less prominent towards the Hope and Kotzebue troughs (Malyshev, et al., 2010). Strike-slip

displacements occurred along reactivated faults in the lower structural complex and the basement, but in some cases the strike-slip faults are newly formed, characterized by different orientation and cross the older faults.

SOURCE ROCK DATA FOR THE RUSSIAN SECTOR OF THE CHUKCHI SHELF

As regards to hydrocarbon potential, the North Chukchi basin has the highest oil prospective, established from similarity with the Arctic Alaska basin of the Alaska North Slope, where currently more than two dozen oil and gas fields were discovered, including the unique Prudhoe Bay field with 3 to 5 billion tons of oil reserves (Orudzheva, et al., 1999).

The source rock prediction was based on public data on geochemical studies over Wrangel Island, the Chukotka Peninsula, the U.S. sector of the Chukchi Shelf, and Alaska North Slope. Oil source rocks were identified in the entire sedimentary interval from Carboniferous to Paleocene. The Lower Carboniferous section (Kekiktuk formation) contains mudstone layers of 0.5-1% TOC. Kerogen is of mixed humus-sapropel and humus types. In Alaska, the Upper Carboniferous-Lower Permian Lisburne Group contains mudstones and clayey limestones of 0.5-1% TOC and kerogen of type II. On Wrangel Island, the Upper Permian interval includes numerous layers of black shales and marls (Kosko and Ushakov, 2003). Geochemical studies of these rocks were not conducted; however, accounting for the preferential basin facies development, we can predict high TOC content of sapropelic type. The Ivishak mudstones are fairly rich in sapropelic and humic-sapropelic organic matter (TOC varies from 0.5 to 3%).

The Shublik clayey limestones and mudstones are the main oil source rocks in the region. TOC in these rocks reaches 8% with kerogen of mainly sapropelic type. The Lower Cretaceous Pebble Shale mudstones also have good oil potential. TOC in them varies from 1.6% to 5.5%, and the kerogen type is II-III. In the Middle-Upper Jurassic Kingak mudstones, TOC varies from 0.5% to 6.47%, with the kerogen type of II-III. The youngest oil source rocks recognized in the region are the Lower Cretaceous Torok mudstones (Aptian-Albian). TOC in these

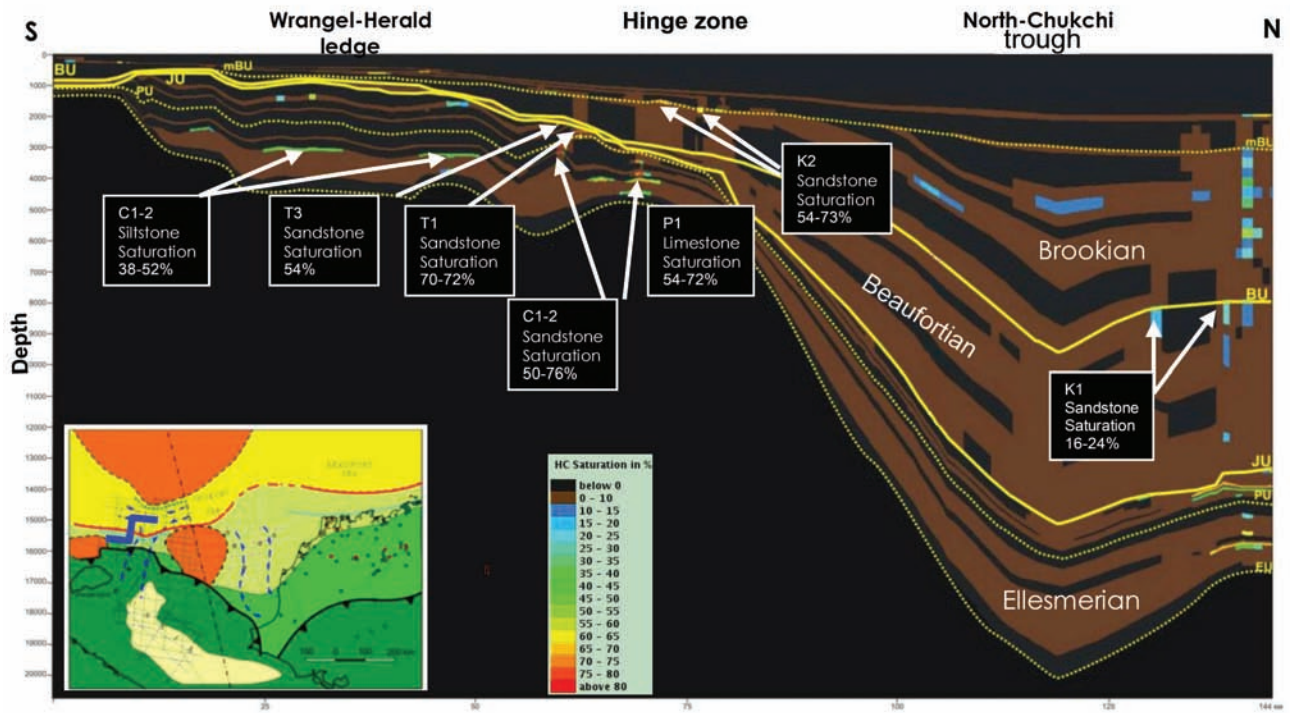


Fig. 3. Present-day hydrocarbon saturation across the North Chukchi basin (south to north cross-section – TemisSuite basin modeling)

rocks is 0.6-2.2% with kerogen of the mixed humus-sapropel type. The overlying Paleogene section includes primarily gas prone rocks. TOC there is up to 5-6% (in some samples - up to 12.3%) mainly due to the humus component.

The distribution of oil source rocks, reservoirs and seals through the section in the offshore region is predicted from the depositional reconstruction and seismic facies analysis. The analysis of the outcrops on the Wrangel Island and Chukchi Sea coast indicated the general facies zoning for the most of the sedimentary section. The main source rock – the Shublik Formation - is predicted over the majority of the North Chukchi basin, except for its depocenter and a part of the southern flank, where Shublik was eroded in Jurassic time. Seismic mapping in the U.S. sector shows that the Shublik Formation in Hanna trough is truncated by unconformities west of 166° west longitude due to erosion over the western Chukchi platform and related isolation from Hanna trough (Sherwood, et al., 1998). However, we believe that the Shublik Formation is preserved in isolated correlative basins in the Russian sector of the Chukchi shelf west of the Chukchi platform uplift where the Shublik Formation is lost to erosion.

MODELING OF PETROLEUM GENERATION, MIGRATION, AND ENTRAPMENT

Our mapping of the present-day geological structure and history of sedimentary basins in the Russian sector of the Chukchi Sea form the basis of two-dimensional hydrocarbon system modeling using the software package TemisSuite. In the absence of actual geochemical data for the Russian offshore sector, we conducted multivariate modeling using reasonable ranges of geochemical parameters (sources rock presence, distribution, thickness, kerogen type, and total organic carbon) consistent with U.S. sector data for correlative source rocks. The heat flow was assigned as the average from existing measurements (50-60 mW/m²). The heat flow was calibrated with the Klondike well data in the U.S. sector of the Chukchi Sea.

The results of 2D-modeling showed that within the Wrangel-Herald Ledge the oil source rocks within the sequence of Upper Paleozoic and older rocks were completely expended for oil prior to Late Jurassic time. The Mesozoic source rocks experienced thermal exposures sufficient for oil generation in Cenozoic time and remain in the oil window at present. Cretaceous-Paleogene source

rocks remain thermally immature.

In the sedimentary section of the North Chukchi basin in the Wrangel-Herald Ledge, the highest oil potential is associated with the Permian, Triassic and Jurassic and Lower Cretaceous intervals (Fig. 3).

Gas accumulations are forecast for the Cretaceous-Paleogene section in the depocenters and on the flanks of the North Chukchi trough. The main risks here are related to the Permian-Triassic clastic reservoirs presence (erosional events could have removed the reservoirs at some of the prospects) and trap integrity in the periods of the Cretaceous and Early Paleozoic erosion events.

In geological hydrocarbon prospects, the North Chukchi basin includes the Andrianov gas prospective zone and Academic oil prospective zone, divided into the Lineiny, Mamontov and West Mamontov prospective regions. The highest oil and gas potential in this case is related to the Academic hydrocarbon-prospective region with eight identified prospects.

CONCLUSIONS: UNDISCOVERED PETRO-LEUM POTENTIAL

A total of about 20 prospects are mapped in the northern shelf of the Chukchi Sea. The estimated hydrocarbon resources are slightly higher than the volumes of the RF Ministry of Natural Resources (2.2 bln ton OE). Despite the estimated higher hydrocarbon potential of the basin, the region is characterized by a very high risk of hydrocarbon accumulation destruction from numerous faults and erosion events. In this regard, further study of the North Chukchi basin is required to assess the erosion magnitude. We recommend the drilling of wells along the Wrangel-Herald fold zone, where the Pre-Upper Cretaceous formations are shallow.

The South Chukchi sedimentary basin seems to be less prospective than the North Chukchi. It includes the Nadezhdin, Onman and Ushakov hydrocarbon-prospective regions (Fig. 5) and is predicted as mainly gas-bearing in the Upper Cretaceous-Paleogene section on structures adjoined

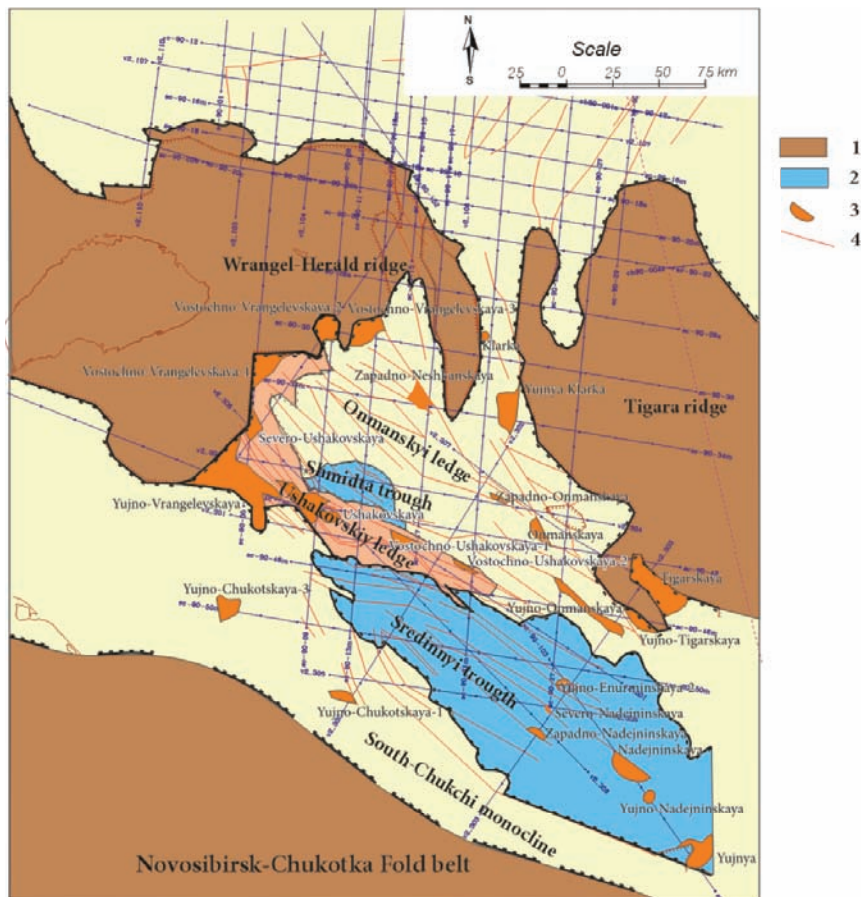


Fig. 4. Tectonic scheme of the South Chukchi basin: 1 – Basement high; 2 – Depressions; 3 - Local structures; 4 – faults.

to subsidence depocenters – particularly the Schmidt and Sredinny troughs. The key risks here are related to the potential for trap destruction in the period of the Pre-Middle Miocene erosion.

REFERENCES

- Brown, David, 2009. Arctic Holds Huge Resource Promise, American Association of Petroleum Geologists AAPG Explorer V. 30, No.7. pp. 6-9.
- Filatova, N.I and Khain, V.E., 2007, Eastern Arctic Tectonics, in Geotectonics,. No. 3, pp. 3-29 (in Russian).
- Kim, B.I., Evdokimova, N.K., Kharitonova, L.Ya., 2009, Geology and petroleum potential of the East Arctic shelf of Russia, in Geology of Polar Regions. Materials of the XLII Tectonic Meeting. V.1. Moscow. GEOS, pp. 266-271 (in Russian).
- Kosko, M.K. and Ushakov, V.I, 2003. Wrangel Island: Geology, Minerageny, Geoecology, VNIIOkeangeologia, St. Petersburg, pp. 137 (in Russian).
- Malyshev, N.A., Nikishin, A.M., Drachev S.S., 2010, The tectonic history of sedimentary basins in the Russian Arctic shelf and adjacent land, in Tectonics and geodynamics of fold belts and Phanerozoic platforms. V.2. Moscow. GEOS, pp. 19-23 (in Russian).
- Orudzheva, D.S., Obukhov A.N., Agapitov D.D., 1999, Prospects for oil and gas exploration in the Chukchi Sea, in Petroleum Geology. No 3, pp. 28-33 (in Russian).
- Sherwood, K.W., Craig, J.D., Lothamer, R.T., Johnson, P.P., and Zerwick, S., 1998, 13. Chukchi Shelf assessment province: in: Undiscovered Oil and Gas Resources, Alaska Federal Off-shore (As of January 1995): Sherwood, K.W., (ed.), U.S. Minerals Management Service, OCS Monograph MMS 98-0054, p. 115-196. A map that shows the extent of the preserved Shublik Formation west of Hanna trough is shown in figure 13.22 on file page 187 in the downloaded document. Available online at Bureau of Ocean Energy Management web-site at http://www.boem.gov/uploadedFiles/BOEM/Oil_and_Gas_Energy_Program/Resource_Evaluation/Resource_Assessment/1995AlaskaResourcesMMS98_0054.pdf.
- Tolson R.B., 1987, Structure and stratigraphy of the Hope Basin, southern Chukchi Seas, Alaska // Geology and resource potential of the continental margin of western North America and adjacent ocean basins: Beaufort Sea to Baja California / D.W. Scholl, A. Grantz, J.G. Vedder (Eds.). Houston, Texas, Circum-Pacific Council for Energy and Mineral Resources, Earth Science Series. V. 6. pp. 59-71.
- Vierzhbitsky, V.E., Sokolov, S.D., Tuchkova, M.I., 2009, Tectonics, structural evolution stages and hydrocarbon potential of the Chukchi Sea shelf (Russian Arctic), in Geology of Polar Regions. Materials of the XLII Tectonic Meeting. V.1. Moscow. GEOS, pp. 85-89 (in Russian).

Zircon geochronology of bottom rocks in the central Arctic Ocean: analytical results and some geological implications

Garrik Grikurov¹, Oleg Petrov², Sergey Shokalsky², Pavel Rekant¹, Alexey Krylov^{1,4}, Anatoly Laiba³, Boris Belyatsky^{1,2}, Mikhail Rozinov² and Sergey Sergeev^{2,4}

¹I.S. Gramberg Research Institute for Geology and Mineral Resources of the World Ocean ‘VNIIOkeangeologia’, 1 Angliysky Ave., 190121 St. Petersburg, Russia

²A.P. Karpinsky Russian Research Geological Institute ‘VSEGEI’, 74 Sredny Prospect, 199106 St. Petersburg, Russia

³Polar Marine Geosurvey Expedition, 24 Pobedy St., 188512 Lomonosov – St. Petersburg, Russia

⁴St. Petersburg State University, 7/9 Universitetskaya Emb., 199034 St. Petersburg, Russia

ABSTRACT

In the past few years sampling of deepwater seabed gained an increasingly important role in studying geological structure of the Arctic Ocean. A common concept of virtually uninterrupted pelagic drape in the Amerasia Basin and exclusively ice-rafted nature of all clastic components that occur in bottom sediments was challenged by recent discoveries of bedrock exposures in the sea floor, while correlation of results of analytical study of bottom samples collected by the Russian expeditions in 2000, 2005 and 2007 with bathymetric environments at respective sites suggested that certain dredged and cored coarse rock fragments appeared meaningful for bedrock characterization if even the source sub-pelagic outcrop was not positively documented. The first results of age determinations of detrital zircons that were extracted from coarse fragments of lithic sedimentary rocks resting on the seabed and in the immediate sub-bottom, as well as of zircons from fragments of magmatic/metamorphic rocks and of zircon grains separated directly from sub-pelagic unlithified sediments are in agreement with published interpretations of the Lomonosov Ridge bedrock as composed of Mesozoic terrigenous sequences; the presence of an older Neoproterozoic(?) – Early-Middle Paleozoic basement is also possible. The Mendeleev Rise bedrock, too, is believed to mainly consist of Paleozoic-Early(?) Mesozoic sedimentary superstructure that may locally rest on the Earliest Paleozoic or even older units. Basaltic rocks likely to originate from the High Arctic Large Igneous Province (HALIP) has not so far been found among the collected fragments but limited loose zircon grains probably derived from broadly contemporaneous magmatic products were recorded

in sub-pelagic sediment along with dropstones of variably metamorphosed Precambrian mafic and granitoid rocks.

INTRODUCTION

Great progress in acquisition of new bathymetric and geophysical data relevant to understanding the geological structure and history of the Arctic Ocean, including the tectonic nature of enigmatic Central-Arctic bathymetric highs, was achieved in recent years by the Arctic countries through their programs for delineation of respective extended continental shelves. However, only limited direct geological information was obtained on the composition of sub-bottom bedrock concealed by almost continuous drape of young sediments. Only at a few sites can the lithic fragments recovered by bottom sampling be interpreted with sufficient confidence as representing *in situ* submarine bedrock, while in most cases they are regarded ice rafted debris (IRD) of questionable derivation.

In search of provenance of lithic and mineral clastic components in bottom sediments we conducted age determinations on zircon crystals of two categories: (1) extracted from the rock fragments and (2) separated directly from hemipelagic sediments. In this paper we present the results of more than 700 zircon U-Pb age measurements completed before 2012. The samples labeled AF00, AF05, AF07 were collected during MS “Akademik Fedorov” cruises Arctic-2000, 2005, 2007, those marked ALR07 were acquired in 2007 on board NIB (nuclear icebreaker) “Rossiya”, and two specimens designated BC were selected for the analysis from clastic material sampled by RV “Polarstern” in the course of ARK-XXIII/3-2008 cruise.

Sampling sites were located on Mendeleev Rise, Lomonosov Ridge, on deep Amundsen Basin seabed at the North Pole, and on the bathyal floor in the southern Podvodnikov Basin (Fig 1). Dredging equipment used during Arctic-2000 expedition was supplemented by box and gravity coring on the Arctic-2005 cruise, whereas RV “Polarstern” and the Arctic-2007 cruises employed different types of coring but did not execute any dredging. Sampling on RV “Polarstern” was controlled by Parasound observations which indicated a continuous presence along the ship track of sub-bottom hemipelagic sediments at least several dozen meters thick (Jokat, 2009). Selection of sampling localities surveyed by Russian vessels was only guided by bathymetric data available at the time of cruises.

Zircon dating was performed by high-resolution SIMS method on SHRIMP-II instrument in the Centre of Isotopic Research at VSEGEI, St. Petersburg, Russia. Zircon grains of different morphologies were measured using regular analytical procedure similar to that described by Williams (1998, and references therein) and reference zircons Temora2 (for U/Pb

ratios) and 91500 (for U content). Each analytical spot had size ca 2x20x25 µm.

DESCRIPTION OF ANALYZED MATERIAL

Zircons in fragments of magmatic and/or metamorphic rocks (Fig. 2)

Almost 200 age determinations, including:

- **Station/sample AF07-01 (North Pole):** five semi-angular to semi-rounded gravel-pebble size fragments (0.5-0.6 – 1.5-2.0 cm) of granitic rocks with indistinct gneissic banding recovered from box cored pelagic mud. Zircons were analyzed by SIMS SHRIMP directly in thin sections (21 measurements).
- **Station ALR07-16:** steep western slope of the Geophysicists Spur. Box cored sediments with abundant small rock fragments of variable composition with unusually high proportions of metamorphic and igneous lithologies. Zircon grains were separated from three little splinters of fine-grained gneiss-like rocks and enabled 15 age determinations.
- **Station/sample BC-299:** Podvodnikov Basin.

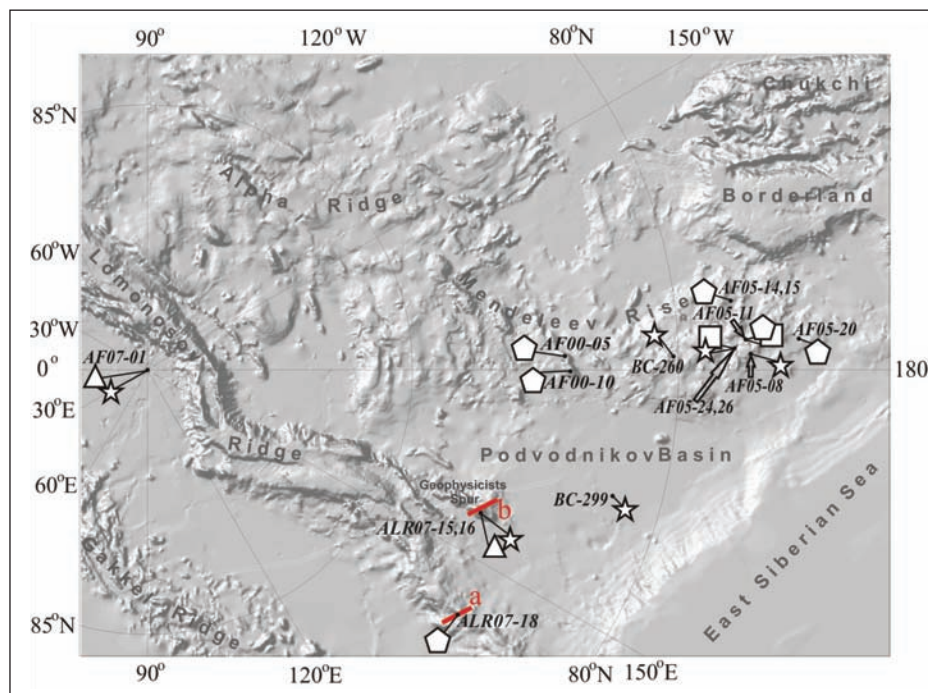


Fig. 1. Location of sampling sites described in this paper. Geological stations designated AF00, AF05 and AF07 were made from MS “Akademik Fedorov” in 2000, 2005 and 2007, respectively, ALR07 from NIB “Rossiya” in 2007, and BC from RV “Polarstern” in 2008. Specimens represented by large fragments and/or pebble-gravel sized debris of zircon-bearing rocks are marked by pentagons (sandstones, siltstones), stars (granitic and gneissic rocks) and squares (metagabbro-dolerites). Triangles indicate samples of hemipelagic sediments. Red lines correspond to the position of small sections of seismic lines shown in Fig. 6.

A single pebble-like fragment of plagiogranite over 2 cm in size from gravity cored sediment (12 U-Pb isotope analyses were made in thin section).

- **Stations/samples AF05-08, AF05-24, AF05-26** (dredges) and **BC-260** (box corer): southern Mendeleev Rise. Scarce fragments of muscovite, biotite and/or two-mica gneissoid granites and plagiogranites, often cataclastically deformed, gravel-pebble sized, semi-angular to semi-rounded at all sites. One specimen (AF05-08) with distinct gneissic banding had noticeably larger size (8-9 cm) and an almost non-abraded shape. Small pieces of regular petrographic thin sections (without cover glasses) containing visible zircon grains were implanted in standard SIMS mounts (over one hundred measurements).
- **Stations/samples AF05-11, AF05-26**: southern Mendeleev Rise, dredges. Three small fragments of metagabbro-dolerites among variable other lithologies (25 zircon age determinations in thin sections).

Detrital zircons extracted from fragments of quartz sandstones (Fig. 3)

Stations/samples AF00-05, 10, AF05-11, 14, 15, 20 – different parts of Mendeleev Rise, station/sample ALR07-18 – Lomonosov Ridge. Numerous sandstone fragments of highly variable size (usually from 1.5-2.0 cm to 10-15 cm, the largest is nearly 40 cm) were recovered by dredges, box and gravity corers and altogether enabled more than 300 zircon age determinations.

Detrital zircons in soft sediments

Station/sample AF07-01 – deepwater seabed at the North Pole, approximately 120 km from the foot of the Lomonosov Ridge. Small portions of soft sediments totaling ~ 300 grams in weight were arbitrary selected from the box cored sample, then mixed and reduced to heavy minerals concentrate which contained about 250 zircon grains. Approximately half of that number appeared unsuitable for age determination (grains too small, or fractured, or filled with inclusions). Unbroken crystals were picked out by hand and analyzed in grain mounts (103 age determinations).

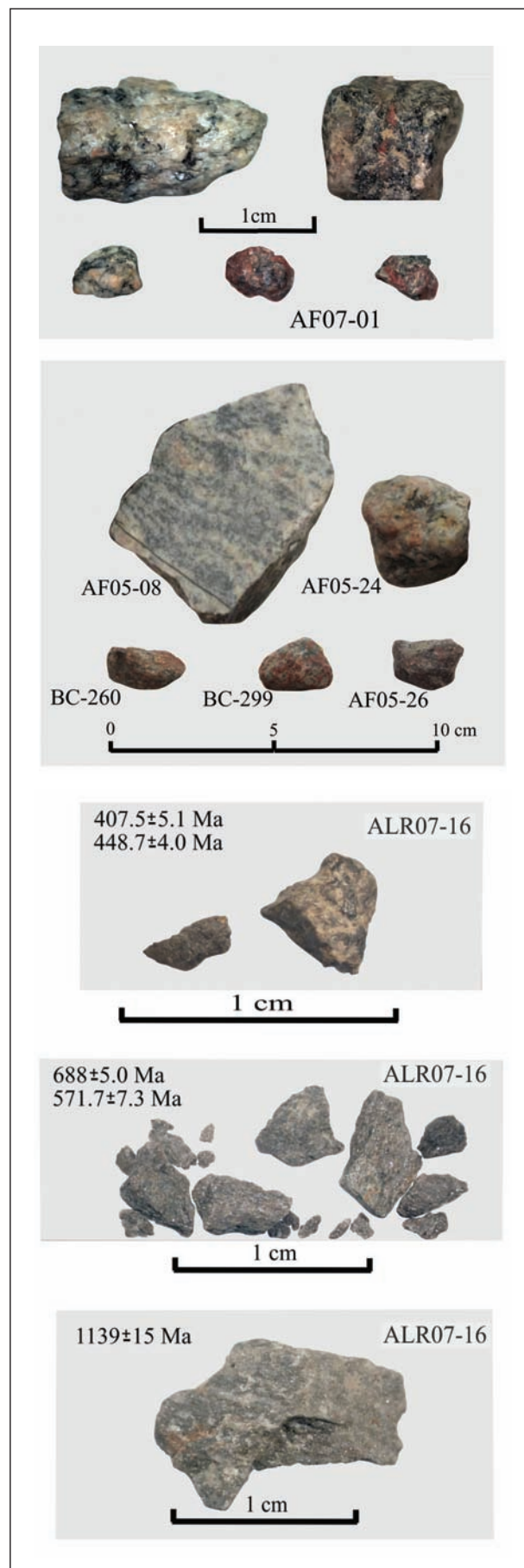


Fig. 2. Morphological appearance of granitoid rock fragments hosting magmatic zircons that were analyzed.



Fig. 3. Examples of the morphological appearance of sedimentary rocks fragments sampled. Arrows indicate the biggest of sandstone fragments dredged at stations AF00-05 & 10 (central Mendeleev Rise) that were selected for age determinations; other debris includes both terrigenous and carbonate rocks some of which are likely to represent IRD. Sandstone specimen ALR07-18 (southern Lomonosov Ridge) was retrieved by gravity core from 55 cm b.s.f.

Station/sample ALR07-15 – steep western slope of the Geophysicists Spur 3 km away from the station ALR07-16. A continuous sub-bottom succession was cored to 9 m below sea floor (b.s.f.) and sampled at ~1 m intervals, each sample up to 500 g in weight providing 200-300 small zircon grains. The first 152 measurements reported in this paper were performed on zircons from 12-14 cm b.s.f., 505-507 cm b.s.f. and 703-705 cm b.s.f. (ca 50 grain analyses for each sample).

SUMMARY OF ANALYTICAL RESULTS

The analytical data are presented in the annex (Tables 1 and 2) and illustrated in Figures 4-5. Only concordant or sub-concordant age data were considered for detrital zircons. A brief description of obtained zircon ages is given below.

Fig. 4 demonstrates the lack of apparent correlation between the ages and morphological characteristics of analyzed zircon grains.

Ages of detrital zircons extracted from fragments of sandstones (Fig. 5A):

A common feature of all analyzed specimens is the prevalence of zircons with ages mainly in ~2000 – 1000 Ma interval (late Paleoproterozoic – Mesoproterozoic). Yet Precambrian zircons in samples AF00-05 and AF00-10 are mostly late Paleoproterozoic (~2000-1700 Ma), whereas the majority of grains in all other sandstones are Mesoproterozoic (~1800-1700 – 1000 Ma). Another peculiarity of AF00-05 & AF00-10 sandstones is the paucity of Archean zircons relative to the amount observed in other studied sandstones and in soft sediments.

One more distinctive feature of the AF00-05 and AF00-10 specimens is the dominating presence of zircons with Paleozoic to early Mesozoic U-Pb ages whose peaks on the histograms closely resemble the major clusters in hemipelagic sediments. In other sandstones zircons with such ages are absent or very poorly defined.

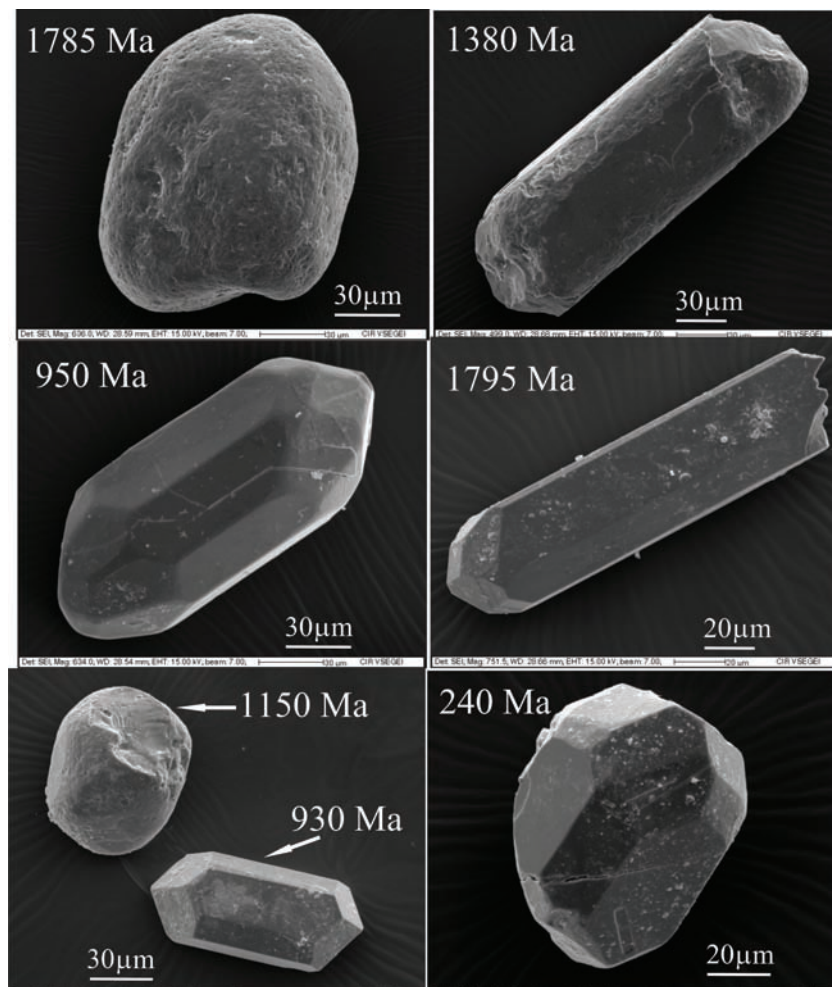


Fig. 4. Selected SE images of zircon crystals from sandstone specimens AF00-05 and AF00-10 showing lack of correspondence between measured U-Pb ages and the degree of grains roundness.

Ages of zircons in fragments of magmatic and metamorphic rocks (Fig. 5B):

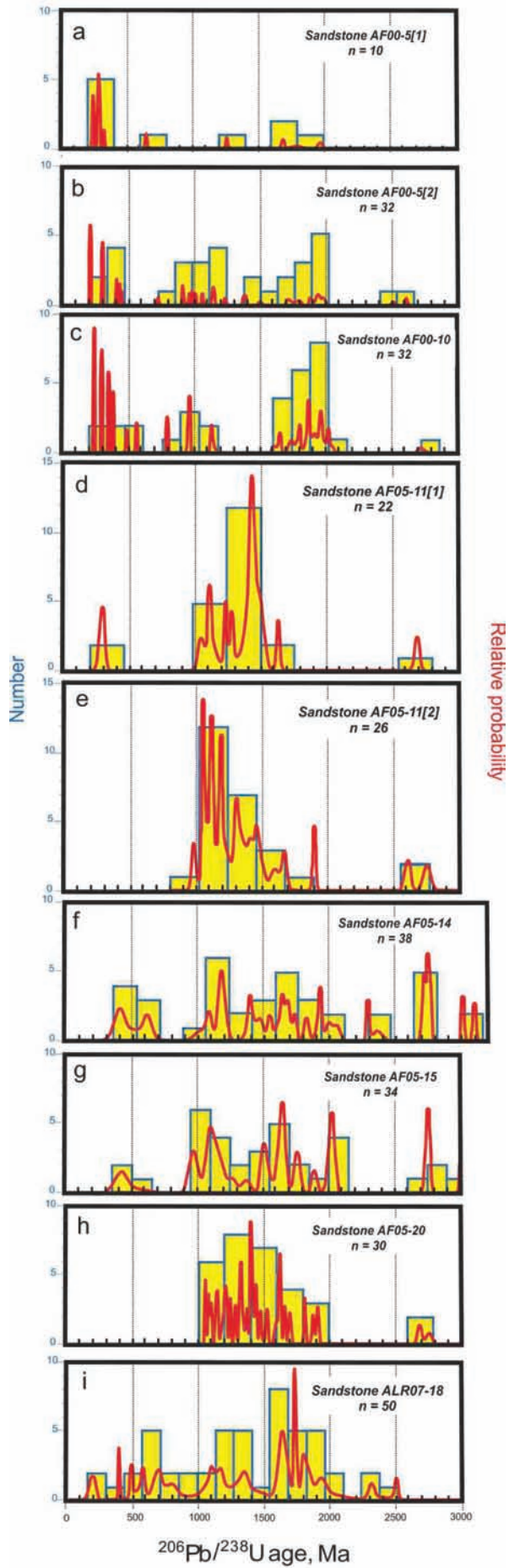
Ages of zircons from granitoid fragments in samples AF07-01, AF05-08, AF05-24, AF05-26 and BC-299 suggest that all listed rocks were mainly crystallized in the Neoproterozoic (2600 – 2700 Ma). AF07-01 specimens additionally point to the possibility that the parental magma for these granitoids was derived from a Mesoarchean (ca. 2900 Ma) crustal source. Indications of Paleoproterozoic overprint are present in all granitoid samples. The largest and least rounded specimen AF05-08 with the most distinct gneissosity was probably also affected by the Latest Neoproterozoic metamorphic event, as suggested by the presence of rare 600-800 Ma zircon grains with secondary rims.

Granitic rock BC-260 contains only late Paleoproterozoic zircons.

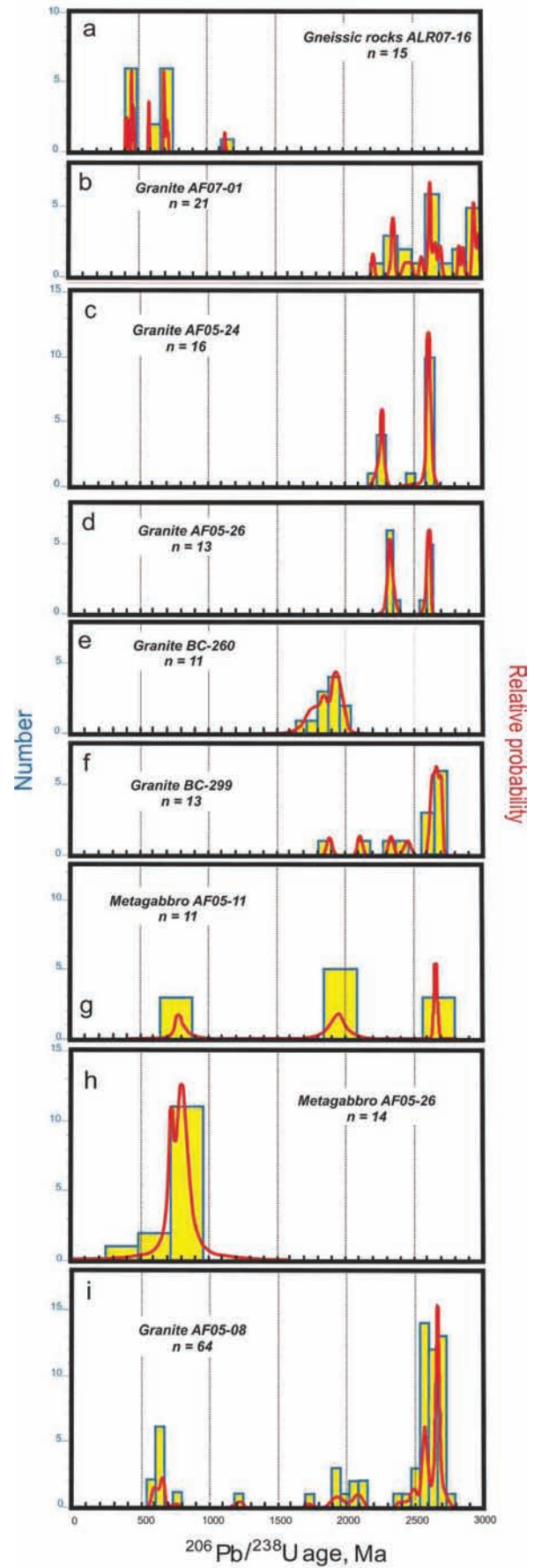
The best estimated value of 790 ± 20 Ma obtained on zircons from metagabbro-dolerite specimens AF05-11 and AF05-26 most likely represents the age of magmatic crystallization. Older values close to 2650 Ma and 1950 Ma are closely comparable to ages determined for the granitic rocks and may reflect the presence of zircons captured by mafic magma from older crustal material.

Zircons from three small fragments of gneiss-like rocks collected on Geophysicists Spur (ALR07-16) displayed ~1140 Ma, ~570-690 Ma ~400-450 Ma ages. The oldest age was obtained (single shot) on a sole grain recovered from one of the fragments; of three grains extracted from the second fragment two showed ~ 690 Ma (six shots), and one ~ 570 Ma (two shots); and two grains from the third splinter exhibited ~ 407 Ma and ~ 448 Ma ages (three measurements on each grain).

A



B



Relative probability

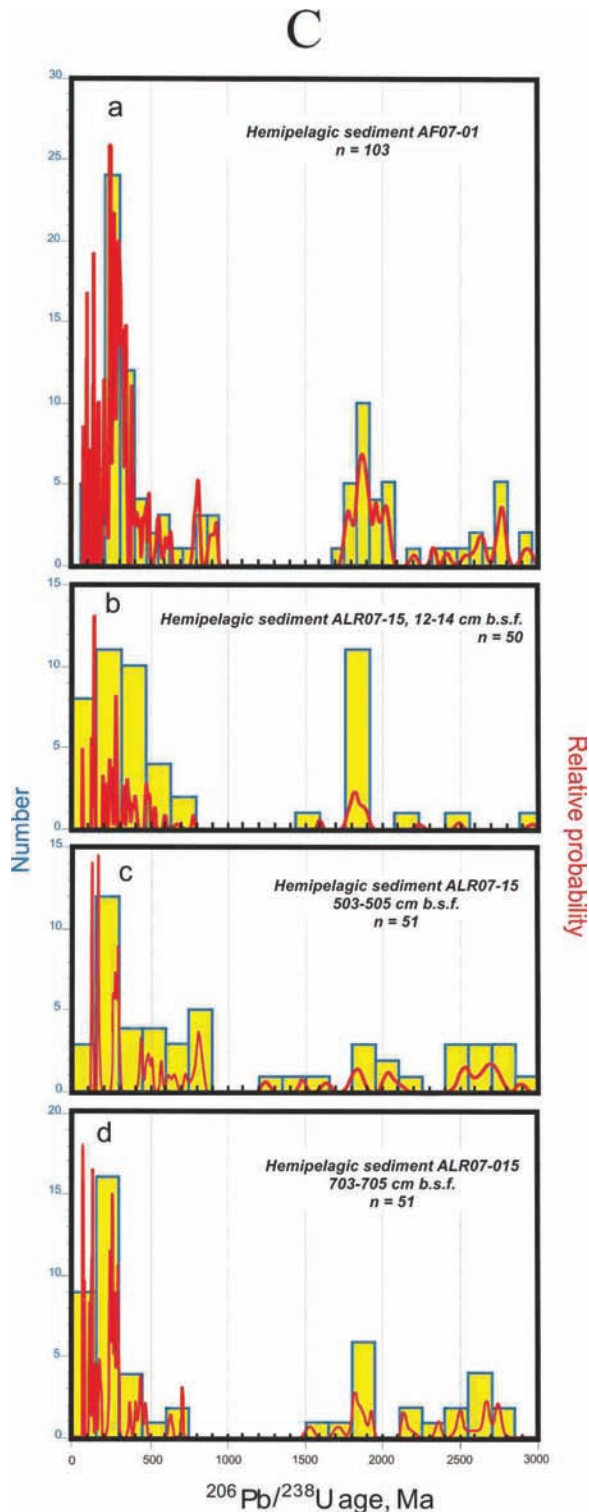


Fig. 5. Distribution of measured zircon ages. A – ages of detrital zircons in sandstone fragments, B – ages of zircons in metamorphosed magmatic rocks, C – ages of detrital zircons in sub-bottom sediments. See text for explanation.

Ages of detrital zircons in Recent sediments (Fig. 5C):

The majority of ages are younger than ~ 500 Ma (Phanerozoic) with lesser peaks in ~ 2000-1800 Ma age interval (late Paleoproterozoic). Neoproterozoic and Meso-Neoproterozoic determinations are subordinate. A distinct age gap is documented between ~ 1800 and 1000 Ma.

DISCUSSION

The presence of basement outcrops not concealed under sub-pelagic cover or accessible for sampling at shallow sub-bottom depth has been reported, with greater or lesser confidence, from several sites located on the Lomonosov Ridge (Grantz et al., 2001), the southern Northwind Ridge (Grantz et al., 1998), on the central and northern Northwind Ridge, seamounts between Alpha and Northwind Ridges and the southern Alpha Ridge (Andronikov et al., 2008; Brumley et al., 2010, 2011; Database for ECS Dredge Samples at NOAA/NGDC), and in the central Alpha Ridge (Clark et al., 2000; Jokat, 2003; Van Wagoner et al., 1986). The coarse debris that can positively be attributed to, or inferred to represent the bedrock, is usually mixed with variable proportions of IRD consisting mainly of quartz-rich terrigenous and carbonate rocks. This IRD was defined by Grantz et al. (2011a) as “... shallow marine Paleozoic carbonates and sandstones ... widely distributed on the seabed of the Amerasia Basin by the basin’s clockwise Beaufort Gyre current system”; the authors (ibid) further concluded that “...sedimentary clasts in the dredges and cores from Mendeleev Ridge belong to an areally extensive suite of glacial erratics that originated in NW Canada...” Our data suggest that such definition is probably excessively all-embracing, and at least some of the coarse clastic material in sampled bottom sediments on the Mendeleev Rise may appear meaningful for characterization of the local bedrock.

Rock specimens interpreted to represent sub-pelagic basement

The sandstone fragments bearing detrital zircons analyzed in the present study were collected in three different areas – the central Mendeleev Rise, the southern Mendeleev Rise and the near-Siberian segment of the Lomonosov Ridge (see pentagons in Fig. 1). These geographic variations are reflected

in the distribution of detrital zircons ages and other characteristics of respective specimens (Fig. 5A).

The largest of all recovered sandstone fragments were dredged on a small, steep-sided bathymetric spur in the central Mendeleev Rise (sites AF00-05 & 10). Three fragments were analyzed and displayed only slightly differing zircon age data (Fig. 5A, a-c) notably dissimilar to those in the sandstones from the southern Mendeleev Rise. The marked distinctions of these data, such as well expressed Paleozoic-Early Mesozoic zircons population, prevalence of Paleoproterozoic ages over Mesoproterozoic determinations and almost total lack of Archean grains, suggest clastic input from the sources independent from those involved in formation of the sandstones dredged farther south. The central sites are also peculiar for the occurrence of fossiliferous Paleozoic limestones (Kaban'kov et al., 2004) not encountered elsewhere in the sampled area. In our view, these features are likely to signify that AF00-05 & 10 sandstone/carbonate debris represents local Paleozoic and Mesozoic (mostly pre-200 Ma?) sedimentary bedrock strata whose upper horizons may be broadly correlative with sub-pelagic basement of the Lomonosov Ridge described by Grantz et al. (2001) and exemplified in our collection by the specimen ALR07-18 discussed below.

A common feature of specimens from the southern Mendeleev Rise is the predominance of Mesoproterozoic detrital zircons (Fig. 5A, d-h). Sandstones AF05-11[2] and AF05-20 which contain only pre-1000 Ma grains can in reality be as old as Neoproterozoic; this may or may not also be true for the specimen AF05-11[1] where the ~ 200-400 Ma zircon ages are probably too rare to be meaningful. However, more numerous ~ 400-600 Ma grains in specimens AF05-14 & 15 (Fig. 5A, f-g) seem to preclude their Precambrian age; these sandstones also contain lesser amounts of Mesoproterozoic grains and a greater number of ancient grains, some of them as old as Mesoarchean.

Unless caused by the shortage of analytical data, such peculiarities may suggest that sandstones collected at stations 14, 15 and those recovered at stations 11 and 20 differ in age and origin, despite geographical proximity of these sites and apparent lithological similarity of the studied rocks. They

also further confirm the dissimilarity of the southern and the central Mendeleev Rise specimens. If corroborated by subsequent studies, these distinctions would seem easier to explain by local derivation of the analyzed rocks than by their ice rafting from remote sources and selective unloading at different Mendeleev Rise locations. For instance, the presence of Archean grains captured in the analyzed sandstones indicates that these rocks could not be derived from the nearest coastal mainland - the Arctic Alaska-Chukotka (AAC) terrane which was shown by Akinin et al. (2012) to lack the Archean juvenile crust.

The Lomonosov Ridge specimen ALR07-18 is composed of coarse quartzose siltstone with carbonate cement. Zircon U-Pb age data (Fig. 5A, i) indicate input from sources ranging in age from Paleoproterozoic to possibly as young as Early Mesozoic. Except some clustering at about the Paleo/Mesoproterozoic boundary, the distribution of ages is relatively flat throughout more than a 2000 Ma time interval suggesting multiple recycling of primary clastic material. Lithological composition of the analyzed rock, its likely post-Triassic depositional age and detrital zircons population are consistent with the characterization of the Lomonosov Ridge bedrock by Grantz et al. (2001). The location of sampling site at the base of steep Lomonosov Ridge slope in close vicinity to the near-bottom high of the acoustic basement (Fig. 6a) and a sharply angular shape of the collected specimen suggest possibility of its derivation from a proximal submarine outcrop.

Among magmatic/metamorphic rock fragments the most likely representatives of bedrock were recovered by box corer at the Geophysicists Spur at site ALR07-16 (Fig. 1, Rekant et al., 2012). Here the unusual abundance of fragments is accompanied by uncommonly large amount (about 50%) of metamorphic rocks which at all other sampling sites are invariably markedly subordinate to unaltered carbonate and terrigenous clasts. Increase in overall concentration of coarse material could be caused by slumping of sediments and washing out of fine particles – the processes likely to occur on a steeply faulted slope (Fig. 6b); however, the remarkably high proportion of magmatic/metamorphic rock fragments is uncharacteristic of IRD and, when considered together with bathymetric profile at

the sampling site, suggests supply from the local bedrock.

All box-cored rock splinters were too small for preparation of thin sections or chemical treatment. So far only three of them that could visually (using binocular microscope) be defined as gneisses of probable diorite composition were analyzed and showed different (~1140, ~570-690 and ~400-450 Ma) ages. In the absence of detailed examination of the mineral composition, metamorphic grade, magmatic vs sedimentary origin, etc. of the samples studied, these ages could be interpreted as indicating that analyzed rocks belong to either the same polymetamorphic assemblage, or are derived from different metamorphic sources. The latter possibility, however, seems highly unlikely, since it would imply transportation of one piece from a Mezoproterozoic provenance, another from a Late Neoproterozoic terrane, and the third from an Early-Middle Paleozoic

area. We therefore prefer the alternative option which allows correlation of the Geophysicists Spur bedrock with the basement assemblages reported from the Northwind Ridge (Brumley et al., 2010, 2011; Database for ECS Dredge Samples at NOAA/NGDC) and characterized by an ancient (no younger than Grenvillian) protolith affected by subsequent events as young as the Caledonian.

Rock fragments of questionable origin

Interpretation of mineral particles and/or relatively small rock pieces in bottom samples as IRD or otherwise relocated matter (e.g. Bischof et al., 1996; Clark et al., 1980; Grantz et al., 2011a; Phillips and Grantz, 2001) in all probability applies to those subordinate fragments in our collection which are characterized by predominantly small size, sub-rounded or pebble-like shape and, in some cases, display apparent association with glacial-dominated

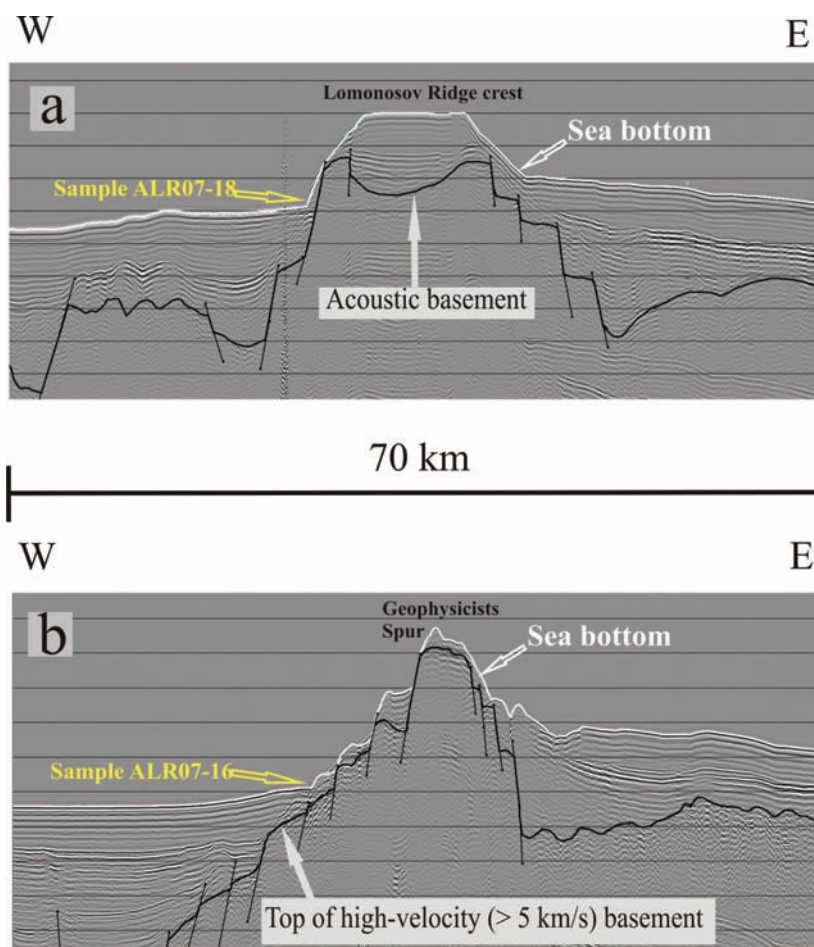


Fig. 6. Fragments of stacked seismic sections showing the position of sampling sites ALR07-18 (a) and ALR07-16 (b) relative to the bathymetry and basement behavior (modified from lines shot during Arctica-2011 cruise). Vertical exaggeration approximately 8:1. See Fig. 1 for the location of imaged sections.

layers in sub-bottom sediments. These features are inherent in the majority of analyzed magmatic rocks, namely the granitic pieces AF07-01, AF05-24 & 26, BC-260 & 299 and metagabbro-dolerites AF05-11 & 26 (Figs. 2 and 5B, b-h) which are therefore interpreted as dropstones of questionable origin.

Specimen AF05-08 (Figs. 2 and 5B, i) is distinct among granitoid rocks being much larger with pronounced gneissic banding and almost unsmoothed shape. Its zircon population is characterized by higher amount of Late Archean zircons and the presence of 600-800 Ma grains with secondary rims suggesting Latest Neoproterozoic overprint. The combination of these features may indicate the provenance more proximal than the source area of other Archean granitoids.

Mineral grains interpreted as IRD

Detrital zircons from soft bottom sediments have so far been studied in only two samples collected on different flanks of the Lomonosov Ridge (stations AF07-01 & ALR07-15, Figs. 1 and 5C). Ages of zircons selected at different levels from the ALR07-15 core appeared barely distinguishable (Fig. 5C, b-d). This can either be attributed to invariability of sources that supplied zircon grains to the sampling site during the time spanned by the cored interval, or may merely reflect intermixing of loose sediments on a steep slope. Other findings attracting attention in Fig. 5C are (1) general similarity of zircon age data obtained in radically diverse geographical and geomorphological environments – site AF07-01 in deepwater Amundsen basin (Fig. 5C, a) vs. site ALR07-15 on a prominent bathymetric spur (Fig. 5C, b-d), (2) presence at both localities of post-Triassic grains not recorded in any of the analyzed rock fragments, and (3) notable absence of Mesoproterozoic zircons which constitute the most characteristic population in the studied sandstone specimens.

The first two observations can be interpreted as signifying either a common source or separate but closely comparable provenances. The latter would at first glance seem represented by proximal Paleozoic-Mesozoic sedimentary bedrock reportedly sampled on the Lomonosov Ridge (Grantz et al., 2001) and, based on interpretation of our zircon data from sandstone specimens, also thought to occur on the

Mendelev Rise, at least in the vicinity of sampling sites in the central part. However, upon closer examination such explanation appears difficult to accept. For the North Pole site it would be hard to imagine how abundant heavy mineral products eroded from the Lomonosov Ridge sedimentary bedrock could be delivered to the sampling locality across more than 100 km of flat deepwater Amundsen Basin, and in case of the Geophysicist Spur our data suggest that the bedrock here is more likely composed of Late Precambrian-Early Paleozoic metamorphic basement than of younger rocks capable of releasing post-500 Ma zircons into pelagic sediment.

Ice rafted zircons in sub-pelagic sediments appear therefore the most likely possibility, if even the light minerals and clay components in these deposits could be supplied to both sampling localities by turbidity currents from a variety of sources, including as distal ones as the Laptev Sea shelf. As shown by Krylov et al. (2008) on the basis of ACEX data, in post-Middle Miocene time zircon was a steady component (6-8%) of the heavy minerals assemblage continuously delivered to the Lomonosov Ridge and adjacent bathymetric deeps by Transpolar ice drift from the Arctic margin of Eastern Asia. Consequently, the Phanerozoic and Neoproterozoic zircons could easily be derived from various geological formations of respective age mapped in this extensive region. The provenance of Early Precambrian zircons is more problematic. They could either be supplied from the same enigmatic shield sources which gave rise to the above mentioned magmatic/metamorphic dropstones, or assumed to originate from younger igneous rocks containing inherited ancient grains that were captured by parental melts.

The youngest detrital zircons in Recent sub-bottom sediments are Late Cretaceous. In all probability they mostly originate from HALIP and/or broadly contemporaneous volcanic products which are exposed on the Circum-Arctic mainland and islands (Akinin and Miller, 2012; Korago et al., 2010) and believed to extend throughout much of the central Arctic Ocean (e.g. Grantz et al., 2011b). However, based on geophysical data the near-Pole to Russia segment of the Lomonosov Ridge is commonly excluded from the area affected by Late Mesozoic volcanic activity and therefore can

hardly serve as a local source for zircons of that age. This further strengthens the notion of their distal derivation and ice rafted nature

The virtual absence in modern deposits of Mesoproterozoic zircons indicates that mineral grains in pelagic sediments were not recycled from sandstones disseminated on the seabed. In case of such recycling the zircon population in sub-bottom layers would be dominated by Precambrian rather than Phanerozoic ages.

CONCLUSIONS

Intensification in recent years of bottom sampling in the central Arctic Ocean was accompanied by implementation of improved methods of site control and state-of-the-art analytical studies of the collected material. This enabled more exact examination of the nature of recovered bottom specimens and expanded the opportunities for interpretation of their lithological and age characteristics in regional geological context.

Our zircon geochronological data suggest that the sandstone/carbonate fragments dredged on the central Mendeleev Rise at sites AF00-05 & 10 most likely represent local Paleozoic and Mesozoic (mainly pre-200 Ma?) sedimentary bedrock units. The youngest of the central Mendeleev Rise sandstones may be broadly correlative with sub-pelagic Mesozoic sedimentary bedrock of the Lomonosov Ridge confirmed by sampling near the North Pole (Grantz et al., 2001) and believed to be exemplified in the Pole to Siberia segment of the ridge by our specimen ALR07-18 of coarse quartzose siltstone.

The presence of post-500 Ma sandstones among the samples from the southern Mendeleev Rise is more questionable, since the analyzed specimens from this area provided so far only a much lower number of zircons younger than 1000 Ma. At the same time, the well expressed population in these rocks of Mesoproterozoic grains is not a sufficient argument in favor of derivation of the analyzed sandstones from local Neoproterozoic bedrock, as assumed by Kaban'kov et al. (2004, 2008, 2012). While not ruled out by the available data, such possibility requires a much stronger confirmation. Distribution of Precambrian grains in detrital zircon population from Cambrian quartzites in the Canadian

Arctic (Hadlari et al., 2012) is very similar to that observed in our specimens of quartzose sandstones from the southern Mendeleev Rise. Consequently, the latter are not necessarily Neoproterozoic and may also be Cambrian or younger, and until their inferred local provenance is constrained with better confidence, the derivation of these rocks from the Canadian provenance and transportation by ice to the Mendeleev Rise will be difficult to disprove.

Zircon geochronology of sandstone debris in bottom sediments from the Mendeleev Rise and the Lomonosov Ridge suggests that these submarine highs are largely underlain by Paleozoic-Early Mesozoic sedimentary bedrock. The latter may in places include Early-Middle Paleozoic fold basement, but the predominance of younger (Middle Paleozoic to Early Mesozoic) platform-type or transitional sequences seems a more likely possibility.

Limited evidence for the presence of older assemblages is provided at the Geophysicists Spur basement high interpreted to consist of metamorphic rocks of possible Grenville-Caledonian affinity.

The source of variably metamorphosed Late Precambrian mafic and Archean granitoid rocks interpreted as dropstones is uncertain. One of many probabilities is that during the glacial maximum they could be scoured by ice from the shallowest blocks of the Lomonosov Ridge some of which may, by analogy with the plateau described by Jackson and Dalh_Jensen et al. (2010), be composed of ancient(?) high-velocity crystalline infrastructure virtually uncovered by sediments.

On the whole, the preliminary geological implications of the present study are consistent with the models proposing significant extension of mature continental crust as a leading mechanism of formation of the Amerasia Basin (Miller et al., 2006; Laverov et al., 2013).

ACKNOWLEDGEMENTS

We thank Dr. Vyacheslav Akinin and anonymous reviewer for constructive comments which highlighted the parts of the text that lacked adequate clarity and prompted respective revisions helping to improve the paper. Participation of A. Krylov in laboratory studies of the bottom samples was partly supported by the RFBR grant 12-05-00364-a.

Table 1. U-Pb SHRIMP-II analytical data.

Analysis number	% ²⁰⁶ Pb _c	ppm U	ppm Th	ppm ²⁰⁶ Pb*	²³² Th/ ²³⁸ U	(1) ²⁰⁶ Pb/ ²³⁸ U Age (Ma) ± abs	(1) ²⁰⁷ Pb/ ²⁰⁶ Pb Age (Ma) ± abs	% Dis.	(1) ²³⁸ U/ ²⁰⁶ Pb* ±%	(1) ²⁰⁷ Pb/ ²⁰⁶ Pb* ±%	(1) ²⁰⁷ Pb/ ²³⁵ U ±%	(1) ²⁰⁶ Pb/ ²³⁸ U ±%	err corr						
Hemipelagic sediments from the North Pole site, sample AF07-01 (89°59'10.9"N, 32°19'13.8"E)																			
79.1	0.00	128	82.3	1.47	0.66	85.2	2.3	286	213	235	75.17	2.7	0.0520	9.3	0.095	9.7	0.0133	2.7	0.28
91.1	0.64	2121	613	30.6	0.30	107	1.0	116	123	9	59.98	1.0	0.0483	5.2	0.111	5.3	0.0167	1.0	0.18
34.1	0.00	126	133	2.24	1.09	132	2.7	672	133	408	48.29	2.1	0.0619	6.2	0.177	6.6	0.0207	2.1	0.31
52.1	0.00	276	105	5.43	0.39	146	2.0	128	98	-12	43.64	1.4	0.0486	4.2	0.154	4.4	0.0229	1.4	0.31
57.1	0.45	488	147	9.78	0.31	148	1.6	80	144	-46	43.01	1.1	0.0476	6.1	0.153	6.2	0.0232	1.1	0.17
27.1	0.00	68.6	52.7	1.62	0.79	175	4.1	126	245	-28	36.31	2.4	0.0485	10	0.184	11	0.0275	2.4	0.22
26.1	0.00	488	1487	11.9	3.15	181	2.4	171	81	-5	35.06	1.3	0.0495	3.5	0.195	3.7	0.0285	1.3	0.36
39.1	0.00	220	102	6.40	0.48	214	3.4	202	96	-6	29.57	1.6	0.0502	4.1	0.234	4.4	0.0338	1.6	0.36
1.1	1.38	893	421	27.0	0.49	220	3.0	270	216	22	28.78	1.4	0.0516	9.4	0.247	9.5	0.0347	1.4	0.14
18.1	0.00	33.2	39.3	1.00	1.22	222	8.0	343	238	54	28.49	3.7	0.0533	11	0.258	11	0.0351	3.7	0.33
12.1	0.00	37.0	58.9	1.16	1.64	231	6.7	284	224	23	27.38	3.0	0.0520	9.8	0.262	10	0.0365	3.0	0.29
30.1	0.00	323	220	11.0	0.70	250	3.4	231	83	-7	25.32	1.4	0.0508	3.6	0.277	3.9	0.0395	1.4	0.36
9.1	0.00	479	157	16.6	0.34	255	3.4	252	75	-1	24.75	1.4	0.0512	3.2	0.285	3.5	0.0404	1.4	0.39
44.1	0.02	775	899	27.0	1.20	256	3.3	259	59	1	24.70	1.3	0.0514	2.5	0.287	2.9	0.0405	1.3	0.45
47.1	1.11	100	177	3.53	1.82	256	5.7	69	303	-73	24.69	2.3	0.0474	13	0.265	13	0.0405	2.3	0.18
45.1	0.00	53.4	143	1.86	2.77	256	6.1	157	184	-39	24.68	2.4	0.0492	7.9	0.275	8.2	0.0405	2.4	0.30
99.1	0.00	612	418	21.5	0.71	258	2.6	288	54	11	24.46	1.0	0.0521	2.4	0.293	2.6	0.0409	1.0	0.39
2.1	0.00	35.6	67.7	1.30	1.97	268	8.6	586	233	118	23.53	3.3	0.0595	11	0.349	11	0.0425	3.3	0.29
93.1	0.58	338	216	12.6	0.66	272	3.3	156	149	-43	23.17	1.2	0.0492	6.4	0.293	6.5	0.0432	1.2	0.19
49.1	1.51	78.2	84.8	2.99	1.12	276	6.8	403	329	46	22.81	2.5	0.0548	15	0.331	15	0.0438	2.5	0.17
31.1	1.41	114	105	4.35	0.95	277	5.2	134	353	-52	22.81	1.9	0.0487	15	0.294	15	0.0438	1.9	0.13
46.1	0.60	172	175	6.52	1.06	278	4.6	228	164	-18	22.72	1.7	0.0507	7.1	0.308	7.3	0.0440	1.7	0.23
75.1	0.00	68.5	73.5	2.62	1.11	281	6.3	566	146	102	22.48	2.3	0.0590	6.7	0.362	7.1	0.0445	2.3	0.32
55.1	0.83	172	405	6.66	2.44	282	3.9	113	157	-60	22.33	1.4	0.0483	6.7	0.298	6.8	0.0448	1.4	0.21
42.1	0.78	144	165	5.59	1.19	283	4.9	235	198	-17	22.25	1.8	0.0509	8.6	0.315	8.7	0.0449	1.8	0.20
51.1	1.01	95.5	110	3.85	1.19	293	5.8	328	245	12	21.52	2.0	0.0530	11	0.339	11	0.0465	2.0	0.19
95.1	0.37	167	162	6.85	1.00	299	4.5	198	170	-34	21.08	1.5	0.0501	7.3	0.327	7.5	0.0474	1.5	0.21
68.1	2.43	52.9	82.1	2.21	1.60	299	7.9	-131	752	-144	21.08	2.7	0.0436	30	0.285	31	0.0474	2.7	0.09
87.1	0.70	142	54.1	5.91	0.39	303	5.0	222	189	-26	20.81	1.7	0.0506	8.2	0.335	8.3	0.0481	1.7	0.20
89.1	0.39	172	93.7	7.20	0.56	306	4.5	318	164	4	20.60	1.5	0.0527	7.2	0.353	7.4	0.0485	1.5	0.21
21.1	0.44	410	367	17.3	0.93	308	4.1	250	122	-19	20.44	1.4	0.0512	5.3	0.345	5.5	0.0489	1.4	0.25
19.1	0.00	63.0	80.9	2.69	1.33	312	6.9	286	153	-8	20.14	2.3	0.0520	6.7	0.356	7.1	0.0496	2.3	0.32
17.1	0.18	698	228	29.8	0.34	312	3.9	305	67	-2	20.14	1.3	0.0525	2.9	0.359	3.2	0.0497	1.3	0.40
15.1	0.00	372	88.7	16.0	0.25	316	4.8	287	81	-9	19.93	1.6	0.0520	3.5	0.360	3.9	0.0502	1.6	0.40
6.1	0.00	112	56.1	4.87	0.52	319	6.3	385	133	21	19.74	2.0	0.0543	5.9	0.379	6.2	0.0507	2.0	0.33
92.1	0.27	568	437	25.0	0.80	321	3.1	340	73	6	19.58	1.0	0.0533	3.2	0.375	3.4	0.0511	1.0	0.30
16.1	0.00	252	202	11.2	0.83	325	5.1	370	90	14	19.34	1.6	0.0540	4.0	0.385	4.3	0.0517	1.6	0.37
40.1	0.34	486	162	22.0	0.35	330	4.3	308	104	-7	19.04	1.3	0.0525	4.6	0.380	4.8	0.0525	1.3	0.28
22.1	0.00	337	533	15.3	1.63	333	4.5	361	65	9	18.89	1.4	0.0538	2.9	0.392	3.2	0.0529	1.4	0.43
38.1	0.68	128	124	5.92	1.00	335	5.6	373	194	11	18.72	1.7	0.0541	8.6	0.398	8.8	0.0534	1.7	0.20
33.1	0.00	387	267	18.0	0.71	339	4.4	294	66	-13	18.51	1.3	0.0522	2.9	0.389	3.2	0.0540	1.3	0.42
76.1	0.39	614	92.1	29.5	0.15	349	3.4	801	63	129	17.96	1.0	0.0658	3.0	0.505	3.2	0.0557	1.0	0.32
88.1	0.21	362	216	17.6	0.62	355	3.2	356	72	0	17.68	0.9	0.0536	3.2	0.418	3.3	0.0566	0.9	0.28
7.1	0.00	206	122	10.0	0.61	355	5.3	362	88	2	17.67	1.5	0.0538	3.9	0.420	4.2	0.0566	1.5	0.37
14.1	0.78	192	92.2	9.47	0.50	357	5.7	332	194	-7	17.54	1.6	0.0531	8.6	0.417	8.7	0.0570	1.6	0.19
58.1	0.08	1365	2762	73.9	2.09	394	2.9	359	36	-9	15.88	0.7	0.0537	1.6	0.466	1.8	0.0630	0.7	0.43
48.1	0.44	213	90.3	11.7	0.44	397	5.8	416	116	5	15.72	1.5	0.0551	5.2	0.483	5.4	0.0636	1.5	0.28
81.1	0.00	86.5	64.1	4.80	0.77	403	8.4	380	117	-6	15.49	2.2	0.0542	5.2	0.483	5.7	0.0646	2.2	0.38
11.1	0.65	262	185	15.3	0.73	422	6.2	395	171	-6	14.80	1.5	0.0546	7.6	0.509	7.8	0.0676	1.5	0.19
25.1	0.00	179	119	10.8	0.69	440	6.6	436	74	-1	14.16	1.6	0.0556	3.3	0.542	3.7	0.0706	1.6	0.42
63.1	0.61	92.6	53.1	6.03	0.59	468	6.4	485	161	4	13.27	1.4	0.0568	7.3	0.591	7.4	0.0754	1.4	0.19
71.1	0.45	279	33.8	18.8	0.13	483	5.5	400	124	-17	12.84	1.2	0.0547	5.6	0.587	5.7	0.0779	1.2	0.21
97.1	0.00	666	362	46.3	0.56	501	4.3	469	34	-6	12.37	0.9	0.0564	1.6	0.629	1.8	0.0809	0.9	0.50
54.1	0.86	43.2	55.6	3.40	1.33	560	11.1	491	209	-12	11.01	2.1	0.0570	9.5	0.713	9.7	0.0908	2.1	0.21
86.1	0.00	44.1	32.4	3.49	0.76	568	12.3	596	128	5	10.85	2.3	0.0598	5.9	0.760	6.3	0.0921	2.3	0.36
78.1	1.74	112	65.9	9.78	0.61	613	9.7	382	272	-38	10.03	1.7	0.0543	12	0.746	12	0.0997	1.7	0.14
8.1	0.00	372	308	33.4	0.86	642	7.9	631	46	-2	9.554	1.3	0.0608	2.1	0.877	2.5	0.1047	1.3	0.52
28.1	0.24	114	28.4	12.9	0.26	796	11	766	75	-4	7.607	1.5	0.0648	3.6	1.173	3.9	0.1314	1.5	0.39
29.1	0.00	46.3	40.6	5.35	0.91	814	14	902	91	11	7.430	1.9	0.0691	4.4	1.282	4.8	0.1346	1.9	0.39
94.1	0.00	62.1	51.6	7.19	0.86	815	13	768	77	-6	7.419	1.7	0.0648	3.7	1.204	4.0	0.1348	1.7	0.42
98.1	0.00	271	66.8	31.6	0.26	822	8.0	765	39	-7	7.352	1.0	0.0647	1.9	1.214	2.1	0.1360	1.0	0.49
24.1	0.25	244	238	31.2	1.01	892	13	870	56	-2	6.739	1.6	0.0680	2.7	1.392	3.1	0.1484	1.6	0.50
5.1	0.00	114	47.7	14.9	0.43	915	14	864	63	-6	6.553	1.6	0.0679	3.0	1.428	3.4	0.1526	1.6	0.47
65.1	0.00	231	37.7	31.0	0.17	936	8.8	935	35	0	6.398	1.0	0.0702	1.7	1.513	2.0	0.1563	1.0	0.51
80.1	0.00	330	183	72.5	0.57	1469	13	1753	18	19	3.908	1.0	0.1072	1.0	3.784	1.4	0.2559	1.0	0.70
32.1	0.06	343	237	86.4	0.72	1658	19	1784	19	8	3.409	1.3	0.1091	1.0	4.410	1.7	0.2933	1.3	0.79
13.1	0.05	466	99.0	121	0.22	1707	18	1793	15	5	3.299	1.2	0.1096	0.8	4.581	1.5	0.		

Table 1. Continued.

Analysis number	% ²⁰⁶ Pb _c	ppm U	ppm Th	ppm ²⁰⁶ Pb*	²³² Th/ ²³⁸ U	(¹) ²⁰⁶ Pb/ ²³⁸ U Age (Ma) ± abs	(¹) ²⁰⁷ Pb/ ²⁰⁶ Pb Age (Ma) ± abs	% Dis.	(¹) ²³⁸ U/ ²⁰⁶ Pb* ±%	(¹) ²⁰⁷ Pb/ ²⁰⁶ Pb* ±%	(¹) ²⁰⁷ Pb/ ²³⁵ U ±%	(¹) ²⁰⁶ Pb/ ²³⁸ U ±%	err corr						
41.1	0.00	1026	307	401	0.31	2419	24	2376	7	-2	2.196	1.2	0.1527	0.4	9.583	1.3	0.4553	1.2	0.94
72.1	0.27	85.3	69.1	35.4	0.84	2537	27	2529	22	0	2.073	1.3	0.1671	1.3	11.11	1.8	0.4824	1.3	0.70
35.1	0.09	122	203	52.5	1.72	2609	30	2646	15	1	2.004	1.4	0.1793	0.9	12.33	1.7	0.4988	1.4	0.84
20.1	0.05	401	116	174	0.30	2634	26	2740	30	4	1.981	1.2	0.1897	1.8	13.21	2.2	0.5048	1.2	0.54
61.1	0.08	164	53.2	71.7	0.34	2651	22	2678	13	1	1.966	1.0	0.1827	0.8	12.82	1.3	0.5087	1.0	0.78
96.1	0.12	419	107	191	0.26	2739	19	2823	9	3	1.889	0.9	0.1996	0.5	14.57	1.0	0.5294	0.9	0.84
67.1	0.32	101	15.5	46.5	0.16	2761	27	2755	18	0	1.870	1.2	0.1915	1.1	14.12	1.6	0.5346	1.2	0.74
62.1	0.00	193	39.0	89.2	0.21	2770	20	2728	10	-2	1.863	0.9	0.1884	0.6	13.94	1.1	0.5368	0.9	0.81
60.2	0.00	151	50.0	70.1	0.34	2780	23	2906	12	5	1.854	1.0	0.2101	0.7	15.62	1.2	0.5392	1.0	0.81
59.1	0.00	412	281	191	0.70	2783	18	2701	10	-3	1.852	0.8	0.1853	0.6	13.79	1.0	0.5398	0.8	0.79
70.1	0.00	46.9	25.7	23.2	0.57	2938	37	2902	21	-1	1.732	1.6	0.2095	1.3	16.68	2.0	0.5773	1.6	0.76
64.1	0.15	51.0	34.5	25.3	0.70	2938	31	2936	17	0	1.732	1.3	0.2139	1.1	17.03	1.7	0.5773	1.3	0.78
Hemipelagic sediments from the Lomonosov Ridge (Geophysicists Spur), sample ALR07-15 (83° N, 156°E), 12-14 cm b.s.f.																			
49.1	2.37	360	154	3.51	0.44	72.8	1.4	-428	10	118	88.11	1.9	0.0388	30	0.061	30	0.0113	1.9	0.06
50.1	0.43	695	218	12.3	0.32	131	1.5	5	150	-2525	48.57	1.1	0.0461	6.0	0.131	6.1	0.0206	1.1	0.18
46.1	--	1046	521	19.3	0.51	137	1.4	226	180	40	46.48	1.1	0.0507	4.1	0.150	4.2	0.0215	1.1	0.25
31.1	0.58	430	662	8.38	1.59	145	1.6	143	174	-1	44.08	1.1	0.0489	7.4	0.153	7.5	0.0227	1.1	0.15
9.1	0.00	199	129	3.90	0.67	145	2.6	170	137	17	43.86	1.8	0.0495	5.9	0.156	6.1	0.0228	1.8	0.29
20.1	0.00	385	98.5	7.66	0.26	148	2.3	159	104	8	43.17	1.6	0.0492	4.5	0.157	4.7	0.0232	1.6	0.33
8.1	3.13	203	92.3	4.19	0.47	148	4.1	375	854	153	42.96	2.8	0.0541	3.8	0.173	3.8	0.0233	2.8	0.07
26.1	0.14	1204	381	24.1	0.33	148	1.7	164	68	11	42.94	1.1	0.0493	2.9	0.158	3.1	0.0233	1.1	0.37
32.1	0.00	507	139	13.9	0.28	202	2.4	205	56	1	31.38	1.2	0.0502	2.4	0.221	2.7	0.0319	1.2	0.45
33.1	--	172	86.6	4.97	0.52	214	2.9	518	174	60	29.64	1.4	0.0577	7.9	0.268	8.1	0.0337	1.4	0.17
2.1	1.14	160	109	5.36	0.70	244	4.8	189	303	-22	25.92	2.0	0.0499	13	0.265	13	0.0386	2.0	0.15
15.1	1.08	373	187	12.6	0.52	245	3.8	246	300	0	25.77	1.6	0.0511	13	0.273	13	0.0388	1.6	0.12
17.1	1.99	131	159	4.60	1.26	253	5.1	204	255	-19	25.00	2.1	0.0502	11	0.277	11	0.0400	2.1	0.18
13.1	0.66	1566	675	55.5	0.45	259	2.7	231	98	-11	24.39	1.0	0.0508	4.3	0.287	4.4	0.0410	1.0	0.24
11.1	0.00	42.8	47.8	1.63	1.15	280	7.4	357	194	28	22.52	2.7	0.0537	8.6	0.329	9.0	0.0444	2.7	0.30
25.1	0.84	542	686	20.9	1.31	281	3.5	242	151	-14	22.45	1.3	0.0510	6.5	0.313	6.7	0.0445	1.3	0.19
27.1	1.40	200	399	7.84	2.06	284	5.1	398	331	40	22.20	1.8	0.0547	15	0.339	15	0.0450	1.8	0.12
29.1	0.88	605	520	23.8	0.89	286	3.4	263	134	-8	22.07	1.2	0.0515	5.8	0.322	6.0	0.0453	1.2	0.20
38.1	0.00	527	327	20.6	0.64	287	3.0	299	44	4	21.96	1.1	0.0523	1.9	0.328	2.2	0.0455	1.1	0.48
3.1	0.00	17.1	28.1	0.77	1.69	329	15.1	1868	147	468	19.09	4.7	0.1143	8.2	0.825	9.4	0.0524	4.7	0.50
21.1	0.50	525	526	23.9	1.03	331	3.9	520	83	57	18.95	1.2	0.0577	3.8	0.420	4.0	0.0528	1.2	0.31
1.1	0.43	536	682	26.2	1.32	355	4.2	438	89	23	17.67	1.2	0.0556	4.0	0.434	4.2	0.0566	1.2	0.29
7.1	0.00	75.6	117	3.78	1.61	365	7.2	495	121	36	17.18	2.0	0.0571	5.5	0.458	5.8	0.0582	2.0	0.35
42.1	1.54	71.4	38.7	3.57	0.56	365	8.8	330	570	-11	17.16	2.5	0.0530	25	0.426	25	0.0583	2.5	0.10
30.1	0.37	283	277	15.2	1.01	389	5.2	409	102	5	16.07	1.4	0.0549	4.5	0.471	4.7	0.0622	1.4	0.29
10.1	0.68	318	410	17.8	1.33	403	5.0	322	151	-20	15.50	1.3	0.0528	6.7	0.470	6.8	0.0645	1.3	0.19
5.1	2.50	181	95.2	10.5	0.54	412	7.4	343	413	-17	15.13	1.9	0.0533	18	0.486	18	0.0660	1.9	0.10
16.1	0.91	174	170	11.5	1.01	475	7.9	594	270	25	13.08	1.7	0.0597	12	0.629	13	0.0764	1.7	0.14
34.1	0.29	410	183	27.0	0.46	476	5.0	386	93	-24	13.06	1.1	0.0544	4.1	0.574	4.3	0.0766	1.1	0.26
22.1	1.41	130	62.1	8.94	0.49	490	8.4	479	287	-2	12.66	1.8	0.0567	13	0.617	13	0.0789	1.8	0.14
14.1	0.36	512	90.7	35.2	0.18	494	5.6	460	80	-7	12.55	1.2	0.0562	3.6	0.617	3.8	0.0796	1.2	0.31
41.1	--	317	317	23.3	1.03	529	5.9	693	55	25	11.70	1.2	0.0625	2.6	0.737	2.8	0.0855	1.2	0.42
12.1	1.22	248	296	20.8	1.23	595	8.2	521	209	-12	10.34	1.4	0.0578	9.5	0.770	9.6	0.0967	1.4	0.15
40.1	0.19	414	73.6	39.1	0.18	673	24	1480	27	57	9.088	3.8	0.0926	1.4	1.405	4.0	0.1100	3.8	0.93
47.1	0.00	307	146	33.6	0.49	774	8.6	771	30	-0	7.843	1.2	0.0649	1.4	1.141	1.9	0.1275	1.2	0.64
4.1	0.32	926	150	224	0.17	1591	14	1919	16	21	3.570	1.0	0.1176	0.9	4.537	1.3	0.2799	1.0	0.76
28.1	0.21	195	122	52.9	0.65	1770	19	1848	28	4	3.163	1.2	0.1130	1.5	4.924	2.0	0.3160	1.2	0.63
35.1	0.03	239	81.3	65.4	0.35	1786	18	1831	15	3	3.133	1.2	0.1120	0.8	4.927	1.4	0.3192	1.2	0.82
39.1	--	179	84.7	49.7	0.49	1805	20	1866	19	4	3.096	1.3	0.1141	1.0	5.083	1.6	0.3230	1.3	0.78
24.1	0.00	222	158	61.9	0.74	1813	19	1873	20	3	3.079	1.2	0.1146	1.1	5.130	1.6	0.3247	1.2	0.74
37.1	0.01	639	156	178	0.25	1815	17	1794	24	-1	3.075	1.0	0.1097	1.3	4.918	1.7	0.3252	1.0	0.62
19.1	0.14	1046	237	295	0.23	1828	16	1878	12	3	3.049	1.0	0.1149	0.7	5.193	1.2	0.3279	1.0	0.82
18.1	0.13	139	93.0	39.6	0.69	1843	22	1859	27	1	3.021	1.4	0.1137	1.5	5.188	2.1	0.3309	1.4	0.68
43.1	--	259	153	73.8	0.61	1847	19	1871	13	2	3.014	1.2	0.1144	0.7	5.235	1.4	0.3317	1.2	0.85
36.1	0.03	882	68.3	255	0.08	1872	16	1901	52	2	2.968	1.0	0.1163	2.9	5.404	3.1	0.3369	1.0	0.33
23.1	0.00	255	134	74.7	0.54	1890	19	1872	19	-1	2.936	1.2	0.1145	1.0	5.378	1.6	0.3406	1.2	0.75
48.1	0.00	192	143	56.7	0.77	1902	21	1883	15	-1	2.913	1.3	0.1152	0.9	5.453	1.6	0.3432	1.3	0.83
44.1	0.00	159	26.5	56.6	0.17	2237	25	2387	15	7	2.410	1.3	0.1537	0.9	8.790	1.6	0.4149	1.3	0.83
6.1	0.08	681	420	276	0.64	2491	21	2645	10	6	2.119	1.0	0.1791	0.6	11.65	1.2	0.4718	1.0	0.87
45.1	--	537	175	270	0.34	2969	26	2946	26	-1	1.710	1.1	0.2154	1.6	17.37	1.9	0.5849	1.1	0.56
Hemipelagic sediments from the Lomonosov Ridge (Geophysicists Spur), sample ALR07-15 (83° N, 156°E), 505-507 cm b.s.f.																			
10.1	0.30	1579	44.8	29.1	0.03	137	2.9	263	81	93	46.70	2.2	0.0515	3.5	0.152	4.1	0.0214	2.2	0.52
37.1	0.87	570	226	10.6	0.41	137	2.1	36	180	-73	46.45	1.5	0.0468	7.4	0.139	7.5	0.0215	1.5	0.20
18.1	0.74	1009	273	19.4	0.28	142	3.0	-52	160	-137	45.04	2.2	0.0451	6.6	0.138	6.9	0.0222	2.2	0.31
26.1	0.00	222	86.2	5.15	0.40	172	4.1	814	86	373	36.99	2.4	0.0662	4.1	0.247	4.8	0.0270	2.4	0.50
23.1	3.86	114	60.7	2.81	0.55	176	5.6	65	920	-63									

Table 1. Continued.

Analysis number	% ²⁰⁶ Pb _c	ppm U	ppm Th	ppm ²⁰⁶ Pb*	²³² Th/ ²³⁸ U	(¹) ²⁰⁶ Pb/ ²³⁸ U Age (Ma) ± abs	(¹) ²⁰⁷ Pb/ ²⁰⁶ Pb Age (Ma) ± abs	% Dis.	(¹) ²³⁸ U/ ²⁰⁶ Pb* ±%	(¹) ²⁰⁷ Pb/ ²⁰⁶ Pb* ±%	(¹) ²⁰⁷ Pb/ ²³⁵ U ±%	(¹) ²⁰⁶ Pb/ ²³⁸ U ±%	err corr						
41.1	0.15	191	242	22.6	1.31	831	12	-5	7.270	1.5	0.0655	1.9	1.243	2.4	0.1376	1.5	0.61		
6.1	0.78	77.0	6.28	14.2	0.08	1246	28	41	4.690	2.4	0.1073	3.8	3.150	4.5	0.2133	2.4	0.54		
33.1	0.00	71.7	33.2	15.9	0.48	1482	22	-1	3.868	1.6	0.0918	1.7	3.274	2.4	0.2585	1.6	0.70		
20.1	0.11	564	314	140	0.58	1636	31	17	3.460	2.2	0.1168	5.6	4.650	6.0	0.2889	2.2	0.36		
24.1	0.30	275	162	77.0	0.61	1815	34	2	3.073	2.1	0.1133	1.4	5.080	2.6	0.3252	2.1	0.84		
12.1	0.15	516	198	145	0.40	1827	34	1	3.050	2.1	0.1128	0.9	5.100	2.3	0.3277	2.1	0.92		
50.1	0.00	100	53.5	28.8	0.55	1861	27	-4	2.988	1.7	0.1093	1.7	5.040	2.4	0.3346	1.7	0.70		
32.1	0.13	156	84.3	49.6	0.56	2029	25	-2	2.702	1.4	0.1226	1.1	6.250	1.8	0.3699	1.4	0.80		
1.1	0.10	551	305	177	0.57	2043	36	-2	2.681	2.1	0.1225	0.7	6.300	2.2	0.3729	2.1	0.95		
19.1	0.06	223	78.5	74.2	0.36	2109	39	-3	2.584	2.2	0.1256	1.0	6.700	2.4	0.3870	2.2	0.92		
22.1	0.11	221	89.4	91.2	0.42	2522	45	6	2.088	2.2	0.1827	0.8	12.06	2.3	0.4790	2.2	0.94		
38.1	0.02	529	203	218	0.40	2529	29	3	2.081	1.4	0.1748	1.4	11.58	2.0	0.4805	1.4	0.71		
9.1	0.35	154	95.4	63.8	0.64	2532	48	4	2.076	2.3	0.1787	1.7	11.85	2.9	0.4810	2.3	0.80		
7.1	0.16	178	101	76.4	0.59	2603	50	2	2.009	2.3	0.1801	0.9	12.35	2.5	0.4970	2.3	0.94		
16.1	0.01	285	159	126	0.58	2665	46	0	1.953	2.1	0.1832	0.6	12.93	2.2	0.5120	2.1	0.96		
13.1	0.03	444	372	196	0.86	2672	47	2	1.947	2.1	0.1879	0.6	13.30	2.2	0.5140	2.1	0.97		
48.1	0.00	236	127	106	0.56	2704	35	0	1.919	1.6	0.1844	1.0	13.25	1.8	0.5212	1.6	0.86		
21.1	0.00	187	103	84.3	0.57	2715	48	0	1.909	2.2	0.1879	0.7	13.57	2.3	0.5240	2.2	0.95		
49.1	0.00	226	235	103	1.08	2752	33	-1	1.878	1.5	0.1882	0.7	13.82	1.6	0.5326	1.5	0.92		
45.1	0.05	336	80.0	164	0.25	2896	34	-3	1.763	1.4	0.1969	0.6	15.40	1.6	0.5672	1.4	0.93		
Hemipelagic sediments from the Lomonosov Ridge (Geophysicists Spur), sample ALR07-15 (83° N, 156° E), 703-705 cm b.s.f.																			
18.2	0.47	832	473	9.17	0.59	82	1.5	236	190	189	78.30	1.9	0.0509	8.1	0.090	8.3	0.0128	1.9	0.23
18.1	1.60	636	503	7.22	0.82	83	1.7	80	310	-4	76.90	2.0	0.0476	13	0.085	13	0.0130	2.0	0.15
22.1	0.45	1078	802	12.9	0.77	89	1.6	-15	190	-117	72.00	1.8	0.0458	8.0	0.088	8.1	0.0139	1.8	0.22
19.1	0.73	281	287	4.69	1.06	123	2.5	155	200	26	51.80	2.1	0.0491	8.4	0.131	8.7	0.0193	2.1	0.24
26.1	2.02	513	101	9.01	0.20	128	2.6	258	310	102	50.00	2.0	0.0514	14	0.142	14	0.0200	2.0	0.15
4.1	0.28	1772	244	33.1	0.14	138	2.3	151	75	9	46.11	1.7	0.0491	3.2	0.147	3.6	0.0217	1.7	0.46
23.1	0.38	732	280	14.0	0.40	141	2.5	113	120	-20	45.08	1.8	0.0483	5.3	0.148	5.6	0.0222	1.8	0.32
33.1	0.40	521	141	10.2	0.28	145	1.5	123	130	-15	43.95	1.1	0.0485	5.4	0.152	5.5	0.0228	1.1	0.19
20.1	1.56	289	83.3	5.80	0.30	147	3.1	311	330	112	43.45	2.2	0.0526	15	0.167	15	0.0230	2.2	0.15
1.1	2.69	243	139	5.55	0.59	165	3.5	13	510	-92	38.63	2.2	0.0463	21	0.165	21	0.0259	2.2	0.10
16.1	0.00	252	113	6.20	0.46	182	3.7	214	99	17	34.85	2.1	0.0504	4.3	0.199	4.8	0.0287	2.1	0.44
14.1	1.67	205	62.5	5.41	0.31	192	4.2	-62	450	-133	33.14	2.2	0.0449	18	0.187	19	0.0302	2.2	0.12
34.1	3.79	155	58.6	5.39	0.39	246	5.1	-439	910	-278	25.64	2.1	0.0390	35	0.208	35	0.0390	2.1	0.06
41.1	1.41	508	318	17.4	0.65	248	2.6	295	250	19	25.46	1.1	0.0522	11	0.283	11	0.0393	1.1	0.10
48.1	4.08	73.1	146	2.58	2.06	249	7.9	459	800	84	25.38	3.2	0.0560	36	0.300	36	0.0394	3.2	0.09
21.1	1.02	247	408	8.78	1.71	259	5.0	92	250	-65	24.37	2.0	0.0479	11	0.271	11	0.0410	2.0	0.18
5.1	4.02	60.2	53.3	2.25	0.91	263	9.2	623	710	137	24.00	3.6	0.0610	33	0.350	33	0.0416	3.6	0.11
44.1	0.60	165	179	5.99	1.12	265	3.8	371	160	40	23.79	1.5	0.0540	6.9	0.313	7.1	0.0420	1.5	0.21
32.1	0.26	940	548	34.5	0.60	269	1.9	267	57	-1	23.43	0.7	0.0516	2.5	0.304	2.6	0.0427	0.7	0.28
17.1	1.54	233	272	8.78	1.21	272	5.5	-30	430	-111	23.16	2.1	0.0455	18	0.271	18	0.0432	2.1	0.12
39.1	0.49	447	588	17.2	1.36	280	2.6	275	120	-2	22.50	1.0	0.0518	5.1	0.317	5.1	0.0444	1.0	0.19
37.1	4.54	88.2	65.3	3.63	0.76	288	7.8	1183	600	311	21.90	2.8	0.0790	30	0.500	31	0.0456	2.8	0.09
11.1	1.07	133	177	5.36	1.38	293	6.1	322	250	10	21.49	2.1	0.0528	11	0.339	11	0.0465	2.1	0.19
8.1	1.77	501	669	20.7	1.38	298	5.4	292	190	-2	21.15	1.9	0.0522	8.4	0.340	8.6	0.0473	1.9	0.21
38.1	0.91	486	212	20.0	0.45	300	2.9	378	200	26	21.02	1.0	0.0542	8.7	0.355	8.8	0.0476	1.0	0.11
28.1	0.19	937	220	47.9	0.24	372	6.0	321	52	-14	16.85	1.6	0.0528	2.3	0.432	2.8	0.0594	1.6	0.59
3.1	0.19	875	1567	49.7	1.85	412	6.5	425	44	3	15.17	1.6	0.0553	2.0	0.503	2.6	0.0659	1.6	0.64
2.1	0.20	906	1702	54.6	1.94	436	6.9	386	58	-11	14.28	1.6	0.0544	2.6	0.525	3.1	0.0700	1.6	0.54
24.1	0.54	218	120	13.4	0.57	442	7.8	445	120	1	14.09	1.8	0.0558	5.2	0.546	5.5	0.0710	1.8	0.33
50.1	2.76	223	112	14.9	0.52	469	6.2	605	250	29	13.24	1.4	0.0600	12	0.625	12	0.0755	1.4	0.12
40.1	1.01	48.6	27.7	4.35	0.59	632	11	774	190	23	9.700	1.9	0.0650	9.2	0.923	9.4	0.1030	1.9	0.20
49.1	0.20	499	414	49.6	0.86	705	5.1	702	45	0	8.654	0.8	0.0628	2.1	1.001	2.2	0.1155	0.8	0.34
6.1	0.05	273	94.6	62.8	0.36	1529	24	1804	18	18	3.736	1.7	0.1103	1.0	4.070	2.0	0.2677	1.7	0.87
25.1	0.07	214	91.8	56.0	0.44	1713	25	1703	20	-1	3.284	1.7	0.1043	1.1	4.381	2.0	0.3045	1.7	0.84
31.1	0.20	226	66.5	63.1	0.30	1814	12	1801	21	-1	3.077	0.8	0.1101	1.1	4.933	1.4	0.3249	0.8	0.55
13.1	0.13	188	121	53.0	0.67	1824	27	1843	21	1	3.057	1.7	0.1127	1.2	5.080	2.0	0.3271	1.7	0.83
15.1	0.12	167	75.0	47.4	0.46	1832	27	1850	20	1	3.041	1.7	0.1131	1.1	5.130	2.0	0.3287	1.7	0.84
7.1	0.12	254	115	72.8	0.47	1855	27	1857	17	0	2.999	1.7	0.1135	1.0	5.219	1.9	0.3334	1.7	0.87
10.1	0.06	202	184	58.8	0.94	1877	27	1871	18	0	2.959	1.7	0.1144	1.0	5.330	1.9	0.3379	1.7	0.86
47.1	0.06	520	101	156	0.20	1926	11	1919	13	0	2.872	0.7	0.1175	0.7	5.642	1.0	0.3481	0.7	0.69
43.1	0.19	642	596	217	0.96	2132	14	2773	8.6	30	2.551	0.8	0.1936	0.5	10.46	0.9	0.3919	0.8	0.82
27.1	0.36	76.1	19.2	26.3	0.26	2169	35	2216	34	2	2.498	1.9	0.1391	2.0	7.670	2.7	0.4000	1.9	0.69
35.1	0.06	231	146	87.4	0.65	2356	17	2366	16	0	2.267	0.9	0.1518	0.9	9.230	1.3	0.4411	0.9	0.69
12.1	0.04	293	73.8	119	0.26	2493	34	2500	10	0	2.117	1.6	0.1643	0.6	10.69	1.7	0.4722	1.6	0.94
30.1	0.02	394	193	160	0.51	2496	15	2495	8.6	0	2.115	0.7	0.1638	0.5	10.68	0.9	0.4729	0.7	0.82
9.1	0.15	146	20.9	62.1	0.15	2583	36	2619	14	1	2.028	1.7	0.1764	0.9	11.99	1.9	0.4929	1.7	0.89
45.1	0.04	282	139	124	0.51	2660	19	2651	11	0	1.958	0.9	0.1798	0.7	12.66	1.1	0.5107	0.9	0.80
36.1	0.06	271	80.7	119	0.31	2667	16	2649	18	-1	1.951	0.7	0.1796	1.1	12.69	1.3	0.5124	0.7	0.55
29.1	0.07	146	103	65.4	0.73	2698	38	2717	19	1	1.923	1.7	0.1871						

Table 1. Continued.

Analysis number	% ²⁰⁶ Pb	ppm U	ppm Th	ppm ²⁰⁶ Pb*	²³² Th/ ²³⁸ U	(1) ²⁰⁶ Pb/ ²³⁸ U Age (Ma) ± abs	(1) ²⁰⁷ Pb/ ²⁰⁶ Pb Age (Ma) ± abs	% Dis.	(1) ²³⁸ U/ ²⁰⁶ Pb ± %	(1) ²⁰⁷ Pb/ ²⁰⁶ Pb ± %	(1) ²⁰⁷ Pb/ ²³⁵ U ± %	(1) ²⁰⁶ Pb/ ²³⁸ U ± %	err corr						
Gneissic rocks from the Lomonosov Ridge (Geophysicists Spur), sample ALR07-16 (83.152° N, 156.105° E)																			
65_1.2	2.67	386	356	21.8	0.95	399	4.5	450	380	13	15.63	1.2	0.0560	8.8	0.493	8.9	0.0639	1.2	0.13
65_1.1	3.27	616	657	35.6	1.10	406	4.3	422	320	4	15.37	1.1	0.0552	7.4	0.495	7.5	0.0650	1.1	0.15
65_1.3	5.23	579	553	35.2	0.99	418	4.6	524	400	26	14.91	1.1	0.0578	9.2	0.534	9.3	0.0669	1.1	0.12
65_2.2	2.47	1572	663	99.2	0.44	446	3.4	532	160	19	13.96	0.8	0.0580	3.9	0.573	3.9	0.0716	0.8	0.20
65_2.3	3.07	1454	622	92.5	0.44	446	3.7	308	230	-31	13.93	0.9	0.0525	5.3	0.519	5.3	0.0717	0.9	0.16
65_2.1	1.38	1675	693	106	0.43	454	3.3	496	120	9	13.71	0.8	0.0571	2.7	0.574	2.8	0.0729	0.8	0.27
9_2.2	0.20	462	325	36.8	0.73	571	4.7	570	86	0	10.80	0.9	0.0591	2.0	0.754	2.2	0.0926	0.9	0.39
9_2.1	0.41	351	211	28.2	0.62	573	5.7	591	200	3	10.75	1.0	0.0597	4.7	0.765	4.8	0.0930	1.0	0.22
9_1.4	0.05	928	49.0	88.9	0.05	681	5.0	645	48	-5	8.972	0.8	0.0612	1.1	0.940	1.4	0.1115	0.8	0.57
9_1.2	0.00	864	27.2	82.8	0.03	682	5.0	702	39	3	8.961	0.8	0.0630	1.0	0.969	1.2	0.1116	0.8	0.62
9_1.1	0.08	704	749	67.7	1.10	684	5.2	682	53	0	8.938	0.8	0.0623	1.2	0.960	1.5	0.1119	0.8	0.55
9_3.2	1.45	126	57.8	12.4	0.47	692	9.2	653	340	-6	8.810	1.4	0.0614	8.0	0.960	8.2	0.1134	1.4	0.17
9_1.3	0.08	313	244	30.8	0.80	699	6.1	688	65	-2	8.734	0.9	0.0624	1.6	0.985	1.8	0.1145	0.9	0.50
9_3.1	0.23	149	63.2	14.9	0.44	708	7.7	679	120	-4	8.616	1.2	0.0621	2.9	0.994	3.1	0.1160	1.2	0.37
4_1.1	0.55	1049	347	175	0.34	1137	7.7	1160	46	2	5.180	0.7	0.0785	1.1	2.088	1.4	0.1929	0.7	0.54
Granitoid fragments from the Podvodnikov Basin, sample BC-299 (81°N, 165°E)																			
5_2.1	2.02	2322	321	416	0.14	1196	7.0	1872	19	57	4.907	0.7	0.1144	1.1	3.217	1.3	0.2038	0.7	0.52
5.1	0.80	573	77.9	143	0.14	1627	9.9	2085	17	28	3.483	0.7	0.1290	1.0	5.110	1.2	0.2871	0.7	0.58
7.1	1.15	1171	372	296	0.33	1643	9.1	2305	17	40	3.446	0.6	0.1464	1.0	5.862	1.2	0.2902	0.6	0.54
5_3.1	1.88	464	66.3	129	0.15	1765	12	2421	23	37	3.176	0.8	0.1566	1.3	6.810	1.6	0.3149	0.8	0.50
mica-5.1	0.95	765	407	277	0.55	2244	15	2615	17	17	2.402	0.8	0.1758	1.0	10.10	1.3	0.4164	0.8	0.60
mica-3.1	0.59	598	195	218	0.34	2267	13	2591	16	14	2.373	0.7	0.1734	1.0	10.08	1.2	0.4214	0.7	0.58
mica-4.1	0.14	502	134	186	0.28	2308	19	2585	16	12	2.323	1.0	0.1728	1.0	10.26	1.4	0.4304	1.0	0.71
6.2	0.89	972	133	367	0.14	2325	14	2652	11	14	2.303	0.7	0.1799	0.7	10.77	1.0	0.4342	0.7	0.73
7_2.1	0.28	619	285	238	0.48	2377	13	2596	13	9	2.243	0.7	0.1740	0.8	10.69	1.0	0.4458	0.7	0.65
6.1	0.08	577	47.6	232	0.09	2473	15	2637	16	7	2.138	0.7	0.1782	1.0	11.49	1.2	0.4677	0.7	0.60
6.3	0.38	696	364	282	0.54	2482	15	2659	10	7	2.129	0.7	0.1807	0.6	11.70	1.0	0.4696	0.7	0.76
7_3.1	0.50	415	157	170	0.39	2498	16	2622	13	5	2.113	0.8	0.1766	0.8	11.53	1.1	0.4733	0.8	0.70
mica-2.1	0.42	341	292	141	0.88	2515	16	2628	14	5	2.096	0.8	0.1774	0.8	11.67	1.2	0.4771	0.8	0.69
Granitoid fragments from the Mendeleev Rise, sample AF05-08 (78°40'N, 179°13'W)																			
1_12.1	1.74	91.0	49.7	7.39	0.56	573	13	644	244	12	10.76	2.4	0.0611	1.1	0.784	1.2	0.0929	2.4	0.21
1_15.1	1.47	84.8	72.5	6.99	0.88	583	15	529	318	-9	10.57	2.6	0.0580	1.4	0.756	1.5	0.0946	2.6	0.18
1_4.1	7.23	14.0	8.42	1.25	0.62	595	38	-127	2004	-121	10.34	6.6	0.0437	81	0.583	81	0.0967	6.6	0.08
1_13.1	0.99	120	140	10.3	1.20	604	13	513	243	-15	10.19	2.3	0.0576	1.1	0.779	1.1	0.0982	2.3	0.20
1_17.1	1.52	79.3	41.7	7.13	0.54	633	16	690	236	9	9.696	2.7	0.0625	1.1	0.888	1.1	0.1031	2.7	0.23
1_3.1	0.37	97.2	60.7	8.73	0.65	638	14	826	140	29	9.605	2.4	0.0666	6.7	0.956	7.1	0.1041	2.4	0.33
1_16.1	1.14	99.5	95.4	9.07	0.99	643	14	784	215	22	9.540	2.4	0.0653	1.0	0.944	1.1	0.1048	2.4	0.22
1_1.1	0.27	668	20.8	61.6	0.03	655	9.3	589	55	-10	9.345	1.5	0.0596	2.5	0.879	2.9	0.1070	1.5	0.51
1_10.1	3.53	39.0	17.7	4.22	0.47	740	31	581	967	-21	8.220	4.4	0.0594	45	0.996	45	0.1217	4.4	0.10
1_6.1	2.41	81.8	36.8	14.8	0.47	1208	27	953	256	-21	4.850	2.4	0.0709	13	2.015	1.3	0.2062	2.4	0.19
1_2.1	0.40	117	70.6	31.0	0.62	1724	30	1780	37	3	3.262	2.0	0.1088	2.0	4.600	2.8	0.3065	2.0	0.70
1_8.1	0.43	148	158	43.9	1.10	1904	30	1978	36	4	2.911	1.8	0.1215	2.0	5.754	2.7	0.3436	1.8	0.67
1_9.1	0.28	266	219	79.6	0.85	1922	27	2037	24	6	2.879	1.6	0.1256	1.4	6.015	2.1	0.3474	1.6	0.76
1_26.1	1.70	95.7	96.4	29.5	1.04	1945	38	2038	71	5	2.839	2.3	0.1256	4.0	6.103	4.6	0.3523	2.3	0.49
1_14.1	0.13	283	72.8	87.5	0.27	1983	27	2036	22	3	2.777	1.6	0.1255	1.2	6.233	2.0	0.3601	1.6	0.79
1_5.1	1.42	98.6	131	32.0	1.37	2041	37	1966	82	-4	2.686	2.1	0.1206	4.6	6.194	5.1	0.3724	2.1	0.41
1_24.1	1.00	522	81.6	17.3	0.16	2087	29	2602	21	25	2.615	1.7	0.1746	1.3	9.203	2.1	0.3824	1.7	0.80
1_7.1	0.81	223	125	74.2	0.58	2095	30	2045	41	-2	2.605	1.7	0.1261	2.3	6.678	2.9	0.3839	1.7	0.58
1_18.1	0.23	651	122	215	0.19	2096	27	2086	15	0	2.602	1.5	0.1291	0.9	6.840	1.8	0.3843	1.5	0.87
2_5.1	0.63	2444	117	944	0.05	2380	20	2564	88	8	2.239	1.0	0.1706	0.5	10.51	1.1	0.4466	1.0	0.88
1_23.2	0.24	1204	8.64	477	0.01	2392	20	2568	11	7	2.225	1.0	0.1710	0.6	10.60	1.2	0.4493	1.0	0.85
2_23.2	0.09	897	8.34	352	0.01	2420	21	2563	11	6	2.195	1.0	0.1705	0.6	10.71	1.2	0.4557	1.0	0.85
1_23.2	0.03	1211	15.2	466	0.01	2433	20	2575	13	6	2.181	1.0	0.1717	0.8	10.86	1.3	0.4586	1.0	0.78
1_21.2	0.02	1383	41.0	558	0.03	2484	21	2565	9.4	3	2.127	1.0	0.1707	0.6	11.07	1.2	0.4701	1.0	0.87
2_14.1	0.25	1216	12.8	495	0.01	2496	22	2586	12	4	2.115	1.1	0.1729	0.7	11.27	1.3	0.4728	1.1	0.82
1_24.2	0.07	1770	62.8	720	0.04	2496	20	2569	8.7	3	2.115	1.0	0.1711	0.5	11.16	1.1	0.4728	1.0	0.88
2_23.1	0.05	328	133	134	0.42	2506	24	2668	14	6	2.104	1.1	0.1816	0.8	11.90	1.4	0.4752	1.1	0.81
1_19.2	0.04	1645	46.7	673	0.03	2509	20	2590	8.7	3	2.101	1.0	0.1733	0.5	11.37	1.1	0.4759	1.0	0.88
2_11.1	0.07	987	10.2	408	0.01	2532	21	2576	8.8	2	2.078	1.0	0.1719	0.5	11.40	1.1	0.4811	1.0	0.88
2_8.1	0.08	1792	44.4	742	0.03	2533	21	2581	8.1	2	2.078	1.0	0.1724	0.5	11.44	1.1	0.4813	1.0	0.90
1_28.1	0.00	132	413	55.2	3.22	2550	43	2696	24	6	2.061	2.1	0.1848	1.4	12.36	2.5	0.4852	2.1	0.82
1_29.1	0.67	221	89.7	93.5	0.42	2564	39	2670	23	4	2.047	1.8	0.1819	1.4	12.25	2.3	0.4884	1.8	0.79
1_23.1	0.59	297	156	126	0.54	2574	37	2651	20	3	2.038	1.7	0.1798	1.2	12.16	2.1	0.4907	1.7	0.82
2_9.1	0.29	797	456	338	0.59	2582	22	2676	10	4	2.030	1.0	0.1826	0.6	12.40	1.2	0.4925	1.0	0.87
2_13.1	0.01	919	9.27	390	0.01	2589	27	2601	19	0	2.023	1.3	0.1745	1.1	11.89	1.7	0.4942	1.3	0.75
1_27.1	0.30	540	19.6	230	0.04	2595	35	2592	16	0	2.018	1.6	0.1736	0.9	11.86	1.9	0.4956	1.6	0.87
2_16.2	0.00	285	143	122	0.52	2608	24	2657	12	2	2.005	1.1	0.1805	0.7	12.41	1.3	0.4987	1.1	0.85
1_23.3	0.66	119	38.9	51.5	0.34	2609	32	2663	27	2	2.005	1.5	0.1811	1.6	12.45	2.2			

Table 1. Continued.

Analysis number	% ²⁰⁶ Pb _c	ppm U	ppm Th	ppm ²⁰⁶ Pb*	²³² Th/ ²³⁸ U	(1) ²⁰⁶ Pb/ ²³⁸ U Age (Ma) ± abs	(1) ²⁰⁷ Pb/ ²⁰⁶ Pb Age (Ma) ± abs	% Dis.	(1) ²³⁸ U/ ²⁰⁶ Pb* ±%	(1) ²⁰⁷ Pb/ ²⁰⁶ Pb* ±%	(1) ²⁰⁷ Pb/ ²³⁵ U ±%	(1) ²⁰⁶ Pb/ ²³⁸ U ±%	err corr						
2_6.1	0.02	1176	678	558	0.60	2836	22	2680	7.8	-5	1.809	1.0	0.1830	0.5	13.95	1.1	0.5527	1.0	0.90
Granitoid fragments from the Mendeleev Rise, sample AF05-24 (79°N, 178°W)																			
2.1	4.38	861	402	184	0.48	1353	16	2604	20	92	4.214	1.3	0.1748	1.2	5.630	1.8	0.2335	1.3	0.73
13.1	3.52	2869	353	714	0.13	1576	7.7	2233	26	42	3.575	0.6	0.1405	1.5	5.362	1.6	0.2769	0.6	0.34
4.1	0.60	949	240	228	0.26	1580	9.0	2603	9.5	65	3.593	0.7	0.1746	0.6	6.687	0.9	0.2777	0.7	0.75
1_1.1	0.89	1450	305	356	0.22	1607	9.0	2246	17	40	3.534	0.6	0.1415	1.0	5.524	1.2	0.2830	0.6	0.55
1_2.1	4.79	2834	856	795	0.31	1731	20	2512	82	45	3.247	1.3	0.1649	4.9	7.030	5.0	0.3080	1.3	0.26
1_1.2	1.61	980	386	272	0.41	1774	21	2267	17	28	3.157	1.3	0.1432	1.0	6.260	1.7	0.3168	1.3	0.81
10.1	0.00	3051	222	876	0.08	1859	8.8	2270	5.1	22	2.992	0.5	0.1435	0.3	6.613	0.6	0.3342	0.5	0.88
1.1	0.78	687	457	205	0.69	1909	9.6	2617	10	37	2.894	0.6	0.1761	0.6	8.367	0.8	0.3446	0.6	0.69
11.1	1.56	1818	170	582	0.10	2007	9.7	2289	13	14	2.725	0.6	0.1451	0.8	7.307	0.9	0.3653	0.6	0.60
3.1	2.21	492	174	165	0.37	2071	59	2636	24	27	2.618	3.3	0.1782	1.4	9.310	3.6	0.3790	3.3	0.92
8.1	0.90	703	302	241	0.44	2145	15	2609	9.5	22	2.524	0.8	0.1753	0.6	9.546	1.0	0.3949	0.8	0.83
5.1	1.66	499	300	174	0.62	2159	16	2627	19	22	2.499	0.9	0.1772	1.1	9.720	1.4	0.3978	0.9	0.61
7.1	0.29	565	472	209	0.86	2301	12	2630	7.9	14	2.328	0.6	0.1775	0.5	10.50	0.8	0.4290	0.6	0.79
6.1	1.33	303	105	121	0.36	2423	14	2624	14	8	2.181	0.7	0.1770	0.9	11.13	1.1	0.4563	0.7	0.62
9.1	0.00	479	115	196	0.25	2512	13	2613	7.3	4	2.098	0.6	0.1758	0.4	11.55	0.8	0.4766	0.6	0.82
12.1	0.26	1042	526	442	0.52	2578	13	2610	14	1	2.032	0.6	0.1754	0.9	11.89	1.0	0.4918	0.6	0.59
Granitoid fragments from the Mendeleev Rise, sample AF05-26 (79°N, 178°W)																			
3.1	0.00	466	375	96.6	0.83	1393	13	2599	22	86	4.144	1.0	0.1742	1.3	5.796	1.6	0.2413	1.0	0.61
1.1	0.64	716	435	151	0.63	1407	12	2325	18	65	4.099	1.0	0.1482	1.0	4.984	1.4	0.2440	1.0	0.68
7.1	1.52	389	405	96.1	1.07	1607	16	2331	28	45	3.533	1.1	0.1487	1.6	5.800	2.0	0.2831	1.1	0.58
5.1	2.26	1147	349	328	0.31	1817	15	2330	18	28	3.072	1.0	0.1486	1.0	6.669	1.4	0.3255	1.0	0.68
10.1	0.46	754	606	222	0.83	1890	16	2339	13	24	2.936	1.0	0.1494	0.7	7.017	1.2	0.3406	1.0	0.80
4.1	0.00	1107	832	340	0.78	1971	16	2602	8.2	32	2.795	1.0	0.1746	0.5	8.610	1.1	0.3577	1.0	0.89
12.1	0.76	577	304	192	0.54	2098	18	2321	27	11	2.600	1.0	0.1479	1.6	7.840	1.8	0.3846	1.0	0.54
8.1	1.93	561	206	192	0.38	2123	18	2353	24	11	2.564	1.0	0.1506	1.4	8.100	1.7	0.3901	1.0	0.57
2.1	0.13	428	545	149	1.32	2194	19	2615	11	19	2.467	1.0	0.1760	0.7	9.840	1.2	0.4054	1.0	0.83
2.2	0.00	423	402	150	0.98	2228	20	2625	10	18	2.422	1.0	0.1770	0.6	10.08	1.2	0.4129	1.0	0.86
6.1	0.00	533	161	198	0.31	2313	19	2624	9.4	13	2.317	1.0	0.1769	0.6	10.53	1.1	0.4316	1.0	0.87
9.1	0.00	352	296	147	0.87	2557	22	2622	11	3	2.054	1.0	0.1767	0.7	11.86	1.2	0.4870	1.0	0.84
11.1	0.17	1079	1451	497	1.39	2762	23	2323	9.4	-16	1.869	1.0	0.1480	0.6	10.92	1.2	0.5350	1.0	0.88
Granitoid fragment from the Mendeleev Rise, sample BC-260 (80°N, 179°30'W)																			
4.1r	2.40	12073	4824	189	0.41	114	6.4	1744	38	1434	56.20	5.7	0.1067	2.1	0.262	6.1	0.0178	5.7	0.94
4.1	2.66	9257	4296	224	0.48	174	1.6	1822	47	947	36.55	0.9	0.1113	2.6	0.420	2.8	0.0274	0.9	0.33
7_3.1	3.12	3431	4078	144	1.23	299	6.3	1705	71	471	21.08	2.1	0.1044	3.8	0.683	4.4	0.0474	2.1	0.49
5.1	1.33	5145	5481	226	1.10	317	2.6	1805	51	469	19.82	0.9	0.1103	2.8	0.767	2.9	0.0504	0.9	0.29
4_2.1	1.30	4308	1904	236	0.46	393	4.7	1850	24	371	15.91	1.2	0.1131	1.3	0.980	1.8	0.0628	1.2	0.69
3.1	1.21	4915	686	280	0.14	410	3.3	1922	23	369	15.24	0.8	0.1177	1.3	1.065	1.5	0.0656	0.8	0.54
6.1	2.35	3530	1132	230	0.33	461	6.3	1892	97	311	13.48	1.4	0.1157	5.4	1.183	5.6	0.0741	1.4	0.25
1.2	1.86	2573	273	289	0.11	777	21	1931	37	148	7.790	2.9	0.1183	2.1	2.091	3.6	0.1282	2.9	0.81
7_2.1	1.16	3043	6097	348	2.07	796	7.9	1968	30	147	7.599	1.0	0.1208	1.7	2.190	2.0	0.1315	1.0	0.53
1.1	0.21	2077	49.7	359	0.02	1178	7.1	1933	30	64	4.985	0.7	0.1184	1.7	3.275	1.8	0.2006	0.7	0.36
7.1	1.42	1392	270	245	0.20	1183	18	1971	35	67	4.957	1.7	0.1210	2.0	3.361	2.6	0.2014	1.7	0.64
Metagabbro-dolerite fragments from the Mendeleev Rise, sample AF05-11 (78°55'N, 177°40'W)																			
31_1.1	0.70	168	67.1	17.9	0.41	750	9.4	818	102	9	8.101	1.3	0.0664	4.9	1.130	5.1	0.1234	1.3	0.26
31_1.2	0.00	253	145	28.8	0.59	801	8.7	811	37	1	7.561	1.2	0.0661	1.8	1.206	2.1	0.1323	1.2	0.54
31_2.1	9.57	412	841	83.2	2.11	1242	14	1904	85	53	4.705	1.3	0.1166	4.7	3.415	4.9	0.2125	1.3	0.26
31_3.1	16.3	486	1152	107	2.45	1248	16	1989	98	59	4.682	1.4	0.1222	5.5	3.599	5.7	0.2136	1.4	0.24
31_3.2	10.4	442	748	149	1.75	1946	27	1958	94	1	2.838	1.6	0.1201	5.3	5.836	5.5	0.3524	1.6	0.29
31_4.1	7.73	1485	1476	370	1.03	1528	15	1923	43	26	3.738	1.1	0.1178	2.4	4.344	2.6	0.2675	1.1	0.43
31_5.1	0.00	95.2	16.0	28.7	0.17	1940	24	1962	30	1	2.848	1.4	0.1204	1.7	5.828	2.2	0.3511	1.4	0.65
31_6.1	0.13	709	224	317	0.33	2700	22	2661	8	-1	1.923	1.0	0.1809	0.5	12.97	1.1	0.5201	1.0	0.90
31_6.2	1.33	1905	102	815	0.06	2577	20	2652	9	3	2.034	1.0	0.1799	0.5	12.19	1.1	0.4915	1.0	0.88
31_7.1	0.15	440	130	197	0.31	2701	22	2673	10	-1	1.921	1.0	0.1822	0.6	13.08	1.2	0.5205	1.0	0.86
32_1.1	0.09	1895	2294	193	1.25	nd	nd	776	20	nd	nd	nd	0.0651	0.9	nd	nd	nd	nd	nd
Metagabbro-dolerite fragments from the Mendeleev Rise (measurements in thin sections), sample AF05-26 (79°N, 178°W)																			
1.1	0.46	6991	24825	445	3.67	nd	nd	720	15	nd	nd	nd	0.0633	0.7	nd	nd	nd	nd	nd
2.1	0.55	1067	557	99.8	0.54	nd	nd	828	30	nd	nd	nd	0.0667	1.4	nd	nd	nd	nd	nd
2.2	0.48	2090	2055	207	1.02	nd	nd	786	21	nd	nd	nd	0.0654	1.0	nd	nd	nd	nd	nd
3.1	0.48	1499	1076	147	0.74	nd	nd	800	28	nd	nd	nd	0.0658	1.3	nd	nd	nd	nd	nd
3.2	0.43	1063	611	105	0.59	nd	nd	816	56	nd	nd	nd	0.0663	2.7	nd	nd	nd	nd	nd
4.1	0.67	1006	263	109	0.27	nd	nd	804	33	nd	nd	nd	0.0659	1.6	nd	nd	nd	nd	nd
5.1	1.14	12374	36736	806	3.07	nd	nd	717	48	nd	nd	nd	0.0633	2.3	nd	nd	nd	nd	nd
6.1	3.52	1729	1117	198	0.67	nd	nd	836	268	nd									

Table 1. Continued.

Analysis number	% ²⁰⁶ Pb _c	ppm U	ppm Th	ppm ²⁰⁶ Pb ₀	²³² Th/ ²³⁸ U	(1) ²⁰⁶ Pb/ ²³⁸ U Age (Ma) ± abs	(1) ²⁰⁷ Pb/ ²⁰⁶ Pb Age (Ma) ± abs	% Dis.	(1) ²³⁸ U/ ²⁰⁶ Pb ± %	(1) ²⁰⁷ Pb/ ²⁰⁶ Pb ± %	(1) ²⁰⁷ Pb/ ²³⁵ U ± %	(1) ²⁰⁶ Pb/ ²³⁸ U ± %	err corr						
2_10.1	0.03	155	55.6	28.3	0.37	1239	7.5	1135	23	-8	4.718	0.7	0.0775	1.1	2.266	1.3	0.2120	0.7	0.50
1_6.1	0.12	310	80.9	57.9	0.27	1263	9.1	1707	26	35	4.612	0.8	0.1057	1.3	3.160	1.5	0.2168	0.8	0.53
2_26.1	0.08	164	70.0	33.7	0.44	1381	10	1387	30	0	4.185	0.8	0.0882	1.6	2.906	1.8	0.2390	0.8	0.47
2_14.1	0.06	210	90.0	43.6	0.44	1394	7.8	1360	17	-2	4.142	0.6	0.0870	0.9	2.896	1.1	0.2414	0.6	0.57
2_21.1	0.16	57.0	30.0	12.9	0.54	1504	16	1581	43	5	3.805	1.2	0.0977	2.3	3.541	2.6	0.2628	1.2	0.45
1_3.1	0.19	372	510	96.2	1.41	1691	11	1839	17	9	3.330	0.7	0.1130	0.8	4.681	1.1	0.3003	0.7	0.66
2_3.1	0.02	365	224	95.6	0.63	1714	9.4	1849	13	8	3.282	0.6	0.1131	0.7	4.749	1.0	0.3047	0.6	0.66
2_13.1	0.05	92.7	44.2	24.7	0.49	1741	14	1744	19	0	3.226	0.9	0.1067	1.0	4.562	1.4	0.3100	0.9	0.65
2_29.1	0.17	107	41.8	29.3	0.40	1778	13	1918	27	8	3.148	0.8	0.1174	1.5	5.144	1.7	0.3177	0.8	0.48
1_5.1	---	27.7	15.0	7.68	0.56	1795	36	1648	81	-8	3.080	2.3	0.1100	3.9	4.924	4.6	0.3247	2.3	0.50
2_24.1	0.02	136	35.0	37.9	0.27	1808	12	1822	22	1	3.089	0.7	0.1114	1.2	4.970	1.4	0.3237	0.7	0.52
2_2.1	0.03	315	126	91.8	0.42	1885	8.9	1997	11	6	2.944	0.5	0.1228	0.6	5.750	0.8	0.3396	0.5	0.66
2_1.1	0.12	78.5	62.8	23.3	0.83	1912	17	1842	27	-4	2.896	1.0	0.1126	1.5	5.361	1.8	0.3453	1.0	0.57
2_20.1	---	335	150	101	0.46	1938	9.0	1933	13	0	2.851	0.5	0.1184	0.8	5.727	0.9	0.3508	0.5	0.58
2_5.1	0.01	255	162	77.4	0.66	1951	11	1997	11	2	2.830	0.7	0.1228	0.6	5.982	0.9	0.3534	0.7	0.72
1_7.1	0.19	207	136	63.8	0.68	1975	15	1979	19	0	2.785	0.9	0.1225	1.0	6.067	1.3	0.3591	0.9	0.67
2_8.1	0.01	115	76.0	35.5	0.68	1976	12	1991	14	1	2.788	0.7	0.1224	0.8	6.051	1.0	0.3587	0.7	0.67
2_17.2	0.14	75.5	55.6	23.5	0.76	1989	15	1993	19	0	2.767	0.9	0.1225	1.1	6.103	1.4	0.3613	0.9	0.63
2_27.1	0.06	151	78.1	62.1	0.53	2514	14	2560	14	2	2.097	0.7	0.1703	0.8	11.20	1.1	0.4770	0.7	0.62
2_7.1	0.02	527	345	226	0.68	2611	8.0	2716	4.4	4	2.003	0.4	0.1870	0.3	12.87	0.5	0.4992	0.4	0.82
Sandstone fragments from the Mendeleev Rise, sample AF00-10 (82°04'N, 179°59'W)																			
15.2	1.71	1929	980	64.2	0.53	241	1.0	552	91	129	26.24	0.4	0.0586	4.2	0.308	4.2	0.0381	0.4	0.10
15.1	1.60	1459	693	60.6	0.49	300	1.4	567	68	89	21.02	0.5	0.0590	3.1	0.387	3.1	0.0476	0.5	0.15
26.1	1.00	1008	172	49.0	0.18	352	1.7	393	74	12	17.83	0.5	0.0545	3.3	0.421	3.4	0.0561	0.5	0.15
5.1	0.66	900	963	47.9	1.11	385	2.5	350	70	-9	16.24	0.7	0.0548	2.6	0.454	3.2	0.0615	0.7	0.21
8.1	1.44	1585	737	109	0.48	490	6.3	1465	44	199	12.64	1.3	0.0925	2.2	1.001	2.7	0.0790	1.3	0.50
3.1	---	436	209	34.3	0.49	564	4.9	481	39	-15	10.91	0.9	0.0587	1.8	0.742	2.0	0.0917	0.9	0.45
20.1	1.15	1799	1466	205	0.84	795	4.2	1539	63	94	7.619	0.6	0.0955	3.3	1.729	3.4	0.1313	0.6	0.17
1.1	0.07	774	373	106	0.50	949	5.5	920	25	-3	6.297	0.6	0.0704	1.0	1.525	1.4	0.1587	0.6	0.46
22.1	0.64	826	32.8	115	0.04	965	3.9	1186	27	23	6.193	0.4	0.0796	1.4	1.772	1.5	0.1615	0.4	0.30
25.1	0.23	151	112	21.0	0.77	965	7.4	995	54	3	6.193	0.8	0.0723	2.7	1.610	2.8	0.1615	0.8	0.29
27.1	0.01	316	159	52.1	0.52	1132	7.0	1154	25	2	5.208	0.7	0.0783	1.2	2.073	1.4	0.1920	0.7	0.48
7.1	---	60.8	40.8	10.2	0.69	1147	17	1013	81	-12	5.094	1.6	0.0795	2.7	1.959	4.3	0.1947	1.6	0.37
21.1	1.24	42.6	73.5	10.5	1.78	1612	19	1668	75	3	3.520	1.3	0.1024	4.1	4.010	4.3	0.2841	1.3	0.31
29.1	0.01	293	132	73.4	0.47	1651	7.8	1664	16	1	3.427	0.5	0.1022	0.9	4.110	1.0	0.2918	0.5	0.52
11.1	0.28	44.8	52.5	11.9	1.21	1731	25	1738	46	0	3.246	1.6	0.1064	2.5	4.518	3.0	0.3080	1.6	0.54
30.1	---	66.7	35.7	17.8	0.55	1739	16	1748	32	1	3.229	1.0	0.1069	1.7	4.565	2.0	0.3097	1.0	0.51
28.1	0.05	132	44.3	36.1	0.35	1785	12	1821	22	2	3.135	0.8	0.1113	1.2	4.896	1.4	0.3190	0.8	0.52
16.1	0.10	436	113	121	0.27	1801	6.3	1858	12	3	3.103	0.4	0.1136	0.7	5.048	0.8	0.3223	0.4	0.53
17.1	0.10	157	67.7	44.9	0.45	1854	23	1932	24	4	3.002	1.4	0.1184	1.4	5.438	2.0	0.3331	1.4	0.73
4.1	0.50	272	76.0	78.9	0.29	1862	14	1884	23	1	2.980	0.9	0.1160	1.1	5.322	1.5	0.3349	0.9	0.58
10.1	---	193	86.9	55.5	0.47	1866	15	1841	20	-1	2.976	0.9	0.1137	1.3	5.209	1.4	0.3357	0.9	0.64
24.1	0.09	634	317	183	0.52	1868	5.8	1966	17	5	2.975	0.4	0.1207	0.9	5.593	1.0	0.3361	0.4	0.36
9.2	---	98.9	32.9	29.2	0.34	1900	20	1877	27	-1	2.910	1.2	0.1169	1.4	5.424	1.9	0.3427	1.2	0.62
13.1	0.27	133	59.0	39.6	0.46	1914	15	1982	23	4	2.893	0.9	0.1218	1.3	5.804	1.6	0.3456	0.9	0.58
14.1	0.09	82.8	58.4	24.8	0.73	1927	16	1962	25	2	2.870	1.0	0.1204	1.4	5.784	1.7	0.3484	1.0	0.57
2.1	0.13	311	141	95.0	0.47	1957	13	1957	15	0	2.816	0.8	0.1207	0.8	5.873	1.1	0.3547	0.8	0.67
19.1	0.05	376	348	115	0.96	1958	8.6	1989	12	2	2.817	0.5	0.1222	0.7	5.982	0.9	0.3550	0.5	0.59
12.1	0.35	207	110	63.4	0.55	1962	11	1980	23	1	2.812	0.7	0.1216	1.3	5.962	1.4	0.3557	0.7	0.46
9.1	---	412	59.5	128	0.15	1988	12	1956	12	-2	2.768	0.7	0.1205	0.7	5.974	1.0	0.3612	0.7	0.72
18.1	0.05	381	183	120	0.50	2018	7.3	2014	11	0	2.720	0.4	0.1239	0.6	6.282	0.7	0.3676	0.4	0.58
23.1	0.19	52.9	22.9	17.0	0.45	2042	19	2034	34	0	2.684	1.1	0.1254	1.9	6.440	2.2	0.3726	1.1	0.50
6.1	---	373	163	168	0.45	2722	27	2706	8.0	-1	1.903	1.2	0.1862	0.5	13.47	1.3	0.5254	1.2	0.93
Sandstone fragments from the Mendeleev Rise, sample AF05-11 (78°55'N, 177°40'W)																			
4_20.1	0.00	22.2	19.2	0.83	0.89	274	20	352	446	28	23.01	7.6	0.0535	20	0.321	21	0.0435	7.6	0.360
4_20.2	0.00	27.6	22.5	1.10	0.84	292	16	492	316	69	21.61	5.5	0.0570	14	0.364	15	0.0463	5.5	0.357
6_3.1	0.63	1984	3426	150	1.78	541	3.4	1598	33	195	11.43	0.7	0.0986	1.7	1.189	1.9	0.0875	0.7	0.353
6_5.1	0.74	2091	926	169	0.46	577	3.0	1489	27	158	10.68	0.5	0.0931	1.4	1.201	1.5	0.0936	0.5	0.360
6_19.1	0.69	1563	446	127	0.29	578	3.4	1124	41	95	10.66	0.6	0.0771	2.1	0.997	2.1	0.0938	0.6	0.286
6_9.1	0.74	1056	945	87.3	0.93	588	3.9	1360	52	131	10.46	0.7	0.0870	2.7	1.146	2.8	0.0956	0.7	0.249
6_8.1	0.65	1056	386	96.3	0.38	646	4.1	1100	52	70	9.483	0.7	0.0762	2.6	1.108	2.7	0.1055	0.7	0.249
6_1.1	0.23	1348	968	124	0.74	655	3.3	1224	26	87	9.344	0.5	0.0811	1.3	1.197	1.4	0.1070	0.5	0.364
6_7.1	0.90	478	322	46.0	0.70	679	6.5	1388	78	104	9.002	1.0	0.0883	4.0	1.352	4.2	0.1111	1.0	0.242
6_20.1	0.23	870	178	84.5	0.21	688	4.6	1192	37	73	8.874	0.7	0.0798	1.9	1.240	2.0	0.1127	0.7	0.351
6_15.1	0.84	186	155	26.5	0.86	979	16	1062	154	8	6.097	1.7	0.0748	7.6	1.691	7.8	0.1640	1.7	0.219
4_2.1	1.95	106	35.9	16.2	0.35	1037	21	1032	216	0	5.731	2.2	0.0737	11	1.772	11	0.1745	2.2	0.197
6_21.1	0.28	670	248	102	0.38	1048	6.6	1067	37	2	5.665	0.7	0.0750	1.9	1.824	2.0	0.1765	0.7	0.344
6_18.1	1.00	167	61.1	25.9	0.38	1057	13	1053	139	0	5.611	1.3	0.0744	6.9	1.828	7.0	0.1782	1.3	0.190
6_4.1	1.88	77.7	45.5	12.2	0.61														

Table 1. Continued.

Analysis number	% ²⁰⁶ Pb _c	ppm U	ppm Th	ppm ²⁰⁶ Pb*	²³² Th/ ²³⁸ U	(¹) ²⁰⁶ Pb/ ²³⁸ U Age (Ma) ± abs	(¹) ²⁰⁷ Pb/ ²⁰⁶ Pb Age (Ma) ± abs	% Dis.	(¹) ²³⁸ U/ ²⁰⁶ Pb* ±%	(¹) ²⁰⁷ Pb/ ²⁰⁶ Pb* ±%	(¹) ²⁰⁷ Pb/ ²³⁵ U ±%	(¹) ²⁰⁶ Pb/ ²³⁸ U ±%	err corr					
4_11.1	1.10	19.7	7.62	4.45	0.40	1489	43	24	3.848	3.3	0.1124	8.9	4.030	9.5	0.2599	3.3	0.344	
4_5.1	1.05	86.0	51.4	19.7	0.62	1509	23	6	3.791	1.7	0.0984	5.8	3.579	6.0	0.2638	1.7	0.286	
4_19.1	0.10	250	221	61.9	0.92	1632	13	1	3.471	0.9	0.1011	1.6	4.016	1.8	0.2881	0.9	0.478	
6_10.1	0.26	146	244	37.3	1.72	1668	19	4	3.386	1.3	0.1059	4.3	4.312	4.4	0.2954	1.3	0.285	
6_26.1	0.11	436	156	128	0.37	1895	11	-2	2.926	0.7	0.1130	1.3	5.328	1.5	0.3418	0.7	0.460	
6_22.1	0.06	201	162	86.2	0.83	2605	22	1	2.008	1.0	0.1769	0.9	12.15	1.4	0.4980	1.0	0.731	
4_18.1	0.26	213	155	95.4	0.75	2697	19	0	1.925	0.8	0.1860	1.0	13.32	1.3	0.5195	0.8	0.630	
6_24.1	0.31	96.6	37.4	44.3	0.40	2751	27	-1	1.878	1.2	0.1879	1.5	13.79	1.9	0.5324	1.2	0.619	
Sandstone fragments from the Mendeleev Rise, sample AF05-14 (79°N, 172°W)																		
4_4.1	7.30	678	166	40.3	0.25	400	4.1	37	15.60	1.1	0.0585	9.5	0.516	9.5	0.0639	1.1	0.11	
4_2.1	0.09	723	314	40.6	0.45	408	2.8	0	15.30	0.7	0.0549	1.4	0.495	1.5	0.0653	0.7	0.46	
2_23.1	0.00	357	338	22.1	0.98	449	4.2	-13	13.88	1.0	0.0544	2.0	0.541	2.2	0.0721	1.0	0.44	
2_9.1	0.06	779	456	49.2	0.60	457	3.6	-6	13.61	0.8	0.0555	1.7	0.562	1.9	0.0735	0.8	0.44	
4_3.1	0.34	578	182	39.0	0.33	486	3.5	7	12.77	0.7	0.0577	2.2	0.623	2.3	0.0783	0.7	0.33	
4_6.1	0.08	517	243	45.7	0.49	630	4.4	-2	9.734	0.7	0.0605	1.2	0.856	1.4	0.1027	0.7	0.51	
2_5.1	0.00	295	56.3	26.7	0.20	644	7.0	-4	9.520	1.1	0.0605	2.2	0.877	2.5	0.1051	1.1	0.46	
2_26.1	0.12	1372	1700	132	1.28	682	6.0	72	8.960	0.9	0.0791	1.0	1.217	1.4	0.1116	0.9	0.67	
2_12.1	2.37	707	71.0	81.4	0.10	791	7.4	80	7.649	1.0	0.0898	2.9	1.617	3.0	0.1305	1.0	0.33	
2_18.1	0.25	130	42.8	19.9	0.34	1055	11	-3	5.624	1.1	0.0732	2.4	1.795	2.7	0.1778	1.1	0.41	
2_21.1	0.05	567	336	87.2	0.61	1061	7.9	2	5.590	0.8	0.0756	1.0	1.864	1.3	0.1789	0.8	0.63	
2_16.1	0.00	21.0	5.06	3.45	0.25	1129	21	-1	5.220	2.0	0.0768	3.5	2.026	4.1	0.1914	2.0	0.50	
2_24.1	0.01	510	211	88.4	0.43	1185	10	-2	4.956	1.0	0.0788	0.9	2.192	1.3	0.2018	1.0	0.73	
2_15.1	0.00	353	112	61.5	0.33	1191	9.3	-1	4.926	0.9	0.0795	1.1	2.225	1.4	0.2030	0.9	0.62	
2_31.1	0.09	362	100	64.3	0.29	1211	9.6	0	4.840	0.9	0.0803	1.1	2.288	1.4	0.2066	0.9	0.61	
4_5.1	0.24	663	248	130	0.39	1321	8.5	5	4.396	0.7	0.0884	0.9	2.772	1.1	0.2274	0.7	0.64	
2_22.1	0.00	123	34.5	26.2	0.29	1422	14	-2	4.053	1.1	0.0888	1.5	3.021	1.9	0.2467	1.1	0.59	
4_1.1	0.00	102	68.7	22.8	0.69	1486	12	-1	3.856	0.9	0.0922	1.2	3.296	1.5	0.2593	0.9	0.60	
2_1.1	0.00	341	96.9	79.5	0.29	1548	12	0	3.684	0.9	0.0957	0.9	3.581	1.2	0.2715	0.9	0.70	
2_19.1	0.11	162	124	39.2	0.79	1594	14	1	3.563	1.0	0.0990	1.3	3.831	1.6	0.2806	1.0	0.60	
2_6.1	0.15	233	142	56.9	0.63	1612	15	70	3.520	1.0	0.1896	0.8	7.428	1.3	0.2840	1.0	0.78	
2_14.1	0.01	388	105	97.1	0.28	1648	12	-1	3.434	0.8	0.1006	0.7	4.039	1.1	0.2912	0.8	0.74	
2_10.1	0.00	248	167	63.0	0.70	1671	14	-1	3.379	0.9	0.1021	1.1	4.167	1.4	0.2959	0.9	0.65	
2_7.1	0.00	235	120	60.9	0.53	1698	13	-1	3.319	0.9	0.1032	0.9	4.287	1.3	0.3013	0.9	0.70	
2_30.1	0.03	291	89.1	77.8	0.32	1747	13	-1	3.212	0.9	0.1058	0.8	4.543	1.2	0.3113	0.9	0.73	
2_13.1	0.10	211	87.8	58.5	0.43	1804	14	1	3.096	0.9	0.1112	1.0	4.951	1.3	0.3229	0.9	0.68	
2_17.1	0.02	423	103	122	0.25	1863	15	10	2.984	1.0	0.1262	1.5	5.830	1.8	0.3351	1.0	0.54	
2_28.1	0.00	86.6	57.8	25.6	0.69	1908	20	0	2.902	1.2	0.1170	1.4	5.560	1.8	0.3445	1.2	0.66	
2_27.1	0.00	408	143	121	0.36	1913	14	19	2.895	0.8	0.1442	0.6	6.871	1.0	0.3455	0.8	0.81	
2_20.1	0.00	448	162	135	0.37	1938	13	-1	2.852	0.8	0.1177	0.6	5.688	1.0	0.3506	0.8	0.79	
2_29.1	0.00	80.5	77.5	25.1	1.00	1994	20	0	2.759	1.2	0.1220	1.3	6.100	1.7	0.3624	1.2	0.68	
2_3.1	--	801	37.0	294	0.05	2293	18	19	2.341	0.9	0.1882	0.4	11.09	1.0	0.4273	0.9	0.91	
2_4.1	0.00	51.2	57.2	19.6	1.16	2382	32	-1	2.237	1.6	0.1504	2.3	9.270	2.8	0.4470	1.6	0.57	
2_2.1	0.00	186	209	78.5	1.16	2571	20	5	2.041	1.0	0.1842	0.7	12.45	1.2	0.4901	1.0	0.81	
2_32.1	0.05	251	15.6	110	0.06	2667	23	3	1.952	1.0	0.1906	0.6	13.46	1.2	0.5123	1.0	0.87	
2_25.1	0.06	403	69.4	183	0.18	2732	18	-1	1.894	0.8	0.1861	0.5	13.54	1.0	0.5278	0.8	0.85	
2_11.1	0.00	202	6.76	96.1	0.03	2834	21	6	1.811	0.9	0.2219	0.6	16.89	1.1	0.5522	0.9	0.85	
2_8.1	0.00	112	40.3	58.6	0.37	3061	29	1	1.645	1.2	0.2344	0.7	19.64	1.4	0.6078	1.2	0.86	
Sandstone fragments from the Mendeleev Rise, sample AF05-15 (78°58'N, 173°56'W)																		
33.1	0.36	939	784	34.0	0.86	265	10	101	23.82	3.9	0.0581	4.4	0.336	5.9	0.0420	3.9	0.66	
31.1	0.00	495	160	28.7	0.33	421	4.2	-7	14.82	1.0	0.0545	2.0	0.507	2.3	0.0675	1.0	0.46	
20.1	0.10	807	160	48.1	0.21	432	3.9	38	0	14.43	0.9	0.0555	1.7	0.530	2.0	0.0693	0.9	0.48
1.1	0.00	249	18.6	34.7	0.08	968	8.3	0	6.169	0.9	0.0716	1.6	1.599	1.9	0.1621	0.9	0.49	
25.1	0.11	479	239	66.9	0.51	969	8.5	-1	6.166	1.0	0.0712	1.4	1.591	1.7	0.1622	1.0	0.56	
17.1	0.00	184	59.1	26.1	0.33	985	10	-2	6.059	1.1	0.0713	1.8	1.623	2.1	0.1650	1.1	0.53	
9.1	0.08	443	191	68.1	0.44	1060	8.6	2	5.597	0.9	0.0757	1.2	1.864	1.5	0.1787	0.9	0.61	
7.1	0.34	105	40.0	16.5	0.39	1080	13	2	5.482	1.3	0.0761	3.0	1.914	3.2	0.1824	1.3	0.39	
21.1	0.00	237	81.4	37.7	0.35	1093	12	1	5.410	1.2	0.0764	1.5	1.947	1.9	0.1848	1.2	0.64	
13.1	0.00	82.0	39.0	13.0	0.49	1096	14	3	5.396	1.4	0.0773	2.4	1.974	2.8	0.1853	1.4	0.51	
27.1	0.00	190	244	30.8	1.33	1115	12	-1	5.297	1.1	0.0762	1.7	1.983	2.0	0.1888	1.1	0.56	
5.1	0.08	209	104	35.5	0.52	1165	11	5	5.050	1.0	0.0781	1.5	2.133	1.8	0.1980	1.0	0.56	
14.1	0.17	212	140	36.5	0.68	1175	12	31	5.000	1.1	0.0955	1.8	2.632	2.1	0.1999	1.1	0.52	
30.1	0.00	179	67.3	31.7	0.39	1212	13	-2	4.836	1.1	0.0795	1.6	2.266	2.0	0.2068	1.1	0.58	
22.1	0.00	154	81.7	29.6	0.55	1299	14	-3	4.481	1.2	0.0828	1.6	2.548	2.0	0.2232	1.2	0.58	
28.1	0.18	158	107	31.5	0.70	1341	14	2	4.322	1.2	0.0875	1.9	2.792	2.2	0.2313	1.2	0.53	
4.1	0.05	406	252	91.0	0.64	1493	11	0	3.837	0.9	0.0936	1.0	3.363	1.4	0.2606	0.9	0.63	
10.1	0.00	164	61.5	37.1	0.39	1508	24	0	3.793	1.8	0.0941	1.3	3.421	2.2	0.2636	1.8	0.81	
3.1	0.06	239	171	57.9	0.74	1600	13	2	3.549	0.9	0.1006	1.0	3.909	1.4	0.2817	0.9	0.67	
23.1	0.13	127	69.3	31.6	0.56	1634	17	0	3.465	1.2	0.1006	1.6	4.002	2.0	0.2885	1.2	0.60	
32.1	--	362	22.4	90.9	0.06	1653	14	0	3.421	1.0	0.1018	1.0	4.105	1.4	0.2924	1.0	0.70	
6.1	0.14	131	159	33.1	1.26	1663	16	-2	3.398	1.1	0.1002	1.6	4.064	1.9	0.2942	1.1	0.58	
16.1	0.05	226	227	58.4	1.04	1698	15	-3	3.319	1.0	0.1016	1.1	4.221	1.5	0.3013	1.0	0.68	
2.1	--	219	174	58.2	0.82	1741	14	1	3.225	1.0	0.1077	1.0	4.606	1.4	0.3101	1.0	0.68	
15.1	0.44	220	160	60.0	0.75	1767	16	-1	3.168	1.0	0.1072	1.5	4.663	1.8	0.3154	1.0	0.58	
24.1	0.00	161	163	47.7	1.05	1911	18	-1	2.898	1.1	0.1157	1.1	5.504	1.6	0.3451	1.1	0.70	
18.1	0.00	263	208	81.2	0.81	1978	17	1	2.785	1.0	0.1							

Table 1. Continued.

Analysis number	% $^{206}\text{Pb}_c$	ppm U	ppm Th	ppm $^{206}\text{Pb}^*$	$^{232}\text{Th}/^{238}\text{U}$	(1) $^{206}\text{Pb}/^{238}\text{U}$ Age (Ma) \pm abs	(1) $^{207}\text{Pb}/^{206}\text{Pb}$ Age (Ma) \pm abs	% Dis.	(1) $^{238}\text{U}/^{206}\text{Pb}^*$ \pm %	(1) $^{207}\text{Pb}/^{206}\text{Pb}^*$ \pm %	(1) $^{207}\text{Pb}/^{235}\text{U}$ \pm %	(1) $^{206}\text{Pb}/^{238}\text{U}$ \pm %	err corr
5.1	0.40	49.6	25.7	9.89	0.54	1341 13	1343 51	0	4.323 1.1	0.0862 2.6	2.750 2.8	0.2313 1.1	0.38
9.1	0.07	138	45.5	28.1	0.34	1373 8.4	1390 20	1	4.213 0.7	0.0883 1.0	2.892 1.2	0.2374 0.7	0.54
19.1	0.12	451	162	94.1	0.37	1400 4.4	1460 11	4	4.123 0.3	0.0916 0.6	3.064 0.7	0.2426 0.3	0.51
28.1	0.03	247	107	51.6	0.45	1400 5.7	1444 15	3	4.121 0.5	0.0909 0.8	3.039 0.9	0.2426 0.5	0.50
23.1	0.10	188	74.8	39.6	0.41	1412 6.5	1455 21	3	4.083 0.5	0.0914 1.1	3.086 1.2	0.2449 0.5	0.42
27.1	0.04	96.7	63.1	20.7	0.67	1432 10	1442 22	1	4.021 0.8	0.0908 1.1	3.113 1.4	0.2487 0.8	0.56
7.1	---	186	88.3	40.1	0.49	1443 6.4	1440 16	0	3.985 0.5	0.0907 0.8	3.138 1.0	0.2510 0.5	0.51
4.1	---	126	61.3	27.7	0.50	1476 8.8	1477 19	0	3.886 0.7	0.0925 1.0	3.281 1.2	0.2573 0.7	0.56
20.1	0.04	164	60.9	37.7	0.38	1524 8.3	1667 16	9	3.751 0.6	0.1023 0.9	3.762 1.1	0.2666 0.6	0.58
14.1	0.35	53.1	38.3	12.9	0.74	1596 12	1590 32	0	3.561 0.9	0.0982 1.7	3.801 1.9	0.2808 0.9	0.45
13.1	0.05	115	112	28.2	1.01	1623 10	1658 18	2	3.494 0.7	0.1018 1.0	4.018 1.2	0.2862 0.7	0.59
21.1	0.01	511	227	126	0.46	1624 4.7	1733 8.1	7	3.490 0.3	0.1061 0.4	4.190 0.5	0.2866 0.3	0.59
10.1	0.06	149	75.3	37.8	0.52	1660 7.7	1684 16	1	3.404 0.5	0.1033 0.9	4.183 1.0	0.2938 0.5	0.52
25.1	0.00	149	45.8	38.5	0.32	1697 9.1	1698 15	0	3.320 0.6	0.1041 0.8	4.323 1.0	0.3012 0.6	0.61
16.1	0.00	302	104	84.2	0.36	1813 6.1	1871 9.2	3	3.080 0.4	0.1145 0.5	5.124 0.6	0.3247 0.4	0.60
3.1	0.08	96.2	52.5	28.0	0.56	1877 10	1917 16	2	2.958 0.6	0.1174 0.9	5.472 1.1	0.3381 0.6	0.57
29.1	0.00	258	255	76.3	1.02	1911 7.7	1906 10	0	2.899 0.5	0.1167 0.5	5.551 0.7	0.3450 0.5	0.65
12.1	---	83.7	67.7	37.1	0.84	2685 14	2681 15	0	1.936 0.6	0.1830 0.9	13.04 1.1	0.5166 0.6	0.57
30.1	0.00	40.1	17.7	18.4	0.46	2757 23	2751 18	0	1.873 1.0	0.1910 1.1	14.06 1.5	0.5338 1.0	0.69

Note:

Dots in the first column separate numbers of analyzed grains from numbers of shots.

Errors marked "+/- abs" and "+/- %" are within 1 sigma.

Pb_c and Pb* indicate common and radiogenic lead, respectively.

Columns (1) designate radiogenic Pb calculated using measured ^{204}Pb .

Relative discordancy (% Dis) is calculated as $100 \times \{[\text{age}(207/206)] / [\text{age}(206/238)] - 1\}$.

Error correlation (err corr) is the correlation of errors for Pb/U isotope ratio.

Table 2. U-Pb analytical data obtained by laser ablation coupled with MC-ICPMS-HR NEPTUNE (Thermo TM). Sandstone fragment from the Lomonosov Ridge, sample ALR07-18 (82°30'N, 140°E)

Analysis number	$^{206}\text{Pb}/^{238}\text{U}$	$\pm 1s, \text{ abs}$	$^{207}\text{Pb}/^{206}\text{Pb}$	$\pm 1s, \text{ abs}$	$^{206}\text{Pb}/^{238}\text{U}$ Age (Ma)	$\pm 1s, \text{ abs}$	$^{207}\text{Pb}/^{206}\text{Pb}$ Age (Ma)	$\pm 1s, \text{ abs}$
1.1	0.2862	0.0032	0.0955	0.0013	1636	21	1533	49
2.1	0.0401	0.0016	0.0630	0.0008	196	17	755	40
3.1	0.1685	0.0066	0.0767	0.0025	878	200	1066	220
4.1	0.1066	0.0011	0.2566	0.0048	662	22	3216	98
5.1	0.1323	0.0062	0.1383	0.0011	568	12	2132	5.3
6.1	0.0618	0.0004	0.0599	0.0011	386	5.6	526	13
7.1	0.3051	0.0026	0.1066	0.0011	1703	33	1709	56
8.1	0.1891	0.0029	0.0793	0.0009	1091	18	1143	21
9.1	0.3257	0.0017	0.1078	0.0002	1832	32	1770	6.8
10.1	0.0302	0.0018	0.0687	0.0012	170	20	818	100
11.1	0.2323	0.0015	0.0794	0.0013	1352	20	1197	35
12.1	0.3223	0.0059	0.1018	0.0008	1840	85	1644	52
13.1	0.3151	0.0013	0.1056	0.0001	1758	28	1729	2.4
14.1	0.1613	0.0096	0.1062	0.0003	933	150	1747	18
15.1	0.1229	0.0057	0.1184	0.0002	689	100	1942	14
16.1	0.3774	0.0061	0.1499	0.0003	2001	88	2334	16
17.1	0.2251	0.0106	0.0958	0.0007	1342	170	1513	38
18.1	0.3328	0.0248	0.1963	0.0041	2001	130	2731	31
19.1	0.0768	0.0010	0.1262	0.0010	479	9.5	2029	9.9
20.1	0.2478	0.0089	0.1084	0.0007	1646	120	1829	22
21.1	0.1918	0.0042	0.0968	0.0044	1169	71	1383	270
22.1	0.2841	0.0014	0.1123	0.0008	1615	29	1820	24
23.1	0.2901	0.0014	0.1061	0.0002	1653	28	1731	13
24.1	0.4707	0.0169	0.1935	0.0008	2376	100	2787	14
25.1	0.1066	0.0011	0.2566	0.0048	1303	76	1652	50
26.1	0.1066	0.0011	0.2566	0.0048	1240	100	1768	14
27.1	0.1176	0.0018	0.1209	0.0003	691	17	1961	5.5
28.1	0.2489	0.0063	0.1052	0.0004	1425	58	1715	7.1
29.1	0.1671	0.0102	0.1194	0.0005	800	30	1953	3.0
30.1	0.4831	0.0035	0.1630	0.0003	2518	56	2502	13
31.1	0.4215	0.0029	0.1548	0.0009	2312	20	2406	37
32.1	0.2801	0.0058	0.1095	0.0002	1587	130	1790	13
33.1	0.1863	0.0060	0.0976	0.0032	1141	97	1501	140
34.1	0.3239	0.0032	0.1964	0.0073	1800	28	2774	90
35.1	0.2673	0.0130	0.1079	0.0010	1379	170	1750	53
36.1	0.0904	0.0015	nd	nd	536	37	nd	nd
37.1	0.2980	0.0031	0.1136	0.0003	1631	26	1861	2.2
38.1	0.2874	0.0010	0.1046	0.0010	1626	23	1725	23
39.1	0.3542	0.0027	0.1150	0.0003	1929	30	1880	6.5
40.1	0.1796	0.0011	0.0761	0.0004	1058	37	1087	35
41.1	0.1908	0.0020	0.0810	0.0022	1126	31	1158	170
42.1	0.2816	0.0138	0.0984	0.0010	1783	130	1655	26
43.1	0.2427	0.0098	0.1129	0.0004	1531	160	1823	25
44.1	0.1549	0.0990	-0.1858	0.4786	583	190	2104	18
45.1	0.3415	0.0036	0.1092	0.0004	1934	44	1770	15
46.1	0.2253	0.0018	0.0972	0.0005	1316	30	1578	56
47.1	0.1134	0.0038	0.0894	0.0007	732	35	1400	21
48.1	0.1867	0.0037	0.1197	0.0002	1161	18	1948	2.7
49.1	0.3046	0.0029	0.1054	0.0003	1740	25	1721	3.1
50.1	0.2865	0.0057	0.1197	0.0006	1614	27	1969	4.3

Note: nd - corresponds to extremely low-Pb content for appropriate estimation of Pb/Pb and U/Pb ratios.

REFERENCES

- Akinin, V.V. and E.L. Miller, 2012. Age and Compositional Trends in the Okhotsk-Chukotka Volcanic Belt. In: D.B. Stone, J.G. Clough, D.K. Thurston (compilers): Abstracts of presentations made at ICAM VI, May 30 – June 2, 2011, Fairbanks, Alaska, UAF Geophysical Institute Report UAG-R-335.
- Akinin, V.V., J.M. Amato, E.L. Miller, E. Gottlieb and G.O. Polzunenkov, 2012. New Geochronological Data on pre-Mesozoic Rocks (Neoproterozoic to Devonian) from the Arctic Part of the Chukotka Peninsula. In: D.B. Stone, J.G. Clough, D.K. Thurston (compilers): Abstracts of presentations made at ICAM VI, May 30 – June 2, 2011, Fairbanks, Alaska, UAF Geophysical Institute Report UAG-R-335.
- Andronikov, A., S. Mukasa, L.A. Mayer, K. Brumley, 2008. First Recovery of Submarine Basalts from the Chukchi Borderland and Alpha/Mendeleev Ridge region, Arctic Ocean. EOS Trans. AGU, 89 (53), Fall Meet. Suppl., Abstract V41D-2124.
- Bischof, J.F., D.L. Clark and J.-S. Vincent, 1996. Origin of ice-rafted debris: Pleistocene paleoceanography in the western Arctic Ocean. *Paleoceanography*, Vol. 11, p. 743-756.
- Brumley, K., E.L. Miller, L.A. Mayer, A. Andronikov, J.L. Wooden, T.A. Dumitru, B. Elliott, G.E. Gehrels and S.B. Mukasa, 2010. Petrography and U-Pb detrital zircon geochronology of metasedimentary strata dredged from the Chukchi Borderland, Amerasia Basin, Arctic Ocean. Abstract T31A-2144 presented at 2010 Fall Meeting, AGU, San Francisco, Calif., 13-17 Dec.
- Brumley, K., E.L. Miller, L.A. Mayer, J.L. Wooden, T.A. Dumitru, 2011. Petrography and U-Pb zircon geochronology of Caledonian age orthogneisses dredged from the Chukchi Borderland, Arctic Ocean. Abstract T51K-07 presented at 2011 Fall Meeting, AGU, San Francisco, Calif., 5-9 Dec.
- Clark, D.L., R.R. Whitman, K.A. Morgan and S.D. Mackey, 1980. Stratigraphy and glaciomarine sediments of the Amerasian Basin, central Arctic Ocean. *Spec. Pap. Geol. Soc. Am.*, 181, p. 1–57.
- Clark, D.L., B.J. Kowallis, L. Gordon Medaris and A.L. Deino, 2000. Orphan Arctic Ocean metasediment clasts: Local derivation from Alpha Ridge or pre-2.6 Ma ice rafting? *Geology*, v. 28, p. 1143-1146.
- Database for ECS Dredge Samples at NOAA/NGDC
- Grantz, A., D. Clark, R. Phillips and S. Srivastava, 1998. Phanerozoic stratigraphy of Nortwind Ridge, magnetic anomalies in the Canada Basin and the geometry and timing of rifting in the Amerasia Basin, Arctic Ocean. *Geol. Soc. Am. Bull.*, v. 110, no. 6, p. 801-820.
- Grantz, A., V.L. Pease, D.A. Willard, R.L. Phillips and D.L. Clark, 2001. Bedrock cores from 89° North: Implications for the geologic framework and Neogene paleoceanography of Lomonosov Ridge and a tie to the Barents shelf. *Geol. Soc. Am. Bull.*, v. 113, no. 10, p. 1272-1281.
- Grantz, A., P.E. Hart and V.A. Childers, 2011a. Geology and tectonic development of the Amerasia and Canada Basins, Arctic Ocean. In: Spencer, A. M., Embry, A. F., Gautier, D. L., Stoupakova, A. V. & Sørensen, K. (eds) *Arctic Petroleum Geology*. Geological Society, London, *Memoirs*, v. 35, p. 771-799, doi:10.1144/M35.50.
- Grantz, A., R.A. Scott, S.S. Drachev, T.E. Moore and Z.C. Valin, 2011b. Sedimentary successions of the Arctic Region (58° to 90° N) that may be prospective for hydrocarbons. In: Spencer, A. M., Embry, A. F., Gautier, D. L., Stoupakova, A. V. & Sørensen, K. (eds) *Arctic Petroleum Geology*. Geological Society, London, *Memoirs*, v.35, p.17–37, doi: 10.1144/M35.2.
- Hadlari, T., W.J. Davis, K. Dewing, L.M. Heaman, Y. Lemieux, L. Ootes, B.R. Pratt and L.J. Pyle, 2012. Two detrital zircon signatures for the Cambrian passive margin of northern Laurentia highlighted by new U-Pb results from northern Canada. *Geological Society of America Bulletin*, v. 124, no. 7-8, p. 1155-1168, doi: 10.1130/B30530.1.
- Jackson, H.R., T. Dahl-Jensen and the LORITA working group, 2010. Sedimentary and crustal structure from the Ellesmere Island and Greenland continental shelves onto the Lomonosov Ridge, Arctic Ocean. *Geophysical Journal International* 182, p. 11–35, doi:

10.1111/j.1365-246X.2010.04604.x

- Jokat, W., 2003. Seismic investigations along the western sector of Alpha Ridge, Central Arctic, Ocean. *Geophys. J. Int.*, v. 152, p. 185–201.
- Jokat, W., 2009. The expedition of the research vessel “Polarstern” to the Arctic in 2008 (ARK-XXIII/3), *Berichte zur Polar- und Meeresforschung* (Reports on Polar and Marine Research), Bremerhaven, Alfred Wegener Institute for Polar and Marine Research, 597, 266 pp.
- Kaban’kov, V.Ya., I.A. Andreeva, V.N. Ivanov V.N., V.I. Petrova, 2004. The geotectonic nature of the Central Arctic morphostructures and geological implications of bottom sediments for its interpretation. *Geotektonika*, no. 6, 33-48 (in Russian). English translation: *Geotectonics*, 2004, vol. 38, part 6, 430-442.
- Kaban’kov, V.Ya., I.A. Andreeva, V.V. Krupskaya, D.V. Kaminsky, E.I. Razuvaeva, 2008. New data on the composition and origin of bottom sediments in the southern Mendeleev Ridge, Arctic Ocean. *Doklady Akademii Nauk*, vol. 419, no. 5, 653–655 (in Russian). English translation: *Doklady Earth Sciences*, 2008, vol. 419A, no. 3, 403-405.
- Kaban’kov, V.Ya., I.A. Andreeva, B.G. Lopatin, 2012. Geology of the Amerasia Sub-Basin. In: *Geological-geophysical features of the Arctic Region. Proc. NIIGA-VNIOkeangeologia*, Vol. 223, Ser. 8 (in Russian). In press.
- Korago, E.A., A.N. Evdokimov and N.M. Stolbov, 2010. Late Mesozoic mafic magmatism of the northwestern Eurasian continental margin. “*VNIOkeangeologia*”, St. Petersburg, 174 pp. (in Russian).
- Krylov, A.A., I.A. Andreeva, C. Vogt, J. Backman, V.V. Krupskaya, G.E. Grikurov, K. Moran and H. Shoji, 2008. A shift in heavy and clay mineral provenance indicates a middle Miocene onset of a perennial sea ice cover in the Arctic Ocean. *Paleoceanography*, v. 23, p. 1-10, PA1S06, doi:10.1029/2007PA001497.
- Laverov, N. P., L.I. Lobkovsky, M.V. Kononov, N.L. Dobretsov, V.A. Vernikovskiy, S. D. Sokolov and E.V. Shipilov, 2013. A geodynamic model of the evolution of the Arctic Basin and adjacent territories in the Mesozoic and Cenozoic and the outer limit of the Russian continental shelf. *Geotectonics*, no. 1, p. 1-35 (in Russian).
- Miller E.L., J.Toro, G. Gehrels, J.M. Amato, A. Prokopyev, M.I. Tuchkova, V.V. Akinin, T.A. Dumitru, T.E. Moore and M.P. Cecile, 2006. New insights into Arctic paleogeography and tectonics from U-Pb detrital zircon geochronology. *Tectonics*, v. 25, no. 3, p. 1-19, doi:10.1029/2005TC001830.
- Phillips, R.L. and A. Grantz, 2001. Regional variations in provenance and abundance of ice-rafted clasts in Arctic Ocean sediments: implications for the configuration of late Quaternary oceanic and atmospheric circulation in the Arctic. *Marine Geology*, v. 172, p. 91-115.
- Rekant, P.V., M.N. Pyatkova, I.D. Nikolaev and E.E. Taldenkova, 2012. Bottom samples from the Geophysicists Spur as lithological representatives of the Lomonosov Ridge basement (Arctic Ocean). *Geology and geoecology of the Euro-Asian continental margins, special issue 4: Geology and mineral resources of the Euro-Asian marginal seas, Moscow, GEOS*, p. 29-40 (in Russian).
- Van Wagoner, N.A., M. Williamson, P. Robinson and I. Gibson, 1986. First samples of acoustic basement recovered from the Alpha Ridge, Arctic Ocean: new constraints for the origin of the ridge, In: Johnson, G. L. & Kaminuma, K. (eds.) *Polar Geophysics. J. Geodyn.*, v. 6, p. 177-196.
- Williams, I.S., 1998. U-Th-Pb Geochronology by Ion Microprobe. In: McKibben, M.A., Shanks III, W.C. and Ridley, W.I. (eds.) *Applications of microanalytical techniques to understanding mineralizing processes. Reviews in Economic Geology*, v. 7, p. 1-35.

The structural integrity of the Lomonosov Ridge with the North American and Siberian continental margins

V. Poselov¹, V. Butsenko¹, A. Chernykh¹, V. Glebovsky¹, H. R. Jackson², D. P. Potter², G. Oakey², J. Shimeld² and C. Marcussen³

¹I.S. Gramberg Research Institute for Geology and Mineral Resources of the World Ocean 'VNIIOkeangeologia', 1 Angliysky Ave., 190121 St. Petersburg, Russia

²Geological Survey of Canada Atlantic, Box 1006 Dartmouth, N.S., B2Y 4A2 Canada

³Geological Survey of Denmark and Greenland (GEUS), Øster Voldgade 10, 1350 Copenhagen K, Denmark

ABSTRACT

The Lomonosov Ridge crosses the Arctic Ocean connecting the North American and Siberian margins. The Ridge consists of a number of linear, parallel topographic highs that deepen toward the adjacent basins where they are buried by sediments. Bathymetric, seismic reflection, refraction, and potential field data show that the structure of the Ridge is continuous with the adjacent continental margins. The sedimentary section on the Lomonosov Ridge can be traced from the North American margin across the Pole to the Siberian margin. A reflection profile shot in the transition from the Siberian margin to the Lomonosov Ridge demonstrates that the strong regional unconformity at the base of the hemipelagic sedimentary unit. The entire sedimentary section and the acoustic basement can be clearly followed from the margin along the Ridge. The continuity of sedimentary and crustal units is confirmed on the coincident wide angle seismic reflection/refraction profile. Magnetic data at the intersection of the Ridge with the North American margin reveal the edge of the Pearya Terrane extending from Ellesmere Island onto the Lomonosov Ridge. Furthermore, with the Eurasia Basin closed the magnetic anomalies associated with Early Cretaceous dyke swarms can be traced from Franz Josef Land via the Lomonosov Ridge to the Alpha Ridge and from the North American polar margin to the Alpha Ridge. The distribution of the dykes suggests that since their emplacement the Lomonosov Ridge has been stable with respect to the North American margin and remained in close proximity to the Barents Sea margin until separation of the North American and Eurasian plates, as predicted by plate reconstructions based on magnetic lineations. The geomorphological and geophysical data presented in the paper do not

support earlier interpretations of the Lomonosov Ridge as a separate microcontinent.

INTRODUCTION

The Lomonosov Ridge, approximately 1700 km long, has a sinuous shape (Fig. 1). The Ridge is named after the Russian polymath Mikhail Vasilyevich Lomonosov. It was first mapped by the Russian high latitude air borne surveys of 1948. In 1954 it was shown on the bathymetric map of the Arctic Ocean (Burkanov 1954). The first bathymetric measurements on the Lomonosov Ridge available in western literature were made close to the pole during the First (1967) and Second (1969) Canadian North Pole expeditions (Weber 1983; Weber and Sweeney 1985).

The Lomonosov Ridge width varies between 50 and 200 km. Its flanks rise steeply from the 3900 - 4200 m deep basins on each side to a depth of typically 1000 - 1300 m below sea level (Weber 1979; Bjork et al. 2007). The steep sides and the saw-toothed crest of the Ridge are typical of continental block faulting. Seismic reflection profiles that show an angular unconformity in the sedimentary section on the Ridge beneath the drilled Tertiary section (Jokat et al. 1992) have a distinct continental character. The refraction velocities on the Ridge are comparable with those on the Barents and Kara seas shelves (Forsyth and Mair 1984), and gravity models controlled by wide angle reflection/refraction (WAR) profiles (Weber and Sweeney 1985) also indicate a continental origin of the Ridge. In addition, the fit of the Lomonosov Ridge morphological configuration with that of the conjugate Eurasia Basin margin suggests that the Ridge is a continental sliver separated by seafloor spreading from the Barents-Kara seas crustal block (e.g. Srivastava and Tapscott 1986).

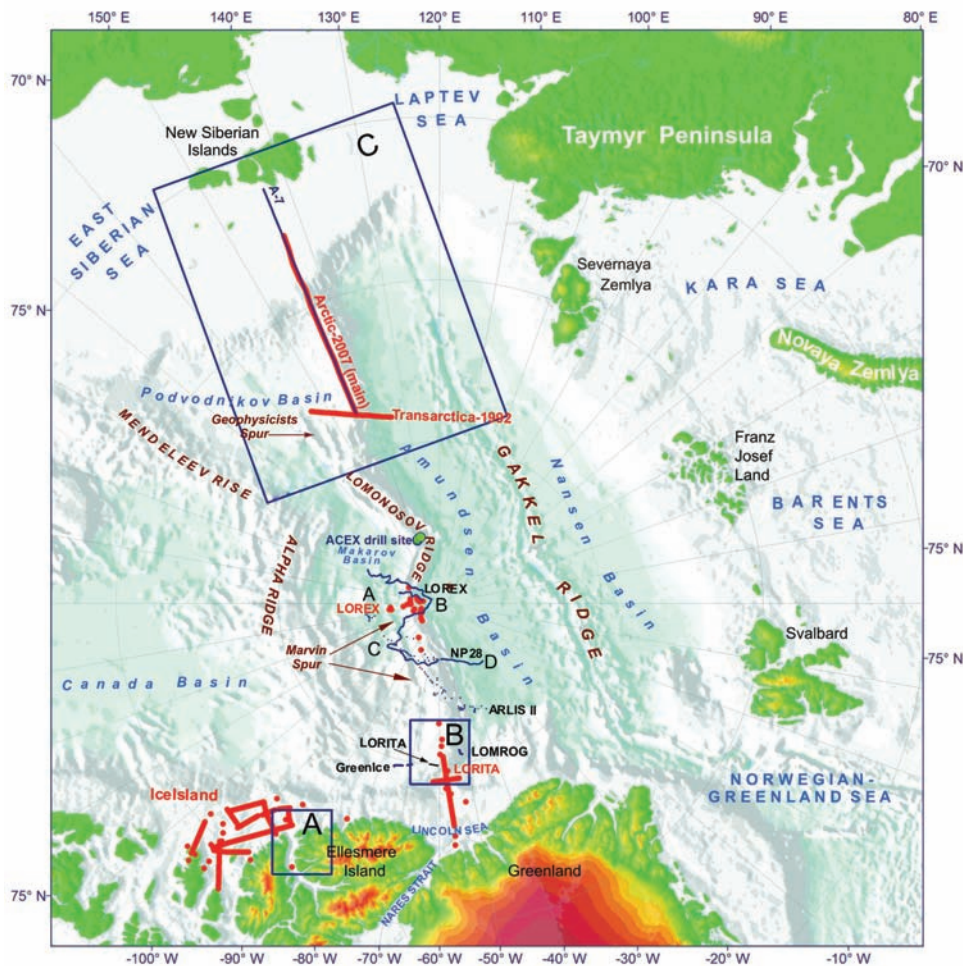


Fig. 1. Bathymetric map of the Arctic Ocean showing the location of seismic reflection lines in black and wide angle reflection/refraction lines in red described in the text. The black boxes labeled A and B are the position of the magnetic surveys shown in Figure 10. The black box labeled C is the location of gravity and magnetic surveys presented in Figure 11.

The Lomonosov Ridge divides the Arctic Ocean into two major deep basins (Fig. 2a): the Eurasia and the Amerasia basins. It has been called a double-sided continental margin (Jokat et al. 1992). The Eurasia Basin with its two sub-basins, the Amundsen and Nansen basins (Fig. 1), was created by Cenozoic sea floor spreading revealed by lineated seafloor spreading anomalies. This is due to the difficulties in interpreting chaotic high amplitude magnetic anomalies associated with the Alpha-Mendeleev ridges, the weak magnetic lineations in the Canada Basin and the scarcity of bedrock samples. Several different geodynamic models have been suggested for the Amerasia Basin, such as rifting of Alaska from the Lomonosov Ridge requiring transform motion along the Queen Elizabeth Islands margin

of North America (e.g. Ostenso 1974). Another transform model has the Siberian margin rifted from the Queen Elizabeth Islands with shearing along the Alaska margin and Lomonosov Ridge (e.g. Herron et al. 1974). The rotational model for the opening of the Amerasia Basin with Alaska rifted away from the Queen Elizabeth Islands margin was first suggested by Carey (1958) and continues to be the option supported by the majority of researches (e.g. Cochran et al. 2006). The rotational model is consistent with paleomagnetic data from Alaska (Halgedahl and Jarrard 1987) and restores Mesozoic geology of the Queen Elizabeth Islands with that on the Alaskan margin (Embry 1990). The rotational option predicts that the Amerasia Basin side of the Lomonosov Ridge is a sheared margin.

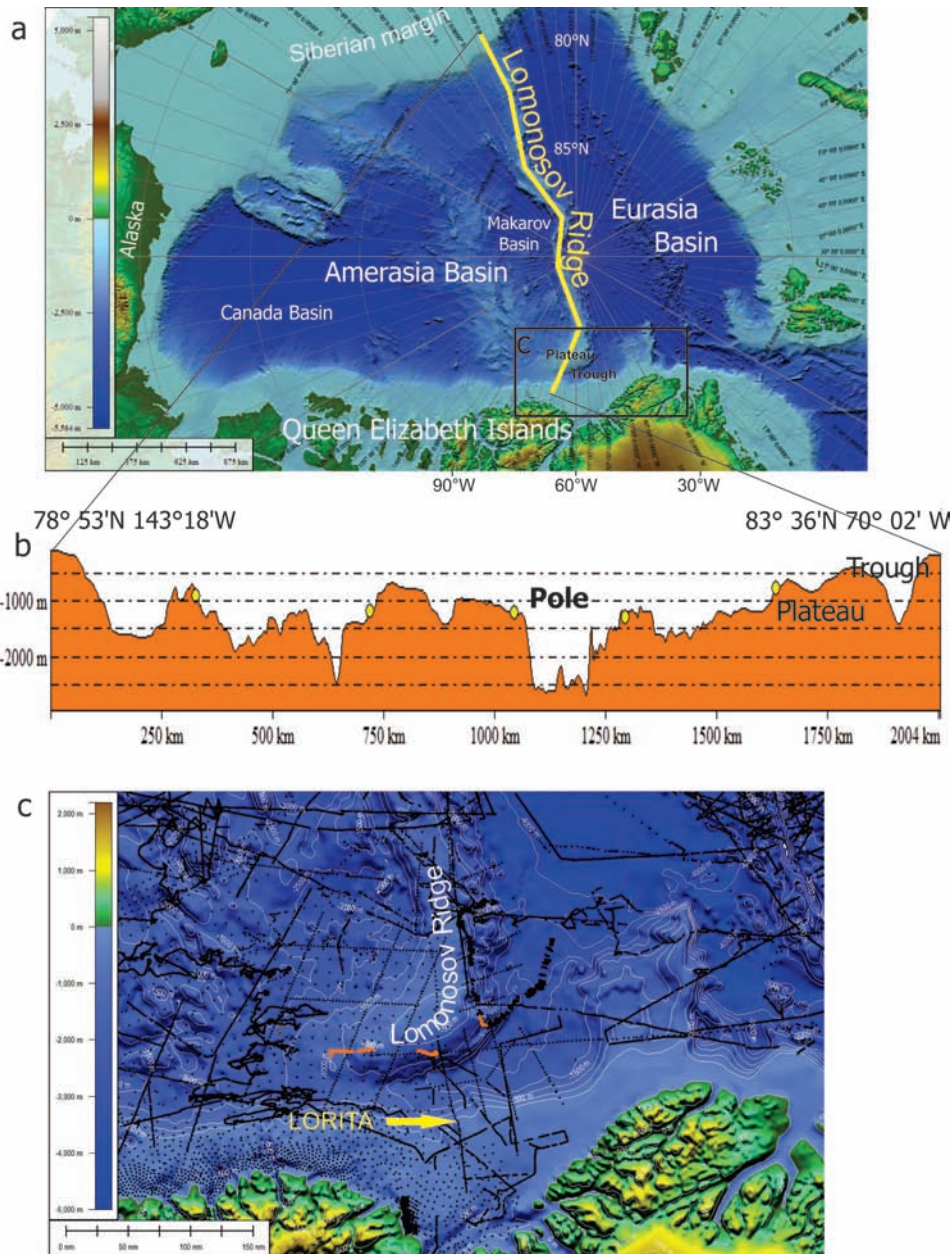


Fig. 2. Bathymetric map of the Arctic Ocean (section ‘a’) with the yellow line along the length the Lomonosov Ridge indicating the position of the bathymetric profile presented in section ‘b’. The black box labeled ‘c’ indicates the region of detailed bathymetric surveys. The dots on section ‘c’ are the locations of spot soundings. The north-south line with closely spaced dots is the location of the LORITA wide angle reflection/refraction profile. The orange short lines are the location of seismic reflection profiles.

Significant new data collected by agencies in Canada, Denmark and Russia over the Lomonosov Ridge (Fig. 1) are presented that provide information on the continental affinities of the Ridge and its transition to the adjacent continental margins. A major question addressed is whether the geophysical data can be explained by plate reconstructions with the Lomonosov Ridge remaining fixed with respect to the continental margins of North America and Siberia, or whether displacement of the Ridge

relative to the margins along major transform faults is required.

In 1992 for the first time, the Polar Marine Geosurvey Expedition (PMGE) under the auspices of the Ministry of Natural Resources and Environment of the Russian Federation carried out WAR observations over the Lomonosov Ridge and the adjacent Amundsen and Podvodnikov-Makarov basins (Fig. 1). In addition, aeromagnetic mapping in a belt 100 km wide was acquired along the WAR profile.

In 2007, VNIIOkeanologia and the Marine Arctic Geological Expedition (MAGE) were charged by the Federal Agency for Mineral Resources of the Russian Federation (Rosnedra) to perform integrated geological and geophysical investigations on the Lomonosov Ridge and the adjacent Siberian Shelf. The range of scientific observations included WAR measurements, multichannel seismic reflection profiling and potential field (gravity and magnetic) measurements in a belt 100 km wide along the WAR line.

The Geological Surveys of Canada (GSC) and Denmark and Greenland (GEUS) acquired WAR data and limited reflection profiling over the junction of the Lomonosov Ridge with the Greenland and Ellesmere Island continental margin in 2006. In 2007 and 2009 on LOMROG I and II ship-based programs, seismic reflection profiles on the Lomonosov Ridge were collected by GEUS that are also shown here.

In this paper the Lomonosov Ridge will be described from the continental shelves towards the North Pole through successive data sets beginning with bathymetry and continuing with data that investigate the sedimentary and crustal structure.

BATHYMETRY

The contours on the International Bathymetric Chart of the Arctic Ocean (IBCAO version 2.0) (Jakobsson et al. 2008) are developed from data gridded at a 2 km interval (Fig. 1). The data distribution is irregular and care must be taken assigning confidence to the mapped features. Due to the perennial ice cover, the bathymetric data on the Lomonosov Ridge adjacent to Greenland and Ellesmere Island consists of spot soundings augmented by sparse submarine single beam profiles and ship based multibeam data. The distribution of recent transects with spot soundings ensures that the representation of the major features in this region is realistic (Fig. 2c).

The bathymetry data reveal several distinct zones from the shelf adjacent to Ellesmere Island along the Lomonosov Ridge towards the North Pole. The shelf is characterized by water depths of less than 500 m. Further seaward a bathymetric trough that reaches a maximum depth of 2300 m and width of 75 km at the position of the LORITA refraction line (Fig. 1 and 2) is distinct. Northward there is a plateau with a minimum water depth of about 500

m. At the 1000 m contour the plateau is about 200 km wide. Further north the Lomonosov Ridge has a width of about 70 km at the 1500 m contour. On a bathymetric profile (Fig. 2b) slightly westward of the location of the LORITA profile, the topography across the trough and over the plateau is not significantly different from the regional variations observed along the length of the Lomonosov Ridge. For instance, greater water depths are observed near the Pole where there is an internal valley in the Ridge or towards the Siberian margin (at about 700 km on figure 2b) where one limb of the sub-parallel ridges that form the Lomonosov Ridge is crossed.

The transition from the Siberian margin to the Lomonosov Ridge (Fig. 1 and 2) is smooth for the first 200 km from the shelf. The water depth increases steadily from about 200 m to 1750 m over about 200 km. Further northward the Lomonosov Ridge is made up of a complex of ridges and basins as seen in the rugged topography. A consistent feature of this region of the Lomonosov Ridge is a series of parallel ridges with a width of over 200 km extending south to at least 82°30' N and, based on gravity data, perhaps to the Siberian Margin (Cochran et al. 2006).

SEISMIC REFLECTION DATA

Near the North American margin

The ice cover in the Arctic Ocean hinders shipping. This is a particular problem for vessels towing seismic reflection equipment. In order to acquire seismic reflection data, a number of different platforms have been used that include drifting ice stations and icebreakers. The data coverage of the Lomonosov Ridge, adjacent to Greenland and Ellesmere Island, where the ice is the thickest and under compression, is limited. Only three seismic reflection profiles have been acquired in this area: the GREENICE and LORITA profiles from drifting ice camps and the ship based LOMROG 1 experiment (Fig. 3).

The length of the profiles varied from 55 km, 32 km to 22 km respectively. The seismic sections from drifting ice camps show that the sedimentary cover increases in thickness with distance away from the centre of the plateau. This is clearly seen on the GREENICE profile (Fig. 3). Near the crest of Lomonosov Ridge (550 m water depth) a thin veneer (0.05 s) of unconsolidated sediments overlies the

acoustic basement that displays occasional dipping reflections. The sedimentary section thickens westward. On the LORITA reflection profile, 70 km to the east of the GREENICE profile and closer to the centre of the plateau (Jackson and Dahl-Jensen et al. 2010), and on the LOMROG profile, the sedimentary section is thin to absent, while basement reflection characteristics are similar to those observed on the GREENICE profile. On all three profiles coherent dipping reflections are visible only near the top of acoustic basement with a velocity of 5.9-6.5 km/s (Jackson and Dahl-Jensen et al. 2010). The limited seismic penetration beneath the thin sedimentary cover is consistent with high velocity rocks. Possible geological interpretations for the acoustic basement are calcareous or basaltic rocks. If calcareous, the dipping units would be due to fault blocks; however there is no indication of faults. The dipping reflectors

observed in all the profiles could also be volcanic flows. When the seismic profiles are viewed in conjunction with the associated high frequency magnetic anomalies, it suggests that the basement is composed of volcanic rocks (Jackson and Dahl-Jensen et al. 2010).

The location of seismic reflection profiles between the plateau and the Pole is shown in Figures 1 and 4. The data were collected by the drifting ice camps NP28 (Langinen et al. 2008) and ARLIS II (Ostenso and Wold 1977) which zigzagged from the Amundsen Basin to Makarov Basin across the Ridge crest. The ARLIS II seismic section shows a flat top of the Lomonosov Ridge with sedimentary thickness of about 500 m thinning toward the Pole where bedrock pierces the seafloor in two locations (Weber and Sweeney 1985). Close to the Pole, steps in the seabed topography suggest block-faulting.

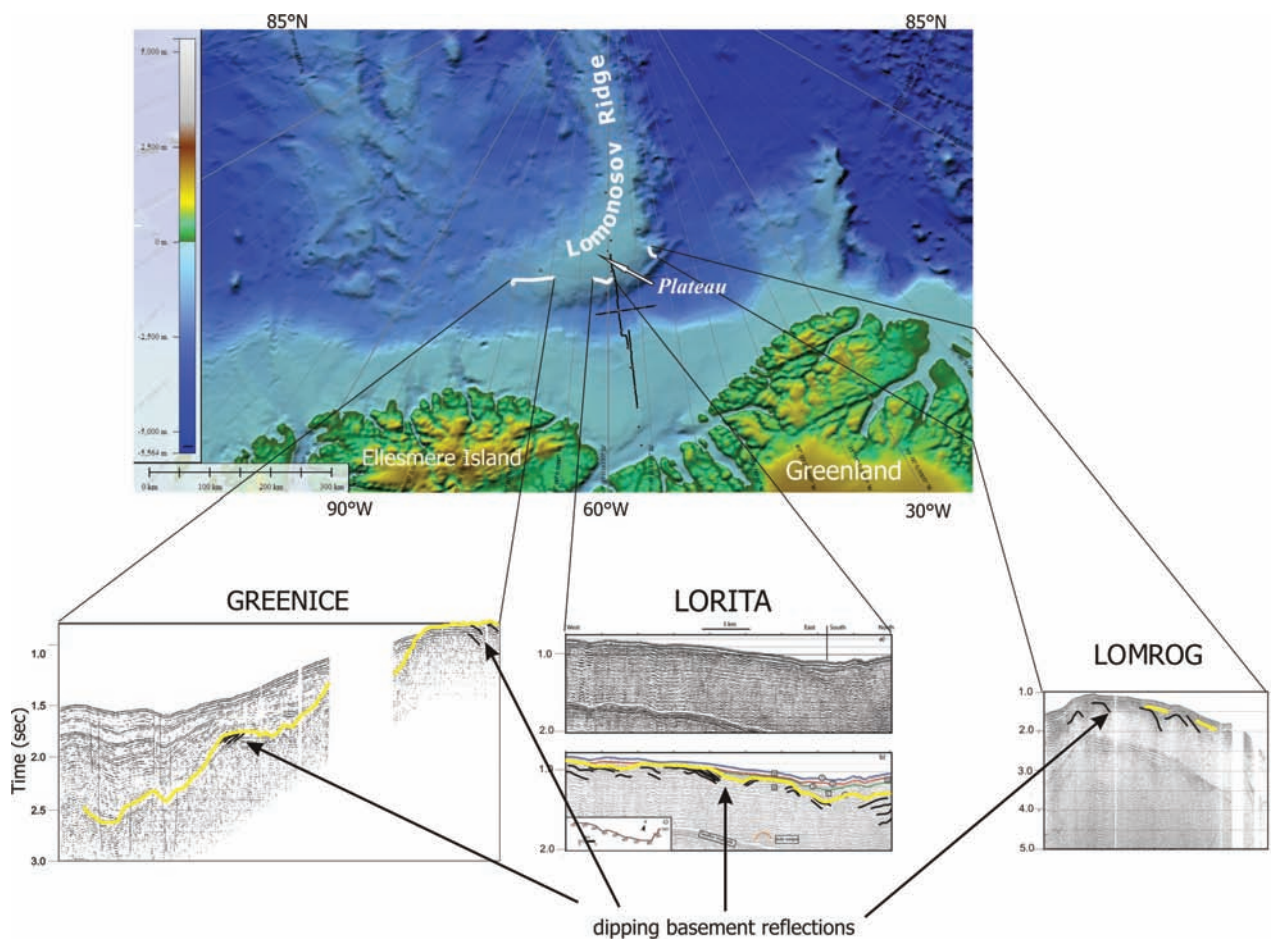


Fig. 3. Location of seismic data on the Lomonosov Ridge plateau and next to the Ellesmere Island and Greenland. The short white lines are the reflection profiles GREENICE (modified from Kristoffersen and Mikkelsen 2006), LORITA (after Jackson and Dahl-Jensen et al. 2010) and LOMROG (data from the LOMROG I experiment). The black line and dots are the position of the receivers and shots from the LORITA refraction profile.

The most continuous reflection data (Fig. 4) were obtained by the drifting ice camp NP28 (Langinen et al. 2008). The drift track crossed the Lomonosov Ridge three times between 88°N and the major bend in the Ridge near the Pole. The steeper continuous slope of the Lomonosov Ridge towards the Makarov Basin contrasts with the several ridges that step down to the Amundsen Basin. On the NP 28 seismic profiles as described by Langinen et al. (2008), a prominent flat-lying composite reflection package is seen from the seafloor to a depth of a few hundred meters. The base of this reflection package is often accompanied by a sharp increase in P-velocity and defines a major discontinuity, called the Lomonosov Unconformity (LU). The underlying reflections are variable in intensity and in dip. Between the LU and acoustic basement there is a variety of units, some highly reflective (with reflections concordant or discordant to the upper units), while others are sporadically reflective. The thickness of these units varies greatly not exceeding 1.5 km.

Marvin Spur

Marvin Spur is a linear ridge 20-50 km wide in the Makarov Basin (Fig. 4). The Marvin Spur is sub parallel to the Lomonosov Ridge at a distance of about 50 km from it on the Amerasia Basin side. The bathymetric depression between the Spur and the Ridge narrows toward the North American polar margin. Seismic lines that cross both the Lomonosov Ridge and Marvin Spur (Langinen et al. 2008, Fig. 4) illustrate their similar sedimentary stratigraphy. Fine-layered sediments, up to 0.5 s (two-way travel time) are visible on top of the Spur that have the same reflection characteristics as identified on the Lomonosov Ridge. Equally low or slightly greater thickness of sedimentary cover was recorded on the Spur by Polarstern-1998 seismic data (Jokat, 2005). On the profile C to D (Langinen et al. 2008) the basement is of variable depth and not well imaged but seems to have a blocky topography. The Spur, on the NP 28 data, appears as an opaque block with no consistent internal seismic structure. The Oden seismic reflection profile crosses the Marvin Spur at its extremity in the northernmost Makarov Basin (Fig. 4). The line is located slightly more distant from the Lomonosov Ridge than point A of the NP 28 profile. The LOMROG profile (Hopper et al.

2009) indicates normal faults in the basement, as well as stratigraphic reflectivity below the basement. The character of the reflectivity implies a continental origin of the crust (Hopper et al. 2009). Gravity data (Cochran et al. 2006) and limited seismic evidence (Langinen et al. 2008) suggest that the Marvin Spur continues in the Makarov Basin beneath the sedimentary section. We believe that the parallel continental feature of the Marvin Spur was formed by fragmentation of the North American section of the Lomonosov Ridge. Towards the North American margin the Marvin Spur merges with the Lomonosov Ridge further supporting a common geological development.

The Lomonosov Ridge from the Pole toward Russia

Due to the lighter ice conditions, from the North Pole to the Siberian margin, more continuous seismic reflection profiles are available, including a lengthy high-resolution line 'A-7' that followed the WAR profile (Fig. 1). From the North Pole towards the Siberian margin, especially between 89°N and 85°N, there are noticeable changes in trend and differences in elevations of blocks in a series of en echelon horsts and grabens oblique to the main ridge (Lomonosov Ridge complex) (Kristoffersen 2001).

Multichannel seismic reflection data 'A-7'

The 'A-7' line (832 km) extended from the New Siberian Islands to 83.5° N (Fig. 1). A Sercel Seal seismic work station and Sercel streamer with an active length of 8,100 m were used as the recording equipment. Bolt airguns with a total volume of 3400 in³ were the seismic source. The recording parameters were: number of channels 648; group length 12.5 m; streamer depth 9 m; geophone group interval 12.5 m; record time 12 s; sample rate 2 ms. Source parameters: shot point spacing 37.5 m; airgun submersion depth 6 m. CDP fold – 108. Navigation was accomplished using the GPS Spectra system with the accuracy of at best 2 m.

The principal feature of the sedimentary cover along the entire line is a unit with distinct hemipelagic reflection characteristics overlying a strong unconformity. This unconformity is associated with the major depositional hiatus recorded in ACEX core data (Backman et al. 2006) and separates the Middle Eocene shallow-water rocks rich in

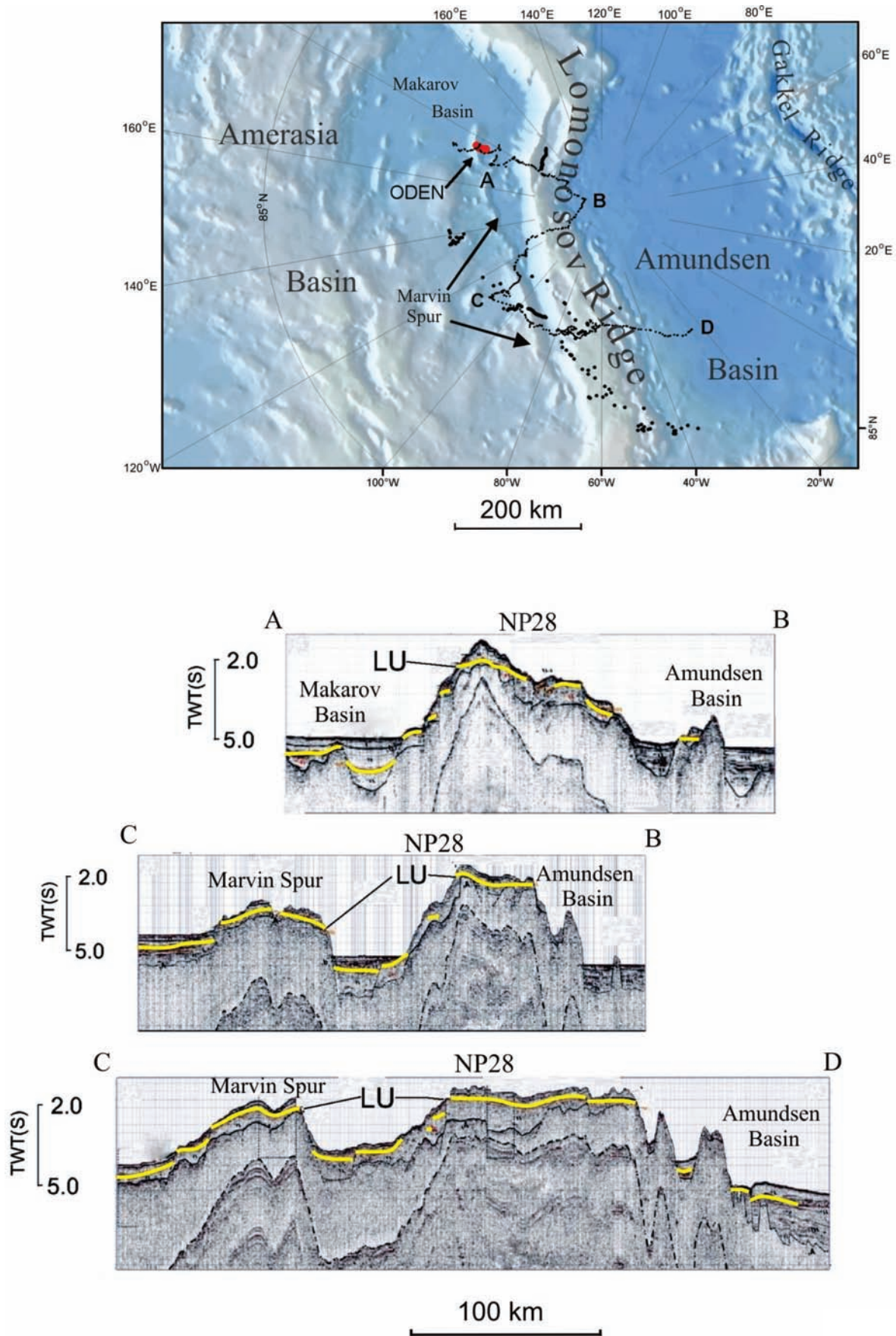


Fig. 4. Location of seismic reflection lines that cross the Lomonosov Ridge north of the plateau. Seismic sections AB, BC and CD are the portions of the NP 28 profile modified from Langinen et al. (2008). The position of the 'Oden' (LOMROG) seismic reflection profile is marked in red (Hopper et al. 2009). LU - the Lomonosov Unconformity.

biogenic material from the Early/Middle Miocene hemipelagic deposits with only minor amount of biogenic remains. This seismic boundary is recorded throughout much of the Central Arctic as a regional pre-Miocene unconformity RU (Butsenko and Poselov 2006) (Fig. 5 and 6a). An older unconformity also observed on ‘A-7’ line is believed to be related to post-Campanian depositional break (PCU). Such identification is based on correlation with the AWI 91090 profile which was tied to the ACEX core data (Bruvoll et al. 2010).

Southward along the Lomonosov Ridge and downslope to the Makarov Basin these unconformities merge, while the character of overlying Miocene-Quaternary hemipelagic unit remains similar to that observed in the northernmost part of ‘A-7’ line. At the approach to the Laptev Sea shelf the merged unconformities are again divided (Fig. 5 and 6a) and can be correlated with unconformities LS1 and LS2 on the Laptev Sea shelf (Franke et al. 2001).

Stratigraphic subdivision of the sedimentary cover along the ‘A-7’ line is based on the age of these major unconformities and enables recognition of 5 units (Fig. 5): (1) pre-Upper Cretaceous, (2) Upper Cretaceous, (3) Paleogene, (4) Miocene and (5) Pliocene-Quaternary. On the Lomonosov Ridge

the Neogene-Quaternary deposits virtually rest on the Upper Cretaceous formations.

Continuous tracing of the Cretaceous-Cenozoic sedimentary units from the Siberian shelf to the Lomonosov Ridge through the transition zone and the persistence of seismostratigraphic and seismic facies characteristics are consistent with the lack of observable displacement in the acoustic basement (Fig. 6b). We interpret this as evidence of the absence of any major structural boundary in the transition zone.

WIDE ANGLE REFLECTION/REFRACTION *North American polar margin*

A summary of a WAR survey along the margin near Ellesmere Island (Fig. 1) by Forsyth et al. (1998) is included for comparison with the data on the Lomonosov Ridge. The Ice Island surveys were conducted southwest of the junction of the Lomonosov Ridge with the margin in 60-km segments with 5-km recorder spacing. The data were modeled by ray tracing. Five velocity units were determined. The shallowest, a 1.9-3.4 km/s unit of unconsolidated to lightly compacted sedimentary rocks interpreted to be clastics of Tertiary age (Forsyth et al. 1998). Beneath this unit is a 4.3-5.2 km/s unit that could be an equivalent of an onshore

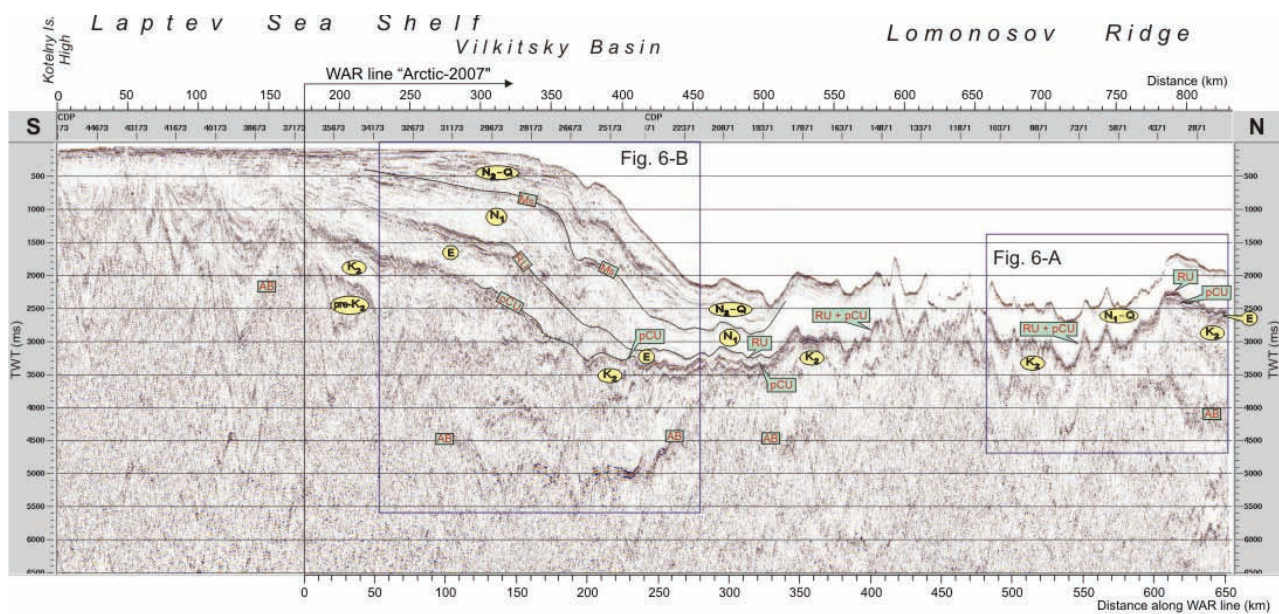


Fig. 5. A-7 multichannel migrated seismic reflection section. AB – acoustic basement, pCU – post-Campanian unconformity, RU – regional pre-Miocene unconformity, Ms – Messinian regression. The unconformities pCU, RU and Ms correspond to LS1, LS2 and LS3 of Franke et al. (2001), respectively. Boxes indicate the sections enlarged in Figure 6.

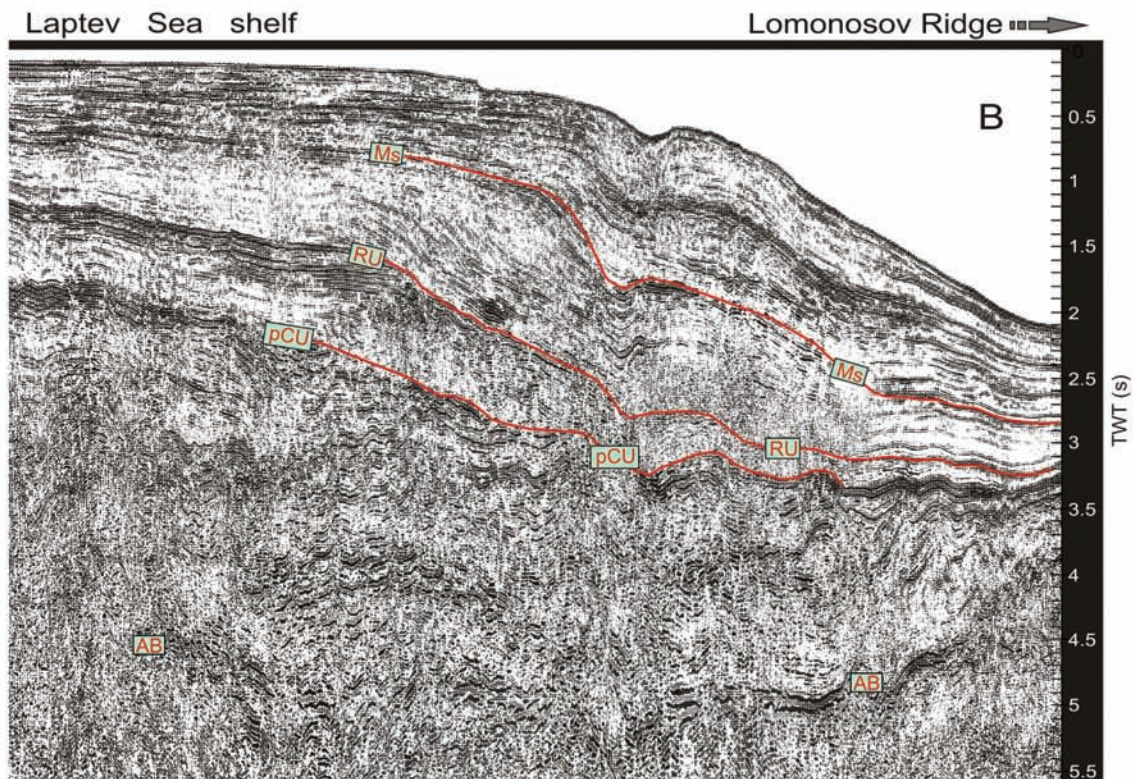
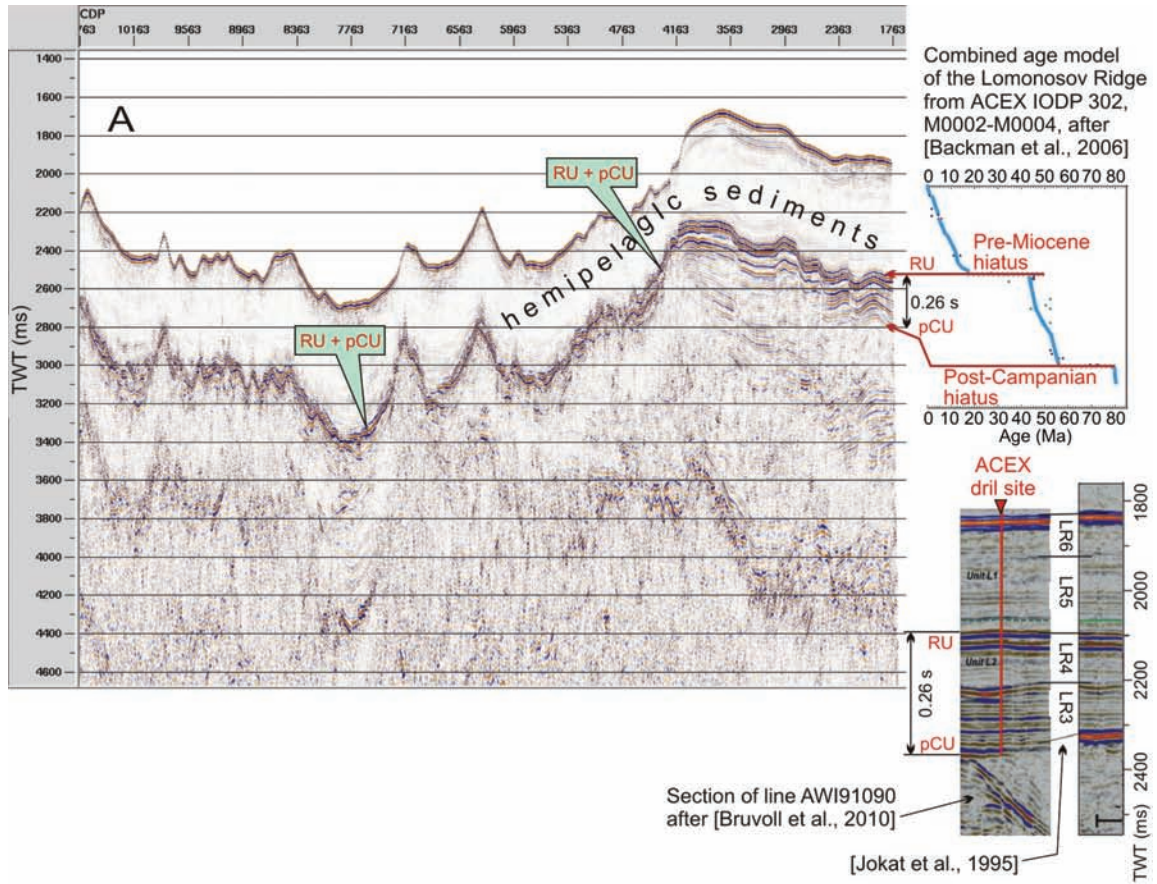


Fig. 6. Enlarged segments of A-7 multichannel seismic reflection profile (see Fig. 5): A – ties of major unconformities to the ACEX core, B - tracing major unconformities from the Lomonosov Ridge to the Laptev Sea shelf. Designation of unconformities is the same as in Fig. 5.

sedimentary sequence in the Sverdrup Basin (Sørensen et al. 2011). A 5.9 km/s unit that may be highly deformed and indurated clastics, carbonates and volcanics of Late Proterozoic to early Paleozoic age overlies a 6.6-6.8 km/s unit interpreted to be the crystalline lower crust (Forsyth et al. 1998). An upper mantle velocity of 8.2 km/s was measured at a depth of 20-25 km.

From the North American Margin to the Plateau of the Lomonosov Ridge

The results of the LORITA experiment are extracted from Jackson and Dahl-Jensen et al. (2010). The 440 km long north-south WAR profile crosses the continental shelf from the Lincoln Sea onto the Lomonosov Ridge. A 110 km east-west profile was run in the trough crossing the north-south line (Fig. 1). On the north-south line 181 receivers were spaced at 1.3 km and a total of 13 shots were fired. The WAR data were used to constrain two dimensional P-wave velocity models. The P-wave models were generated using the ray-tracing code RAYINVR and accompanying inversion and amplitude modeling code (Zelt 1999).

The modeling of the north-south WAR line identified three sedimentary units on the southern section of the line. The upper two layers with velocities of 2.1-2.2 km/s and 3.1-3.2 km/s are correlated with the Arctic continental terrace wedge. Below a seaward dipping interface predicted to be a regional unconformity, velocities in the range 4.3-5.2 km/s similar to those in the Mesozoic to Paleozoic Sverdrup Basin onshore have been determined. A layer with a velocity of 5.5-5.9 km/s underlies the inferred sedimentary strata on the continental shelf and can be traced seaward until it pinches out at a basement high on Lomonosov Ridge. This velocity is consistent with metasedimentary rocks of Late Proterozoic to early Paleozoic age seen in the onshore Sverdrup Basin at the same stratigraphic level (Jackson and Dahl-Jensen et al. 2010).

On the plateau of the Lomonosov Ridge (Fig. 2 and 3), the sediment cover is <1 km. The basement velocities are 5.9-6.5 km/s (Jackson and Dahl-Jensen et al. 2010). Consistent with the WAR results, the short seismic reflection profiles (Fig. 3) penetrated only a thin veneer of sediments overlying basement with internal dipping reflections. This seismic data

in combination with the associated high frequency magnetic anomaly pattern suggests basaltic rocks near the surface (Jackson and Dahl-Jensen et al. 2010).

The crustal velocities flanking the basement high are in the range of 6.4-6.7 km/s. The information on the gradients is dependent on the depth of the penetration of the diving waves. Diving rays at about 15 km depth and at a range of 350 km indicate subtle changes in the crustal velocities northward. On the north end of the line, unreversed diving waves reach a maximum depth of 16.5 km that also constrain the top of the lower crust beneath the high. The Moho depth varies substantially from 20 to 27 km shallowing beneath the trough and deepening towards the continent and the plateau.

Near the North Pole

A WAR profile called LOREX (Fig. 1) was completed with 6 shots and 10 seismic recorders that were deployed on both a cross and a strike line on the Lomonosov Ridge near the North Pole (Mair and Forsyth 1982; Forsyth and Mair 1984). The location of the shots and receivers were verified with water wave arrival times. The shot-to-recorder distances are accurate to 500 m. Ray tracing was done on the cross line and synthetic models were computed on the strike line. Due to the small number of shots and receivers and the 10-20 km spacing between them, there is little velocity control on the sediments at the seafloor. The reversed arrivals along the strike of the Lomonosov Ridge were modeled with two layers: a 5 km thick velocity layer of 4.7 km/s underlain by a 15-20 km thick velocity layer of 6.6 km/s (Mair and Forsyth 1982). An upper mantle velocity of 8.3 km/s was indicated by a few arrivals. The modeling of the cross line suggests Moho depth of about 28 km with a steeper slope on the Makarov Basin side than on the Eurasia Basin side.

The Pole to the Siberian margin

Wide-angle refraction/reflection data 'Transarctica-1992'

The 280 km long 'Transarctica-1992' WAR line crosses the Lomonosov Ridge from the Amundsen Basin to the Podvodnikov-Makarov basins at about 83.5°N (Fig. 1). The observations were made using twenty 'Taiga' analogue recorders placed on the ice at 4-6 km intervals. The energy was sourced from

TNT charges between 100 and 1200 kg, depending on the position of shot points relative to the recorders. The average distance between shots was 40 km. The maximum offset reached 200 km.

Analogue WAR data were digitized at 8 ms sample rate and processed using ProMAX 2D software. To improve the data quality, true amplitude recovery and minimum-phase bandpass filtering of 1-2-7-9 Hz were applied. Interpretation of the data was based on ray-tracing, and modeling of synthetic wave field. For these purposes, RAYINVR and the accompanying amplitude modeling software TRAMP (Zelt, 1999) were used.

The results of WAR data interpretation along the ‘Transarctica-1992’ line are presented (Fig. 7). Ray-tracing of seismic waves from selected shot points, synthetic wave fields generated from segments of the final model, the corresponding seismic records with superposition of calculated time-distance curves of reflected and refracted waves, and seismograms without interpretation of the wave field are shown

(Poselov et al. 2012). Errors bars for picking of the arrivals are shown in Table 1.

Several groups of waves were discerned and interpreted on seismic records: P-waves reflected from the intra-mantle boundary (Pm1P), from the Moho discontinuity (PmP) and from the top of the upper crust (PBP), and P-waves refracted in the upper mantle (Pn), in the upper crust (Pg) and in the layer PMS that occupies an intermediate position between the crystalline crust and the uppermost sedimentary layer.

The top of this “in-between” layer forms the acoustic basement on the reflection profile A-7 and also throughout the greater part of the Alpha-Mendelev Ridge and Podvodnikov-Makarov Basin area. The layer occupying similar position in crustal section and demonstrating comparable seismic characteristics was identified in the southern section of LORITA WAR profile and interpreted as a metasedimentary unit correlative to Franklinian assemblages (Jackson, Dahl-Jensen et al., 2010).

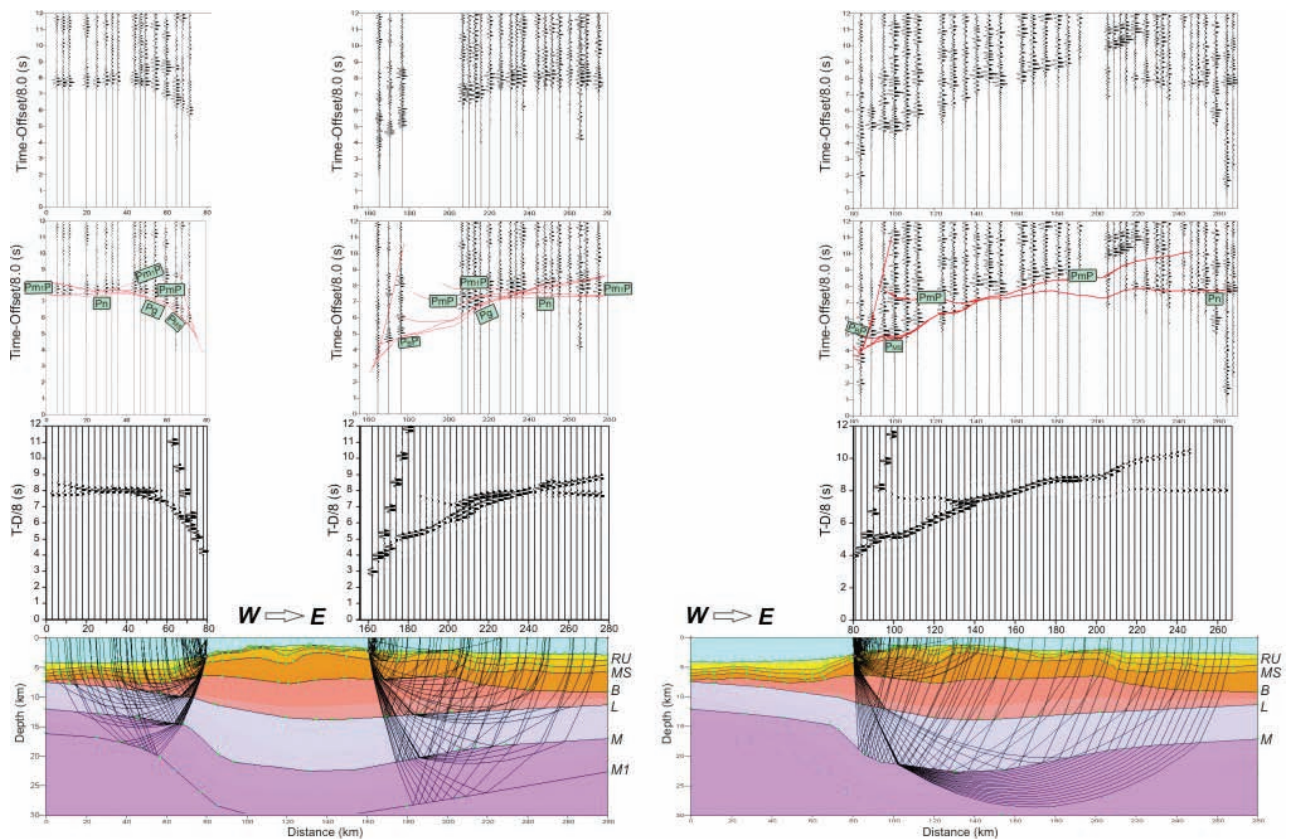


Fig. 7. Transarctica-1992 wide angle reflection/refraction profile, ray tracing and synthetic modeling. Major boundaries: RU - Regional unconformity, IL - Top of Intermediate layer, B - Top of Upper crust, L - top of Lower crust, M - Moho, M1- intra-mantle boundary

Conceivably, the seismic parameters of this layer may at different locations correspond to folded and mildly metamorphosed sedimentary units, or undeformed but highly compacted sedimentary rocks (e.g. quartzitic sandstones, dolomites), or sediments

interleaved with volcanic flows or sills. Until the nature of that layer in the Pole to Siberia segment of the Lomonosov Ridge is understood with better confidence, we shall tentatively apply the definition proposed in LORITA model and refer to this unit as presumably Paleozoic to Early Mesozoic in age and 'metasedimentary' in composition (ms unit).

The main feature of the wave field is the presence of atypically strong Pn waves which may be due to their interference with Pm1P waves (as indicated by the synthetic modeling). The resulting velocity model of the Earth's crust along the 'Transarctica-1992' line is presented in Figure 8a.

Three sedimentary sequences, of which two upper ones are separated by a regional unconformity, are identified in the model. The upper sequence is characterized by i.e. velocities 1.6-2.6 km/s; the middle one, by i.e. velocities 3.6-3.9 km/s and the lower one, by i.e. velocities 4.2-4.5 km/s. Total thickness of the sequences reaches a maximum of ~3 km over a subsided block of the Lomonosov Ridge. On the top of the Ridge, it does not exceed ~1 km. The crust below the sedimentary sequences consists

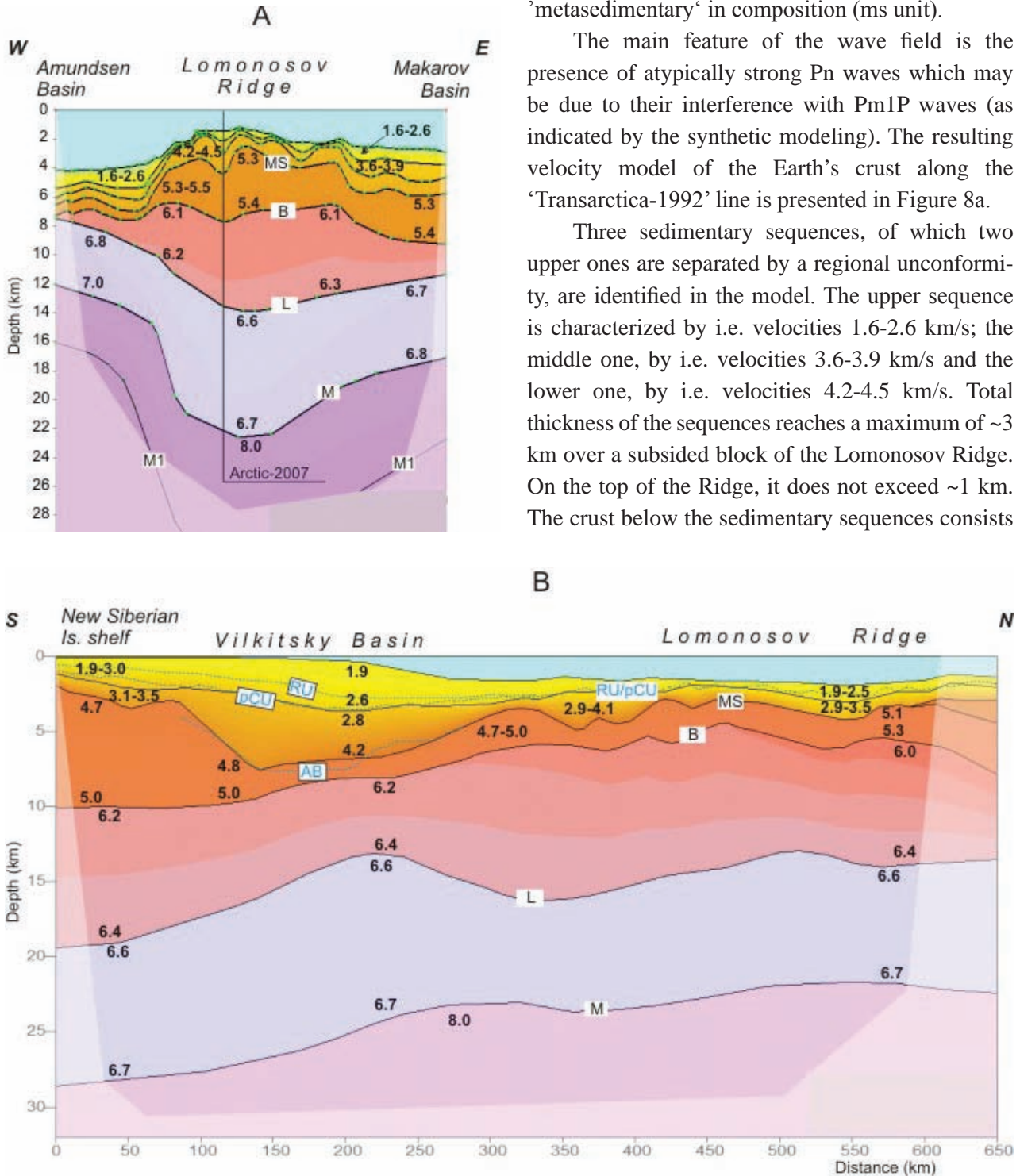


Fig. 8. Velocity models of the crust: (a) along Transarctica-1992 wide angle reflection/refraction profile, (b) along A-7 multichannel seismic reflection line and Arctic-2007 WAR profile. Major boundaries: MS - top of "metasedimentary" layer, B - top of upper crust, L - top of lower crust, M - Moho, M1- intra-mantle boundary. Bold digits – P-wave velocities (km/s), blue dotted lines – position of unconformities time/depth converted from A-7 multichannel seismic reflection profile (see Fig. 5 for designations).

of three velocity layers. Velocity parameters of the 'metasedimentary' layer (MS) are characterized by 5.3-5.5 km/s. Its thickness varies from ~1 km under the Amundsen Basin to ~4.5 km across the Lomonosov Ridge. In the Makarov Basin, it reaches a thickness of 3.0-3.5 km. The upper crust is characterized by velocities of 6.1-6.3 km/s and a thickness of between 6 and 7 km across the Ridge. Velocities in the lower crust do not exceed 6.7 km/s. The thickness of the lower crust varies within 7-9 km across the Ridge. Depth to the Moho discontinuity ranges from ~22 km at the Lomonosov Ridge crest to ~17 km and ~12 km beneath the Makarov and Amundsen basins, respectively. The intra-mantle reflections are coming from a depth of greater than 30 km under the Ridge, and from ~23 km and ~15 km in the Makarov and Amundsen basins, respectively.

WAR data 'Arctic-2007'

The 650 km long 'Arctic-2007' WAR line was shot along the Lomonosov Ridge from 83.5°N to the Siberian shelf north of the New Siberian Islands (Fig. 1). Data were recorded from ice stations. Thirty recording instruments were spaced at intervals of 5 km. TNT charges weighed from 200 to 1000 kg. The average spacing between shot points was 50 km. The maximum offset reached was 250 km.

Digital WAR data (sample rate 8 ms) were processed by using ProMAX 2D software. To improve data quality, true amplitude recovery for the offset and minimum-phase bandpass filtering of 2-3-6-8 Hz were applied. The approach to the interpretation of WAR data was similar to that applied for 'Transarctica-1992' line. The resulting model is presented in Figure 8b.

The results of WAR data interpretation along the 'Arctic-2007' line are shown in figure 9. The ray-tracing of seismic waves from selected shot points, synthetic wave fields generated by the final model, the corresponding seismic records superimposed with the calculated time-distance curves of reflection and refraction waves, and seismograms without interpretation of the wave field are presented. In addition, errors bars for picking of the arrivals are shown in Table 1.

On the seismic records, P-wave refractions in the upper crust (Pg), refractions in the upper mantle (Pn), reflections from the Moho discontinuity (PmP)

as well as shot lineups of P-waves reflected from the top of the upper (PBP) and lower (PLP) crust are interpreted. A common feature of the WAR data is the lack of refraction waves passing through the lower crust in the first arrivals, as a result of which the velocities in the lower crust were estimated only from PmP waves.

The resulting 'Arctic-2007' velocity model (Fig. 8b) was controlled by multichannel seismic reflection data. Two sedimentary sequences are separated by a regional unconformity. The upper sequence is characterized by velocities from 1.9-3.0 km/s on the shelf to 1.9-2.5 km/s on the Lomonosov Ridge; the lower one, by velocities from 3.1-3.5 km/s on the shelf to 2.9-4.1 km/s on the Lomonosov Ridge and 2.9 to 3.5 km/s farther to the North Pole. Total thickness of the sequences reaches the maximum of ~7 km in the depocentre of the Vilkitsky Basin; on the Lomonosov Ridge, it does not exceed ~2 km. Consolidated crust consists of three velocity layers: 'MS', upper and lower crust. Velocity parameters of 'MS' are characterized by a lateral variability from 4.8-5.0 km/s on the shelf to 5.1-5.3 km/s on the Lomonosov Ridge. Thickness of the layer varies laterally from ~7 km on the shelf to ~1.5 km under the shelf edge; on the Lomonosov Ridge, it reaches a thickness of 3.5 km. The upper crust is characterized by velocities of 6.0-6.4 km/s and the thickness is 6-7 km. Velocities in the lower crust do not exceed 6.7 km/s. The thickness of the lower crust varies within 9-12 km. Depth to the Moho discontinuity ranges from 28 km on the shelf to 22-23 km on the Lomonosov Ridge.

According to the WAR data, all sedimentary sequences and consolidated crustal layers are continuous from the outer shelf of the Laptev - East Siberian Seas to the Lomonosov Ridge.

POTENTIAL FIELD DATA

Near North America

Of particular interest is the magnetic signature associated with the plateau of the Lomonosov Ridge and its onshore extension (Miles 2002; Damaske and Estrada 2006; Oakey et al. 2012) (Fig. 10). The linear magnetic anomalies highlighted in white on Figure 10b are present from near shore to the plateau. Oakey et al. (2012) have interpreted them as Cretaceous intrusives. These linear anomalies terminate against

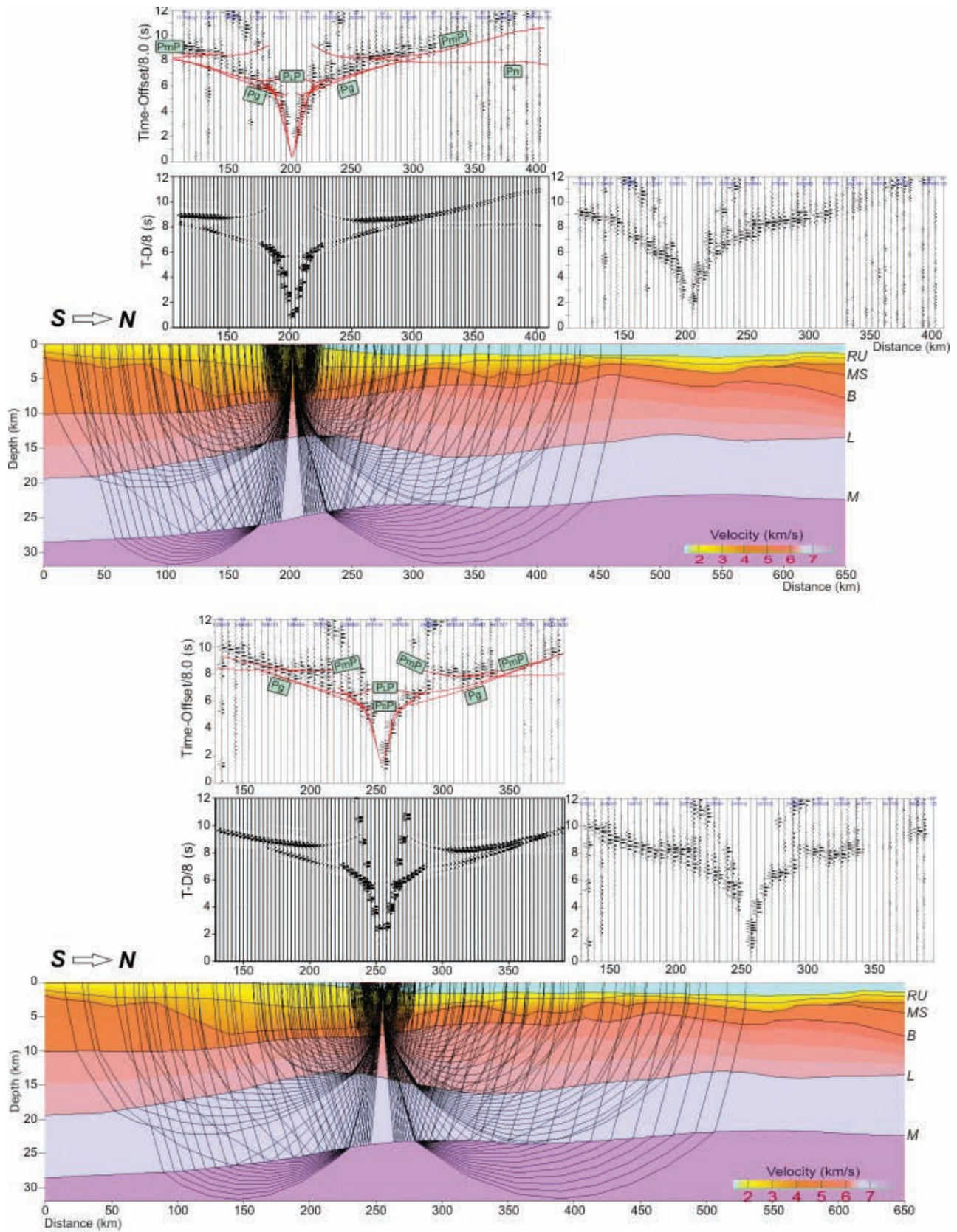


Fig. 9. Arctic-2007 wide angle reflection/refraction data: ray tracing and synthetic modeling. Major boundaries: RU-Regional Unconformity, IL - Top of Intermediate layer, B - Top of Upper crust, L - top of Lower crust, M – Moho.

Table 1. Number of observations (no. of shots, no. of picks), RMS misfit between calculated and picked arrival travel times, dominant phases for individual waves.

Line/Wave	No. of shots	No. of picks	RMS misfit(s)	Phase(s)
Transarctic-1992 line (digitized analog data)				
Sed. refractions	6	9	0.179	0.10
Metased. refractions	9	29	0.120	0.10
Upper Crust top reflections	7	22	0.160	0.10
Upper Crust refractions	12	40	0.116	0.10
Lower Crust top reflections	6	15	0.111	0.10
Lower Crust refractions	5	23	0.091	0.12
PmP	12	60	0.121	0.14
Pn	11	63	0.103	0.13
All observations (shots/traces)	14/280	261		
Arctic-2007 line (digital data)				
Sed. refractions	6	22	0.121	0.12
Metased. refractions	9	15	0.115	0.12
Upper Crust top reflections	11	34	0.095	0.12
Upper Crust refractions	18	120	0.114	0.13
Lower Crust top reflections	18	70	0.102	0.13
Lower Crust refractions	0			
PmP	20	167	0.111	0.17
Pn	14	48	0.106	0.16
All observations (shots/traces)	23/690	476		

a series of SSW-NNE trending magnetic highs that can be traced from Clements Markham Inlet (CMI) on Ellesmere Island to the southeastern edge of the Lomonosov Ridge. Oakey et al. (2012) suggest that this bounding feature marks the easternmost extension of the Pearya Terrane. Onshore, the Pearya Terrane (Trettin 1991) has a limited geographical extent of 300 km on Ellesmere Island.

The magnetic data show additional onshore/offshore correlations (Fig. 10b). There is a high amplitude positive circular anomaly (marked with a 'V' in a yellow circle) about 25 km in diameter surrounded by shorter wavelength linear anomalies (shown in yellow on Figure 10b). The circular anomaly is enclosed by the 500 m contour, and the

linear anomalies by the 1000 m bathymetric contour. Onshore Ellesmere Island at the westernmost extent of the Pearya Terrane, there is a similar magnetic pattern (Fig. 10a and 10d) that is known to be caused by the Hansen Point Volcanic complex. The onshore volcanic complex is a 1000 m thick sequence of flows, pyroclastic rocks, and intercalated fluvial and marine clastic sedimentary rocks and coal (Trettin and Parrish 1987). The igneous rocks are bimodal, partly alkaline (Estrada et al. 2006). A WAR experiment offshore of the Hansen Point Volcanic complex (Asudeh et al. 1989) measured a value of 5.0 km/s at the seabed overlying a 5.8 km/s unit that is described as basement. These high velocities near the seafloor were unlike the lower velocities obtained

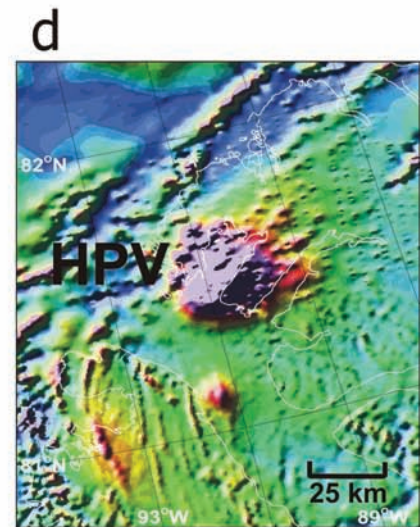
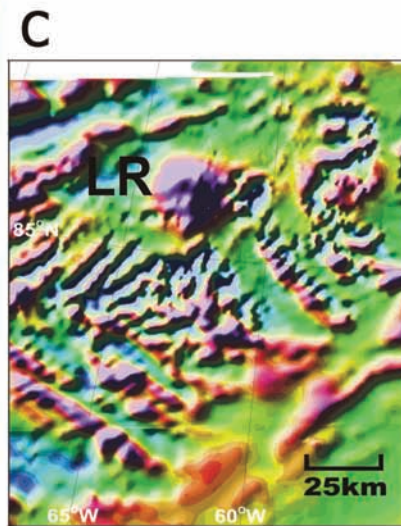
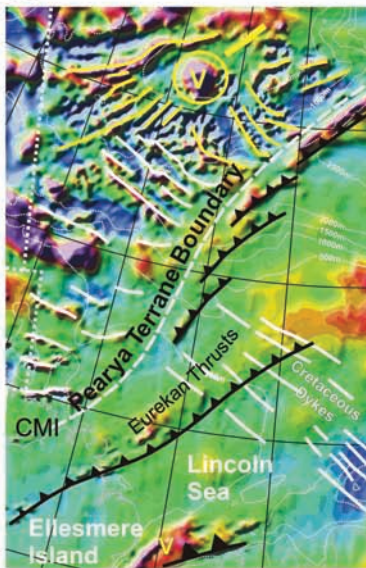
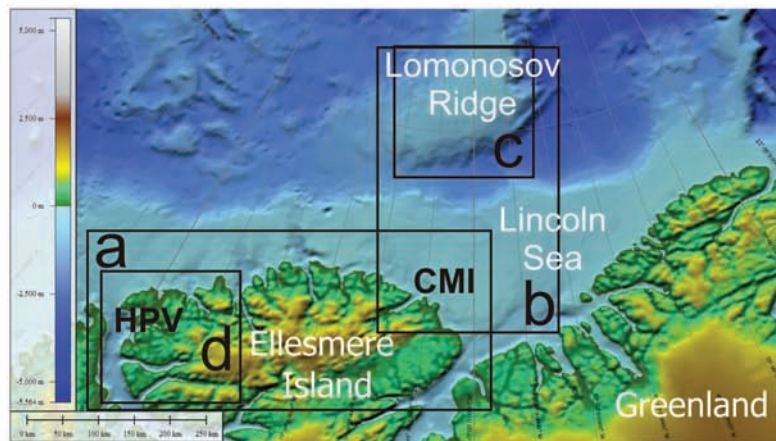
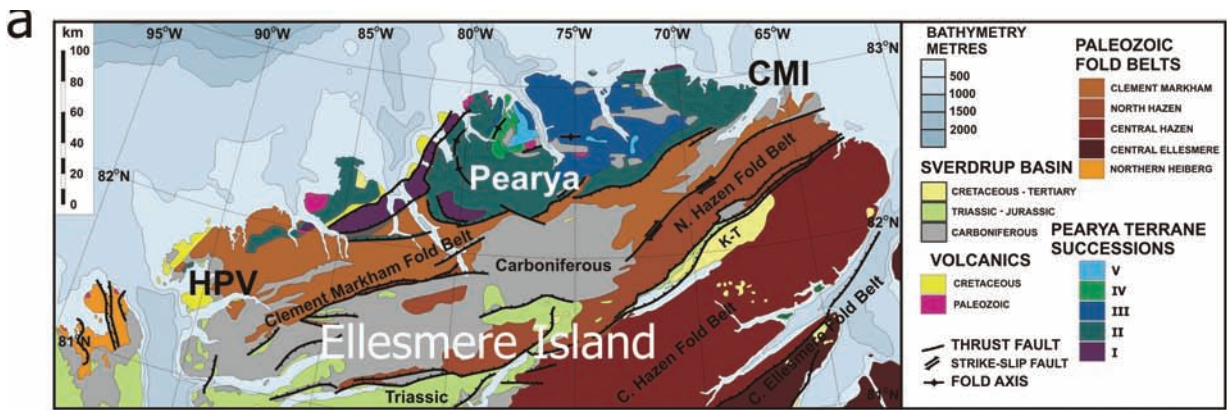


Fig. 10. Geological and bathymetric maps with 3 enlargements of magnetic surveys near the junction of the Lomonosov Ridge with the North American margin. Figure 10a illustrates the geology of northern Ellesmere Island for comparison with the magnetic anomalies. The black boxes labeled 'a', 'b', 'c' and 'd' on bathymetric map indicate relative positions of the geology map and the magnetic maps. CMI-Clements Markham Inlet, HPV- Hansen Point Volcanics, LR-Lomonosov Ridge, V-Volcanics

elsewhere on the margin at this depth. On the plateau of the Lomonosov Ridge near the circular magnetic anomaly, velocities of 5.9 km/s were recorded at the seafloor.

By analogy, based on the similar unique magnetic signatures of the plateau and the Hansen Point Volcanic complex, the consistent refraction velocities, and the proximity of the Pearya Terrane, we suggest that the plateau on the Lomonosov Ridge was caused by a magmatic event similar to the Hansen Point Volcanic complex modifying older continental crust.

High amplitude long wavelength magnetic anomalies associated with the Lomonosov Ridge to the north of the plateau are similar to those observed over the southern Makarov basin and the adjacent Alpha Ridge. Kristoffersen and Mikkelsen (2006) mention two sets of reflectors on the plateau of the Lomonosov Ridge and another set 600 km to the

North along the Ridge (Kristoffersen 2001) at a depth of 600 m below the seabed that were interpreted as basaltic flows. Døssing et al. (2013) are able to trace magnetic anomalies from the edge of this section of the Lomonosov Ridge to the Alpha Ridge. We suggest that the magmatic event that is associated with the Alpha Ridge also affected the Lomonosov Ridge from the Pole to the margin of North America.

Near The Siberian Margin

Potential field data coverage in the area of transition from the Lomonosov Ridge to the Siberian margin is irregular (Fig. 11). Line spacing during airborne magnetic surveys conducted here between 1962 and 2007 varied dramatically, as well as RMS observation and navigation errors (Fig. 11a). Gravity information was also merged from different available data sources characterized by unequal accuracy (Fig. 11b). The best quality data were obtained within

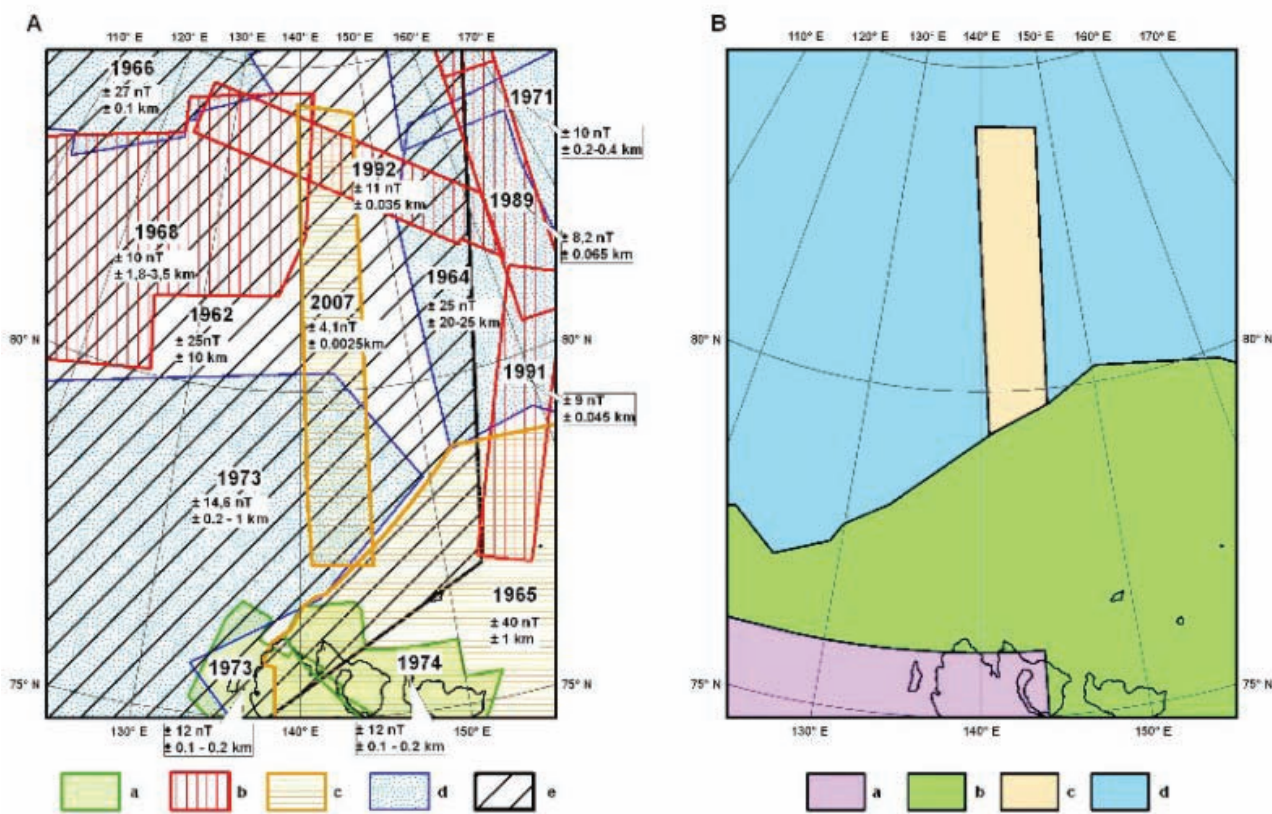


Fig. 11. Potential field data coverage near the junction of the Lomonosov Ridge with the Siberian margin. A) Airborne magnetic surveys with track line spacing: a) 2-5 km, b) 5 km, c) 10 km, d) 20-40 km, e) 40-50 km; the year of activity, RMS observation error (nT) and navigation error (km) are indicated for each survey. B) Gravity data sources: a) State free-air gravity anomaly map of the USSR at scale 1: 1,000,000; b) geophysical database to the State geological map of Russia at scale 1:1,000,000; c) results of 2007 airborne gravity survey; d) Arctic Gravity Project (Kenyon et al., 2008; <http://earth-info.nga.mil/GandG/wgs84/gravitymod/egm96/egm96.htm>).

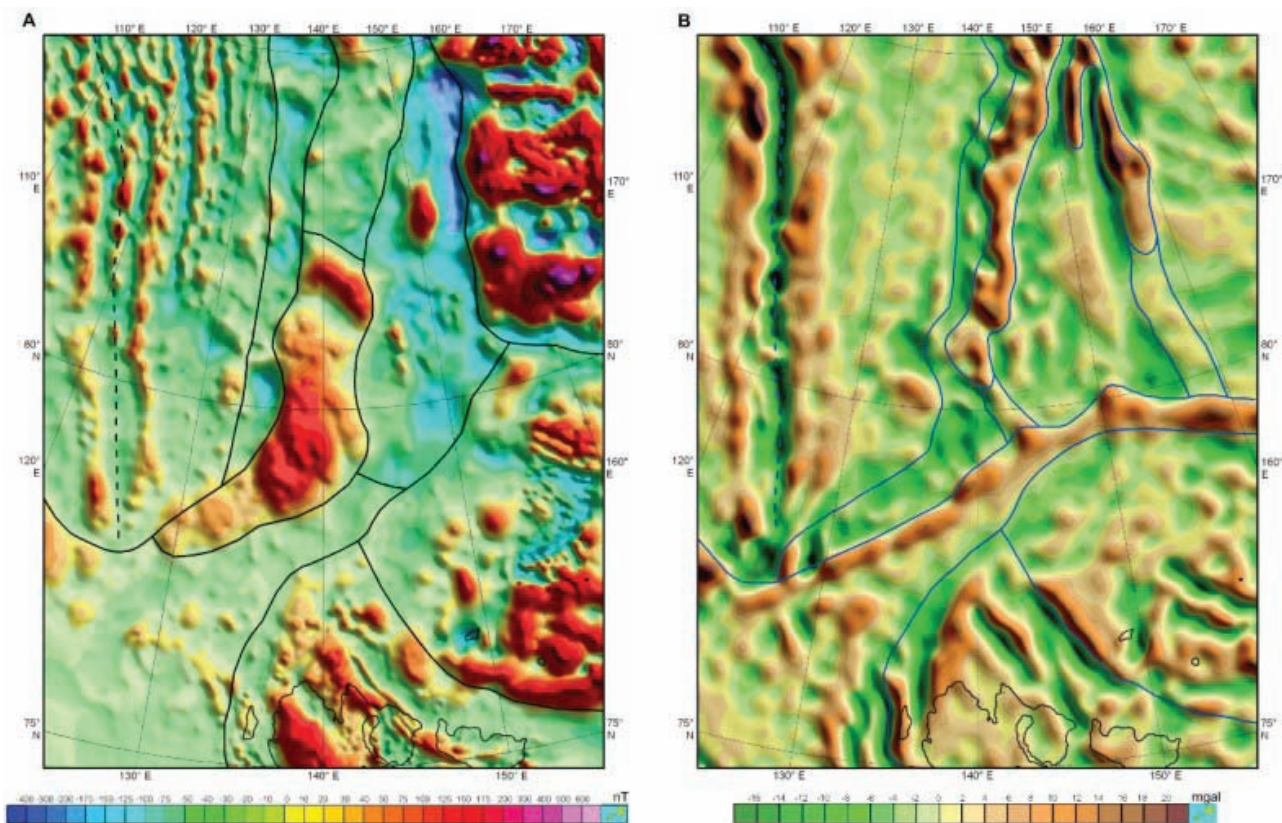


Fig. 12. Magnetic anomalies (A) and local Bouguer gravity anomalies (B) in the area indicated by box ‘C’ in Figure 1. Boundaries of potential field domains are shown by solid lines. The Gakkel Ridge axis is marked by a dashed line.

the corridor surveys performed along WAR lines ‘Arctica-2007’ and ‘Transarctica-1992’ described above.

All available magnetic and gravity information was processed, adjusted and converted to grids of magnetic and free-air gravity anomalies with cells size of 2×2 and 3×3 km. Bouguer gravity anomalies were calculated using IBCAO grid (Jakobsson et al. 2008). Local Bouguer anomalies were computed as the difference between Bouguer gravity anomalies and their upward continuation to 20 km. Several grids of magnetic and Bouguer gravity anomaly transformations, such as vertical and total horizontal gradients, tilt-transformations, upward continuations were computed as additional tools for potential fields interpretation.

Analysis of the above information was carried out manually using GIS ArcMap v.9.2. Magnetic and gravity datasets were first considered independently and then correlated on the basis of sketch maps of magnetic and local Bouguer anomalies each showing the respective main features of potential fields zoning expressed as boundaries of differing

domains (Fig. 12). The boundaries whose positions appeared matching or closely comparable on both maps were interpreted as reflecting the limits of major tectonic provinces and/or morphostructural features which are shown in figure 13 taking into account the above considered seismic evidence and available geological data.

The oceanic Eurasia Basin stands out for displaying a linear magnetic and gravity signature symmetrical relative to the Gakkel Ridge spreading axis. Between anomaly 24 and the base of the Lomonosov Ridge marked by distinct magnetic and gravity gradients, this signature fades out indicating the ocean-continent transition zone.

The crest and eastern spurs of the Lomonosov Ridge are clearly reflected in the gravity field, whereas the magnetic signature over the Lomonosov Ridge and the Laptev Sea shelf is rather flat and inexpressive, except the area around 80°N with intensive positive anomalies. The origin of these anomalies is unknown. Their interpretation may, perhaps, be facilitated by the notion of a similar pattern of the magnetic field on the conjugate side

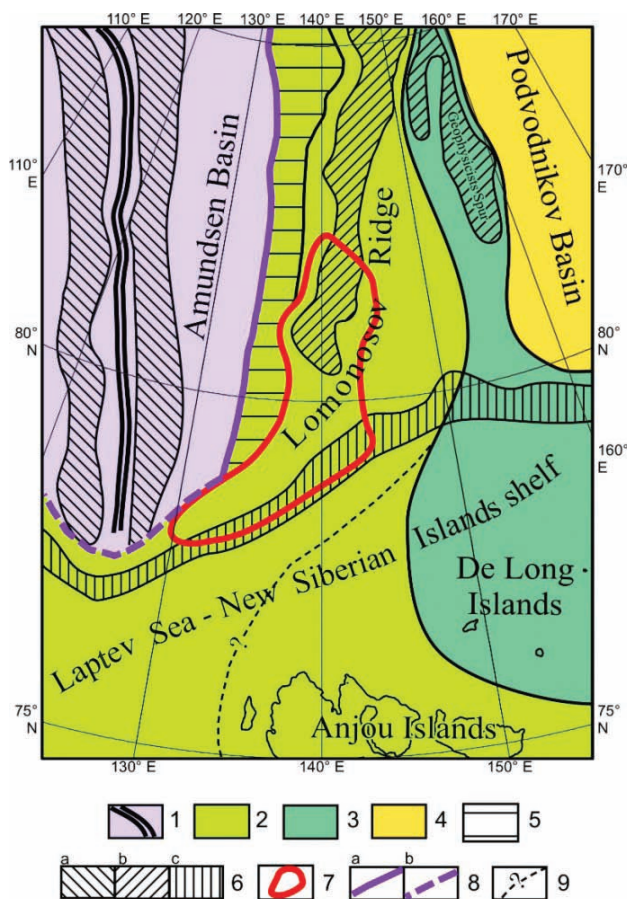


Fig. 13. Structural provinces and features near the Siberian margin. 1 – Cenozoic oceanic crust and the Gakkel Ridge spreading axis; 2-5 – rifted continental crust: 2 – Anjou Islands and its inferred continuation in the Laptev Sea and on the Lomonosov Ridge, 3 – De Long Islands province and its inferred continuation to the Geophysicists Spur, 4 – Podvodnikov Basin province, 5 – continent-ocean transition zone; 6 – linear gravity highs associated with a) the Gakkel Ridge, b) crestal parts of the Lomonosov Ridge and adjacent spurs, c) shelf edge effect; 7 – outline of prominent positive magnetic anomalies in the southern Lomonosov Ridge; 8 – position of the continent-ocean boundary a) as defined by Chron 24, b) speculative; 9 – potential field gradient interpreted as internal fault boundary within the Anjou Islands province.

of the southern Eurasia Basin at the submarine prolongation of the Taymyr structures.

The “Serny Transfer”, or “Khatanga-Lomonosov Fracture Zone”, etc. postulated in many works (e.g. Franke et al. 2001; Drachev et al. 2003; Engen et al. 2003) coincides with a narrow gravity high that evidently follows the Siberian shelf edge. For that reason we interpreted this high as resulting from “shelf edge effect” whose expression in local Bouguer anomalies may be mainly caused by insufficient accuracy of the IBCAO grid.

The area of New Siberian Islands and the surrounding shelf is characterized by general similarity of magnetic and gravity anomaly patterns. The discordance that can be observed between the Anjou Islands and the De Long Islands potential field domains (Fig. 13) is consistent with the different ages of these provinces (Mesozoic and Late Neoproterozoic-Early Paleozoic, respectively). Based on geological and geochronological evidence from the near-Pole Lomonosov Ridge (Backman et al. 2006; Grantz et al. 2001) and the Geophysicists Spur (Grikurov et al., this volume), we interpret

both these provinces to extend northward from the Siberian shelf as shown in figure 13. We also assume that potential field gradients that appear to restrict the Anjou Islands block on the west do not manifest a division between different structural terranes but rather mark an internal boundary within a single tectonic province underlain by the Mesozoic fold basement which is exposed on Anjou Islands but rifted and subsided in the Laptev Sea Basin.

The Podvodnikov Basin domain is remarkable for contrasting magnetic signature which is expressed in alternating high-amplitude positive and negative anomalies that strike almost orthogonally to the Lomonosov Ridge. An explanation of such a strong magnetic signal in a deep-water basin with subsided, intensely stretched and thinned high-velocity crustal layers (Lebedeva-Ivanova et al. 2011) is not readily available. At present it can only be assumed that the anomalies are caused by deeply submerged very strongly magnetized magmatic sources whose formation must have occurred in extensional environment and could be associated with, or independent of the emplacement of HALIP.

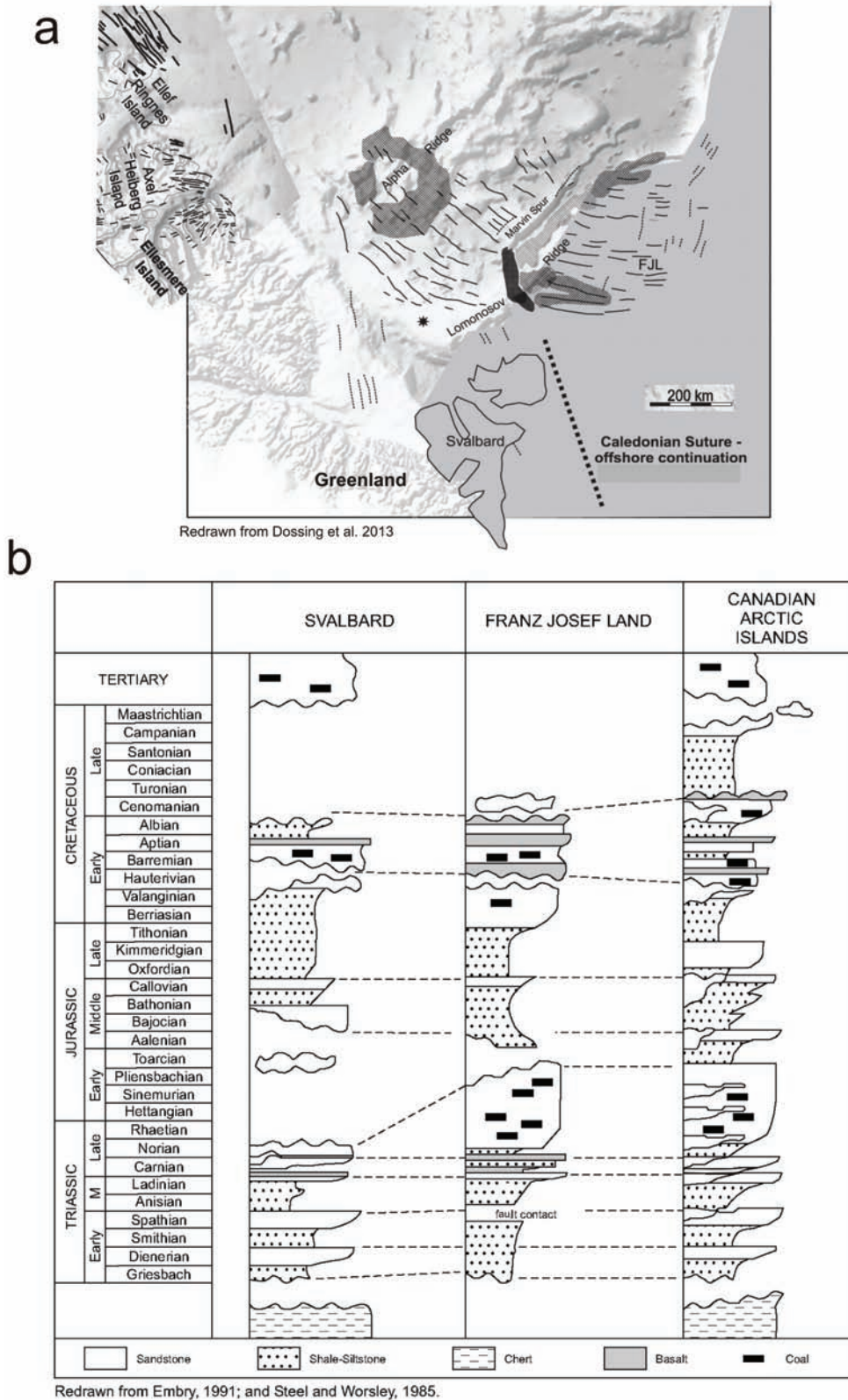


Fig. 14. a) Plate reconstruction at anomaly 25 with the position of the Lomonosov Ridge relative to Franz Josef Land (FJL), Svalbard, Greenland and Ellesmere, Axel Heiberg and Ellef Ringnes islands. Circular region of high intensity long wavelength anomalies marked in dark gray on the Alpha Ridge is the focus of radiating linear magnetic anomalies shown by black lines and interpreted as dykes based on their onshore correlations. The star on the Lomonosov Ridge is the position of the circular magnetic anomaly shown in figure 10b and c. The darkest gray area that reaches from the Marvin Spur across the Lomonosov Ridge to the margin north of Svalbard traces a broad magnetic low. b) Mesozoic stratigraphy of the Svalbard, Franz Josef Land and Canadian Arctic Islands illustrating the similarity of volcanic-sedimentary sections and the age of unconformities.

DISCUSSION

Plate reconstructions for the Arctic and the North Atlantic oceans have been published on extensive magnetic and morphological data bases that define the magnetic anomalies and fracture zones (Srivastava and Tapscott 1986; Rowley and Lottes 1988; and Gaina et al. 2002). The reconstructions place the Lomonosov Ridge adjacent to the Barents and Kara margins prior to sea floor spreading in the Eurasia Basin (Fig. 14a). These reconstructions were performed with the Lomonosov Ridge remaining fixed to the North American plate. Because the pole of rotation for the North American and Eurasian plates is not accurate enough to be a point but is determined within an error ellipse, the motion of the Lomonosov Ridge relative to the North American and Siberian margins, if any, is less than the available constraints.

Gaina et al. (2002) calculate 600 km of extension in the Laptev Sea which is consistent with the width of the central Eurasia Basin but probably is an overestimate for its narrowing continuation on the Siberian shelf. The evidence for the extension in the Laptev Sea is predicted by the plate reconstructions as summarized by Pulvertaft and Dawes (2011), and numerous extensional features in the area (rifts, extensional faults) are documented by geological and geophysical observations (e.g. Drachev 2000; Franke et al. 2001; Sekretov 2001) suggesting the propagation of the Gakkel Ridge spreading axis into continental crust that underlies the Laptev Sea. The rift activity has occurred over a long period from at least the Maastrichtian to present (e.g. Engen et al. 2003). Recent mapping indicates that the main rift underlying the Laptev Sea lies off-line from the Gakkel Ridge, and there is the possibility that 150-200 km of displacement between the Gakkel Ridge and the landward focus of extension may be accommodated by rift transfer (Engen et al. 2003) which took place beneath the shelf along a strike-slip fault within continental crust. We presume that the separation of continental crust due to seafloor spreading in the Eurasia Basin was manifested as a stretching regime on the continental margin of the Laptev Sea. Here the extension appeared sufficient to match the width of immediately adjacent oceanic opening in the southernmost Eurasia Basin, and the Siberian segment of the Lomonosov Ridge

developed in geological uniformity with the adjacent part of the Siberian shelf. The absence of movement of the Lomonosov Ridge relative to the Siberian margin is indicated by the lack of present-day seismic activity in their junction zone (Engen et al. 2003).

Moore et al. (2011) interpret the Lomonosov Ridge as a microcontinent on the assumption that it is separated from the Siberian margin by a fault that would be difficult to detect because of the more than 1 km of Cenozoic sedimentary cover. However, the reflection profile 'A-7' that extends from the Lomonosov Ridge to the shelf penetrates well below the Cenozoic cover and shows that the sedimentary cover and acoustic basement are continuous across the transition zone. This is confirmed by the coincident WAR profile that also shows the continuity of the crustal layers.

A transform fault is also predicted (Moore et al. 2011) at the junction of the Ridge with the North American margin based on the bathymetry profile from the margin to the Ridge and the interpretation of a short WAR profile with a poorly constrained lower crust (Forsyth et al. 1994); the authors also ignore the results of the more detailed WAR (Jackson and Dahl-Jensen et al. 2010) that shows continental crust beneath the trough. Furthermore, Oakey et al. (2011) clearly show the magnetic lineations (Fig. 10) that are not displaced by a fault boundary and can be traced from onshore across the shelf, the trough and the plateau of the Lomonosov Ridge.

In addition, Døssing et al. (2013) describe magnetic anomalies that radiate from the Alpha Ridge onto the Queen Elizabeth Islands (Ellesmere Island, Axel Heiberg and Ellef Ringnes islands) and towards Greenland, and from the Alpha Ridge to Franz Josef Land and Svalbard (Fig. 14a). Based on the onshore continuation of the linear magnetic anomalies, they are interpreted to be caused by dykes formed in the Early Cretaceous. The pattern of the dykes establishes the position of the margins prior to seafloor spreading in the Eurasia Basin and prior to or early in the opening of the Amerasia Basin. Reconstructed dyke swarms are accurate indicators for the position of continents prior to sea floor spreading because they provide piercing points that can be matched (Buchan and Ernst 2006). Thus, Moore et al. (2011) suggestion of a transform

fault between the Lomonosov Ridge and the Queen Elizabeth Islands margin is not supported by the available magnetic and geological data.

Mair and Forsyth (1982) correlated the velocity structure of the Lomonosov Ridge with that of the Barents Sea at 76°N and the Kara Sea at 78°N and 82°N. The velocity section of Franz Josef Land based on seismological data shows the sedimentary layer (3.2 km/s) on top of crustal layers 4.7-4.8 km/s, 5.7 km/s and 6.6-6.7 km/s with depth to Moho in the range 22-28 km (Dibner 1998). The 5.7 km/s layer recorded on Franz Josef Land is missing in the LOREX section on the Lomonosov Ridge, possibly due to the geometry and low resolution of the LOREX refraction profile. However, the 5.7 km/s layer is observed on the LORITA WAR velocity model, and the velocities of 5.3-5.5 km/s and 4.8-5.3 km/s are recorded on Transarctic-1992 and Arctic-2007 WAR profiles, respectively. Thus, the velocities of the crustal layers and depth to Moho are similar on the conjugate margins and are consistent with the plate reconstructions predicting that the Lomonosov Ridge was rifted from the Barents and Kara seas margin.

Also of interest are the lower crustal velocities that do not exceed 6.8 km/s along the length of the Lomonosov Ridge or on the adjacent margins. This velocity limit is typical of Paleozoic continental crust (Holbrook et al. 1992). The depth to Moho for the Lomonosov Ridge varies from 22 to 28 km and is also consistent with the crustal thickness range of other continental margins.

The plate reconstructions indicate that prior to seafloor spreading in the Eurasia Basin the Lomonosov Ridge was in proximal position to the Queen Elizabeth Islands, Greenland, Svalbard and Franz Josef Land (Fig. 14a). Before the plate reconstructions were well established, striking lithological similarities were observed in the Late Paleozoic to Mesozoic sections of the Sverdrup Basin, northeast Greenland, Franz Josef Land and Svalbard (Embry 1994; Harland 1997, Nassichuk and Davies 1980; Fig 14b). Thus, the plate reconstructions in context of the circum Arctic geology predict that the Lomonosov Ridge was a part of the Paleozoic to Mesozoic basin continuous between the Barents-Kara seas and the North American margins.

CONCLUSIONS

The improved bathymetric data for the Lomonosov Ridge accompanied by seismic reflection profiles indicate that the Ridge consists of a number of elongated sub-parallel continental fragments; for example, the Marvin Spur between the Pole and the North American margin and the en echelon ridges from the Pole towards the Siberian margin. An exception to this morphological character is observed near the margin of Ellesmere Island and Greenland where the widest part of the Ridge is occupied by a plateau. Based on tracing the Clements Markham Fault offshore and the occurrence of similar circular magnetic anomalies onshore and offshore, the plateau is interpreted as a geological counterpart of the Pearya Terrane affected by volcanic activity. The position of the Lomonosov Ridge relative to the Ellesmere Island margin is thought to be stable based on magnetic anomalies attributed to dykes. On the reconstruction at anomaly 25 these dykes can be traced from the Queen Elizabeth Islands and from Franz Josef Land to the Alpha Ridge.

On the Siberian margin a seismic reflection profile that extends from the shelf along the Lomonosov Ridge is interpreted with seismic reflectors continuing from onshore to offshore without faulting. Furthermore, the accompanying WAR velocity model shows that sedimentary and crustal velocities can be followed across the margin onto the Ridge. The presence in Bouguer anomalies of shelf edge effect can be explained by insufficient accuracy of the bathymetric grid and does not necessitate the existence of a sharp structural junction. The lack of present-day seismicity indicates the absence of active faulting, and plate reconstructions are readily accomplished without a transform fault between the Ridge and the margin.

The upper crustal velocities on the Lomonosov Ridge near the North Pole are similar to those observed on Franz Josef Land. The lower crustal velocities from the Queen Elizabeth Islands margin along the Lomonosov Ridge to the Siberian margin all show values of 6.8 km/s or less typical of rifted lower continental crust. This is consistent with plate reconstructions that would place the Lomonosov Ridge prior to seafloor spreading in the Eurasia Basin against the margins of the Barents and Kara seas. The plate reconstructions also show the proximity of the

North American and the Barents-Kara seas margins which is substantiated by the similar stratigraphy of the Queen Elizabeth Islands, Svalbard and Franz Josef Land from the Carboniferous to the late Cretaceous time.

ACKNOWLEDGEMENTS

The Geological Surveys of Canada (GSC), the Geological Survey of Denmark and Greenland (GEUS) and the Federal Agency for Mineral Resources of the Russian Federation (ROSNEDRA) are thanked for their ongoing support to collecting and processing of the difficult to acquire Arctic data sets presented here. Dieter Franke and an anonymous reviewer provided insightful comments that helped to improve the paper.

REFERENCES

- Asudeh, I., D.A. Forsyth, R.A. Stephensen, A.F. Embry, H.R. Jackson., and White, D.A., 1989. Crustal structure of the Canadian Polar margin: results of the 1985 seismic refraction survey. *Canadian Journal of Earth Sciences*, 26, p. 853-866.
- Backman, J., Moran K., McInroy, D.B., Mayer, L.A. and Expedition 302 Scientists, 2006. *Proceedings of the Integrated Ocean Drilling Program*, volume 302, p. 1-115.
- Bjork, G., Jakobsson, M. Rudels, B. Swift, J.H. Anderson, L., Darby, D.A. Backman, J. Coakley, B., Winsor, P., Polyak, L., and Edwards, M., 2007. Bathymetry and deep-water exchange across the central Lomonosov Ridge at 88-89°N. *Deep Sea Research I*, 54, p. 1197-1208.
- Bruvoll, V., Kristoffersen, Y., Coakley, B.J. and Hopper, J., 2010. Hemipelagic deposits on the Mendeleev and Alpha sub-marine ridges in the Arctic Ocean: acoustic stratigraphy, depositional environment and inter-ridge correlation calibrated by the ACEX results. *Marine Geophysical Research* 31, 149-171. doi:10.1007/s11001-010-9094-9.
- Buchan, K.L. and Ernst, R. E., 2006. Giant dyke swarms and the reconstruction of the Canadian Arctic islands, Greenland, Svalbard and Franz Josef Land. In: Hanski, E., Mertanen, S., and Ramo, T. (eds). *Dyke Swarms: Time Markers of Crustal Evolution*, p. 27-48.
- Burkanov, V. 1954. *New Soviet discoveries in the Arctic*. Moscow Foreign Languages Publishing House, 60 pp.
- Butsenko V.V. and Poselov V.A., 2006. Regional paleotectonic interpretation of seismic data from the deep-water central Arctic. In: R.A. Scott and D.K. Thurston (eds.) *Proceedings of the Fourth International conference on Arctic margins (ICAM IV)*, p. 125-131.
- Carey, S.W., 1958. The tectonic approach to continental drift. In: S. W. Carey (ed.) *Continental Drift - A Symposium*. University of Tasmania, Hobart, p. 177-363.
- Cochran, J.R., Edwards, M.H. and Coakley, B.J., 2006. Morphology and structure of the Lomonosov Ridge, Arctic Ocean. *Geochemistry Geophysics Geosystems*, 7(5), p. 1-26, doi: 10.1029/2005GC001114.
- Damaske, D. and Estrada, S., 2006. Correlation of aeromagnetic signatures and volcanic rocks over northern Greenland and the adjacent Lincoln Sea. In: R.A. Scott and D.K. Thurston (eds.) *Proceedings of the Fourth International conference on Arctic margins (ICAM IV)*, p. 224-232.
- Dibner, V.D., 1998. *Geology of Franz Josef Land*. Meddelelser Nr. 146, Norsk Polarinstitut, Oslo, 190 pp.
- Døssing, A., Jackson, H. R., Matzka, J., Einarrson, I., Rasmussen, T.M., Olesen, A. V., and Brozena, J.M., 2013. On the origin of the Amerasia Basin and the High Arctic Large Igneous Province – Results of new magnetic data. *Earth and Planetary Science Letters*, 363, p. 219-230.
- Drachev, S.S., 2000. Laptev Sea rifted continental margin: modern knowledge and unsolved questions. *Polarforschung*, 68, p. 41-50.
- Drachev S. S., Kaul N., and Beliaev, V. N., 2003. Eurasia spreading basin to Laptev shelf transition: structural pattern and heat flow. *Geophysical Journal International*, 152, p. 688-698.
- Embry, A., 1990. Geological and geophysical evidence in support of the hypothesis of anticlockwise rotation of northern Alaska. *Marine Geology*, 93, p. 17-329.
- Embry, A., 1994. Mesozoic stratigraphy of Franz

- Josef Land Archipelago, Arctic Russia – a literature review. In: Thurston, D., Fujita, K. (eds.), Proceedings of the 1992 International Conference on Arctic Margins, p. 15- 20.
- Engen, Ø., Eldhom, O. and Hilmar, B., 2003. The Arctic Plate Boundary. *Journal of Geophysical Research* 108 (B2), 2075, p. 1-17, doi: 10.1029/2002JB001809.
- Estrada, S. Piepjohn, K., Henjes-Kunst F. and Von Gosen, W., 2006. Geology, magmatism and structural evolution of the Yelverton Bay Area, Northern Ellesmere Island, Arctic Canada. *Polarforschung*, 73, p. 59-75.
- Forsyth, D.A. and Mair, J. A., 1984. Crustal structure of the Lomonosov Ridge and the Fram and Makarov basins near the North Pole. *Journal of Geophysical Research*, 89, p. 473-481.
- Forsyth, D.A., Argyle, M., Okulitch, A. and Trettin, H.P., 1994. New seismic, magnetic and gravity constraints on the crustal structure of the Lincoln sea continent-ocean transition. *Canadian Journal of Earth Sciences*, 31, p. 905-918.
- Forsyth, D.A., I. Asudeh, D. White, H.R. Jackson, R.A. Stephensen, A.F. Embry, and Argyle, M., 1998. Sedimentary basins and basement highs beneath the polar shelf north of Axel Heiberg and Meighen islands. *Bulletin of Canadian Petroleum Geology*, 48, p. 12-29.
- Franke, D., Hinz, K., and Oncken O., 2001. The Laptev Sea Rift. *Marine and Petroleum Geology*, 18, p. 1083-1127.
- Gaina, C., Roest, W.R. and Muller, R. D., 2002. Late Cretaceous - Cenozoic deformation in northeast Asia. *Earth and Planetary Sciences Letters*, 197, p. 73-286.
- Grantz, A., Pease, V.L., Willard, D.A., Phillips, R.L. and Clark, D.L., 2001. Bedrock cores from 89° North: Implications for the geological framework and Neogene paleoceanography of the Lomonosov Ridge and a tie to the Barents Shelf. *Geological Society of America Bulletin*, 113, p. 1271-1281.
- Grikurov, G., Petrov, O., Shokalsky, S., Rekant, P., Krylov, A., Laiba, A., Belyatsky, B., Rozinov, M., and Sergeev, S., this volume. Zircon geochronology of bottom rocks in the central Arctic Ocean: analytical results and some geological implications.
- Halgedahl, S. L. and Jarrard, R. D., 1987. Paleomagnetism of the Kuparuk River Formation from oriented drill core: Evidence for rotation of the Arctic Alaska Plate. In: I.L. Tailleux and P. Weimer (eds.) *Alaskan North Slope geology*, 2, p. 581-617.
- Harland, W. B., 1997. *The Geology of Svalbard*. Geological Society, London, Memoir 17, 521 pp.
- Herron, E.M., Dewey, J.F. and Pitman, W.P., 1974. Plate tectonic models for the evolution of the Arctic. *Geology*, 4, p. 377-380.
- Holbrook, S.W., Mooney, W.D. and Christensen, N.I., 1992. The seismic structure of the deep continental crust in continental lower crust. In: F. M. Fountain, R. Arculus and R.W. Kay (eds.), *Developments in Geotectonics*, Elsevier, p. 1-42.
- Hopper, J., Funck, T., Marcussen, C. Jackson, H.R. and Shimeld J., 2009. Arctic Tectonic Puzzles: the Makarov Basin, Marvin Spur, and the Lomonosov Ridge. American Geophysical Union Fall Meeting, abstract #T51A-1491.
- Jackson, H.R. Dahl-Jensen, T. and the LORITA working group, 2010. Sedimentary and crustal structure from the Ellesmere Island and Greenland continental shelves onto the Lomonosov Ridge, Arctic Ocean. *Geophysical Journal International*, 182, p. 11–35, doi: 10.1111/j.1365-246X.2010.04604.x
- Jakobsson, M., Macnab, R., Mayer, L., Anderson, R., Edwards, M., Hatzky, J., Schenke, H-W., and Johnson, P., 2008. An improved bathymetric portrayal of the Arctic Ocean: Implications for ocean modeling and geological, geophysical and oceanographic analyses. *Geophysical Research Letters*, 35, L07602, doi:10.1029/2008GL033520.
- Jokat, W., Uenzelmann-Neben, G., Kristoffersen, I. and Rasmussen, T.M., 1992. Lomonosov Ridge - A double-sided continental margin. *Geology*, 20, p. 887-890.
- Jokat, W. 2005. The sedimentary structure of the Lomonosov Ridge between 88°N and 80°N: Consequences for tectonic and glacial processes. *Geophysical Journal International*, 163, p. 698–726, doi: 10.1111/J.1365-246X.2005.02786.x
- Kenyon, S., R. Forsberg, and B. Coakley, 2008.

- New Gravity Field for the Arctic. EOS, Transactions AGU, 89 (32), p. 289-290, doi:10.1029/2008EO320002.
- Kristoffersen, Y., 2001. An ODP-site survey on Lomonosov Ridge during Arctic Ocean 2001. Swedish Polar Secretariat Yearbook 2001, p. 64-66.
- Kristoffersen, Y. and Mikkelsen, N., 2006. On sediment deposition and nature of the plate boundary at the junction between the submarine Lomonosov Ridge, Arctic Ocean and the continental margin of Arctic Canada/North Greenland. *Marine Geology*, 225, p. 265-278.
- Langinen, A.E., Lebedeva-Ivanova, N.N., Gee, D.G. and Zamansky, Yu.Ya., 2008. Correlations between the Lomonosov Ridge, Marvin Spur and the adjacent basins of the Arctic Ocean based on seismic data. *Tectonophysics*, 472, p. 309-322, doi: 10.1016/j.tecto.2008.05.029.
- Lebedeva-Ivanova, N., Gee, D.G. and Sergeev, M.B., 2011. Crustal structure of the East Siberian continental margin, Podvodnikov and Makarov basins, based on refraction seismic data (TransArctic 1989-1991). In: Spencer, A.M., Embry, A.F., Gautier, D.L., Stoupakova, A.V. & Sorensen, K. (eds.) *Arctic Petroleum Geology*. Geological Society, London, Memoirs, 35, p. 395-411, doi:10.1144/M35.26.
- Mair, J. A. and Forsyth, D. A., 1982. Crustal structure of the Lomonosov Ridge and the Fram and the Makarov Bains near the North Pole. *Journal of Geophysical Research*, 89, p. 473-481.
- Miles, W. F., 2002. Areomagnetic data remediation, Axel Heiberg Island and eastern Canada Basin, Nunavut-Northwest Territories. Geological Survey of Canada Open File Report 2003-069054.
- Moore, T.E., Grantz, A., Pitman, J.K. and Brown, P.J., 2011. A first look at the petroleum geology of the Lomonosov Ridge. In: Spencer, A. M., Embry, A. F., Gautier, D. L., Stoupakova, A. V. & Sørensen, K. (eds.) *Arctic Petroleum Geology*. Geological Society, London, Memoirs, 35, p. 751-770, doi:10.1144/M35.44.
- Nassichuk, W.W. and Davies, G.R., 1980. Stratigraphy and sedimentation of the Otto Fiord Formation - a major Mississippian-Pennsylvanian evaporate of subaqueous origin in the Canadian Arctic Archipelago. *Geological Survey of Canada Bulletin*, 286, 87pp.
- Oakey, G., Damaske, D. and Nelson, B., 2012. Geology and volcanism along the Canadian Arctic margin: New constraints from aeromagnetic mapping. International Polar Year 2012 Conference, Montreal, Canada.
- Ostenso, N.A., 1974. Arctic Ocean margins. In: C.A. Burk and C.L. Drake (eds.): *Geology of continental margins*, Springer, New York, p. 753-763.
- Ostenso, N.A., and Wold, R.J., 1977. A seismic and gravity profile across the Arctic Ocean Basin. *Tectonophysics*, 37, p. 1-24.
- Poselov, V.A., Avetisov, G.P., Butsenko, V.V., Zholondz, S.M., Kaminsky, V.D., and Pavlov, S.P., 2012. The Lomonosov Ridge as a natural extension of the Eurasian continental margin into the Arctic Basin. *Russian Geology and Geophysics*, 53(12), p. 1276-1290.
- Pulvertaft, T.C.R. and Dawes, P.R., 2011. North Atlantic spreading axes terminate in the continental cul-de-sacs of Baffin Bay and the Laptev Sea. *Canadian Journal of Earth Sciences*, 48, p. 593-601, doi:10.1139/E11-004.
- Rowley, D. B. and Lottes, A., 1988. Plate kinematic reconstruction of the North Atlantic and Arctic: Late Jurassic to Present. *Tectonophysics*, 155, p. 73-120.
- Sekretov, S.B., 2001. Eurasia Basin – Laptev Sea geodynamic system: Tectonics and structural evolution. *Polarforschung*, 69, p. 51-44.
- Srivastava, S.P. and Tapscott, C.R., 1986. Plate kinematics of the North Atlantic. In: Vogt, P.R. and Tucholke, B.E. (eds.), *The Western North Atlantic Region, The Geology of North America*, M, Geological Society of America, Boulder, CO, p. 379-404.
- Sørensen, K., Gautier, D., Pitman, P., Jackson, H.R. and Dahl-Jensen, T., 2011. Geology and petroleum potential of the Lincoln Sea Basin, offshore North Greenland. In: Spencer, A. M., Embry, A. F., Gautier, D. L., Stoupakova, A. V. and Sørensen, K. (eds.) *Arctic Petroleum Geology*. Geological Society, London, Memoirs, 35, 673–684, doi:10.1144/M35.44.
- Trettin, H.P., 1991. The Proterozoic to Late Silurian record of Pearya, Chapter 9 in *Geology of the*

Innuitian Orogen and Arctic platform of Canada and Greenland. In: H.P. Trettin (ed.) Geological Survey of Canada, no. 3 (also Geological Society of America, The Geology of North America v. E), p.241-291.

Trettin, H.P. and Parrish, R., 1987. Late Cretaceous bimodal magmatism, northern Ellesmere Island: isotopic age and origin. *Canadian Journal of Earth Sciences*, 24, p. 257-275.

Weber, J. R., 1979. The Lomonosov Ridge experiment: 'LOREX 79'. *EOS, Transactions of the American Geophysical Union*, 60, p. 715-721.

Weber, J. R., 1983. Maps of the Arctic Basin Sea Floor: A History of Bathymetry and its Interpretation. *Arctic*, 36, p. 121-142.

Weber, J. R. and Sweeney, J. F., 1985. Reinterpretation of Morphology and Crustal Structure in the Central Arctic Ocean Basin. *Journal of Geophysical Research*, 90, p. 663-677.

Zelt, C.A., 1999. Modelling strategies and model assessment for wide-angle seismic traveltimes data. *Geophysical Journal International*, 9, p. 183-204.

The Arctic-2010 cruise: bathymetric survey for delineation of the extended continental shelf of the Russian Federation in the Arctic

Sergey Alekseev¹, Ivan Glumov², Andrey Morozov³, Konstantin Stavrov¹, Andrey Zen'kov¹, and Denis Zhilin⁴

¹State Research Navigation-Hydrographic Institute (OJSC GNINGI) St.Petersberg, Russia

²Severnaya Neftegazovaya Kompaniya Open Joint-Stock Company (Severneftegas OJSC), Moscow, Russia

³Russian Federal Agency for Subsoil Use, Rosnedra, Moscow, Russia

⁴HYDRO-C, Joint Stock Company, Russia

ABSTRACT

Having ratified the United Nations Convention on the Law of the Sea (UNCLOS) in 1997, the Russian Federation began exploration to specify the outer limit of the continental shelf in the Arctic Ocean. In December 2001, Russia was the first State to present a Submission on the limit of the continental shelf in this region, prepared in compliance with the requirements of UNCLOS, to the Secretary General of the United Nations. In June 2002 the Commission on the Limits of the Continental Shelf prepared its decision concerning the Claim of the Russian Federation and recommendations for its further development.

Starting from 2002, work was conducted with the aim to prepare the revised Submission to the UN Commission. To address bathymetry aspects, digital hydrographic databases were developed and 2D and 3D bathymetric models of the submarine relief for the Arctic Ocean were created. When preparing the materials for the planned 2013 revised Submission to the UN Commission on determining the outer limit of the continental shelf in the Arctic, it became clear that additional complex hydrographic and geophysical surveys were required—approximately 12,000 linear kilometers. To achieve this, the expedition used the research vessel (RV) “Akademik Fedorov” in combination with the “Yamal,” one of the most powerful nuclear-powered icebreakers, in heavy ice conditions.

The bathymetric survey in the central part of the Arctic Ocean was conducted to obtain the additional data on the submarine relief using a preplotted grid of bathymetric profiles to be used for delimitation of the Russian continental shelf in the Arctic Ocean.

For the first time, the bathymetric survey in this

area of the Arctic Ocean was carried out along the predefined rectilinear bathymetric profiles created according to of the technical guidance of the UN Commission on the Limits of the Continental Shelf.

For a period of 77 days, an enormous volume of work was carried out. The cruise covered a total distance of 23,100 km and the survey was carried out for a total distance of 13,304 linear km, including:

- 9300 linear km for bathymetric survey along the main lines;
- 4004 linear km for bathymetric survey on transits between the main lines;
- 760 km of seismic survey;
- 128 hydrological stations;
- 8 ice reconnaissance operations.

INTRODUCTION

In 1997 the Russian Federation ratified the United Nations Convention on the Law of the Sea and started the explorations intended to specify the outer limit of the continental shelf in the Arctic Ocean. In December 2001 Russia was the first State to present the Submission on the limit of the continental shelf in this region prepared in compliance with the requirements of the Convention to the Secretary General of the United Nations.

In June 2002 the UN Commission on the Limits of the Continental Shelf prepared its decision concerning the submitted Claim of the Russian Federation. The commission recommended further research on the submitted claim. From 2002 the work was conducted with the aim to prepare a revised Submission to the UN Commission and decided to submit a revised claim by 2013 on the outer limit of the continental shelf in the Arctic. When preparing the claim, it became evident that an additional

12,000 linear kilometers of complex hydrographic and geophysical surveys including 9000 kilometers of multibeam bathymetric data were required in the Arctic.

This resulted in a significant hydrographic survey carried out in 2010 in the Arctic by the Russian Federation. A survey was carried out for a period of 77 days covering an astonishing total distance of 23,100 kilometers in ice conditions and acquired 9300 linear km of bathymetry along the main lines (Figure 1) and an additional 4004 linear km of bathymetry on transit lines for a total of 13,304 linear km of multibeam data as well as 760 km of seismic data, occupied 128 hydrological stations and carried out 8 ice reconnaissance operations.

THE ARCTIC SURVEY

The survey was scheduled to be performed during one survey season, from; July until October 2010. Due to the ice- and weather-conditions at this high latitude in combination with the size of the project this became an extremely complicated and challenging task. The research vessel “Akademik Fedorov” was mobilized, in order have the right platform for the survey, together with the nuclear

powered icebreaker “Yamal” in order to be able to operate under these heavy ice conditions. Also two helicopters were present, Mi-2 and Mi-8T for further assistance. The survey area, as well as the co-ordinates of the bathymetric sailing directions that had to be covered by the fleet, were defined by the Scientific-technical project team according to the requirements of the UN Commission on the Limits of the Continental Shelf.

The bathymetric survey was carried out by the State Research Navigation-Hydrographic Institute (OJSC “GNINGI”) under a Russian State contract; with the Federal Agency on the Use of the Earth’s Interior (“ROSNEDRA”) on the commercial tender basis. During the cruise bathymetric surveys were carried out. Over 9000 kilometers of survey lines for use in substantiating the outer limit of the continental shelf were collected during the journey.

HYDROMETEOROLOGICAL CONDITIONS

Ice conditions were favorable during the entire period of the survey. The work was conducted mainly in one-year old ice with thicknesses of 1.5 - 2 m and concentrations of 90 – 100 % (9/10-10/10 ice cover). However, in the southern part of the eastern sector,

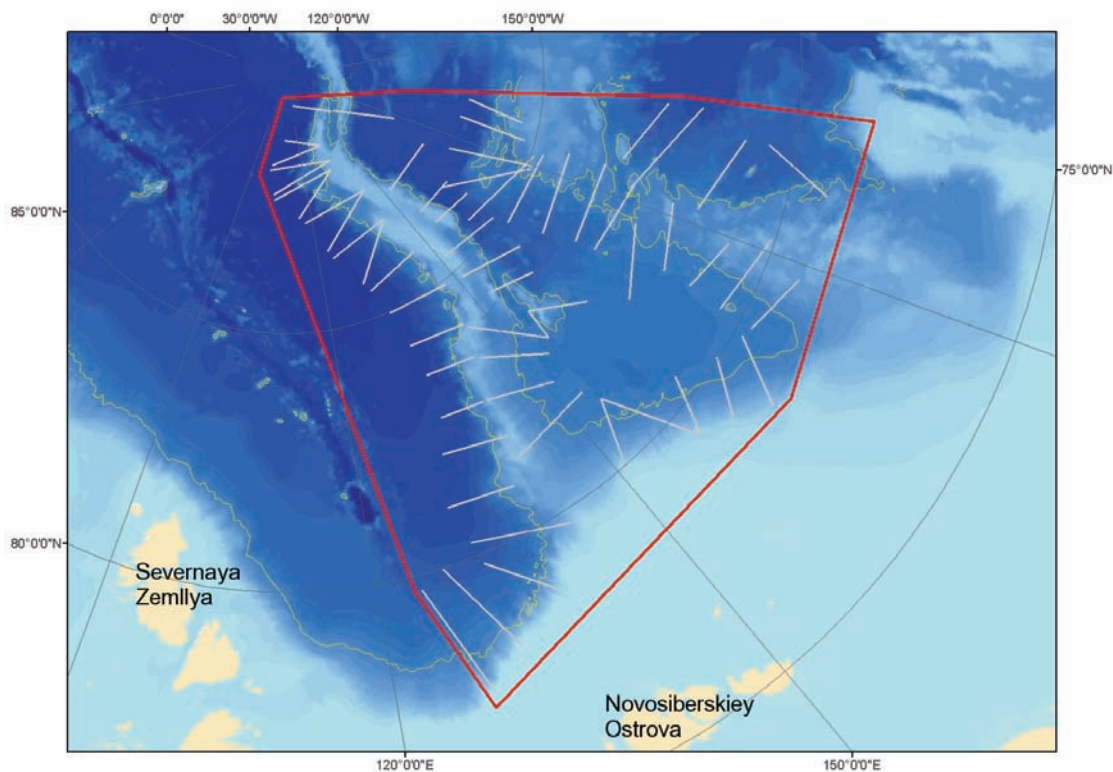


Fig. 1. Map of survey area (outlined in red) showing multibeam transects (transit lines are not shown) containing parts of the Lomonosov and Mendeleev Ridges. White contour shows 2500m depth, and transect lines.

old ice fields up to 4 m thick were encountered within the younger ice. The air temperature during the period did not fall below -18°C degrees.

SURVEY MOBILIZATION

From May 30 until July 7, 2010 the multibeam echo sounder Kongsberg EM 122 was installed on board of the “Akademik Fedorov” at the Turku Repair Yard Ltd..

The bathymetric system consisted of the following components:

- Kongsberg EM122 multibeam echo sounder;
- Kongsberg SIS acquisition software;
- Kongsberg EA 600 single-beam echo sounder;
- Kongsberg TOPAS subbottom profiler with a single-beam echo sounder option;
- Kongsberg Seapath 330 (GPS/GLONASS) primary navigation positioning system;
- C-NAV 2050R secondary navigation positioning system;

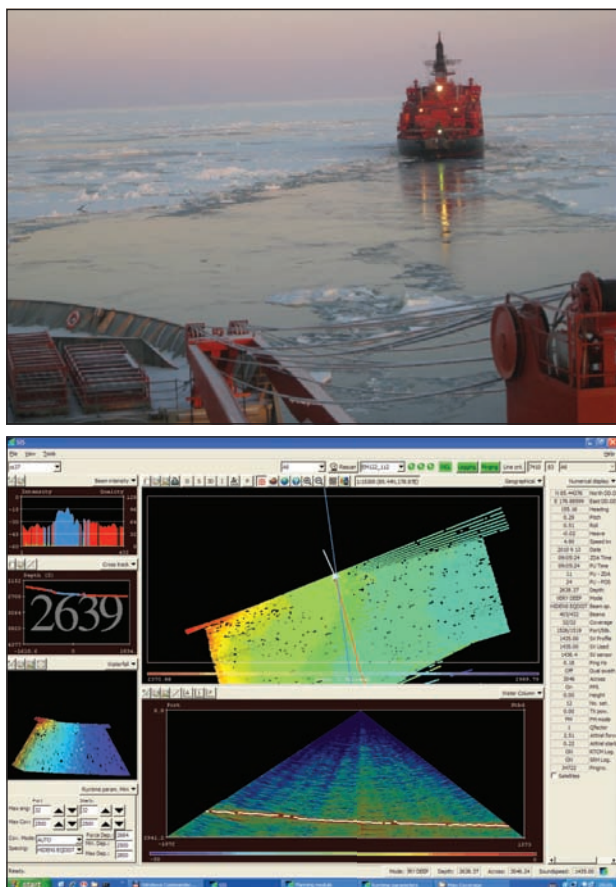


Fig. 2. Example of data acquisition on board of RV “Akademik Fedorov.” Swath width shown is approximately 3000m across. Depths range from 2300m (red) to 3000m (deep blue). Location of the detailed profile shown is about 85.4°N and 178.9°E.

- an integrated navigation and hydrographic system Quality Integrated Navigation System (QINSy);
- bathymetric data processing using CARIS HIPS&SIPS Professional and CARIS LOTS.

After installation, a harbor acceptance test of the complete survey outfit was carried out followed by the final sea acceptance in a test area in the Norwegian Sea under supervision of Kongsberg representatives. The Kongsberg representatives compiled a service report that included the description of the test, the results of the calibrations and qualification survey. The survey system on board of the “Akademik Fedorov” was accepted for operation after the analyses of sea trial results.

The icebreaker “Yamal” was also mobilized with the Qinsy software suite. This way the icebreaker could navigate along the pre-planned routes ahead of the “Akademik Fedorov”. Via telemetry, the navigation information on position, speed, distance, and direction were exchanged between the two vessels and displayed online.

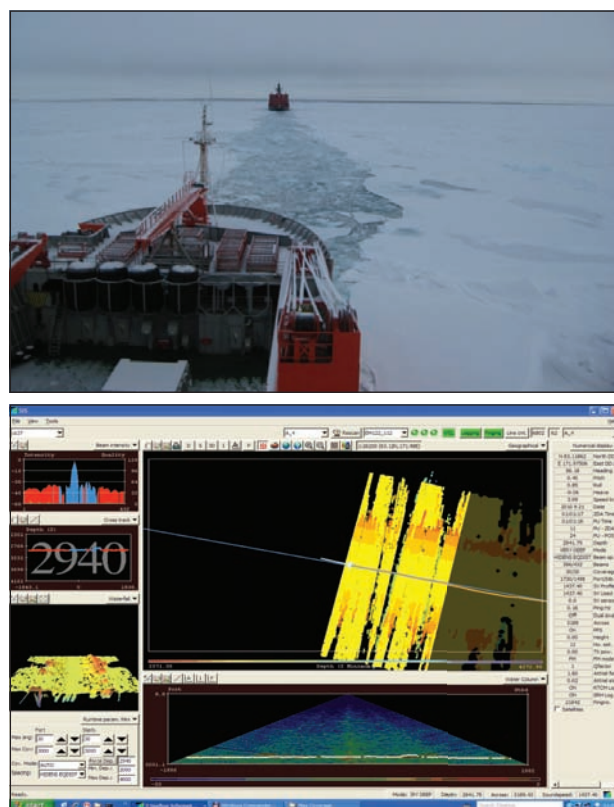


Fig. 3. Data acquisition on board of RV “Akademik Fedorov” with influence of ice conditions. The main swath width is about 3200m across, depths are from 1000m (red) to 4200m (deep blue). The detailed section at 2940m is located at 83.1°N, 172°E.

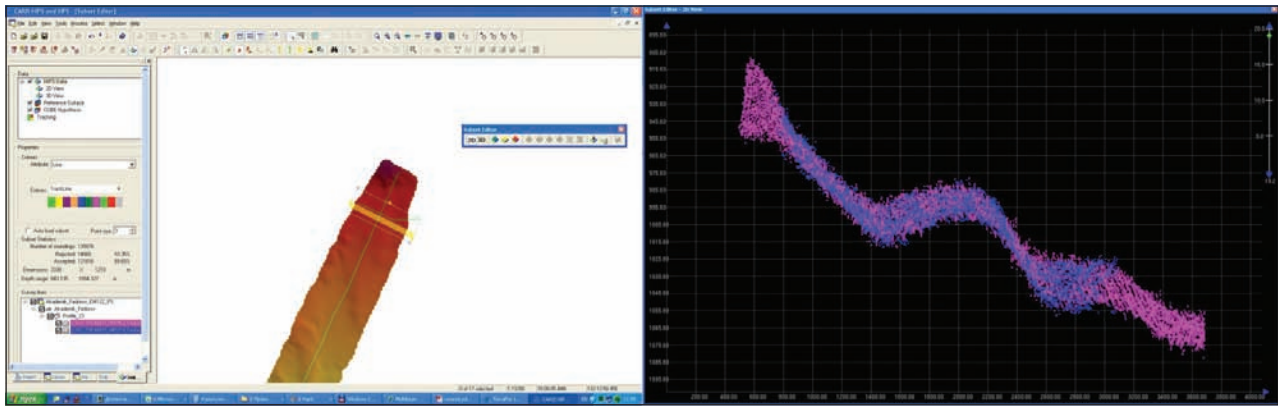


Fig. 4. Example of cross check analyses in CARIS HIPS/SIPS software. The right hand block shows depth vs distance with the corresponding section perpendicular to it. The locality is 78°N, 132.1°E. The matching of these two profiles shows no discrepancies, and thus validates the calibration parameters.

It was essential to enter the parameters of the sound velocity profiles (SVP) in the multibeam echo sounder system. The hydrological measurements were made in the course of the hydrographic surveys on regular basis at least once a day. A total of 128 oceanographic samples were taken of which 29 samples using the Midas Valeport probes to obtain the sound velocity profile, and 99 samples using the expendable XCTD probes.

The strong changes in course direction, ship's engine, machinery, as well as, the ice influenced the data reception by the multibeam echosounder. Noises negatively influenced the quality of the acquired data and in some cases even resulted in data loss.

QUALITY CONTROL

Before the start of the project, calibration tests were performed. In the course of the survey the quality of the bathymetric data was regularly

validated. Data from multibeam cross lines were compared to cross lines of the single-beam echo sounder data.

The results of the different mentioned SVP sensor models, MIDAS VALEPORT and XCTDs, were compared with each other in order to ensure data integrity and quality. At the end of the project, calibration tests were carried out again. No changes in the calibration parameters were detected during the survey.

A designated quality control group on board carried out the data analysis and performed data processing. The team was making use of the latest versions of CARIS HIPS Professional and Fledermaus Professional and Geocap processing software. The team corrected the multibeam data disturbances caused by the ice. While processing, the team also ensured that the acquired data met the data quality standards and specifications of UN

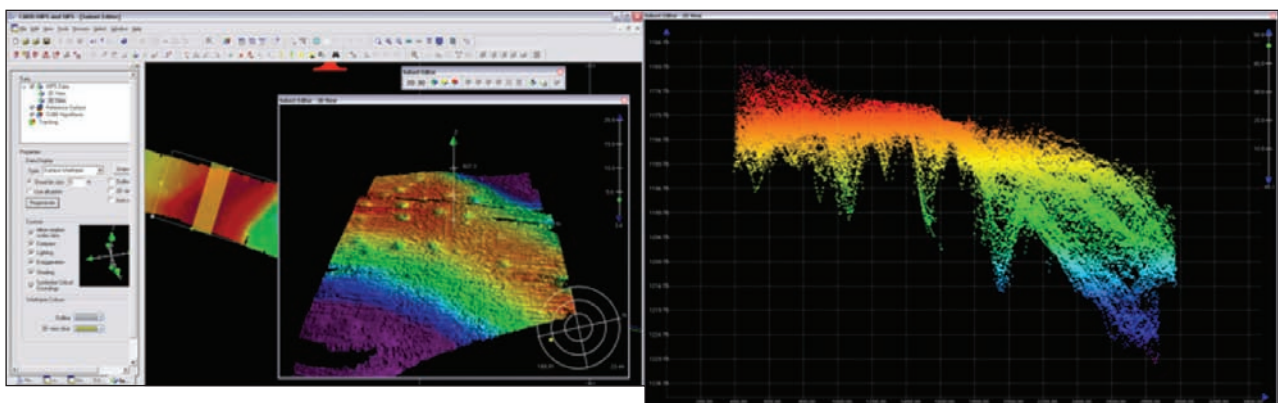


Fig. 5. Analyses of multibeam data in CARIS HIPS/SIPS software. Note the pock marks on the crest of the rise.

Commission on the Limits of the Continental Shelf. The defined standards were based on IHO S-44, Order 2 (IHO, 2008). As a result, the quality of the multibeam survey data was assured along all 59 survey lines.

Geocap and CARIS LOTS software were used for accurate determination of the foot of the slope (FOS) and calculation of the continental shelf boundary limits 60 miles or 100 kilometers from the FOS. These calculations were based on the Scientific and Technical Guidelines of the UN Commission on the Limits of the Continental Shelf. http://www.un.org/depts/los/clcs_new/commission_documents.htm#Guidelines

During multibeam processing, the main task was to provide the operational quality control of the initial data and data cleaning of erroneous measurements and disturbances, evaluation of the processing results and resolving of the remaining ambiguities.

The preliminary evaluation of the data accuracy and quality of the multibeam echo sounder was carried out after the preliminary onboard processing by means of the statistical comparison of the data from the main survey lines obtained by the multibeam echo sounder with the check lines data obtained by the multibeam echo sounder, single-beam echo sounder and subbottom profiler with the option of a single-beam echo sounder.

For additional control, digital terrain models (DTM) based on the CUBE algorithm were created and analyzed using processed data (Figures 7 and 8).

For quality control of positioning data, the offset differences between primary and the secondary positioning systems was monitored. Also positioning of Seapath 330 data was logged in RINEX format by SIS hydrographic software. During onshore processing this data was processed using TerraPos software by Terratec to improve the positioning accuracy. The processed navigation data

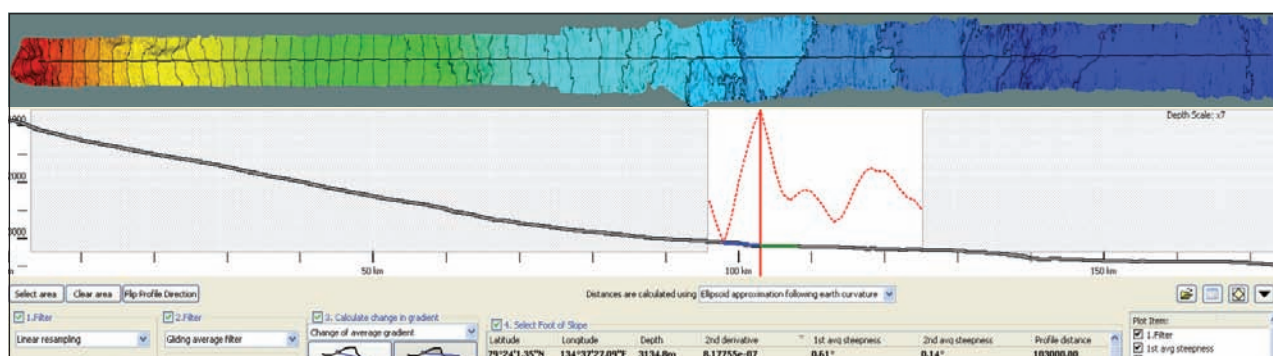


Fig. 6. Example of determination of Foot of Slope in Geocap. Selection of Foot of Slope based on the first derivative of changes in the slope. The foot of slope in this profile is at 71.2°N, 134.4°E.

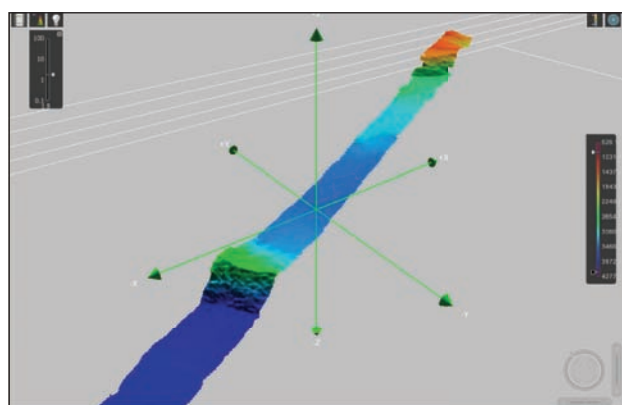


Fig. 7. Example of DTM in 3D mode in CARIS HIPS/SIPS software.

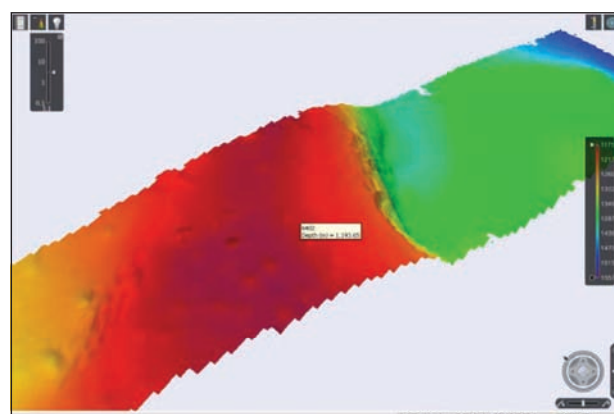


Fig. 8. Example of DTM in 3D mode in CARIS HIPS/SIPS software.

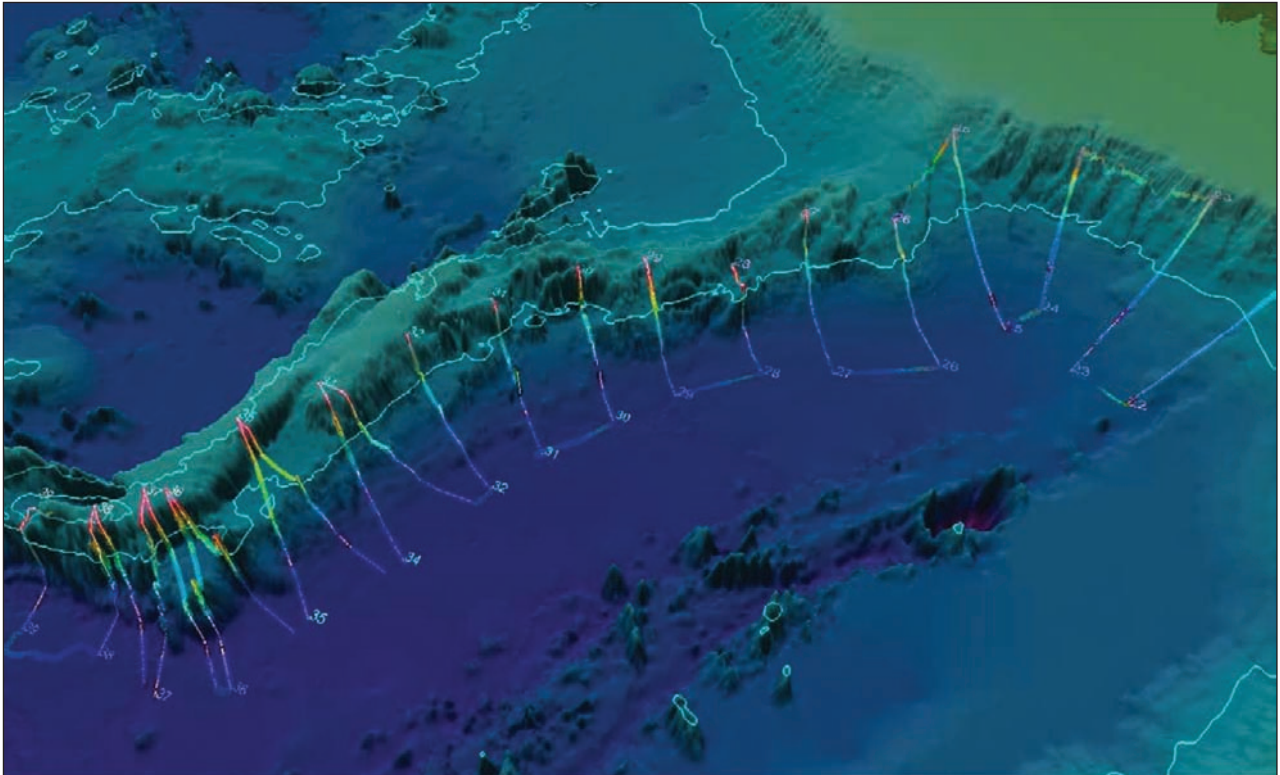


Fig. 9. The path of the multibeam survey on the west slope of the Lomonosov ridge (3D visualization). Note the white 2500m contour line outlining the Lomonosov, Alpha and Mendeleev Ridges

was imported into CARIS HIPS and statistically the original positioning data and processed positioning data were compared in order to determine the accuracy of the processed positioning information.

RESULTS OF THE EXPEDITION

According to quality assessment the acquired data complied well within the required standards in IHO S-44 Order 2 (IHO, 2008) and thus falling within the specified requirements of the UN Commission. The first stage of the survey in the framework of the State task for determination and substantiation of the outer limits of the Russian Federation's continental shelf in the Arctic Ocean was completed according to the set time limits.

REFERENCES

International Hydrographic Organization, 2008. Standards for Hydrographic Surveys 5th Edition, February 2008, Special Publication No. 44, Published by the International Hydrographic Bureau, Monaco. 28 p.

Early evolution stages of the arctic margins (Neoproterozoic-Paleozoic) and plate reconstructions

V. A. Vernikovsky^{1,2}, D. V. Metelkin^{1,2}, A. E. Vernikovskaya¹, N. Yu. Matushkin^{1,2}, L. I. Lobkovsky³, E. V. Shipilov⁴

¹Trofimuk Institute of Petroleum Geology and Geophysics, Siberian Branch of the RAS, 3, Akademika Koptyuga Prosp., Novosibirsk, Russia, 630090

²Novosibirsk State University, 2, Pirogova St., Novosibirsk, Russia, 630090

³Shirshov Institute of Oceanology of the RAS, 36, Nahimovsky Prosp., Moscow, Russia, 117997

⁴Polar Geophysical Institute, Kola Science Centre of the RAS, 15, Khalturina St., Murmansk, Russia, 183010

ABSTRACT

In this paper we offer paleoreconstructions for key structures of the Arctic based on the synthesis of geosstructural, geochronological and new paleomagnetic data bearing upon the Late Neoproterozoic and the Paleozoic histories of the Taimyr fold belt and Kara microcontinent. These tectonic features are part of a greater continental mass that we term “Arctida”, with an interesting history of breakup and reassembly that is constrained by our new data and synthesis. In the Central Taimyr accretionary belt fragments of an ancient island arc (960 Ma) have been discovered, and the paleomagnetic pole for the arc approximates the synchronous (950 Ma) pole for the Siberian paleocontinent. For the Kara microcontinent we demonstrate its evolution in the Early Paleozoic and its collision with Siberia in the Late Paleozoic. These data along with an extensive published paleomagnetic database for the cratons of Laurentia, Baltica, Siberia, and Gondwana are the basis for the presented paleotectonic reconstructions. The migrations of those Arctida tectonic blocks that lack paleomagnetic data are reconstructed based on geologic information.

INTRODUCTION

The current structure of the Arctic Ocean is determined by the position of the Amerasian (Canadian) and Eurasian basins, whose formation took place as a result of significant tectonic processes in the Late Mesozoic – Cenozoic. However it is impossible to understand relatively recent and modern tectonic displacements without analyzing previous tectonic events.

The discovery of Precambrian metamorphic complexes among the main structures of the

Arctic Region led to the suggestion that in the Late Precambrian a paleocontinent – termed “Arctida” – existed between Laurentia, Baltica and Siberia (Zonenshain, Natapov, 1987). In the classic presentation it is composed of several blocks of continental crust, whose relicts are now located in the Arctic (Fig. 1): the Kara block, the New Siberian block (the New Siberian Islands and the adjacent shelf), the North Alaska and Chukotka blocks, as well as small fragments of the Inuit Fold Belt in northern Greenland (Peary Land, the northern part of Ellesmere and Axel Heiberg islands) and the blocks of the underwater Lomonosov and Alpha-Mendeleev Ridges (Zonenshain, Natapov, 1987; Zonenshain et al., 1990). In the modern interpretation, aside from these fragments, Arctida also includes parts of Barentsia, which includes the structures of the Svalbard and the Timan-Pechora plates (Vernikovsky, 1996; Kuznetsov et al., 2007).

Late Precambrian and Paleozoic global tectonic history is defined by the breakup of Rodinia, the evolution of newly formed oceanic basins and the formation of Pangea as a result. Many paleotectonic schemes and reconstructions have been composed for the Late Precambrian – Paleozoic stages of the plates interactions (Scotese and McKerrow, 1990; Dalziel, 1991,1997; Hoffman, 1991; Powell et al., 1993; Condie and Rosen, 1994; Torsvik et al., 1996; Golonka, 2002; Golonka et al., 2003; Cocks and Torsvik, 2002; Lawver et al., 2002; Li et al., 2008; Pisarevsky et al., 2008, Metelkin et al., 2012). However, when dealing with the details of the evolution of separate lithosphere segments, including those of the Arctic Region, there are still many unsolved, debatable and ill-founded reconstructions. This is true mainly for the deciphering of the initial

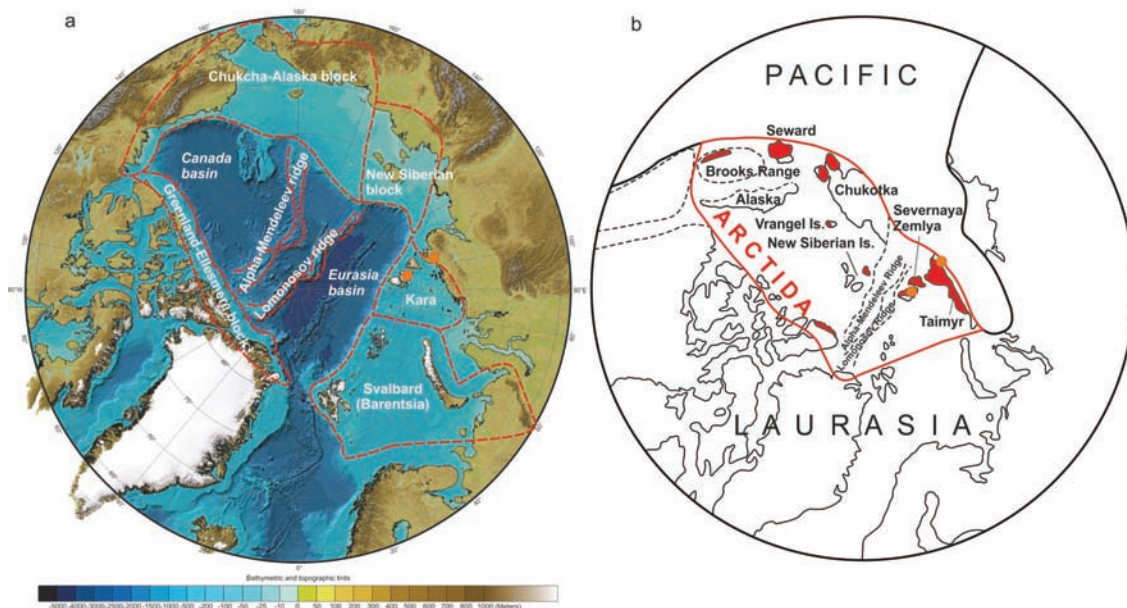


Fig. 1. (a) The main blocks, microcontinents, plates, and basins of the Arctic on the International Bathymetric Chart of the Arctic Ocean and (b) a reconstruction for the Early Jurassic, showing the Precambrian Arctic blocks (in red), amalgamated into the Arctida continent, which is attached to Laurasia (Zonenshain and Natapov, 1987; Zonenshain et al., 1990). The approximate location of the field study area within the Taimyr folded area is shown by orange dots.

structure of Arctida, the reasons and mechanisms of its breakup, the drift trajectories of the continental blocks that composed it. The very existence of oceanic basins that supposedly separated the paleocontinents is uncertain. All these are largely debatable topics, especially the early stages of the Arctic Region tectonic evolution – the Late Precambrian and the Early Paleozoic, which are the subject of this paper. In this study we have attempted to integrate the available geologic and geophysical material for the early evolution stages of the Arctic Ocean in the form of a series of paleotectonic reconstructions, as well as to create a new development model for the structures of Arctida.

The determination of the relative positions of the blocks composing Arctida could be done with paleomagnetic data. However, such data are very sparse for the Late Precambrian and the Paleozoic. For the entire Arctic Region the IAGA Global Paleomagnetic Database counts no more than 30 paleomagnetic determinations. Nearly all of the available data represent the Late Paleozoic and Early Mesozoic of the Barentsia and Greenland-Ellesmere regions. There are no data for the New Siberian Islands and the territories of Chukotka and Northern Alaska, which represent most of the classic

Arctida area. Reliable paleomagnetic determinations for the Neoproterozoic-Paleozoic time interval are available only for fragments of a 960 Ma island arc from Central Taimyr (Vernikovsky et al., 2011) and for which the paleomagnetic pole is comparable to the approximately synchronous pole of Siberia from (Pavlov et al., 2002). There are other reliable data for the Kara microcontinent: this includes three paleomagnetic poles for 500, 450 and 420 Ma (Metelkin et al., 2000; 2005). It is these data that are placed at the core of our paleotectonic reconstructions along with the extensive paleomagnetic database for the Laurentia, Baltica, Siberia and Gondwana cratons (Pechersky and Didenko, 1995; Torsvik et al., 1996; Smethurst et al., 1998; McElhinny and MacFadden, 2000; Wingate and Giddings, 2000; Pavlov et al., 2002; Torsvik and Van der Voo, 2002; Meert and Torsvik, 2003; Metelkin et al., 2007, 2012; Li et al., 2008). The paleogeographic position of the cratons is corrected (within confidence limits for paleopoles) in accordance with the general model and available global reconstructions, including structures of the Arctic sector (Scotese, 1997; Lawver et al., 2002, 2011; Golonka et al., 2003, 2006; Kurenkov et al., 2005; Cocks and Torsvik, 2002, 2007).

THE OLDEST ISLAND ARC COMPLEX OF CENTRAL TAIMYR

The Central-Taimyr accretionary belt is located between two large continental blocks – the Siberian craton on the south and the Kara microcontinent on the north (Fig. 2a). It is composed of paleo-island arc fragments, granite-metamorphic terranes, passive continental margin terranes of mainly carbonate composition and ophiolites, which were amalgamated and accreted to the Siberian craton in the Late Neoproterozoic and then unconformably overlain by a Vendian (Ediacaran) – Early Carboniferous cover (Uflyand et al., 1991; Vernikovskiy, 1996; Khain et al., 1997; Vernikovskiy and Vernikovskaya, 2001; Pease et al., 2001). In this model a significant role is played by ophiolites and island arcs, whose zircons U–Pb age has been established in the interval of 755–730 Ma from plagiogranites, gabbros and volcanogenic rocks (Vernikovskiy et al., 1994; 2004). However, no paleomagnetic data have been obtained for the 755–730 Ma rocks. Investigations carried out in the North-Eastern Taimyr in recent years allowed us to identify an older (960 Ma) paleo-island arc complex in the Central Taimyr accretionary belt and to establish its location at the time of formation by using paleomagnetic data.

The studied area of the Three Sisters Lake (Fig. 2b) is the junction zone of Zhdanov formation rocks (Zabiyaka et al., 1986) and mainly volcanogenic rocks previously included in the Borzov (Bezzubtsev et al., 1986) or Laptev (Zabiyaka et al., 1986) formations. Zhdanov formation rocks are mainly terrigenous (greenish-grey and grey sandstones, siltstones, black and dark-grey phyllites with separate layers of carbonate rocks, andesite-basalts, acid effusive rocks and their tuffs), metamorphosed in greenschist facies conditions. Borzov/Laptev formation rocks (metamorphosed basalts, andesites, dacites, plagioryhodacites) are host to plagiogranites and plagiogranite porphyry. Both formations are intruded by slightly metamorphosed gabbro-dolerite sills and dikes with thicknesses ranging from tens of centimeters to hundreds of meters which compose a wide dike belt with a total length of over 100 km. The Zhdanov and Borzov/Laptev formations are overlain by the coarse-grained terrigenous deposits of the Oktyabrsk formation. In the studied region the rocks that compose the island arc are tectonically

composited with sedimentary and volcanogenic-sedimentary deposits that we consider to have formed in an adjoining back-arc basin.

In the study area andesites, dacites, and plagioryhodacites are the dominant rock types in the paleo-island arc complex. These rocks range from dark-grey with a lilac hue to bottle-green, sometimes with 2–4 mm phenocrysts of plagioclase, quartz and less frequently of subordinate potassium feldspar. Andesites are distinguished by their fine-grained matrix textures and by the presence of suites of ore minerals. Hypabyssal rocks are represented by metamorphosed plagiogranite porphyry with medium-grained matrix texture and consisting mainly of quartz and plagioclase. Plagiogranites also contain hornblende and clinopyroxene. Secondary minerals are albite, chlorite, biotite, carbonate, and epidote. These rocks are often schistose and highly fractured and veined. Diabases and gabbrodolerites are fine- and medium-grained and intensely amphibolized.

The studied acid-intermediate volcanic and intrusive rocks are attributed to the tholeiitic magmatic series. They have weakly or moderately fractionated REE spectra ($(La/Yb)_N = 3.3–11.5$) with small negative Eu anomalies ($Eu/Eu^* = 0.7–0.9$), the total REE concentration is 330–781 ppm. On the spider diagrams the rocks are enriched in La, Ce and also Th and U and depleted in Sr, Ti, P, Ta, and Nb. For the island arc metabasites the total REE concentration varies in a wider interval from 233–375 to 1290 ppm. They can have small Eu anomalies ($Eu/Eu^* = 0.9–1.1$), whereas the $(La/Yb)_N$ ratio values vary widely from 1–3.5 to 36.6. The REE spectra are flat, typical of MORB and close to those of island arc basalts. The established Rare Earth and other trace elements distribution types for the entire complex are similar to those of the igneous rocks of Neoproterozoic island arc of other Taimyr regions (Vernikovskiy et al., 1994, 2004).

We performed U–Pb isotopic analysis utilizing a multicollector Finnigan MAT-261 mass spectrometer and the Sm, Nd, Rb, and Sr analysis – on a 7-collector Triton T1 mass spectrometer at the Institute of Precambrian Geology and Geochronology of the RAS, St. Petersburg (Russia).

The accessory zircons from a plagioryhodacite and a plagiogranite are semitransparent and

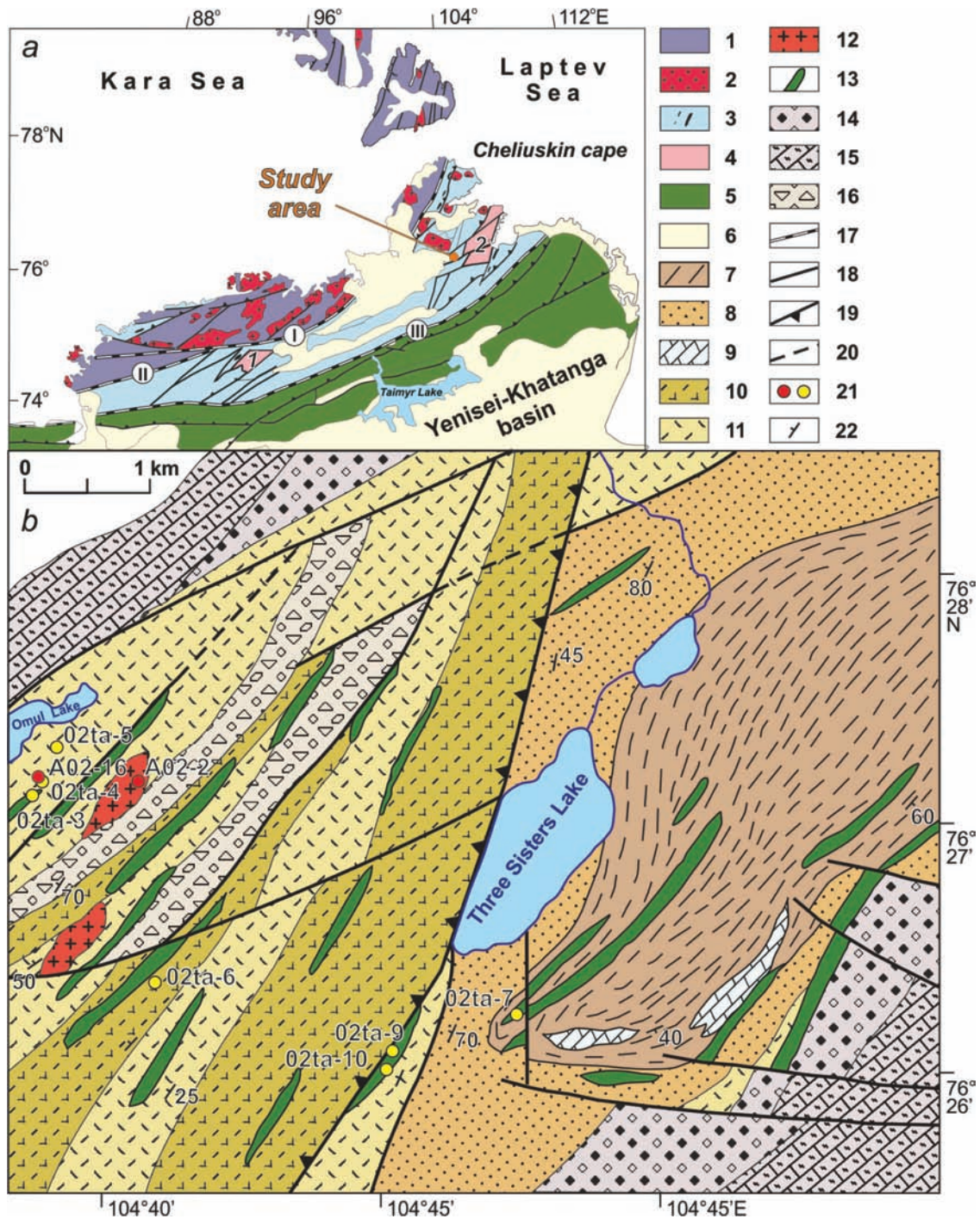


Fig. 2. (a) The Three Sisters Lake study area location on the tectonic scheme of the Taimyr folded area; and (b) a geologic map of the Three Sisters Lake study area composed using the data of Bezzubtsev et al., (1986); Zabiya et al., (1986); and Vernikovskiy (1996). 1–6 – Tectonic elements and geodynamic complexes on the tectonic scheme shown on the regional map (a): 1 – Kara microcontinent (NP–PZ); 2 – collisional granitoids (300–264 Ma, after Vernikovskiy et al., (1995; 1998)); 3 – Central Taimyr accretionary belt (NP) including 4 – Mamont-Shrenk (1) and Faddey (2) cratonic terranes; 5 – South Taimyr folded belt (PZ–MZ); 6 – overlapping sedimentary complex. 7–16 – Neoproterozoic rocks shown on the geological map (b): 7–9 – Zhdanov formation including: 7 – black phyllites and siltstones; 8 – sandstones and siltstones with subordinate interbeds of phyllites; 9 – lenses of limestones and dolomites; 10–11 – Borzov/Laptev formation including: 10 – andesites, dacites, subordinate basalts and andesite-basalts; 11 – plagioryhodacites; 12 – intrusions of plagiogranites; 13 – gabbro-dolerite sill; 14–16 – overlapping strata of Oktyabrsk formation including: 14 – quartz and polymict conglomerates; 15 – oligomict and quartz sandstones and gritstones; 16 – polymict and quartz conglomerates, breccias. 17–21 – faults and other symbols shown in both maps (a) and (b): 17 – sutures: I – Main Taimyr, II – Diabasovy, III – Pyasina-Faddey; 18 – normal faults, reverse faults, strike slip faults, 19 – thrusts; 20 – inferred faults; 21 – sampling sites for geochronological (red) and paleomagnetic (yellow) investigations; 22 – strata bedding.

transparent subidiomorphic pink crystals of prismatic and short-prismatic shape. The morphological particularities of the zircon grains indicate their magmatic origin. The isotopic composition points of the studied zircons from a plagioryhodacite (sample A02-16) are approximated by a regression line, where the upper intersection with the concordia corresponds to the age 966 ± 5 Ma and the lower intersection corresponds to 279 ± 30 Ma, with $MSWD = 0.84$ (Vernikovskiy et al., 2011). At the same time the isotopic composition points for the zircon residue after acid treatment with longer exposition is located on the concordia, and its concordia age is 961 ± 3 Ma ($MSWD = 0.72$, probability = 0.4) and can be accepted as the most precise crystallization time estimate for the studied zircons.

The isotopic composition points for 20 untreated zircon grains from a plagiogranite (sample A02-2) and for two residues after acid treatment form a discordia whose upper intersection with the concordia corresponds to the age of 989 ± 41 Ma, and the lower one – 508 ± 410 Ma, $MSWD = 0.05$. The mean age value, calculated from the $^{207}\text{Pb}/^{206}\text{Pb}$ ratio of the three fractions of the studied zircon grains correspond to 969 ± 17 Ma and is close to the age value obtained from the upper intersection with the discordia. This age estimate may be used as the most precise one (Vernikovskiy et al., 2011).

Sm–Nd isotopic data for island arc acid intrusive and volcanic rocks of the Three Sisters Lake region yield a Mesoproterozoic model age: $T_{\text{Nd}}(\text{DM})$ varies from 1170 to 1219 Ma. These data as well as Rb–Sr isotopic investigations indicate a predominance of a mantle component in the magmatic sources of these rocks: $\epsilon\text{Nd}_{(967-961)} = 5.1-5.2$ and $(^{87}\text{Sr}/^{86}\text{Sr}_0) = 0.70258-0.70391$ (Vernikovskiy et al., 2011).

The paleomagnetic analysis was performed on the apparatus of the Paleomagnetic Center in the Laboratory of Geodynamics and Paleomagnetism of the IPGG SB RAS (Novosibirsk). The hardware system comprises new generation measurers including a 2G Enterprises Superconductive Magnetometer (USA) with built-in AF-demagnetizer and an HSM superconductive spinner-magnetometer (Germany), as well as the well-known JR-4 and JR-6 spin-magnetometers (Czech Republic) and other instruments, placed in a shielded room. The investigation includes a detailed stepwise

thermal demagnetization (T -demagnetization) and/or alternating field demagnetization (AF -demagnetization) of all studied samples until their complete demagnetization.

The experimental results were processed with specialized software products that use standard techniques for component analysis (Butler, 1992); and various modifications of the fold test (McFadden, 1990; Watson and Enkin, 1993, Enkin, 2003) and reversal test (McFadden and McElhinny, 1990) for dating the magnetization components. The sample collection includes volcanic as well as intrusive rocks of the paleo-island arc complex (Fig. 2b). One site (02ta-4) corresponds to an outcrop of plagioryhodacites (sample A02-16), which has been dated by U-Pb method. The studied rocks are characterized by relatively low values of natural remnant magnetization, NRM (tens of mA/m, thousands for one outcrop) and a high magnetic susceptibility - about 10^{-3} SI units. For the analysis of the NRM components T -, and AF -demagnetization were used. Typical orthogonal plots are given in Fig. 3. Most of the samples are characterized by two often unidirectional components – a titanomagnetite component with a blocking temperature T_B of about 400°C and a magnetite component with $T_B \sim 580^\circ\text{C}$. Distinctive particularities in the NRM vector behavior during the demagnetization of rocks from various outcrops are mainly due to the input of the titanomagnetite and magnetite components. In some samples the component of characteristic remnant magnetization ($ChRM$; shown as dashed lines in vertical plane projections (open circles), Fig. 3) is exactly registered in a high temperature interval $400-580^\circ\text{C}$, and the almost complete demagnetization of others is reached with the heating to 400°C or lower. In the last case (lower right in Fig. 3) the AF -demagnetization is more informative. The value of the median destructive field (MDF) is no more than $20-30$ mT, and the complete demagnetization is reached by the impact of the alternating magnetic field no more than 100 mT. The established average $ChRM$ directions are given in Table 1 (In situ and Tilt corrected). The primary nature of the $ChRM$ can be substantiated by positive results of the reversals and fold tests. The upper five of the studied sample groups have a normal polarity, the mean direction in stratigraphic coordinates: $D = 319.2$, $I = 13.7$,

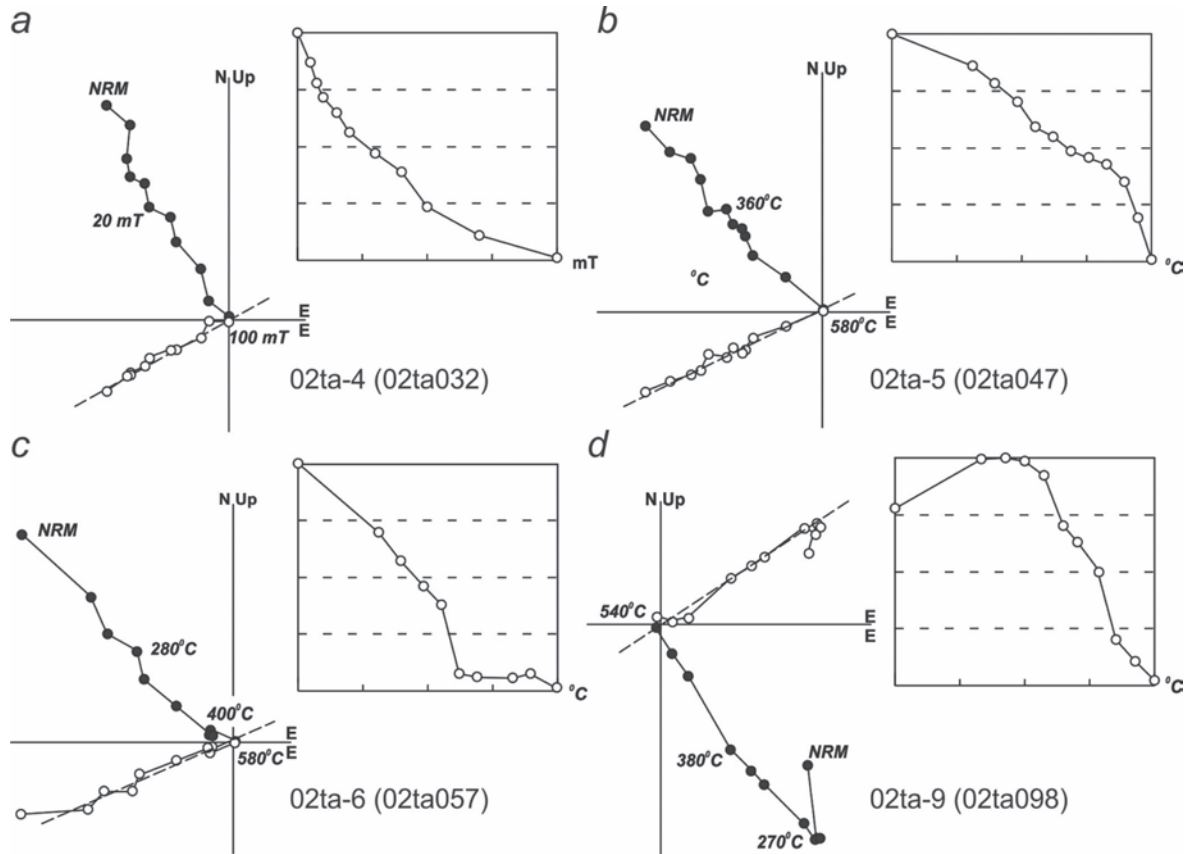


Fig. 3. Typical orthogonal plots in tilt-corrected coordinates and corresponding *NRM* vs. *T(AF)* graphs based on the results of *T*- and *AF*-demagnetization: (a) dacite from site 02ta-4 (sample number 02ta032); (b) rhyolite from site 02ta-5 (sample number 02ta047); (c) andesite from site 02ta-6 (sample number 02ta057); gabbro-dolerite from site 02ta-9 (sample number 02ta098). Solid dots represent projections of vector endpoint on the horizontal plane, and the open ones – on the vertical plane, the dashed line shows the stable *ChRM* component.

Table 1. Paleomagnetic directions and coordinates of virtual geomagnetic poles of the studied 960-Ma volcanogenic formation from the Three Sisters Lake region

Site numbers, rock type	<i>n/N</i>	In situ		Tilt corrected		<i>k</i>	α_{95}	VGPole			PL
		<i>D</i> (°)	<i>I</i> (°)	<i>D</i> (°)	<i>I</i> (°)			<i>PLat</i>	<i>PLong</i>	<i>dp/dm</i>	
02ta-3, gabbro-dolerite	10/11	70.0	86.1	323.9	16.3	374.1	2.5	19.1	322.7	1.3/2.6	8.3±1.9
02ta-4, dacite	8/10	152.5	88.0	319.5	16.9	118.9	5.1	18.8	327.3	2.7/5.3	8.6±3.8
02ta-5, rhyolite	10/10	327.5	89.4	320.1	14.4	75.4	5.6	17.6	326.5	2.9/5.7	7.3±4.1
02ta-6, andesite	7/10	209.4	80.5	310.7	18.1	92.7	6.3	17.9	336.5	3.4/6.5	9.3±4.7
02ta-7, gabbro-dolerite	9/12	300.4	-82.0	321.7	2.3	38.5	8.4	11.7	324.1	4.2/8.4	1.2±5.9
02ta-9, gabbro-dolerite	8/10	85.8	-69.1	138.9	-17.9	89.1	5.9	19.2	328.2	3.2/6.1	9.2±4.4
02ta-10, gabbro-dolerite	10/10	94.6	-74.0	144.8	-17.6	72.8	5.7	20.0	322.0	3.1/5.9	9.0±4.3
Mean		264.2	81.2	320.0	14.8	127.3	5.4	17.8	326.8	$A_{95}=4.0$	7.5±4.0

Note: *n/N* – ratio of the number of samples, used in the statistics, to the total number of studied samples; *D* – declination in degrees; *I* – inclination in degrees; *k* – precision parameter, α_{95} – 95% confidence limit, *VGPole* – the virtual geomagnetic pole coordinates (the inverted positions of the poles are given); *PLat* – latitude, *PLong* – longitude, *dp/dm* – semiaxes of the confidence circle of paleomagnetic pole; the mean pole is calculated as the average from the *VGPole* batch where A_{95} - 95% confidence limit; PL – paleolatitude for the reconstructed block in northern hemisphere.

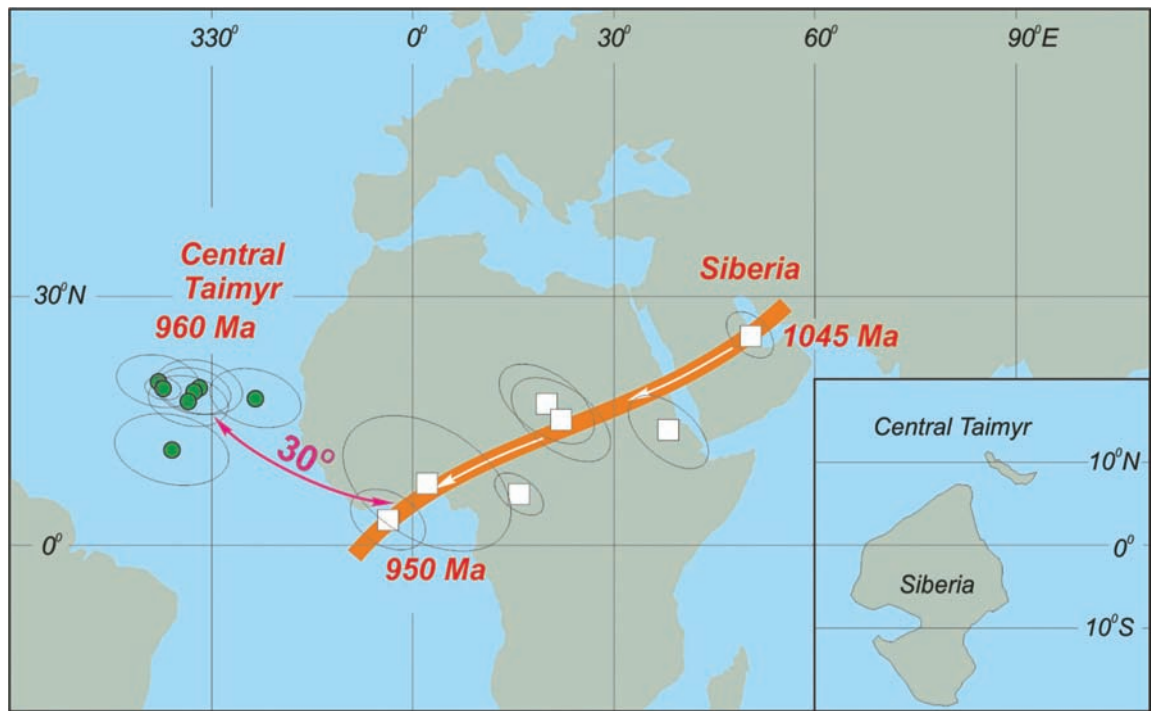


Fig. 4. The relative positions of the calculated Central Taimyr 960 Ma paleomagnetic poles (Table 1, circles) and APWP of Siberia for the time period 1,045–950 Ma by (Pavlov et al., 2002) and a paleogeographic reconstruction (inset) of the Central Taimyr margin and Siberia at 960 Ma.

$k = 100.8$, $\alpha_{95} = 7.7$. A reverse polarity has been established for two outcrops (sample numbers 02ta-9 and 02ta-10, table 1) of gabbro-dolerite sill, with the mean direction being: $D = 141.9$, $I = -17.8$, $k = 414.8$, $\alpha_{95} = 12.3$. The angle between the means of the normal and reverse polarity is $\gamma = 4.8^\circ$ with $\gamma_C = 9.4^\circ$ as the critical value. The precision parameter (k) is significantly higher in the stratigraphic coordinates (the ratio $k_s/k_g = 43.8$ is higher than the critical value – 4.16 for $n = 7$ at the 99% confidence level), the optimal concentration of magnetic directions (when k is maximum) is found at $109 \pm 4\%$ untilting. The correlation test (McFadden, 1990) is positive: the test parameter (distribution function) ξ_1 in stratigraphic coordinates – 3.166 exceeds the critical value at 95% confidence level – 3.086, at the same time in geographic (in situ) coordinates ξ_1 is 2.552, which is lower than the critical value. The main stage of deformations of the island arc complexes of Central Taimyr corresponds to the ~600 Ma boundary (Vernikovskiy, Vernikovskaya, 2001), therefore we can safely assume that the 960 Ma age of the established *ChRM* is pre-Ediacaran (630-542 Ma; Walker and Geissman, 2009). In all probability the

ChRM corresponds to the time of formation of these rocks at 960 Ma or in the Early Neoproterozoic.

The mean paleomagnetic pole for the Central Taimyr rocks (Table 1; P_{Lat}=17.8, P_{Long}=326.8, A₉₅=4.0) is close to synchronous poles for Uya series sedimentary rocks in the Uchuro-Maya region in the south-east of the Siberian craton, hosting basic intrusions (Pavlov et al., 2002). The age of those intrusions is substantiated by results of Sm–Nd, 942 ± 19 Ma (Pavlov et al., 2002) and U–Pb, 947 ± 7 , 1005 ± 4 Ma (Rainbird et al., 1998) dating. The angular divergence in the poles position, considering the confidence interval, is equal to $31.7^\circ \pm 4.3^\circ$ in paleolongitude and $-8.7^\circ \pm 3.7^\circ$ in paleolatitude (Fig. 4). Consequently, the island arc whose relicts are preserved in the modern structure of the Three Sisters Lake region was located in some distance away from the Taimyr margin of Siberia at the time of its formation. Judging by the difference in synchronous paleomagnetic latitudes, the Central Taimyr island arc could have been separated from the Siberian continent by a back-arc basin 550–1,380 km wide (Fig. 4). During the back-arc basin's closure the arc must have been rotated for ~30°

clockwise. From these observations, we reach the following conclusions:

1. 960 m.y. ago the paleo-island arc of Central Taimyr was located in the subequatorial zone, near the northern margin of Siberia, and had a sublatitudinal strike. The sizes of the back-arc basin that existed between the arc and the continent at this time could reach 556–1,378 km incorporating the estimated error in paleomagnetic determinations.
2. The established age of the island arc in the Central Taimyr indicates that the transformation of the passive continental margin regime into an active one in the north of Siberia took place as early as the beginning of the Neoproterozoic (1 Ga). It is of fundamental significance for paleotectonic reconstructions of Siberia's position within the framework of Rodinia because it does not allow the joining of the Taimyr margin with the Canadian margin of Laurentia as it is assumed in alternative reconstructions (Dalziel, 1991; Hoffman, 1991).

3. The accretion of the island arc to the craton incorporated mutual rotation around a vertical axis, which implies the existence of a significant strike-slip component in the kinematics of the accretion process in the north of Siberia in the Late Precambrian.

THE KARA MICROCONTINENT DURING THE PALEOZOIC

The Kara microcontinent (or Kara plate) is one of the largest fragments of the ancient Arctida paleocontinent (Fig.1). Therefore the problems related to the reconstruction of its formation, kinematics and interactions with other continental blocks are very important for the understanding of the entire Arctic region. The Kara microcontinent's Precambrian basement is heterogeneous, which is consistent with refraction velocities ranging from 5.7 to 7.1 km/s (Bogolepov et al., 1991). According to individual seismic soundings, the crust thickness in the Kara microcontinent may exceed 40 km, with a 14–16-km-thick lower crust. The sedimentary

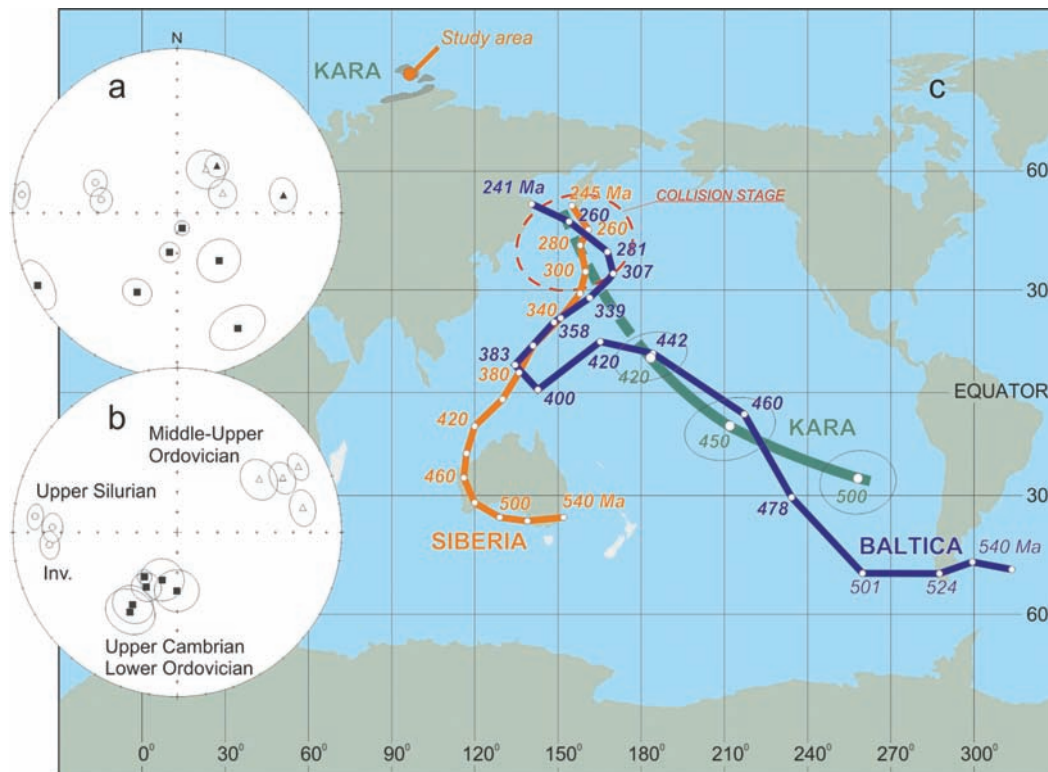


Fig. 5. (a) Paleomagnetic site mean directions in situ; and (b) tilt corrected; and (c) APWP for the Kara microcontinent and its comparison with APWP for Siberia by (Pechersky and Didenko, 1995) and APWP for Baltica by (Torsvik et al., 1996). Modified after (Metelkin et al., 2005).

section includes two units. The lower unit is up to 14 km thick and is apparently composed of Late Cambrian–Ordovician and Silurian to Permian carbonate, evaporate, and terrigenous deposits (Kaban'kov, Sobolevskaya., 1981; Kaban'kov et al., 1982). The upper unit, as thin as 2 km, consists of Triassic–Jurassic sequences.

Analysis of geostructural, paleomagnetic, geochronological and biostratigraphic data showed that the Kara microcontinent was tectonically isolated from neighboring continents in the Early Paleozoic (Fig.5) and collided with Siberia at ~300 Ma or in the Carboniferous (Vernikovskiy et al., 1995; 1998; 2004; Metelkin et al., 2000; 2005; 2012, Shipilov, Vernikovskiy, 2010). The 300 Ma collision is thought to have closed an oceanic basin that once separated Kara from Siberia and the Central Taimyr island arc that collided with the Siberian continent at ~600 Ma. The Northern Taimyr forms the collision belt between the Kara microcontinent on the north and the Central Taimyr/Siberian amalgamation on the south. The absence of Middle-Late Paleozoic ophiolite and island arc complexes in the Northern Taimyr is therefore curious.

We propose a reconstruction of the Early Paleozoic history of the Kara microcontinent as part of the amalgamation of the Arctida paleocontinent. Our reconstruction describes the mechanism of the 300 Ma collision of Kara with Siberia and the subsequent collision-caused deformation processes in the amalgamation of the greater Pangea supercontinent that was culminated in Permian time or ~280 Ma (Fig. 9) (Metelkin et al., 2011; 2012, Vernikovskiy et al., 2011).

Our paleotectonic analysis is based on paleomagnetic and geochronological data. The results indicate that the collision between Siberia and the Kara microcontinent was an oblique event. The orogen that was formed can be characterized as a transform orogen (Metelkin et al., 2005). During the Early Paleozoic and prior to the collision Kara moved northward on a system of large transform faults from the sub-tropic zone of the southern hemisphere to the subequatorial latitudes of the northern hemisphere while at the same time rotating counter clockwise, whereas the Siberian plate underwent a clockwise rotation (e.g., Fig. 8, 450 Ma).

The oppositely directed rotation of the interacting

Kara and Siberian continental masses led to their oblique convergence and “soft” collision. In the Late Silurian – Devonian, when there still was a “lens” of oceanic crust between the Siberian and Kara plates (Fig. 6, 430–400 Ma; Fig. 8, 420 Ma), the margins of the converging continents escaped significant shortening while sliding along the transforms and maintaining intact margins (Fig. 6, 430–400 Ma). It is possible that the oceanic crust was partially subducted beneath the Siberian plate; however the strike-slip processes were dominating. As a result the supra-subductional geologic complexes are lacking. The continent-microcontinent collision took place in the Late Carboniferous and culminated in the Permian (Fig. 6, panel for Carboniferous-Permian). The Carboniferous-Permian (300–260 Ma) collision re-deformed the Central Taimyr island-arc complex that was originally deformed when it accreted to the Siberian continent at 600 Ma.

In the course of oblique collision there was a thickening of the crust, accompanied by folding which migrated to the south-west (in modern geographic coordinates), regional metamorphism, and the formation of collisional granites (Vernikovskiy et al., 1995; Pease, 2001). As a result of compression in the frontal part of the Kara tectonic domain there was a gradual exhumation of the deeper parts of the crust of the deformed plate.

The transform faults which controlled the collision of the Kara and Siberia continental masses gradually evolved into thrust faults as shortening progressed. The oblique collision may have evolved into a more orthogonal-directed collision because of far-field interactions with the nearby continental masses of Laurentia, Baltica, Alaska-Chukotka, and Svalbard (Fig. 9). The most important among these thrusts is the Main Taimyr fault zone (Fig. 6), which can be regarded as the main suture of the Late Paleozoic Taimyr orogen. The progressing compression and the associated crustal thickening led to the “collapse” – fast thrusting and imbrication of the crust and post-collisional granitoid magmatism (Vernikovskiy et al., 1998) on the Main Taimyr thrust which separates the Central and North Taimyr zones.

This geodynamic paleoreconstruction for the Kara microcontinent shows the need and significance of such studies for the entire Arctic.

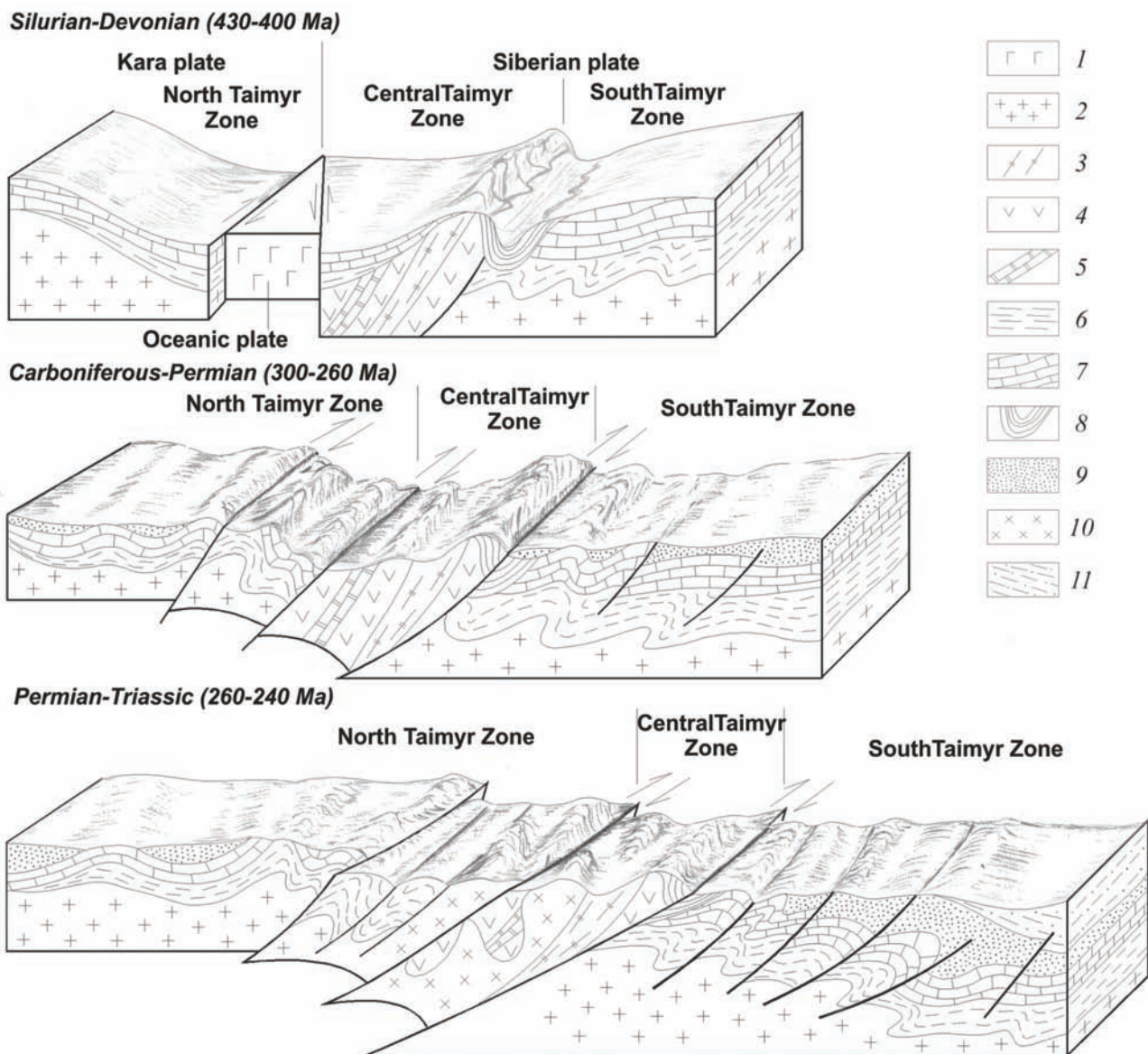


Fig. 6. A model for the structure transformation of the Siberian Taimyr margin during the interaction with the Kara microcontinent. 1 – oceanic complexes; 2 – Early Precambrian complexes of the Kara microcontinent and Siberian craton crystalline basement; 3–5 – Late Precambrian complexes of the Central Taimyr accretion zone: 3 – gneissic from cratonic terranes, 4 – volcanogenic-sedimentary from island arc terranes with ophiolites, 5 – carbonate shelf of passive continental margin terranes; 6 – Neoproterozoic-Cambrian flyschoid deposits of the Kara and Siberian continental margins; 7 – Paleozoic mainly carbonate shelf deposits (Ordovician-Silurian on the Kara microcontinent and Ordovician-Early Carboniferous on the Taimyr Siberian margin); 8 – Ediacaran-Early Carboniferous hemipelagic argillaceous-carbonate and black-schists deposits of the Pyasina-Faddey abyssal trough; 9 – Late Paleozoic mainly terrigenous deposits (Devonian and Carboniferous-Permian for Kara and Late Carboniferous-Permian for Southern Taimyr); 10 – Late Paleozoic (300–260 Ma) collisional granitoids; 11 – Triassic sandy-agrillaceous deposits, including the trap complex in the front of the Late Paleozoic orogen (basal horizons of the Mesozoic-Cenozoic Yenisey-Khatanga basin).

SPECULATIVE PALEOTECTONIC RECONSTRUCTIONS FOR THE ARCTIDA PALEOCONTINENT AND THE GREATER ARCTIC DURING LATE NEOPROTEROZOIC – PERMIAN TIME

Cryogenian (~750 Ma)

The Cryogenian is marked by the breakup stage of Rodinia – the supercontinent that formed around 1 Ga. According to current interpretations, the breakup of Rodinia began as soon as ~950 Ma and continued for a very long time until the Ediacaran (630–542 Ma) (Li et al., 2008). We join with Li et al., (2008) in believing that most of the classic Arctida blocks were composited into a continuous belt from fragments originating in diverse settings including the present-day northern margin of Laurentia, the former (750–650 Ma) southern margin of Siberia, and the present-day north-eastern margin of Baltica (Fig. 7, 750 Ma).

The Svalbard plate has a Grenvillian (1.3–1.0 Ga) basement, which has been confirmed by the identification of Grenvillian complexes on Spitsbergen (Gee et al., 1995) and on Novaya Zemlya (Korago et al., 2004). This allows us to infer the formation of Svalbard from collisional events during the establishment of Rodinia. On the basis of paleomagnetic data, Baltica is usually positioned in paleoreconstructions in such a way that in modern geographic coordinates the Grenvillian Sveconorwegian structures serve as the northern “ending” of the Grenvillian structures of Laurentia’s eastern margin. The Meso-Neoproterozoic fold belts of Amazonia are oriented in a linear fashion along Laurentia’s Grenvillian margin (Cawood and Pisarevsky, 2006). In this context it is logical to suppose that the Svalbard orogen structures form the northern (present-day) extension of the Grenville belt that marks the collisions between Laurentia, Baltica, and Amazonia that formed northern Rodinia.

Paleoproterozoic(?) crystalline complexes of the Kara microcontinent basement are known on the Severnaya Zemlya archipelago (Proskurnin, 1999; Proskurnin and Shul’ga, 2000) and in the northern part of the Taimyr Peninsula (Vernikovskiy and Vernikovskaya, 2001). The sedimentary cover on the Kara microcontinent is floored by Late Neoproterozoic flyschoid deposits which are overlain by a Paleozoic (Ordovician to Early

Carboniferous) sequence composed of carbonates, evaporates and terrigenous formations that indicate an epicontinental shelf regime. The structure of the gravity, magnetic, and other geophysical fields for the Kara microcontinent differ significantly from adjacent plates or blocks. The Kara microcontinent thus appears to form an independent block with a distinct internal structure.

Despite the distinctive differences between the geologic and geophysical structures of the Kara microcontinent and the Svalbard plate, the emplacement history and evolution of their modern margin (St. Anna Trough and North Siberian Sill) display a characteristic dextral strike-slip component, which was probably inherited from the Neoproterozoic-Paleozoic transform boundary between Svalbard and Kara (Shipilov and Vernikovskiy, 2010). From these observations we speculate that in the Meso-Neoproterozoic (Cryogenian) structure of Arctida (during the formation of Rodinia) the Kara microcontinent was located between the Greenland-Ellesmere block and the Svalbard block, from the latter possibly separated by a strike-slip fault system (Fig. 7, 750 Ma).

In our reconstruction the Early Precambrian structures of Arctida’s Greenland-Ellesmere block correspond to their current position near the Canadian margin of Laurentia. Our reconstruction infers that the Alaska-Chukotka block was located in close proximity to the Greenland-Ellesmere block and they did not change their positions as the northern (present-day) margin of Laurentia throughout the period 750–255 Ma. The detachment of the Alaska-Chukotka tectonic element from Laurentia occurred in the Jurassic (202–146 Ma), as part of the opening of the Canada basin (Grantz et al., 1998, Lawyer et al., 2002, Alvey et al., 2008). The Alaska-Chukotka tectonic element later collided with the Verkhoyan-Kolyma Siberian plate along the South Anyui (Novosibirsk-Chukotka) suture (Sokolov et al., 2002; 2009).

Unlike earlier models, our reconstruction does not include the New Siberian Islands and the Laptev Sea continental shelf (New Siberian block) in the structure of Meso-Neoproterozoic Arctida. The Neoproterozoic-Paleozoic evolution of the New Siberian block took place in a passive continental margin setting (Kuzmichev, 2009). The Paleozoic

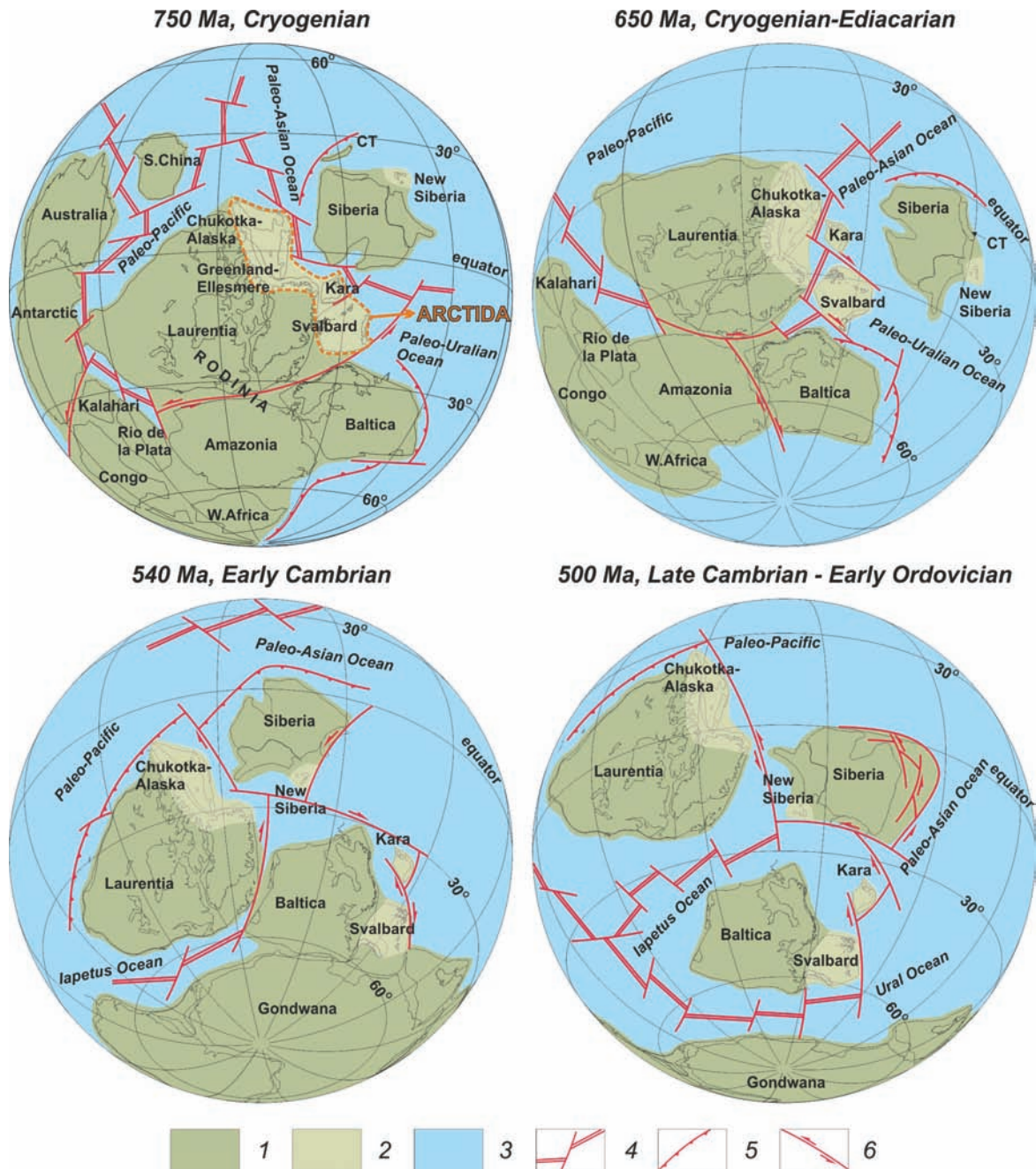


Fig. 7. Plate tectonic reconstructions for the evolution of Arctida and its dispersed fragments (Chukotka-Alaska, Kara, and Svalbard) from the Neoproterozoic to the Early Ordovician. 1 – continental masses; 2 – continental blocks of Arctida; 3 – oceanic basins; 4 – inferred position of spreading zones; 5 – active continental margins; 6 – general strike of the transform/strike-slip zones with indicated strike-slip kinematics.

geological complexes that exist on the New Siberian Islands are amazingly similar to the deposits of the Cis-Verkhoyan and South-Taimyr margins of Siberia. The lack of a pronounced tectonic suture in the Laptev shelf allows us to infer the genetic unity of the Paleozoic complexes of the New Siberian block and the north-eastern Siberian margin. Thus in our model in the Cryogenian the New Siberian block

was located far from the other Arctida blocks and during the Paleozoic it evolved as a part of the north-eastern (in geographic coordinates) Siberian margin.

According to our model, strike-slip displacements took a major role in the process of Rodinia's breakup and basically conditioned the tectonic dispersal of the supercontinent (Metelkin et al., 2007, 2012; Vernikovskiy et al., 2009). The

accepted position of the Siberian craton is based on paleomagnetic data for the south of Siberia (Metelkin et al., 2007, 2012) and is supplemented by data for the Taimyr margin (Vernikovskiy et al., 2011). The latter indicate that Central Taimyr island arcs were situated to the north from the Arctic margin of Siberia since 960 Ma. Consequently, at the time of a unified Rodinia (> 950 Ma) and later its breakup the Siberian northern margin should have been facing a paleo-ocean (Fig. 7, 750 Ma). The paleogeographic position of the Arctica subcontinent was to the southwest relative to Siberia and straddling the equator (Fig. 7, 750 Ma). The position of Kara, Svalbard and Alaska–Chukotka within Arctica is debatable and taken from (Li et al., 2008).

Cryogenian-Ediacaran (~650 Ma)

By the beginning of Ediacaran the Arctica subcontinent on the northern margin of Laurentia had moved south of the equator to subtropical latitudes (Fig. 7, 650 Ma). Some Arctica blocks were probably involved at this time in the breakup and dispersal of Rodinia, including the detachment of Baltica from Rodinia. Many examples show that the Rodinia breakup was accompanied by the shredding of the Rodinia margin into independent terranes such as the Kara microcontinent and the Svalbard plate. At the base of the Paleozoic sedimentary cover of those plates Late Precambrian riftogenic troughs and basins are present, which are clearly revealed by seismic measurements (Shipilov and Vernikovskiy, 2010).

At the same time on the eastern periphery of Baltica (Timan-Ural margin) the evolution of an active subduction zone can be inferred (Kuznetsov et al., 2007). Oblique subduction on one side of the Svalbard plate and extension on the other caused a transform regime of its displacement and interaction with the Kara plate.

Early Cambrian (~540 Ma)

Traces of the Cadomian orogenic event on the territory of Barentsia (Puchkov, 2003; Kuznetsov et al., 2007) in our opinion relate directly to the evolution of the Arctica structures. We believe this event to be a result of the collision between the Timan margins of Baltica (present-day northeast margin) with the Svalbard plate. From this time Barentsia was

joined to the East-European paleocontinent (Fig. 7, 540 Ma). The collision was structurally manifested in the formation of the divergent Timan-Pechora orogen. Its existence is confirmed by a deep cut-out of the Late Precambrian complexes in the basement of the Timan-Pechora sedimentary basin and by an outstanding unconformity in the base of the Paleozoic sedimentary cover (Kuznetsov et al., 2007). The 540 Ma collision was accompanied by the emplacement of I-type granitoid plutons, characterized by isotopic dates from 695 to 515 Ma (Kuznetsov et al., 2007). Kara continued to experience a mainly transform displacement relative to Svalbard. The transform/strike-slip regime characterized the entire north-eastern Siberian margin (in geographic coordinates) and its displacements relative to distant Laurentia and Baltica. On the boundary between Laurentia and Baltica the Iapetus Ocean began to open (Fig. 7, 540 Ma).

Late Cambrian – Early Ordovician (~500 Ma)

By the Cambrian-Ordovician boundary (488 Ma) an active spreading regime widened the Iapetus oceanic basin (Fig. 7, 500 Ma). The breakup of the continental crust along the eastern (in present-day coordinates) Baltica margin and the formation of the Ural oceanic basin began at this time (Puchkov, 2003). Thus Baltica on almost all its periphery (except the north) was surrounded by young oceanic spreading centers whose growth dynamic set up a counter-clockwise rotation of the plate, which is confirmed by paleomagnetic data (Torsvik et al., 1991; Cocks and Torsvik, 2002). The northern Baltica margin including Svalbard was separated from Siberia by large-scale strike-slip faults, which caused a gradual drift of the Kara block towards Siberia (Metelkin et al., 2005).

Late Ordovician (~450 Ma)

The Iapetus oceanic basin began to close at the end of the Middle Ordovician. Active subduction occurred widely on all of the margins of the continents that surrounded the Iapetus Ocean. Baltica began its movement across Iapetus toward Laurentia. The Svalbard-Baltica margin and Kara located on its periphery were drawn significantly closer to the Taimyr margin of Siberia by mainly multidirectional rotation of these continental masses.

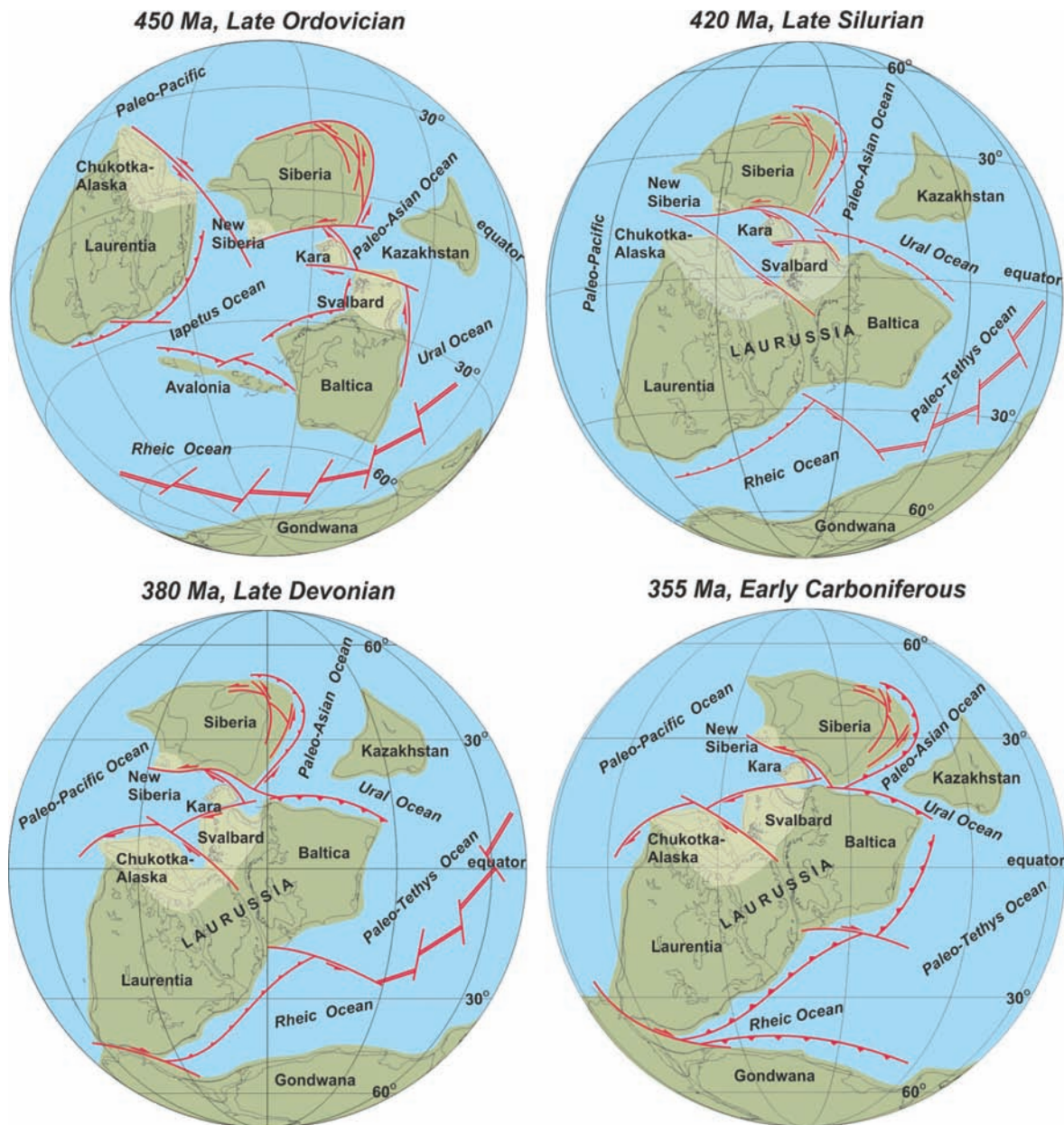


Fig. 8. Plate tectonic reconstructions for the evolution of Arctida's dispersed fragments from the Late Ordovician to the Early Carboniferous. See legend keys on Fig. 7.

This entire system continued its general drift towards the equator (Fig. 8, 450 Ma and 420 Ma).

Late Silurian – Late Devonian (~420–380 Ma)

During this time the collision between Laurentia and Baltica (Laurussia) took place (Golonka et al., 2003). Along with the formation of the Scandinavian orogen the Caledonian orogeny also affected Svalbard and the north-eastern Greenland margin, later spreading along the Greenland-Ellesmere area

of Laurentia. Thus, by the end of the Silurian the Ellesmere-Alaskan margin of Laurentia we infer the existence of an active subduction zone where the relicts of the Iapetus Ocean were consumed. The Kara microcontinent already was approaching the Taimyr margin of Siberia (Metelkin et al., 2005). The early stages of the Kara-Siberia collision occurred along a transform fault. The inferred transform fault collision mechanism does not exclude the existence of oceanic crust fragments between the Siberian

continent and the Kara microcontinent. Apparently there also existed a narrow space of oceanic crust between Svalbard and Kara. The Ural margin of Baltica and the south-western Siberian margin were characterized by intense subduction magmatism, which indicates the closure of the Ural and Paleo-Asian oceanic basins that were separated by the Kazakhstan plate (Fig. 8, 420 Ma). The collisions of the Siberian and Baltic plates took place along strike-slip faults within their modern arctic margins. As a result it was already the mid-Paleozoic (~380 Ma) when the component Arctic blocks of Arctida were reassembled into their Cryogenian (~750 Ma) configuration. By this time the Arctida blocks were located near the equator (Fig. 8, 380 Ma). By the end of the Devonian the Arctida assemblage formed a continental “bridge” between Siberia and Laurussia (Laurentia/Baltica). According to our reconstructions and available paleomagnetic data for the Early Paleozoic of the Kara microcontinent (Metelkin et al., 2005) we are inclined to believe that the Siberian margin in the Silurian-Devonian did not have any common boundaries with Laurussia. On the west, an embayment of the Paleo-Pacific Ocean separated the Siberian and Laurussia continental blocks during subsequent Paleozoic evolution. The Siberia and Laurussia plates were closest to each other by the end of the Silurian. The transform regime was dominating along all continental margins of Arctida at ~380 Ma. Strike-slip faults accommodated the sliding of Siberia and Kara to the east along the north-western (in paleogeographic coordinates) margin of Laurussia. This displacement widened the embayment facing the Paleo-Pacific Ocean into a wide marginal sea basin lapping the margins of Alaska-Chukotka, Svalbard, Kara, and New Siberia–Cis-Verkhoyan. It is probable that the inferred strike-slip displacements were driven by seafloor spreading Paleo-Pacific Ocean. To the east, subduction and the closing of the Paleo-Pacific and Ural Oceans added to the retreat of Siberia (and the Arctic blocks sutured to its margin) away from the Alaska-Chukotka margin of Laurentia.

Early Carboniferous (~355 and 330 Ma) and Late Carboniferous (~305 Ma)

The Carboniferous period witnessed the closing of the oceanic basins that divided the continental

masses of Laurussia (Baltica and Laurentia), Siberia, and the Kazakhstan composite terrane. These collisions culminated with the formation of Laurasia – the supercontinent that along with Gondwana formed Pangea at the Carboniferous-Permian boundary (Fig. 9, 280 Ma) (Zonenshain et al., 1990; Golonka, 2002).

At the beginning of the Carboniferous (355 Ma) the main blocks of Arctida (e.g., the Alaska-Chukotka, Svalbard, Kara, and New Siberian blocks) and the related continental margins of Laurentia, Baltica and Siberia occupied the space between the equator and 30° N. This entire paleo-shelf was tectonically stable and underwent a slow “opening” caused by the eastward retreat of Siberia. The main cause for this retreat probably was seafloor spreading in the Paleo-Pacific Ocean. The closing of the Paleo-Asian and Ural Oceans as well as the progressive narrowing of the Rheic and Paleo-Tethys Oceans was essentially complete by ~305 Ma. These collisions and the interactions with the Paleo-Pacific Ocean on the western side of the Laurasian continental agglomerate contributed to the transform-fault regime of the paleo-shelf described above and to the clockwise rotation of the system (Fig. 8, 355 Ma and Fig. 9, 330 Ma).

By the Late Early Carboniferous (330 Ma) all the continents continued drifting northwards, moving closer to each other. for the final amalgamation of continental masses into a unified supercontinent began in Late Carboniferous time (Fig. 9, 305 Ma). Subduction of the Ural Ocean at the northeast Baltica margin was completed (Puchkov, 2003). The Paleo-Asian Ocean collapsed in a regime of oblique subduction (Dobretsov, 2003; Windley et al., 2007). At the end of the Early Carboniferous (Fig. 9, 330 Ma), collision tectonics began at the Taimyr margin of Siberia (Vernikovskiy et al., 1995; Vernikovskiy, 1996). At Taimyr, the collision proceeded as a soft interaction between sialic masses in oblique impact conditions with them rotating relatively to each other (Metelkin et al., 2005, 2012). Geochronological data indicates that as early as in the Late Carboniferous (305 Ma) syn-collisional calc-alkaline granitoids began to intrude Taimyr (Vernikovskiy et al., 1995; Pease, 2001). Paleomagnetic data, described above, forms the chief evidence for the inferred strike-slip component of Taimyr deformation. Thus, large-

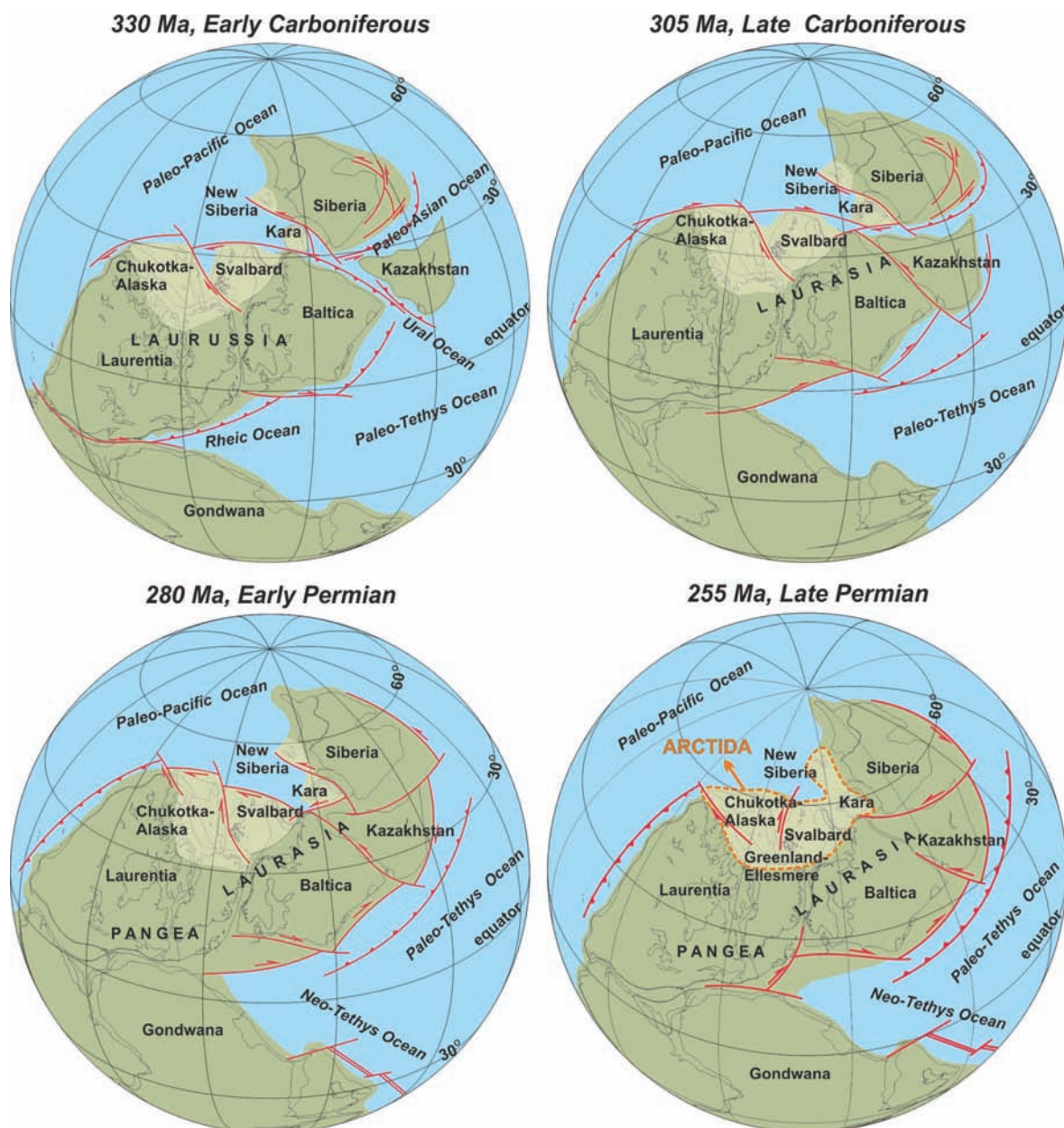


Fig. 9. Plate tectonic reconstructions for the evolution of Arctida and its dispersed fragments from the Early Carboniferous to the Late Permian. See legend keys on Fig. 7.

scale strike-slip fault zones, along which Kara “slid” during the entire Paleozoic, in the end led to the collision between the Kara microcontinent and the Siberian continent and subsequent formation of the fold-and-thrust structure of the Taimyr – Severnaya Zemlya folded area (located in Fig. 1b).

Early to Late Permian (280–255 Ma)

At the beginning of the Late Carboniferous (Fig. 9, 305 Ma) the main continental collisions involved in the formation of Pangea had already started (Zonenshain et al., 1990; Golonka, 2002; Metcalfe,

2002; Dobretsov, 2003). The Carboniferous-Permian boundary (280 Ma) is the time when the Laurasia and Gondwana blocks united in a single supercontinent – Pangea (Fig. 9, 280 Ma). The deformations caused by the collision and orogenic events continued within Laurasia, related mostly to strike-slip displacements along old sutures. Available paleomagnetic data indicate that the intraplate strike-slip displacements between rigid tectonic units of Eurasia (the Siberian and East European cratons) continued until the Cenozoic (Metelkin et al., 2010, 2012). By the end of the Permian (Fig. 9, 255 Ma)

the mainly transform-fault-driven amalgamation of the Kara – New Siberian and Svalbard – Novaya Zemlya continental margins into a single shelf structure was accomplished (Shipilov, 2003; 2008). The collisions caused the curved structure of the Pay-Khoy – Novaya Zemlya area (Korago et al., 1992; Scott et al., 2010).

Thus the Permian-Triassic boundary can be considered as the time of the second formation of Arctida or “Arctida-II”. Arctida-II is located in Pangea’s northern edge near the 60th parallel, occupying the moderate and sub-polar regions of the Northern Hemisphere (Fig. 9, 255 Ma). Subsequently, in the Mesozoic as a result of the opening of the Amerasian basin, the large Alaska-Chukotka block was rifted away from the Greenland-Ellesmere margin (Grantz et al., 1998). Its collision with the Cis-Verkhoyan Siberian margin in the Cretaceous along the South Anyui suture (Drachev et al., 1998; Sokolov et al., 2002; 2009; Kuzmichev, 2009) established the main structural features of the current arctic shelves of the Eurasian and North-American continents (Natalin, 1999; Khain et al., 2009).

CONCLUSION

We infer the existence at two different times of two Arctic subcontinents comprised of essentially the same crustal fragments. The first subcontinent, “Arctida-I” broke apart and the fragments were dispersed through independent plate movement paths before being reassembled as the second subcontinent, “Arctida-II.”

Arctida-I was an amalgamation of Mesoproterozoic terranes that “welded” together elements of Laurentia, Siberia and Baltica within the Rodinia supercontinent at 1 Ga. The Rodinia disintegration caused the breakup of Arctida-I into independent tectonic fragments which experienced highly diverse displacement paths over the next 720 million years (1,000 to 280 Ma). The evolution of Neoproterozoic and Paleozoic oceanic basins between these tectonic fragments led to their reorganization into a new configuration in Arctida-II – a Late Paleozoic subcontinent which again “welded” together the continental masses of Laurentia, Siberia and Baltica within Pangea. The breakup of Arctida-II in the Mesozoic and the

Cenozoic with the formation of the north Atlantic basin and the Amerasian and Eurasian basins of the Arctic Ocean led to a significant redistribution of the continental masses, especially in the north-eastern part of the modern Arctic and to the formation of the modern shelves of the Eurasian and North-American continents.

Our paleotectonic reconstructions will of course be improved after further investigations. For this purpose complex geostructural, geochronological, paleontological and especially paleomagnetic data will be of paramount importance.

REFERENCES

- Alvey, A., Gaina, C., Kuszniir, N.J., Torsvik, T.H., 2008. Integrated crustal thickness mapping and plate reconstructions for the high Arctic. *Earth and Planetary Science Letters*, 274, 310–321.
- Butler, R.F., 1992. *Paleomagnetism: magnetic domains to geologic terrains*. Backwell Sci. Publ., Oxford, 319.
- Bezzubtsev, V.V., Zalyaleev, R.Sh., Sakovich, A.B., 1986. Geological map of Gorny Taimyr Scale 1: 500,000, Explanatory Note. Krasnoyarsk, 177 (in Russian).
- Bogolepov, A.K., Shipilov, E.V., Yunov, A.Y., 1991. Geophysical characteristics of the Barents-Kara region deep structure. Proc. Intern. Seminar on Tectonics of the Barents Sea – Kara Sea Region. NIIMorgeophysica. IKU, Inter. Groupe, Norway, Trondheim.
- Cawood, P.A., Pisarevsky, S.A., 2006. Was Baltica right-way-up or upside-down in the Neoproterozoic? *J. Geol. Soc. London*, 163, 753–759.
- Cocks, L.R.M., Torsvik, T.H., 2002. Earth geography from 500 to 400 million years ago: a faunal and palaeomagnetic review. *J. Geol. Soc.*, 159, 631–644.
- Cocks L.R.M., Torsvik T.H. Siberia, the wandering northern terrane, and its changing geography through the Palaeozoic // *Earth Sci. Rev.*, 2007, v.82, p. 29–74.
- Condie, K.C., Rosen, O.M., 1994. Laurentia–Siberia connection revisited. *Geology*, 22, 168–170.
- Dalziel, I.W.D., 1991. Pacific margins of Laurentia and East Antarctica–Australia as a conjugate

- rift pair: evidence and implications for an Eocambrian supercontinent. *Geology*, 19, 598–601.
- Dalziel, I.W.D., 1997. Neoproterozoic – Paleozoic geography and tectonics: review, hypothesis and environmental speculation. *Geol. Soc. Am. Bull.*, 109, 16–42.
- Drachev, S.S., Savostin, L.A., Groshev, V.G., Bruni, I.E., 1998. Structure and geology of the continental shelf of the Laptev Sea, Eastern Russian Arctic. *Tectonophysics*, 298, 357–393.
- Gee, D.G., Johansson, A., Ohta, Y., Tebenkov, A.M., Krasilschikov, A.A., Balashov, Y.A., Larionov, A.N., Gannibal, L.F., Ryungenen, G.I., 1995. Grenvillian basement and a major unconformity within the caledonides of nordaustlandet, Svalbard. *Prec. Research*, 70(3–4), 215–234.
- Golonka, J., 2002. Plate tectonics map of the Phanerozoic. In: Kiesling, W., Flügel, E., Golonka, J. (eds.), *Phanerozoic reef patterns*. *SEPM Spec. Publ.*, 72, 21–75.
- Golonka, J., Bocharova, N.Y., Ford, F., Edrich, M.E., Bednarczyk, J., Wildharber, J., 2003. Paleogeographic reconstruction and basins development of the Arctic. *Mar. Petrol. Geol.*, 20(3–4), 211–248.
- Golonka J., Krobiski M., Pajak J., Nguyen Van Giang, Zuchiewicz W. *Global Plate Tectonics and Paleogeography of Southeast Asia*. Faculty of Geology, Geophysics and Environmental Protection, AGH University of Science and Technology, Arkadia, Krakow, Poland, 2006, 128 p.
- Grantz, A., Clark, D.L., Phillips, R.L., Srivastava, S.P., Blome, C.D., Gray, L.B., Haga, H., Mamet, B.L., McIntyre, D.J., McNeil, D.H., Mickey, M.B., Mullen, M.W., Murchey, B.I., Ross, C.A., Stevens, C.H., Silberling, N.J., Wall, J.H., Willard, D.A., 1998. Phanerozoic stratigraphy of Northwind Ridge, magnetic anomalies in the Canada Basin, and the geometry and timing of rifting in the Amerasia basin, Arctic Ocean. *Geol. Soc. Am. Bull.*, 110, 801–820.
- Dobretsov, N.L., 2003. Evolution of structures of the Urals, Kazakhstan, Tien Shan, and Altai-Sayan region within the Ural-Mongolian Fold Belt (Paleo-Asian ocean). *Russ. Geol. Geophys.*, 44(1–2), 5–27.
- Enkin, R.J., 2003. The direction-correction tilt test: an all-purpose tilt/fold test for paleomagnetic studies. *Earth and Planetary Science Letters*, 212, 151–166.
- Hoffman, P.F., 1991. Did the breakout of Laurentia turn Gondwana inside out? *Science*, 252, 1409–1412.
- Kaban'kov, V.Ya., Sobolevskaya, R.F., 1981. Late Precambrian-Early Paleozoic history of the Taimyr–Severnaya Zemlya folded area. In: *Tectonics of the Baikalian (Riphean) Strata of Siberia*. IGiG SO AN SSSR, Novosibirsk, 55–62 (in Russian).
- Kaban'kov, V.Ya., Rogozov, Yu.G., Makar'ev, A.A., 1982. Upper Proterozoic stratigraphy of Bolshevik Island (Severnaya Zemlya). In: *Geology of the Severnaya Zemlya Archipelago*. Sevmorgeo, Leningrad, 5–22 (in Russian).
- Khain, V.E., Gusev, G.S., Khain, E.V., Vernikovskiy, V.A., Volobuyev, M.I., 1997. Circum-Siberian Neoproterozoic Ophiolite Belt. *Ophioliti*, 22(2), 195–200.
- Khain, V.E., Polyakova, I.D., Filatova, N.I., 2009. Tectonics and petroleum potential of the East Arctic Province. *Russ. Geol. Geophys.*, 50(4), 334–345.
- Kirschvink, J.L., 1980. The least-squares line and plane and the analysis of paleomagnetic data. *Geophysical Journal of the Royal Astronomical Society*, 62, 699–718.
- Korago, E.A., Kovaleva, G.N., Il'in, V.F., Pavlov, L.G., 1992. The Tectonics and Metallogeny of the Early Kimmerides of Novaya Zemlya. Nedra, Leningrad.
- Korago, E.A., Kovaleva, G.N., Lopatin, B.G., Orgo, V.V., 2004. *The Precambrian Rocks of Novaya Zemlya*. Geological Society, London, *Memoirs*, 30, 135–143.
- Kurenkov S.A., didenko A.N., Simonov V.A., Lubnina N.V. Geodynamic formation conditions of the paleospreading complexes of the Ural-Mongolian belt / *Proc. GIN. Iss. 561, Studies on regional tectonics. V. 2: Kazakhstan, Tian-Shan, Polar Ural, M.: Nauka, 2005. 249 P.* (in Russian)
- Kuzmichev, A.B., 2009. Where does the South Anyui suture go in the New Siberian Islands and Laptev Sea?: Implications for the Amerasia

- basin origin. *Tectonophysics*, 463, 86–108.
- Kuznetsov, N.B., Soboleva, A.A., Udoratina, O.V., Gertseva, O.V., Andreichev, V.L., 2007. Pre-Ordovician tectonic evolution and volcano–plutonic associations of the Timanides and northern Pre-Uralides, northeast part of the East European Craton. *Gondwana Research*, 12, 305–323.
- Lawver, L.A., Grantz, A., Gahagan, L.M., 2002. Plate kinematic evolution of the present Arctic region since the Ordovician. In: Miller, E.L., Grantz, A., Klemperer, S.L. (eds.) *Tectonic Evolution of the Bering Shelf–Chukchi Sea–Arctic Margin and Adjacent Landmasses*. *Geol. Soc. Amer., Spec. Pap.*, 360, 333–358.
- Lawver L.A., Gahagan L.M. and Norton I. Palaeogeographic and tectonic evolution of the Arctic region during the Palaeozoic // *Geological Society, London, Memoirs*, 2011; v.35; p. 61-77.
- Li, Z.X., Bogdanova, S.V., Collins, A.S., Davidson, A., Waele, B.De., Ernst, R.E., Fitzsimons I.C.W., Fuck, R.A., Gladkochub, D.P., Jacobs, J., Karlstrom, K.E., Lul, S., Natapov, L.M., Pease, V., Pisarevsky, S.A., Thrane, K., Vernikovskiy, V., 2008. Assembly, configuration, and break-up history of Rodinia: A synthesis. *Precam. Res.*, 160, 179–210.
- Meert J.G., Torsvik T.H. The making and unmaking of a supercontinent: Rodinia revisited // *Tectonophysics*, 2003, v.375, p.261–288.
- McElhinny M.W., MacFadden P.L. *Paleomagnetism: continents and oceans*. San Diego, Academic Press, CA, 2000, 386 p.
- McFadden, P.L., 1990. A new fold test for paleomagnetic studies. *Geophys. J. Int.*, 103, 163–169.
- McFadden, P.L., McElhinny, M., 1990. Classification of reversal test in paleomagnetism. *Geophys. J. Int.*, 103, 725–729.
- Meert J.G., Torsvik T.H., 2003. The making and unmaking of a supercontinent: Rodinia revisited. *Tectonophysics*, 375, 261–288.
- Metcalfe I., 2002. Permian tectonic framework and palaeogeography of SE Asia. *J. Asian Earth Sci.*, 20, p.551–566.
- Metelkin, D.V., Kazansky, A.Yu., Vernikovskiy, V.A., Gee, D.G., Torsvik, T., 2000. First paleomagnetic data on the Early Paleozoic rocks from the Severnaya Zemlya Archipelago and their geodynamic interpretation. *Russ. Geol. Geophys.*, 41(12), 1767–1772.
- Metelkin, D.V., Vernikovskiy, V.A., Kazansky, A.Yu., Bogolepova, O.K., Gubanov, A.P., 2005. Paleozoic history of the Kara microcontinent and its relation to Siberia and Baltica: paleomagnetism, paleogeography and tectonics. *Tectonophysics*, 398, 225–243.
- Metelkin, D.V., Vernikovskiy, V.A., Kazansky, A.Yu., 2007. Neoproterozoic evolution of Rodinia: constraints from new paleomagnetic data on the western margin of the Siberian craton. *Russ. Geol. Geophys.*, 48(1), 32–45.
- Metelkin, D.V., Vernikovskiy, V.A., Kazansky, A.Yu., 2011. Siberia – from Rodinia to Eurasia. In Closson, D. (ed.) *Tectonics*, In Tech, Rijeka, Croatia, 103–136.
- Metelkin, D.V., Vernikovskiy, V.A., Kazansky, A.Yu., 2012. Tectonic evolution of the Siberian paleocontinent from the Neoproterozoic to the Late Mesozoic: paleomagnetic record and reconstructions. *Russ. Geol. Geophys.*, 53(7), 681–694.
- Natalin, B.A., Amato, J.M., Toro, J., Wright, J.E., 1999. Paleozoic rocks of northern Chukotka Peninsula Russian Far East: implications for the tectonics of the Arctic region. *Tectonics*, 18, 977–1003.
- Pavlov, V.E., Gallet, Y., Petrov, P.Yu., Zhuravlev, D.Z., Shatsillo, A.V., 2002. Uy series and late Riphean sills of the Uchur-Maya area: isotopic and palaeomagnetic data and the problem of the Rodinia supercontinent. *Geotectonics*, 36, 278–292.
- Pease, V., 2001. East European Craton margin source for the allochthonous Northern Terrane of Taimyr, Arctic Siberia. *EOS Transactions, American Geophysical Union*, 82, Fall Meeting Suppl., Abstract T32B-0892.
- Pease, V., Gee, D., Vernikovskiy, V., Vernikovskaya, A., Kireev, S., 2001. The Mamont-Shrenk terrane: a Mesoproterozoic complex in the Neoproterozoic accretionary belt of Central Taimyr, Northern Siberia. *Terra Nova*, 13, 270–280.
- Pechersky D.M., Didenko A.N. The Paleosian

- ocean: petromagnetic and paleomagnetic information concerning its lithosphere. M.:OIFZ RAN, 1995. 298 P. (in Russian).
- Pisarevsky, S.A., Natapov, L.M., Donskaya, T.V., Gladkochub, D.P., Vernikovskiy, V.A., 2008. Proterozoic Siberia: a promontory of Rodinia. *Precam. Res.*, 160, 66–76.
- Powell, C.M., Li, Z.X., McElhinny, M.W., Meert, J.G., Park, J.K., 1993. Paleomagnetic constraints on timing of the Neoproterozoic breakup of Rodinia and the Cambrian formation of Gondwana. *Geology*, 21, 889–892.
- Proskurnin, V.F., 1999. Concerning the problem of angular unconformities in the Upper Precambrian and Lower Paleozoic of the Severnaya Zemlya archipelago. In: Simonov, O.N. (ed.). *Bowels of Taimyr. Norilsk*, 68–76, (in Russian).
- Proskurnin, V.F., Shul'ga, Yu.D., 2000. Geological structure of the pre-Mesozoic basement, magmatic formations. In: Gramberg, I.S., Ushakov, V.I. (eds.). *Severnaya Zemlya—geology and mineral resources. VNIIOkeangeologia*, St. Petersburg, 31–44 (in Russian).
- Puchkov, V.N., 2003. Uralides and Timanides, their structural relationship and position into geological history of Ural-Mongolian fold-thrust belt. *Russ. Geol. Geophys.*, 44(112), 28–39.
- Rainbird, R.H., Stern, R.A., Khudoley, A.K., Kropachev, A.P., Heaman, L.M., Sukhorukov, V.I., 1998. U–Pb geochronology of Riphean sandstone and gabbro from southeast Siberia and its bearing on the Laurentia–Siberia connection. *Earth Planet. Sci. Lett.*, 164, 409–420.
- Scotese, C.R., McKerrow, W.S., 1990. Revised world map and introduction. In: McKerrow, W.S., Scotese, C.R. (eds.). *Palaeozoic Paleogeography and Biogeography*, *Geol. Soc. London Mem.*, 12, 1–21.
- Scotese C.R. *Paleogeographic Atlas / PALEOMAP Progress Report 90-0497*, 1997, Department of Geology, University of Texas at Arlington, Arlington, TX, 45 pp.
- Scott, R.A., Howard, J.P., Guo, L., Schekoldin, R., Pease, V., 2010. Offset and curvature of the Novaya Zemlya fold-and-thrust belt, Arctic Russia. In: Vining, B.A., Pickering, S.C. (eds.). *Petroleum Geology: From Mature Basins to New Frontiers – Proceedings of the 7th Petroleum Geology Conference*, 645–657.
- Shipilov, E.V., 2003. Interference of tectonic-geodynamic regimes in Permian-Triassic evolution of the Arctic periphery of North Eurasia. *Dokl. Earth Sci.* 393A(9), 1215–1219.
- Shipilov, E.V., 2008. Generations of spreading basins and stages of breakdown of Wegener's Pangea in the geodynamic evolution of the Arctic Ocean. *Geotectonics*, 42(2), 105–124.
- Shipilov, E.V., Vernikovskiy, V.A., 2010. The Svalbard–Kara junction: structure and geodynamic history *Russ. Geol. Geophys.*, 51, 1–13.
- Smethurst, M.A., Khramov, A.N., Torsvik, T.H., 1998. The Neoproterozoic and Paleozoic paleomagnetic data for the Siberian Platform: from Rodinia to Pangea. *Earth Sci. Rev.*, 43, 1–24.
- Sokolov, S.D., Bondarenko, G.Ye., Morozov, O.L., Shekhovtsov, V.A., Glotov, S.P., Ganelin, A.V., Kravchenko-Berezhnoy, I.R., 2002. The South Anyui suture: facts and problems to solve In: Miller, E.L., Klemperer, S., Grantz, A. (eds.). *Tectonic evolution of the Bering shelf – Chukchi sea – Arctic margin and adjacent landmasses*, *Geol. Soc. of America Spec. Paper* 360. 209–224.
- Sokolov, S.D., Bondarenko, G.Ye., Layer, P.W., Kravchenko-Berezhnoy, I.R., 2009. South Anyui suture: tectono-stratigraphy, deformations, and principal tectonic events. *Stephan Mueller Special Publication Series “Geology, geophysics and tectonics of Northeastern Russia: a tribute to Leonid Parfenov”*, 4, 201–221.
- Torsvik T.H., Ryan P.D., Trench A., Harper D.A.T., 1991. Cambrian-Ordovician paleogeography of Baltica. *Geology*, 19, 7–10.
- Torsvik, T.H., Smethurst, M.A., Meert, J.G., Van der Voo, R., McKerrow, W.S., Brasier, M.D., Sturt, B.A., Walderhaug, H.J., 1996. Continental break-up and collision in the Neoproterozoic and Palaeozoic – a tale of Baltica and Laurentia. *Earth Sci. Rev.*, 40(3–4), 229–258.
- Torsvik T.H. and Van der Voo R. 2002, Refining Gondwana and Pangea palaeogeography: estimates of Phanerozoic non-dipole (octupole)

- fields // *Geophys. J. Int.*, v.151(3), p.771–794.
- Uflyand, A.K., Natapov, L.M., Lopatin, V.M., Chernov, D.V., 1991. To the Taimyr tectonic nature. *Geotectonika*, 6, 76–93, (in Russian).
- Vernikovskiy, V.A., 1996. Geodynamic evolution of Taimyr fold area. Novosibirsk, Siberian Branch RAS, SPC UIGGM, 203, (in Russian).
- Vernikovskiy, V.A., Vernikovskaya, A.E., Lyapunov, S.M., Neimark, L.A., Proskurnin, V.F., Chernykh, A.I., 1994. Petrology, geochemistry, and tectonic settings of plagiogranites of the Chelyuskin Ophiolite Belt. *Int. Geol. Rev.*, 36, 961–974.
- Vernikovskiy, V.A., Neimark, L.A., Ponomarchuk, V.A., Vernikovskaya, A.E., Kireev, A.D., Kuzmin, D.S., 1995. Geochemistry and age of collision granitoids and metamorphites of the Kara microcontinent (Northern Taimyr). *Russ. Geol. Geophys.*, 36, 46–60.
- Vernikovskiy, V.A., Sal'nikova, E.B., Kotov, A.B., Ponomarchuk, V.A., Kovach, V.P., Travin, A.V., 1998. Age of post-collisional granitoids, North Taimyr: U-Pb, Sm-Nd, Rb-Sr and Ar-Ar data. *Dokl. RAN*, 363, 375–378 (in Russian).
- Vernikovskiy, V.A., Vernikovskaya, A.E., 2001. Central Taimyr accretionary belt (Arctic Asia): Meso–Neoproterozoic tectonic evolution and Rodinia breakup. *Prec. Res.*, 110, 127–141.
- Vernikovskiy, V.A., Vernikovskaya, A.E., Pease, V.L., Gee, D.G., 2004. Neoproterozoic orogeny along the margins of Siberia. *Geol. Soc. London Mem.*, 30, 233–247.
- Vernikovskiy, V.A., Kazansky, A.Yu., Matushkin, N.Yu., Metelkin, D.V., Sovetov, J.K., 2009. The geodynamic evolution of the folded framing and the western margin of the Siberian craton in the Neoproterozoic: geological, structural, sedimentological, geochronological, and paleomagnetic data. *Russ. Geol. Geophys.*, 50, 380–393.
- Vernikovskiy, V.A., Metelkin, D.V., Vernikovskaya, A.E., Matushkin, N.Yu., Lobkovsky, L.I., Shipilov, E.V., 2011. Early stages of evolution of the arctic margins (Neoproterozoic–Paleozoic) and plate reconstructions. *Origins of Northeastern Russia: Paleomagnetism, Geology, and Tectonics. ICAM-VI. Abstracts*, Fairbanks, Alaska, CD.
- Vernikovskiy, V.A., Metelkin, D.V., Vernikovskaya, A.E., Sal'nikova, E.B., Kovach, V.P., Kotov, A.B., 2011. The Oldest Island Arc Complex of Taimyr: Concerning the Issue of the Central Taimyr Accretionary Belt Formation and Paleogeodynamic Reconstructions in the Arctic. *Doklady Earth Sciences*, 2011, 436(2), 186–192.
- Walker, J.D., and Geissman, J.W. (compilers), 2009. *Geologic time scale: Geological Society of America*, doi: 10.1130/2009.CTS004R2C.
- Watson, G.S., and Enkin, R.J., 1993. The fold test in paleomagnetism as a parameter estimation problem. *Geophys. Res. Lett.*, 20, 2135–2137.
- Windley B.F., Alexeiev D., Xiao W., Kröner A., Badarch G., 2007. Tectonic models for accretion of the Central Asian Orogenic Belt. *J. Geol. Soc. Lond.*, 164(1), 31–47.
- Wingate M.T.D., Giddings J.W. Age and palaeomagnetism of the Mundine Well dyke swarm, Western Australia implications for an Australia-Laurentia connection at 755 Ma // *Precam. Res.*, 2000, v.100, p.335–357.
- Zabiyaka, A.I., Zabiyaka, I.D., Vernikovskiy, V.A., Serdyuk, S.S., Zlobin, M.M., 1986. *Geological Structure and Tectonic Evolution of Northeastern Taimyr*. Nauka, Novosibirsk, 144p.
- Zonenshain, L.P., Natapov, L.M., 1987. The Arctic tectonic history. In: *Topical Problems of Geotectonics*. Nauka, Moscow, 31–57 (in Russian).
- Zonenshain, L.P., Kuz'min, M.I., Natapov, L.M., 1990. *Geology of the USSR: A Plate Tectonic Synthesis*, Geodyn. Ser. 21, Page, B.M. (ed.), AGU, Washington, D.C.

3D geodynamics of Arctic region and model of Amerasia Basin formation

L.I. Lobkovsky¹, M.V. Kononov¹, V.E. Verzhbitsky¹, I.A. Garagash², and V.D. Kotelkin³

¹P.P. Shirshov Institute of Oceanology, Russian Academy of Sciences, Moscow, Russia

²O. Yu. Shmidt Institute of Physics of the Earth, Russian Academy of Sciences, Moscow, Russia

³M.V. Lomonosov Moscow State University, Moscow, Russia

ABSTRACT

The authors suggest a new quantitative approach to describe Arctic region evolution that is based on joint 3D modeling of upper mantle flows and elastic-plastic lithosphere deformations. During Tithonian-Aptian time in the Arctic region there existed a subduction zone characterized by a particular bend and consisting of two branches - South Anyui and Pacific. Stable subduction formed an upper-mantle convective cell with a downwelling close to the subduction zone and an upwelling on the opposite side of Arctida. This configuration of Arctic region mantle flows result in a pattern of stresses and diffuse lithosphere deformations that could be responsible for Chukchi plateau-Novosibirsk (New Siberian) Islands block-Chukotka and Arctic Alaska being torn apart from Arctic Canada and moving away from it. These deformations are responsible for diffusion spreading and Canada Basin formation. Following South Anyui ocean closing and Chukotka-Eurasia collision about 120 Ma the subduction zones were reorganized. New configuration of upper mantle flows led to extension and formation of the Basin and Rise Province, which included Alpha-Mendeleev Rise, Lomonosov Ridge, and Podvodnikov-Makarov basins. Given the proposed model, it is reasonable to believe that Lomonosov Ridge, Alpha-Mendeleev Rise, and the Makarov and Podvodnikov basins must be natural extensions of the mainland margins of Eurasia and North America, which in compliance with Article 76 of the 1982 United Nations Convention on the Law of the Sea, creates a fundamental geological rationale to justify the extension of the limits of the continental shelf for Russia, Canada and Denmark.

INTRODUCTION

Plate Tectonics, a new geological paradigm that came into being in the second half of the 1960s, is known to have owed its success largely to its simple method of quantifying global tectonic processes based on the kinematics of rigid rotation of lithospheric plates on the Earth's surface. This explains Plate Tectonics' attractiveness to geologists, which created the illusion that motions and interaction of lithospheric plates could be described by hit-and-miss adjustment of their parameters of rotation about certain Eulerian poles while disregarding convection currents in the mantle. This also explains the weakness of the new paradigm, since the real-life non-rigid behavior of the lithosphere calls for its numerical description - first, by applying the deformable solid mechanics methods (the theories of elasticity, plasticity, brittle destruction, etc.) and, second, through a necessarily combined analysis of lithospheric deformations and currents in the underlying mantle.

This paper offers a way to overcome the plate tectonic contradictions by rejecting the methodology of kinematic description of rigid rotation of lithospheric plates in favor of the direct numerical modeling of 3D deformations in the lithosphere jointly with the modeling of sublithospheric mantle currents. This new approach is being developed based on a case study of the geodynamic evolution of the Arctic region in the Mesozoic.

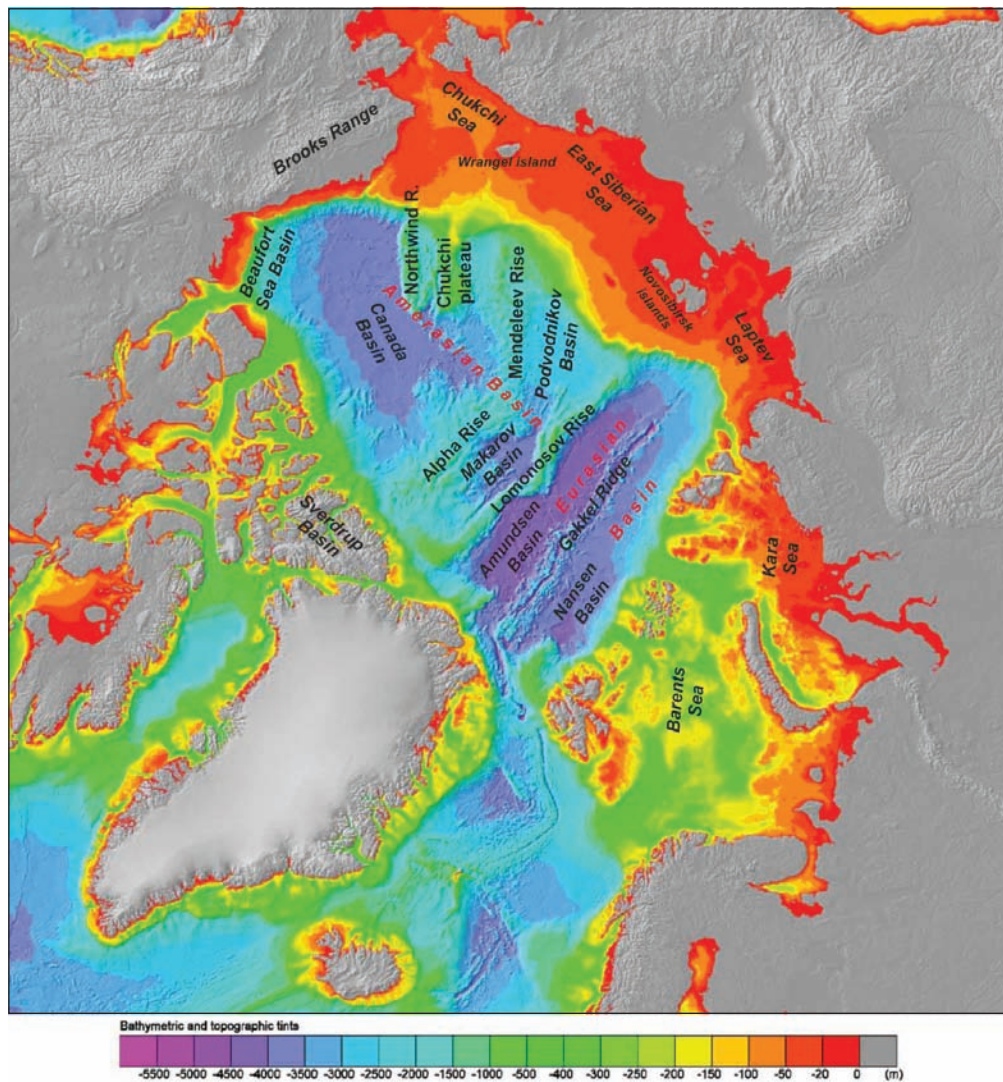


Fig. 1. Principal geomorphological features of the Arctic Ocean, after (<http://www.ngdc.noaa.gov/mgg/bathymetry/arctic/currentmap.html>)

TECTONIC AND GEODYNAMIC ANALYSIS

Principal geomorphological features and geological structures of the Arctic

The main geomorphological (Fig.1) and geological structural elements (Fig.2) of the Arctic region are: (i) Mesozoic and Cenozoic oceanic basins (Eurasia Basin with the Nansen and Amundsen basins and the Gakkel Ridge, the Amerasia Basin with the Canada, Makarov, and Podvodnikov basins and the Lomonosov Ridge, Alpha and Mendeleev submarine Rises); (ii) large shelf seas and adjacent land areas containing deep sedimentary basins that started subsiding at different times beginning in the Late Paleozoic (Barents Sea and Kara Sea basins, the Laptev, East Siberian, and Chukchi seas of the Eurasian margin, the Beaufort Sea basin rimming

from the south the Canada basin, the Sverdrup Basin in the Canadian Arctic Archipelago); (iii) continental basement incorporating ancient shields (Baltic, Anabar, and Canadian), their overlying Late Precambrian and Paleozoic cratonic cover, fold belts (Caledonian, Uralian, Taymyr, Timan, Inuit, Verkhoyansk-Chukotkan, and North Alaskan) separating the ancient cratons (East European, Siberian, and North American).

Given the spreading origin of the Gakkel Ridge, proved on the basis of the established system of Cenozoic magnetic lineations (e.g Karasik, 1973; Shreider, 2004) and the Eurasia Basin as a whole, there is hardly any doubt as to the continental origin of the Lomonosov Ridge, which split off from the Barents-Kara passive margin through rifting that

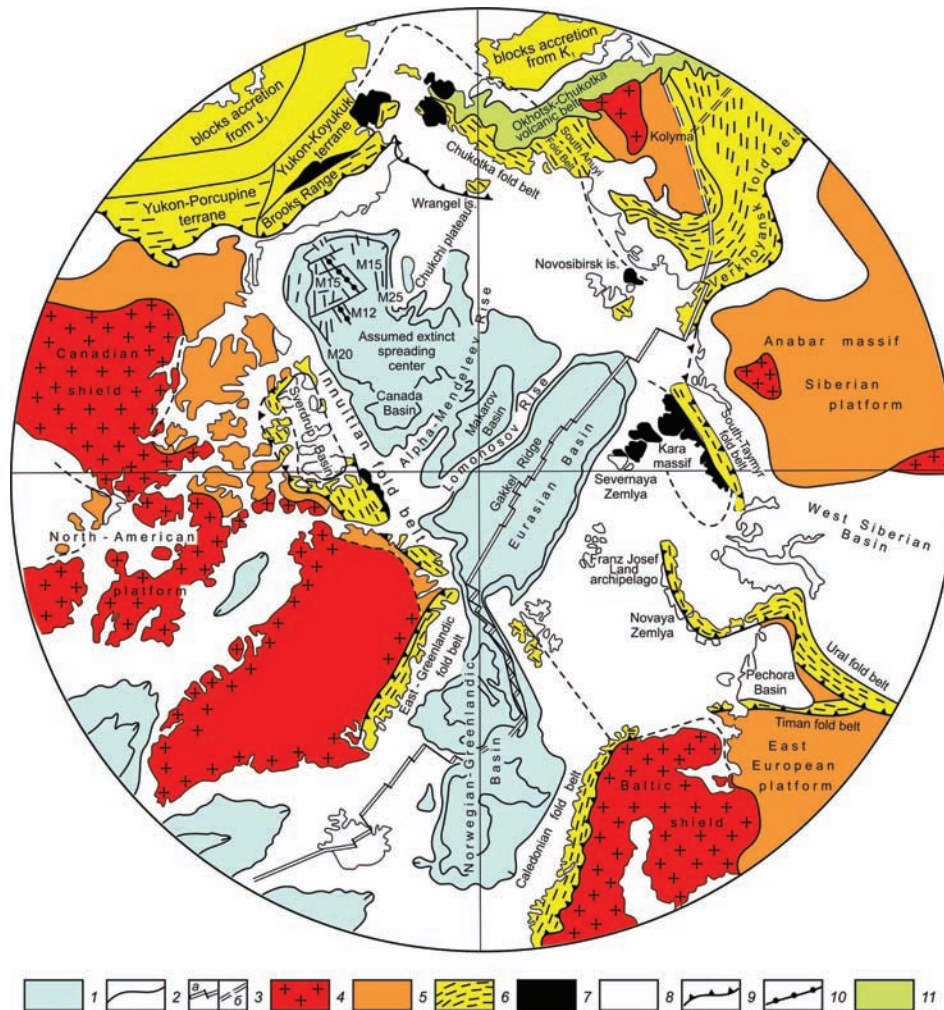


Fig. 2. Principal geological structures of the Arctic (after Zonenshain and Natapov, 1987). 1) oceanic basin deeper than 2000 m; 2) 2000 m and 3000 m isobaths; 3) active spreading center (a = proven, b = diffuse or inferred); 4) shield; 5) craton; 6) orogenic belt; 7) ancient massif - remnant of the Arctida continent; 8) Mesozoic and Cenozoic sedimentary basins; 9) folding front; 10) fossil spreading axis; 11) Okhotsk-Chukotka volcanic belt.

passed into spreading in the Paleocene (Khain, 2001, Khain et al., 2009). Similarly the oceanic nature of at least most part of Canada basin is now widely accepted (e.g. Taylor et al., 1981; Grantz et al., 1998). At the same time, the origin of the Alpha-Mendeleev Rise, as well as the Makarov basin, still remains a matter of heated debate among the international community of Arctic geologists and geophysicists (Bogdanov, 2004).

At least four principal groups of models exist to explain the origin of the Alpha-Mendeleev Rise: (i) a mid-ocean ridge model (Demenitskaya, 1975; Karasik, 1974); (ii) a model calling for a supra-subduction zone volcanic island arc (Herron et al., 1974; Zonenshain and Natapov, 1987); (iii) a model for a hot spot that created a within-plate volcanic

plateau with oceanic crust (Jokat et al., 2007); and (iv) a continental fragment model (Pushcharovsky, 1976; Zamansky et al., 2002; Poselov et al., 2002; Kaban'kov et al., 2004; Lebedeva-Ivanova et al., 2006; Miller et al., 2008; Miller and Verzhbitsky, 2009).

With regards to the Makarov basin, the spectrum of ages for its formation as per the different authors (Taylor et al., 1981; Rowley and Lottes, 1988; Weber and Sweeney, 1990; Shipilov, 2004) ranges from Late Cretaceous - Paleocene (71-56 Ma (Shreider, 2004)) to Late Jurassic - Neocomian (Gurevich and Merkuriev, 2007); we have used the geologic time scale (Gradstein et al., 2012) in this paper. In recent works, based on structural-geological and radiometric studies in the northern

Chukotka Peninsula (Miller et al., 2008; Miller and Verzhbitsky, 2009), flood basalts of Bennett Island (Fedorov et al., 2005) and Indigirka extensional belt of Aptian-Early Paleogene age, traceable along one line with Makarov Basin and Novosibirsk (New Siberian) Islands (Trunilina et al., 1999; Parfenov and Kuzmin, 2001) an Aptian-Albian age (~117-108 Ma) for the Makarov basin formation is proposed.

To understand the structure and evolution of the Arctic region let us briefly discuss the geological data.

Geological data of the Arctic region and concept of Arctida paleocontinent

On the tectonic scheme of the Arctic (Fig.2) the ancient Precambrian blocks of continental crust within the framework of Canada and Eurasia oceanic basins are visible. According to the early ideas of Shatsky (1965), these blocks and Canada Basin are

fragments of the ancient Hyperborea craton. Later, Zonenshain and Natapov (1987) described a plate tectonic model for the evolution of the Arctic region that “closed” the oceanic areas of the Eurasia and Canada basins (the latter according to the rotational model) and called the resulting vast continental block during Late Jurassic time the Arctida paleocontinent (Fig. 3). Thus, they further developed the notion of an ancient continent playing an essential role in Arctic evolution. Note that later Embry (1992) gave the name Crockerland to continental land, which was eroded during Triassic period and supplied detrital material to the south to Sverdrup Basin.

According to Khain et al. (2009), present-day geological and geophysical data show that fragments of the Neo-Proterozoic Arctida craton, destroyed during Paleozoic-Cenozoic evolution, currently occupy almost the entire circumpolar area, cropping out in the continental rim of the Arctic oceanic basins

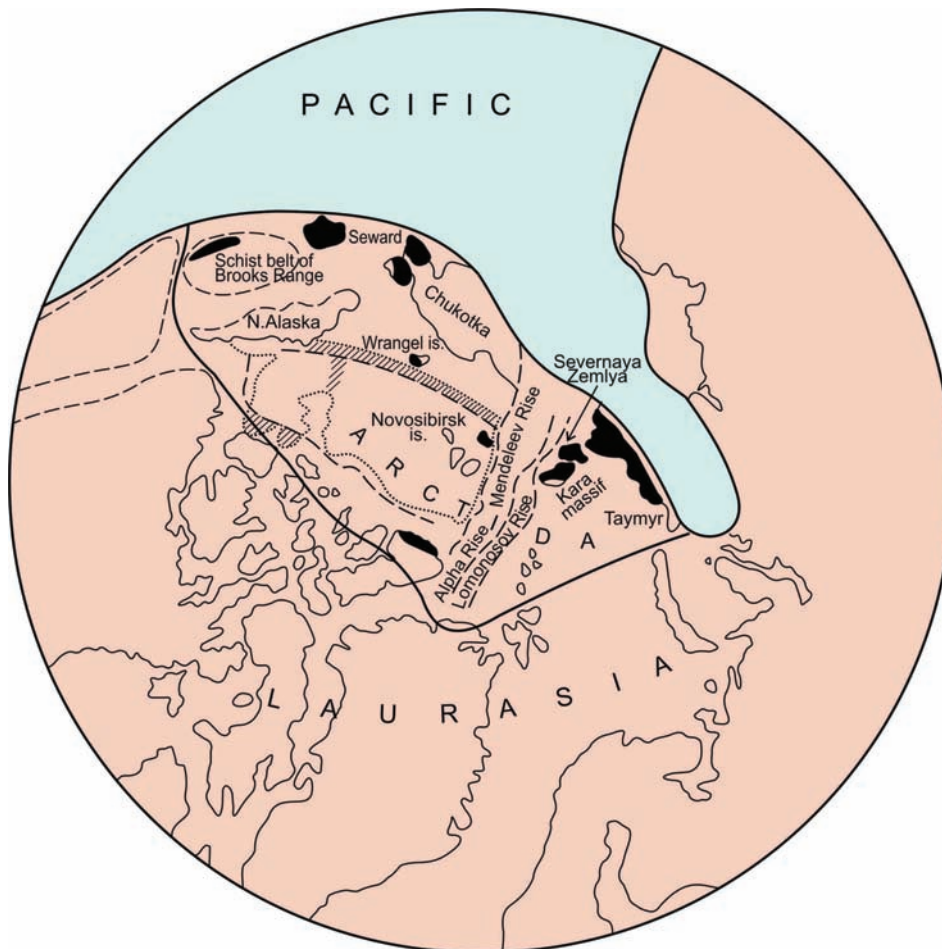


Fig. 3. Early Jurassic reconstruction showing ancient Arctic massifs (black) fused into the Arctida continent which amalgamated with Laurasia (Zonenshain and Natapov, 1987).

in the Novaya Zemlya Archipelago, in the Taymyr Peninsula, in the Kara massif, in the Novosibirsk Islands, in the De Long Archipelago, in Wrangel Island, in the Seward Peninsula, in the Brooks Range, in Peary Land, in the Canadian Arctic Archipelago, and elsewhere. The structural boundaries of the Arctida continent block are represented by fold belts (Fig.2): Timan belt of the Baikalian orogeny (Kuznetsov et al., 2010), Caledonides in northern Norway and Svalbard (Gee et al., 1995), Ellesmerides (Late Caledonides): North Greenland fold belt (Soper and Higgins, 1987), Hazen fold belt (Klaper, 1990 ; Trettin, 1994 ; Patchett et al., 1999), Central Ellesmere fold belt (Trettin, 1994 ; Patchett et al., 1999), Caledonides of Parry islands fold belt (Fox, 1985 ; Harrison and Bally, 1988), Late Kimmerides of Novosibirsk Islands, Wrangel Is., Herald - Brooks fold-and-thrust belt (Zonenshain et al., 1990a,b, Khain et al., 2009), Hercynides of Taimyr, Novaya Zemlya and Urals fold-and-thrust belts (Zonenshain et al., 1990a,b; Khain et al., 2009). They separate Arctida respectively from Baltika and Laurentia paleocratons, partly from the structures of the Paleopacific Ocean, Siberian craton and West Siberian platform.

In general, the identification of fragments of the Arctida continent is rather difficult because of its later significant reworking by the Mesozoic and Cenozoic orogenic events. The fragments of the Arctida craton can be assumed within the submarine ridges and rises: Lomonosov, Alpha-Mendeleev, Chukchi Plateau, and on the shelves of the Arctic seas - Laptev, East Siberian, Chukchi, and as well as the Alaska-Chukotka block (microplate).

The structure of the Arctida craton (Khain et al., 2009) is most fully revealed in Svalbard and northern Greenland (Peary Land). The craton has two main structural units, separated by a sharp structural unconformity: Archean- Mesoproterozoic crystalline basement (Svalbard and Peary Land) and the Neoproterozoic - Lower Paleozoic sedimentary cover (Novosibirsk Islands, De Long Archipelago, Peary Land). On the New Siberian Islands the sedimentary cover of the craton is revealed, beginning with the Ordovician carbonates (Parfenov and Kuzmin, 2001). Two structural unconformities corresponding to Skandian and Ellesmerian orogenic phases of adjacent structures are revealed within the

cover (Khain et al., 2009).

On Wrangel Island in the Wrangelian complex of very diverse composition (Kos'ko et al., 1993, 2003), the following rocks can be presumably related to shelf cover of Arctida: Neoproterozoic - Cambrian marbles, arkosic sandstones and shales, which underwent deformation and metamorphism to greenschist - amphibolite facies during the Baikalian orogeny. This cover of Arctida is unconformably overlain by Silurian - Carboniferous clastic-carbonate sediments. It is notable that there is also the volcanic and clastic unit of Middle-Late Devonian - an indicator of widespread structural reorganization (Khain et al., 2009).

Similar in composition, shelf cover is known for the Chukchi Peninsula and Northern Alaska, where it forms a series of north-vergent nappes and thrust sheets, overlying the Alaska-Chukotka fragment of Arctida. To the east, on the Seward Peninsula of Alaska, the Upper Proterozoic-Lower Paleozoic Nome Group is distinguished (Patric and McClelland, 1995). The latter is as heterogeneous in composition as the Wrangelian complex mentioned above (Kosko et al., 2003; Khain et al., 2009).

The sedimentary cover of Arctida on the Seward Peninsula likely includes metamorphosed shales, arkoses, marbles (with the Ordovician conodonts) the lower part of which is intruded by orthogneisses with a Neoproterozoic age of the protolith. Similar Late Proterozoic and Paleozoic rocks of the Arctida craton cover continue in the Brooks Range, where they represent a part of the Central Zone and Schist Belt of Kimmerian (Mesozoic) orogen. It is notable that the shelf cover within the greater part of the Arctida continent is weakly deformed except for the of De Long Islands where this cover is complicated by Cretaceous magmatic domes (Khain et al., 2009).

Thus, taking into consideration the age of deformation, Arctida continent collided with the Baltica craton along the Timan orogenic belt during the Baikalian orogeny; during the Caledonian and Ellesmerian Orogeny time it collided with Laurentia along northern Norway - Svalbard, Northern Greenland, Ellesmere Island, and the Franklinian mobile belt of the Canadian Arctic Archipelago; during Hercynian time it collided with the West Siberian platform and the Siberian craton along the Ural, Novaya Zemlya, Taimyr fold belts. Finally, as

a result of the breakup of the Arctida (opening of the Canada Basin) in the Early Cretaceous, the South Anyui suture was formed as a result of a collision with the Asian margin and the Brooks fold belt due to the collision of the Arctic Alaska margin of Arctida with island arc terranes of the Pacific.

Plate tectonic reconstructions for the Arctic region: Analysis of contradictions and the transition to a new paradigm - Tectonics of Deformable Plates

Let us briefly review the geologic history of the Arctic region based on plate tectonic reconstructions, mainly following the fundamental work by Zonenshain and Natapov (1987). Many plate tectonic models for the Arctic region have been proposed in the literature (eg. Karasik, 1968; Churkin, 1972, 1973; Ostenso and Wold, 1973; TAILLEUR, 1973; Herron et al., 1974; Zonenshain et al., 1978; Vogt et al., 1979; Taylor et al., 1981; Karasik et al., 1983; Savostin et al., 1984; Grantz and May, 1984; Burke, 1984; Jackson and Johnson, 1984). Most reconstructions for the Arctic region hypothesize that from the Devonian to the mid-Cretaceous, the North American and Eurasian continents were parts first of the Euramerica megacontinent and then of the Laurasia megacontinent. In the Late Cretaceous, the North Atlantic started opening, with the divergence of the North American and Eurasian continental plates. Their relative positions in the above process are established from the pattern of magnetic lineations in the North Atlantic and from the final fit of continental boundaries.

As per the classical plate tectonic view, the current geodynamic situation in the Arctic region is controlled by the interaction of only two lithospheric plates - Eurasian and North American, separated by a divergent boundary. The instantaneous pole of divergence of the plates (the pole of their relative rotation), according to Savostin et al., 1984, is located at 59.5°N, 141.2°E. A mid-oceanic spreading Ridge (Reykjanes - Kolbeinsey - Mohns - Knipovich - Gakkel Ridges) strikes from Iceland through the center of the Norwegian-Greenland and Eurasia basins, to abut into the continental shelf of the Laptev Sea. Further location of the boundary between the North American and Eurasian plates remains as yet unclear. In other words, it is still a matter of debate how to connect the end of the NW

branch of the North American plate boundary (the Aleutian subduction zone in the Pacific) with the end of its Arctic branch (the Gakkel Ridge in the Arctic Ocean).

Most researchers believe that the spreading Gakkel Ridge penetrates directly into the Eurasian continent as a rift zone on the Laptev Sea shelf (Zonenshain et al., 1990a,b; Gramberg et al., 1990). This concept comes in several options. One is that the rift boundary merges with the graben of the Lena River mouth and then crosses the Verkhoyansk Range (Grachev, 1973; Zonenshain et al., 1990a,b). According to another one, this boundary is located further east, running into the mouth of the Indigirka and from there stretching via the Moma rift, into the area of the Shelikhov Bay in the Sea of Okhotsk (Fig.4). Other hypothetical routes were also proposed for the plate boundary connecting the Gakkel Ridge with the Sea of Okhotsk shelf and Kamchatka. Under any of the options, to close the hypothetical boundary between the North American and Eurasian plates, it has to be extended eastward and connected with the Komandorsky Shear and the Aleutian subduction zone.

This, however, meets serious complications. First, the Okhotsk-Chukotka Volcanic Belt is not cut by any known Cenozoic faults of NW strike that could be interpreted to represent a plate boundary. Second, there are no traces of active Cenozoic structures, cutting at right angles the Central Kamchatka rift and the Miocene volcanic belt of the Central Kamchatka Range, that could also be viewed as evidence of a plate boundary running across Kamchatka. Some evidence for the recent (post-Early Miocene) small-offset sinistral strike-slip displacements along the faults of NW strike was obtained for Karaginsky Island in the East Bering Sea region only (Verzhbitsky et al., 2005).

At present time we observe the elongated zone of seismicity, which is considered as the boundary of the North American and Eurasian plates from the mouth of the Lena River to Kamchatka. However, this belt is not morphologically expressed, especially in its southern part from the southern spurs of the Moma mountains and Cherskii Range to the east coast of Kamchatka.

Throughout all this seismicity zone grabens are found only in the northern part of the Lena River

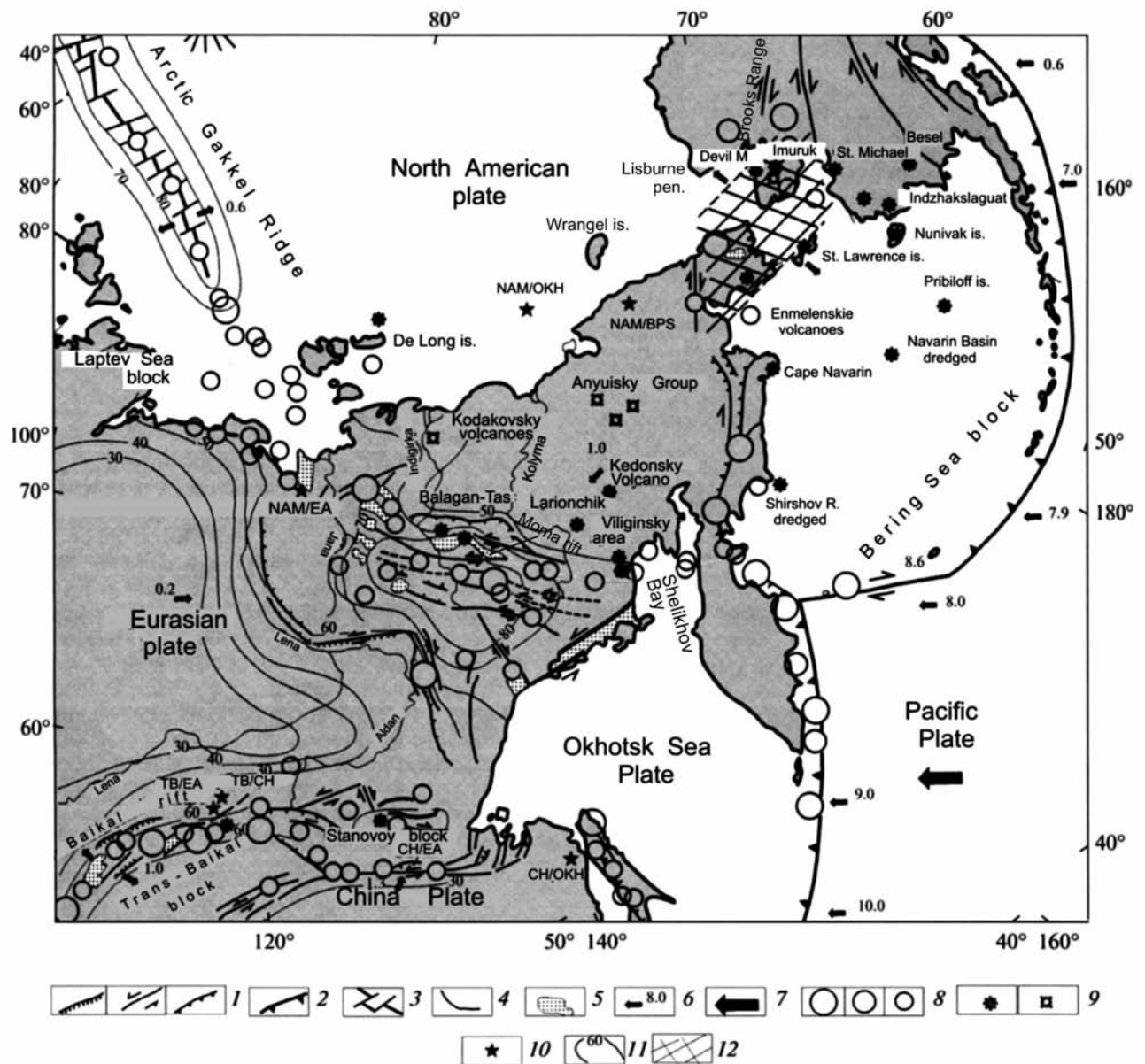


Fig. 4. Sketch map showing modern geodynamics of NE Asia and Alaska, after (Kovalenko et al., 2010). 1) active fault: normal fault, strike slip, thrust, respectively, 2) boundary of lithospheric plates; 3) axial zone of the Gakkel spreading Ridge; 4) passive (inactive) fault; 5) Cenozoic basin; 6) direction and velocity of motion of a separate block, cm/year; 7) direction and velocity of lithospheric plate motion, cm/year; 8) focal mechanisms of earthquakes with $M > 7.0$, 6.0-6.9, and < 6.0 , respectively; 9) Cenozoic volcanism, respectively: chiefly alkaline mafic and ultramafic lavas; subalkaline mafic lavas; 10) poles of rotation of plates and blocks: BPS = Bering Sea block (plate); CH = Chinese plate; EA = Eurasian plate; OKH = Sea of Okhotsk plate; NAM = North American plate; 11) heat flow, mW/m^2 ; 12) Bering Sea rift

delta and between the middle flows of the Yana and Indigirka River (Fig. 4). The southernmost graben, containing a quaternary volcano Balagan-Tas, is located between the Chersky Range and Moma Mountains (Fig. 4). Further towards the Kamchatka Peninsula the boundary is not observed in a geological structure. For seeing this fact it is enough to look at geological (Geological ..., 2008) or tectonic (Geodynamics ..., 2006) (Fig. 5) maps of NE Russia.

This indicates that the boundary is quite young, not mature. Note that according traditional plate tectonics point of view, the boundary between North American and Eurasian plates could be delineated here from 110 Ma to present, but certainly for at least for the last 65 million years, from the time of opening of the Eurasia Basin. From our point of view it is hard to believe that for 110 Ma this boundary in Eurasia was seismically active without forming visible geological structures.

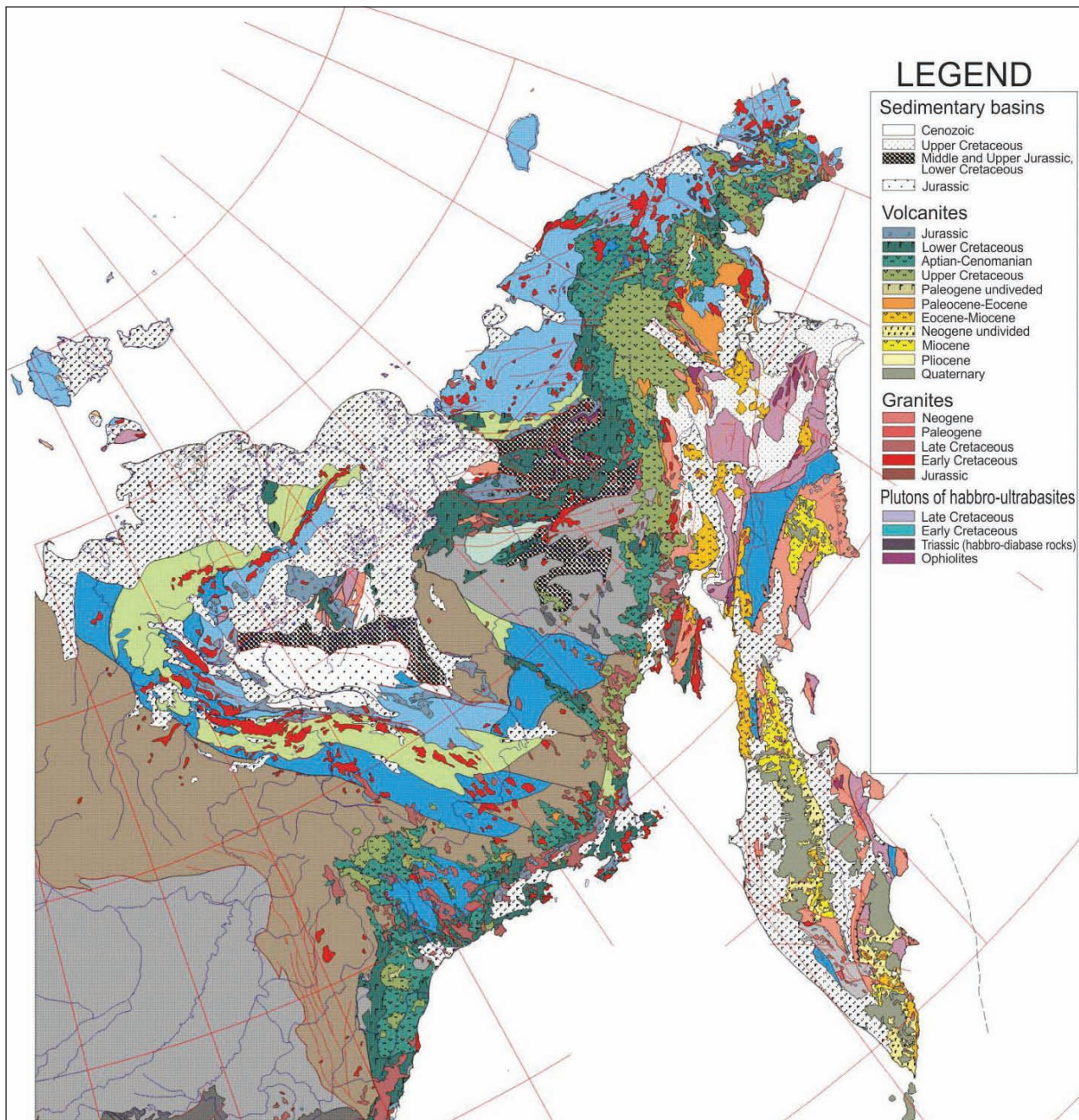


Fig. 5. Tectonic map of Northeastern Russia (Geodynamics ..., 2006).

In general, maybe we should consider whether or not seismicity is a sign of a plate boundary without proper morphological expression. In our case we must assume the existence of boundary from 110 Ma. We suggest that the North American and Eurasian plates are not completely separated in continental Northeastern Eurasia, and are only in the process of break-up.

The question remains: how far back in the geological history can we assume that the above boundary has acted as a diffuse plate boundary between Eurasia and North America? Let us

consider the age of the southernmost structural unit of the boundary from the mouth of the Lena River to Kamchatka: the timing of formation of the Moma graben is referred as Miocene (Grachev, 1973). Thus, we can assume that the formation of the lithosphere plate boundary within the Eurasian continent to towards Kamchatka only started 20-30 million years ago. Prior to this time, during the period 110-30 Ma, the boundary was in a very different place. Probably it was located far to the north in the East Siberian shelf region (Bogdanov et al., 1995). Presently, this boundary is revealed as a rift system, but is not

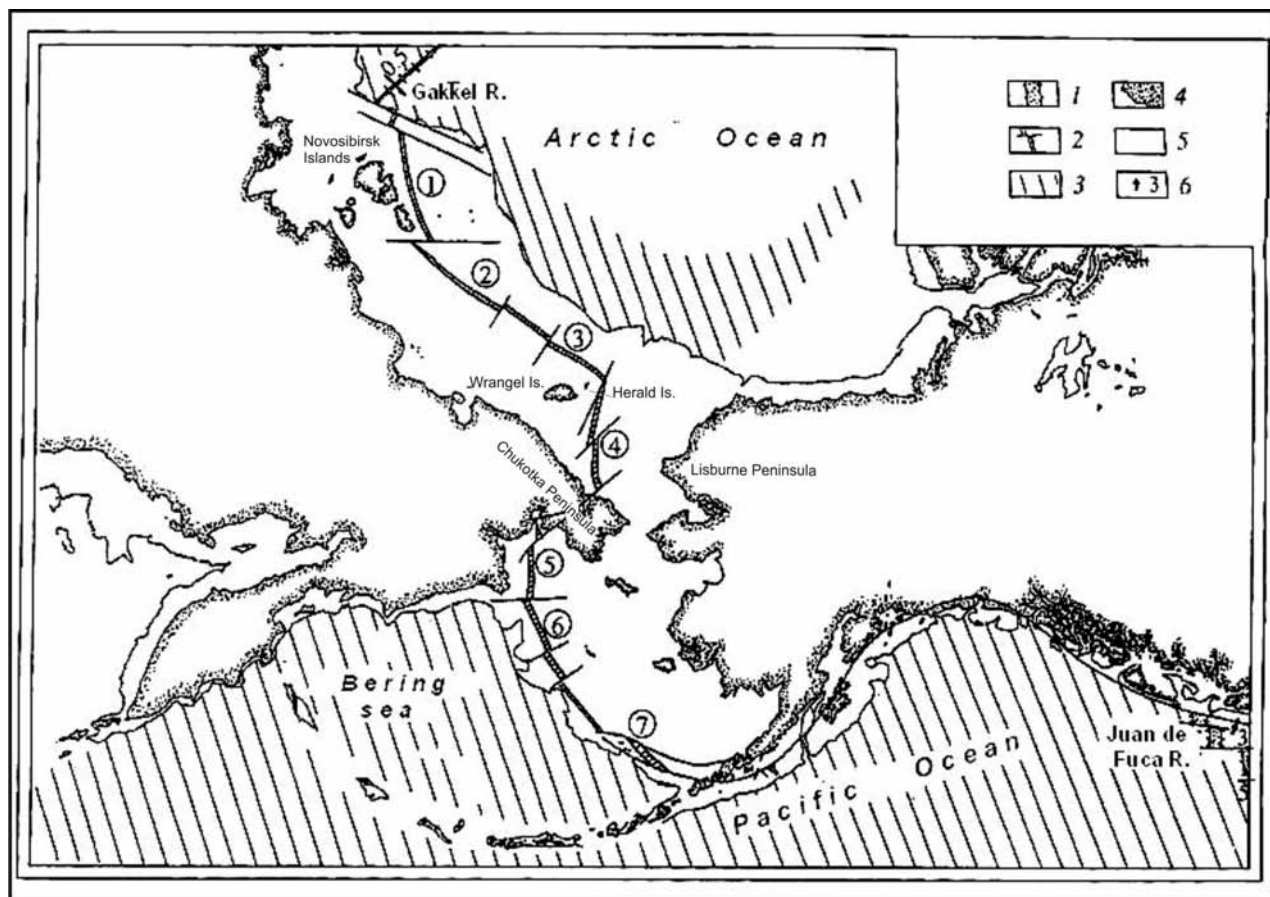


Fig. 6. Inferred boundary of the Eurasian and North American plates on the Arctic shelf (after Bogdanov et al., 1995). Location of Cenozoic rifts of the Eastern Arctic. 1) mid-ocean ridge; 2) Cenozoic rift; 3) area with oceanic crust; 4) land; 5) continental shelf; 6) spreading velocity (cm/year). Circled number (rift): 1 = Anjou, 2 = Novosibirsk, 3 = Vilkitsky, 4 = South Chukotka, 5 = Anadyr, 6 = Navarin, 7 = St. George.

expressed in seismic activity (Fig.6).

It should be noted that the Eastern Arctic system of shelf rifts is well manifest in the magnetic and gravity fields, but they do not disrupt continental crust and show almost no seismic activity. It is more likely that this system is a within-plate megashear consisting of a chain of rifts and transform faults, along which slow displacements of adjoining crustal blocks occur. Despite the lack of present-day seismicity along the rifted system we consider it as the transform (transtensional) fault boundary of movement of Amerasia block, including Lomonosov and Alpha-Mendeleev Ridges, Chukchi Borderland, Canada Basin, Alaska relative to Eurasia in Late Cretaceous-Cenozoic.

In summary, this brief review of studies striving to locate the boundary between the Eurasian and North American plates in the eastern part of the Arctic region, it is reasonable to conclude that presently there is no tangible boundary (single, linear

and well-defined by tectonic pattern) between the major lithospheric plates. In other words, we have no grounds to believe that the Eurasian and North American plates are completely separated from one another in terms of the classical plate tectonics. Their separation is only partial (along the divergent boundary in the North Atlantic and in the Western Arctic), and they still remain integral in the eastern part of the Arctic region (Fig.4). It is conceivable that as the deformation processes keep evolving, the boundary between the plates will finally develop to the point of complete separation of these plates, which may yet take dozens of million years. From thence follows the inapplicability of the methodology of calculating the motions of crustal and lithospheric blocks of Eurasia and North America based on plate tectonic tenets, especially in the Arctic region.

Let us now dwell on some implications of plate tectonic calculations for the Arctic region, performed in the framework of the classical plate tectonic

paradigm. In compliance with it, tectonic evolution of the Arctic in the Mesozoic and Cenozoic was chiefly controlled by the interaction of two plates, Eurasian and North American (Herron et al., 1974). The initial calculations of the parameters of their motions (Pitman and Talwani, 1972) already showed that during the opening of the North Atlantic, the Arctic plates must have converged, for which reason Herron and co-workers (1974) defined the Alpha Rise as a compression structure.

A later work of Zonenshain and Natapov (1987) presented differential parameters of motions for the Eurasian and North American plates, shedding light on their interaction in the Arctic. According to these calculations, between 110 and 55 my ago, the pole of the relative rotation for the North American and Eurasian plates was situated in the area of Greenland and Ellesmere Island. Accordingly, in the direction of the Atlantic the plates were diverging, and in the direction of the North Pole and from there to the Bering Strait they were converging. In the Chukchi Sea plate convergence amounted to 900 km, and in the area of the northern part of Ellesmere Island it was 350 km. Therefore, in the Late Cretaceous - Paleocene time in the Arctic there must have existed structures resulting from the convergence of North America and Eurasia (Herron et al., 1974). The proposed compression belt is seen in the fold front stretching from the Brooks Range via the Lisburne Peninsula to Herald I. and Wrangel I., to pass into the Mendeleev and Alpha Rises. To accommodate a 1000 km convergence one cannot avoid assuming that, apart from continental shortening, 900 km of oceanic crust of the Canada basin was consumed in the subduction zone with the formation of a volcanic arc. In the work of Zonenshain and Natapov (1987) it was proposed that the Alpha-Mendeleev Rise is a Late Cretaceous volcanic arc with characteristic calc-alkaline magmatism, beneath which the Canada basin lithosphere was subducting. This resulted in the formation of the Makarov oceanic basin through backarc spreading. A similar model is used in a recent paper by J. Golonka (2011).

These are some implications of applying the methodology of kinematic calculations to the interaction of the Eurasian and North American plates in the Arctic region. It should be noted that a whole range of conclusions thus obtained are at odds with

the available geological and geophysical data. This applies primarily to the proposed subduction origin for the Alpha-Mendeleev Rise and the Makarov Basin. There are no data on calc-alkaline magmatism in the Alpha or Mendeleev Rises, on compressional structures in these rises, or on consumption of any considerable volumes of lithosphere of the Canada basin beneath them. On the contrary, the totality of data currently available provides convincing evidence of extensional structures existing on the Alpha and Mendeleev Rises and of their rift origin (Rowley and Lottes, 1988; Miller and Verzhbitsky, 2009; Lobkovsky et al., 2010, 2011). A seismic reflection profile across the Lomonosov Ridge, Makarov Basin and Mendeleev Rise shows a complete undisturbed sedimentary section of Mesozoic/Cenozoic age (Jokat et al., 2013). Seismic reflection data for the Makarov Basin show no evidence of compressional features consistent with the Lomonosov Ridge moving as a microplate in the Cenozoic. Thus the main compressional features in the describing part of Arctic region (Novosibirsk-Chukotka-Brooks fold and thrust belt) were formed before the opening of Makarov Basin (i.e. before Aptian time according to our estimations).

Jokat et al. (2013) proposed that the Amerasia Basin moved as a single tectonic plate during the opening of the Eurasia Basin. We believe that in accordance with these data one can talk about movement of Amerasia single plate from the time of formation of the Makarov Basin. Aptian-Albian basaltic rocks of the De Long magmatic dome, outcropping on Bennett Island (De Long Archipelago) (Fedorov et al., 2005) can be considered as onshore geological evidence of the early opening of Makarov Basin, as well as the Indigirka extensional belt of Aptian-Early Paleogene age, located approximately along on line with the Makarov Basin and Novosibirsk islands (Trunilina et al., 1999; Parfenov and Kuzmin, 2001; Miller and Verzhbitsky, 2009).

Therefore, the formation of compressional structures on the site of the Lomonosov Ridge, Makarov Basin and Mendeleev Ridge can theoretically be assumed for Early Cretaceous (pre-Aptian) time during the formation of the South Anyui suture can be expected. This conclusion is in a good agreement with our point of view since

we underscore that, according to the kinematic calculations of the interaction between Eurasian and North American plates (Pitman and Talwani, 1972; Herron et al., 1974; Zonenshain and Natapov, 1987; Rowley and Lottes, 1988) in the central Arctic and Eurasia the compressional setting was proposed for time interval ~ 110-55 Ma and subsequently the existence of a subduction zone under the Alpha - Mendeleev Ridge, due to a the pole of rotation for the Eurasian and North American plates in Greenland and on Ellesmere Island. However geological data indicate the formation of extensional structures in the central Arctic region at this time show no evidence of the existence of a paleo-trench along the border of Alpha Mendeleev Ridge. These geological facts limit the applicability of rigid lithosphere plate tectonics.

The analysis of the other reconstructions for the North Atlantic and the Arctic (Bullard et al., 1965; Le Pichon et al., 1977; Sclater et al., 1977; Srivastava and Tapscott, 1986; Srivastava et al., 1985; Savostin et al., 1986, Rowley and Lottes, 1988; Roest, Srivastava, 1989; Lawver et al., 1990; Gaina et al., 2002; Brozena, et al., 2003; Glebovsky et al., 2006) all call for a 500 to 1400 km compression in the Arctic region between 110 and 56 my ago. The latter researchers (Rowley and Lottes, 1988) attempted to achieve the best computer-aided visual fit of magnetic lineations, transform faults, and boundaries of continental blocks. They managed to reduce the shortening in the Arctic ocean to 170 km by reinterpreting, in some cases, the observed order of magnetic lineations (e.g., in the Labrador Sea). However, if we turn to the continental geology of Eurasia, we will be confronted with the same sort of inconsistencies. Indeed, according to (Rowley and Lottes, 1988), the differential pole of rotation for the NAM/EUR plates was situated in the southern part of the Podvodnikov Basin (81.62°N, 170.67°E), which implies a compression regime at that time (110-56 Ma) on the Eurasian continent from the Laptev Sea to the sea of Okhotsk shore (e.g., near the Alazeya River about 280 km of compression was inferred).

Thus following the traditional kinematic reconstructions one should look for traces of the Arctic plate boundary between North America and Eurasia along which for a time interval 110-56 m.y. the estimates of plate convergence varies from 500 to

1400 km. The examples of relatively young Mesozoic and Cenozoic compressional structures on the periphery of the Arctic Ocean are well-known: New Siberian – Chukotka/Wrangell – Lisburne – Brooks Range fold belt, the Eurekan orogen combining West Spitsbergen fold belt and northern Ellesmere Island mountain belt and their offshore continuations.

The prominent New Siberian – Chukotka/Wrangell – Lisburne – Brooks Range fold belt can be considered as a typical interplate collisional fold belt. It is widely known that it was mainly formed in Late Jurassic - Middle Cretaceous and was mostly completed in Aptian-Albian time (Drachev, 2002; Drachev et al., 2011; Kos`ko et al., 1993; Moore et al., 2002; Miller and Hudson, 1991; Sokolov et al., 2002, 2009). We believe that the fold belt was formed a result of the Arctida dispersal. The formation of the fold belt was related to collision of the Chukotka – Novosibirsk block with the edge of Eurasia and also the Arctic Alaska block with terranes of Central Alaska. At this time neither Chukotka nor Alaska were integral parts of the Eurasian and North American plates. In general the belt as a whole is older than 110 million years.

The Eurekan orogen is a fold and thrust belt that extends from West Spitsbergen across northernmost Greenland and into Ellesmere Island and the eastern Canadian Arctic Archipelago. The West Spitsbergen Fold Belt and northern Greenland structures (Lyberis and Manby, 1993) are suggested to be the result of a Paleocene-Eocene (~ 65-34 Ma) sheared and rifted margin setting during the opening of the Norwegian-Greenland Sea. The belt was definitely formed due to transpressional development of a transform boundary of the North American and Eurasian plates along the DeGeer (Hornsund) fracture zone (Faleide et al., 1993). Small-scale tectonic structures studied on Ellesmere and Axel Heiberg Islands show that there are two successive and independent stress regimes related to the Eurekan Orogeny (Lepvrier et al., 1996). The oldest, a minor event, is related to a NE-ENE orientation of the maximum stress axis. It is likely corresponds to the sinistral oblique-slip motion of Greenland with respect to Ellesmere Island which mainly occurred between magnetic anomalies 25 and 24 (Late Paleocene - Early Eocene; ~ 56.5-53.5 Ma) and supports the hypothesis of distributed shear during the early stage of the Eurekan Orogeny.

The youngest, a major stress regime recorded in the uppermost Middle Eocene (possibly to Early Oligocene) rocks of the synorogenic Eureka Sound Group, is compressional and is characterized by a WNW-ESE (eastern Axel Heiberg Island) to NNW-SSE (northern Ellesmere Island) orientation of the maximum horizontal stress axis. It can be correlated with the northwestward convergent motion of Greenland toward Ellesmere Island between magnetic anomalies 21 and 13 (Middle Eocene - Early Oligocene; ~ 48-33.5 Ma). Structural evidence for the initial Late Cretaceous-Paleocene counter-clockwise rotation of Greenland with respect to the Canadian Shield between anomalies 34 (Campanian) and 25 (Late Paleocene) has not been found (Lepvrier et al., 1996). Thereby all these Eureka structures are transpressional and were mostly formed in the relatively younger period of time in Paleocene-Eocene, thus they don't represent the deformations formed at the "real" convergent plate boundary.

The Beaufort Fold Belt is of greatest interest to us. This thrust and fold belt was revealed by a seismic survey above the detachment plane at a depth of about 15 km is located within the Beaufort-Mackenzie Basin at the southern margin of the Canada Basin (Helwig et al., 2010, Dinkelman et al., 2008). The Upper Cretaceous-Miocene (~100-5 Ma) sedimentary rocks are involved in folding and faulting. These deformations are related to both gravity sliding and Brooks-Range orogeny-related compression from northeastern Alaska (Dinkelman et al., 2008); the belt is also distinctly delineated by a near latitudinal negative gravity anomaly. In our opinion, the Beaufort Fold Belt is the intraplate deformation zone and is not connected with the convergent plate boundary of the North American and Eurasian plates. The belt represents also the example of deformation of the upper sedimentary cover, but not deformation of the whole lithosphere or subduction of the one plate beneath another as a result of a convergence (Laverov et al., 2013). It is also clearly visible on the seismic sections (Dinkelman et al., 2008) that deep sub-detachment crust is cut by series of small-offset normal faults (i.e. weakly deformed). It is important to emphasize that the Miocene rocks (Dinkelman et al., 2008) are involved into folding here, therefore the deformation took place very recently.

We believe that the formation of the intraplate Beaufort fold belt and Alaskan orocline (formed by Brooks Range and Lisburne Hills fold belts) took place during Late Cretaceous-Miocene as a result of displacement of the Amerasian fragment of Arctida continent (including Lomonosov Ridge, Podvodnikov and Makarov Basins, Alpha-Mendeleev Rise, Canada Basin and Arctic Alaska block) along the transform fault zones on the Canadian Arctic Islands and the Arctic Asia continental shelf margin toward the Pacific subduction zone. In other words this process of Amerasian block movement was the cause of shortening in the Alaskan marginal segment.

Thus, after considering all the compressional structures of the peripheral parts of the Arctic region, we found that none of them are suitable for a convergent boundary of the North American and Eurasian plates. And again, it would presumably have to pass through the central part of the Arctic and northeast Asia.

On the contrary, during this time period (110-56 Ma) it was an area of formation of mainly extensional and shear structures (except for some local ones). Note that the concept of Rowley and Lottes (1988) is in disagreement with geological and structural data, including the development of the Lower Indigirka Aptian- Early Paleogene extension belt (Trunilina et al., 1999; Parfenov and Kuzmin, 2001) and the Aptian-Albian pulse of strong roughly E-W extension in the Central Chukotka (Miller and Verzhbitsky, 2009).

The above inconsistencies, in our opinion, cannot be reconciled in the framework of the classical plate tectonic concept. To overcome them, it is necessary to reject certain basic tenets of this concept, such as: (i) rheology of rigid plates, (ii) the practice of applying kinematic calculations of rigid plate interactions using Eulerian poles of rotation.

This unavoidably entails the issue of expanding the classical plate tectonic paradigm and formulating a new, more realistic generalizing concept, capable of adequately describing global and regional geological processes. We propose to term this generalizing concept tectonics of deformable lithospheric plates, to emphasize that it succeeds the classical paradigm, while introducing the key word deformable.

The essence of the new concept proposed here is that instead of the methodology of kinematic

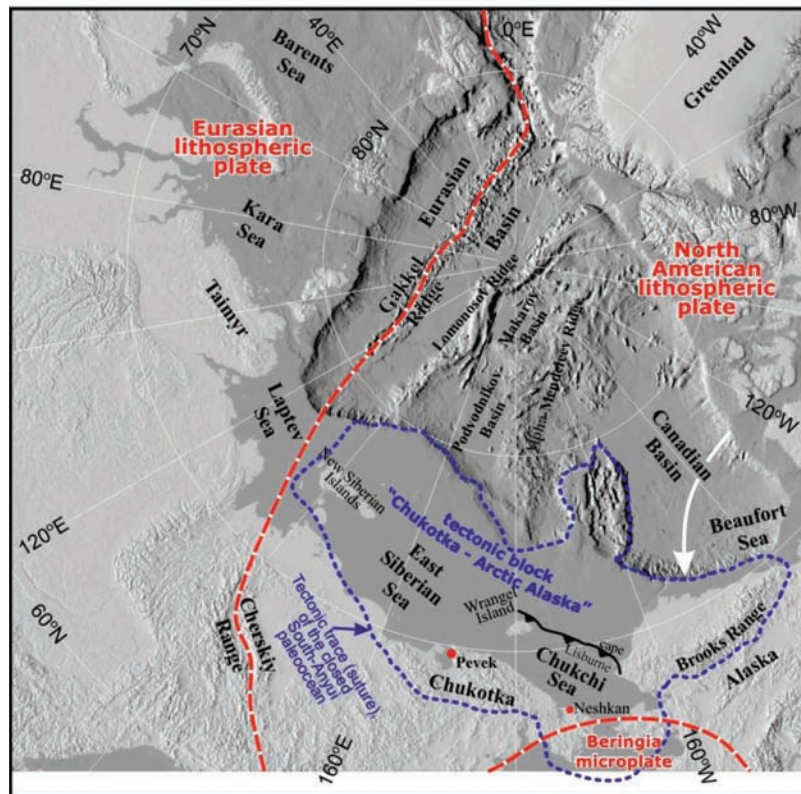


Fig. 7. Principal geographic and tectonic features of the Arctic (based on the map from Miller et al. (2006), modified and supplemented after Lander et al. (1994), Imaev et al. (2000) and Mackey et al. (1997)). Red dashed line shows idealized boundaries of modern lithospheric plates. Blue dashed line shows position of the “Chukotka - Arctic Alaska” microplate. White arrow corresponds to idealized path of plate motion of the “Chukotka – Arctic Alaska” microplate in the course of opening of the Canada Basin. Topographic base, IBCAO

descriptions of the rotation of rigid plates on the sphere with the use of Eulerian poles, we propose to employ a mathematical (numerical) analysis of 3D elastoplastic deformation of the lithosphere combined with a numerical analysis of sublithospheric mantle currents. It should be noted that this transition to a new paradigm was impossible until the researchers could start using computer-aided modeling of 3D deformation in the lithosphere and the modeling of 3D mantle currents. By combining these two modern lines of numerical analysis we can now suggest the methodology for the concept of the tectonics of deformable lithospheric plates with upper-mantle currents beneath.

In preparing the Arctic reconstructions we used Eulerian poles of rotation to restore the position of main stable continental platforms and thus produced a “support framework” for reconstructions. The smaller continental blocks, such as the Lomonosov Ridge, Podvodnikov and Makarov Basins, Alpha-Mendeleev Rise, New Siberian Islands and Arctic Alaska block were moved within this framework and

in accordance with the accepted geodynamic model and with the available regional geological data. Following the estimates (Miller and Verzhbitsky, 2009) the possibilities of 100 % - 150 % of extension of these blocks were suggested in order to avoid possible overlaps and gaps.

Geological and geophysical data and geodynamic reasons for creating a numerical model for Mesozoic and Cenozoic evolution of the Arctic

In view of the above, under the popular “rotation model” (e.g. Grantz et al., 1998; Sokolov et al., 2002; 2009), it is assumed that in the Jurassic-Cretaceous time the Arctic’s geodynamic development was largely controlled by the “Chukotka - Arctic Alaska” microplate, whose breaking off from the Canadian Arctic Archipelago and collision with Eurasia brought about the formation of the Arctic Canada Basin, closure of the South Anyui paleo-ocean, and the formation of fold-and-thrust belts stretching from Novosibirsk Islands via Chukotka to the Brooks Range in Alaska (Fig. 7). According

to the results presented in Miller and Verzhbitsky (2009), immediately upon the termination of collisional processes at the end of the Neocomian, in Aptian-Albian time, the area of Central Chukotka suffered strong roughly E-W directed extension, approximately across the strike of the Makarov Basin, situated some distance north (Fig. 8). Because the opening of the Eurasia Basin through rifting that evolved into spreading started later, in the Late Cretaceous and Paleocene (Drachev, 2000; Drachev et al., 1998; Gaina et al., 2002) and based on the various geological data, the authors Miller and Verzhbitsky, (2009) proposed that the earlier Aptian-Albian lithospheric extension coincided with the formation of a more ancient basin with a similar trend, namely, the Makarov Basin (see Fig. 8).

In addressing the age and origin of the zone of inner rises and basins in the Arctic Ocean, one should bear in mind the existence in eastern Yakutia of the rather long (~ 500 km) N-S trending Lower Indigirka extensional (rift) belt of Aptian - Early

Paleogene age, first established by Stavsky (1982) and studied more recently by Trunilina et al. (1999) and Parfenov and Kuzmin (2001). The existence of a structure of this type agrees well with the assumed Aptian-Albian time for the inception of the Makarov Basin and suggests that rifting of the lithosphere of the Central Arctic region kept evolving in the Late Cretaceous synchronously with the evolution of the Okhotsk-Chukotka Volcano-Plutonic Belt, which marks the now fossil subduction zone of the Asian margin active up to the Early Paleogene.

Therefore, as a first approximation, the Late Mesozoic - Cenozoic evolution of the central part of the Arctic region falls in two principal geodynamic phases, with different stress fields in the lithosphere. The first phase (from the Late Jurassic to the Aptian) was characterized by a stress field with a significant NS tensile component, which resulted in the Novosibirsk-Chukotka-Alaska system of Arctida blocks breaking off from the North American continent, in the southward movement of Chukotka

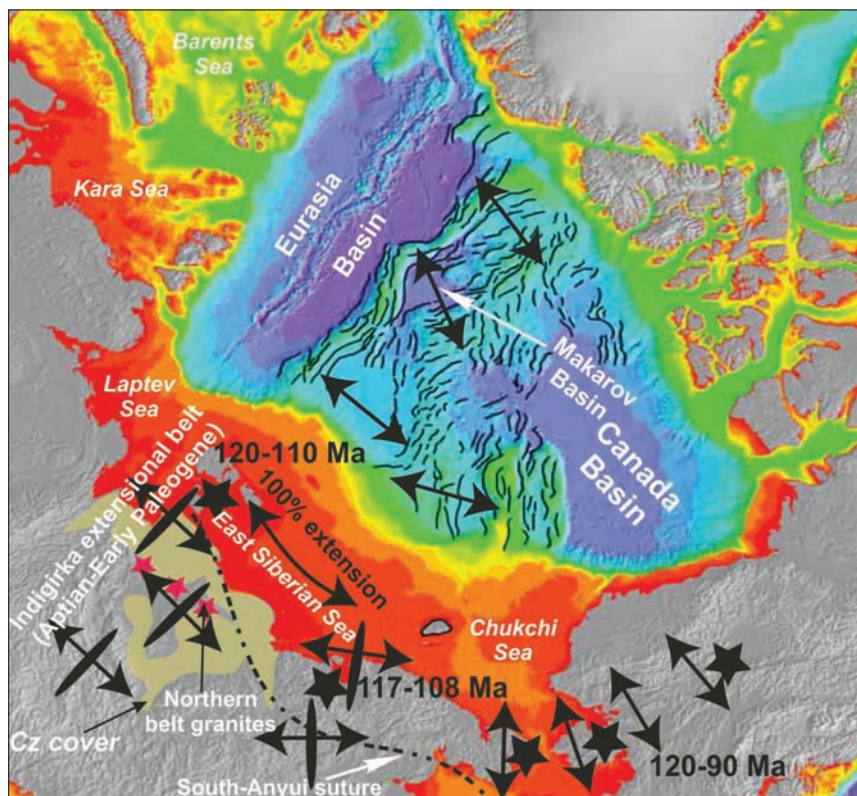


Fig. 8. Model for the opening of the Makarov Basin in the Aptian-Albian based on radiometric and structural data (modified after Miller and Verzhbitsky (2009) using (Parfenov and Kuzmin, 2001)). Solid asterisks show areas of postcollisional magmatic activity, numerals correspond to its age. Elongated solid ellipse = averaged strike of dikes and other extension features, arrows of different directions – direction of postcollisional extension. Thin solid lines on the Lomonosov and Alpha-Mendeleev Rises and on the Chukchi borderland mark inferred normal faults. Thick dotted line shows position of the South Anyui suture.

and its collision with the Eurasian margin due to the closure of the South Anyui paleo-ocean, and in the opening of the oceanic Canada basin.

The second phase of the evolution effectively started with the establishment of a postcollisional EW tensile stress field in the Aptian (~ 120 Ma). In the Aptian-Albian and in the Late Cretaceous this stress field shaped the lithospheric rift structures in the Central Arctic, including the Makarov and Podvodnikov basins, as well as the Alpha-Mendeleev Rise (see Fig. 8). This extensional stress field covered a vast territory in the Arctic region: New Siberian Islands - Indigirka extensional belt -Chukotka region - Seward Peninsula - Brooks Range, most likely due to influence of an upper mantle convection cell. In the Cenozoic, this same stress field gave rise to spreading in the Eurasia Basin with the Lomonosov

Ridge splitting off from the edge of the Barents-Kara shelf.

In addressing the geodynamic reasons for creating a numerical model for the Mesozoic evolution of the Arctic region, let us first discuss the likely driving forces responsible for the opening of the Canada basin in the Late Jurassic - Early Cretaceous (i.e., long before the growing North Atlantic spreading boundary propagated into the Arctic). Here, it should be noted primarily that the Arctic portion of the North American plate (incorporating the Arctida continent) in the Triassic and Jurassic was surrounded by two pale-oceans: the Pacific (Paleo-Pacific) and the South Anyui ocean, with the latter separating the Canadian margin of the North American plate from the Siberian margin of the Eurasian plate (Fig. 9). Starting at least from

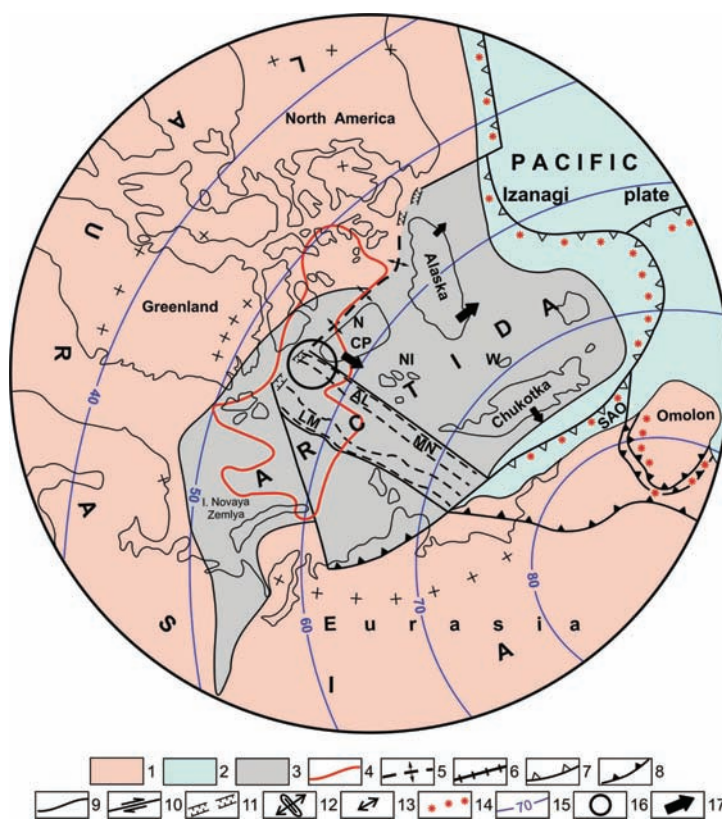


Fig. 9. 150 Ma paleogeodynamic reconstruction for the Arctic (Late Jurassic, Kimmeridgian/Tithonian). Legend for Figs. 9 and 13-16. 1) Continental crust area; 2) Oceanic crust area; 3) Arctic mantle plume magmatism on continental crust; 4) Arctic mantle plume magmatism on oceanic crust; 5) Spreading axis; 6) Fossil spreading axis; 7) Subduction zone; 8) Thrust zone; 9) Major strike slip zone or transform fault; 10) Strike slip sense, where known; 11) Rift; 12) Sheeted dikes polarity and extension direction with age, Ma; 13) Extension direction from structural data with age, Ma; 14) Island arc or marginal volcanic belt magmatism; 15) Paleomagnetic latitude; 16) Calculated position of the Iceland plume (after Lawver et al., 2002); 17) Direction of motion of the Arctida blocks relative to Laurasia. Lettering: AL = Alpha Rise, LM = Lomonosov Rise, MN = Mendeleev Rise, N = Northwind Ridge, NI = Novosibirsk Islands, TFAC = Central fragment of the Arctida continent, CR = Chukotka Rise, SAO = South Anyui ocean, SAS = South Anyui suture, W = Wrangel Island.

the Jurassic, the ongoing subduction of the Paleo-Pacific lithosphere was accompanied by subduction in the South Anyui ocean. It is thus only natural to assume that the main driving force responsible for the opening of the Canada basin in the Late Jurassic - Early Cretaceous was large-scale sinking of mantle material in the linked subduction zones consuming the lithosphere of the NW Pacific and the South Anyui ocean.

The intense and continuous mantle sinking in this region starting at the latest in the Jurassic is corroborated by modern seismic tomography data (Zhao, 2009; Zhao et al., 2009; Zhao et al., 2010). The mantle cross-sections show how the cold material sinking in subduction zones, upon reaching the transitional zone between the upper

and lower mantle, merges in this zone with the extensive horizontal layer of cold mantle material, which spreads far (for thousands of kilometers) beneath the Eurasian continent (Fig.10). In our opinion, this image clearly shows the development of an upper mantle convection cell, whose lower horizontal branch flows under the continent along the transitional zone between the lower and upper mantle, while the upper branch creates a return current of material under the lithosphere toward the Pacific subduction zone, leading to the extension of continental lithosphere and related upper mantle plume magmatism (Faccena et al., 2010).

From the standpoint of the proposed numerical model for the evolution of the Arctic region, the acquired seismic images of the mantle support the

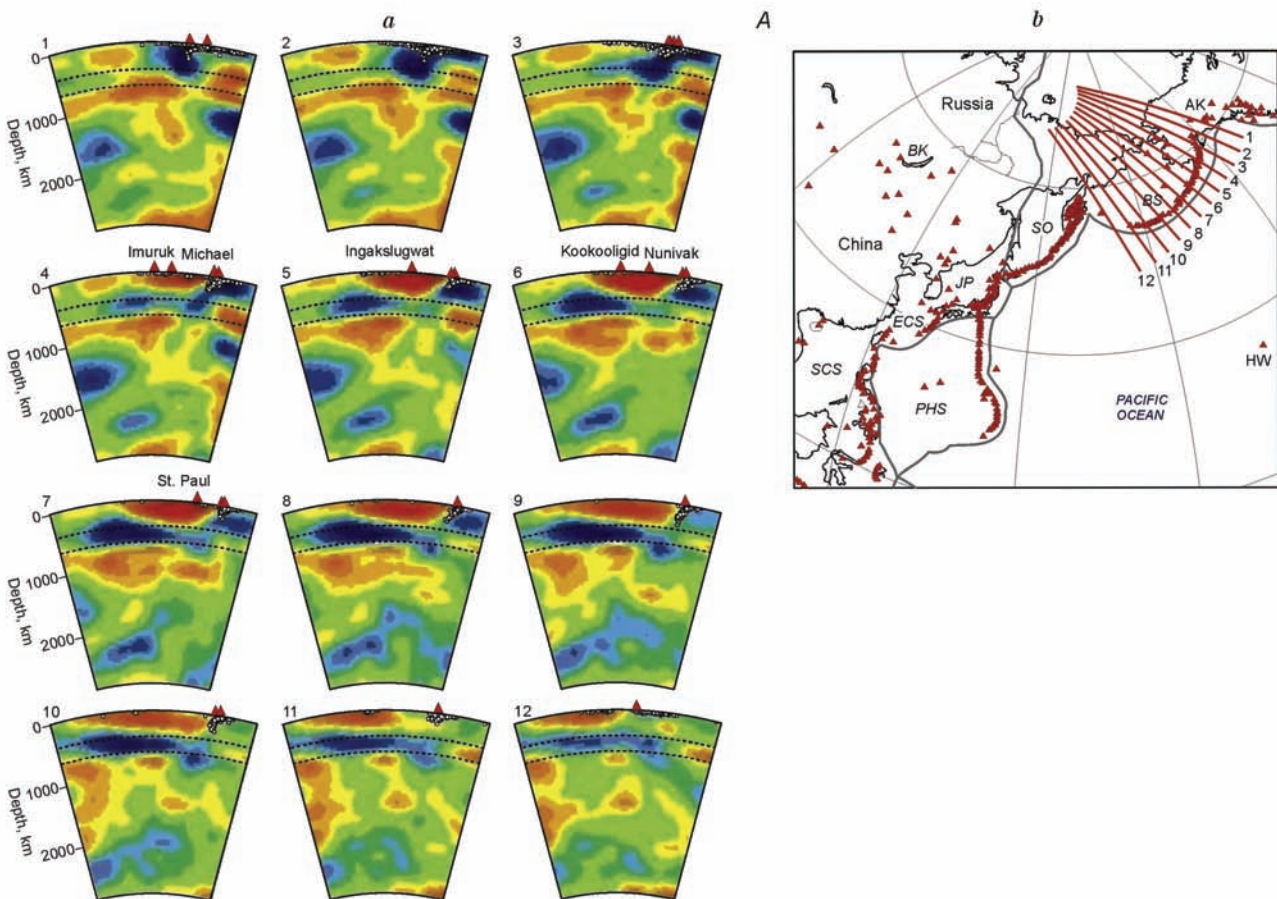
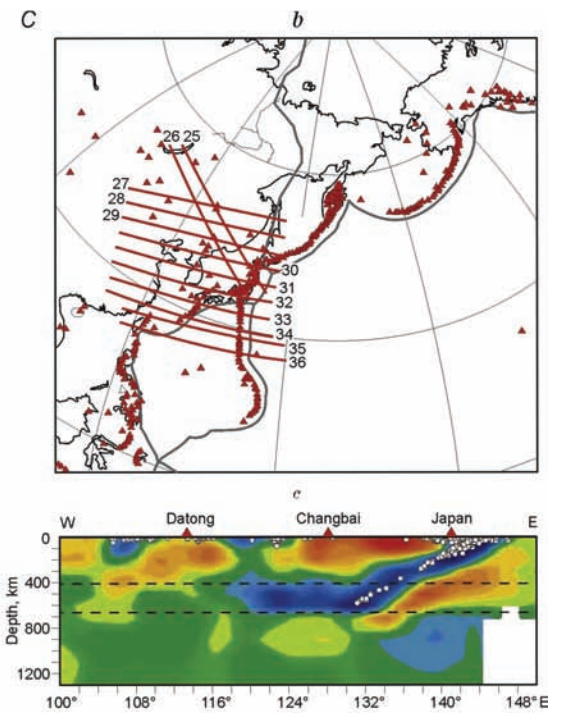
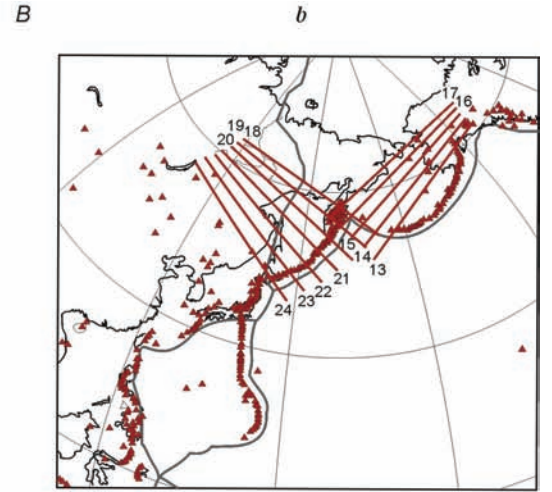
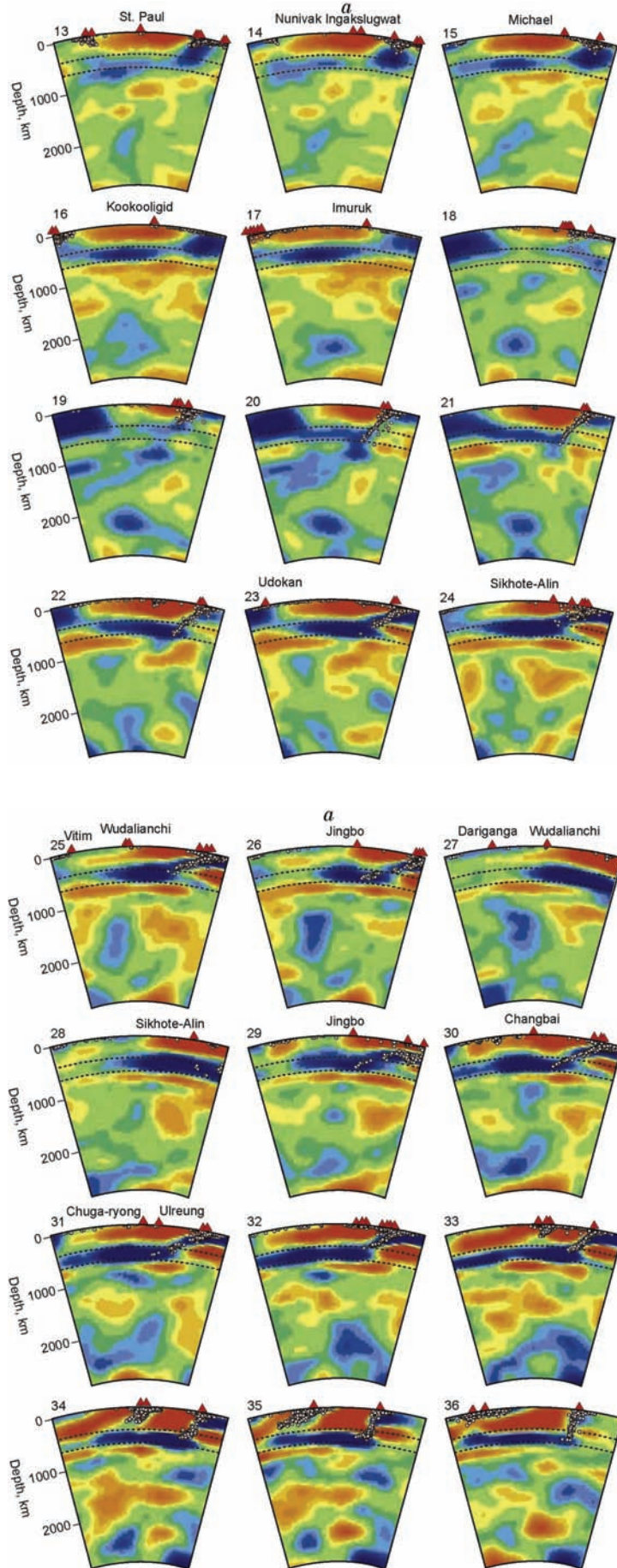


Fig. 10. Vertical cross-sections through the mantle displayed as P-wave tomograms along transects (a), which are shown in the inset (b); vertical cross-section through the mantle beneath Eastern Asia directed W-E displayed as a regional P-wave tomography image (c) (after Zhao et al., 2010). (a), (c) red and blue coloring(respectively), high and low seismic velocities; the maximum amplitude of velocity anomalies: a = 1%, c = 2%. White circle = earthquake within 100 km of a transect, red triangle = active volcano. Dashed line shows the boundary of abrupt change in seismic parameters at 410 and 670 km depths. b = thin red lines in the inset show plate boundary. Ak= Alaska, LB =Lake Baikal, BS = Bering Sea,ECS = East China Sea, HW = Hawaii, SJ =Sea of Japan, PHS = Philippine Sea, SCS =South China Sea, SO = Sea of Okhotsk. Transect nos. 25-36 run through Japanese Islands, Sea of Japan, and Eastern Asia.

Fig. 10. Continued.



basic tenet of the model, that the main driving force of lithospheric deformations in the Arctic was the return sublithospheric flow of mantle material to the subduction zones of the Paleo-Pacific and the South Anyui ocean (Fig.11).

It is logical to assume that such sinking of mantle material induced a compensatory ascending

upper mantle current, manifested in the Western and Central Arctic as the so-called Mesozoic Arctic plume (Shipilov, 2008; Shipilov et al., 2009; Filatova and Khain, 2009). This areal diffuse magmatism, which is mirrored in this province's "disperse-isometric" pattern of magnetic anomalies (Fig. 12), is highly typical of flood volcanic provinces.

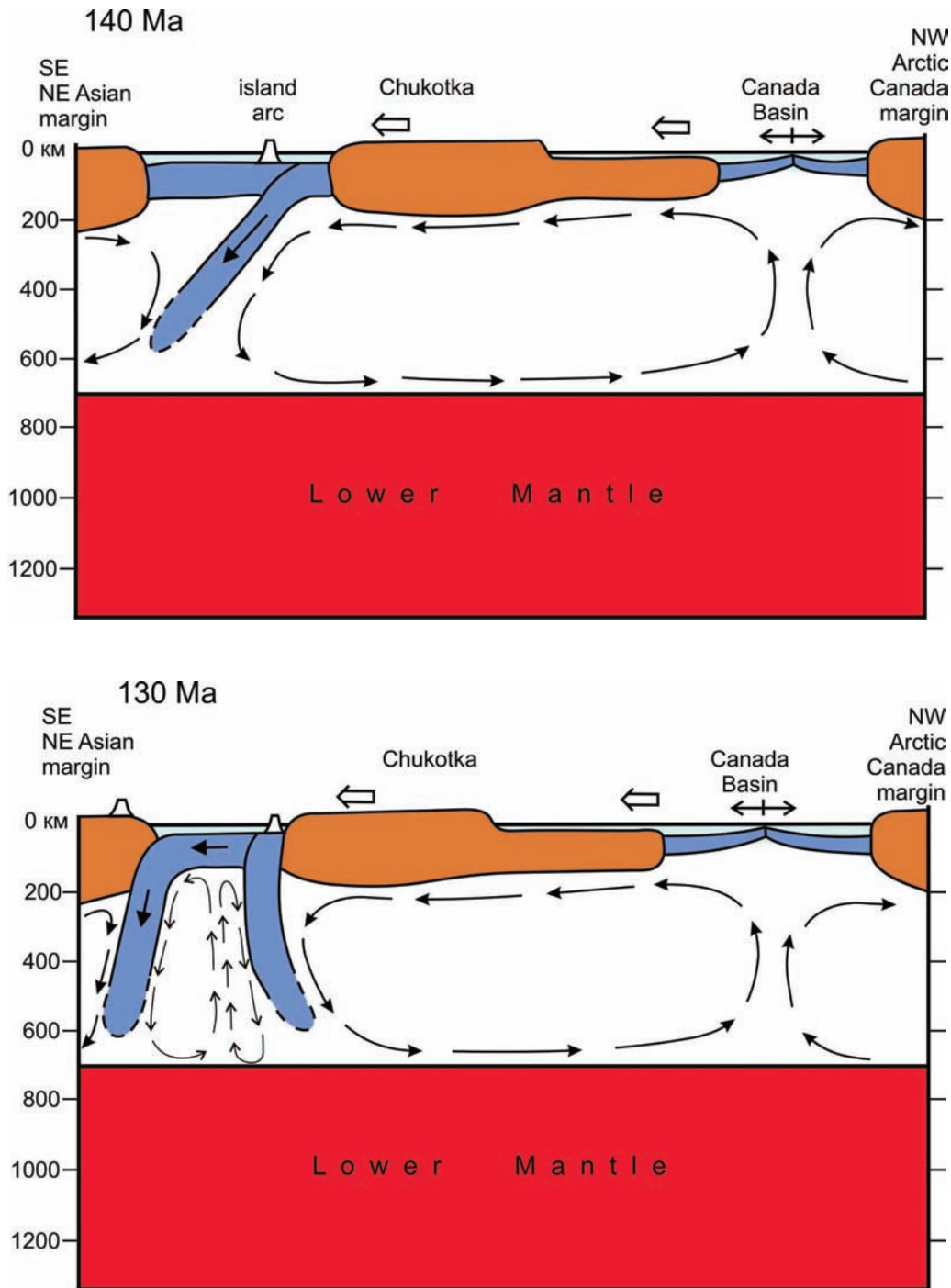


Fig. 11. Model of upper mantle return flow of upper mantle convection cell dragging blocks of Arctida towards to subduction zone existed during Late Cretaceous - Paleogene in Arctic region. a) for 140 Ma, b) for 130 Ma. c) for 90 Ma, d) for 55 Ma. GkR = Gakkel Ridge, LmR = Lomonosov Rise, MkB = Makarov Basin, Al-MnR = Alpha-Mendeleev Rise.

Fig. 9 also shows the province of Jurassic-Cretaceous intraplate magmatism. The main field is located on the edge of the Barents Sea as well as in the Central Arctic (Lomonosov, Alpha-Mendelev Rise, and Makarov and Podvodnikov Basins according to the magnetic field map by Gaina et al. (2010) (see Fig. 12)) just in front of the proposed upper mantle cell.

Thus, we see that spatial distribution of intraplate magmatism in the surrounding areas supports the proposed model of the upper mantle cell.

The second geodynamic reason for creating a numerical model for the evolution of the Arctic is that, in keeping with the concept of tectonics of deformable lithospheric plates, we consider

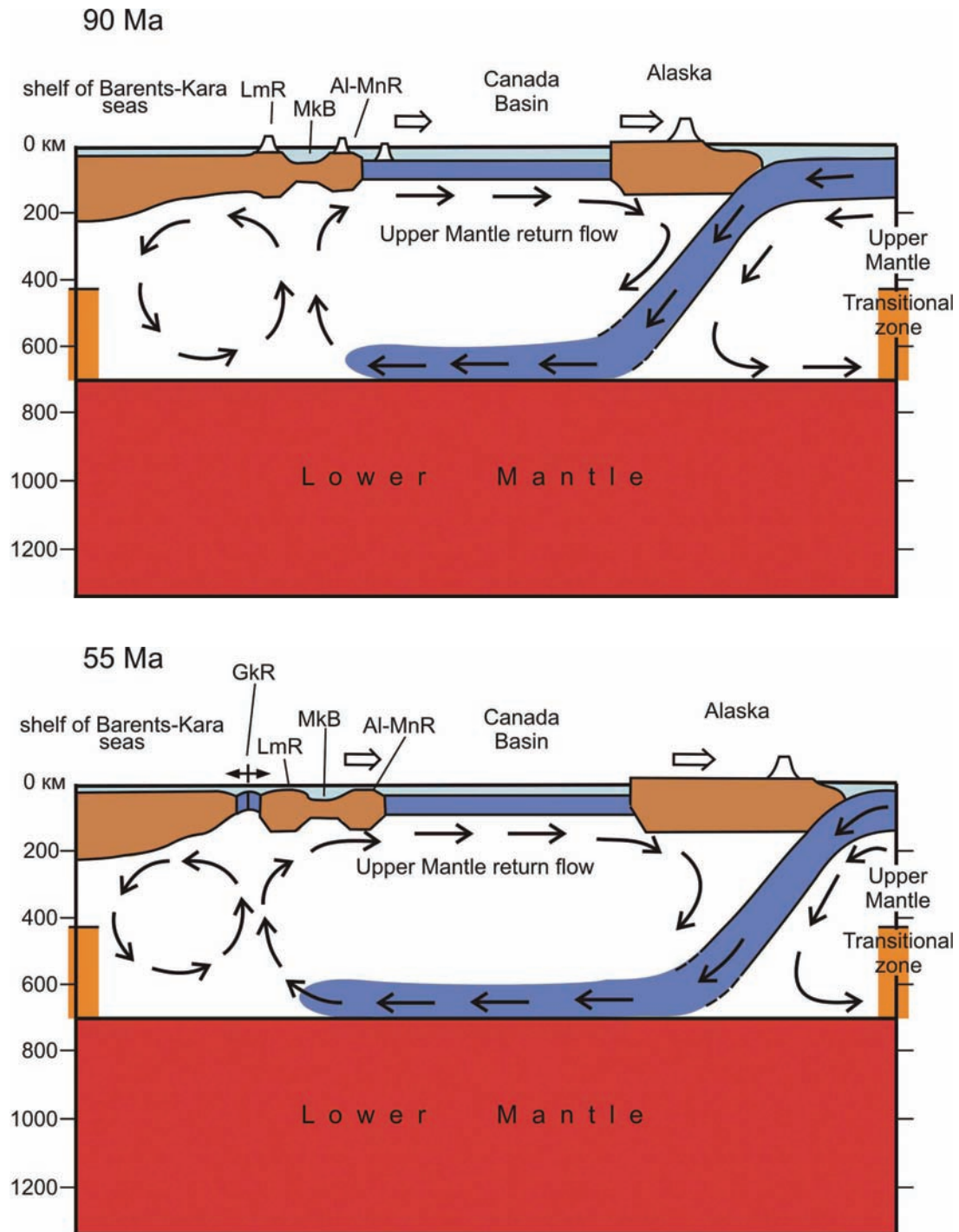


Fig. 11. Continued.

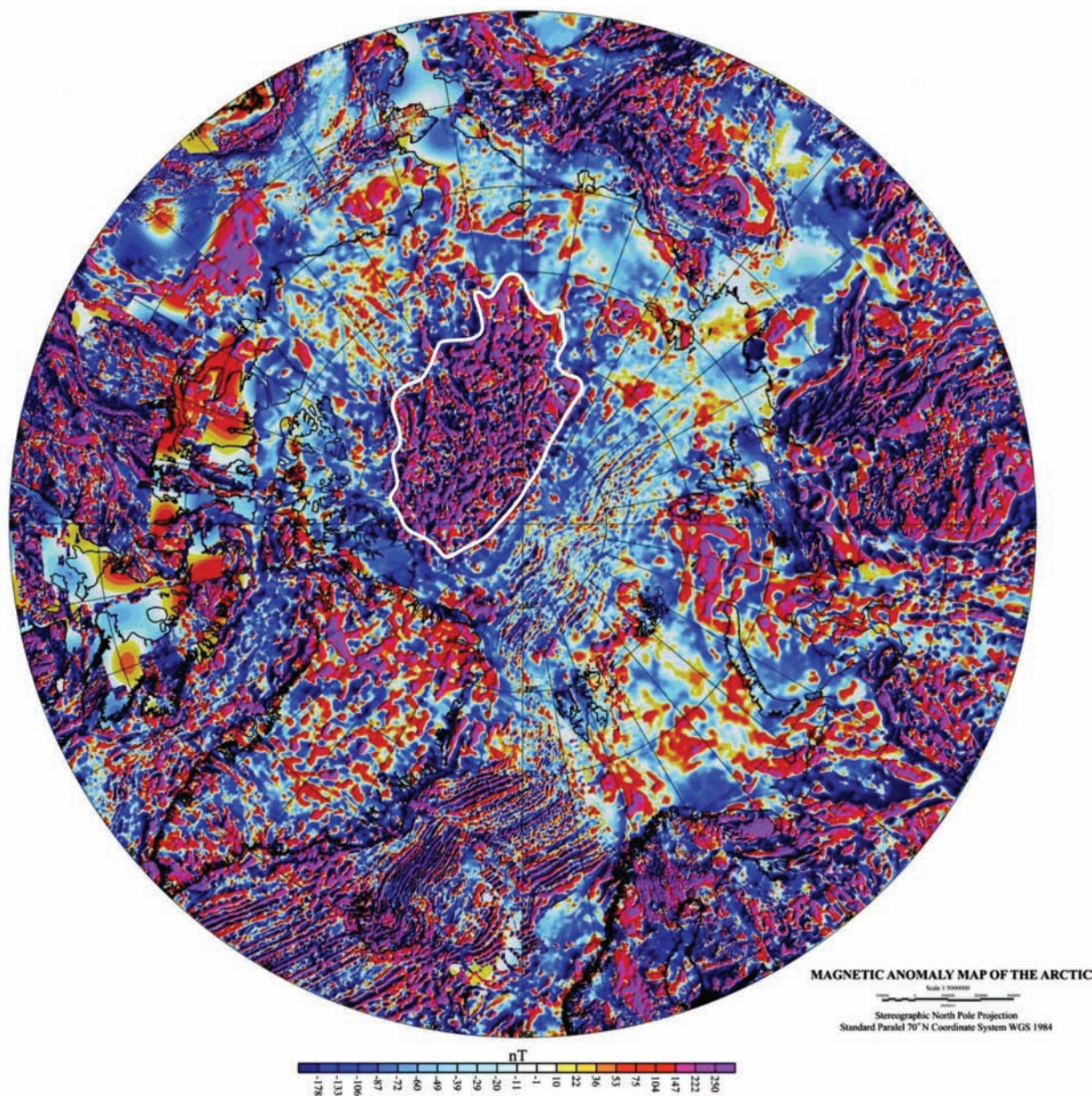


Fig. 12. The anomalous magnetic field of the Arctic (Gaina et al., 2010). The “disperse-isometric” region of anomalies is outlined by white solid line.

diffuse (plastic) deformations in the lithosphere of the disintegrating Arctida, with its constituent continental blocks (in particular, Novosibirsk Islands, Chukotka, and Alaska) moving in different directions. In this context the popular model of Grantz et al. (1998) for counterclockwise rigid rotation of the Chukotka-Alaska microplate, with the pole of rotation in the Mackenzie delta and with the Canada Basin forming behind this microplate, has some apparent constraints. Accordingly, in the model for diffuse lithospheric deformations, the oceanic crust of the Canada Basin is generated

through the so-called diffuse spreading, which does not involve the formation of a single linear zone of lithospheric divergence.

The third geodynamic reason for the proposed model is that the occurrence of a strong roughly latitudinal E-W direction (for 130°E-170°E meridians) of lithospheric extension in the study region in Aptian-Albian time, directly following the termination of the collision of the Novosibirsk-Chukotka massif with the Eurasian margin (Miller and Verzhbitsky, 2009), is explained by the fact that the downdragging effect of the subduction zone of

the South Anyui ocean, upon its closure, was largely diminished, while the ongoing large-scale mantle sinking in the NW Pacific subduction zone created a strong drag effect from the mantle cell in a roughly EW direction. It is this protracted effect of the lithosphere being dragged to the NW Pacific mantle sinking zone that controlled the entire subsequent evolution of tectonic structures of the Arctic region, in particular, the sequential formation of the Alpha and Mendeleev rises, the Makarov and Podvodnikov basins, the Gakkel spreading Ridge, the Lomonosov Ridge, and the Nansen and Amundsen basins.

Paleogeodynamic reconstructions for the Arctic region in the Late Jurassic – Early Cretaceous

The model we have been developing is illustrated with paleogeodynamic reconstructions for the following time slices: 150, 140, 130, 120, and 110 Ma. These time slices mark the crucial phase of tectonic development of the Arctic region. The reconstructions were created relative to a fixed Eurasian continent. The North American and Eurasian plates, as mentioned above, were parts of a single megacontinent of Laurasia (Zonenshain and Natapov, 1987) until the Middle Cretaceous (ca. 120 Ma), when these plates separated in the southern North Atlantic (Herron et al., 1974). This was preceded by a protracted period of rifting between these plates, which started as early as the Late Carboniferous-Permian (Mjelde et al., 1998; Faereth and Lien, 2002). At about 120 Ma, a divergent boundary between these plates started forming. Full-fledged spreading in the North Atlantic, however, started considerably later: ca. 63 Ma in the Labrador Sea (chron C27) (Chalmers, 1991; Chalmers and Laursen, 1995) and ca. 56 Ma in the Iceland region (chron C25r) (Larsen, 1988). After the initial opening of the Norwegian-Greenland sea in the Paleocene (Thanetian) (56 Ma), the mid-ocean spreading ridge very slowly propagated for some 20 my northward along the Spitzbergen strike slip zone, forming (in a transtensional environment) the strongly asymmetrical spreading pattern (Crane et al., 1991). The formation of the ridge is dated by different methods to ca. 36 Ma (Vogt et al., 1982; Crane et al., 2001). By some estimates, north of the Knipovich Ridge, spreading started in the Early Miocene at ca. 23 Ma (Boebel, 2000), and in the

Fram Strait it began in the Early Pliocene at ca. 5 Ma (Ritzmann et al., 2002). All this time starting from the Late Thanetian (i.e., from continental crust breakup in the North Atlantic), in the Eurasia Basin (Glebovsky et al., 2006) an independent divergent spreading boundary between the Eurasian and North American plates was active. Further extension of this boundary into the Eurasian continent or along a mega-transform zone running along the edge of the continent, as mentioned above, is not clearly identified. To use our approach, currently there is no continuous boundary separating the Eurasian and North American plates in the Eastern Arctic. Instead, we are dealing with a large area with diffuse deformation in the crust and lithosphere with a variety of tectonic movements, such as strike slips, pull apart movements, overthrusting, etc., which can be adequately described in terms of an elastoplastic lithosphere model which accounts for rheologic stratification of the lithosphere. The paleogeodynamic reconstructions below provide a kinematic basis for further calculations of stress fields and lithospheric deformations in the Arctic for different phases of its Jura-Cretaceous evolution.

A 150 Ma paleogeodynamic reconstruction (Late Jurassic - Kimmeridgian/Tithonian) shows the beginning of the opening of the Canada Basin and implies the onset of the Mesozoic phase of destruction of the Arctida craton (Fig.9). As noted above, the breakoff of the Novosibirsk-Chukotka-Alaska group of blocks of the Arctida craton from the North American continent was caused by the drag effect from subduction zones combined with the impact from the Arctic upper mantle plume, located (judging from magmatic manifestations) near the junction zone of Arctida with the North American plate (Shipilov and Karyakin, 2010, Shipilov and Vernikovskiy, 2010). The age span of activity of this plume was rather wide, embracing the 205-105 Ma interval, and possibly covering a later period up to 80-65 Ma (Burov et al., 1976; Karyakin and Shipilov, 2008, 2009; Karyakin et al., 2009, 2010; Komarnitsky and Shipilov, 1991; Tarakhovskiy et al., 1982; Stolbov, 2002; Shipilov and Karyakin, 2010; Bailey and Rasmussen, 1997; Campsie et al., 1988; Dibner, 1998; Gayer et al., 1966; Jansa and Pe-Piper, 1988; Silantyev et al., 2004; Worsly et al., 1986).

Of course this general time period should be divided into multiple relatively short plume events. For example, high-precision radiometric studies carried out for Franz Joseph Land Archipelago (Pumhösl, 1998; Piskarev et al., 2009; Shipilov and Karyakin, 2011; Corfu, et al., 2013) define the following magmatic events: 196 -189 Ma, 159 - 152 Ma, 150 - 148 Ma, 138 - 117 Ma. The twenty-two K-Ar determinations for Svalbard basaltic intrusions (Burov et al., 1976) revealed the age interval of 198-93 Ma with the two peaks of magmatic activity as old as 144 ± 5 to 105 ± 5 Ma. At the same time the high-precision methods shows the following age numbers: for Svalbard - 133 Ma and 124.7–123.3 Ma (Shipilov and Karyakin, 2011; Corfu, et al., 2013), Northern Greenland - 82-85 Ma, 70.5-68.5 Ma, 67.2-65 Ma, and 64-58 Ma (Larsen, 1982; Estrada et al., 2001; Kontak et al., 2001; Tegner et al., 2011; Thorarinsson et al., 2011); Canadian Arctic Archipelago - 129-126 Ma, 113 Ma, 101-91

Ma, 84-80 Ma, 77 Ma, 65-58 Ma (Villeneuve and Williamson, 2003; Estrada et al., 2010; Estrada and Henjes-Kunst, 2004, 2013).

As mentioned above, the main mechanical cause for the Arctida blocks to split off from the North American plate was the action of the sublithospheric mantle current, whose downwelling branch was confined to the subduction zones making an arc that embraced the Arctida craton in the South Anyui ocean and in the NW Pacific, with the ascending branch being associated with the plume. The horizontal mantle current component, directed to the South Anyui subduction zone, dragged the Chukotka - Novosibirsk Islands block to the southeast, toward Eurasia, along a major strike-slip fault that rimmed the Alpha-Mendelev Rise from the east. Synchronously, the mantle current component directed to the subduction zone at the NW Pacific margin, led to a rotation motion of the Alaska block in an easterly direction. Hence, these two

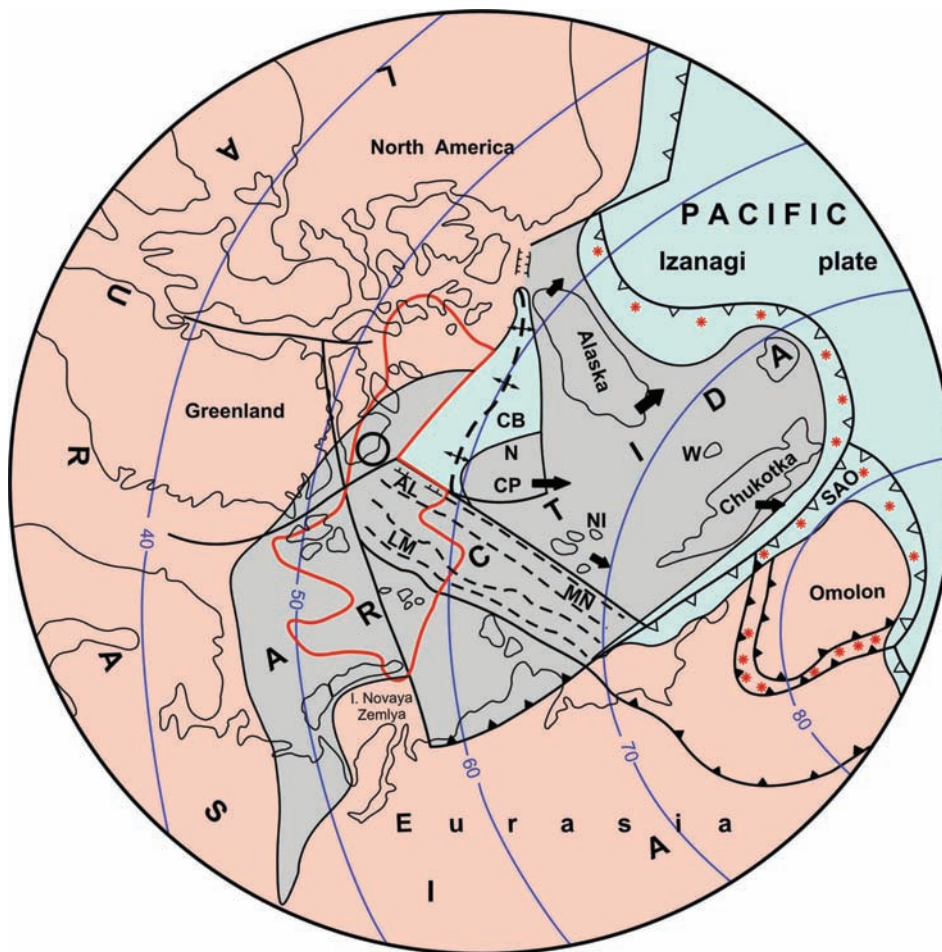


Fig. 13. 140 Ma paleogeodynamic reconstruction for the Arctic (Early Cretaceous, Berriasian) (for caption, see fig. 9)

blocks were dragged by divergent mantle currents in opposite directions. Between them, a large zone of tensile and dextral transtensional deformation arose. The eastern flank of the Alpha-Mendeleev Rise likely started forming precisely at that time under transtensional conditions (Fig.9).

A 140 Ma paleogeodynamic reconstruction (Early Cretaceous, Valanginian, Fig. 13) visualizes the initial stage of the opening of the Canada Basin, caused by the dragging apart of the blocks of Chukotka-Novosibirsk Islands and Alaska due to mantle sinking in subduction zones of the South Anyui ocean and the Pacific. Chukotka moved relative to Eurasia with a considerable dextral strike slip component. The plume magmatic activity was perceptibly weaker than in the Late Jurassic. This was the time of the beginning of the collision of major continental massifs, currently fused into the composite Omolon block, with the Siberian passive margin of Eurasia composed of terrigenous deposits

of the Verkhoyansk complex - the Uyandina-Yasachnaya island arc, the Chersky Range block, the Alazeya-Oloy and Prikolymy blocks (Zonenshain et al., 1990a,b).

A 130 Ma paleogeodynamic reconstruction (Early Cretaceous, Late Hauterivian, Fig.14). Diffuse spreading in the Canada Basin went on. The Omolon continental megablock was being actively pressed into the Verkhoyansk passive margin, with accompanying deformations and generation of granite melts. The South Anyui ocean was almost closed. In the Early Cretaceous, the plume magmatic activity considerably increased (Karyakin and Shipilov, 2008, 2009; Karyakin et al., 2010). The velocity of the plate motion of the outboard Izanagi plate, which interacted with the Eurasian plate from the Pacific side, increased sharply from 3 to 20 cm/year. The direction of convergence of the Izanagi plate with Eurasia changed from chiefly oblique to orthogonal (Engelbreton et al., 1984).

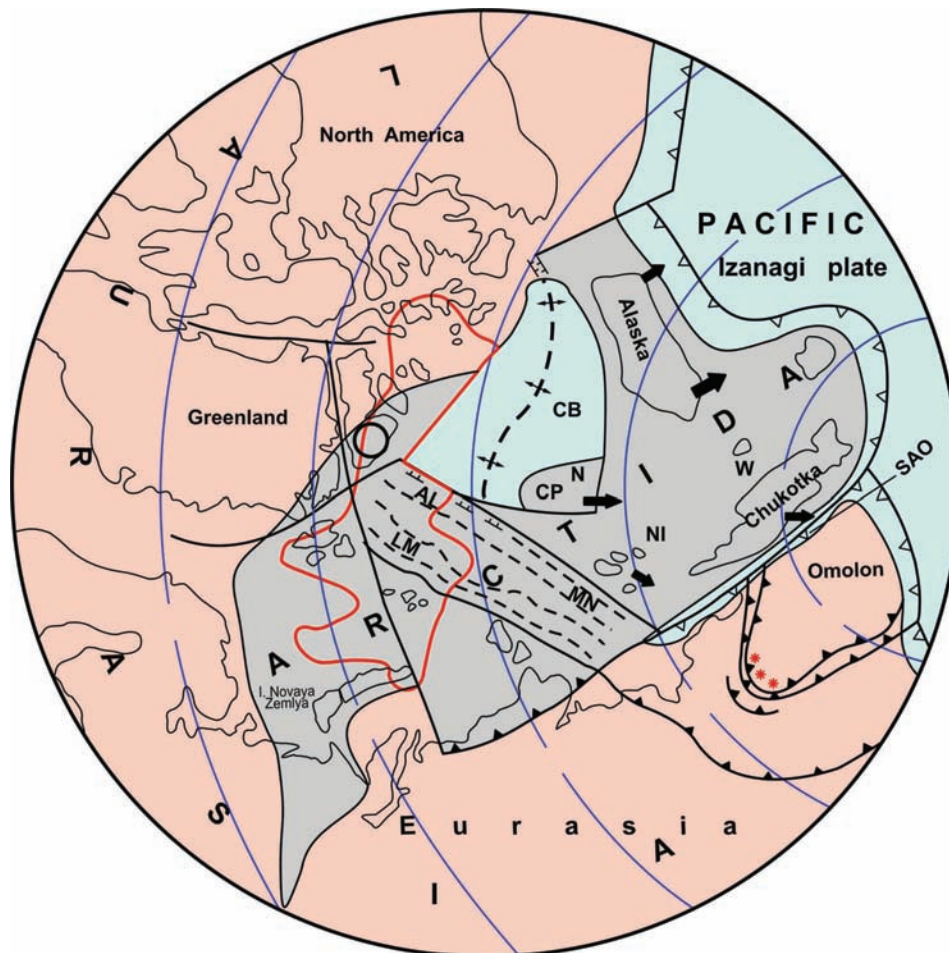


Fig. 14. 130 Ma paleogeodynamic reconstruction for the Arctic (Early Cretaceous, Hauterivian) (for caption, see fig. 9)

This boosted the collision of the Omolon megablock with the Siberian shelf and also likely made for a faster closure of the South Anyui ocean as a result of the collision of Chukotka and Siberia.

A 120 Ma paleogeodynamic reconstruction (Early Cretaceous, Middle Aptian, Fig.15) shows the phases of the final closure of the South Anyui ocean and the collision of Chukotka with Eurasia along the South Anyui suture. This terminated diffuse spreading in the Canada Basin and dramatically slowed down the sinking of mantle material in the South Anyui zone. Meanwhile, active sinking of the mantle material coming from the Pacific side continued in the subduction zone, creating a roughly EW directed drag effect in the lithosphere of the Eastern and Central Arctic. As a result, blocks of the once whole Arctida started moving along major strike slips toward the Pacific. It was then that the stress field changed its direction by about 90° (Miller and Hudson, 1991; Miller and Verzhbitsky, 2009)

giving rise to extension and rifting in the Makarov-Podvodnikov-Alpha-Mendeleev system of basins and ridges constituting the central fragment of the Arctida continent. The plume magmatic activity in the Arctic region went on, although on a smaller scale. The collision of the Omolon megablock with Eurasia kept evolving, giving rise to folding and thrusting(?) in the Verkhoyansk terrigenous complex of Siberia and intensifying granite magmatism in the Kolyma belt.

A 110 Ma paleogeodynamic reconstruction (Early Cretaceous, Early Albian, Fig.16). By that time, collisional events in the South Anyui suture zone stopped, as did the principal folding in the Verkhoyansk fold belt. The fold structures that formed in Eastern Siberia were overlain by the nascent Okhotsk-Chukotka volcanic belt. It marked the position of the newly formed large subduction zone which plunged under the continent.

The Arctic region remained the area of vigorous

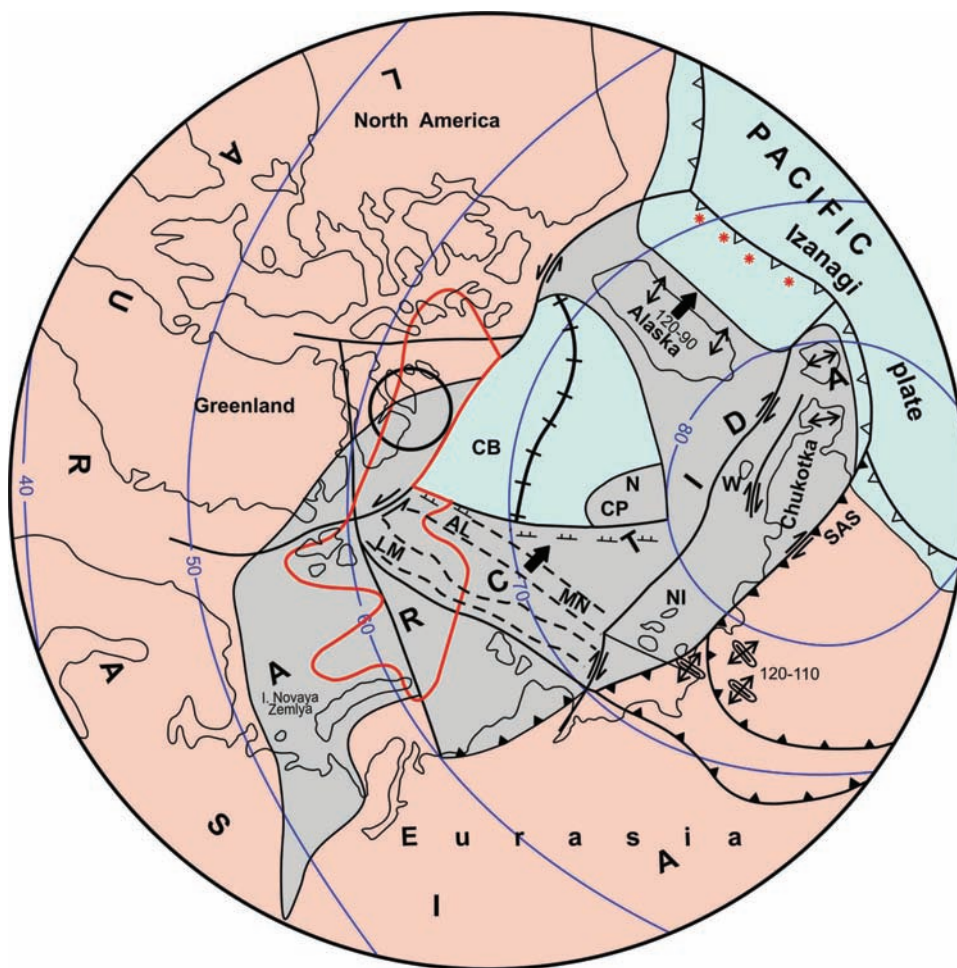


Fig. 15. 120 Ma paleogeodynamic reconstruction for the Arctic (Early Cretaceous, Aptian)(for caption, see fig. 9)

extension and rifting (in the direction of the Pacific) in the Makarov-Podvodnikov-Alpha-Mendelev system of basins and ridges and in the Canada basin. This situation persisted until the Eurasia Basin started opening and the Lomonosov Ridge broke off from the Barents-Kara shelf. As a result, the central continental fragment of Arctida, consisting of tectonic features such as the Lomonosov Ridge and Alpha-Mendelev Rises as well as the Makarov and Podvodnikov basins, became surrounded on two sides by basins with oceanic crust.

It is quite logical to extend the magmatic activity of the Arctic plume at 110 Ma, which is recorded in various structures rimming the Arctic Ocean, into the central “Makarov-Podvodnikov-Alpha-Mendelev basins and ridges province,” in view of the predominance of lithospheric extension in the Central Arctic. The assumption that within-plate magmatism was confined to the rift-related area of attenuated continental lithosphere of the

central region of basins and rises in the Arctic Ocean is corroborated by the anomalous magnetic field in this region, showing a “finely disperse” isometric pattern of anomalies, typical of flood volcanic zones on the continents (Poselov et al., 2008). Although within the entire central magmatic province of the Arctic Ocean only one radiometric age of 82 Ma is firmly established (Initial ..., 1985), this age most likely marks the termination of magmatic activity in this province.

It seems to make sense to compare our proposed reconstructions with reconstructions of the Arctic from the recent publication by Golonka (2011). In general Golonka’s reconstructions reproduce the model of formation of Alpha-Mendelev Rise by L.P. Zonenshain and L.M. Natapov (1987), who regarded this structure as an island arc with the subduction of Canada Basin oceanic crust under it. In the frame of this interpretation, Makarov Basin is a back-arc basin. However, as we showed earlier, this

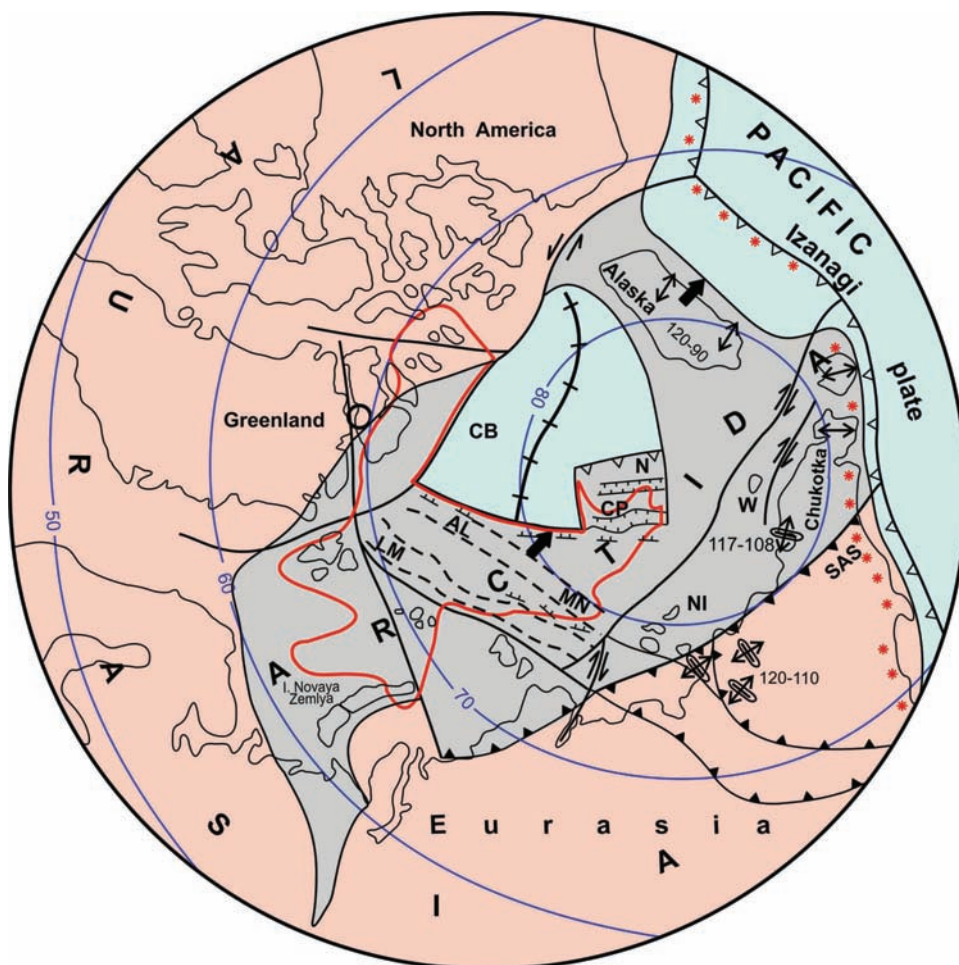


Fig. 16. 110 Ma paleogeodynamic reconstruction for the Arctic (Early Cretaceous, early Albian) (for caption, see fig. 9)

model contradicts the observed onshore and offshore structural data. There is no trench structure on the eastern slope of Alpha-Mendeleev Rise. According to the data instead of thrusting and a compressional regime throughout the central Arctic during Cretaceous and Paleogene time, there are regional extension conditions (Rowley and Lottes, 1988; Miller and Verzhbitsky, 2009). Furthermore on the Eurasian margin according to Golonka's model we should expect sinistral strike slip faults, but actually while analyzing concrete geological materials, we generally find dextral strike slip faults. These are in particular observed along the whole South Anyui suture (Sokolov et al., 2009) and along the structural trend of Wrangel Island (Verzhbitsky et al., 2012).

Thus, actual structural data support our model of the Amerasia Basin formation. Our model uses the movement of continental blocks along huge extended strike slip faults (along the dextral strike slip faults on the Eurasian margin and sinistral strike slip faults on the North American margin) towards the subduction zone in the Pacific Ocean.

DISCUSSION

Tectonics of deformable plates, seismic tomography, and 3D geodynamics

The approach to the analysis of tectonic and geodynamic processes we are developing, as mentioned above, implies the transition to a combined numerical description of deep (mantle) and surface (lithospheric/crustal) processes. Note that for a long time (from the end of the 1960s to the beginning of this century), mathematical models were mostly created for deep and surface processes separately despite the obvious simplistic and non-holistic character of such approach. The underlying causes of the above non-holistic description of natural processes were chiefly as follows: (i) lack of a universal model for the geomedium enabling combined descriptions of deep mantle currents with viscous rheology of the material and surface deformations and destruction of a heterogeneous lithosphere with nonlinear elastoplastic rheology; (ii) incompleteness of our knowledge of the deep structure of the Earth and actual movements of its constituent parts; (iii) insufficient development of computer technologies and numerical methods for the modeling of complex 3D movements and

deformation of the geomedium.

Lately the situation started improving. Primarily, it is worthwhile to note the significant advances in the study in the inner structure of the Earth using seismic tomography methods. For a number of large regions worldwide, high resolution seismic tomography images of the structure of the Earth interior have been obtained that allow one to "see" the mantle convection structure, which is an absolutely necessary element for the accurate formulation of the problem of modeling of regional geodynamic processes. Thus, for example, impressive results from a seismic tomography "show-through" of the mantle for northeastern Asia with its surrounding marginal seas of the NE Pacific have recently been published in a series of works by Zhao (2009), Zhao et al. (2009) and Zhao et al. (2010).

It is obvious that high-resolution seismic tomography of the mantle currently becomes a necessary element in creating realistic geodynamic models for the evolution of specific regions of the Earth, because, in principle, it allows the construction of geometric models of the convective cells of mantle currents in a given region. In addition, the available functionalities of 3D numerical modeling of viscous mantle currents make it possible to calculate the field of velocities and associated stresses operating at the base of the lithosphere. In their turn, the currently available methods of numerical modeling of 3D elastoplastic deformations in a rheologically heterogeneous stratified lithosphere provide the possibility to postulate conditions and loads at the base of the lithosphere and at the boundaries of the study region, to calculate the stress-deformed state of the lithosphere and explain the formation and evolution of its principal structures.

We are thus witnessing the emergence of a generalizing methodology for numerical descriptions of regional tectonic processes, based on the concept of tectonics of deformable lithospheric plates. These in turn can be matched with the data from seismic tomography of the mantle and 3D modeling of mantle currents.

To summarize, the performed paleogeodynamic reconstructions and numerical calculations of the stress-deformed state of the Arctic lithosphere for different phases of its Mesozoic evolution suggest the following conclusion on the origin of the central

tectonic structures of the Arctic Ocean. There is every reason to believe that the principal structures of the Central Arctic, namely, the Lomonosov Ridge, the Alpha and Mendeleev Rises, the Podvodnikov and Makarov Basins, the Chukchi Plateau, etc., are fragments of the ancient Arctida craton, surviving in the course of geological evolution. Starting at least from the Cretaceous, this craton connected the North American and Eurasian continental margins. Given the above picture of geological evolution of the Arctic region, it is reasonable to conclude that the Lomonosov Ridge, just like the Alpha-Mendeleev Rise together with the Makarov and the Podvodnikov Basins in-between, must be the natural extensions of the mainland margins of Eurasia and North America, which, in compliance with Article 76 of the 1982 United Nations Convention on the Law of the Sea, creates a fundamental geological rationale to justify the extension of the limits of the continental shelf (LCS) into the Arctic Ocean for Russia, Canada, Denmark and USA.

REFERENCES

- Bailey, J.C. and M.H. Rasmussen, 1997. Petrochemistry of Jurassic and Cretaceous tholeiites from Kong Karls Land, Svalbard, and their relation to Mesozoic magmatism in the Arctic. *Polar Research*. Oslo, 16, 1, 37-62.
- Boebel, T., 2000. Airborne topography and gravimetry: system and application to Fram Strait, Svalbard and Northeast Greenland. *Reports on Polar and Marine Research*, 366, 1-120 p.
- Bogdanov, N.A., 2004. Tectonics of the Arctic Ocean. *Geotektonika*, 4, 21-42 (in Russian).
- Bogdanov, N.A., Khain, V.E., and E.V. Shipilov, 1995. The system of Cenozoic rifts of the Eastern Arctic and its possible implications. *Doklady Ross. Akad. Nauk*, 345, 1, 84-86 (in Russian).
- Brozena, J., Childers, V., Lawver, L., Gahagan, L., Forsberg, R., Faleide, J., and O., Eldholm, 2003. New aerogeophysical study of the Eurasia Basin and Lomonosov Ridge: implications for basin development. *Geology*, 31, p. 825.
- Bullard, E.C., Everett, J.E. and A.G. Smith, 1965. The Fit of the Continents around the Atlantic. *Phil. Trans. R. Soc., A*, 258, 41-75.
- Burke, K., 1984. Plate tectonic history of the Arctic. In: *Geology of the Arctic*. Moscow. Proc. 27 Int. Geol. Congress, Coll. 04, 159-167.
- Burov, Yu.P., Krasilshchikov, A.A., Firsov, L.V., and B.A. Klubov, 1976. *Geology of Spitzbergen*. Leningrad, NIIGA, 117-125 (in Russian).
- Campsie, J., Rasmussen, M.H., Hansen, N., Liebe, C.J., Laursen, J., Brochwicz-Levinski, W. and L. Johnson, 1988. K-Ar ages basaltic rocks collected during a traverse of the Frans Josef Land Archipelago (1895-1896). *Polar Research*. Oslo, 6, 2, 173-177.
- Chalmers, J.A. and K.H. Laursen, 1995. Labrador Sea: the extent of continental crust and the timing of the start of sea-floor spreading. *Mar. Petrol. Geol.*, 12, 205-217.
- Chalmers, J.A., 1991. New evidence on the structure of the Labrador Sea Greenland continental margin. *J. Geol. Soc. London*, 148, 899-908.
- Churkin, M. (Jr.), 1972. Western boundary of the North American continental plate in Asia. *Geol. Soc. Am. Bull.*, 83, 1027-1972.
- Churkin, M. (Jr.), 1973. Geologic concepts of Arctic Ocean Basin. In: Pitcher, M.G. (ed). *Arctic Geology*. AAPG Memoir, 19, 485-499.
- Corfu, F., Polteau, S., Planke, S., Faleide, J. I., Svensen, H., Zayoncheck, A., and N. Stolbov, 2013. U-Pb geochronology of Cretaceous magmatism on Svalbard and Franz Josef Land, Barents Sea Large Igneous Province. *Geological Magazine*, 1-9.
- Crane, K., Doss, H., Vogt, P., Sundvor, E., Cherkashov, G., Poroshina, I. and D. Joseph, 2001. The role Spitsbergen shear zone in determining morphology, sedimentation and evolution of the Knipovich Ridge. *Mar. Geophys. Res.*, 22, 153-205.
- Crane, K., Sundvor, E., Buck, R. and F. Martinez, 1991. Rifting in the Northern Norwegian-Greenland Sea: thermal tests of asymmetric spreading. *J. Geophys. Res.*, 96, 14529-14550.
- Demenitskaya, R.M., 1975. *The Earth crust and mantle*. 2nd Edition. Moscow, Nedra, 1-312 (in Russian).
- Dibner, V.D., 1998. *Geology of Franz Josef Land*. Oslo, Norsk Polarinstitutt Meddelelser, 146, 1-190.

- Dinkelman, M.G., Kumar, N., Helwig, J., Emmet, P., and J. Granath, 2008. Highlights of petroleum and crustal framework of the Beaufort-Mackenzie Basin: Key Results from BeaufortSPAN East Phases I and II Surveys // Canadian Society Exploration Geophysicists (CSEG) Recorder, 33, 9, 22–25.
- Drachev, S.S., 2000. Tectonics of the rift system of the Laptev Sea floor. *Geotektonika*, 6, 43-58 (in Russian).
- Drachev, S.S., 2002. Fundament tectonics of the Laptev Sea shelf. *Geotektonika*, 6, 60-70 (in Russian).
- Drachev, S.S., 2011. Tectonic setting, structure and petroleum geology of the Siberian Arctic offshore sedimentary basins. In: Spencer, A. M., Embry, A. F., Gautier, D. L., Stoupakova, A. V. and K. Sorensen (eds) *Arctic Petroleum Geology*. Geological Society, London, *Memoirs*, 35, 369-394.
- Drachev, S.S., Savostin, L.A., Groshev, V.G. and I.E. Bruni, 1998. Structure and geology of the continental shelf of the Laptev Sea, Eastern Russian Arctic. *Tectonophysics*, 298, 357–393.
- Embry, A.F., 1992. Crockerland - the northwest source area for the Sverdrup, Canadian Arctic Islands. In Vorren, T.O., Bergsager, E., Dahl-Stammes, Holter, E., Johansen, B., Lie, E., and T.B. Lund, (eds.) *Arctic Geology and Petroleum Potential, Volume 2: Norwegian Petroleum Society Special Publication: Elsevier, Amsterdam*, 205-216.
- Engebretson, D., Cox, A. and R.G. Gordon, 1984. Relative motions between oceanic plates of the Pacific Basin. *J. Geophys. Res.*, 89, B12, 10291-10310.
- Estrada, S., and F. Henjes-Kunst, 2004. Volcanism in the Canadian High Arctic related to the opening of the Arctic Ocean. *Zeitschrift der Deutschen Geologischen Gesellschaft*, 154, 4, 579-603.
- Estrada, S., and F. Henjes-Kunst, 2013. 40Ar-39Ar and U-Pb dating of Cretaceous continental rift-related magmatism on the northeast Canadian Arctic margin. *Zeitschrift der Deutschen Gesellschaft für Geowissenschaften*, 164, 1, 107-130.
- Estrada, S., Henjes-Kunst, F., Melcher, F., and F. Tessensohn, 2010. Palaeocene alkaline volcanism in the Nares Strait region: evidence from volcanic pebbles. *Int. J. Earth Sci.* 99, 863–890.
- Estrada, S., Höhndorf, A., F. Henjes-Kunst, 2001. Cretaceous/Tertiary volcanism in North Greenland: the Kap Washington Group. *Polarforschung*, 69, 17-23.
- Faccenna, C., Becker, T.W., Lallemand, S. and Y. Lagabrielle, 2010. Subduction-triggered magmatic pulses: A new class of plumes? *Earth Planet. Sci. Lett.*, 299, 54–68.
- Faerfærth, R.B. and T. Lien, 2002. Cretaceous evolution in the Norwegian Sea – a period characterized by tectonic quiescence. *Marine and Petroleum Geology*, 19, 1005-1027.
- Faleide, J. I., Vågnes, E., and S.T. Gudlaugsson, 1993. Late Mesozoic-Cenozoic evolution of the south-western Barents Sea in a regional rift-shear tectonic setting. *Marine and Petroleum Geology*, 10, 3, 186-214.
- Fedorov, P. I., Fleurov, G. B., and D.I. Golovin, 2005. New ages and composition data for volcanic rocks of the island Bennett (Eastern Arctic). *Doklady of the Earth Sciences*, 400, 5, 666-670.
- Filatova, N.I. and V.E. Khain, 2009. structures of the central Arctic and their relations with the Mesozoic Arctic plume. *Geotektonika*, 6, 24-51 (in Russian).
- Fox, F. G., 1985. Structural geology of the Parry Islands fold belt. *Bull. Can. Petrol. Geol.*, 33, 306-340.
- Gaina, C., Roest, W., Müller, R.D., 2002. Late Cretaceous–Cenozoic deformation of northeast Asia. *Earth Planet. Sci. Lett.*, 197, 273–286.
- Gaina, C., Saltus, R., Aaro, S., Damaske, D., Ebbing, J., Forsberg, R., Glebovsky, V., Johnson, K., Jonberger, J., Koren, T., Korhonen, J., Litvinova, T., Oakey, G., Olesen, O., Petrov, O., Pilkington, M., Rasmussen, T., Schreckenberger, B., Smelror, M., Harrison, C., St-Onge, M., Tella, S., Paul, D., Lynds, T., Strelnikov, S., Shokalsky, S., Lopatin, B., Wilson, F., Hults, C., Bergman, S., Solli, A. and H. F. Jepsen, 2010. Circum-Arctic Mapping Project: New Magnetic Anomaly map Linked to the Geology of the Arctic. Scale 1:5000000. Stereographic North Pole projection. Standard parallel 70° N coordinate system WGS 1984. In:

- www.congrex.nl/09c24/S2_Posters/S2_P13_Gaina_paper.pdf
- Gayer, R.A., Gee, D.G., Harland, W.B., Miller, J.A., Spall, H.R., Wallis, R.H. and T.S. Winsens, 1966. Radiometric age determination on rocks from Spitsbergen. Oslo, Norsk Polarinstitut Skrifter, 137, 1-39.
- Gee, D.G., Johansson, Å., Ohta, Y., Tebenkov, A. M., Balashov, Y. A., Larionov, A. N., Gannibal, L.F., and G.I. Ryungenen, 1995. Grenvillian basement and a major unconformity within the Caledonides of Nordaustlandet, Svalbard. *Precambrian Research*, 70, 3, 215-234.
- Geodynamics, magmatism and metallogeny of Eastern Russia. Book 1. Dal'nauka, 2006, 1-572 (in Russian).
- Geological map of Far East Region of Russian Federation. 2008 (<http://www.vsegei.ru/ru/info/gisatlas/dvfo/okrug/geol.jpg>) (in Russian).
- Glebovsky V. Yu., Kaminsky V. D., Minakov A. N., Merkur'ev S. A., Childers V. A., and J. M. Brozena, 2006. Formation of the Eurasia Basin in the Arctic Ocean as inferred from geohistorical analysis of the anomalous magnetic field. *Geotectonics*, 4, p. 21-42.
- Golonka, J., 2011. Phanerozoic palaeoenvironment and palaeolithofacies maps of the Arctic region. In: Spencer, A. M., Embry, A. F., Gautier, D. L., Stoupakova, A. V. and K. Sorensen (eds) *Arctic Petroleum Geology*. Geological Society, London, Memoir, 35, 79-129.
- Grachev, A.F., 1973. The Moma continental rift. In: *Geophysical methods of exploration in the Arctic*, 8, 56-75 (in Russian).
- Gradstein, F. M., Ogg, J. G., & Schmitz, M. (Eds.). (2012). *The Geologic Time Scale 2012*, 2-volume set. Elsevier, Oxford, UK; Amsterdam, Netherland; Waltham MA, USA, 1-1144.
- Gramberg, I.S., Demenitskaya, R.M., and S.B. Sekretov, 1990. The system of rift-related grabens of the Laptev Sea shelf as a missing link in the rift belt of the Gakkel Ridge – Moma rift. *Doklady Akad. Nauk SSSR*, 311, 3, 689–693 (in Russian).
- Grantz, A. and S.D. May, 1984. Sedimentary basins and geologic structure of the continental margin north of Alaska. *Geology of the Arctic*. Moscow. Proc. 27 Int. Geol. Congress, Coll. 04, 105-118.
- Grantz, A., Clark, D. L., Phillips, R. L. and S.P. Srivastava, 1998. Phanerozoic stratigraphy of Northwind Ridge, magnetic anomalies in the Canada basin, and the geometry and timing of rifting in the Amerasia basin, Arctic Ocean. *Geol. Soc. Am. Bull.*, 110, 801-820.
- Gurevich, N.I. and S.A. Merkuriev, 2007. Evolution of the northern part of the Amerasia Basin, Arctic Ocean, from geophysical data. In: *Geology of oceans and seas. Abstracts XVII Int. School on Marine Geology, Moscow, IV*, 62-64 (in Russian).
- Harrison, J. C. and A. W. Bally, 1988. Cross-sections of the Parry Islands fold belt on Melville Island, Canadian Arctic Islands; implications for the timing and kinematic history of some thin-skinned decollement systems. *Bull. Can. Petrol. Geol.*, 36, 311-332.
- Helwig, J., Kumar, N., Dinkelman, M. G., and P. Emmet, 2010. Three Segments of the Arctic Continental Margin, Beaufort Sea, Canada: Deep Seismic Profiles of Crustal Architecture. Abstract Presented at GeoCanada, 1-4.
- Herron, E.M., Dewey, J.F. and W.C. Pitman, 1974. Plate tectonic model for the evolution of the Arctic. *Geology*, 2, 377-380.
- Initial geological report on CESAR - the Canadian Expedition to study the Alpha Ridge Arctic Ocean, 1985. In: Jackson, H.R., Mudie, P.J. and S.M. Blasko (ed) *Geol. Survey Canada, Paper*, 84-22, 1-177.
- Jackson, G.P. and G.L. Johnson, 1984. Structure and history of the Amerasian Basin. *Geology of the Arctic*. Moscow, Proc. 27 Int. Geol. Congress, Coll. 04, 85-104.
- Jansa, L.F., and G. Pe-Piper, 1988. Middle Jurassic to Early Cretaceous igneous rocks along Eastern North American continental margin. *Amer. Assoc. Petrol. Geologists Bull.*, 72, 3, 347-366.
- Jokat, W., Ickrath M., and J. O'Connor, 2013. Seismic transect across the Lomonosov and Mendeleev ridges: Constraints on the geological evolution of the Amerasia Basin, Arctic Ocean. *Geophys. Res. Lett.* doi: 10.1002/grl.50975.
- Jokat, W., O'Connor, J. and R. Muhe, 2007. Alpha-Mendeleev Ridge: An oceanic Cretaceous large igneous province? In: *Fifth International*

- Conference on Arctic Margins. Tromso, Norway (3-7 September, 2007) Abstracts and Proceedings, 47.
- Kaban'kov, V.Ya., Andreeva, I.A., Ivanov, V.N., and V.I. Petrova, 2004. On the geotectonical nature of the system of the Central Arctic morphostructures and geological significance of seafloor sediments in defining this nature. *Geotektonika*, 6, 33-48 (in Russian).
- Karasik, A.M., 1968. Magnetic lineations of the Gakkel Ridge and the origin of the Eurasian Subbasin in the Arctic Ocean. *Geophysical methods of investigation in the Arctic*. Leningrad, NIIGA, 9-19 (in Russian).
- Karasik, A.M., 1973. The anomalous magnetic field of the Eurasian Subbasin in the Arctic Ocean. *Doklady Akad. Nauk SSSR*, 211, 1, 53-57 (in Russian).
- Karasik, A.M., 1974. Eurasian Basin of the Arctic Ocean from the plate tectonic standpoint. In: *Problems of the geology of polar regions of the Earth*. Leningrad, NIIGA, 23-31 (in Russian).
- Karasik, A.M., Savostin, L.A., and L.P. Zonenshain, 1983. Parameters of motion of the lithospheric plates in the Eurasian Basin of the Arctic Ocean. *Doklady Akad. Nauk SSSR*, 273, 5, 1191-1196 (in Russian).
- Karyakin, Yu.V. and E.V. Shipilov, 2008. Geochemical characteristics and the $^{40}\text{Ar}/^{39}\text{Ar}$ age of magmatic rocks of the Franz Joseph Land Archipelago. In: *General and regional problems of tectonics and geodynamics*. Proceedings XLI Tecton. Conf. Moscow, GEOS, 1, 389-393 (in Russian).
- Karyakin, Yu.V. and E.V. Shipilov, 2009. Geochemical fingerprints and the $^{40}\text{Ar}/^{39}\text{Ar}$ age of basaltic magmatism of Alexandra Land, Northbrook, Hooker, and Hayes islands (Franz Joseph Land Archipelago). *Doklady Ross. Akad. Nauk*, 425, 2, 1-5 (in Russian).
- Karyakin, Yu.V., Lyapunov, S.M., Simonov, V.A., Sklyarov, E.V., Travin, A.V., and E.V. Shipilov, 2009. Mesozoic magmatic complexes of the Franz Joseph Land Archipelago. In: *Proceedings XLII Tecton. Conf. Moscow, GEOS*, 257-263 (in Russian).
- Karyakin, Yu.V., Sklyarov, E.V., Travin, A.V., and E.V. Shipilov, 2010. The age and composition of basalts of the central and southwestern parts of the Franz Joseph Land Archipelago. In: *Tectonics and geodynamics of fold belts and cratons of the Phanerozoic*. Proceedings XLIII Tecton. Conf. Moscow, GEOS, 1, 293-301 (in Russian).
- Khain, V.E., 2001. *Tectonics of continents and oceans (the year 2000)*. Moscow, Nauchnyi Mir, 1-606 (in Russian).
- Khain, V.E., Filatova, N.I., and I.D. Polyakova, 2009. Tectonics, geodynamics, and hydrocarbon potential of the Eastern Arctic seas and their continental rim. *Trudy Geol. Inst. Ross. Akad. Nauk. Moscow, Nauka*, 601, 1-227 (in Russian).
- Klaper, E.M., 1990. The mid-Paleozoic deformation in the Hazen fold belt, Ellesmere Island, Arctic Canada. *Can. J. Earth Sci.*, 27(10), 1359-1370, 10.1139/e90-146.
- Komarnitsky, V.M. and E.V. Shipilov, 1991. New geological data on the Barents Sea magmatism. *Doklady Akad. Nauk*, 320, 5, 1203-1206 (in Russian).
- Kontak, D.J., Jensen, S.M., Dostal, J., Archibald, D.A., and T.K. Kyser, 2001. Cretaceous mafic dyke swarm, Peary Land, northernmost Greenland: geochronology and petrology. *Canadian Mineralogist* 39, p.997-1020.
- Kos'ko, M.K., Cecile, M.P., Harrison, J.C., et al., 1993. Geology of Wrangel Island, between Chukchi and East Siberian Seas Russia. *Geol. Surv. Canada Bull.*, 461, 1-101.
- Kos'ko M.K., Avdunichev V.V., Ganelin V.G., A.Yu. Opeskunov, M.G. Opeslunova, et al., 2003. *The Wrangel Island: geological structure, minerogenesis, environmental geology: Ministry of Natural Resources of RF, All-Russia Research Institute for Geology and Mineral Resources of the World Ocean*. – SPb., VNIIOkeangeologia. 137 p. (in Russian).
- Kovalenko, V.I., Yarmolyuk, V.V., and O.A. Bogatkov, 2010. The modern supercontinent North Pangea and geodynamic causes of its formation. *Geotektonika*, 6, 8-23 (in Russian).
- Kuznetsov, N.B., Natapov, L.M., Belousova, E.A., O'Reilly, S.Y. and W.L. Griffin, 2010. Geochronological, geochemical and isotopic study of detrital zircon suites from late Neoproterozoic clastic strata along the NE

- margin of the East European Craton: implications for plate tectonic models. *Gondwana Research*, 17, 583-601.
- Larsen, H.C., 1988. A multiple and propagating rift model for the NE Atlantic. Morton, A.C. and L.M. Parson (eds) *Early Tertiary volcanism and the opening of the NE Atlantic*. *Publ. Geol. Soc.*, 39, 157-158.
- Larsen, O., 1982. The age of the Kap Washington group volcanics, North Greenland. *Bull. Geol. Soc. Denmark*, 31, 49-55.
- Laverov, N. P., Lobkovsky, L. I., Kononov, M. V., Dobretsov, N. L., Vernikovskiy, V. A., Sokolov, S. D., and E.V. Shipilov, 2013. A geodynamic model of the evolution of the Arctic basin and adjacent territories in the Mesozoic and Cenozoic and the outer limit of the Russian Continental Shelf. *Geotectonics*, 47, 1, 1-30.
- Lawver, L.A., Müller, R.D., Srivastava, S.P., and W. Roest, 1990. The Opening of the Arctic Ocean, in *Geologic History of the Polar Oceans: Arctic Versus Antarctic*, U. Bleil and J. Thiede (eds.), from the NATO Symposium (October, 1988) in Bremen, West Germany, pp. 29-62.
- Le Pichon, X., Sibuet, J. C. and J. Francheteau, 1977. The fit of the continents around the North Atlantic Ocean. *Tectonophysics*, 38, 3-4, 169-209.
- Lebedeva-Ivanova, N.N., Zamansky, Y.Y., Langinen, A.E., and M.Y. Sorokin, 2006. Seismic profiling across the Mendeleev Ridge at 82° N: Evidence of continental crust. *Geophys. J. Int.*, 165, 527-544.
- Lepvrier, C., van Berkel, J. T., and W. M. Schwerdtner, 1996. Early Tertiary Eureka palaeostresses in the Eastern Sverdrup Basin (Ellesmere and Axel Heiberg Island, Canadian Arctic Islands). *Tectonophysics*, 255, 3, 229-241.
- Lobkovsky, L.I., Garagash, I.A., Kononov, M.V., Verzhbitsky, V.E. and V.D. Kotelkin, 2010. Tectonics of the deformable lithospheric plates and geodynamic evolution of the Arctic region in the Mesozoic-Cenozoic. In: *Geology and geocology of Eurasian continental margins*. Moscow. GEOS, 2, 8-40 (in Russian).
- Lobkovsky, L.I., Verzhbitsky, V.E., Kononov, M.V., Shreider, A.A., Garagash, I.A., Sokolov, S.D., Tuchkova, M.I., Kotelkin, V.D., and V.A. Vernikovskiy, 2011. A geodynamic model for the evolution of the Arctic region in the Late Mesozoic-Cenozoic and the problem of the outer boundary of the continental shelf of Russia. *Arktika. Ekologiya i ekonomika*, 1, 104-115 (in Russian).
- Lyberis, N., and G. Manby, 1993. The West Spitsbergen Fold Belt: The result of Late Cretaceous-Palaeocene Greenland-Svalbard convergence?. *Geological Journal*, 28, 2, 125-136.
- Miller, E. L., Soloviev, A., Kuzmichev, A., Gehrels, G., Toro, J. and M. Tuchkova, 2008. Jura-Cretaceous foreland basin deposits of the Russian Arctic: Separated by birth of Makarov Basin? *Norwegian Journal Geology*, 88, 227-250.
- Miller, E.L. and T.L. Hudson, 1991. Mid-Cretaceous extensional fragmentation of a Jurassic-Early Cretaceous compressional orogen, Alaska. *Tectonics*, 10, 4, 781-796.
- Miller, E.L. and V.E. Verzhbitsky, 2009. Structural studies near Pevek, Russia: Implications for formation of the East Siberian Shelf and Makarov Basin of the Arctic Ocean In: Stone, D. B., Fujita, K., Layer, P. W., Miller, E. L., Prokopiev, A. V. and J. Toro, (eds) *Geology, geophysics and tectonics of Northeastern Russia: a tribute to Leonid Parfenov*. EGU Stephan Mueller Publication Series, 4, 223-241. (www.stephan-mueller-spec-publ-ser.net/4/223/2009/)
- Mjelde, R., Digranes, P., Shimamura, H., Shiobara, H., Kodaira, S., Brekke, H., Egebjerg, T., Soerenes, N. and T. Thorbjørnsen, 1998. Crustal structure of the northern part of the Voring Basin, mid-Norway margin, from wide-angle seismic and gravity data. *Tectonophysics*, 293, 175-205.
- Moore, Th.E., Dimitru T.A., Adams K.E. et al, 2002. Origin of the Lisburne Hills-Herald Arch structural belt: stratigraphic, structural, and fission-track evidence from the Cape Lisburne area, Northwestern Alaska. In: Miller, E. L., Grantz, A., and S. L. Klemperer (eds) *Tectonic evolution of the Bering Shelf-Chukchi Sea-Arctic Margin and adjacent landmasses*. *Geol. Soc. Amer. Special Paper*, Boulder, 360, 77-109.

- Ostenso, N.A. and R.J. Wold, 1973. Aeromagnetic evidence for origin of Arctic Ocean Basin. In: Pitcher, M.G. (ed). *Arctic Geology*. AAPG Memoir, 19, 506-516.
- Parfenov, L.M. and M.I. Kuzmin (eds), 2001. *Tectonics, geodynamics, and metallogeny of the territory of the Sakha Republic (Yakutia)*. Moscow, MAIK Nauka/Interperiodica, 1-571 (in Russian).
- Patchett, P.J., Roth, M.A., Canale, B.S., de Freitas, T.A., Harrison, J.C., Embry, A.F., and G.M. Ross, 1999. Nd isotopes, geochemistry, and constraints on sources of sediments in the Franklinian mobile belt, Arctic Canada. *April. Geol. Soc. Amer. Bull.*, 111, 578-589, doi:10.1130/0016-7606(1999)111.
- Patrick, B. E., and W.C. McClelland, 1995. Late Proterozoic granitic magmatism on Seward Peninsula and a Barentian origin for arctic Alaska–Chukotka. *Geology*, 23, 1, 81-84.
- Piskarev, A. L., Heunemann, C., Makar'ev, A. A., Makar'eva, A. M., Bachtadse, V., M. Aleksyutin, 2009. Magnetic parameters and variations in the composition of igneous rocks of the Franz Josef Land archipelago. *Izvestiya, Physics of the Solid Earth*, 45, 2, 150-166 (in Russian).
- Pitman, W.C. and M. Talwani, 1972. Sea floor spreading in the North Atlantic. *Geol. Soc. Am. Bull.*, 83, 619-646.
- Poselov, V.A., Gramberg, I.S., Murzin, R.R., Butsenko, V.V., Kaminsky, V.D., Sorokin, M. Yu., and Yu.E. Pogrebitsky, 2002. The structure and boundary of the continental and oceanic lithospheres of the Arctic Basin. In: Dodin, D.A. and V.S. Surkov (eds) *The Russian Arctic: Geological history, metallogeny, geoecology*. St. Petersburg, VNIIOkeangeologiya, 121-133 (in Russian).
- Poselov, B.A., Butsenko, V.V., Verba, V.V., Zholondz, S.M. and A.I. Truhalev, 2008. Rises of the Amerasia Subbasin in the Arctic Ocean and their likely counterparts in the Atlantic. In: *60 years in the Arctic, Antarctic, and the world ocean*. St. Petersburg, VNIIOkeangeologiya, 275-304 (in Russian).
- Pumhösl, H., 1998. Petrographische und geochemische Untersuchungen an den Deckenbasalten der Insel Salisbury, Franz Joseph-Land, russische Arktis. University of Vienna, Master thesis, 1-120.
- Pushcharovsky, Yu.M., 1976. Tectonics of the Arctic Ocean. *Geotektonika*, 2, 3-14 (in Russian).
- Ritzmann, O., Jokat, W., Mielde, R. and H. Shimamura, 2002. Crustal structure between the Knipovich Ridge and the Van Mijenfjorden (Svalbard). *Mar. Geophys. Res.*, 23, 379-401.
- Roest, W.R., and S.P. Srivastava, 1989. Seafloor spreading in the Labrador Sea: a new reconstruction. *Geology* 17, 1000–1004.
- Rowley, D.B. and A.L. Lottes, 1988. Plate-kinematic reconstructions of the North Atlantic and Arctic: Late Jurassic to Present. *Tectonophysics*, 155, 73-120.
- Savostin, L.A., Natapov, L.M., and A.P. Stavsky, 1984. Mesozoic paleogeodynamics and paleogeography of the Arctic region. In: *Proceeding 27 Int. Geol. Congress, Paleooceanology. Colloquium K. 03*. Moscow, Nauka, 3, 172-187 (in Russian).
- Savostin, L.A., Sibuet, J.C., Zonenshain, L.P., Le Pichon, X. and M.J. Roulet, 1986. Kinematic evolution of the Tethys belt from the Atlantic Ocean to the Pamirs since the Triassic. *Tectonophysics*, 123, 1-4, 1-35.
- Sclater, J.G., Hellinger, S. and C. Tapscott, 1977. The paleobathymetry of the Atlantic Ocean from the Jurassic to the present. *J. Geol.*, 85, 509—552.
- Shatsky, N.S., 1965. *Selected papers*. Moscow, Nauka, I-IV (in Russian).
- Shipilov, E. V., Y.V. Karyakin, 2011. The Barents Sea magmatic province: geological-geophysical evidence and new ⁴⁰Ar/³⁹Ar dates. *Doklady Earth Sciences*, 439, 1, 955-960 (in Russian).
- Shipilov, E.V. and V.A. Vernikovskiy, 2010. The structure of the junction area of the Svalbard and Kara plates and geodynamic settings of its formation. *Geologiya i geofizika*, 51, 1, 75-92 (in Russian).
- Shipilov, E.V. and Yu.V. Karyakin, 2010. Mesozoic basaltoid magmatism of the Barents Sea continental margin: Geodynamic settings of the early phase of the Arctic Ocean opening (from the results of investigations in the archipelagoes of the Franz Joseph Land and Spitzbergen). In: *Structure and history of development of the*

- lithosphere. Moscow, Paulsen, 312-330 (in Russian).
- Shipilov, E.V., 2004. On the tectono-geodynamic evolution of the Arctic continental margins in the epochs of young ocean formation. *Geotektonika*, 5, 26-52 (in Russian).
- Shipilov, E.V., 2008. Generations of spreading basins and the phases of the breakup of the Wegenerian Pangea in the geodynamic evolution of the Arctic Ocean. *Geotektonika*, 2, 1-23 (in Russian).
- Shipilov, E.V., Karyakin, Yu.V., and G.G. Matishov, 2009. The Barents-Amerasia Jurassic-Cretaceous superplume and the initial phase of geodynamic evolution of the Arctic Ocean. *Doklady Ross. Akad. Nauk*, 426, 3, 1-4 (in Russian).
- Shreider, A.A., 2004. Magnetic lineations of the Arctic Ocean. *Okeanologiya*, 44, 7668-777 (in Russian).
- Silantyev, S.A., Bogdanovskii, O.G., and P.I. Fedorov, 2004. Intraplate magmatism of the De Long Islands. *Rus. J. Earths Sci.*, 6, 3, 1-31.
- Sokolov, S. D., Bondarenko, G. Ye., Layer, P. W., and I.R. Kravchenko-Berezhnoy, 2009. South Anyui suture: tectono-stratigraphy, deformations, and principal tectonic events. *Stephan Mueller Spec. Publ. Ser.*, 4, 201-221.
- Sokolov, S.D., Bondarenko, G.Ye., Morozov O.L., Shekhovtsov V.A., Glotov S.P., Ganelin A.V. and I.R. Kravchenko-Berezhnoy, 2002. South Anyui suture, northeast Arctic Russia: Facts and problems to solve. In: Miller, E.L., Grantz, A., and S.L. Klemperer (eds) *Tectonic evolution of the Bering Shelf-Chukchi Sea-Arctic Margin and adjacent landmasses*. Boulder, Colorado, GSA Special Paper, 360, 209-224.
- Soper, N. J. and A. K. Higgins, 1987. A shallow detachment beneath the North Greenland fold belt: implications for sedimentation and tectonics. *Geological Magazine*, 124, 05, 441-450.
- Srivastava, S.P. and C.R. Tapscott, 1986. Plate kinematics of the North Atlantic. In: Vogt, P.R. and B.E. Tucholke (eds) *Geology of North America Series. The Western North Atlantic Region*. Geol. Soc. Am. Boulder, Colorado, M, 379-404.
- Srivastava, S.P., 1985. Evolution of the Eurasian Basin and its implications to the motion of Greenland along Nares Strait. *Tectonophysics*, 114, 29-53.
- Stavsky, A.P., 1982. The Lower Indigirka rift zone: A new element of the structure of the NE USSR. *Doklady Akad. Nauk SSSR*, 262, 6, 1443-1446 (in Russian).
- Stolbov, N.M., 2002. On the issue of the age of flood magmatism of the Franz Joseph Land Archipelago from radiometric data. In: *Geological and geophysical characteristics of the lithosphere of the Arctic region*. St. Petersburg, VNIIOkeangeologiya, 4, 199-202 (in Russian).
- Tailleux, I.L., 1973. Probable rift origin of the Canada Basin. In: Pitcher M.G. (ed) *Arctic Geology*. AAPG Memoir, 19, 526-535.
- Tarakhovskiy, A.N., Fishman, M.V., Shkola, I.V. and V.L. Andreytchev, 1982. The age of the flood volcanics of the Franz Joseph Land. *Doklady Akad. Nauk SSSR*, 266, 4, 965-969 (in Russian).
- Taylor, P.T., Kovacs, L.C., Vogt, P.R. and G.L. Johnson, 1981. Detailed aeromagnetic investigations of the Arctic Basin. *J. Geophys. Res.*, 86, 6323-6333.
- Tegner, C., Storey, M., Holm, P. M., Thorarinsson, S. B., Zhao, X., Lo, C. H., and M. F. Knudsen, 2011. Magmatism and Eureka deformation in the High Arctic Large Igneous Province: 40Ar-39Ar age of Kap Washington Group volcanics, North Greenland. *Earth and Planetary Science Letters*, 303, 3, 203-214.
- Thorarinsson, S. B., Holm, P. M., Tappe, S., Heaman, L. M., and C. Tegner, 2011. Late Cretaceous-Palaeocene continental rifting in the High Arctic: U-Pb geochronology of the Kap Washington Group volcanic sequence, North Greenland. *Journal of the Geological Society*, 168, 5, 1093-1106.
- Trettin, H.P., 1994. Pre-Carboniferous geology of the northern part of the Arctic Islands: Hazen Fold Belt and adjacent parts of Central Ellesmere Fold Belt, Ellesmere Island. *Geol. Surv. Canada Bull.*, 430, 1-248.
- Trunilina, V.A., Roev, S.P., Orlov, Yu.S., and V.S. Oksman, 1999. Magmatism of different geodynamic settings (the junction zone of the

- Verkhoyansk margin of the Siberian continent and the Kolyma-Omolon microcontinent). Yakutsk, Nauchn. Tsentr. Sib. Otd. Ross. Akad. Nauk, 1-158 (in Russian).
- Verzhbitsky V.E., Shapiro M.N., Solov'ev A.V. and Goldyrev A.E., 2005. New Data on the Structure of the Accretionary Prism in Karaginskii Island (Bering Sea) // Transactions (Doklady) of the Russian Academy of Sciences/Earth Science Section. Vol. 405, No. 8. p. 1150-1154.
- Verzhbitsky, V.E., S.D. Sokolov, E.M. Frantzen, A. Little, M.I. Tuchkova, and L.I. Lobkovsky, 2012, The South Chukchi Sedimentary Basin (Chukchi Sea, Russian Arctic): Age, structural pattern, and hydrocarbon potential, in D. Gao, ed., Tectonics and sedimentation: Implications for petroleum systems: AAPG Memoir 100, p. 267 – 290.
- Villeneuve, M. and M.C. Williamson, 2003. ⁴⁰Ar-³⁹Ar dating of mafic magmatism from the Sverdrup Basin Magmatic Province. Proc. IV Intern. Conf. Arctic Margins. Anchorage: MMS, 206–215.
- Vogt, P., Kovacs, L.C., Bornero, L.C. and S.P. Srivastava, 1982. Assymetric geophysical signatures in the Greenland-Norwegian and the southern Labrador Seas and the Eurasia Basin. Tectonophysics, 89, 95-160.
- Vogt, P., Taylor, P., Kovacs, L. and G. L. Johnson, 1979. Detailed aeromagnetic investigation of the Arctic Basin. J. Geophys. Res., 84, 1071-1089.
- Weber, J. R. and J.F. Sweeney, 1990. Ridges and basins in the Arctic Ocean. In: Grantz, A., Johnson, L. and J.F. Sweeney (eds) The Geology of North America V. L. The Arctic Ocean Region. Geol. Soc. America, Boulder, CO., 305-336.
- Worsly, D., Ada, O.J., Dalland, A., Elverhøi, A. and A. Thon, 1986. The Geology History of Svalbard. Stavanger, Statoil, 1-121.
- Zamansky, Yu.Ya., Ivanova, N.N., Langinen, A.E., and M.Yu. Sorokin, 2002. Seismic investigations during the Arctica-2000 expedition. In: Geological and geophysical characteristics of the lithosphere of the Arctic region. St. Petersburg, VNIIOkeangeologiya, 4, 11-24 (in Russian).
- Zhao, D., 2009. Multiscale seismic tomography and mantle dynamics. Gondwana Res., 15, 297-323.
- Zhao, D., Piraino, F. and L. Liu, 2010. Mantle structure and dynamics under Eastern Russia and adjoining regions. Geologiya i geofizika, 51, 9, 1188-1203 (in Russian).
- Zhao, D., Tian, Y., Lei, J., Liu, L. and S. Zheng, 2009. Seismic image and origin of the Changbai intraplate volcano in East Asia: Role of big mantle wedge above the stagnant Pacific slab. Phys. Earth Planet. Inter., 173, 197-206.
- Zonenshain, L. P., Kuzmin, M. I., and L. M., Natapov, 1990b. Geology of the USSR: a plate-tectonic synthesis. AGU Geodynamics Series, 21, 1-242.
- Zonenshain, L.P. and L.M. Natapov, 1987. Tectonic history of the Arctic. In: The topical problems of geotectonics. Moscow, Nauka, 31-57 (in Russian).
- Zonenshain, L.P., Kuzmin, M.I., and L.M. Natapov, 1990a. Plates tectonics of the USSR territory. Moscow, Nedra, Book 1 —1-328, Book 2 — 1-334 (in Russian).
- Zonenshain, L.P., Natapov, L.M., Savostin, L.A., and A.P. Stavsky, 1978. Plate tectonics of Northeastern Asia in connection with the opening of the Arctic Basin and North Atlantic. Okeanologiya, 18, 6, 38–47 (in Russian).



Отпечатано на КФ ВСЕГЕИ. Заказ 80000432.